Peritumoral cortex : electrophysiological signals

Belén Díaz-Fernández

Sorbonne Université

Ecole doctorale 158, Cerveau, Cognition et Comportement (ED3C)

Centre Interdisciplinaire de Recherche en Biologie (CIRB) – Collège de France
Équipe du Dr. N. Rouach : Interactions Neurogliales dans la Physiopathologie Cérébrale
Laboratoire Imagerie Biomédicale (LIB)
Équipe du Dr. V. Marchand-Pauvert : Connectivité Neurale et Plasticité

Peritumoral cortex : electrophysiological signals

Presenté par Belén Diaz-Fernandez

Thèse de doctorat de Neurosciences

Dirigée par Gilles Huberfeld et Michel Le Van Quyen

Présentée et soutenue publiquement le 24/10/2023

Devant un jury composé de :

Pr. Nathalie Kubis PU-PH, Université Paris Cité	Présidente du Jury
Dr. Catalina Alvarado-Rojas Associate professor, Universidad Javeriana	Rapportrice
Pr. François Ducray PU-PH, Université Lyon 1	Rapporteur
Dr. Christian Bénar DR, Inserm	Examinateur
Dr. Gilles Huberfeld Praticien chercheur, Hopital Fondation A. de Roschtchild	Directeur de thèse
Dr. Michel Le Van Quyen DR, Inserm	Directeur de thèse

A la mémoire de Laurent Capelle,

Acknowledgements

Après un peu plus de quatre ans cette période touche à sa fin. Je me souviens encore de mes doutes sur mon futur à la fin du clinicat. Maintenant j'en suis sûre d'avoir pris la bonne décision de m'embarquer dans cette aventure.

Tout d'abord, je tiens à remercier l'ensemble des membres de mon jury d'avoir accepté d'évaluer mes travaux. Je remercie particulièrement le Dr. Catalina Alvarado-Rojas et le Pr. François Ducray d'avoir accepté d'être mes rapporteurs. Merci également au Pr. Nathalie Kubis et au Dr. Christian Bénard d'avoir accepté d'être mes examinateurs.

Je tiens ensuite à remercier mes directeurs de thèse. Michel, merci de m'avoir introduit au fascinant monde des HFO et à l'importance des nuances. Gilles, merci pour tes enseignements : non seulement cliniques et scientifiques, mais aussi appliqués à la vie en général. Merci pour ta patiente infinie et pour m'avoir encouragé à creuser plus et aller plus loin quand je commençais à fatiguer. Merci à tous les deux pour m'avoir transmis la passion pour les neurosciences.

Nathalie, merci de m'avoir accueillie dans ton équipe au Collège de France et pour tes questions toujours intéressantes aux labmeetings.

Véronique, merci de m'avoir ouvert les portes du LIB et pour ton soutien à chaque fois qu'on a échangé par email ou qu'on s'est vue en personne.

Cette thèse n'aurait jamais eu lieu sans l'aide des neurochirurgiens. Laurent, j'aurais tellement aimé pouvoir te remercier en personne, mais tu nous as quitté trop tôt. Merci pour ces moments vraiment sympas au bloc opératoire, pour être toujours à l'écoute et si aidant avec tout. Johan, merci de m'avoir si bien accueilli à Sainte-Anne, pour ton perfectionnisme et pour vouloir toujours trouver le meilleur emplacement pour « les électrodes de Belén ». Merci à tout l'équipe de la Pitié : Bertrand, Karine, Fred, Fatima, Medhi, Jugurtha. Merci aussi à l'équipe de Sainte-Anne : Alexandre merci pour ton aide avec les repaires neuroanatomiques, Edouard, et le formidable équipe d'infirmerie.

Un énorme merci à Vivianne et Bénédicte, je suis vraiment ravie d'avoir fait votre connaissance grâce à cette thèse. Merci pour votre gentillesse sans limites et pour avoir était toujours si bienveillantes.

Merci à Panaxium pour son soutien. Merci à tous pour l'incroyable accueil que vous m'avez fait lors de mes visites en Aix, et de vous avoir intéressé toujours aux avancés de ma thèse. Pierre, merci pour tes enseignements sur le monde industriel, c'est toujours enrichissant d'avoir un autre regard complémentaire.

Gracias a Alejandro y Patricia, mis mentores en Vall d'Hebron. Gracias por haberme animado a cambiar Barcelona por Paris y a hacer una verdadera tesis.

This thesis wouldn't be the same without my amazing desk colleagues.

Alesya, thanks for everything, your contagious scientific spirit, and your great advices. Thanks also to Anorak and the kids for the good moments shared around a (not strictly veggie) barbecue.

Don David, gracias por los ataques caticardia que nos hemos pegado de las risas. Porque siempre se avanza mas lejos en equipo, que cada uno por su cuenta. La tesis no hubiera sido lo mismo sin los partidos de tenis en streaming, las canciones de Rosalia y las cerves en el Sena.

Juan, gracias por tus enseñanzas sobre el fascinante mundo del deep learning y por los Doritos en momentos de crisis, espero que la experiencia de tesis que comienzas ahora sea tan increible como la que he vivido yo.

Nivitha and Kyrill, I hope your stay in the team will give you plenty of professional success and good moments.

A mes anciens collocs de bureau, A.K.A « The Cave », Rachel, Augustin, Eléonore, Léa, Yoni et Julien. Merci pour ces grands moments partagés ensemble au tour des tothems et pour avoir apporté un grain de folie à mon expérience au Collège.

Rachel, merci pour ton accueil dès le second numéro un. Mon passage au Collège n'aurait pas été le même sans toi. J'ai énormément apprécié nos discussions au jap pour « nous actualiser ». Maintenant t'es la prochaine, mais je suis sûre que tu vas cartonner.

Augustin, merci pour les discussions et bons moments partagés. Grace à toi j'ai pu découvrir l'univers fascinant de la cantine.

Julien, merci pour la bonne ambiance et pour être toujours disponible pour aider.

Pascal, merci pour les bons moments et pour ton aide précieuse avec les complexités de l'immunohistochimie.

Elena, merci pour ton aide et conseils avec les tissus humains et MEA.

Giamp, merci pour m'avoir montré les mécanismes du bi-photon et pour ta bonne humeur pérenne.

Je remercie aussi à tous les gens avec lesquelles j'ai pu partager mon temps pendant ces quatre ans : Edmon, Eléonor, Jeff, Anna, Josine, Noémie, David, Isabelle, Daria, Laure, Armelle, Arthur, Anaïs, Assumpta, Jérôme, Martine, Anne Cécile, Marc, Katia, Rodrigo.

Un grand merci à Claudie et Vincent, sans eux tout aurait été beaucoup plus compliqué. Je remercie également Nicole et Sophie qui m'ont aidé à traverser le labyrinthe burocratique.

Ces dernières années n’aurait pas été les mêmes sans le soutien de ma famille parisienne. Grazie à Guilia et Leo pour les voyages partagés ensembles, les dimanches à Fonta et les 80 km d’Arcachon. Grazie anche à Filo et Aurora, pour les promenades aux Buttes Chaumont, les concerts, festivals e i fegatini.

A toute la belle équipe « Calle 13 », en spécial à Esther et Luca pour faire que le 4eme et le 6eme soient vraiment proches. Merci pour les bons moments partagés ensembles.

Gracias a Nur y Miguel, sin vosotros no hubieran sido lo mismo esos partidos insufribles de la seleccion ni las discusiones post-electrorales.

Grazie a la mia famiglia italiana, Francesca, Pier e Marce per essere sempre cosi accogliente.

Gracias a mis padres y a Maria, porque sin ellos no habria llegado hasta aqui. Por el apoyo incondicional, por haberme animado siempre a hacer lo que queria y a conocer el mundo.

Nico, gracias por haberme acompañado y animado siempre. Por ser una inspiracion no solo a nivel cientifico, sino en el resto de facetas de la vida. Porque el futuro sigue siendo nuestro.

-*“A smooth sea never made a skilled sailor”*-

Franklin D. Roosevelt

Summary

Introduction

1. Brain gliomas

Tumors are characterized by excessive and uncontrolled growth of abnormal cells. Primary brain tumors encompass a diverse group, including benign and malignant tumors. They account for approximately 2% of all tumors and comprise over 100 different types of neoplasms. Gliomas are the most common primary brain tumor (Louis et al., 2021). They seem to originate from various cell types, such as neural stem cells and unipotent progenitors (Llaguno & Parada, 2016). This thesis focuses explicitly on adult diffuse gliomas, excluding gliomatosis cerebrii, type I gliomas, and midline and cerebellum gliomas.

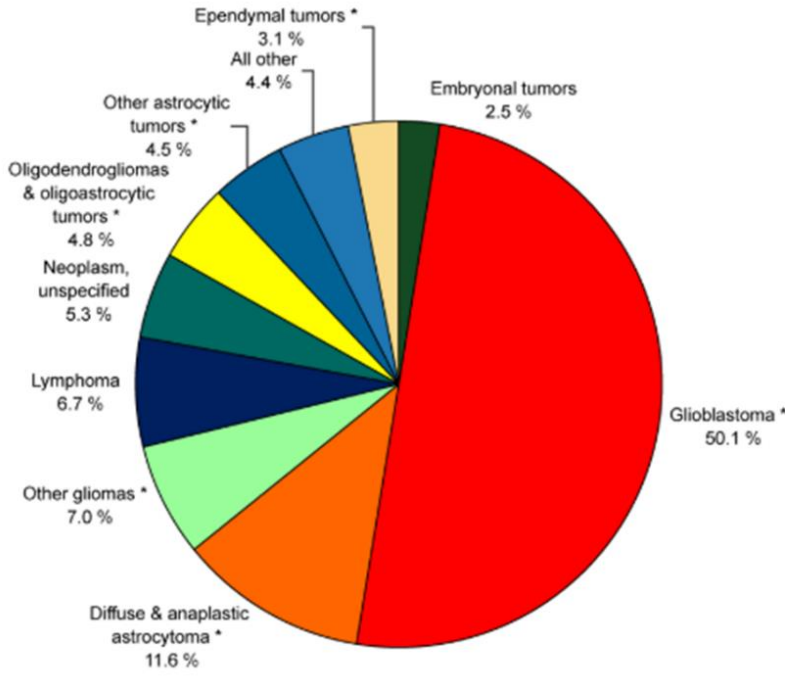

Figure 1: Relative frequency of malignant primary brain tumors (126.345 patients) from the CBTRUS Statistical Report 2022.

1.1. Epidemiology, etiology, and risk factors

Diffuse gliomas are the most frequent primary brain tumor (Salari et al., 2023). The global annual incidence of gliomas is approximately six cases per 100.000 individuals (Michael Weller et al., 2021). The Central Brain Tumor Registry of the United States (CBTRUS) collects comprehensive population-based data on primary brain tumors. According to the 2022 report, which includes data from 2015 to 2019, gliomas accounted for approximately 24% of all primary brain tumors and 61.7% of malignant primary brain tumors. The

updated World Health Organization (WHO) brain tumor classification distinguishes between astrocytoma, oligodendroglioma, and glioblastoma (GB) (Louis et al., 2021). GB are the most prevalent among all gliomas, representing 14.2% of all tumors and 59.2% of all gliomas (Figure 1) (Ostrom et al., 2022). In France, gliomas are estimated at eight cases per 100.000 individuals (Bauchet et al., 2007). According to the French Brain Tumor Data Base (FBTDB), gliomas account for 42,4% of all primary brain tumors (Zouaoui et al., 2012).

Specifically, the incidence of astrocytoma in the USA is reported to be 0.46 per 100.000 individuals per year. Oligodendrogliomas have an incidence of 0.23 per 100.000 individuals per year. GB exhibits the highest incidence at 3.26 per 100.000 individuals annually (Ostrom et al., 2022). GB also carries the worst prognosis, with only 6.9% of patients surviving five years after diagnosis (Ostrom et al., 2022). Mean survival rates vary, ranging from ten years in the case of low-grade gliomas to just 15 months for GB (Claus et al., 2015).

Although gliomas are typically sporadic, certain factors can increase the risk of developing a glioma. These factors can be classified into non-modifiable and modifiable. In the non-modifiable factors group, sex, age, and ethnicity are noteworthy. Male individuals have a higher risk of developing a glioma than females, with a ratio of 1.6 to 1 in the case of GB (Ostrom et al., 2022; W. Yang et al., 2019). Additionally, females have better outcomes (Ostrom et al., 2018). While the underlying reasons for these differences are not yet fully understood, they could be partially explained by the fact that male astrocytes are more prone to RB1 inactivation, which increases the induction of a stem-like cell phenotype and accelerates the growth rate, in comparison to female astrocytes (Sun et al., 2014). Age is considered a significant risk factor for developing GB, with its incidence increasing over time and peaking between 75 and 84 years (Colopi et al., 2023). Moreover, Caucasian individuals present a twofold higher risk of developing GB, whereas Hispanic or Black individuals have a lower risk (Tamimi & Juweid, 2017).

Patients with specific genetic syndromes also have a higher risk of developing glioma, which accounts for approximately 1% of glioma cases (Bondy et al., 2008). The most common syndromes associated with high glioma risk are neurofibromatosis type 1 (NF1), tuberous sclerosis, Li-Fraumeni syndrome, and Turcot syndrome. NF1 is caused by a germline mutation in the tumor suppressor gene NF1 (17q11.2). The protein neurofibromin plays a role in the MAPK, mTOR, and Akt pathways. Li-Fraumeni syndrome is characterized by an autosomal mutation in the TP53 tumor suppressor gene (17p3). Patients with this syndrome may develop multiple cancers, including sarcoma, breast cancer, acute leukemia, or brain tumors. Tuberous sclerosis results from an autosomal mutation in either TSC1 (9q34) or TSC2 (16p13). Turcot syndrome type 1 is associated with the APC mutation (5q21), while Turcot syndrome type 2 is linked to hMSH2 (2p16), hMLH1 (3p21.3), and hPMS2 (7p22) mutations. Other less common syndromes with an increased risk of glioma include neurofibromatosis type 2 (Merline, 22q12), Gorlin syndrome (PTCH, 9q22.3), and Cowden syndrome (PTEN, 10q23.3) (Almairac et al., 2010; Bondy et al., 2008).

Genome-wide association studies (GWAS) have identified several polymorphisms associated with glioma susceptibility. For example, the rs1412829-G allele in the CDKN2B gene and the rs6010620-G allele in the REL1 gene have been implicated (Claus et al., 2015; Shete et al., 2009; Wrensch et al., 2009) (Table 1). Besides the previously mentioned

genetic syndromes and polymorphisms, approximately 5% of glioma patients exhibit familiar clustering. In these cases, first-degree relatives of glioma patients have a twofold increased risk of developing a brain tumor, mainly if the tumor manifests at a younger age (Malmer et al., 2003).

Candidate Gene (chromosome location)	Risk Allele	Magnitude of Association*	Risk Allele Frequency†	Putative Functional Significance	Associated Glioma Subtypes
TERC (3q26.2)	rs1920116-G	+	0.72	Increased telomere length	HGG
TERT (5p15.33)	rs2736100-C	+	0.51	Increased telomere length	All glioma subtypes
EGFR (7p11.2)	rs2252586-A	+	0.27	Unknown	All glioma subtypes
EGFR (7p11.2)	rs11979158-A	+	0.82	Unknown	All glioma subtypes
CCDC26 (8q24.21)	rs55705857-G	+++	0.046	microRNA site	Oligodendroglial tumors & *IDH*-mutated astrocytic tumors
CDKN2B/ANRIL (9p21.3)	rs1412829-G	+	0.43	Unknown	Astrocytic tumors of all grades
PHLDB1 (11q23.3)	rs498872-A	+	0.31	Unknown	*IDH*-mutated gliomas
TP53 (17p13.1)	rs78378222-C	++	0.014	Alteration of polyadenylation signal impairs *TP53* mRNA processing	All glioma subtypes
RTEL1 (20q13.33)	rs6010620-G	+	0.76	Unknown	All glioma subtypes

* Magnitude of Association: +++ represents OR ≥ 5.0, ++ represents 2.0 ≤ OR < 5.0, and + represents 1.0 < OR < 2.0.
† Allele frequency in Caucasians, extracted from HapMap CEPH (Centre d'Etude du Polymorphisme Humain) data where available.

Table 1: Glioma-associated susceptibility polymorphisms detected by GWAS. From Claus et al, 2015.

Numerous studies have been published regarding the modifiable factors, often yielding contradictory results. The following factors have been identified as the most relevant:

- Diagnostic ionizing radiation does not increase the risk of developing glioma. However, high doses of radiation administered in the head-neck area to treat other neoplasms increase the risk of developing GB (Bondy et al., 2008).
- Electromagnetic fields, such as those created by mobile phones, do not increase the likelihood of developing gliomas (Schüz et al., 2022)
- Atopic diseases and allergies act as protective factors, reducing the risk of developing GB by approximately 40% (Tamimi & Juweid, 2017; Wiemels et al., 2002).
- Anti-inflammatory drugs are also associated with a protective effect against GB (Ferreira et al., 2021; Kast, 2021; Lopes et al., 2021).
- Abdominal obesity can increase glioma risk in diabetic and non-diabetic patients (Sang et al., 2023).
- While further research is needed to fully understand curcumin's protective effect in humans, some promising studies have demonstrated its cytotoxic effect on glioma cell cultures (Shi et al., 2021; Wong et al., 2021).

1.2. Classification

1.2.1. Previous classification

In 2021, the WHO updated its classification of brain tumors. The previous classification was published in 2016 (Louis et al., 2016). In 2016 classification, diffuse astrocytic and oligodendroglial tumors encompassed astrocytoma (diffuse or anaplastic), oligodendroglioma (diffuse or anaplastic), GB, diffuse midline glioma and

oligoastrocytoma (diffuse or anaplastic). Astrocytoma and GB could be categorized as IDH-mutated, IDH-wildtype (IDH-WT), or not otherwise specified (NOS), while oligodendroglioma could be classified as IDH-mutated or NOS.

1.2.2. Principles in the classification evolution

One of the main revisions in the new classification is the distinction of gliomas based on the age of onset into a pediatric-type and an adult-type, as they exhibit distinct genetic, epigenetic, and clinical characteristics. The adult-type diffuse gliomas include astrocytoma, oligodendroglioma, and GB, based on the IDH status. Histological and molecular criteria determine the classification among these types. The changes in the new classification primarily involve taxonomy, nomenclature, and grading. The previous classification, which consisted of 15 different glioma groups, has been streamlined into three main entities: IDH-mutated astrocytomas, IDH-mutated and 1p/19q-codeleted oligodendrogliomas, and IDH-WT GB.

In the updated classification, the term "anaplastic" is no longer used, and the previously referred to "anaplastic astrocytoma or oligodendroglioma" are now term "grade 3 astrocytoma or oligodendroglioma". The group "oligoastrocytoma" has also been removed from the classification, as it has been reclassified into different groups based on their molecular profile. The frequency of "not otherwise specified (NOS)" and "not elsewhere classified (NEC)" has decreased due to the implementation of molecular diagnosis.

Molecular criteria play a pivotal role in the new classification. The main criterion use is the status of the isocitrate dehydrogenase (IDH) gene, distinguishing between mutated and wild-type (WT) forms. Astrocytomas and oligodendrogliomas are IDH-mutated tumors, whereas GB are IDH-WT tumors (Louis et al., 2021).

1.2.2.1. IDH mutation

Astrocytoma and oligodendroglioma exhibit mutations in the enzyme IDH. The IDH enzyme family, consisting of three forms – IDH1, IDH2, and IDH3- participates in the Krebs Cycle. IDH1 and 2 form homo-dimers, while IDH3 is a hetero-tetramer. IDH1 is localized in the cytoplasm and peroxisomes of cells, whereas IDH2 and 3 are found within the mitochondrias (Joseph et al., 2006; Leighton et al., 1969). Under normal conditions, these three forms catalyze the oxidative decarboxylation of isocitrate into α-ketoglutarate (αKG), consuming NADP+ and releasing NADPH and CO_2 (Solomou et al., 2023). However, when IDH is mutated, αKG is converted into D2-HydroxyGlutarate (D2HG) (figure 2). This mutation is therefore associated with a gain of function. IDH 1/2 mutations are not exclusive to gliomas; they have also been observed in other tumors, including chondrosarcoma (20–80%) (Amary et al., 2011; Lu et al., 2013), cholangiocarcinoma (6–30%) (Farshidfar et al., 2017; Kipp et al., 2012), or acute myeloid leukemia (Mardis et al., 2009). Nevertheless, gliomas display the highest frequency of IDH mutations. IDH 3 mutations have not been associated with any tumor (Al-Khallaf, 2017). IDH1/2 mutation is one of the earliest events in gliomagenesis. A study in serial biopsies from the same patients has consistently demonstrated that IDH mutation always occurs before acquiring TP53 mutation or p1-q19 codeletion (Watanabe et al., 2009).

The most common IDH mutation observed in glioma patients is the IDH1-R132H. In this mutation, the amino acid arginine at position 132 is replaced by a histidine, switching the

protein configuration from an open structure to a closed form. This alteration reduces the enzyme's affinity for isocitrate while increasing its affinity for αKG. IDH1/2 mutations are characterized by monoallelic changes, resulting in both WT and mutated monomers in the enzyme. Consequently, the WT monomer catalyzes the conversion of isocitrate into αKG, while the mutated monomer converts αKG into D2HG (Figure 2) (Dang et al., 2009; Solomou et al., 2023).

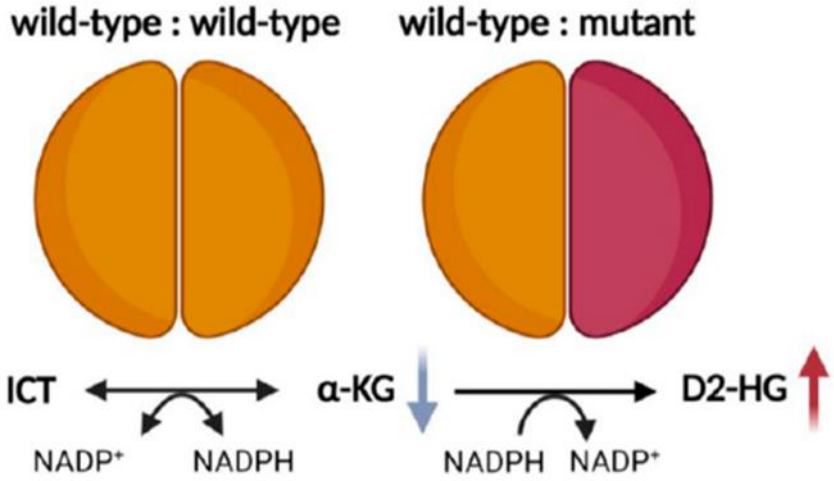

Figure 2: IDH-WT and IDH-mutated dimers representation. The IDH-mutated form contains one WT monomer and a second mutated monomer. From Solomou et al 2023.

Interestingly, patients with different mutations from the R132H mutation in IDH1 appear to exhibit distinct clinical characteristics. While their median overall survival may be similar, patients with non-R132H mutations tend to have a younger mean age at diagnosis and a higher frequency of a family history of cancer (22.2% vs. 5.1% in R132H IDH1 patients). Additionally, multicentric tumor locations are more commonly observed in non-R132H IDH1 mutations (4.8% vs. 0.9% in R132H IDH1). Among the non-canonical IDH1 mutants, astrocytomas are more frequently involved (65.6% vs. 43% in R132H IDH1), while IDH2 mutations are more commonly associated with oligodendrogliomas (85% vs. 48.3%) (Poetsch et al., 2021).

D2HG is an oncometabolite not only because gliomas produce it but also because it actively contributes to gliomagenesis. Firstly, D2HG plays a role in the hypermethylation of DNA and histones by inhibiting histone lysine demethylases (KMDs) and 10-11-translocation-methylcytosine (TET) enzymes (Chowdhury et al., 2011; Xu et al., 2011). Secondly, the mutation leading to D2HG accumulation increases oxidative stress (Gilbert et al., 2014; Latini et al., 2005) and impairs DNA repair mechanisms (Lu et al., 2017; Sulkowski et al., 2017). In patients without IDH mutation (IDH-WT), D2HG brain concentration is minimal since it is only produced as an erroneous byproduct in the Krebs cycle. However, in patients with IDH mutations, D2HG reaches high intracellular and extracellular concentrations, ranging from 5-35 µmol per gram of tumor (Dang et al., 2009). D2HG is not confined to the tumor; it diffuses and can be detected in cerebrospinal fluid (CSF). In a study conducted on glioma patients CSF, the mean concentration was 0.427 mmol/L in IDH-WT patients and 7.439 mmol/L in IDH1/2 mutated patients (Kalinina et al., 2016). A recent study has

shown that CSF D2HG concentration decreases after surgery and chemoradiation treatment in regularly monitored patients, suggesting the potential of CSF D2HG as a biomarker for monitoring IDH-mutated gliomas (Riviere-Cazaux et al., 2023). A mathematical model-based study indicated that extracellular concentrations of up to 3 mM D2HG can be found as far as two cm from the tumor core in IDH1/2 mutated patients (Linninger et al., 2018). Non-conventional neuroimaging techniques such as MRI-spectroscopy enable the quantification of D2HG in the brain, but with reduced spatial resolution due to the voxels size (Andronesi et al., 2012).

In addition to its intracellular effects, D2HG also exhibits extracellular actions. Patients with IDH1/2 mutations, found in astrocytomas and oligodendrogliomas, have a higher frequency of seizures. These types of tumors are associated with seizures in 60-85% of patients, whereas in GB, the seizure frequency is situated at around 35% of patients (Huberfeld & Vecht, 2016; Pallud et al., 2014, 2022). Moreover, IDH1/2 mutated patients also have a higher incidence of pharmacoresistant epilepsy (Correia et al., 2021).

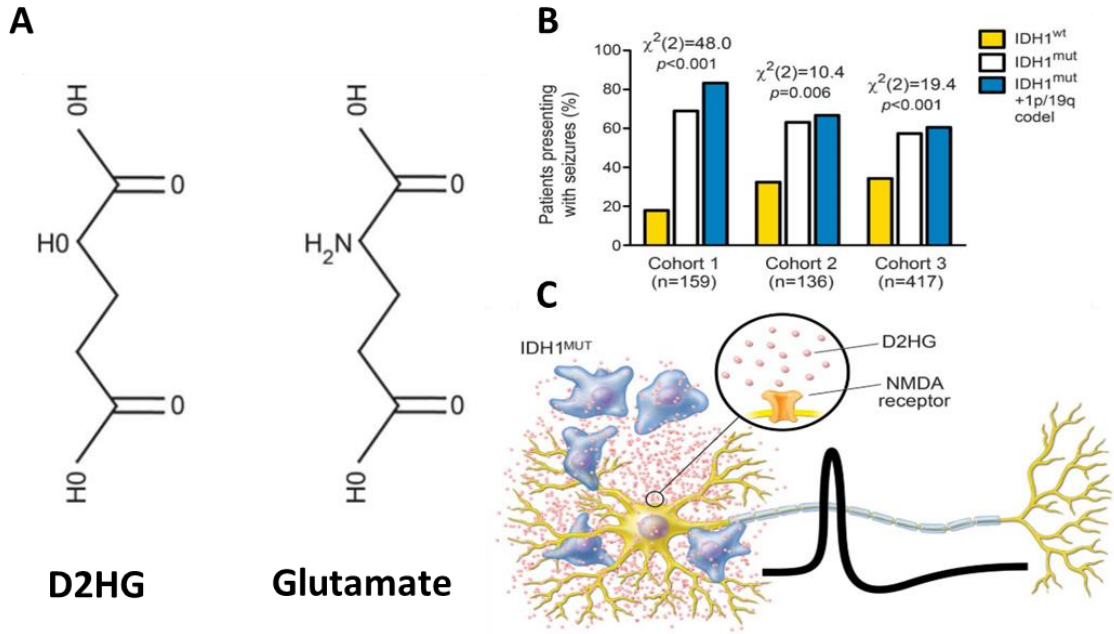

Figure 3: IDH mutation and D2HG
A: D2HG and Glutamate molecules.
B: Patients presenting with seizures: astrocytoma (white), oligodendroglioma (blue), and GB (yellow).
C: D2HG can stimulate NMDA receptors.
From Chen et al, 2017.

The structure of the D2HG molecule bears significant similarity to glutamate (Glu) (Figure 3). This similarity enables D2HG to activate Glu receptors but D2HG acts as a weak agonist. Through the stimulation of NMDA receptors, D2HG can increase neural activity and, consequently, the frequency of seizures (Armstrong et al., 2016; Chen et al., 2017; Lange et al., 2021; Liubinas et al., 2014; Yang et al., 2014). However, the epileptogenesis

effects of IDH1/2 mutations are not solely attributed to the stimulation of NMDA receptors. Recent studies have shown that D2HG enhances neural firing by stimulating NMDA receptors and upregulating the mTOR pathway in adjacent neurons. The elevation in neuronal firing was attenuated in glioma cell lines by applying mTOR inhibitors (Mortazavi et al., 2022).

Nevertheless, the D2HG role is considerably more complex than described. At low concentrations (millimolar scale), D2HG presents agonist effects on NMDA receptors (Kölker et al., 2002). At higher concentrations (3-10 mM), at least ins neuronal cultures, there is also an increase in neuronal burst firing (Chen et al., 2017). However, in an ex-vivo model using human peritumoral slices, D2HG inhibits spontaneous interictal discharges (IIDs) and ictal-like events (ILEs), acting as an antagonist on AMPA signaling. We hypothesize that D2HG and Glu compete for binding sites on the AMPA receptor.

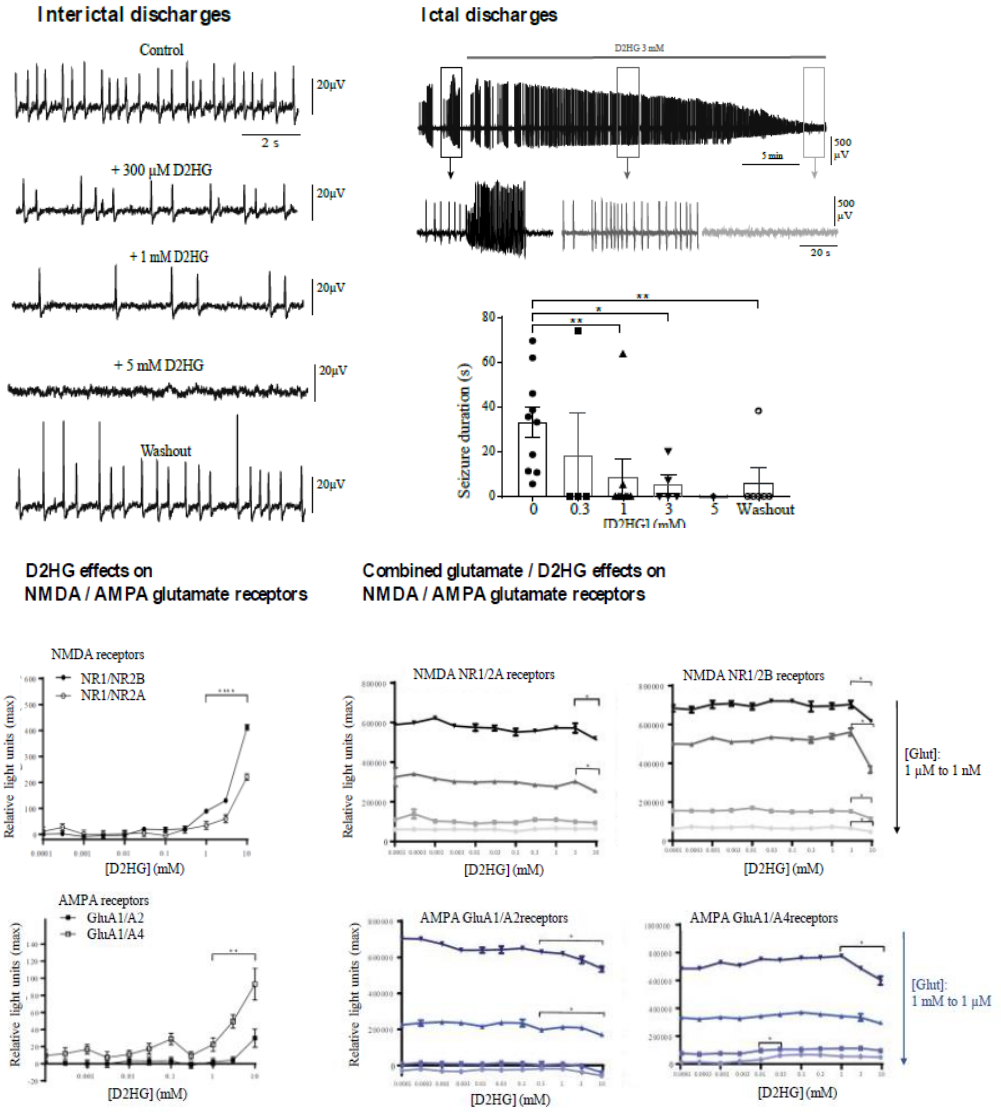

Figure 4: D2HG effects on extracellular and intracellular recordings.
A: D2HG effect on IIDs and ILEs.
B: D2HG effects on NMDA and AMPA Glu receptor under different Glu concentrations.
Unpublished data from our team.

To investigate this hypothesis, a preliminary study was conducted by expressing functional AMPA and NMDA receptors on the surface of HEK cells (cells derived from human embryonic kidney cells). The effects of increasing D2HG concentrations on AMPA and NMDA receptors were tested with or without glutamate. In the absence of Glu, high concentrations of D2HG exhibited agonist effects on NMDA and AMPA receptors. In contrast, in the presence of high concentrations of Glu, a competitive antagonist effect was observed (unpublish data from our team) (Figure 4).

Glu is implicated not only in the genesis of epileptic activities but also in tumor growth, cell division, and migration by stimulating autocrinally (glioma cells releasing themselves glutamate) AMPA and NMDA receptors. The subsequent increase in intracellular Ca^{+2} levels induces cell division via MAPK, Akt, and Focal Adhesion Kinase pathways (de Groot & Sontheimer, 2011). Therefore, we can expect that the structural similarity of D2HG also influences these pathways. However, IDH-mutated patients present longer survivals compared to IDH-WT patients. In the case of GB, the median survival is 15 months, while IDH1/2 grade 4 astrocytomas have a median survival of 31 months (Yan et al., 2009). A study conducted on 189 glioma patients demonstrated that IDH1/2 mutations were associated with more prolonged survival (Houillier et al., 2010). That seems counterintuitive since Glu enhances tumor growth, but patients with higher D2HG levels present longer survival rates. That suggests that D2HG cannot present exclusively Glu agonistic effects. Since D2HG acts as a weak competitive agonist, depending on the glutamate / D2HG balance, a reduction of glutamatergic effects by D2HG is suggested.

Another extracellular effect of D2HG is the inhibition of platelet aggregation. Glioma patients have a high risk of developing venous thromboembolisms (Jo et al., 2023; Perry, 2012; Timp et al., 2013). Approximately 30% of GB patients experience thrombotic events (Kayser-Gatchalian & Kayser, 1975; Ruff & Posner, 1983). In contrast, IDH1/2 mutated astrocytomas and oligodendrogliomas rarely develop thrombosis (Jo et al., 2023). In 2016, a study conducted on human platelets demonstrated that the addition of D2HG strongly and rapidly suppressed platelet aggregation by reducing intracellular Ca^{+2} accumulation by 72% and decreasing the levels of the procoagulant tissue factor (Unruh et al., 2016). However, this is not the sole mechanism implicated in the inhibition of platelet aggregation. The suppression of podoplanin, a sialoprotein that enhances platelet activation, may also be associated with the reduced risk of venous thromboembolism in IDH-mutated patients and their longer survivals (He et al., 2023; Riedl et al., 2017). However, when and where D2HG interacts with platelets is uncertain since low-grade IDH-mutated gliomas do not present a disruption in the blood-brain barrier. Platelets accumulation in tumors is known to increase their aggressivity but this link has not been studied yet in gliomas.

Given that patients with IDH1/2 mutations present distinct clinical characteristics, including longer survivals, a higher frequency of epilepsy, and a lower occurrence of venous thrombotic events, these discrepancies have led to the current WHO brain tumor classification, which divides adult-type diffuse gliomas based on their molecular IDH status.

1.2.3. Histology

Astrocytoma, oligodendroglioma, and GB exhibit differences in histology allowing for classification into different grades. Astrocytomas are graded from 2 to 4, while oligodendrogliomas are graded from 2 to 3. Glioblastomas are always classified as grade 4 tumors.

Tumor cells in astrocytomas can display varying degrees of nuclear atypia. They express GFAP and the transcriptional factor Olig2. From a molecular perspective, astrocytomas typically carry IDH 1 or IDH2 mutations without co-deletion of chromosomes 1p and 19q. Approximately 90% of IDH mutations correspond to the IDH1 R132H mutation, which can be rapidly assessed through immunohistochemistry (Capper et al., 2009). However, 10% of mutations require sequential gene analysis for accurate diagnosis. The presence of p53 and ATRX mutation is also common. Astrocytomas can be classified into WHO grades 2, 3, or 4. The previously used term 'anaplastic' for grade 3 has been removed in the new classification and GB IDH-mutant is now classified as astrocytoma grade 4.

Grade 2 astrocytomas are characterized by low to moderate cellularity. The nuclei of the tumor cells are usually oval and monomorphic. There is either no mitotic activity, or it is extremely rare. Grade 3 astrocytomas show increased mitoses, although a clear threshold to differentiate grade 2 from 3 is currently lacking. The cellularity is high, and nuclear atypia is commonly observed (Figure 5). Grade 4 are characterized by necrosis and/or neovascular proliferation. In addition to the histological criteria, the CDKN2A/B status allows for the direct classification of astrocytomas into grade 4, even in the absence of neoangiogenesis or necrosis, as tumors with this mutation exhibit more aggressive clinical behavior and shorter survival (Appay et al., 2019). Even within the grade 4 group, tumors presenting CDKN2A/B mutations show a worse outcome (Korshunov et al., 2019).

Tumor cells in oligodendroglioma are monomorphic, with round-shaped nuclei that exhibit a pale perinuclear area resembling fried eggs. Microcalcifications are frequently observed. Molecularly, they present an IDH 1 or IDH2 mutation, along with a co-deletion of chromosomes 1p and 19q. While the TERT promoter is commonly mutated in oligodendrogliomas, its mutation alone is insufficient for diagnosis as it can also occur in some astrocytomas. ATRX and p53 mutations are typically absent. Oligodendrogliomas can be classified into grades 2 or 3 based on their histological characteristics. The terms "oligoastrocytoma" and "anaplastic oligodendroglioma" have been removed from the updated classification. Grade 2 oligodendrogliomas exhibit a low number of mitoses, and low Ki-67 proliferation index. Grade 3 display high cellularity with nuclear atypia, necrosis, neoangiogenesis, and increased mitotic activity. They may contain gemistocytic cells characterized by nuclei at the periphery and rounded cytoplasm.

GB are the most common adult-type diffuse glioma. They present as highly diffuse astrocytomas with necrosis and/or microvascular proliferation. Tumor cells in GB exhibit a heterogeneous morphology, typically appearing as rounded and small cells with nuclear atypia. They infiltrate the brain parenchyma and the subpial space in some cases. GB are always IDH-WT and usually exhibit a TERT promoter mutation and EGFR amplification. Mitotic activity is significantly elevated in all GB. The presence of microvascular

proliferation and the formation of pseudo-palisading or geographic areas of tumor necrosis are frequent features.

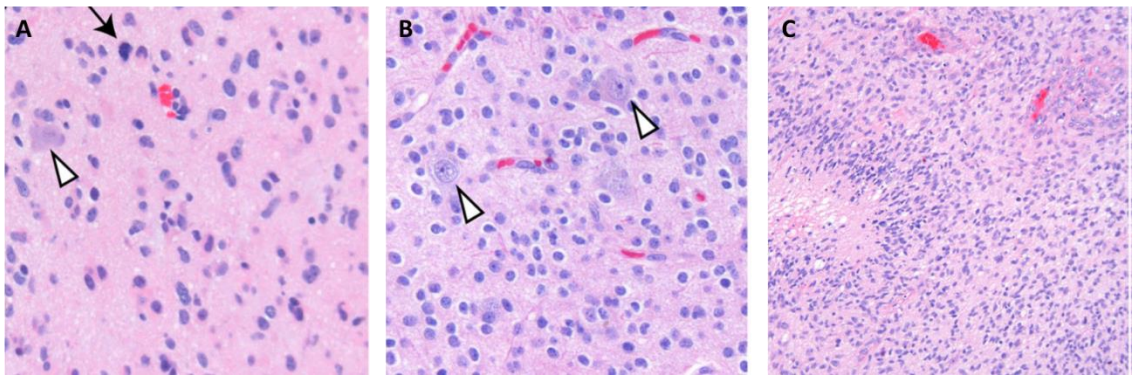

Figure 5: Glioma's histology.
A: Grade 3 astrocytoma showing mitotic activity (black arrow).
B: Grade 2 oligodendroglioma with rounded nuclei and perinuclear clearing.
C: GB with palisade necrosis and endothelial proliferation.
From Wood et al, 2019.

1.3. Topography

Diffuse gliomas predominantly occur in the supra tentorial region (86%), with a smaller percentage found in the brainstem (4.1%) and cerebellum (1.5%). Within the supratentorial region, diffuse gliomas' location correlates with each lobe's surface area. Therefore, the most common location is the frontal lobe, followed by the temporal lobe. There are no significant differences in lateralization, as both hemispheres exhibit an equal distribution (Larjavaara et al., 2007).

In a study conducted on 102 grade 2 gliomas, the authors reported that astrocytomas primarily occurred in the fronto-temporal-insular lobes, while oligodendrogliomas were more commonly located in the deep white matter (Latini et al., 2020). In a larger cohort of 1509 low-grade gliomas (LGG), approximately 50.3% of the tumors were located in the frontal lobe, followed by the temporal (18.2%) and the insula (16%). Furthermore, 45.5% of patients had involvement of multiple lobes (Pallud et al., 2014).

LGGs are frequently located near functional areas (Numan et al., 2022). A comparative study of LGG and GB locations showed that 82.6% of LGG were situated within functional areas, whereas only 53.9% of GB were found in such regions. Specifically, secondary functional areas like the supplementary motor area or the insula exhibited a higher prevalence of LGG (Duffau & Capelle, 2004). A recent study published last year demonstrated that gliomas tend to occur more frequently in brain regions characterized by higher levels of brain activity in healthy individuals. The brain activity levels were measured using magnetoencephalography (MEG) in 65 healthy controls (Numan et al., 2022).

1.4. Clinical symptoms

The onset symptoms of gliomas can vary and include epileptic seizures, neurological deficits, headaches, intracranial hypertension, and neuropsychological impairment. However, these symptoms are not specific to glioma and require neuroimaging to determine the underlying etiology. In some cases, gliomas may be incidentally discovered during a neuroimaging examination performed for other reasons. Most LGGs are diagnosed in young adults who present with an epileptic seizure, while GB are typically diagnosed in older individuals who experience progressive neurological impairment due to increased intracranial pressure (Capelle et al., 2013; Pallud et al., 2014).

When dedicated neuropsychological tests are conducted before surgery, approximately half of the patients exhibit neurocognitive impairment, such as deficits in attentional processing, psychomotor speed, or executive functions (Lemaitre et al., 2022). The patients' emotional well-being may also be affected (Lemaitre et al., 2021).

1.4.1. Epilepsy

1.4.1.1. Definition

Epilepsy is “a disorder of the brain characterized by an enduring predisposition to generate epileptic seizures and by the neurobiological, cognitive, psychological, and social consequences of this condition”. This initial conceptual definition of epilepsy was established in 2005 by a Task Force of the International League Against Epilepsy (ILAE). They also defined an epileptic seizure as “a transient occurrence of signs and/or symptoms due to abnormal excessive or synchronous neuronal activity in the brain” (Fisher et al., 2005). In clinical practice, patients were typically diagnosed with epilepsy if they experience two unprovoked seizures separated by more than 24 hours.

In 2014, an updated definition of epilepsy was introduced, which states that epilepsy can be diagnosed based on one of the following criteria: “(i) at least two unprovoked (or reflex) seizures occurring more than 24 hours apart, (ii) one unprovoked (or reflex) seizure and a probability of further seizures similar to the general recurrence risk (at least 60%) after two unprovoked seizures over the next ten years, (iii) a diagnosis of an epilepsy syndrome” (Fisher et al., 2014). Epilepsy is one of the most frequent neurological disorders, affecting approximately 7.6 per 1000 individuals over their lifetime (WHO 2019, Epilepsy: a public health imperative. Geneva: World Health Organization; 2019).

There is a strong association between epilepsy and gliomas. Tumor-related epilepsy (TRE) is highly prevalent among glioma patients, with seizure occurrence at diagnosis ranging from 35 to 89 % of cases (Huberfeld & Vecht, 2016; Pallud et al., 2014, 2022). The presence of epileptic seizures significantly impacts patients' quality of life, even when the tumor is under control (Klein et al., 2003). The frequency and characteristics of seizures depend on factors such as tumor histology, molecular profile, growth rate, and specific location. The following sections will focus on TRE rather than epilepsy in general.

1.4.1.2. Epidemiology

Brain tumors account for approximately 4% of all cases of epilepsy (van Breemen et al., 2007). In individuals over 65, around 10-15% of newly diagnosed epilepsy cases are attributed to brain tumors (Hamilton & Kernick, 2007). Epileptic seizures are a common symptom among glioma patients, particularly in those with LGGs. More than 80% of glioma patients experience an epileptic seizure as their initial symptom (Sherman et al., 2011; Zhong et al., 2015). Typically, younger patients without other neurological symptoms are diagnosed with glioma following their first seizure, while older patients often present with subacute neurological deficits that may be followed by a seizure (Zhong et al., 2015).

The prevalence of epilepsy varies depending on the histological diagnosis. Astrocytomas have an epilepsy prevalence ranging between 57 and 89% in different studies, while oligodendrogliomas have a prevalence ranging between 57 and 91% (Nataf et al., 2005; You et al., 2012; Zhong et al., 2015). GB patients generally exhibit a lower frequency of seizure, around 30 to 38% (Audrey et al., 2022; Chang et al., 2008). The aggressiveness of the tumor influences the presence of epilepsy. LGGs have a higher probability of causing seizures (Lee et al., 2010). Approximately 60 to 89% of grade 2 patients experience seizures, while the frequency decrease to 50-60% for grade 3 patients and 25-50% for grade 4 patients (de Groot & Sontheimer, 2011; van Breemen et al., 2007). IDH1/2 mutation is associated with a higher incidence of seizures, observed in 80 to 85% of patients (Chen et al., 2017; Vecht et al., 2014; Zhong et al., 2015). In an extensive series of 1509 LGGs patients, 90 % presented with seizures at diagnosis (Pallud et al., 2014).

But how can we explain these differences between LGGs and GBs epilepsy frequency? The differences in their epileptogenic nature depend first on their growth speed. LGGs exhibit slow growth, allowing for the formation of epileptic networks within the surrounding tissue (the peritumoral tissue). In contrast, the rapid growth of GBs leads to symptoms related to increased intracranial pressure, such as neurological deficits. GBs may induce seizures through different mechanisms, such as hemosiderin deposition or deafferentation due to neural cell death. Moreover, LGGs present an IDH1/2 mutation, enhancing the probability of presenting seizures, while GB are IDH-WT. The specific mechanisms of epileptogenesis will be further discussed in the upcoming chapter.

However, the risk of developing seizures seems to be higher in LGGs and HGGs presenting cortical invasion. Conversely, tumors located in deeper structures are associated with a lower epilepsy risk (Chaichana et al., 2009; Englot, Berger, et al., 2012; Lee et al., 2014; Liang et al., 2016; Rudà et al., 2012).

Approximately 20 to 30% of GB patients experience poor seizure control despite trying two or more antiseizure medications (ASM) (Kerkhof & Vecht, 2013; Kwan et al., 2010). For grade 2 glioma patients, poor seizure control rates range from 15% to 40% (Jo et al., 2020; Pallud et al., 2014). Pharmacoresistance is more common in IDH-mutated patients (Correia et al., 2021). Factors such as longer time to diagnosis, prolonged seizure duration, focal simple semiology, tumor location inside a functional area, and involvement of temporal and insular regions are associated with pharmacoresistance at diagnosis (Chang et al., 2008; Pallud, Audureau, et al., 2014). Seizure control decreases as the oncological disease progresses (Pallud et al., 2014; Sizoo et al., 2010; Taphoorn et al., 2010). Patients with a pharmacoresistant TRE at diagnosis typically remain pharmacoresistant, while

10.5% of patients with well-controlled epileptic seizures may develop pharmacoresistance over time (Figure 6) (Pallud et al., 2014). Poor seizure control significantly impacts the patient's quality of life (Klein et al., 2003).

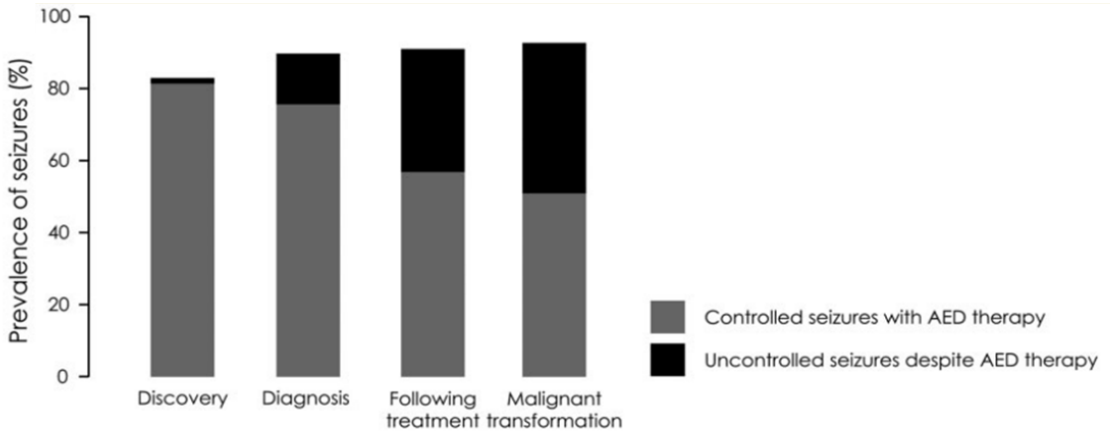

Figure 6: Prevalence of controlled and uncontrolled epileptic seizures during glioma evolution. From Pallud et al 2014.

Pharmacoresistance in TRE is a complex phenomenon influenced by multiple mechanisms. Among these mechanisms, the overexpression of ATP-binding transporter family proteins plays a significant role. These membrane pumps are responsible for regulating the transport of various molecules across the endothelial membrane. Specifically, the multidrug-resistance gene MDR and the multidrug-resistance-related protein (MRP1), which are also expressed in the apical surface of other barrier tissues such as the liver and intestines, can reduce the concentration of certain ASM and antineoplastic treatments at the extracellular and intracellular level (Alms et al., 2014; Calatozzolo et al., 2012). Another member of the family, the breast-cancer resistance protein (ABCG2), is also overexpressed in brain glioma (Aronica et al., 2005). This overexpression can impact the concentrations of carbamazepine, oxcarbazepine, eslicarbazepine, phenytoin, phenobarbital, lamotrigine, and felbamate. However, the impact on medications such as levetiracetam and valproate is relatively less pronounced as they are less affected by MDR1 overexpression (Newton et al., 2006; Zhang et al., 2011). However, pharmacoresistance also depends of the target of current ASMs which rather act by reducing neuronal firing or by increasing inhibition rather than focusing on seizure initiation mechanisms.

1.4.1.3. Semiology

In LGGs, secondary generalized seizures are the most common seizure type, accounting for 30% to 70% of cases, followed by focal seizures without alteration of consciousness (10% to 24%), and focal seizures with alteration of consciousness (7 to 12%) (Lee et al., 2010; Breemen et al., 2009). However, a large study involving 1509 LGG reported only

5.3% of patients presenting generalized seizures (Pallud et al., 2014). Pharmacological control of seizures is generally higher in patients with secondary generalized seizures (74%) and lower for those with focal seizures without alteration of consciousness (53%) (Englot et al., 2011).

For GBs patients, the most prevalent seizure type is secondary generalized seizures, ranging from 42.3% to 62%. Focal seizures without loss of consciousness occur in 18.3% to 40.6% of patients, while focal seizures with loss of consciousness were present in 10% to 28% (Flanigan et al., 2017; Kerkhof et al., 2013; Lee et al., 2010, 2014; Liang et al., 2016; Toledo et al., 2015; Yang et al., 2016). Status epilepticus, the most severe form of epilepsy, is also possible as the oncological disease progresses and affects approximately 10% of patients, particularly in the advanced stages of the disease (Kerkhof & Vecht, 2013). Diagnosing non-convulsive status epilepticus in glioma patients can be challenging, as its symptoms may be mistaken for tumoral progression. In a recent retrospective study of 108 glioma patients, 5% were found to have non-convulsive status epilepticus (Kaneoka et al., 2023).

1.3.1.4. Morphological characteristics of gliomas presenting with seizures

The location of the tumor can also influence the development of TRE. Astrocytoma TRE is often associated with the involvement of the temporal or insular lobes, while oligodendrogliomas that provoke epilepsy are more frequently located in the frontal lobe. Deep locations, such as the pericallosal regions, typically do not cause seizures as they primarily induce symptoms through their mass effect (Lee et al., 2010; You et al., 2012). In GBs patients, the regions more commonly associated with seizures are the temporal and parietal lobes (Chaichana et al., 2009; Flanigan et al., 2017; Lee et al., 2014; Liang et al., 2016).

Regarding tumor size, LGGs presenting with seizures tend to have larger volumes compared to tumors without seizures. On the other hand, GBs with seizures typically have smaller tumor volumes. In a retrospective study examining the morphological characteristic of GBs associated with seizures, epileptic patients had a mean volume of 31.1 cm^3, while non-epileptic patients had a mean volume of 58.8 cm^3 (Berendsen et al., 2016; Flanigan et al., 2017; Lee et al., 2010). Additionally, smaller peritumoral edema was found to be associated with seizures, possibly because pro-epileptogenic molecules such as Glu are more concentrated when edema is less prominent (Dührsen et al., 2019). The larger volumes observed in LGGs imply longer growth times, while the smaller volumes in GBs may reflect slower growth rates. This suggests that epileptogenesis requires time, and slower-growing gliomas are more prone to the development of seizures.

1.3.1.5. Impact on the prognosis

The presence of epileptic seizures is associated with longer overall survival (Chaichana et al., 2009; Chang et al., 2008; Fan et al., 2018; Flanigan et al., 2017). In a comprehensive study involving 1509 LGGs patients, the presence of TRE at diagnosis was associated with longer malignant progression-free survival and overall survival. Patients with TRE survived for an average of 92.3 ± 69.1 months after diagnosis, while non-epileptic patients survived for an average of 51.1 ± 38 months from diagnosis (Pallud et al., 2014).

Specifically, patients presenting with a single seizure before surgery had better survival outcomes (Mirsattari et al., 2011).

Another study conducted on GBs patients demonstrated that epileptic patients had a mean survival of 13.2 months, while non-epileptic GBs had a mean survival of only 8.4 months (Berendsen et al., 2016). A recent work showed a mean survival of 21 months when epileptic patients received levetiracetam during chemoradiothery treatment (Johan Pallud et al., 2021). However, it is important to consider whether this effect is exclusively related to epilepsy itself or if other confounding factors are involved. In the case of LGGs, epilepsy is strongly associated with IDH1/2 mutations, which are also favorable prognostic factors (Houillier et al., 2010; Zhong et al., 2015). For GBs, seizures are associated with younger patients and smaller tumoral sizes. Although epilepsy is a good prognosis factor, the recurrence of epilepsy after more than six months of seizure freedom is a strong indicator of tumor progression in approximately 50% of LGGs patients and about 67% of GBs patients (Chang et al., 2008).

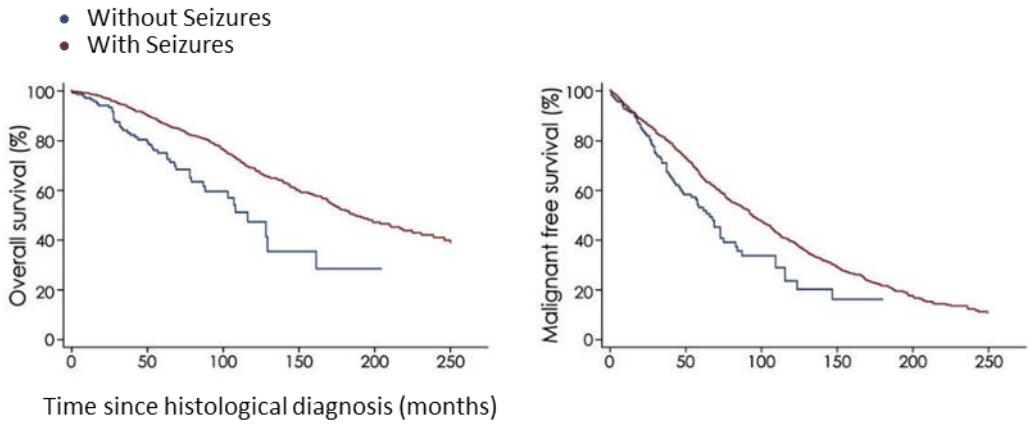

Figure 7: Survival and malignant free survival curves in patients with seizures (red), and without seizures (blue).
From Pallud et al, 2014.

The relationship between epilepsy and overall survival can also be influenced by specific ASM that have shown the potential to improve tumor control. One of the first ASM showing a beneficial effect on overall survival was Valproate (VPA). VPA inhibits histone deacetylase, which leads to chromatin structure opening and exposes DNA to the effects of chemotherapy agents, such as temozolomide, or radiotherapy. A post hoc analysis of the temozolomide clinical trial revealed that patients receiving chemoradiotherapy combined with VPA had a median survival of three months longer than those receiving chemoradiotherapy without VPA (Weller et al., 2011). Another study involving 143 glioma patients compared using VPA or levetiracetam (LEV) as monotherapy. Patients receiving temozolomide with VPA had a median survival of 69 weeks, while patients without VPA had a median survival of 61 weeks (Kerkhof et al., 2013). However, it is essential to note that VPA's enzyme-inhibiting properties can lead to side effects, such as thrombocytopenia and other bone marrow toxicities, which can be problematic for patients undergoing chemotherapy or requiring surgery.

LEV, an inhibitor of the transcription of MGMT (a DNA repair protein), has been shown to play a modulatory role in survival by increasing the sensitivity of tumor cells to temozolomide (Bobustuc et al., 2010). In a study of 103 GBs patients, LEV treatment was a significant prognostic factor for overall survival (HR 0.31). Patients treated with LEV and temozolomide had a median overall survival of 25.7 months compared to 16.7 months in patients receiving temozolomide alone (Kim et al., 2015). A retrospective study involving 408 GBs patients, testing the effects of nine different ASM effects on survival, demonstrated that only LEV significantly impacted survival. LEV patients have a mean survival of 21 months compared to 16 months in patients not receiving LEV. However, a limitation of the study could be the small number of patients receiving ASM other than LEV (322 patients treated with LEV, 218 with VPA, 83 with gabapentin, 76 with topiramate, 50 with phenytoin, 40 with lamotrigine, 39 with oxcarbazepine, 31 with pregabalin, 14 with carbamazepine, three with clobazam, three with phenobarbital, one with lacosamide, and one with perampanel) (Ryu et al., 2019). A recent study involving 460 GBs patients showed that patients who received LEV throughout the entire duration of chemoradiotherapy had longer survival (21 months) compared to patients who received LEV partially (16.8 months) or not at all (16 months) (Pallud et al., 2022). The advantages of LEV in TRE include its ease of use, fast titration, lower rate of side effects, and lack of interactions with chemotherapy.

A newer ASM, Perampanel (PER), modulates glutamatergic signaling by inhibiting AMPA receptors. Recent studies have demonstrated that functional synapses between tumor cells and surrounding neurons can enhance tumor growth via functional AMPA synapses (Venkataramani et al., 2019; Venkatesh et al., 2019). Furthermore, in vitro studies on tumor cell cultures have shown that PER can induce high levels of apoptosis in glioma cells. This apoptotic effect exhibits synergy with the use of temozolomide. However, the expression of certain proteins, such as SERPINE1, by tumor cells can decrease the apoptotic effect of PER (Salmaggi et al., 2021; Tatsuoka et al., 2022). PER is generally well tolerated, has low side effects in patients with TRE (Rossi et al., 2023; Damavandi et al., 2023) and is efficient on TRE (Huberfeld & Vecht, 2016).

1.5. Complementary exams

1.5.1. Neuroimaging

Neuroimaging plays a crucial role in the diagnosis of gliomas. While histological analysis after a biopsy remains the gold standard for definitive diagnosis, neuroimaging can accurately indicate glioma presence. It also helps rule out other neurological conditions such as stroke, inflammatory amyloid angiopathy, metastases, or abscesses. Neuroimaging is essential in determining whether a glioma can be surgically removed and is crucial in surgical planning. Throughout the course of the disease, neuroimaging is also vital for monitoring patients and detecting early signs of tumor relapse.

1.5.1.1. Magnetic Resonance Imaging

Magnetic resonance imaging (MRI) is an essential examination in the preoperative diagnosis of gliomas. It allows for visualization of the tumor's spatial extension, structure, and localization. In most cases, MRI is considered the gold standard neuroimaging examination for evaluating gliomas unless there are contraindications, such as the presence of pacemakers. MRI offers various morphological sequences, including T1-weighted, T2-weighted, FLAIR (fluid-attenuated inversion recovery), and T1-weighted imaging with gadolinium (GD). These sequences provide valuable information about the tumor's characteristics. In addition to the morphological sequences, other specialized sequences provide insights into the tumor's metabolism, such as diffusion-weighted imaging (DWI), perfusion imaging, and spectroscopy. The recommended routine protocols for 3T-MRI in glioma evaluation typically included high-resolution T1-weighted imaging before and after GD administration, T2-weighted imaging after GD injection, T2-weighted FLAIR imaging and DWI (Ellingson et al., 2015).

Gliomas typically appear as hypo or iso signals in T1-weighted MRI sequences and hypersignal in T2-weighted and FLAIR sequences. The appearance of the lesion can be heterogeneous, indicating the presence of various features such as bleeding, calcifications, variable densities, cysts, or necrosis. The lesion is often surrounded by extracellular edema, and its enhancement after GD injection can provide important prognostic information. Abnormalities are generally larger in T2-weighted/FLAIR sequences compared to T1-weighted sequences (Henker et al., 2019). GD enhancement is the marker of HGGs with aggressive behavior. However, in a 927 WHO grade 2 glioma study, GD enhancement was observed in 16% of patients. The study identified three patterns of GD enhancement: patchy and faint, nodular, and ring-like. The patchy and faint pattern was the most common at diagnosis, while the ring-like pattern was not present at that stage. The nodular pattern was associated with shorter survival (Pallud et al., 2009). Additionally, GD enhancement volume greater than 4 cm^3 is associated with shorter overall survival (Tofts et al., 2007). Molecular GBs often does not exhibit GD enhancement. A recent study found that half of the 31 molecular GBs cases showed a gyriform infiltration pattern, which was never seen in IDH mutant glioma (Mesny et al., 2022). Susceptibility-weighted sequences (SWI) can provide visualization of diamagnetic substances (such as calcium) and paramagnetic substances (such as deoxygenated hemoglobin). SWI is useful for visualizing hemorrhages, calcifications, and neovascularization within gliomas.

Perfusion-weighted sequences (PWS) using GD injection can generate perfusion maps with different parameters, including cerebral blood volume (CBV), cerebral blood flow (CBF), mean transit time (MTT), and time to peak (TTP). In gliomas, these maps enable the quantification of microvascularization and neoangiogenesis. Several studies have demonstrated a correlation between glioma grade and relative CBV (rCBV) values (Boxerman et al., 2020; Hirschler et al., 2023). A study involving 146 glioma patients showed that higher rCBV values were associated with shorter survival (McCullough et al., 2018). In another case report, rCBV maps were used to differentiate non-infiltrated from tumor areas. Areas with zero to low rCBV corresponded to non-tumor regions, while high rCBV values were observed in aggressive and early recurrence sites (Connelly et al., 2021).

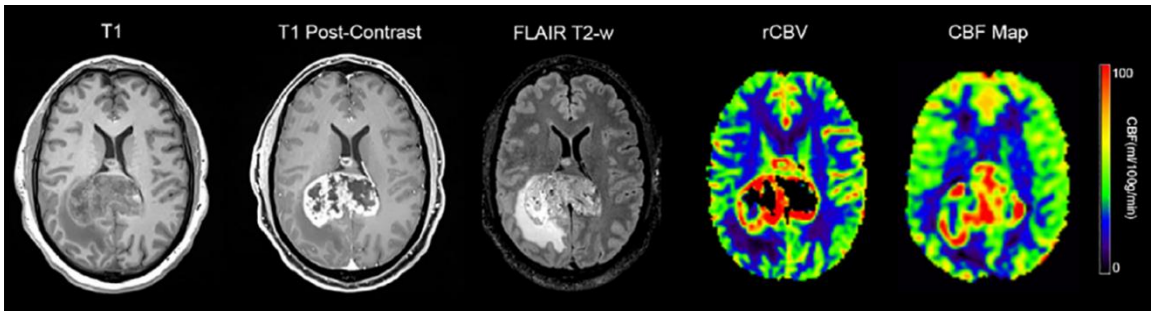

Figure 8: Example from a 48-year-old patient with a GB.
From Hirschler et al, 2023

Arterial spin labeling (ASL) sequence, on the other hand, quantifies CBF using the magnetic labeling of arterial blood water as a tracer instead of GD (Alsop et al., 2015). The quantitative use of ASL allows for measuring relative tumor blood flow (rTBF). In a GBs patients study, lower TBF values were associated with longer overall survivals (Mao et al., 2020; Yoo et al., 2020). Furthermore, ASL can be valuable for differential diagnosis purposes, aiding in the distinction between glioma and primary CNS lymphoma, non-neoplastic brain lesions, or metastases (Razek et al., 2019).

Brain water undergoes free Brownian movement, which is influenced by the microarchitecture of the tissue. Parameters such as cellularity, viscosity, or tortuosity of the extracellular space impact the movement of water molecules, making diffusion quantification a valuable marker for pathology assessment. Using the apparent diffusion coefficient (ADC), DWI measures the impedance of water molecule diffusion. Diffusion tensor imaging (DTI) is another commonly used technique that provides fractional anisotropy (FA) or mean diffusivity (MD) values. FA introduces directionality to the dispersion of diffusion. In regions where water can diffuse freely, FA approaches 0, while in densely packed axonal fibers where diffusion occurs primarily along a single axis, FA values approach 1.

ADC values have demonstrated the ability to distinguish between LGGs and HGGs with high sensitivity (85%) and specificity (80%). LGGs typically exhibit normal or increased ADC values, whereas HGGs display lower ADC values (Price et al., 2011; Zhang et al., 2017). Moreover, in IDH1 mutated gliomas, ADC values tend to be higher compared to IDH-WT patients (Wang et al., 2021). In a recent study, ADC values were higher in tumoral tissue compared to the surrounding marginal tumoral area in IDH-mutated patients, while no such difference was observed in IDH-WT patients (Fujita et al., 2021).

In the past decade, newer imaging techniques, such as proton magnetic resonance spectroscopy (1H-MRS), have gained prominence. It allows for the detection of different metabolites, including N-acetyl-aspartate (NAA), creatine (Cr), choline (Cho), myoinositol (mI), Glu, glutamine (Gln), gamma-aminobutyric acid (GABA), glutathione (GSH), lactate (Lac), lipid (Lip), and even the oncometabolite D2HG (Andronesi et al., 2012; Öz et al., 2014). NAA is predominantly found in neurons and is considered a neuronal density and function marker. It directly reflects the functional state of neurons, and its levels decline with reduced cell metabolism or neuronal loss (Birken & Oldendorf, 1989). The Cr

spectrum provides information about cellular energy status. Cho is primarily located in glial cells and is proposed as a marker for membrane turnover and activation of astrocytes and microglia (Chang et al., 2013). mI is a marker of activated glial cells (Buonocore & Maddock, 2015; Zhu & Barker, 2011). Lac peak indicates hypoxic conditions and anaerobic metabolism, while the Lip peak reflects the presence of necrosis (Buonocore & Maddock, 2015). The intensity of a metabolite peak is proportional to the concentration of this metabolite within the voxel.

1H-MRS has proven to be a valuable tool in differentiating gliomas from other brain lesions, such as demyelinating lesions, metastasis, and primary CNS lymphoma. In glioma, specific metabolic changes can be observed using 1H-MRS. Elevated levels of Cho often indicate increased cell density and accelerated membrane turnover in gliomas. Decreased levels of NAA suggest neuronal degeneration or loss. Cr levels may decrease, while Lac and Lip levels may increase, particularly in GBs, reflecting hypoxic conditions, necrosis, and metabolic impairment. The detection of D2HG using 1H-MRS has emerged as a useful method for assessing the IDH-mutated status in gliomas, as IDH mutations lead to D2HG production (Andronesi et al., 2012). However, the challenge lies in distinguishing D2HG from other spectral peaks, such as Glu and Gln, and there is currently no established cutoff value for differentiating IDH-mutated gliomas from IDH-WT (Pope et al., 2012). Another limitation of 1H-MRS is its long acquisition time, which may restrict its clinical application. However, it can detect metabolic changes even without structural damage (Croteau et al., 2001). However, despite the promising role of 1H-MRS, the overlap of spectra in different conditions stresses the importance of interpreting it in the context of conventional imaging findings.

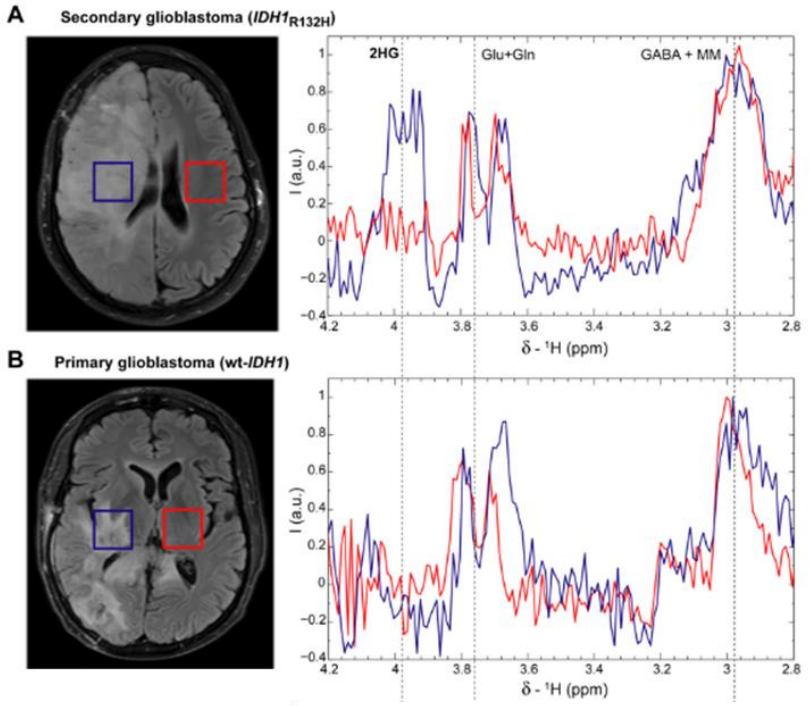

Figure 9: MRS spectra in GB patients at 3 T.
A: Secondary GB patient with IDH1R132H mutation (astrocytoma WHO grade 4 following the new classification).
B Glioblastoma IDH-WT.
From Andronesi et al 2012.

MRI is valuable for initial diagnostic purposes and for follow-up of glioma patients. Monitoring radiological changes over time allows for the measurement of tumor growth rate. A study involving 143 WHO grade 2 glioma patients found that LGGs presented an average growth rate of 4 mm per year (Johan Pallud et al., 2006). In HGGs, the tumor volume increase observed on MRI is much faster. WHO grade 3 astrocytomas demonstrated a growth rate of over 8 mm per year, while GBs exhibited a staggering growth rate of over 100 mm per year (Párraga & Pallud, 2012). Furthermore, the increase in rCBV has been identified as a marker of malignant transformation (Dhermain et al., 2010; Price et al., 2011).

In the last few years, new MRI sequences have been developed in imaging research centers; although they are not currently used routinely in clinical settings, they hold great promise for the future. One such technique is Chemical Exchange Saturation Transfer (CEST) imaging, which enables the detection of proteins, peptides, and small molecules that are not easily detectable with conventional MRI due to their low concentration in tissue. Amide Proton Transfer (APT)-CEST imaging is the most extensively studied among the various CEST techniques. In HGG, protein, and peptide concentrations are increased within the tumor compared to the surrounding tissue (Vinogradov et al., 2013; Zhang et al., 2018). The use of APT-CEST in the presurgical evaluation of aggressive non-enhanced gliomas is of great interest as it can aid in distinguishing tumors from healthy tissue (Su et al., 2022; Warnert et al., 2022). A recent study based on APT-CEST on 7T-MRI demonstrated increased Glu concentration at the peritumoral level. Accurate Glu detection can help to define the extent of the peritumoral infiltrated area, leading to better surgical planning (Neal et al., 2019). Another CEST technique, gluco-CEST, examines the tissue perfusion parameters using a glucose injection instead of GD (Zu et al., 2017). Like PWI, gluco-CEST enables the measurement of local blood flow, vascular permeability, and extracellular space volume. However, it is important to note that CEST techniques require extensive postprocessing analysis and validation on larger cohorts to establish their reliability and clinical utility.

MR-elastography and radiomics are emerging MRI techniques still in the developmental stage. MR-elastography focuses on studying tissue viscosity and stiffness. Gliomas are generally softer than normal-appearing brain tissue (Pepin et al., 2018). A recent meta-analysis of 68 glioma patients demonstrated that WHO grade 2 gliomas exhibited a 34% reduction in stiffness compared to healthy tissue. In contrast, the decline was 14% for grade 3 gliomas and 17% for GB (Bunevicius et al., 2020). Radiomics, on the other hand, uses artificial intelligence methods to extract quantitative features from conventional structural and diffusion MRI data obtained in clinical settings. These extracted features are then used in machine-learning prediction models to establish correlations between imaging characteristics with tumor genotypes.

The development of 7T-MRS holds promise for improved quantification of D2HG and better characterization of metabolites such as Glu, Gln, and Gly. The higher signal-to-noise ratio (SNR) at 7T increases sensitivity and specificity in detecting and quantifying these metabolites. However, it is important to note that although the SNR is improved, the spatial resolution is only slightly enhanced with 7T-MRS (Mccarthy et al., 2022). Further technical advancements are necessary before its widespread use in clinical settings. These improvements may address challenges such as optimization of image quality, ensuring reproducibility, and standardizing protocols.

1.5.1.2. Positron Emission Tomography

Positron emission tomography (PET) is a well-established molecular imaging technique in clinical practice. It provides a non-invasive visualization and quantification of various physiological processes such as perfusion, proliferation, and metabolism. PET utilizes biological compounds that are labeled with positron-emitting radionuclides. It is often used in conjunction with MRI to provide complementary information. Different radiotracers are employed for PET imaging. These include:

-18F-fluoro-D-glucose (FDG): this radiotracer is commonly used to assess tissue glucose metabolism. It reflects the uptake of glucose and provides information about cellular metabolism.

-11C-methyl-methionine (MET): MET evaluates amino acid transport and protein synthesis.

-18F-fluoroethyl-L-tyrosine (FET): FET is used for imaging amino acid transport and uptake.

-18F-fluoro-L-thymidine (FLT). FLT is a radiotracer used to measure cellular proliferation. It provides insights into the rate of DNA synthesis and can be useful in assessing tumor growth.

-18F-fluoro-L-phenylalanine (FDOPA). FDOPA assesses amino acid transport and protein synthesis.

In 2018, a collaborative effort between the European Association of Nuclear Medicine (EANM), the Society of Nuclear Medicine and Molecular Imaging (SNMMI), the European Association of Neuro-Oncology (EANO), and the working group for Response Assessment in Neuro-Oncology with PET (PET-RANO) led to the publication of practical guidelines for the acquisition, reconstruction, and quantification of gliomas using PET with radiolabeled amino acids and glucose (Law et al., 2019).

Among the radiotracers used in PET imaging, FDG is the most frequently employed. Its widespread use is still mainly attributed to the limited availability of amino acid tracers. FDG has a longer half-life (110 minutes), which makes him easily transportable to centers that may not have an on-site cyclotron. Gliomas exhibit high expression of GLUT1, a glucose transporter protein, leading to FDG uptake. However, it is important to note that the healthy brain also expresses GLUT1, resulting in the physiological uptake of FDG. This physiological uptake reduces the signal-to-noise ratio (SNR) when assessing gliomas using FDG PET.

It is worth mentioning that the use of amino acids tracers, such as MET, FET, FLT, and FDOPA, has gained prominence in glioma imaging due to their higher SNR compared to FDG. These tracers specifically target amino acid transport and protein synthesis, providing more specific information related to tumor metabolism and proliferation. However, they have a limitation due to the short half-life of 11C, which is only 20 minutes. This restricts their use to a center equipped with a cyclotron, where the radiotracer can be produced on-site (Price, 2010). A meta-analysis showed that FET and MET tracers present higher

sensitivity (90% and 93%, respectively) and specificity (85% and 82%) compared to FDG (84% sensitivity and 84% specificity) in differentiating treatment-related changes from tumor progression (de Zwart et al., 2020). However, both MET and FET can potentially underestimate the extent of the tumor when compared to FDG (Price et al., 2009).

PET can aid in the initial diagnosis of gliomas by providing information about tumor grade and selecting appropriate biopsy sites. High FDG uptake is associated with higher tumor grades and aggressive behavior (Dhermain et al., 2010). Similarly, high MET uptake is observed in HGGs (Arbizu et al., 2012). Although all the tracers can contribute to the differential diagnosis, FET presents higher sensitivity and negative predictive value in differentiating gliomas compared to FDG (Brendle et al., 2022). A recent study has shown that FET is a promising marker for visualizing infiltrated peritumoral areas far from the contrast-enhancing region. Biopsies obtained from areas of high FET uptake, even if placed at more than 3 cm from the GD enhancement, contained tumor infiltration (Furtak et al., 2021).

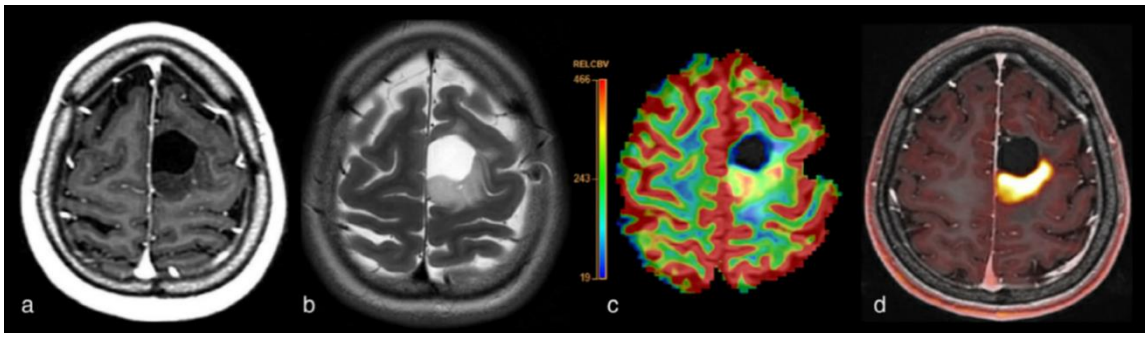

Figure 10: FET-PET-MRI of a 28-year-old female with a resected oligodendroglioma and a tumor relapse.
A: Post-GD T1 weighted sequence.
B: T2.
C: rCBV map.
D: FET-PET overlaid on post-GD T1.

Combined with MRI metrics, PET imaging with amino acid tracers can predict molecular status. For example, an increase in FDG uptake has been observed in 1p-19q co-delected gliomas (Price, 2010). In another study of 52 glioma patients, FET-PET combined with PWI was able to differentiate IDH mutated 1p-19q co-delected oligodendroglioma patients from GB (Song et al., 2021). Furthermore, a recent study showed that FET-PET and MRI could predict IDH1 and 1p-19q mutations in 89% and 98% of cases, respectively (Haubold et al., 2020). FDOPA and MET can also predict IDH1 mutation and 1p-19q co-delection (D. Kim et al., 2019; Tatekawa et al., 2020).

Accurate tumor delimitation is capital in radiotherapy (RT) planning as it aims to deliver a maximal radiation dose to the tumor while minimizing the dose to healthy surrounding areas. GD-MRI is commonly used in RT planning, but tumor cells can extend beyond the regions of enhancement. In a clinical trial, FDOPA-guided RT has improved overall survival in GB patients (Laack et al., 2021). Conversely, FET presents the advantage of

better delineating highly infiltrated areas than PWI and T1-GD MRI sequences (Dissaux et al., 2020; Lohmann et al., 2019).

PET imaging can also assist during follow-up to monitor treatment efficacy and the progression of tumors. It helps in the differentiation between a tumor relapse and treatment-related changes (TRC). Based on T2-weighted, FLAIR, and T1-GD sequences, the commonly used RANO criteria may not accurately differentiate tumor relapse from TRC, as both can exhibit enhancement on imaging. MET is highly sensitive to tumor relapse (Deuschl et al., 2018). A meta-analysis involving 1734 patients showed that FET, MET, and FDOPA have sensitivities of 78%, 78%, and 70%, respectively, for detecting tumor recurrence (Cui et al., 2021). FET accurately identifies pseudo-progression with 87% of sensitivity and 100% of specificity when performed ten days after the appearance of a suspicious MRI finding (Werner et al., 2021). FDG can help differentiate radionecrosis (which typically shows no increase in FDG uptake) from tumor relapse (which presents with a high FDG uptake) (Price, 2010).

Combining MRI and positron emission tomography (PET) into a single system, known as MRI-PET, offers the advantage of simultaneously acquiring structural and functional information. This integrated imaging modality overcomes the limitation of PET, lacking anatomical information. The anatomical information from MRI improves image registration and motion correction (Jadvar & Colletti, 2014). Nowadays, they are available in larger hospitals. Having MRI and PET capabilities in a single system improves the image's quality and diagnostic value and offers patients convenience. With MRI-PET, patients do not need to return for a separate PET scan, reducing their time in the hospital.

1.5.2. Electroencephalogram

Electrical currents generated by neuronal synaptic activity induce an extracellular electrical field potential (FP), which can be measured remotely by electroencephalography (EEG). EEG has been used for many years in glioma diagnosis. In fact, in 1946, Walter and Dovey proposed using EEG to delineate brain tumors before the advent of CT scans (Walter & Dovey, 1946). However, the abnormalities we can find on EEG are not specific to gliomas (Hasegawa & Aird, 1963; Munari et al., 1985). Interictal abnormalities are not very frequent on scalp EEG. Glioma patients can exhibit various EEG anomalies, including interictal spikes, spikes and waves, delta waves, or electrical silence (Gastaut et al., 1979). Nevertheless, the use of EEG in TRE has decreased in importance due to the advances in neuroimaging and the revised definition of epilepsy by the ILAE. According to the new definition, a single seizure and evidence of a tumor on neuroimaging is sufficient to diagnose a patient with epilepsy.

The most frequent findings on gliomas' EEG are delta waves. They are likely attributed to deafferentation and high cellularity within the tumor (Lairy-Bounes & Dreyfus-Brisac, 1950). Several studies have described slow activity at the tumor level, both in EEG and stereo EEG (sEEG). Electrodes placed directly above the tumor location have shown increased delta power (Munari et al., 1985; Nagata et al., 1985; Newmark et al., 1983). A study performed in 1962 reported that only 5% of glioma patients had a normal EEG, and approximately 70% of gliomas presented with abnormalities suggesting a space-occupying

lesion (Gonzalez & Elvidge, 1962). This study was done before the widespread of MRI; thus, the diagnosed gliomas nowadays are smaller. So higher proportions of normal EEG can probably be found today.

Regarding the EEG characteristics of seizures in TRE, limited research is available. One study conducted with chronic subdural grids implanted for five days in pharmacoresistant glioma patients found that the seizure onset zone was located at distance from the tumor border, with half of the cases exhibiting seizure onset at more than 15 mm from the tumor (Mittal et al., 2016). This observation highlights the involvement of the surrounding peritumoral tissue in the epileptogenesis process and suggests that epileptic activity may extend beyond the visible tumor boundaries.

Indeed, while the primary role of EEG in glioma patients is to evaluate epileptic activity, there have been studies exploring its potential as a non-invasive tool to assess the prognosis of glioma patients. Recently, a study described that glioma IDH-WT patients with periodic lateralized discharges or electrographic seizures on EEG were associated with shorter survival (mean 12.5 months vs. 19.9 months) (Tobochnik et al., 2022). However, it is the only study of this kind performed on glioma patients, so larger studies are needed to confirm their findings.

1.5.3. Magnetoencephalography

Magnetoencephalography (MEG) is a non-invasive technique that measures the magnetic fields generated by the intracellular currents resulting from neuronal synaptic activity in the brain. In contrast to EEG, which measures extracellular FP, MEG directly measures the intracellular currents produced by the apical dendrites (Shibasaki et al., 2007). One advantage of MEG is that the magnetic fields measured by MEG are not significantly influenced by the scalp, unlike the electrical signals measured by EEG. MEG provides a high spatial resolution with a millisecond temporal resolution. However, MEG systems can be expensive compared to EEG systems, limiting their availability and widespread use.

Glioma patients also present different patterns of functional resting-state connectivity, with a disruption in their small-world network organization (Bosma et al., 2008). Small-world networks refer to an efficient balance between local clustering and the global interaction of brain regions. The persistence of the increase of theta frequency after surgical removal of glioma is associated with uncontrolled epileptic seizures (Douw et al., 2011). A study including 25 glioma patients showed that LGGs present a decrease in network synchronization in the theta frequency range, while HGGs did not show significant changes compared to controls. The authors suggested that LGGs and HGGs may have different network organizations due to their differences in growth patterns (van Dellen et al., 2012). Pathological levels of synchronization were observed within the tumor, and MEG can be a useful tool for detecting these changes and localizing interictal discharges (Wilson et al., 2012).

1.6. Treatment

1.6.1. Base of epilepsy treatment

The treatment of TRE is not analogous to focal epilepsy treatment, considering cancer co-therapies and specific side-effect profiles. The ILAE has defined epilepsy as a condition where there is a high risk (> 60%) of seizure recurrence after a single seizure (Fisher et al., 2014). Following this definition, ASM should be initiated after the first seizure in glioma patients. Since certain types of gliomas, such as astrocytomas and oligodendrogliomas, have a prevalence of seizures exceeding 60%. In such cases, the question arises whether prophylactic ASM treatment should be initiated. However, the current evidence does not provide robust support for the effectiveness of prophylactic therapy in preventing the development of epilepsy in glioma patients (Glantz et al., 2000). It is important to consider that ASM can have side effects and a cognitive impact on patients, and glioma patients are more prone to develop side effects. To shed more light on this topic, the ongoing Seizure PRophylaxis IN Glioma (SPRING) trial will randomize 806 glioma patients to receive either levetiracetam (500 mg twice daily for two weeks, followed by 750 twice daily) or placebo before surgery, continuing the treatment up to a year post-surgery. The primary endpoint will be the one-year risk of the first seizure, with secondary endpoints including time to first seizure, survival, and quality of life measures (https://www.springtrial.org.uk).

The effect of ASM in preventing epileptogenesis is not very robust. However, epileptogenesis and tumor growth present shared mechanisms such as GABA and Glu signaling impairment (Huberfeld & Vecht, 2016). In 2019, two independent studies showed for the first time the presence of functional AMPA synapses from surrounding neurons to tumor cells (Venkataramani et al., 2019; Venkatesh et al., 2019). The synaptic activation of AMPA receptors in glioma cells increased tumor growth. Consequently, it is plausible to hypothesize that ASM, which can modulate AMPA receptor activity, may also impact tumor growth. For example, perampanel, an AMPA receptor blocker, reduced glioma cells' proliferation and motility in vitro (Venkataramani et al., 2019). A recent retrospective study of 460 glioma patients showed that those receiving LEV during chemoradiotherapy presented longer overall survival (21 months) compared to patients who never received LEV (16 months) (Pallud et al., 2022). However, another study performed on 1800 GB patients showed no improvement in survival associated with ASM use (Happold et al., 2016). These conflicting findings highlight the need for further studies to confirm whether specific ASM usage can truly benefit glioma patients in terms of survival.

Management of TRE is indeed a complex task, as it involves considerations of the potential interactions between ASM and chemotherapy treatments and the high incidence of pharmacoresistance in glioma patients. The primary goal of TRE treatment is to achieve seizure control, thereby improving the patient's quality of life (Weller et al., 2012). A large number of ASM are effective in monotherapy in focal epilepsy. When selecting the most appropriate ASM for an individual patient, factors such as the patient's specific characteristics, comorbidities, risk of side effects, and potential drug interactions must be considered.

Levetiracetam (LEV) monotherapy achieves seizure freedom in 60–100% of patients. One of the advantages of LEV is its good tolerability, and it has been reported to improve cognitive function in approximately 20–25% of patients (De Groot et al., 2013; Helmstaedter & Witt, 2008). Its most frequent adverse effect is irritability, which leads to discontinuation in less than 5% of patients (Mbizvo et al., 2012). Additionally, LEV has the advantage of having a low potential for drug interactions (Bénit & Vecht, 2016). A recent retrospective study performed on 460 GB patients showed that those treated with LEV during chemotherapy had longer overall survival (21 months) compared to patients who never received LEV (16 months) (Pallud et al., 2022). Considering its effectiveness, lack of significant drug interactions, and good tolerability, LEV is the preferred choice for monotherapy in the management of TRE (De Bruin et al., 2021; Maschio et al., 2011; Vacher et al., 2023).

Lamotrigine (LTG) has shown superiority as a monotherapy in focal epilepsy compared to carbamazepine, oxcarbazepine, topiramate, and gabapentin (Marson et al., 2007). When comparing LTG to LEV, studies have not found significant differences in efficacy or tolerability (Rosenow et al., 2012). The main limitation can be its slow titration compared to LEV.

Valproic acid (VPA) monotherapy reduces seizures in 55–78% of glioma patients (Kerkhof et al., 2013). One advantage of VPA is its limited cognitive adverse effects and its potential positive effects as a mood stabilizer (Bodalia et al., 2013; Chen et al., 2023). However, VPA is associated with side effects such as tremors, weight gain, and thrombocytopenia. When combined with certain chemotherapeutic agents like temozolomide and lomustine, the risk of thrombocytopenia may increase (Weller et al., 2011). Nevertheless, the clinical consequences of thrombocytopenia are often moderate (Tinchon et al., 2015). Exposure to valproic acid during pregnancy has been associated with an increased incidence of autism and other neurodevelopmental disorders (Bromley et al., 2014; Christensen et al., 2013). VPA is known to be a teratogenic drug and has been associated with a higher risk of neural tube defects, cleft lip and palate, cardiovascular abnormalities, genitourinary defects, developmental delay, endocrinological disorders, and limb defects (Vajda et al., 2023).

When monotherapy is insufficient to achieve seizure control, the following therapeutic option is to consider polytherapy, which involves adding a second ASM while continuing the first one (Brodie & Sills, 2011). A retrospective study on GB patients has shown that simultaneous use of LEV and VPA achieved seizure freedom in 60% of patients who did not respond to monotherapy (Kerkhof et al., 2013). The lowest possible dose of ASM must be used to minimize potential side effects and cognitive dysfunction (Vecht et al., 2014; Witt & Helmstaedter, 2013).

Lacosamide (LCS) is an ASM that has shown effectiveness and tolerability in TRE patients (Rudà et al., 2020; Saria et al., 2013). It has also demonstrated antitumoral effects in glioma cells ex vivo (Rizzo et al., 2017). Perampanel (PER) acts as a selective antagonist of AMPA receptors. It is effective and well-tolerated as an add-on therapy in TRE (Huberfeld & Vecht, 2016). In vitro studies have shown promising antitumor activity of PER, but clinical data on its antitumor effects are limited (Maschio et al., 2019; Damavandi et al., 2023). Brivaracetam (BRV) can be used in focal epilepsy as an add-on therapy. It shares a similar mechanism of action with LEV but has some differences in its pharmacological profile. BRV has demonstrated safety and efficacy in TRE (Maschio et al., 2020). Like LCS, it has also shown antitumoral effects in glioma cells ex vivo (Rizzo et al., 2017). Cenobamate

(CNB), a potentiator of persistent voltage-gated sodium channels and a GABAergic coupound, has recently been approved for treating adult focal epilepsy. While CNB has shown efficacy and tolerability in patients with refractory epilepsy, its specific use and effects in glioma patients have not been extensively studied yet (Peña-Ceballos et al., 2023; Villanueva et al., 2023; Wheless, 2020).

Vagus Nerve Stimulation (VNS) can be a potential treatment for patients with TRE who have intractable seizures and are not candidates for tumor resection surgery. A retrospective study conducted on 16 glioma patients with VNS showed that 50% of patients experienced an improvement in seizure frequency, and seizure frequency decreased in 65% of patients with stable tumors (Patel et al., 2013). Those results are similar to the efficacy rates found in other types of epilepsy. However, a limitation of using VNS in glioma patients is that they regularly need to realize MRI and a specialist to turn off the leads before the scan.

ASM enzymatic inducers such as carbamazepine, phenytoin, and phenobarbital should be avoided in TRE because they compromise the efficacy of chemotherapy, which may affect survival. These medications increase the activity of cytochrome P450, which can result in decreased antitumor effect of chemotherapy and potential drug toxicity (Brodie et al., 2013). On the other hand, eslicarbazepine and valproic acid can cause enzyme inhibition, which results leading to increased toxicity of chemotherapy drugs that are substrates for cytochrome P450 or UDP-glucuronosyltransferase (UGT) enzymes unless dose adjustments are applied (Bénit & Vecht, 2016).

1.6.2. Surgery

1.6.2.1. Objectives

Maximal surgical resection, also called supra-total resection, is the first-line treatment of glioma patients, preceding the administration of chemotherapy and radiotherapy. On the one hand, supra-total resection aims to prolong the overall survival of patients by removing the highest quantity of tumor cells. It also delays malignant transformation (Capelle et al., 2013; Molinaro et al., 2020). However, it is essential to note that brain gliomas are incurable, despite significant advances in treatment in recent years. Patients invariably experience relapse, with a new glioma emerging near the surgical cavity. This capacity of relapse displayed by gliomas is attributed to tumor cells placed outside the MRI abnormalities, in an area referred to as “the peritumoral tissue” (Pallud et al., 2010; Zetterling et al., 2016). The challenge lies in determining the extent of this peritumoral tissue, which can be located far from the tumor border, sometimes at even more than 2 cm. Moreover, this peritumoral tissue may be situated within eloquent regions we cannot remove, as glioma cells present a tendency to be placed in functional areas (Duffau & Capelle, 2004).

On the other hand, supra-total resection also aims to improve the patient’s quality of life by preventing new neurological deficits and aiding in seizure control. Since gliomas cannot be cured by surgery, reducing the risk of postoperative deficits is as important as the extent of resection (Weller et al., 2021). Supra-total resection must carefully consider the presence of functional areas surrounding the tumor that should not be removed, as doing so could result in the patient experiencing neurological impairment after the surgery. Additionally,

as mentioned earlier, glioma patients frequently present epileptic seizures, significantly impacting their quality of life. Supra-total resection is one of the main factors implicated in achieving seizure freedom after surgery (Klein et al., 2003; Still et al., 2019). Therefore, we can conclude that the surgery has two goals: oncological and epileptological.

1.6.2.2. Awake surgery

To test the functionality of the surrounding peritumoral tissue and ensure its safety for removal or preservation, glioma surgery is performed under awake conditions. The pioneer of this approach was Wilder Penfield in 1937, during epilepsy surgery. In the 1970s, George Ojemann introduced systematic testing to identify eloquent areas using a biphasic current (Whitaker & Ojemann, 1977). Glioma lesions located within or near functional areas may be considered suitable candidates for this type of surgery. Previously contraindications, such as a significant mass effect or a previous dural scar, are no longer considered absolute contraindications (Gogos et al., 2020; Sauvageot et al., 2023).

Preoperative evaluation techniques such as MRI-DTI, functional MRI, or MEG are not entirely accurate in excluding the presence of a function in a cortical area. Furthermore, brain shift during craniotomy can displace the functional areas detected preoperatively by more than 1 cm (Nimsky et al., 2005).

The most frequent approach for awake glioma surgery is the “asleep-awake-asleep” technique (Gogos et al., 2020). Initially, patients are placed under general anesthesia with propofol. Local anesthesia is infiltrated around the head holder pins. The head’s position depends on the tumor's location. Once the craniotomy is performed, the dura mater is opened and fixed to expose the cortical surface. The awake phase starts at this stage: propofol administration is discontinued, and the patient gradually wakes up. Functional mapping can begin when the patient is fully awake and cooperative. Once the mapping is complete, the resection process starts. As the neurosurgeons proceed with the resection, they conduct subcortical mapping in parallel. Some centers, such as Sainte Anne Hospital, employ the “four-hands technique”: while one neurosurgeon cuts, the other tests the subcortical bundles. After the resection is finished, the patient is placed back under anesthesia, and the dura mater, scalp, and skin are closed.

An extensive meta-analysis involving 8091 glioma patients demonstrated that awake surgery extended the surgical indications for gliomas situated within eloquent areas, leading to an improvement in the resection rates (75% vs. 58%) and a decrease in postsurgical neurological deficit (3.4% vs. 8.2%) (De Witt Hamer et al., 2012) (Figure 11).

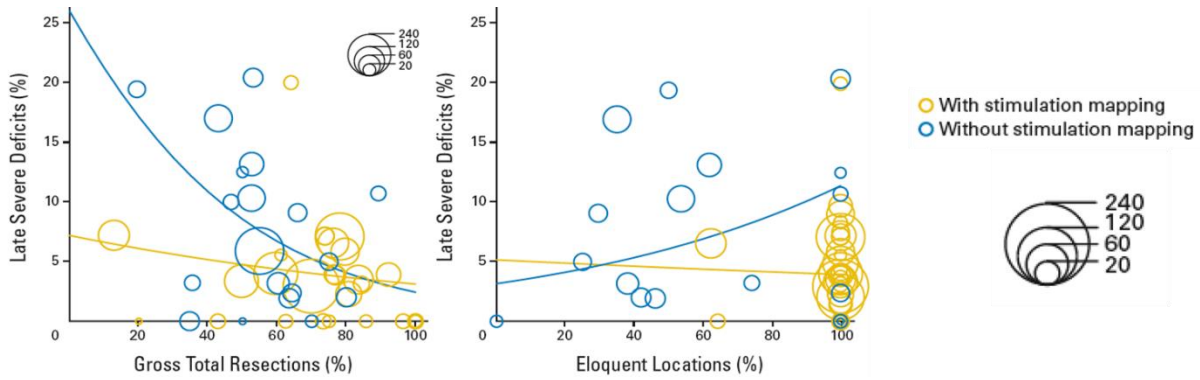

Figure 11: Meta-analysis including 8091 glioma patients comparing awake to anesthetized surgery. From De Witt Hamer, et al. 2012.

1.6.2.2.1. Supra-total approach

The current approach involves performing a supra-total resection to remove isolated tumor cells placed in the peritumoral area, outside the MRI abnormalities, by removing a security margin of 1-2 cm around the tumor (Silva et al., 2022). Two studies characterizing biopsies inside and outside the abnormal MRI areas have demonstrated the presence of tumor cells beyond the tumor boundaries (Pallud et al., 2010; Zetterling et al., 2016). During surgery, the neurosurgeon is unaware of the presence of these cells, as their detection is possible only through histopathological analysis after a biopsy. Tumor growth occurs in the peritumoral area, where glioma cells detach from the macroscopic core and propagate into the healthy tissue. This peritumoral area is also where epileptogenesis takes place. In a series of TRE patients, seizures always originated from the peritumoral area, sometimes up to 2 cm from the tumor border (Mittal et al., 2016). Moreover, in LGGs, the cycling tumor cell fraction is higher at the periphery compared to the center of the tumor, suggesting that removing peripheral areas could delay tumor recurrence (Gerin et al., 2013). Long-term follow-up of patients has shown that supra-total resection leads to significantly larger overall survivals in both LGGs and HGGs (Duffau, 2016; Freyschlag et al., 2018; Molinaro et al., 2020). Recently, a series of LGGs revealed that supra-total resection was associated with longer overall survival and longer malignant progression-free survival (Rossi et al., 2021). Even in complex scenarios, such as elderly patients with GB, the supra-total resection proves to be superior to partial resection (Han et al., 2020). Traditionally, the extent of resection has been the main endpoint of the surgery. However, quantifying residual tumoral volume is a valuable predictive marker for relapse. Therefore, the resection must be systematically and objectively calculated post-surgery based on MRI findings (Capelle et al., 2013; Karschnia et al., 2021; Roelz et al., 2016).

In incidentally discovered gliomas, early resection has been shown to improve the survival rate (Ius et al., 2022). Neurocognitive disturbances are present in 60% of incidentally discovered gliomas when subjected to fine cognitive testing (Cochereau et al., 2016). Since the tumor and the peritumoral area are smaller in these cases, the chances of performing a

supra-total resection without postoperative impairment are higher. Moreover, chemotherapy may be more efficient due to the tumor's reduced molecular heterogeneity. Given these considerations, some authors have raised the possibility of performing screening for glioma in the general population (Mandonnet et al., 2014). Based on a previous study that showed a centered MRI onset of gliomas at 30 years using a biomathematical model (Gerin et al., 2012), the suggested screening should be conducted between the ages of 20 and 40 years (Mandonnet et al., 2017).

1.6.2.2.2. Perioperative Image

In the last decades, significant advancements have been made in neurosurgery, leading to new techniques to aid neurosurgeons in tailoring the limits of the resection. These techniques include perioperative echography, perioperative MRI, neuronavigation, and 5-ALA fluorescence. By leveraging these innovative tools, neurosurgeons can operate more complex cases with greater precision and efficiency, ultimately resulting in reduced morbidity and mortality rates (Barker & Linskey, 2004).

Echography

Perioperative echography is a precious tool due to its cost-effectiveness, real-time capability, and ease of implementation in the operative theater. It may aid in enhancing resection rates and reducing residual tumor volume. However, the neurosurgeon needs to undergo proper training, as inter-operator variability remains a significant limitation (Moiraghi & Pallud, 2020). One of the most important advantages of perioperative echography is its ability to overcome brain shift issues that can occur after craniotomy. It provides real-time feedback, allowing neurosurgeons to adjust during surgery to achieve optimal outcomes. The image quality can decline during resection due to the reduction in the sound-to-noise ratio between tumor remnants and reactive tissue changes (Munkvold et al., 2018). New developments have been made in the perioperative echography field. Coupling perioperative echography with preoperative MRI has shown the potential to improve supra-total resection rates further while reducing postoperative morbidity (Liang et al., 2019).

Perioperative MRI

Perioperative MRI remains relatively underused in France due to its complexity in the operative theater. Nonetheless, certain teams have demonstrated the utility of perioperative-MRI in increasing resection rates in 40% of cases and the number of supra-total resections (Mohammadi et al., 2014; Pamir et al., 2010). In a prospective study involving 100 glioma patients undergoing surgery with perioperative MRI guidance, a median extent of resection reaching 100% was achieved in all the locations except for the insula (Leroy et al., 2019).

A recent technological advancement, the low-field portable MRI, shows promising potential for use during glioma surgery. It provides a similar resolution to conventional 3T-MRI but a significantly lower cost (Campbell-Washburn et al., 2023). Clinical studies are needed to prove their utility in glioma resection.

Neuronavigation

Perioperative neuronavigation relies on stereotaxic principles (Willems et al., 2006). It uses external anatomical head references to replicate the MRI, enabling neurosurgeons to precisely locate their pointers in relation to MRI references. This technique improves the identification of small and subcortical lesions. However, a primary limitation is the lack of real-time information, as brain shifts can occur during craniotomy, particularly in HGGs. Despite this, neuronavigation contributes to increasing rates of supra-total resection, leading to improved survival rates in HGGs patients (Kurimoto et al., 2004). A unique randomized trial investigating the effectiveness of neuronavigation demonstrated that surgeries performed with neuronavigation obtained a smaller mean amount of residual tumor (13,8% vs. 28,9% in surgeries without neuronavigation) (Willems et al., 2006).

5-ALA fluorescence

While intraoperative fluorescence-guided surgery using 5- aminolevulinic acid (5-ALA) is not widely used in France, many neurosurgical teams worldwide employ this technique (Guyotat et al., 2016). The use of 5-ALA is based on the capacity of glioma cells to transform 5-ALA into protoporphyrin X, a fluorescent substance (Duffner et al., 2005). Before surgery, patients receive 5-ALA intravenously. During the resection, an optic system integrated into the surgical microscope allows the identification of fluorescent areas, indicating the presence of tumor cells (Zhang et al., 2017). To visualize the low levels of fluorescence in LGG, a confocal microscope is needed (Sanai, Snyder, et al., 2011). The first prospective study demonstrating its utility was conducted on HGGs (Stummer et al., 2006) and showed a significant increase in resection rates. In HGGs, the level of fluorescence is high (95.4% in GBs), making this technique suitable for enhancing tumor visualization. However, for LGGs, the level of fluorescence is lower (26.3%), limiting the applicability of this technique (Ishihara et al., 2007; Ji et al., 2019).

Fluorescein has emerged as another fluorophore used to improve glioma surgery guidance and detect glioma cells. A recent study demonstrated that using fluorescein significantly increased the supra-total resection rate compared to the non-fluorescein group (45.9% vs. 19.6%, $P = 0.003$). Additionally, the postoperative residual tumor volume was significantly lower in the fluorescein group than in the non-fluorescein group (0.40 [0.12-7.11] cm^3 vs. 4.76 [0.44-11.00] cm^3, $P = 0.020$) (Xi et al., 2023).

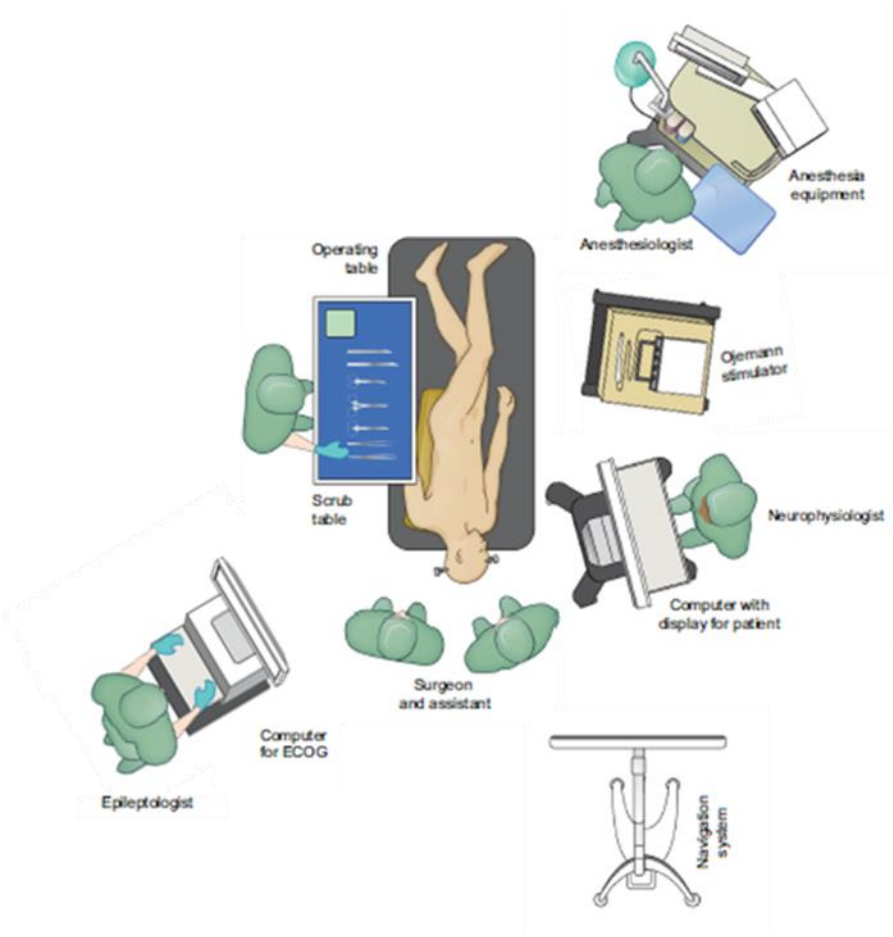

Figure 12: Overview of the operative room.
From de Gogos, et al. 2020.

1.6.2.2.3. Functional mapping

Delineating the real boundaries of glioma presents challenges, as tumor cells are often found beyond the visible MRI abnormalities (Pallud et al., 2010). In glioma surgery, the primary approach involves removing as much peritumoral tissue as possible, making anatomical guidance insufficient. Instead, surgical decisions rely on the functionality of the surrounding brain areas. Therefore, when gliomas are located around or within functional regions, preoperative functional testing is crucial to avoid postsurgical neurological impairment (Duffau et al., 2005; Pallud, Mandonnet, et al., 2017). Notably, brain functional locations exhibit interindividual variability, particularly in cases of slow tumor growth, which can cause functional areas to relocate due to neuronal plasticity, especially at the cortical level (Hugues Duffau, 2017; Johan Pallud et al., 2018). Various technologies are available to test the functionality of cortical and subcortical areas, with electrical direct stimulation being the most commonly used method.

Direct electrical stimulations

Direct electrical stimulations aid in testing cognitive and neurological functions in awake patients during glioma surgery. The method involves applying electrical stimulation directly to the cortex (or subcortical structures) for 4 seconds at low intensity (biphasic impulse at 60 Hz, 1 ms, 2-6 mA) using bipolar electrode contacts separated by 5 mm (Duffau, 2007; Mandonnet et al., 2010). Simultaneously, the patients undergo evaluation by a neuropsychologist or speech therapist. Although this technique has been employed for over 40 years, the underlying cellular mechanisms responsible for functional impairment remain unknown. In specific brain regions, such as the primary motor cortex, electrical stimulations induce function, eliciting clonic movements on the contralateral side, whereas, in language-related areas, they impair speech production. Throughout the surgical resection, stimuli are repeated as necessary, as debulking the lesion may reveal eloquent brain areas (Pallud et al., 2019). This personalized approach allows for supra-total resection minimizing the risk of postoperative impairment, as demonstrated in a meta-analysis involving 8091 glioma patients (De Witt Hamer et al., 2012). A more recent series, including 107 awake glioma surgeries, reported resection rates exceeding 90% in 85.7% of grade 2, 61.4% of grade 3 gliomas, and 85.7% of GBs (Pallud & Dezamis, 2017).

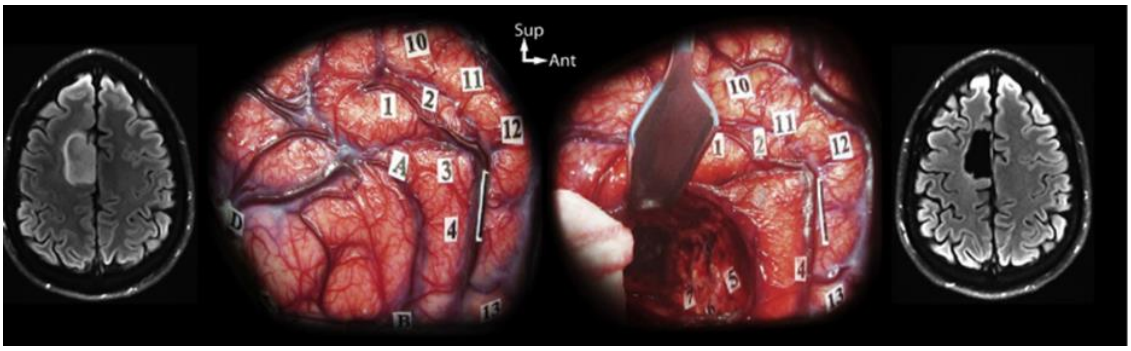

Figure 13: Functional-based surgery for gliomas located close to or within motor networks. From Pallud et al 2017.

1.6.2.2.4. Perioperative neurophysiological monitoring

Direct electrical stimulations can induce seizures in 9-20% of patients (Alimohamadi et al., 2023; Duffau, 2007). To localized interictal activities and monitor the presence of induced after-discharges or electrical seizures, simultaneous recording of brain activity using Electrocorticography (ECoG) is employed. ECoG has a long history, with its initial recordings made by Wilder Penfield in Montreal in the 1950s. The technique involves placing macroelectrode grids (between 0.4 to 1 cm in diameter) with six to 64 contacts directly in contact with the cortical surface once the patient is fully awake. A monopolar or bipolar montage can be used, with a reference electrode placed at the scalp level near the craniotomy (Trebuchon et al., 2012).

One limitation of the functional mapping performed by EDS is that this type of mapping is only efficient in the eloquent cortex, which represents approximately 30% of the cortical

surface. Complex functions dependent on associative areas cannot be adequately delineated with such tools. Different electrophysiological biomarkers, such as gamma activity, can be recorded with ECoG and used in conjunction with EDS mapping to address this limitation. Gamma oscillations have been observed during various cognitive processes, including visual perception (Lachaux et al., 2000), motor function (Engelhard et al., 2013), selective attention (Müsch et al., 2014), speech processing (Basirat et al., 2008), and memory-related processes (Jensen et al., 2007). An increase in gamma amplitude reflects local cortical activation and is associated with enhanced neural firing (Mukamel et al., 2005; Ray et al., 2008). Consequently, recording gamma-evoked activity during tasks shows promise as a functional mapping technique. A meta-analysis including 129 patients implanted with sEEG electrodes reported that gamma activity increases during language tasks in the functional cortex. This increase enables the precise location of functional speech areas previously defined by electrical stimulation (Arya et al., 2018).

Motor-evoked potentials (MEP) represent another valuable tool for localizing the functional motor cortex. Notably, at the primary motor cortex, MEP exhibits a phase reversal. Likewise, the somatosensory primary cortex can be localized using somatosensory-evoked potentials (SSEP) (Romstöck et al., 2002). Recently, cortico-cortical evoked potential has been employed during awake surgery for functional mapping purposes (Boyer et al., 2021).

1.6.3. Radiotherapy

Radiotherapy ideally aims to improve local tumor control without provoking neurotoxicity in healthy brain areas. The initiation of radiotherapy typically occurs 3-5 weeks after surgery, with the exact timing influenced by histology, age, and residual tumor volume (Press et al., 2020). The gross tumor volume, which includes the residual tumor volume and the surgical cavity, is assessed using T1, T2, and FLAIR MRI sequences. A safety margin of 1-2 cm is added to encompass tumor cells invading the peritumoral area, ensuring comprehensive treatment (Niyazi et al., 2016). However, structures like the optic nerves, optic chiasm, lenses, retinae, brainstem, cochlea, pituitary, and hippocampi are delineated to be spared from radiotherapy due to their high risk of toxicity. The standard radiotherapy regime involves a daily fraction of 1.8-2 Gy, with a total dose of 50 to 60 Gy (Weller et al., 2021). Older patients and those with poor prognoses can receive higher doses per fraction with a lower total dose (Roa et al., 2004). Following the completion of radiotherapy, an MRI examination should be conducted 3-4 weeks later to establish a baseline for monitoring tumor evolution (Weller et al., 2021).

1.6.4. Chemotherapy

Temozolomide is the most frequently used chemotherapy agent, which has shown efficacy and a favorable safety profile. It can penetrate the blood-brain barrier and acts as a DNA alkylating agent (Ricard et al., 2012). Its main side effect is thrombocytopenia; hepatic function must also be monitored. However, it generally has a favorable safety profile (Stupp et al., 2005). Another chemotherapy regimen is PCV, which includes procarbazine, CCNU (lomustine), and vincristine. Alkylating agents from the nitrosourea class (lomustine, carmustine) can induce delayed leukopenia and thrombocytopenia. Carmustine use has been associated with pulmonary fibrosis (Weller & Le Rhun, 2020). Carmustine can also be directly implanted in the post-surgical cavity during surgery. It diffuses over several mm

around the surgical cavity some weeks before initiating radiochemotherapy (Roux et al., 2023).

Bevacizumab, a monoclonal antibody against VEGF, targets neovascular proliferation in HGG. It can be used alone or in combination with irinotecan, which inhibits topoisomerase 1 (Ricard et al., 2012; Weller et al., 2021).

1.6.5. Tumor treating fields

Tumor treating fields (TTF) is an approved treatment for GB patients. It consist in applying alternating electric fields suing transducer arrays situated outside the scalp at low intensity and intermediate frequency to alter tumor cells division (Kirson et al., 2004, 2007). The underlying mechanisms is the alteration of the polarization of the cell membranes. After TTF application we obtain abnormal mitotic figures and membrane breaking (Voloshin et al., 2016). Moreover, there exists a synergic effect between TTF and chemotherapy (Clark et al., 2017; Kirson et al., 2009).

1.7. Natural evolution

1.7.1. Care challenges: epilepsy and survival

As illustrated previously, there is a connection between epilepsy and survival. The presence of epileptic seizures is associated with longer survivals, even in cases where patients experience only a single seizure (Chaichana et al., 2009; Chang et al., 2008; Fan et al., 2018; Flanigan et al., 2017; Mirsattari et al., 2011). As the glioma progresses, epilepsy also develops at a higher frequency among patients, with an increased number experiencing seizures and developing pharmacoresistance.

1.7.2. Epilepsy prognostic factors

Temporal, parietal, and insular cortical involvement are associated with a higher risk of seizures in LGGs (Kerkhof & Vecht, 2013; Pallud et al., 2014). The presence of IDH1/2 mutations is also associated with a higher risk of epilepsy development compared to IDH-WT patients (Kerkhof & Vecht, 2013). In HGGs, temporal lobe involvement and cortical locations were linked to a higher risk of seizures, while larger tumor volumes were less associated (Chaichana et al., 2009; Kerkhof & Vecht, 2013). The strongest predictor of seizure freedom six months after surgery is supra-total resection. (Kerkhof & Vecht, 2013; Rudà et al., 2012). Patients whose seizures were controlled by ASMs preoperatively had better seizure control after surgery.

1.7.3. Oncology

1.7.3.1. Tumor relapse

Tumor relapse occurs systematically after oncological treatment, regardless of the histology, justifying the need for clinic-radiological follow-up of the patients. There is no standard treatment for tumor relapses (Ricard et al., 2012). Treatment decisions should be discussed in a multidisciplinary meeting. Both LGG and HGG demonstrate clear benefits from reoperation, with the extent of resection being the strongest predictor of overall survival (Chaichana et al., 2013; Duffau, 2022; Hamdan & Duffau, 2021; Quick et al., 2014; Shofty et al., 2020; Uppstrom et al., 2016). LGG treated with repeated surgery can achieve an overall survival of 18 years (Hamdan & Duffau, 2021). In HGG, carmustine wafers can be implanted perioperatively (Roux et al., 2023). Post-surgery, the treatment approach depends on histology and previous treatments. Patients may receive first or second-line chemotherapy, antiangiogenic treatment (Bevacizumab alone or combined with Irinotecan), or a new radiotherapy schedule (Weller et al., 2021).

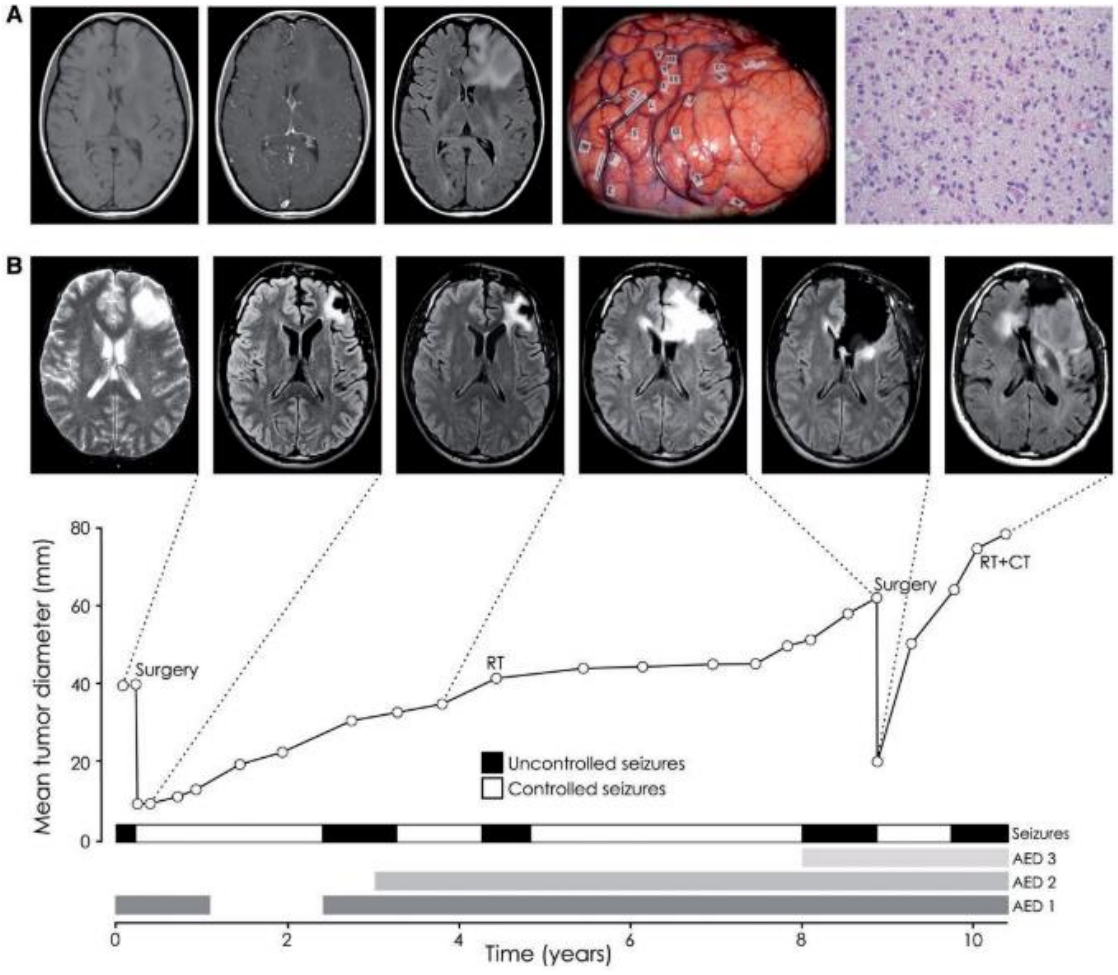

Figure 14: Natural evolution of glioma
From Pallud, et al. 2014.

1.7.3.2. Malignant transformation

LGGs progressively evolve towards a higher-grade glioma. The time to malignant transformation can vary significantly between patients (Pallud et al., 2006). Progression-free survival can range from 3 to 10 years, with 30 to 90% of patients showing no malignant transformation at 5 years (Capelle et al., 2013). Radiologically, we can observe an increase in the growth rate, new contrast-enhanced areas, edema, and mass effect. Histologically, there is an increase in proliferation rates such as Ki67, neoangiogenesis outbreak, destruction of the brain parenchyma, and increased migration. These changes can lead to several clinical consequences for patients, including worsening epileptic seizures, increased intracranial pressure, or the development of new neurological deficits. Malignant transformation precedes the patient's death.

1.7.3.3. Survival

Despite the advances made in chemoradiotherapy and the new development of new surgical tools, the outcome for patients with gliomas remains fatal without a possible cure. However, there have been improvements in overall survival and quality of life. In LGG, overall survival has expanded from 8 to 15 years in various studies, with 40 to 88% of survival at 5 years (Capelle et al., 2013; Lebrun et al., 2004). HGG's mean overall survival ranges between 2 and 7 years, with 15-75% survival at 5 years (Van Den Bent et al., 2013). In GB patients, the mean overall survival varies from 12 to 18 months, with 27% survival at 2 years and less than 10% survival at 5 years (Stupp & Roila, 2009; Stupp et al., 2005).

1.7.3.4. Prognostic factors

Several prognostic factors have been identified in LGG. Among them, the age, the presence of epilepsy, the presence of neurological impairment, the tumor size, the displacement of the midline, functional areas involvement, the histology, and the extent of surgical resection are associated with overall survival (Capelle et al., 2013; Pallud et al., 2006, 2009). In an extensive series of 1097 LGG cases, age over 55, tumor location outside the frontal lobe, and tumor volume over 100 cm^3 were independently associated with worse outcomes. Conversely, supra-total resection and the presence of epilepsy were found to be independent factors for favorable outcomes (Capelle et al., 2013). Regarding HGG, age, tumor location, tumor volume, and extent of resection are also good prognostic factors. In GB, the prognosis worsens with higher age (Chaichana et al., 2009; Sanai, Polley, et al., 2011).

IDH mutated status, the presence of MGMT methylation, or the co-delection 1p-19q are also prognostic factors. IDH-mutated patients have a better prognosis, regardless of their tumor grade (Ducray et al., 2011; Sanson et al., 2009; Van Den Bent et al., 2013). Patients with 1p19q co-deletion respond better to radio and chemotherapy (Ducray et al., 2011). MGMT methylation improves GB's response to chemotherapy and radiotherapy (Hegi et al., 2005). It is an independent factor of good prognosis (Stupp & Roila, 2009; Stupp et al., 2005).

2. Peritumoral tissue

2.1. Definition

Diffuse brain gliomas, as the name evokes, are poorly circumscribed and heterogeneous tumors that progressively infiltrate the brain. Numerous studies have already reported the presence of tumor cells outside MRI abnormalities. The first study, conducted in 1987, searched for the presence of infiltrative tumor cells in five stereotactic biopsies taken from normal T2-weighted MRI regions surrounding grade 2 astrocytomas. In three of the samples, infiltrative tumor cells were found (Kelly et al., 1987). Subsequently, in another study, tumor cells outside the T2 abnormality areas were detected in five LGG (Watanabe et al., 1992). A third study identified tumor cells in eight out of 18 patients whose biopsy trajectories were taken from areas with normal T2 signal intensity (Price et al., 2006). In 2010, a study including 16 oligodendrogliomas found mitotic tumor cells beyond MRI-defined abnormalities in all patients. The highest density of tumor cells was observed between 10 to 20 mm beyond the macroscopic MRI limits (Pallud et al., 2010). Finally, in 2016, another study also identified tumor cells beyond the MRI abnormalities in five patients. This time, tumor cells were detected at a maximum distance of 14 mm from the macroscopic MRI abnormalities (Zetterling et al., 2016).

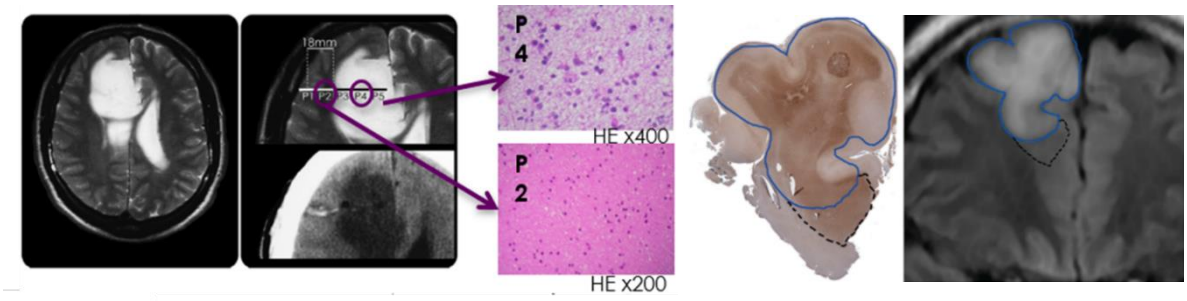

Fig 15: Tumor cells outside MRI abnormalities.
Left: From Pallud et al, 2010.
Right: From Zetterling et al, 2016.

The peritumoral tissue can be defined as the peripheral area of the glioma that appears macroscopically normal but exhibits microscopic tumor infiltration. This virtual space can extend at least 20 mm beyond the MRI abnormalities. The presence of isolated tumor cells in the peritumoral tissue explains the recurrence of gliomas at the resection margin after surgery. This phenomenon also elucidates the prognostic significance of the extent of resection, which is now recognized as one of the primary prognostic factors in gliomas (Silva et al., 2022).

But the peritumoral tissue is not only characterized by such tumoral infiltration. Functional neuronal disturbances are another hallmark. TRE originates from the peritumoral area due

to the microenvironment disturbances caused by tumor cells, including glutamatergic and GABAergic impairment (Chen et al., 2017; Pallud & McKhann, 2019). Supra-total resection affects the oncological prognosis and impacts the control of TRE, underscoring the crucial role of the peritumoral area in the oncological and epileptological outcomes. More over specific plasticity phenomenon and interactions between glioma cells and neurons have been more recently revealed (Venkataramani et al., 2023, Krishna et al., 2023, Huang-Hobbs et al., 2023).

2.1.1. Identification

Currently, the only way to detect the presence of infiltrative tumor cells in the peritumoral area is through histological analysis following a biopsy or a resection. We lack a tool to detect infiltrative tumor cells before or during surgery, or at least their interactions with the local microenvironment, which means that the extent of the peritumoral area remains unknown. Neurosurgeons are unaware of the presence of tumor cells beyond the MRI abnormalities, which is why the surgical approach involves supra-total resection. This area of research is of great interest, particularly in neuroimaging, where numerous studies aim to develop new imaging modalities for identifying infiltrative tumor cells (Bontempi et al., 2021; Roodakker et al., 2019). A study conducted on LGG demonstrated that changes in ADC values preceded structural MRI changes and were associated with tumor progression (Chen et al., 2018), suggesting that radiomic analysis could be useful in detecting peritumoral cells. PET imaging has also shown potential in aiding tumor delimitation. In a prospective study, the combination of MRI-ADC and FET PET demonstrated better detection of glioma infiltration compared to structural MRI and FET PET in HGG. However, for LGG, FET PET was not found to be part of the optimal imaging combinations, and its accuracy was lower than that of FLAIR MRI (Verburg et al., 2020).

However, these techniques alone are not sufficient. Various strategies have been explored, such as using 5-ALA to detect the presence of infiltrative tumor cells in HGG, as described earlier. The limitation is that the visualization provided by 5-ALA is time-consuming and limited to areas exposed within the resection cavity. It does not enable the visualization of all tumor cells in the peritumoral area.

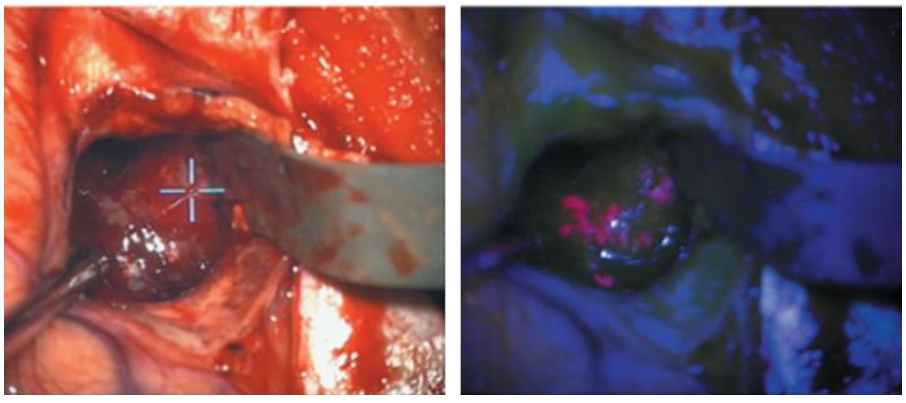

Fig 16: Intraoperative detection of protoporphyrin X fluorescence.
From Valdés et al, 2015.

Since tumor cells profoundly affect the peritumoral microenvironment and cause GABAergic and glutamatergic signaling impairment, neurophysiology offers valuable

tools for measuring this disbalance. In vivo, ECoG recordings conducted on glioma patients have demonstrated differences between the tumor and healthy tissue in terms of the canonical frequency bands of the power spectrum (Boussen et al., 2016). Recently, there has been a growing interest in studying the aperiodic components of the power spectrum, such as the offset and slope, which have been explored in various pathologies like schizophrenia or Parkinson's disease (Belova et al., 2021; Donoghue et al., 2020; Ghinda et al., 2021; Molina et al., 2020). However, there is limited knowledge regarding their association with gliomas and the surrounding tissue. Specifically, the slope of the power spectrum is considered a marker of the excitation-inhibition balance (Gao et al., 2017; Jiang et al., 2022; Molina et al., 2020), known to be crucial in both epileptic and glioma growth processes (Huberfeld & Vecht, 2016). Additionally, previous studies from our group have shown, using ex vivo extracellular recordings from human peritumoral glioma slices, that high-frequency oscillations (HFO) colocalized with the presence of the infiltrative tumor cells (Pallud, Le Van Quyen, et al., 2014).

2.1.2. Challenges

As mentioned earlier, the peritumoral area plays a critical role in tumor growth and epileptogenesis, both of which are of utmost importance for patients. Tumor growth is a significant concern because the presence of infiltrative tumor cells that we cannot detect leads to inevitable recurrence, making it challenging to cure gliomas. Epileptogenesis, on the other hand, dramatically impacts the patient's quality of life. Since the disease is not curable, one of the primary objectives in glioma treatment is to maintain or improve their quality of life. Finally, specific interactions between peritumoral neurons and infiltrative tumor cells affect glioma growth (Venkataramani et al., 2023, Krishna et al., 2023, Huang-Hobbs et al., 2023).

When treating gliomas, surgery is one of the first-line treatments. Whenever possible, the approach involves performing a supra-total resection, aiming to remove the maximum amount of infiltrative peritumoral cells allowed by the functional areas surrounding the tumor while avoiding any neurological impairment to the patient. The definition of complete resection includes the removal of the T2/FLAIR hyperintensities (Karschnia et al., 2021). The current approach, known as supra-total resection, goes beyond that by incorporating a "security margin" around the tumor, which is the largest margin allowed by the surrounding functional areas.

Although the latest Cochrane review stated that there are no randomized controlled trials to determine the best surgical approach (Jiang et al., 2017), numerous reviews and meta-analyses have confirmed the association between the extent of resection and the overall survival (Brown et al., 2019; Di Carlo et al., 2020; Hervey-Jumper & Berger, 2019). In a study involving 15 patients who underwent supra-total resection compared to 29 patients with total resection, it was found that the supra-total resection group exhibited a reduction in malignant transformation (Yordanova et al., 2011). More recently, another study demonstrated that supra-total resection was achieved in 32.3% of 449 LGGs, with only 0.68% of patients experiencing permanent neurological deficits (Rossi et al., 2019). Furthermore, the same authors reported in a study of 319 LGG that only 5.4% of patients who underwent supra-total resection experienced progression, compared to 82.4% of those who underwent partial/subtotal resection, with a mean follow-up of 7 years (Rossi et al., 2021).

In clinical practice, the surgical approach for glioma surgery has evolved from an anatomical, neuroimaged-based to a "connectome-based surgery". This approach aims to achieve a maximal security margin while considering the surrounding functional areas. The goal is to strike a balance between oncological outcomes and functional preservation. Supra-total resection, which involves the largest possible supramarginal removal while maintaining functional boundaries and minimizing postsurgical impairment, represents the highest level of onco-functional balance (De Witt Hamer et al., 2012).

TRE is a complex condition involving multiple factors and mechanisms, which will be discussed in more detail later. Seizures arise from the peritumoral tissue and can occur even up to 2 cm from the tumoral borders (Mittal et al., 2016).

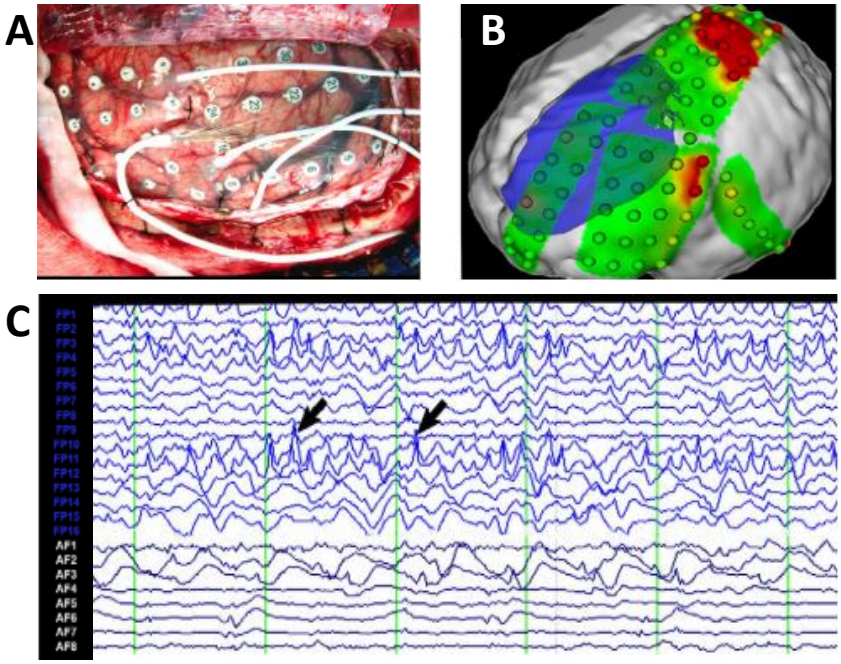

Figure 17: Perioperative ECoG recording.
A: ECoG grid.
B: SOZ is located at the peritumoral level (red).
C: Interictal spikes.
From Mittal et al, 2016.

Ex vivo electrophysiological recordings conducted on human peritumoral slices have demonstrated that epileptic activities originate from the peritumoral neocortex infiltrated by glioma cells rather than from the glioma core (Pallud, Le Van Quyen, et al., 2014).

It is now widely accepted that larger extents of resection are associated with improved postoperative seizure control (Capelle et al., 2013; Duffau, 2016; Pallud, Audureau, et al., 2014; Yordanova et al., 2011). In a review of 346 gliomas, postoperative seizure control was associated with EOR ≥91% and/or residual tumor volume ≤19 cm^3 (Still et al., 2019). Another study involving 449 gliomas demonstrated that the supra-total resection group had improved epilepsy control (91.7%) compared to the non-supra-total group (77.5%), along with a consistent decrease in the frequency of seizures (Rossi et al., 2021). The number of

ASM required to obtain seizure control also decreased after surgery, suggesting that removing the peritumoral area containing infiltrative tumor cells leads to better long-term epileptic outcomes (Rossi et al., 2021).

2.2 Epilepsy

2.2.1 Mechanisms

2.2.1.1 GABA

$GABA_A$ receptors are ionotropic channels consisting of 5 subunits from 8 families (α, β, γ, δ, ε, θ, μ, and ρ). The inner channel of the receptor is permeable to anions, particularly Chloride (Cl^-) and bicarbonate (HCO_3^-) ions (Bormann et al., 1987). The receptor possesses various binding sites for different ligands, including benzodiazepines and barbiturates. The channel opens upon the binding of two GABA molecules at the extracellular site. In mature neurons, intracellular Cl^- concentration is low (around 4 mM) and high extracellularly (around 100 mM) (Kaila, 1994).

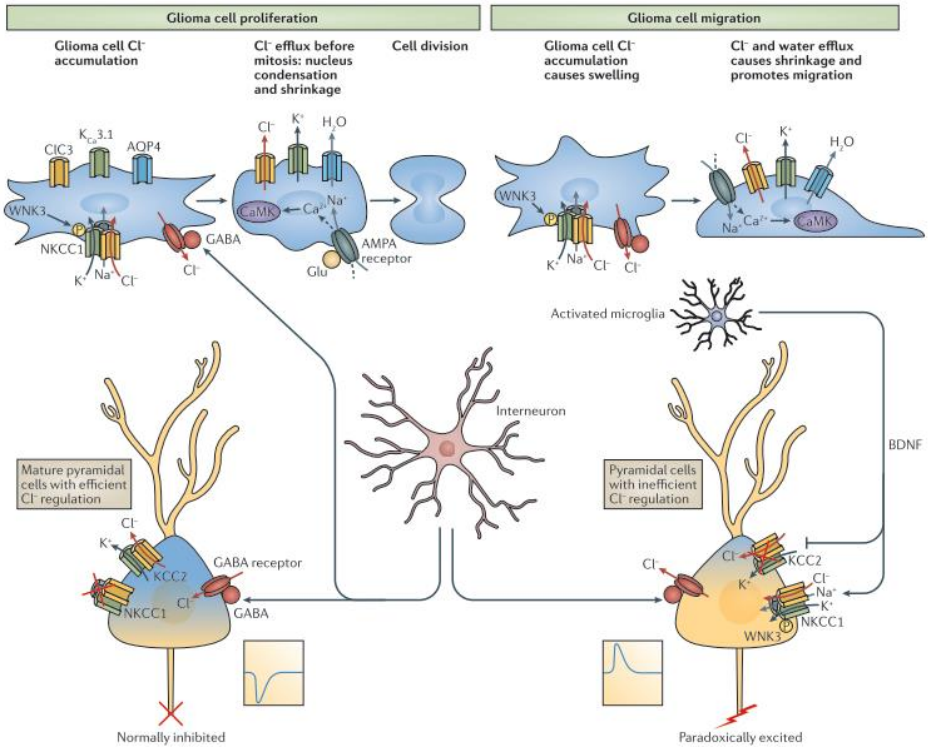

Figure 18: GABA dysregulation in glioma.
From Huberfeld and Vecht 2016.

Under these conditions, when the GABA receptor opens, the ionic gradient causes Cl^- to enter the cell, where it is less concentrated, resulting in hyperpolarization. The electric gradient counterbalances this force. Since the inside of the cell is negatively charged, anions are repelled outward. The combination of these two forces generates the electrochemical

gradient, which drives Cl^- movement either into or out of the cell. For a given intracellular and extracellular Cl^- concentration, a membrane potential opposes this electrochemical gradient, known as the inversion potential. If the membrane potential exceeds the inversion potential, Cl^- will move into the cell, leading to hyperpolarization. Conversely, if the membrane potential is lower than the inversion potential, Cl^- will exit the cell, resulting in depolarization (Rheims et al., 2008; Spitzer, 2010). Therefore, GABA stimulation can induce either hyperpolarization or depolarization depending on the intracellular Cl^- concentration and membrane potential.

GABA concentrations are higher at the tumor core compared to the peritumoral tissue (Bianchi et al., 2004). However, gliomas exhibit a decrease in GABAergic synaptic density. The excess of extracellular Glu downregulates neuronal $GABA_A$ receptors (Buckingham & Robel, 2013). Moreover, the peritumoral cortex experiences a loss of GABA interneurons and GABA synapses (Haglund et al., 1992; Marco et al., 1997).

In healthy mature neurons, Cl^- concentration is regulated by the co-transporter KCC2, which facilitates Cl^- efflux along with K^+ efflux (maintained by K^+ gradient), and by the repression of the cotransporter NKCC1, which promotes Cl^- influx along with Na^{2+} and K^+ influx (mediated by Na^{2+} gradient) (Liu et al., 2019). Under normal conditions, GABA activation allows Cl^- to enter the neuron into the extracellular space, resulting in hyperpolarization. However, in the peritumoral tissue, activated microglia and tumor cells secret BDNF (Coull et al., 2005), which enhances NKCC1 expression and downregulates KCC2 co-transporters (Campbell et al., 2015; Conti, et al., 2011; Pallud, Le Van Quyen, et al., 2014). Additionally, NMDA activity suppresses KCC2, thereby exacerbating Cl^- dysregulation (Lee et al., 2011).

This leads to an increased concentration of Cl^- inside neurons. Approximately 60% of pyramidal cells present an altered Cl^- homeostasis in gliomas (Pallud et al., 2014; Campbell et al., 2015). Consequently, Cl- exits the neuron when the GABA receptor is activated, resulting in depolarization (Campbell et al., 2011). It's worth noting that GABA depolarization is not exclusive to gliomas. It also contributes to epileptiform activities in various pathologies, including hippocampal sclerosis (Muñoz et al., 2007; Palma et al., 2006, Huberfeld et al., 2007), tuberous sclerosis (Talos et al., 2012) or cortical dysplasia (Cepeda et al., 2012, Blauwblomme et al., 2019).

2.2.1.2 Glutamate

Glu receptors play a crucial role in various biological responses. They can be categorized as ionotropic or metabotropic receptors. Among the ionotropic receptors, we find N-methyl-D-aspartate (NMDA) (subunits NR1, NR2A, NR2B, NR2C, NR2D, NR3A and NR3B), α-amino-3-hydrocy-5-methyl-4-isoxazolepropionic acid (AMPA) (with the subunits GluR1, GluR2 GluR3 and GluR4), and kainate (subunits GluR5, GluR6, GluR7, KA1, KA2).

The NMDA receptor is composed of four transmembrane subunits that form a hetero-tetramer. Typically, it consists of two GluN1 and two GluN2 or GluN3 subunits (Hansen et al., 2018). However, there are different types of subunits encoded by specific genes: one for GluN1 (GRIN1), four for GluN2 (GRIN 2A, 2B, 2C, and 2D,) and two for GluN3 (GRIN 3A and 3B). Alternative splicing of the GRIN1 gene can produce eight different

isoforms (Traynelis et al., 2010). During brain maturation, there is a shift from the predominant GluN2B subunit to the GluN2A isoform (Matta et al., 2011). However, in epileptic tissues, this shift is reversed (Gholami et al., 2020; Müller et al., 2013). Stimulation of NMDA receptors triggers the opening of a nonselective ion channel to cations. The channel can be blocked by extracellular magnesium (Mg^{2+}) and zinc (Zn^{2+}) ions, which are removed when the neuron is depolarized. The influx of Ca^{2+} through the NMDA receptor channel triggers intracellular signaling pathways, leading to synaptic plasticity processes involved in memory and learning. NMDA also plays a role in generating epileptic activities by facilitating neuronal stimulation. However, excessive stimulation of NMDA receptors and the resulting excessive influx of Ca^{2+} into the cell can induce excitotoxicity through the activation of caspase pathways (Lange et al., 2021).

AMPA receptors are hetero-tetramers composed of four subunits encoded by four different genes: GRIA1, GRIA2, GRIA3, and GRIA4, which encode the GLUR1, GLUR2, GLUR3, and GLUR4 subunits, respectively. Each subunit contains a binding site for Glu, but the channel only opens when two binding sites are occupied. The current flow through the channel increases if more binding sites are occupied. The channel is permeable to cations, such as Na^{2+}, K^{+}, and Ca^{2+}. The presence of the GluA2 subunit influences the permeability of the channel to Ca^{+2}. When GluA2 is present, the channel is impermeable to Ca^{2+}, whereas its absence renders it permeable to Ca^{2+}. In adult synapses, GluA2 undergoes mRNA editing through the enzyme adenosine deaminase, resulting in the edited form that renders the channel impermeable to Ca^{2+} (Wright & Vissel, 2012). In gliomas, the Glu2A subunit is commonly expressed in its non-edited form, which allows for Ca^{2+} permeability (Brocke et al., 2010; Maas et al., 2001; Venkataramani et al., 2019; Venkatesh et al., 2019). This altered expression of GluA2 in gliomas promotes migration and proliferation of tumor cells (Ishiuchi et al., 2002). In many GB, the expression of GluA2 is lacking, resulting in AMPA receptors that are permeable to Ca^{2+} (Stepulak et al., 2009). The absence of GRIA2 expression has been associated with a poor prognosis in GB (Colman et al., 2010). The opening and closing of the AMPA receptor channel occur rapidly, within 1 ms, allowing for fast excitatory synaptic transmission (Traynelis et al., 2010). Due to their involvement in fast excitatory synaptic transmission, AMPA receptors are implicated in TRE.

Kainate receptors consist of five types of subunits GluK1, GluK2, GluK3, KA1, and KA2. They are organized into tetramers. GluK 1, GluK2, and GluK3 can form homomers, whereas KA1 and KA2 always require the presence of GluR subunits (Hollmann & Heinemann, 1994). The kainate receptor channel allows the passage of Na^{+} and K^{+}. Compared to NMDA and AMPA receptors, kainate receptors are less distributed in the brain, and their function, especially in glioma, is less understood. While they play a minor role in synaptic signaling, kainate receptors can impact neurotransmitter release when stimulated autocrine (Mayer, 2005; Song & Huganir, 2002). This autocrine stimulation can accelerate glioma progression (Lyons et al., 2007).

Metabotropic Glu receptors belong to the group C family of G-protein-coupled receptors. They can be organized into three groups: group one (mGlu1 and mGlu5), group two (mGlu2 and mGlu 3), and group three (mGlu4, mGlu6, mGlu7 and mGlu8). Groupe one metabotropic receptors are mainly found postsynaptically and are coupled to the enzyme phospholipase C. Once the receptor is activated, the associated G protein dissociates, and the coupled phospholipase C hydrolyzes phosphatidylinositol-4,5 biphosphate in the cell membrane to generate diacylglycerol and inositol triphosphate (IP3). IP3 can trigger the opening of Ca^{2+} channels in the endoplasmic reticulum, increasing Ca^{2+} concentrations in

the cytoplasm. This activation can also stimulate protein kinase C (PKC), which may phosphorylate downstream targets. Groups two and three metabotropic receptors are presynaptic and decrease NMDA receptor activity by inhibiting cyclic adenosine monophosphate synthesis through activating G proteins. The G proteins associated with metabotropic receptors can impact the PI3K/AKT and MAPK signaling pathways, which are essential for the regulation of cell survival and proliferation (Nakada et al., 2011). GB cells express all the different metabotropic receptors (Stepulak et al., 2009). However, mGluR3 is reported to have the highest expression level in GB (Wirsching et al., 2020).

After its binding to synaptic Glu receptors at the postsynaptic level, Glu can be transported back to the presynaptic neuron or taken up by glial cells for buffering and recycling. Glu buffering primarily occurs through the action of Na^+-dependent transporters, EAAT1 or EAAT2, also named Glt-1 and Glast, respectively. Under normal conditions, the extracellular Glu concentration is approximately 25 nM (Herman et al., 2011). However, extracellular Glu concentrations can be significantly increased in the tumor and peritumoral areas. Studies have reported that extracellular Glu levels in these areas can be up to 100 times higher than normal levels (de Groot & Sontheimer, 2011), and in some patients, Glu concentrations as high as 100 µM have been reported (Marcus et al., 2010).

Indeed, the increase in extracellular Glu levels in gliomas can be attributed to various mechanisms. Unlike astrocytes that typically buffer Glu, glioma cells release Glu. In culture conditions, a monolayer of glioma cells can produce Glu concentrations of 500 µM after 12 hours (Ye et al., 1999). Additionally, the decrease in adenosine signaling in glioma cells plays a role in the dysregulation of Glu homeostasis. Adenosine is usually released into the extracellular space through the pannexin 1 channels. However, pannexins are downregulated in glioma cells, leading to a decrease in extracellular adenosine levels (Dossi, Vasile, et al., 2018). Low adenosine levels result in decreased activation of presynaptic adenosine receptors, increasing Glu release. This dysregulated adenosine-Glu interplay further contributes to the elevated extracellular levels of Glu in gliomas (De Groot et al., 2012).

In addition to the dysregulation of Glu transporters EAAT 1 and EAAT 2 in peritumoral astrocytes (Ye et al., 1999; Yuen et al., 2012), other factors contributed to the impaired buffering of extracellular Glu. Microglia, when activated, also exhibit decreased expression of EAAT2, further contributing to the impaired buffering of extracellular Glu (Buckingham & Robel, 2013). The downregulation of EAAT2 expression is particularly pronounced in GB, while LGG tends to maintain higher levels of EAAT2 (De Groot et al., 2005). Moreover, glioma cells themselves present an upregulation in the cystine-glutamate transporter (xCT), which imports cystine into glioma cells in exchange for Glu. This upregulation of xCT is driven by hypoxia due to a fast-growing (Long et al., 2020). Inside the glioma cells, cystine is transformed into glutathione, an antioxidant that protects tumor cells (de Groot & Sontheimer, 2011; Takano et al., 2001; Ye et al., 1999). However, this process leads to a net release of Glu into the extracellular space, further contributing to elevated Glu levels. Gliomas with IDH 1/2 mutations can also produce high intra and extracellular D2HG concentrations. D2HG, due to its structural similarity to Glu, can have an agonist glutamatergic effect, as described earlier in chapter one (Andronesi et al., 2012; Yan et al., 2009).

The elevated Glu concentration in gliomas has various biological effects, primarily by stimulating its different receptors. It enhances epileptic activities by stimulating NMDA and AMPA receptors, promoting the emergence of synchronous epileptic discharges (Watkins & Sontheimer, 2011). A murine glioma xenograft model study demonstrated a correlation between increased Glu levels and the presence of epileptic activities (Buckingham et al., 2011). Higher Glu levels have also been linked with the presence of TRE (Yuen et al., 2012). Patients with IDH1/2 mutations and those overexpressing the xCT transporter are commonly associated with seizures, likely due to excessive NMDA and AMPA receptors stimulation. Furthermore, the excessive stimulation of NMDA receptors can trigger excitotoxicity, leading to neuronal death and creating space for tumor cell expansion. Excessive NMDA stimulation results in sustained Ca^{2+} influx, triggering the caspase pathway and ultimately leading to apoptosis in postsynaptic neurons (Noch & Khalili, 2009; Sontheimer, 2003). As the space within the skull is limited, brain tumors require room to grow. Neuronal and glial death by excitotoxicity creates space for invasive tumor cells (Ye et al., 1999).

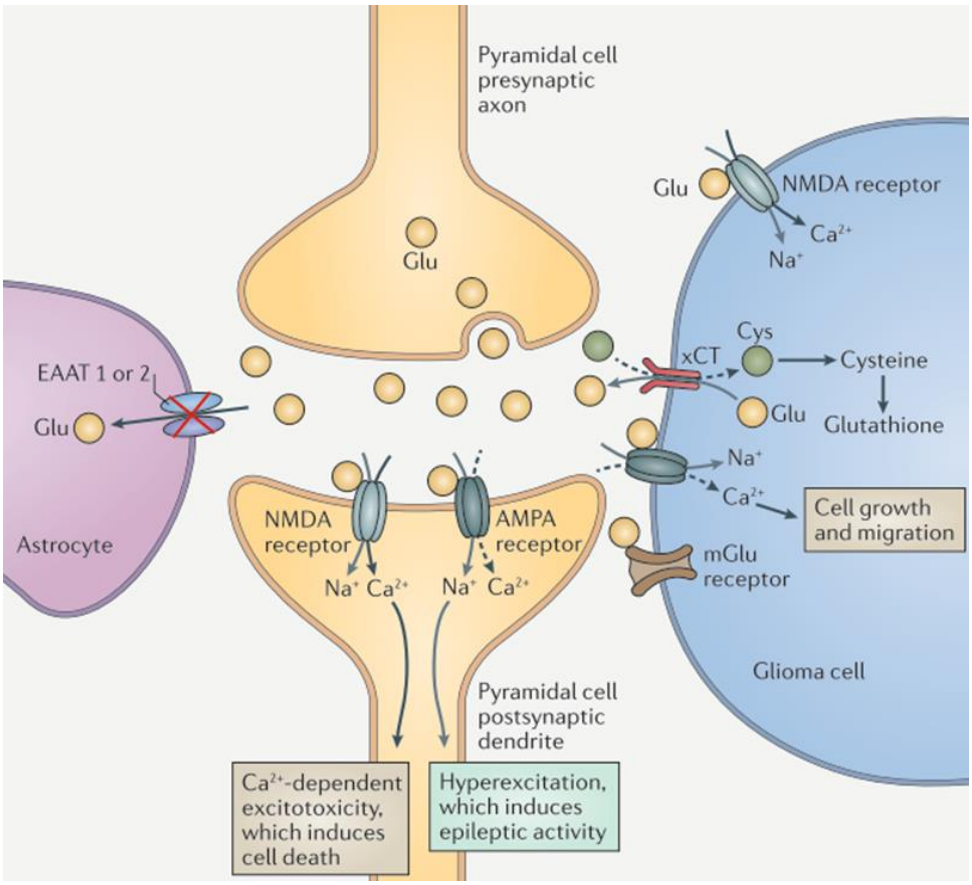

Figure 19: Glutamatergic signaling impairment in gliomas.
From Huberfeld and Vecht, 2016.

The PI3K-mTOR pathway modulates cell growth, proliferation, cell morphology, longevity, and migration (Cases-Cunillera et al., 2022). The mTOR pathway is activated in peritumoral tissues from epileptic patients, while Western Blots analysis have shown that

mTOR and S6k protein are inactivated in glioma patients without TRE (Yuan et al., 2017). The mTOR pathway alterations can contribute to epilepsy by affecting axonal and dendritic growth and altering neuronal excitability (Lipton & Sahin, 2014; Schubert-Bast et al., 2019). In gliomas, hyperactivation of the mTOR pathway can occur due to changes in the PI3K-Akt pathway and PTEN mutations (Knobbe et al., 2002). Stimulation of NMDA and AMPA receptors, as well as activation of G proteins coupled to metabotropic Glu receptors, can activate the PI3K-Akt pathway, leading to epileptogenesis and tumor growth (Lyons et al., 2007; Yuen et al., 2012). Moreover, the oncometabolite D2HG can induce changes in cells' metabolic profile, including alterations in the Krebs cycle and hypermetabolic phenotypes (Böttcher et al., 2018; Carbonneau et al., 2016). D2HG inhibits alpha KG-dependent dioxygenases (Garrett et al., 2018; Yang et al., 2012), resulting in altered protein interactions and gene expression and impacting the metabolic profile of the cell and activity (Yuan et al., 2013). The activation of the mTOR pathway has been associated with the presence of D2HG (Crino, 2016). Probably more mechanisms are implicated in mTOR activation, and more studies are needed to decipher new activation pathways. In a recent study using tumor slices from IDH-mutated patients with a pharmacoresistant TRE, metabolic alterations in the peritumoral cortex induced by mTOR activation driven by D2HG played a crucial role in TRE. In the study, the mTOR inhibitor, rapamycin, reduced neuronal firing, highlighting the potential therapeutic implications of targeting the mTOR pathway in TRE (Mortazavi et al., 2022).

Astrocytes are a key component of the synapse. In addition to their supportive functions, they are also involved in synaptic transmission and act as modulators of neurons (Rouach et al., 2008). Astrocytes can be modulated by neuronal activity, typically through the action of Glu (Haydon, 2001). Interestingly, they can also release Glu themselves (Angulo et al., 2004). Moreover, astrocytes can extrude ATP, which is converted into adenosine. Adenosine, in turn, inhibits Glu release by activating presynaptic A1 adenosine receptors (Pascual et al., 2005). Additionally, astrocytes clear the neurotransmitters from the synaptic cleft, and they are responsible for K^+ homeostasis. Kir 4.1 astrocytic channels are responsible for buffering extracellular K^+ (Olsen & Sontheimer, 2008; Zurolo et al., 2012). Following sustained neuronal activity, extracellular K^+ concentration increases, leading to hyperexcitability (Heinemann et al., 1977). Given the small size of the perisynaptic space, rapid control of K^+ levels is crucial, as a single action potential can increase K^+ concentration by up to 1 mM (Buckingham & Robel, 2013). Under normal conditions, astrocytes efficiently uptake excessive K^+, and through their gap junctions, K^+ is redistributed within the astrocytic network towards areas with lower K^+ concentrations (Walz, 2002). However, Kir 4.1 channels are barely expressed at the cell membrane in glioma cells, resulting in extracellular K^+ accumulation (Higashimori & Sontheimer, 2007; Zurolo et al., 2012). Kir 4.1 are internalized to the nucleus because glioma cells require high intracellular K^+ concentrations for migration and proliferation, (Olsen & Sontheimer, 2008). Moreover, the peritumoral cortex of epileptic glioma patients also exhibits alterations in glial gap junctions, for example, an increase in connexin 43 protein, suggesting an enlargement in astrocytic gap junctions (Aronica et al., 2001; Beaumont & Whittle, 2000).

Recently, it has been demonstrated that in GB, approximately 5% of cells form networks displaying autonomous periodic Ca^{2+} activity (Osswald et al., 2015). These rhythmic Ca^{2+} waves can potentially influence tumor growth by activating the MAPK and NF-KB pathways (Hausmann et al., 2023). Therefore, investigating the behavior of autonomous

GB cells and their possible contribution to epileptogenesis holds significant research interest.

2.2.1.3 Non-synaptic mechanisms

The tumor growth can significantly impact the surrounding brain tissue and disrupt its normal functioning. LGG with TRE usually presents larger volumes than patients without TRE (Lee et al., 2014), suggesting that a longer growth period allows for modifying the surrounding tissue, ultimately leading to epilepsy (de Groot & Sontheimer, 2011). The slow and progressive growth over the course of years can result in the isolation of cortical areas by deafferentation, which ultimately contributes to epileptogenicity (Beaumont & Whittle, 2000). While pyramidal cells may survive the deafferentation process, there is a more prominent loss of parvalbumin-interneurons, causing a reduction in inhibitory signaling (Daumas-Duport et al., 1997; Senner et al., 2004). Consequently, there is an imbalance between excitation and inhibition within the affected brain regions (Beaumont & Whittle, 2000; Haglund et al., 1992; Marczynski, 1998). On the other hand, GB, known for its rapid growth, can induce severe vascular changes due to the peritumoral edema and mass effect leading to ischemia (Beaumont & Whittle, 2000; Rosati et al., 2009; Shamji et al., 2009). GB are prone to bleeding and necrosis, which can induce epileptogenesis (Shamji et al., 2009). However, since there is no clear association between the edema, mass effect, necrosis, and TRE, the tumor-specific characteristics seem less important than the synaptic interactions between the tumor and the surrounding tissue in TRE (Beaumont & Whittle, 2000; van Breemen et al., 2007).

The peritumoral pH is significantly elevated in the tumor and surrounding areas compared to the normal cortex (Beaumont & Whittle, 2000). This alkalization of the local environment increases the likelihood of seizures through several mechanisms. Firstly, it reduces GABA conductance (Pasternack et al., 1992). Secondly, it removes inhibition on NMDA receptors (Tang et al., 1990). Lastly, it blocks inward K^+ currents (Moody, 1984) and favors gap-junction coupling.

The alteration of the blood-brain barrier (BBB), especially in HGG, allows the release of various molecules into the brain parenchyma, including albumin, growth factors, and immunoglobulins (Buckingham & Robel, 2013). The released albumin is taken up by astrocytes, which triggers the downregulation of the Kir 4.1 K^+ channels (Ivens et al., 2007).

GAP junctions facilitate direct electric communication between cells very fast, without the delay associated with synaptic transmission. The assemblage of connexins forms the GAP channels. The opening and closing of the channel can be modulated by intracellular Ca^{2+}, pH, and voltage. Connexin 36 is specific to neurons, while astrocytes can express connexin 30 and 43. Gap junctions are important during development, and their number decrease in adulthood. In adult stages, they are predominantly expressed in interneurons (Traub et al., 2011). Since GAP junctions contribute to the synchronization of pyramidal cells or interneurons, they may be implicated in epileptogenesis (Beierlein et al., 2000).

Ephaptic transmission, on the other hand, involves the synchronization of neurons that are oriented in parallel. This synchronization occurs due to the electric field generated by the

neuronal activity in the membrane potential of nearby dendrites (Jefferys, 1995). Ephaptic transmission could represent an additional mechanism implicated in TRE.

Proinflammatory molecules, including cytokines and interleukins, can lead to endothelial damage resulting in seizures (Gust et al., 2017; Mostofa et al., 2017).

2.2.2 Ictogenesis

Ictogenesis is the process leading to a seizure in a brain that has already undergone the epileptogenesis process. While epileptogenesis may take years, ictogenesis typically lasts for tens of minutes. Seizures are characterized by abnormal, excessive, and hypersynchronous neuronal activity, accompanied by symptoms and signs that can persist from seconds to minutes.

In vivo studies have shown that seizure onset patterns recorded through sEEG can be highly complex (Lagarde et al., 2019). Researchers have identified eight seizure onset patterns in sEEG recordings of the mesial temporal lobe and neocortical epilepsies. These patterns are:

- The low voltage (< 30 µV) fast activity oscillations (> 14 Hz) pattern (LVFA) pattern.
- LVFA pattern preceded by a preictal spiking of 5-20 seconds consisting of rhythmic spikes at low frequency (≤3 Hz), high amplitude.
- LVFA pattern preceded by a short (< 5 seconds) burst of polyspikes at >12 Hz with high amplitude.
- LVFA preceded by a slow wave or baseline shift
- Low frequency (6 – 14 Hz) rhythmic spikes or spike waves with high amplitude.
- Sharp theta/alpha activity with progressive increasing amplitude
- Sharp beta activity with sinusoid activity with progressive increasing amplitude
- Delta-brush, with bursts of low-amplitude gamma activity upon delta sinusoidal activity

In ex vivo experiments, we can induce ictal-like events (ILE) in animal and human brain slices using several approaches that enhance neuronal excitability. One such method involves increasing the extracellular K^+ concentration. Additionally, reducing the concentrations of Ca^{2+} or Mg^{2+}, alkalization, or 4AP (K^+ channel blocker) application, are other techniques used to induce ILE (Huberfeld et al., 2011). It is essential to consider the limitations and potential artifacts associated with experimental slice preparation. While slice models provide valuable insights into neuronal and network properties, they do not fully replicate the in vivo microenvironment and connectivity.

Ex vivo models provide a valuable approach to studying the ictogenesis process, as they allow us to overcome the temporal limitation associated with long recordings required for studying these processes. By inducing ILE in acute and chronic epileptic models, researchers can gain quick access to the seizure initiation period. While animal models have been very important to increase our understanding of ictogenesis, it is essential to note that animal conditions may not precisely mirror those in humans (Milior et al., 2023). However, human tissue offers a more accurate representation of human epilepsy. In the context of glioma, it is possible to have access to the excess tissue that is not essential for diagnosis and study it ex vivo. The surgical procedure is not modified due to the use of human tissue, and only the excess security margin surrounding the tumor is used. Gliomas, since they are

highly epileptic tumors, provide a good model for studying ictogenesis. Epileptic activities are typically initiated in the peritumoral area, likely in areas infiltrated by tumor cells (Mittal et al., 2016; Pallud et al., 2015), rather than in the tumor core. Therefore, studying peritumoral brain slices allows a more focused examination of ictogenesis.

In ex vivo peritumoral human slices, we find two different ILE patterns (Dossi, Blauwblomme, et al., 2018; Huberfeld et al., 2011, Pallud et al., 2014):

- The low voltage (< 30 µV) fast activity oscillations (> 14 Hz) pattern (LVFA) pattern.

- The hypersynchronous (HS) pattern that starts directly with rhythmic, high-amplitude discharges lacking initial fast discharges.

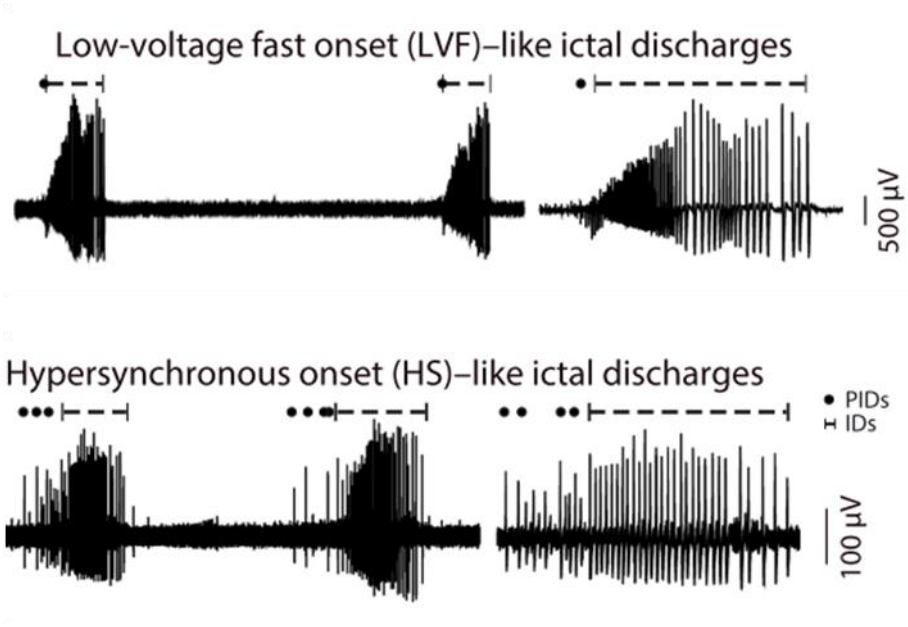

Figure 20: Ex vivo human ILE patterns.
From Dossi et al, 2018.

During the interictal period, which is much longer than the duration of seizures, spontaneous interictal discharges (IIDs) are observed. Due to their brief duration, ranging from 10 to 100 ms, IIDs do not provoke obvious paroxysmal symptoms in patients (De Curtis & Avanzini, 2001). However, recent studies have shown that IIDs can affect memory consolidation during sleep, inducing an alteration in cognitive functioning (Okadome et al., 2022). Traditionally, IIDs are a biomarker of epileptogenicity, but their precise role of IIDs is not yet totally understood since several studies have shown that IIDs rate decrease before seizures (Karoly et al., 2016) and increases after seizures (Gotman & Marciani, 1985). Moreover, a higher IIDs rate is associated with longer periods to the first seizure in intracranial recordings (Goncharova et al., 2016). In vivo recordings such as EEG, sEEG, and ECoG capture IIDs in the form of spikes. These spikes can be observed in the peritumoral tissue rather than in the tumor (Mittal et al., 2016; Tran et al., 1997). In vitro studies using peritumoral human tissues can present spontaneous IIDs. IIDs are a marker of tissue's epileptogenicity since they are not observed in non-epileptic tissues (Dossi,

Blauwblomme, et al., 2018). IIDs are triggered by interneuron spiking, depolarizing almost 65% of pyramidal cells (Pallud et al., 2014).

The preictal state is the transitional period between the interictal state and the seizure onset (Richardson & Jefferys, 2011). The preictal period is crucial for anticipating seizures since seizures tend to occur in temporal clusters rather than randomly, both in animals and humans (Karoly et al., 2021; Williams et al., 2009). Non-linear analysis methods have been applied to preictal EEG and sEEG recordings, revealing changes in brain activity in the minutes to hours leading up to a seizure (Lehnertz & Litt, 2005; Litt & Lehnertz, 2002). Hemodynamic changes, such as increased regional cerebral blood flow, have also been detected before seizure onset (Baumgartner et al., 1998). An increase in the BOLD fMRI signal was observed before seizure beginning (Federico et al., 2005). Furthermore, changes in heart rate (Kerem & Geva, 2005) and clinical prodromes, such as self-prediction of a seizure or noise sensitivity, have been reported during this transitional period (Cousyn et al., 2021). These various indicators suggest that detectable physiological and clinical changes precede a seizure, allowing for potential seizure anticipation and prediction. Microelectrodes recordings have shown that neuronal activity changes in the minutes before the seizure (Lambrecq et al., 2017; Stead et al., 2010). But not all the neurons fire before seizures (Truccolo et al., 2011).

Predicting the occurrence of seizures remains a complex task, but significant progress has been made in seizure forecasting over the last decade. One notable advancement is the application of machine learning algorithms. These algorithms analyze various features, including non-EEG-based data such as heart rate changes, behavioral changes, physiological biomarkers, or cyclic circadian and ultradian patterns (Stirling et al., 2021). However, these algorithmic approaches often do not consider the underlying physiopathology of seizures. Seizure forecasting models primarily focus on pattern recognition (Mormann et al., 2007).

However, the transition between the interictal period and the beginning of a seizure occurs remains poorly understood nowadays. Ex vivo, towards the transition to an ILE, a new kind of discharge progressively appears: the preictal discharges (PIDs) (Huberfeld et al., 2011). PIDs gradually emerge when we increase the excitability of the tissue in the minutes that precede the onset of the ILE. PIDs are characterized by high amplitude field potential (FP). Throughout the temporal evolution of the preictal period, PIDs show a progressive increase in amplitude until reaching full development. In the seconds preceding the ILE, PIDs present clustering (Huberfeld et al., 2011). Similar patterns of PIDs have also been observed in vivo on sEEG human recordings (Huberfeld et al., 2011; Lagarde et al., 2019).

PIDs depend on glutamatergic signaling (Huberfeld et al., 2011). When $GABA_A$ antagonists such as bicuculline or picrotoxine are applied, they block IIDs but not PIDs. This indicates that PIDs have a different underlying mechanism than IIDs. Furthermore, the NMDA receptor antagonist AP5 has been found to prevent the formation of PIDs, suggesting that NMDA receptor-mediated plasticity mechanisms play a role in the emergence of PIDs. However, once PIDs are fully established, the application of AP5 does not affect their maintenance. This suggests that NMDA signaling is unnecessary to maintain PIDs once fully developed. On the other hand, AMPA receptor antagonist NBQX has been shown to suppress PID, indicating that AMPA receptor-mediated glutamatergic signaling is involved in both the generation and maintenance of PIDs (Huberfeld et al., 2011).

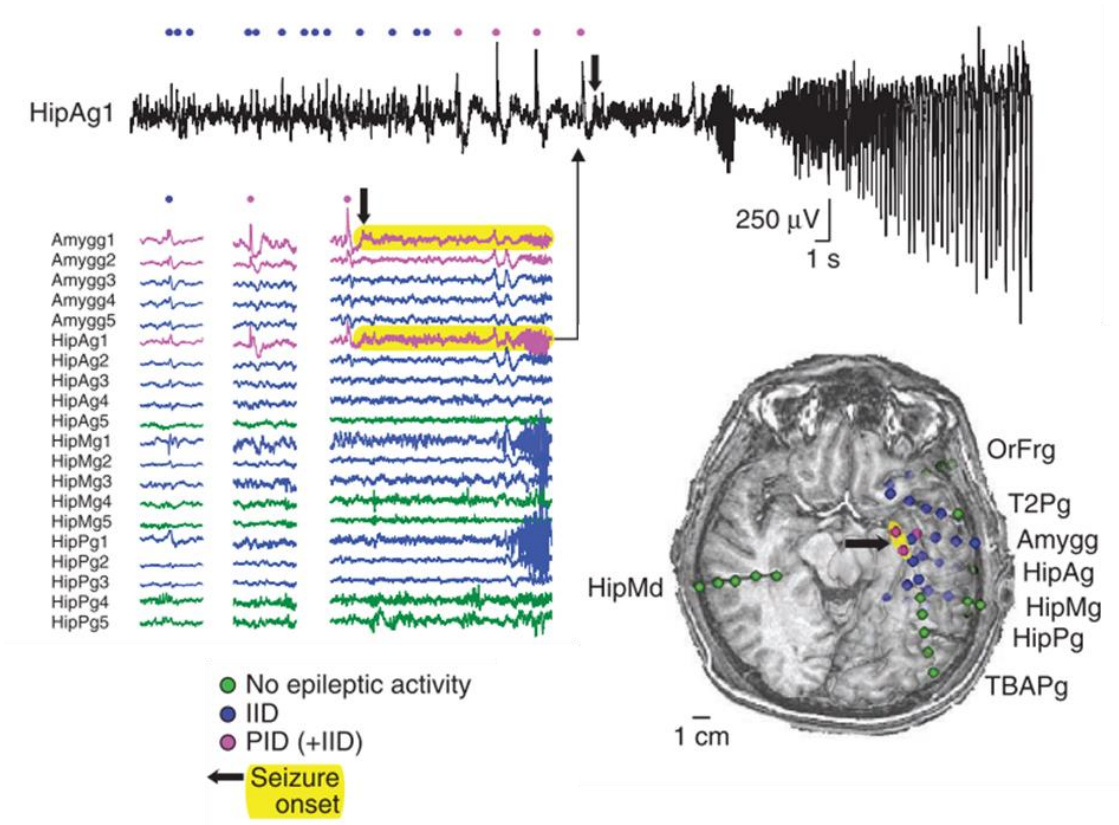

Figure 21: PIDs progressively appear in the minutes preceding a seizure and are similar to in vivo recordings.
From Huberfeld et al, 2011.

Glutamatergic signaling primarily depends on pyramidal cells. We already know that pyramidal cells fire during seizures, but their contribution to ictogenesis is still a matter of debate. Optogenetics, a technique involving light-sensitive ion channel expression in specific cell populations, has provided valuable insights into brain functioning (Boyden et al., 2005). By using optogenetic approaches, it has been shown that we can induce seizures by stimulating pyramidal cells (Cela et al., 2019; Losi et al., 2016). During PIDs, a significant number of the pyramidal cells fire. This firing is maximum when we approach the beginning of the ILE (Jensen & Yaari, 1997). However, at the onset of the ILE, pyramidal cells remain silent while interneurons exhibit their maximal firing (Ziburkus et al., 2006), suggesting that interneurons are responsible for seizure initiation. The dynamics

and interactions between pyramidal cells and interneurons during ictogenesis are complex and still require further investigation.

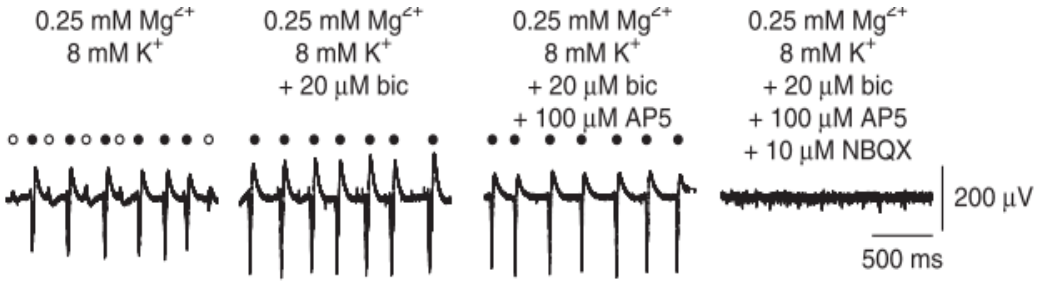

Figure 22: Glu signaling is implicated in PIDs genesis
From Huberfeld et al, 2011.

Under normal conditions, GABA stimulation has antiepileptic effects. In the seconds preceding the onset of an ILE and during its initial phase, interneurons increase their firing in animal models (Lillis et al., 2012; Ziburkus et al., 2006) and in humans (Elahian et al., 2018). Even in models with enhanced Glu signaling, such as the 0 Mg^{2+} model, pyramidal activation is preceded by interneuron firing (Parrish et al., 2019).

Optogenetic activation of interneurons has been shown to induce seizures. Activation of all interneurons in the somatosensory cortex leads to seizures (Chang et al., 2018). Similarly, selective stimulation of specific populations of interneurons, such as parvalbumin in the hippocampus (Sessolo et al., 2015) or somatostatin interneurons in the entorhinal cortex (Yekhlef et al., 2015), can also induce seizures. Pharmacological inactivation of interneurons using the µ-opioid agonist DAGO has been found to suppress ILE in human peritumoral slices (Pallud, Le Van Quyen, et al., 2014).

But how can interneurons trigger seizures? Several mechanisms may be implicated. One mechanism involves the depolarizing effect of GABA under certain conditions. As described previously in the epileptogenesis chapter, GABA stimulation can also present a depolarizing effect, depending on Cl^- homeostasis. Under normal physiological conditions, GABA binding to $GABA_A$ receptors results in Cl^- influx, leading to hyperpolarization. However, under pathological conditions, as in glioma, Cl^- homeostasis can be impaired due to alterations in Cl^- transporters NKCC1 and KCC2. This disruption results in elevated intracellular Cl^- levels, causing Cl^- efflux when the GABA channel opens, inducing depolarization. This depolarizing effect of GABA has been observed in 65% of peritumoral pyramidal cells (Pallud, Le Van Quyen, et al., 2014). Pyramidal cells without Cl^- homeostasis alteration fire during the IIDs but do not start the IIDs.

During epileptogenesis, there is evidence of a progressive loss of interneurons, including a decrease in parvalbumin interneurons in gliomas (Daumas-Duport et al., 1997; Senner et al., 2004). However, the remaining interneurons can reorganize their axonal connections. It has been observed in the hippocampus that there is a decrease in dendritic inhibition and an increase in somatic inhibition (Cossart et al., 2001; Wittner et al., 2005). This GABAergic reorganization allows a precise time window during which pyramidal cells can

fire. Therefore, coordinated interneuron inhibition by gap junction (Skinner et al., 1999) can lead to synchronized pyramidal firing (Cobb et al., 1995; Wenzel et al., 2019).

GABA depolarizing effects may appear more prominent in slices than in vivo conditions. This could be attributed to the slicing process itself, which can result in the release of intracellular components such as K^+ and Glu, as well as the deafferentation of cells (Conti, et al., 2011).

During ictogenesis, sustained neuronal activity can increase extracellular K^+ levels. In high extracellular K^+ conditions, the KCC2 transporter, responsible for maintaining low intracellular Cl^- levels, can reverse its directionality. This reversal of the KCC2 transporter leads to an influx of both K^+ and Cl^-, contributing to the depolarizing effects of GABA (Payne, 1997). In line with this, $GABA_A$ receptor antagonists have been shown to suppress ILE (Behr et al., 2014; Huberfeld et al., 2011).

Several factors that are important in epileptogenesis can also impact ictogenesis, including the increase in extracellular K^+, Ca^{2+} decrease, osmolarity changes, and ephaptic transmission. The K^+ increase can be attributed to the increased neuronal firing of interneurons and pyramidal cells. As interneurons fire at an increased frequency, the continuous opening of the GABA channel leads to Cl^- influx. To maintain Cl^- homeostasis, the KCC2 transporter releases K^+ along with Cl^- (Viitanen et al., 2010). Astrocytes also contribute to the regulation of extracellular by actively removing K^+ following GABA astrocytic stimulation (Fraser et al., 1995). Furthermore, the EAAT2 transporter, responsible for the uptake of Glu, releases at the same time K^+ (Bjørnsen et al., 2007). Downregulation of Kir 4.1, a K^+ inwardly-rectifying channel, has been observed in gliomas, potentially further impacting K^+ homeostasis.

Extracellular Ca^{2+} levels are decreased due to the increase in K^+ levels. The elevated K^+ levels can lead to increased excitability and subsequent entry of Ca^{2+} into the cells (Heinemann et al., 1977). Osmolarity modifies the size of the extracellular space (Fox et al., 2007). During the period of neuronal activity, cells can swell, decreasing the extracellular space and favoring seizures (Fox et al., 2007). The decrease of extracellular space results in increased concentrations of ions and neurotransmitters in the extracellular environment, potentially exacerbating neuronal excitability. Moreover, ephaptic transmission can be more efficient when the extracellular space is reduced. A smaller extracellular space allows for faster and more efficient synchronization of larger populations of neurons, contributing to the spread and propagation of seizure activity (Buzsáki et al., 2012).

2.2.3 Epileptogenicity biomarkers

The different epilepsy biomarkers will be further developed in the next chapter. The traditional biomarker of epileptogenicity are IIDs (Gallotto & Seeck, 2022). The brain region where we can detect the presence of IIDs is known as the irritative zone. However, we know that in pharmacoresistant patients, it is not enough to remove the irritative area to achieve seizure control. The seizure onset zone (SOZ) presents better outcomes when it is removed. The epileptogenic zone was first described by Luders in 1993 as “the area of cortex that is necessary and sufficient for initiating seizures and whose removal (or disconnection) is necessary for the complete abolition of seizures” (Luders et al, 1993).

2.3 Tumor growth

2.3.1 Mechanisms involving neuronal interactions

In the previous chapters, I have explained how the tumor microenvironment influences neurons. Dysregulations provoked by tumor cells, as for example, the excess of Glu release, can lead to epilepsy and neuronal death. But the interactions between neurons and tumor cells are bidirectional. Neuronal activity can also promote tumor growth (Bikfalvi et al., 2023; Venkataramani et al., 2019, 2022; Venkatesh et al., 2019). Intrinsic cellular mechanisms and the surrounding microenvironment regulate glioma growth. In this chapter, I will develop how neuronal activity can enhance tumor growth.

As described before, gliomas present a dysregulation of glutamatergic signaling. Different mechanisms increase the tumor and peritumoral Glu concentrations, such as the release of Glu by tumor cells, the downregulation in astrocytic Glu buffering, the extrusion of Glu by the xCT system, and the structural similarity of D2HG with Glu molecule. Glutamatergic signaling impairment can provoke seizures and promote tumor growth (de Groot & Sontheimer, 2011).

In physiological conditions, brain AMPA and NMDA receptors function as ion channels and play essential roles in activating intracellular signal pathways, leading to tumor proliferation. AMPA receptors can trigger intracellular signaling cascades, including the mitogen-activated protein kinase (MAPK) pathway (Reddy et al., 2003) and the Akt pathway (Ishiuchi et al., 2007). Activation of the MAPK pathway can regulate cellular processes such as cell proliferation, differentiation, and survival. The Akt pathway is involved in promoting cell survival and inhibiting apoptosis. Similarly, NMDA receptors can regulate multiple intracellular signaling pathways, including mTOR-S6 kinase, AKT, and MAPK (Lenz & Avruch, 2005). These pathways control protein synthesis, cell growth, and survival. In gliomas, those effects are enhanced due to the increase of Glu concentration and the overexpression of Glu receptors, including not only NMDA (Stepulak et al., 2009) and AMPA (Colman et al., 2010) but also metabotropic receptors two and three (Arcella et al., 2005).

Glioma cells can exploit autocrine AMPA stimulation to promote their own proliferation and invasive behavior (Piao et al., 2009; Reddy et al., 2003). The autocrine activation of AMPA receptors of glioma cells provokes a Ca^{2+} influx since they lack the expression of the GluR2 subunit, making them permeable to Ca^{2+} (de Groot & Sontheimer, 2011). The overexpression of GluR subunits in glioma AMPA receptors further contributes to their tumorigenic properties. Activating AMPA receptors leads to the upregulation of β1-integrin and focal adhesion kinase (FAK), which are proteins involved in cell adhesion to the extracellular matrix. This increased adhesion to extracellular matrix collagen enhances glioma cells' motility and invasive potential, allowing them to spread and infiltrate surrounding brain tissue (de Groot & Sontheimer, 2011; Piao et al., 2009). Additionally, autocrine AMPA stimulation induces cellular detachment, promoting their migration both in ex vivo and in vivo conditions (Piao et al., 2009).

The activation of AMPA receptors increases the intracellular Ca^{2+} levels, activating the PI3K/Akt pathway by promoting EGFR expression (Schunemann et al., 2010). The PI3K/Akt pathway is crucial for the expression of the malignant phenotype of glioma (Knobbe et al., 2002). Dysregulation of membrane receptor tyrosine kinases, including EGFR, PDGFR, and IGF-1R, activates the Ras/MAPK pathway and contributes to glioma growth and progression (Besson & Yong, 2001).

Similarly, NMDA receptors are also overexpressed in glioma cells (Stepulak et al., 2009), and their autocrine stimulation promotes glioma proliferation and motility (Lyons et al., 2007; Takano et al., 2001). Intracellular Ca^{2+} increase induced by NMDA receptor activation increases glioma proliferation (Rzeski et al., 2001). Interestingly, inhibition of the NMDA receptor has been shown to decrease glioma growth (Rzeski et al., 2001). Furthermore, NDMA excessive stimulation triggers neuronal excitotoxicity, to make space for tumor invasion (Buckingham et al., 2011).

Despite this increase in Glu signaling, IDH-mutated patients generally have a better oncological prognosis than IDH-WT gliomas. But inhibiting mutated IDH functions improves prognosis, at least progression free survival from 27.7 months vs. 11.1 months (Mellinghoff et al., 2023). The exact role of D2HG in this context is still not fully understood, and its interactions with Glu signaling are complex. It has been shown that D2HG can act as a Glu agonist, contributing to the increase in Glu signaling in IDH-mutated patients. This increased Glu signaling can lead to a higher frequency of epilepsy in these patients. On the other hand, Glu signaling is also associated with tumor growth and invasion, as discussed previously. However, we could think that IDH-mutated patients will present more aggressive tumors and shorter overall survival. But this is not the case, IDH-mutated patients show better oncological prognosis, which looks paradoxical. The interplay between D2HG and Glu signaling may have complex and opposing effects on tumor behavior. It is possible that D2HG could influence glioma growth and survival in a manner that counteracts the pro-tumorigenic effects of increased Glu signaling. Maybe D2HG can act differently in the presence or absence of Glu, as explained in the first chapter. Deciphering all various effects of D2HG and IDH mutations will help distinguishing favorable vs deleterious ones.

GABA signaling impairment also contributes to tumor growth and invasion in gliomas. The dysregulation of Cl^- levels in tumoral and peritumoral areas results in a GABA depolarizing effect. Usually, GABA acts as an inhibitory neurotransmitter, causing hyperpolarization of neuronal membranes. However, in gliomas, the dysregulated Cl^- levels result in a depolarizing effect, leading to the opening of GABA channels and the efflux of Cl^- ions to the extracellular space. That provokes that the intracellular medium becomes hypoosmotic compared to the extracellular level. As a result, water exits the cells through aquaporin channels, causing the glioma cells to shrink (McCoy & Sontheimer, 2007). This volume decrease is associated with the initiation of the premitotic phase of the cell cycle (Cuddapah et al., 2012). The volume changes of glioma cells aid in their migration through small spaces along the fiber bundles and perivascular spaces (Ernest et al., 2005; Habela et al., 2009; Watkins & Sontheimer, 2011). Glioma cells are also expressing the Cl^- importer NKCC1 which increases intracellular concentrations of Cl^- during the intermitotic period (Ernest et al., 2005; Garzon-Muvdi et al., 2012; Haas & Sontheimer, 2010; Habela et al., 2009). NKCC1 expression correlates with GB severity (Garzon-Muvdi et al., 2012). A huge Cl^- extrusion through various channels precedes both mitosis and migration (Cuddapah et al., 2012), triggered by Ca^{2+} signals generated by AMPA and bradykinin receptors

activation (Lyons et al., 2007). Expression of $GABA_A$ receptors by tumors reduces their ability to accumulate Cl^- (leaking by activated $GABA_A$ channels) which counteracts theses mechanisms.

Glioma cells present long membrane protrusions, the tumor microtubes. They are driven by pathways involved in neuroplasticity and neurodevelopment, which suggests that the tumor cells hijack normal cellular mechanisms to create these structures (Osswald et al., 2015). The microtubes allow glioma cells to communicate with each other via gap junctions (Osswald et al., 2015; Winkler & Wick, 2018). This communication network within the tumor is known as the glioma network. The presence of gap junctions and Ca^{2+} wave communication between glioma cells can enhance their collective behavior (Hausmann et al., 2023) and make the tumor more resistant to conventional treatments such as chemotherapy and radiotherapy (Venkataramani et al., 2019; Venkatesh et al., 2019; Weil et al., 2017). The glioma network also plays a role in tumor recurrence after surgery. Even if some tumor cells are removed during surgery, the remaining network of interconnected cells can repair and regrow, leading to tumor recurrence (Weil et al., 2017)

This year it was shown that GB networks include a small tumor population (1-5% of glioma cells) presenting autonomous rhythmic Ca^{2+} oscillations, referred to as "autonomous pacemaker cells". This subpopulation is highly connected to other glioma cells. These Ca^{2+} activities activate MAPK and NF-KB pathways, leading to tumor growth. The whole network viability depends on these "autonomous pacemaker cells". Physical ablation and genetic or pharmacological interference with these cells lead to a reduction in tumor growth in mice, with an increase in overall survival. This discovery paves the way for new drug targets (Hausmann et al., 2023). As this discovery was made in preclinical mouse models, further research and validation in human glioma samples will be essential to confirm the relevance of these findings in human patients.

Neuronal activity can also enhance tumor growth by increasing the expression of neuroligin- 3, which activates the PI3K-mTOR pathway in glioma cells (Venkatesh et al., 2015). Neuroligin-3 also triggers its autocrine secretion and induces synaptic gene expression in glioma cells (Venkatesh et al., 2017), suggesting that gliomas were probably implicated in synaptic processes. Finally, in 2019, using patch-clamp recordings of glioma cells, AMPA-like excitatory postsynaptic potentials were found, indicating the presence of functional synapses between neurons and glioma cells, which were found at the microtube level. In animal and human samples, those synapses were found in approximately 10% of glioma cells. These synapses consisted of AMPA receptors with edited GluA2 subunits that allow Ca^{2+} influx. They are probably reminiscent of the synapses on normal oligodendroglial precursor cells (Bergles et al., 2000). Synaptic connections between distant neuronal populations and glioma cells have been found recently, emphasizing the interconnected nature of glioma growth and neuronal activity (Huang-Hobbs et al., 2023). Optogenetics's AMPA activation on glioma cells in vivo was responsible for tumoral mitosis and migration (Venkatesh et al., 2019). On the other hand, proliferation and motility were reduced by the AMPA receptor antagonist perampanel and anesthesia (Venkataramani et al., 2019). Another in vivo mouse study found that increased neuronal activity around the tumor modulates tumor growth. If pyramidal cells increase their activity, the tumor grows, whereas if the interneuron population is more active, the tumor growth is slower (Tantillo et al., 2020). Glioma cell also presents other properties of normal astrocytes, such as the K^+ activity-dependent currents (Kuffler, 1967; Venkatesh et al.,

2019). Those activities are amplified by gap junction connections at the microtube level, forming an electrical network of glioma cells.

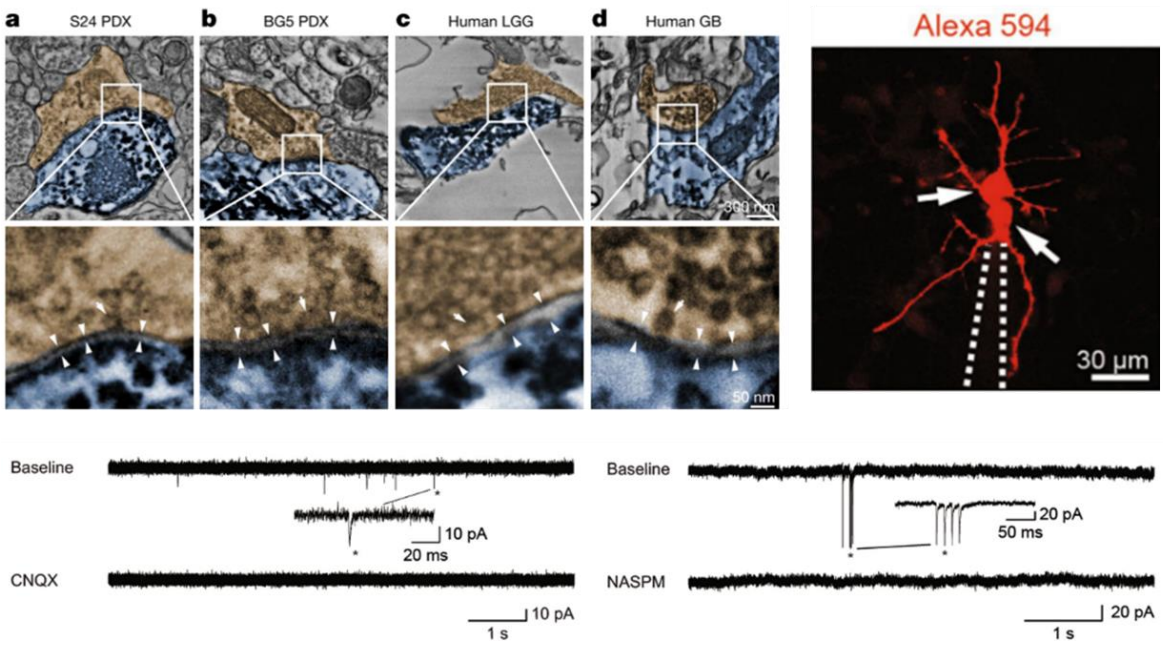

Figure 23: Functional AMPA synapses between neurons and glioma cells.
From Venkataramani et al, 2019.

Gliomas are very heterogeneous, with different subpopulations of tumor cells. This year, a study focused on determining how the different tumor subpopulations confer varying degrees of functional connectivity and how these disparities influence patient tumor growth. The authors obtained samples of GB tissues exhibiting diverse functional connectivity patterns, assessed by MEG recordings. Initially, employing bulk RNA sequencing analyses, they observed that areas with high connectivity (HC) displayed an upregulation of genes involved in neural circuit assembly. These genes included axon pathfinding genes (NTNG1), synapse-associated genes (SYNPO), and synaptogenic factors (THBS1). Then, through single-cell sequencing analysis of biopsy samples from regions with either HC or low connectivity (LC), they discovered that glioma cells from HC areas expressed higher levels of THBS1 than tumor cells from LC regions (Krishna et al., 2023). HC areas exhibited increased presynaptic and postsynaptic neuronal puncta compared to LC areas. Extracellular recordings from co-cultures of neurons and tumor cells expressing high levels of TSP1 (encoded by the THBS1 gene) revealed heightened neuronal activity and network synchrony in cultures with elevated TSP1 expression. Moreover, a fivefold increase in proliferation was observed in HC tumor cells co-cultured with murine neurons. In a murine xenografted model using HC or LC glioma cells, mice implanted with HC cells presented shorter survivals. It was also the case for patients with HC areas (71 weeks) compared to those without HC (123 weeks). Therefore, they concluded that HC areas manifest different synaptogenic and neurotropic phenotypes and promote tumor growth (Krishna et al., 2023).

On the other side of the coin, it remains uncertain whether neurons must be in close proximity to tumor cells to foster tumor growth. This year, another study demonstrated that

contralateral neurons with callosal projections actively promote tumor growth and infiltration in GB. The stimulation of these neurons placed in the contralateral hemisphere over two months led to a decrease in the median survival of mice (51 days) compared to mice receiving saline (95 days) (Huang-Hobbs et al., 2023). Stimulated mice also exhibited larger infiltrations. The disconnection of the corpus callosum halted the increase in infiltration rates. Single-cell RNA analysis of tumor cells under contralateral stimulation showed the presence of different subpopulations. The subpopulation localized in the infiltrating area expressed genes associated with glutamatergic synapses and axon guidance (Huang-Hobbs et al., 2023).

In conclusion, the integration of glioma cells into neuronal circuits provokes a vicious circle. Glioma cells increase neuronal activity, inducing epilepsy. Subsequently, they take advantage of this neuronal activation to promote their growth. The higher the activation of neuronal activity, the greater the stimulation of tumor growth (Krishna et al., 2023). However, clinical observation contradicts this notion, as patients with epilepsy present better oncological outcomes with slower growth rates. This paradox is similar to what was previously described when discussing the effects of Glu, which can boost both epilepsy and tumor growth. Therefore, is epilepsy genuinely represented by a continuous increase in neuronal activity? Or does its hyperactivity only appear during short periods, such as during the seizure and the preictal period, while during the interictal period, epileptic areas display lower activity levels, as suggested by the hypometabolism found in PET imaging of epileptic lesions? (Otsuki, 2004).

2.3.2 Biomarkers

The primary current biomarkers indicating the presence of tumor cells include the fluorescence of 5-ALA, Glu detection using APT-CEST, and detection of D2HG with 1H-MRS.

As described in Chapter 1, several neurosurgical teams employ intraoperative fluorescence surgery guided by 5- aminolevulinic acid (5-ALA) to detect tumor cells (Stummer et al., 2006). This technique relies on the ability of glioma cells to convert 5-ALA into protoporphyrin X, a fluorescent substance (Duffner et al., 2005). Before surgery, the patients receive 5-ALA intravenously. During the resection, an optic system integrated into the surgical microscope aids in identifying fluorescent areas where tumoral cells can be located (Zhang et al., 2017). However, the fluorescence level is significantly higher in HGG than in LGG, making this technique unsuitable for LGG resection (Ishihara et al., 2007; Ji et al., 2019). To visualize the low levels of fluorescence in LGG, a confocal microscope is required (Sanai, Snyder, et al., 2011), rendering this technique time-consuming

In IDH-mt gliomas, we can detect the presence of tumoral and peritumoral D2HG using 1H-MRS (Andronesi et al., 2012). Nevertheless, distinguishing D2HG from other spectral peaks, such as Glu and Gln, is a major challenge. There is currently no established cutoff value for differentiating IDH-mutated gliomas from IDH-WT (Pope et al., 2012). Moreover, spatial resolution in 1H-MSR is suboptimal, as the voxels used typically have a 3 cm^3 volume, leading to the inclusion of healthy tissue within the voxel and potentially impacting the results.

Given the significantly elevated Glu concentrations near tumor cells, detecting Glu through APT-CEST holds a substantial interest (Su et al., 2022; Warnert et al., 2022). A recent study employing APT-CEST demonstrated increased Glu concentration at the peritumoral level. Accurate Glu detection can help to delineate the extent of peritumoral infiltrated areas, leading to improved surgical planning (Neal et al., 2019).

Moreover, high-frequency oscillations (HFO) represent a promising candidate for detecting the presence of tumor cells. In a study performed on human peritumoral slices, HFO were found to be colocalized with the presence of infiltrative tumor cells. Interestingly, macroscopic tumors did not exhibit HFOs, and the rate of HFO occurrence was higher in highly infiltrated areas (Pallud, Le Van Quyen, et al., 2014). These findings suggest that HFO hold potential as an ex vivo biomarker of tumor infiltration. However, further investigations are needed to validate these results in an in vivo setting.

2.4 Towards a common treatment of epilepsy and tumor growth

2.4.1 Pharmacological targets

As described earlier, epilepsy and tumor growth share common mechanisms, primarily involving dysregulation in Glu and GABA signaling and overstimulation of the mTOR pathway. Therefore, targeting the different mechanisms involved in both processes could be a potential approach to treating simultaneously epilepsy and tumor growth. Numerous preclinical studies have explored the potential of blocking Glu transporters and receptors to improve seizure control and slow tumor growth. Several mechanisms contribute to the extracellular increase of Glu levels, including the upregulation of the xCT transporter, the downregulation of EAAT 1/2 channels, and D2HG production in IDH-mutated patients. xCT transporter imports glycine to convert it into glutathione while extruding Glu. One pharmacological agent used to block the xCT system is sulfasalazine, a drug approved for treating Crohn's disease. Sulfasalazine has been found to inhibit glioma cell invasion (Lyons et al., 2007) and proliferation (Chung & Sontheimer, 2009; Chung et al., 2005) in culture conditions. In mouse models, intracranial application of sulfasalazine has also decreased tumor growth (Lyons et al., 2007). Moreover, using small interfering RNA to block the xCT system in culture reduced the amount of extracellular Glu and the excitotoxic effect (Savaskan et al., 2008; Takano et al., 2001). Sulfasalazine may decrease epileptic activity also in ex vivo glioma mice slices (Buckingham et al., 2011). Recent evidence suggests that inhibiting the xCT transporter may improve epilepsy control not only in glioma models but also in different types of epilepsy, such as temporal lobe epilepsy, in mice (Leclercq et al., 2019). Furthermore, EAAT 1/2 transporters are downregulated in gliomas, reducing the buffering of extracellular Glu. The β-lactam antibiotic ceftriaxone has been found to increase EAAT2 expression, leading to a decrease in glioma cell growth (De Groot et al., 2005) and an antiepileptic effect in mouse models (Zaitsev et al., 2019). The EAAT2 gene is regulated by the peroxisome proliferator-activated receptor (PPAR-γ), a transcriptional regulator factor. Consequently, targeting PPAR-γ could enhance EAAT2 expression and reduce extracellular Glu concentrations (Ching et al., 2015), thus potentially decreasing epileptic activities and tumor growth (De Groot et al., 2005). PPAR- γ agonists have been shown to reduce epileptic discharges by blocking nicotinic acetylcholine

receptors (Saha et al., 2014). Additionally, these agonists can inhibit metalloproteinases, which are essential for migration over the extracellular matrix, and the JAK-STAT pathway implicated in tumor growth (Ellis & Kurian, 2014). An interesting study demonstrated that diabetic patients with GB who received PPAR- γ agonists (thiazolidinediones) had a median survival of 19 months, compared to patients without PPAR-γ who had a mean survival of 6 months (Grommes et al., 2010).

This year, the results of a double-blind, phase 3 trial comparing vorasidenib, a dual inhibitor of the mutant IDH1 and IDH2 enzymes (Konteatis et al., 2020), versus placebo on grade 2 IDH-mutated gliomas were published (Mellinghoff et al., 2023). A total of 331 patients were enrolled in the clinical trial. Patients receiving vorasidenib had a mean progression-free survival of 27.7 months, compared to 11.1 months in the placebo group. However, the effect of vorasidenib on TRE was not studied in this trial.

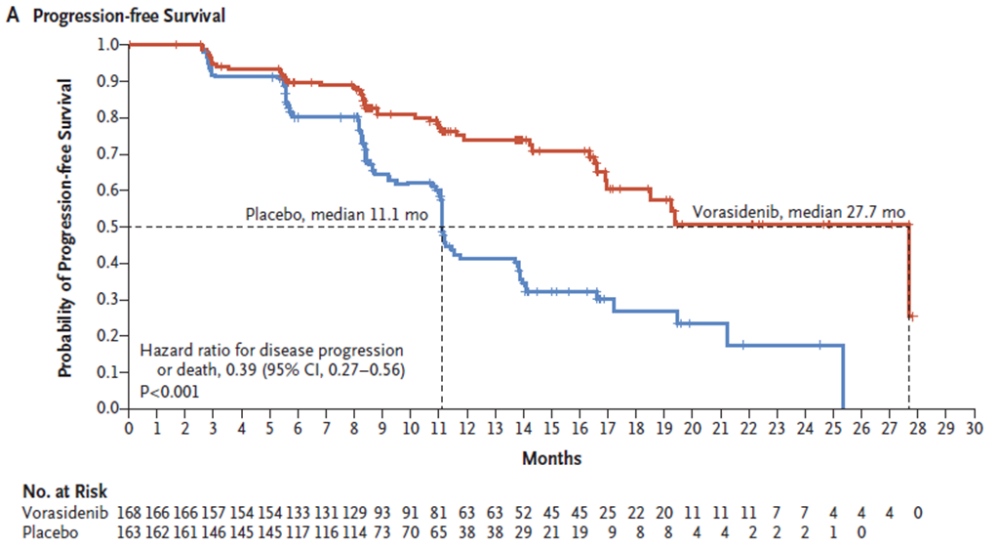

Figure 24: Progression free survival of patients treated with vorasidenib (red) compared to placebo (blue).
From Mellinghoff et al, 2023.

It is also possible to inhibit the Glu receptor using an antagonist, and perampanel is a known antagonist of AMPA receptors. Perampanel is already approved and used as an add-on therapy for focal epilepsy. Several studies, including a recent clinical trial performed on 36 TRE patients, have shown that perampanel is effective in seizure control and is well tolerated (Coppola et al., 2020; Izumoto et al., 2018; Maschio et al., 2019; Vecht J Neurooncol 2017). Furthermore, PER has obtained promising results in reducing tumor growth in vitro (Lange et al., 2019) and in vivo in rodents (Lange et al., 2020). However, the data on patients are limited, as only one study shows its possible effect on tumor growth control (Izumoto et al., 2018). The recent discovery of functional AMPA synapses between glioma cells and neurons suggests that perampanel may have additional value in blocking tumor growth (Venkataramani et al., 2019; Venkatesh et al., 2019). An ongoing multicentric clinical trial named GLUGLIO is currently investigating the efficacy of add-

on anti-glutamatergic molecules such as gabapentin, sulfasalazine, and memantine, in combination with temozolomide and compared to temozolomide alone in GB patients. The trial began in January and aims to enroll 120 patients. The primary endpoint of the trial is progression-free survival at six months. The trial will conclude in 2026 (Glutamate Inhibitors in Glioblastoma - Full Text View - ClinicalTrials.Gov, n.d.). NMDA receptor antagonists are potential targets for fighting epilepsy and tumor growth. In vitro studies and rodent glioma models have shown that NMDA antagonists, such as dizocilpine, memantine, and riluzole, can decrease glioma proliferation (Rzeski et al., 2001; Yohay et al., 2014). However, human studies on these agents are yet to be conducted.

Targeting Cl^- transporters appears to be a promising approach to improve epilepsy control and protect against tumor growth. Cl^- homeostasis is impaired in gliomas, and the NKCC1 transporter is upregulated. The use of the NKCC1 antagonist bumetanide has shown potential benefits in preventing volume changes in glioma cells that are necessary for proliferation and migration, reducing their invasiveness in culture and mice (Ernest et al., 2005; Haas & Sontheimer, 2010). Bumetanide has also demonstrated its ability to enhance the antitumoral activity of temozolomide by extruding K^+ and Cl^- from glioma cells, leading to shrinkage and apoptosis (Algharabil et al., 2012). Moreover, NKCC1 has shown promise ex vivo against epilepsy, not only for TRE (Pallud, Le Van Quyen, et al., 2014) but also for other types of epilepsies such as hippocampal sclerosis (Huberfeld et al., 2007) or cortical dysplasias (Blauwblomme et al., 2019). Some human in vivo studies has reported suppression of seizures in neonates and adults using bumetanide (Eftekhari et al., 2013; Kahle et al., 2009). However, the development of bumetanide analogs may be necessary, as another clinical trial was halted due to serious adverse effects (Pressler et al., 2015). Another potential target is enhancing KCC2 activity. However, a study performed on rats has shown that while it normalized Cl^- levels, it also increased seizure-like activity ex vivo, probably due to the increase of extracellular K^+ (Gagnon et al., 2013).

Everolimus and rapamycin are mTOR inhibitors that induce cell cycle arrest and apoptosis. They have already been shown to reduce growth rates in gliomas in animal studies (Sami & Karsy, 2013). In a mouse xenografts GB model, rapamycin inhibits the growth of glioma cells, and the mice receiving rapamycin doubled their overall survival compared to mice without rapamycin (Arcella et al., 2013). Tuberous sclerosis patients with alterations of the mTOR pathway frequently present pharmacoresistant epilepsy. The use of everolimus in these patients has improved seizure control and reduced tumor growth (Overwater et al., 2019).

As described earlier, some antiseizure medications have shown the potential to improve tumor control. VPA inhibits histone deacetylase, opening chromatin structure and exposing DNA to the effects of chemotherapy agents, such as temozolomide or radiotherapy. Patients receiving chemoradiotherapy in combination with VPA presented longer survivals than those without VPA (Weller et al., 2011). Patients receiving temozolomide with VPA had a median survival of 69 weeks, while patients without VPA had a median survival of 61 weeks (Kerkhof et al., 2013). Other histone deacetylase inhibitors, such as vorinostat and belinostat, have shown antioncogenic effects in hematological and solid tumors (Brodie & Brandes, 2014).

LEV, by inhibiting the transcription of MGMT, has been shown in several studies to play a modulatory role in survival by increasing the sensitivity of tumor cells to temozolomide (Bobustuc et al., 2010). In a recent study involving 460 GB patients, it was found that

patients who received LEV throughout the entire duration of chemoradiotherapy presented longer survival (21 months) compared to patients who received LEV partially (16.8 months) or not at all (16 months) (Pallud et al., 2022). LCS is well tolerated and effective in TRE. LCS has inhibitory activity on histone deacetylase and has shown antitumoral effects in glioma cells in vitro (Rizzo et al., 2017). Also, BRV is effective as an add-on therapy in TRE and has demonstrated an antioncogenic impact in vitro on glioma cultures, probably due to its similarity to LEV (Rizzo et al., 2017).

2.4.2 Oncological treatments as antiepileptic drugs

Not only ASM may demonstrate an antioncogenic effect, but oncological treatments such as surgery, chemotherapy, and radiotherapy have also shown potential benefits for seizure control (Vacher et al., 2023).

2.4.2.1 Surgery

Surgical resection emerges as the primary determinant for achieving seizure control in glioma patients. Multiple studies have demonstrated favorable seizure-free rates, ranging from 63 to 87%, following surgery for LGG (Chang et al., 2008; Englot, Han, et al., 2012; Luyken et al., 2003; Pallud, Audureau, et al., 2014), and 77% in HGG (Chaichana et al., 2009). Remarkably, supra-total resection yields superior seizure outcomes than partial resections (Englot, Han, et al., 2012). A retrospective analysis focusing on LGG with epilepsy revealed an 80% resection threshold for achieving seizure control (D. S. Xu et al., 2018). Conversely, another study reported a higher threshold of 91% resection coupled with less than 19 ml of residual volume (Still et al., 2019). Moreover, early resection is more advantageous in improving seizure control than delayed intervention (Solomons et al., 2020).

2.4.2.2 Radiotherapy

Radiotherapy constitutes another significant intervention contributing to epilepsy control in gliomas. A randomized phase III clinical trial performed on LGG patients demonstrated that the early application of a total dose of 65 Gy in 30 fractions resulted in seizure freedom for 75% of patients, compared to 59% when radiotherapy was applied at a later stage (Van Den Bent et al., 2005). A series involving LGG and HGG showed that 77% of patients experienced reduced seizure frequency at three months, with 32% achieving seizure freedom one year after radiotherapy (Rudà et al., 2013).

Despite its efficacy, radiotherapy can induce inflammation, potentially exacerbating seizures during treatment. A recent prospective study evaluating seizure frequency during radiotherapy treatment and up to six weeks later in HGG has found that 45% of patients experienced a worsening in seizure frequency during the treatment course (Rades et al., 2022).

2.4.2.3 Chemotherapy

Chemotherapy has also demonstrated efficacy in improving seizure control, even though randomized trials are lacking. Several studies have shown that temozolomide treatment

results in seizure reduction in 50-60% of LGG, with seizure freedom achieved in 13-55% of cases (Koekkoek et al., 2015; Pace et al., 2003; Sherman et al., 2011). Moreover, the improvements in epilepsy control manifest before observable changes in the tumor (Koekkoek et al., 2016).

3. Electrophysiological approach of the peritumoral tissue

3.1. In vitro

3.1.1. Extracellular recordings

Initially, extracellular recordings of the peritumoral tissue were conducted in animal models. The most commonly used animal glioma model is the mice xenograft model. Immunocompromised mice are injected with glioma cells obtained from glioma patients. After the injection, a tumor progressively develops in the mice's brains. However, we can get models derived from HGG cells but not from LGGs due to the difference in tumor growth rates since they have a very slow proliferation rate (Dasgupta et al., 2023).

One of the first works dedicated to the electrophysiology of the peritumoral tissue in xenografted mice was done in 2011. First, to decipher the mechanisms implicated in seizure generation, the authors studied in vivo EEG recordings. They observed spontaneous interictal EEG activity in 37% of glioma mice but none in the control group. The authors also studied ex vivo slices, conducting extracellular recordings of layers II/III. They found that approximately 23% of peritumoral slices displayed spontaneous IIDs, lasting 100-500 ms, when perfused with artificial CSF (a-CSF). No IIDs were observed in control animals (Buckingham et al., 2011).

In another similar study, also performed in xenografted mice peritumoral slices, spontaneous IIDs were demonstrated in 30% of slices, with none of the controls displaying IIDs. The authors also observed that glioma slices' input/output curves (consisting of the application of increasing stimulation and recording of the postsynaptic potential evoked by the stimuli) presented larger responses than controls. Furthermore, higher stimulation intensities evoked greater amplitudes in glioma mice slices compared to controls, indicating increased excitability in peritumoral areas (Campbell et al., 2012).

In mice, it is possible to induce ictal-like events (ILE) with 0 Mg^{2+}-aCSF, even in controls. The authors induced ILE using 0 Mg^{+2}-aCSF in both groups, but glioma mice slices presented seizures before (6 minutes after the removal of Mg^{2+}) than control slices (14 minutes after Mg^{2+} removal). The frequency of ILE was higher in glioma mice slices compared to controls (3.7 events /minute vs. 1.4 events/minute). Interestingly, the application of sulfasalazine blocked ILE without affecting IIDs (Campbell et al., 2012). In another mice slice study, ILE was induced using a 0 Mg^{2+} model. The ILE initiation site was outside the tumor core in all the slices (~200–800 µm from the tumor border) (Senner et al., 2004).

However, there are other glioma animal models, for example, gliomas induced using genetic manipulation with retrovirus with the Cre system. Recently, a genetic GB mice model was used to study the peritumoral area. The authors recorded ex vivo slices with multielectrode arrays (MEA). Using 0 Mg^{2+} aCSF perfusion, the tumor, infiltrated

peritumoral tissue, and healthy regions showed an increase in firing rates compared to the control slices. The frequency of ILE was higher in glioma slices (40 events) than in control slices (5 events). The ILE onset electrode was at the infiltrated margin in 50% of cases and the peritumoral region in 36.9% of patients (Gill et al., 2021). These results provide clear evidence of hyperexcitability in the peritumoral area, which can display epilepsy markers such as IIDs. Moreover, induced ILE arises from the peritumoral tissue rather than from the tumor itself.

Using human tissue instead of animal models allows for a more accurate study of the pathophysiological underlying mechanisms involved in epileptogenesis. However, due to limited access to peritumoral human samples, only three studies performed on human peritumoral slices have been published. In the first one, using extracellular recordings, the authors found that approximately 70% of peritumoral slices presented spontaneous IIDs in superficial layers, while no IIDs were observed in controls. The authors also demonstrate that IIDs were blocked with $GABA_A$ and AMPA antagonists, suggesting that IIDs depend on both GABA and Glu signaling. IIDs were characterized by a mean amplitude of 57.9 µV, a mean time to peak of 24.4 ms, and a mean frequency of 0.9 Hz. In 40.7% of the slices, high-frequency oscillations (HFO) were found nested inside the IIDs, presenting a mean frequency of 250 Hz. Notably, HFO were never recorded from the tumor or areas without IIDs. An increase of excitability using 0.25 mM Mg^{2+} and 8 mM K^+ aCSF was used to induce ILE. ILE were present in 37% of slices, displaying two characteristic patterns: LVFA or HS. The mean delay until the arrival of the first ILE was 34 min. One difference compared to mice models was that control slices did not present ILE under proepileptic conditions. During the transition to the ILE onset, preictal discharges (PIDs) progressively emerge. $GABA_A$ antagonists were not able to suppress PIDs. However, the application of bumetanide, an NKCC1 antagonist, blocked IIDs and ILE without affecting PIDs. In conclusion, the authors suggested that the peritumoral neocortex can generate two types of epileptic activities: IIDs and PIDs. The first one depends on GABA and Glu signaling, while PIDs rely on AMPA mechanisms. ILE depends on GABA signaling, and probably depolarizing GABA effect is implicated in its generation, which is likely associated with Cl^- accumulation in pyramidal cells due to synchronous PIDs activity (Pallud, Le Van Quyen, et al., 2014).

The second study also reported spontaneous IIDs in 77% of peritumoral slices, with no IIDs recorded from non-epileptic slices. The Western blot analysis of slices generating IIDs showed an activation of the mTOR pathway (Yuan et al., 2017).

The most recent study compared extracellular recordings from human slices among glioma, focal cortical dysplasia (FCD), and DNET. IIDs were more frequent in gliomas (75% of peritumoral slices) compared to FCD (33%) and DNET (37.5%). All three pathologies developed ILE when exposed to 0 Mg^{2+} 6-8 K^+ aCSF with similar probability, delays to ILE onset, and ILE duration. The two ILE patterns were equally present in all three pathologies, with a predominance of LVFA pattern in gliomas and HS pattern in FCD (Dossi, Blauwblomme, et al., 2018).

3.1.2. Intracellular recordings

One of the most significant recent discoveries in neuro-oncology was the identification of functional AMPA synapses between neurons and glioma cells at the peritumoral level in

2019, independently reported by two different research groups. To investigate the functionality of these synapses identified through electron microscopy, whole-cell patch-clamp recordings were made in slices from the xenografted mice model, in which glioma cells were labeled with GFP. Glioma cells were grafted in the hippocampus, specifically in the CA1 region. GFP cells were recorded after stimulation of the Schaffer collaterals. Voltage-clamp recordings showed that Schaffer stimulation evoked excitatory postsynaptic currents (EPSCs), while current-clamp recordings determined that these inward currents were depolarizing. Further experiments with tetrodotoxin, a voltage-gated Na^+ blocker, effectively suppressed EPSCs, indicating that they were induced by neuronal activity. Moreover, the current-voltage curves showed a reversal potential at 0 mV and facilitation with paired stimuli, suggesting the involvement of AMPA signaling in EPSCs. NBQX, an AMPA receptor antagonist, successfully blocked EPSCs (Venkatesh et al., 2019). Concurrently, similar work was performed using mice xenografted model and the human tissue obtained from GB patients. In this study, the authors marked GB cells by applying 5-ALA preoperatively and then patching glioma cells, revealing similar EPSCs (Venkataramani et al., 2019). The application of CNQX also inhibited EPSCs. As the AMPA receptor subunit GluA2 is not edited in glioma cells, rendering the receptor permeable to Ca^{2+}, both teams tested the presence of Ca^{2+} permeability using the selective blocker NASPM. The two teams observed a significant decrease in EPSCs, suggesting that they depend on Ca^{2+}-permeable AMPA receptors (Venkataramani et al., 2019; Venkatesh et al., 2019).

Both studies also reported the presence of spontaneous slow inward currents (SICs), lasting over one second, in co-culture conditions and on mice slices. In normal astrocytes, SICs are excitatory events caused by Glu due to the activations of extrasynaptic NMDA receptors and inward K^+ currents due to an excess of extracellular K^+ (Sibille et al., 2014). NASPM, the Ca^{2+}-permeable AMPAR inhibitor, did not modify SICs. On the other hand, CNQX inhibited SICs but did not completely suppress them, suggesting that different conductance besides AMPA might be involved in SICs (Venkataramani et al., 2019; Venkatesh et al., 2019). The application of AP5, an NMDA antagonist, did not modify SICs either, but they were suppressed by TTX, indicating that neuronal activity was necessary to induce SICs. Therefore, SICs likely depend on multiple conductances with an important role played by AMPA receptors (Venkatesh et al., 2019). Interestingly, an increase in extracellular K^+ induced SICs even with neuronal activity blocked, and the application of barium, which blocks inward K^+ channels, aborted SICs. These findings suggest that it is not the neuronal activity that triggers SICs but rather the increase of extracellular K^+ due to neuronal activity (Venkatesh et al., 2019).

Glioma cells displaying SICs exhibit a low input resistance, indicating the presence of extensive gap junction coupling. When filling with biocytin glioma cells presenting with SICs, it diffused over interconnected cells, confirming their communication through gap junctions (Venkatesh et al., 2019). The application of gap-junction blockers such as GAP26, GAP 27, carbenoxolone, or meclofenamate reduced SICs amplitude and increased the cell input resistance, suggesting that the organization of the glioma network is involved in the generation of SICs (Venkataramani et al., 2019; Venkatesh et al., 2019). Among all the recorded cells (n=643), approximately 5-10% presented EPSCs, while 40% exhibited SICs following neuronal activity (Venkatesh et al., 2019). These data suggest that increased extracellular K^+ concentration can induce glioma depolarization.

In a previous study on xenografted mice slices, researchers investigated the contribution of glutamatergic mechanisms to epileptogenicity at the peritumoral level. Perfusing slices with 0 Mg^{2+}-aCSF to enhance excitability and using whole-cell patch-clamp recording, they observed that neurons in xenografted slices exhibited shorter latencies to the first epileptiform discharge compared to controls (12 minutes vs. 26 minutes). To determine if the xCT system contributed to epileptogenicity, they added 250 µM sulfasalazine to the 0 Mg^{2+}-aCSF perfusion. This resulted in a reduction in the amplitude and duration of the events. The residual activity was blocked with 50 µM of AP5. These results suggest that the excitability threshold of peritumoral cells can be reduced due to an increase in extracellular Glu at the peritumoral level. Furthermore, the application of 20 µM Glu in ACSF induced epileptiform activity in 66% of the xenografted slices but in none of the control slices (Buckingham et al., 2011).

Regarding GABA signaling, intracellular recordings from pyramidal cells during IIDs showed that 35% received hyperpolarizing synaptic events at resting potential, whereas 65% received depolarizing synaptic events. No pyramidal cells fired before IIDs onset. The input resistance and resting membrane potential were similar in hyperpolarized or depolarized pyramidal cells. On the other hand, interneuron recordings showed that they fired before IIDs onset and continued their activation during IIDs. To test if interneurons contributed to IIDs generation, they were hyperpolarized using a µ-opiate receptor agonist (DAGO) that blocked IIDs, indicating that interneurons indeed have a significant role in the generation of IIDs (Pallud, Le Van Quyen, et al., 2014).

3.2. In vivo ECoG

Peritumoral brain activity can also be recorded using electrocorticography (ECoG) with strips or grids during glioma surgery. Electrodes with diameters ranging from 4 mm to 10 mm are directly applied over the exposed cortex. This technique does not add invasiveness to the surgery since the electrodes do not penetrate the cortical surface. Wilder Penfield was the pioneer of this technique in the 1950s.

ECoG is employed to monitor the induction of seizures through direct electrical stimulations. Early seizure detection allows the neurosurgeon to abort the propagation of the seizure by locally applying cold serum, which immediately interrupts the seizure propagation. Generalized seizures could be dramatic during the surgery due to the uncontrolled movement of the patient and the post-critical drowsiness. ECoG also enables the detection of after-discharges, which alter the normal functioning of a brain area and make the interpretation of EDS difficult. Therefore, ECoG serves as a security tool during awake surgery.

Furthermore, ECoG can record spontaneous IIDs, making it a valuable tool for identifying biomarkers of epileptogenesis during epilepsy or tumor surgery. Thanks to ECoG recordings, we know that IIDs can be recorded at the peritumoral level rather than from the tumor core (Hirsch et al., 1966; Tran et al., 1997). Chronic ECoG recordings of pharmacoresistant TRE patients have shown that seizure onset zones are situated in the peritumoral tissue, more than 15 mm from the tumor border (Mittal et al., 2016).

Since the differentiation of tumor versus peritumoral areas is based on imaging, the electrophysiological characterization of these compartments has not been extensively studied. An ECoG study involving 16 glioma patients recently showed differences in the canonical frequency bands between the tumor and the surrounding area. The results indicated an increase in delta frequency within the tumor and a decrease in all the other frequency bands (Boussen et al., 2016). Additionally, this study showed higher connectivity inside the tumor compared to the surrounding areas.

3.2.1. Technologies

3.2.1.1. Macroelectrodes

Currently, ECoG is performed using macroelectrodes, which typically have a diameter ranging from 0.4 to 1 cm. These electrodes are organized in either strips or grids, with the number of electrodes varying from four to 64. The thickness usually ranges from 0.5 to 1 mm (Wyler et al., 1984). Among the most frequently used brands, DIXImedical and AdTech stand out. Both brands have obtained a CE mark for human use, indicating compliance with European health and safety standards. These electrodes are composed of metal, typically platinum or iridium.

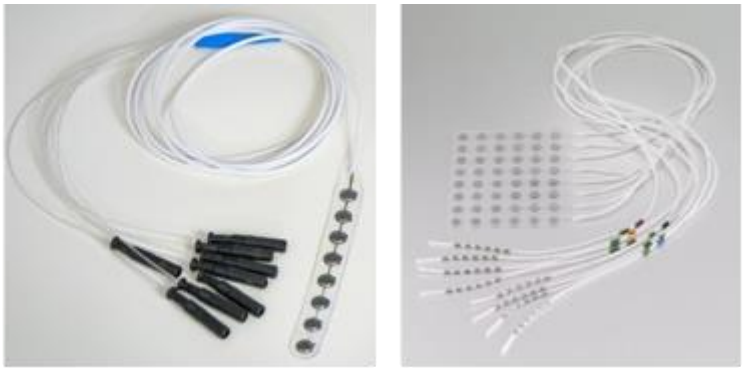

Figure 25: Macro strip (DIXImedical) and grid (AdTech) used for ECoG

Macroelectrodes present several limitations. First, due to their thickness, they are rigid and cannot fully conform to the cortical surface, which may be highly convex in some cases. This lack of complete contact with the cortical surface increases impedance, making low amplitude activities less visible. Moreover, during surgery, the brain presents slight pulsatile movement. If the electrodes are not firmly attached to the surface, it can induce a pulsatility artifact, leading to misinterpretation of false delta activity.

One major drawback of macroelectrodes is their limited spatial resolution; very local activities can be omitted. These electrodes can only record activities generated by a large volume. Since the cortex is functionally organized in columns of 400 µm (Mountcastle, 1957), macroelectrodes lack the spatial resolution to capture this information. To record cortical dynamics, electrodes smaller than 40 µm are needed (Lambrecq et al., 2017; Van Quyen et al., 2016).

3.2.1.2. Microelectrodes

The ideal device for recording electrophysiological activities with ECoG needs to present an increased spatial resolution while maintaining minimal invasiveness. Spatial resolution can be modulated by the size of the electrodes and the interelectrode spacing. A much higher spatial resolution can be achieved by miniaturizing both of these factors.

Nowadays, microelectrodes recordings are used for research purposes in epileptic patients. Two different approaches have been employed. The first approach involves using cortical penetrating arrays, such as Utah arrays implanted in the cortex. The second one uses bundles of 3-4 microelectrodes at the tip of deep sEEG electrodes. Both microelectrodes allow for the simultaneous recording of FP and single-neuron action potentials. Action potentials provide local information at a microscale, giving insights into the activity of individual neurons. On the other hand, FP reflect the synchronization of neuronal populations, providing mesoscale information. However, it is essential to consider that FP can be influenced by remote brain networks, providing macroscale information.

Utah arrays are silicon-based MEA that can be implanted in vivo, either perioperatively or chronically. Microelectrodes can be made of stainless steel or tungsten. However, one limitation of metallic electrodes is their rigidity, which can potentially cause microlesions and glial scars (Fernández et al., 2014). Due to the extremely high density of brain microvascularisation and the microelectrodes being densely arranged, microbleeding and micro ischemic lesions are possible (Fernández et al., 2014). A Utah array consists in 96 silicon penetrating needles that record activities from the tip of each needle. These arrays allow for high-density recording. However, their fixed position and an area of recording limited to 4.2 mm^2 result in suboptimal spatial resolution. Each needle has a diameter of 40 µm. They can be implanted for long periods, making them suitable for acute and chronic recordings. They can record interictal activities, microseizures (Stead et al., 2010), and HFO (Bragin et al., 2002). Additionally, due to their spatial resolution, they can record MUA and FP simultaneously (Schevon et al., 2012). Their clear limitation is that they are invasive and can only be used in brain areas where resection is certain.

Indeed, sEEG microelectrodes have been used for research in pharmacoresistant epileptic patients, and two different configurations are used in France. In the first configuration, 40 µm microelectrodes extend beyond the tip of the macro sEEG electrodes (Lambrecq et al., 2017). In the second one, two or three tetrodes extend 3 mm away from the macrowire between the first and second macrocontact (Curot et al., 2023). In both cases, spatial resolution is also a limitation since the position of the microelectrodes is fixed once implanted, and they do not present high number of contacts.

However, the use of microelectrodes presents some drawbacks. A reduction of the contact area involves an increase in the impedances. To address this limitation, researchers have turned to conductive polymers such as PEDOT:PSS, which can help to improve impedances (Malliaras & Abidian, 2015). The development of organic conductive polymers represents a significant advancement in bioelectronics. These new technologies, using biocompatible organic materials, make possible the downsizing of the electrodes while achieving even better quality recordings.

Traditional metal-based electronics are not well-suited to measure ionic changes, essential for biological communication, especially in neurons where ionic currents are crucial in brain communication. Semiconducting materials are not ideal for measuring these ionic changes and can suffer from issues like surface oxidation, which can decrease signal transduction. The main advantage of organic conductive polymers is that they present electrical and ionic conductivity, improving signal quality.

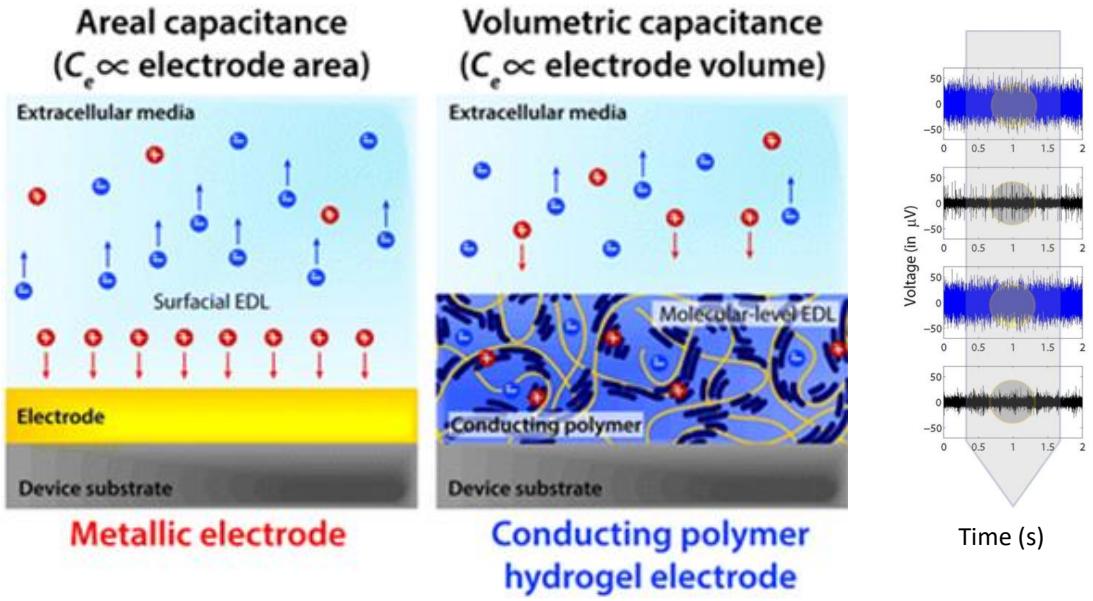

Figure 26: Difference between a metallic and a conducting polymer electrode. Impedance from metallic electrode (blue) and conducting polymer electrode (black).
From Ludwig et al, 2011.

3.2.1.2.1. PEDOT:PSS

The most used organic component in microelectrode fabrication is the conducting polymer poly-3,4-ethylene-dioxythiophene/polystyrene sulfonate (PEDOT:PSS), but other polymers such as poli-3-hexiltiofen (P3HT), polypyrrole (PPy), polietilenglicol (PEG), polyaniline (PANI) and polyvinyl tiofen (PVT) can also be used. PEDOT:PSS microelectrodes, often referred to as NeuroGrid, are embedded in a biocompatible ultrathin parylene support with a thickness ranging from 4 to 12 µm. This design makes them highly flexible and conformable to the cortical surface (Khodagholy et al., 2016). The development of these organic conductive polymer-based microelectrodes has opened new possibilities for recording neuronal activity and has been successfully used in human subjects (Khodagholy et al., 2015).

PEDOT:PSS is an excellent material for bioelectronics due to its numerous advantageous properties. It offers stability (Feron et al., 2018), high conductivity, and resistance to physical deformation (Khodagholy et al., 2013). Moreover, its biocompatibility (Inal et al., 2018) and prolonged stability in cell culture conditions (Dijk et al., 2020) make it a reliable choice for biomedical applications. In recent years, PEDOT:PSS has also been widely applied in various bioelectronic devices, such as electrodes (Inal et al., 2018; Yao et al., 2015), a variety of biosensors (de Mel et al., 2008), metabolite sensing (Pappa et al., 2018),

barrier-tissue integrity assessment (Rivnay et al., 2015), drug delivery (Simon et al., 2009) organic electrochemical transistors (Shen et al., 2016), and small bioelectrode coatings (Povlich et al., 2013). Its lack of toxicity has been tested in vitro in endothelial cells, fibroblasts, and human neurons (Amorini et al., 2017; Ramuz et al., 2014).

The loose structure of PEDOT: PSS allows charges to move freely, making it conductive. Moreover, metal ions within the CSF environment can interact with the polymer, changing its conductivity (Mantione et al., 2017). The main advantage of using PEDOT:PSS as a lining in microelectrodes is that it reduces impedance values compared to naked metallic electrodes. In electronics, the size of the electrode contacts influences impedance: smaller contact size leads to higher impedance values. PEDOT:PSS overcomes this limitation and improves impedance values when used in microelectrodes, making it an ideal choice for bioelectronic applications.

Impedance

When discussing electrodes, one of the key factors that significantly affect recording quality is the impedance of the electrode. Impedance refers to the opposition an electrode presents to the flow of electric current. In simpler terms, it measures the electrode's ability to conduct an electric current. The electrode impedance comprises two main components: the contact resistance and the electrochemical impedance. The contact resistance decreases when the radius of the electrode increases (Ludwig et al., 2011). On the other hand, the electrochemical impedance depends on the efficiency of electric and ionic exchange between the electrode and the surrounding medium. In electrodes coated with PEDOT:PSS, the electrochemical impedance is reduced due to improved ionic conductance. Impedance modifies recordings due to shunt loss and increased noise (Najafi et al., 1990). To minimize shunt loss, it is important to enhance the adherence of the electrode to the cortical surface. Therefore, using thinner and more flexible grids can result in lower impedances. The noise is due to the random fluctuation of ions in the medium (Hassibi et al., 2004).

Signal to noise ratio

Besides impedance, the signal-to-noise ratio (SNR) is crucial in obtaining reliable measurements. In any recording setup, what we are truly interested in measuring is the brain’s signal. At the same time, the noise includes various unwanted disturbances, such as background electrical noise from external sources and other artifacts like movements.

One of the critical challenges in improving SNR is identifying and mitigating artifacts arising from electrode movements, eye blinking, heart rate, and other sources that can be significantly larger in amplitude compared to brain activities, especially when dealing with low-amplitude signals like HFO. To enhance SNR, minimizing external noise from the electrical environment, such as the 50 Hz noise often present in power lines, is essential. Turning off unnecessary equipment like cell phones, computers, and monitors can help to reduce this interference. However, alternative strategies must be employed in an environment like an operative theater, where multiple noise sources cannot be switched off (e.g., perfusion, echographer, electric stimulations, monitors). One approach to dealing with specific frequencies is using a notch filter, which can suppress frequencies within a particular range. Additionally, postprocessing techniques can be employed after data acquisition to remove some artifacts, such as eye movements (Croft & Barry, 2000).

3.2.1.2.2. Other conductor polymers

One of the advantages of PEDOT is its versatility in being associated with PSS and other conjugated polymeric materials (Mantione et al., 2017). For instance, PEDOT-sulfonate (PEDOT-S) has been used to introduce electronic functionality in plants (Stavrinidou et al., 2015), which could potentially be used for collecting energy from photosynthesis. The combination of PEDOT with polydioxythiophenes could be revolutionary in tissue engineering. This union could improve material flexibility and enhance molecule transport (Green et al., 2010). Moreover, glycosaminoglycans, such as hyaluronic acid, heparin, and chondroitin sulfate, can be doped to PEDOT, providing several benefits. This coupling helps soften the interface between rigid electrodes and biological tissues and offers anti-inflammatory effects (Mantione et al., 2016). PEDOT:biopolymer materials can serve as scaffolds for cellular growth, including neurons, due to their biocompatibility and conductivity (Del Agua et al., 2018).

Recently, silk-based electrodes have been coated with PEDOT doped with toluene sulfonate (PEDOT:pTS). The electrode gains increased flexibility by combining silk and PEDOT:pTS, while the PEDOT:pTS lining reduces impedance. A study recording with this electrode successfully measured gamma band activity in the embryonic chick brain with a high SNR. The authors could perform electrical stimulation using this innovative electrode (Watanabe et al., 2017).

3.2.1.2.3. Microelectrodes Contributions

MicroECoG is a promising technology aimed at improving the spatial resolution of cortical recordings, enhancing the SNR, and minimizing invasiveness. To improve the quality of the recordings, new biocompatible materials are being explored to avoid brain damage. Advances in microfabrication technology have enabled the creation of microelectrodes smaller than 20 µm, integrated into ultrathin (4 µm) parylene matrix. Organic polymers, specially PEDOT:PSS coating, have shown positive results in reducing electrode impedance while maintaining biocompatibility in animal studies (Castagnola et al., 2015; Ludwig et al., 2011). Long-term animal implantation, lasting up to three months, have shown that chronic recordings are feasible without compromising recording quality or causing cortical lesion at the implantation site (Tybrandt et al., 2018). Increasing the number of contacts improves spatial resolution, and organizing microelectrodes in tetrodes allows for the measure of single-neuron activity and the possibility of performing spike-sorting. Their thinness improves their flexibility and adherence to the cortical surface.

MicroECoG offers a unique opportunity to explore brain activity at macro and microscales. Not only will it be useful to decipher the underlying mechanisms of multiple diseases, but also to understand the normal functioning of the brain. MicroECoG recording using Utah arrays have already allowed the identification of cognitive processing mechanisms (Quiroga et al., 2005), the study of sleep oscillations (Van Quyen et al., 2016), and robotic neuroprosthetics control (Collinger et al., 2013).

MicroECoG is not only valuable for epilepsy research but also in cognitive research and brain-machine interface development. However, nowadays, microelectrodes can be used only for research purposes. No commercialized solutions are available, and the smallest commercial system available is CorTec AirRay grids, with a one mm diameter and a

maximum of 80 contacts on soft silicon. Table 2 summarizes all the possible commercial ECoG solutions.

Offer		Properties				
Company	Product	High channel count (>64)	High resolution (electrode ø <0,5mm)	Ultra-conformability	Low impedance	Micro electrodes recording capacities
PMT CORPORATION		✓	✗	✗	✗	✗
DIXI medical		✗	✗	✗	✗	✗
AD-TECH		✓	✗	✗	✗	✗
NeuroOne		✓	✗	✓	✗	✗
neuroWISE		✓	✗	✓	✓	✗
CorTec Thinking ahead		✓	✓	✓	✓	✗

Table 2: Comparative table of the available ECoG electrodes.

3.2.1.2.4. MicroECoG uses in humans

Two U.S.A research teams have already used microECoG in patients for research purposes. The first team employed a microECoG grid containing microelectrodes of 30 µm in diameter, with PEDOT:PSS lining, referred to as "NeuroGrid", which was just 4 µm thick (Khodagholy et al., 2015). In their pioneering study, they successfully performed microECoG recordings in two patients undergoing epilepsy surgery. Despite the brain's inherent pulsatility, the NeuroGrid remained stable on the cortical surface due to its flexibility and the hydrophobic nature of parylene. This allowed them to record ripples and MUA activity (Khodagholy et al., 2015). A year later, they improved their previous work by using more contacts (up to 240) arranged in a tetrode organization. They also introduced small perforations in the parylene matrix to enhance proper CSF circulation over the cortical area. A study involving five patients obtained MUA in all the patients, even during general anesthesia (Khodagholy et al., 2016).

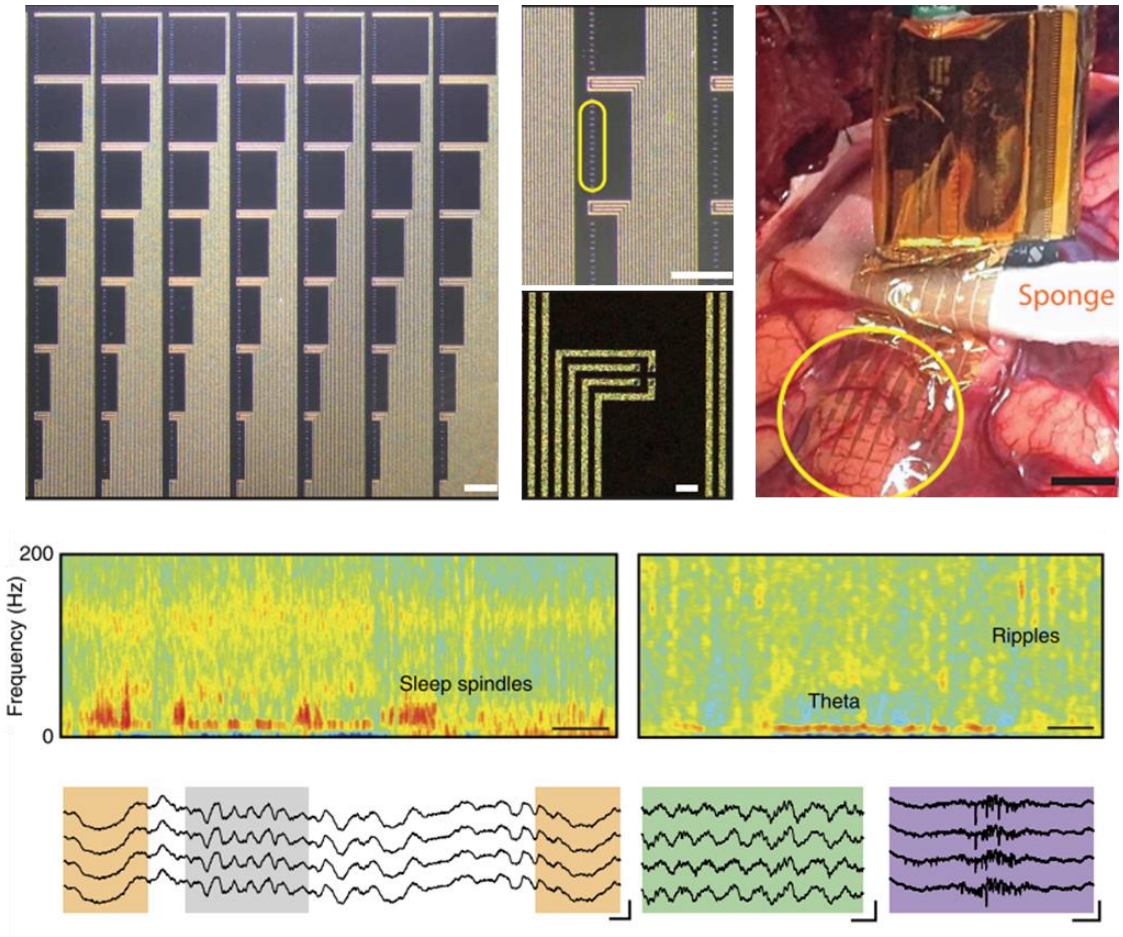

Fig 27: Neurogrid recording in an epileptic patient, showing ripples.
From Khodagholy et al, 2015, 2016.

The second team used microECoGs fabricated with liquid crystal polymer, chosen for its resistance and low water permeability. They employed 200 µm diameter electrodes coated with platinum-iridium to reduce impedance (Dyconex, Switzerland). With this setup, the authors could record high gamma activity during acoustic and motor tasks in two patients using a 244-channel array (Chiang et al., 2020). Using similar microelectrodes, the same authors performed microECoG on nine patients undergoing epilepsy surgery. In this study, they identified 143 microseizures in seven out of nine patients. These microseizures were detectable in adjacent contacts (mean of three contacts) or single channels. The average duration of the microseizures was 5.9 seconds (Sun et al., 2022). This year, the same group has published a study reporting the presence of HFO in seven perioperative microECoG. They could identify ripples (from 80 to 250 Hz) and fast ripples (from 250 to 600 Hz). They compared microECoG recordings with conventional ECoG and found that 47% of HFO were detectably on a single microelectrode. HFO appearing in multiple contacts were limited to a 0.95 mm radius. Moreover, they estimated that macrocontacts could capture merely 44% of the HFO detected with microcontacts (Barth et al., 2023).

3.2.2. Biomarkers

3.2.2.1. Epileptogenesis

3.2.2.1.1. Interictal discharges (IID)

IIDs have long been considered a valuable biomarker for epilepsy. Their detection is routinely used in EEG for epilepsy diagnosis and to localize the brain regions involved in seizures. These regions where IIDs are observed are referred to as the irritative zone (IZ) (Rosenow & Lüders, 2001). While IIDs are uncommon in glioma patients, ECoG enables the recording and delineation of IZ during surgery (Tran et al., 1997).

However, it is essential to note that the complete removal of the IZ does not necessarily guarantee a favorable epilepsy outcome (Schwartz et al., 1997; Tran et al., 1997). In cases where IIDs are frequently observed, such as focal cortical dysplasia or tuberous sclerosis, ECoG can be helpful to tailor the extent of IIDs to aid in surgical planning (Palmini et al., 1995; Tripathi et al., 2010). For glioma patients, where the primary objective is to improve the patient's quality of life, resecting the areas with IIDs resection can be beneficial. A retrospective study demonstrated that glioma patients who underwent ECoG-guided surgery achieved better seizure control after surgery, with 74% of patients presenting Engel I class at one year, compared to 38% of patients without ECoG-guided surgery (Yao et al., 2018).

Nevertheless, the value of integrating the epileptic activity detected by intraoperative ECoG into the resection strategy remains a topic of debate (Boetto et al., 2016; Yao et al., 2018).

3.2.2.1.2. Epileptogenic zone

In 1956, Wilder Penfield had already recognized that epilepsy was not solely associated with a lesion but also involved the "structurally and functionally disturbed but still viable surrounding gray matter", which he termed the "epileptogenic lesion". However, determining the extent of this dysfunctional surrounding cortex remained a challenge. Years after Penfield, Jasper and Rasmussen emphasized that not all spikes held the same significance, and they pointed out that the IZ was broader than the epileptogenic lesion, rendering it unsuitable for precise epileptogenic lesion definition (Jasper et al., 1961; Rasmussen, 1983).

The term epileptogenic zone (EZ) was introduced by Talairach and Bancaud in 1965. They defined the EZ as "the site of the beginning of the epileptic seizures and their primary organization" (Talairach & Bancaud, 1966). As sEEG evolved, more invasive recordings became feasible, allowing researchers to localizing the network responsible for the patient's seizures.

In the 1990s, Luders defined the EZ as "the area of cortex that is necessary and sufficient for initiating seizures and whose removal (or disconnection) is necessary for the complete abolition of seizures". This definition represented a conceptual understanding of the EZ, but there was no direct method for measuring its extent at that time. The challenges in assessing the EZ were reflected in surgical outcomes, which did not always achieve seizure

freedom. During that period, other important concepts were introduced to refine our understanding of epilepsy and guide surgical interventions:

-The seizure onset zone (SOZ) was defined as the area where the seizures started. Its resection was necessary to achieve seizure freedom, but it was recognized that the EZ extended beyond the boundaries of the SOZ.

-The epileptogenic lesion refers to a visible lesion responsible for epilepsy. However, removing the epileptogenic lesion alone was not sufficient to control seizures.

-The irritative zone describes the cortical area generating interictal spikes.

-The symptomatogenic zone represented the area of the cortex that produced symptoms and signs when activated by a seizure.

-The functional deficit zone comprised cortical areas that exhibited dysfunction during the interictal period, which could be detected using neuropsychological tests and functional neuroimaging.

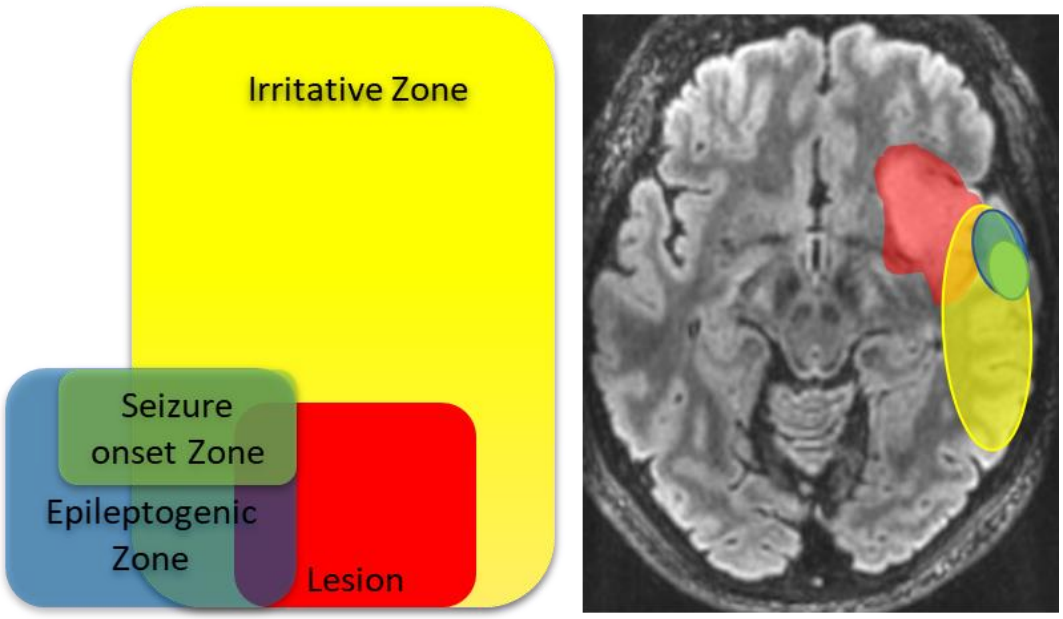

Figure 28: Representation of the different structures and zones involved in epilepsy.

In the 2000s, epilepsy started to be considered a network disease, with the growing understanding that it involves functionally and anatomically connected brain structures and regions that interact bilaterally. Spencer introduced the definition of the EZ as a network "A network [is] a functionally and anatomically connected, bilaterally represented, set of cortical and subcortical brain structures and regions in which activity in any one part affects activity in all the others" (Spencer, 2002). But the challenge was still there, how to delimitate the extension of the EZ. New biomarkers appeared, such as HFO, that were related to EZ (Bragin et al., 1999). But it was not until 2008 that the first quantitative

measure of the EZ appeared. In sEEG recordings, the SOZ typically exhibited “rapid discharges” spanning a range of frequencies from beta to gamma (Talairach & Bancaud, 1966). Building on this observation, Bartolomei proposed the epileptogenicity index (EI), which was based on the content of fast activities and the delay of involvement of the area in the seizure onset (Bartolomei et al., 2008). The rationale behind the EI was that more epileptogenic areas would present rapid discharges earlier in the seizure. High EI values were typically recorded in regions implicated in the initiation of seizures.

In the last two decades, HFO have been considered as a potential marker of the EZ. This topic will be developed later in this chapter.

3.2.2.1.3. Synchronization

Since epilepsy is a network disease, functional connectivity between different brain areas can provide insight into how these areas are organized within a pathologic network (Stam et al., 2016). Given that seizures represent an excessive and hypersynchronous neuronal state, measuring synchronization may offer clues about the regions more susceptible to trigger seizure activity (Jiruska et al., 2013).

Synchrony can be estimated using methods such as linear correlation or coherence. Various techniques can be employed, including time lag, phase locking values, entropy, and non-linear analysis. In the results chapter, we used the phase locking value to study the synchronization between electrodes placed in the tumor, peritumoral, and healthy neocortex. The phase locking value evaluates the coherence between two different signals. PLV is calculated by taking the absolute value of the mean phase difference between two signals computed as a function of the frequency (Nunez et al., 1997). Higher PLV indicates greater synchrony between signals (Lachaux et al., 2003).

3.2.2.1.4. Spectrum aperiodic components

The investigation of aperiodic components of the power spectrum, such as the offset and slope, have been studied in several pathologies like schizophrenia or Parkinson's disease. However, there is comparatively less knowledge about their role in gliomas and their surrounding tissue (Belova et al., 2021; Donoghue et al., 2020; Ghinda et al., 2021; Molina et al., 2020). In particular, the slope of the power spectrum is believed to serve as an indicator of the excitation-inhibition balance (Gao et al., 2017; Jiang et al., 2022; Molina et al., 2020), a critical factor in both epileptic and glioma growth processes (Huberfeld & Vecht, 2016).

A recent study on temporal lobe epilepsy patients implanted with sEEG has shown that the seizure onset zone is characterized by steeper slope values (Jiang et al., 2022). Hence, it is worthwhile to investigate how the aperiodic components of the power spectrum behave in the tumor compared to the peritumoral and healthy areas.

3.2.2.1.5. HFO

In the last two decades, a new biomarker of epileptogenesis has garnered significant interest within the epilepsy community. HFO at 200 Hz were identified in 1992 in healthy rat’s hippocampi during slow-wave sleep and immobility tasks (Buzsáki et al., 1992). These

oscillations ranging from 80 to 250 Hz, were called ripples. Some years later, Bragin observed HFO between 200 and 500 Hz in the hippocampus and entorhinal cortex of epileptic rats and in nine epileptic patients. These oscillations, ranging from 250 to 500 Hz, were referred to as fast ripples (Bragin et al., 1999). They were recorded in areas smaller than 1 mm^3. In the epileptic patients, spontaneous ripples were bilaterally detected in six out of nine patients, only during slow wave sleep or resting state with eyes closed. Among the six patients presenting ripples, FR were present in areas identified as the EZ. In both cases, HFO were recorded using microelectrodes of 40 µm diameter.

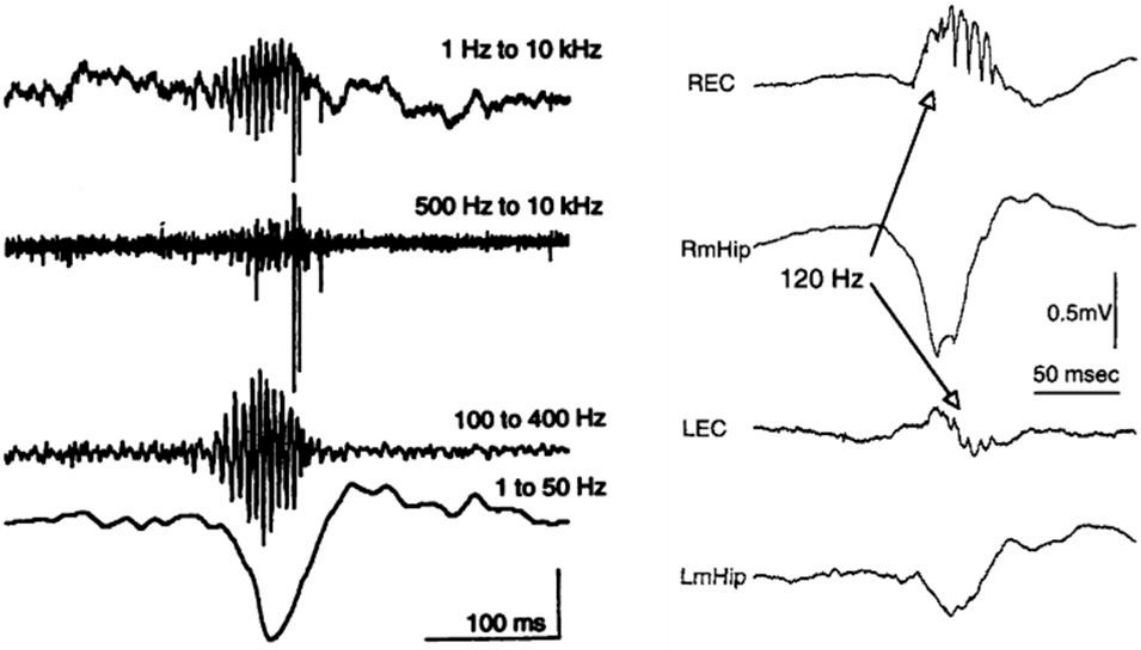

Figure 29: First ripple and fast ripple description.
From Buzsaki et al, 1992 and Bragin et al, 1999.

Several mechanisms contribute to HFO formation. Ripples may arise due to inhibitory postsynaptic currents (IPSCs), reflecting the proper functioning of inhibitory networks under normal conditions. However, in epilepsy, inhibitory networks progressively lose their efficacy as seizures spread, leading to ripples caused by the synchronous firing of pyramidal cells, which can fire up to a frequency of 300 Hz (Ibarz et al., 2010). On the other hand, FR can reflect the pathological bursting of pyramidal cells in the presence of a disrupted inhibitory network (Ibarz et al., 2010; Trevelyan et al., 2007). Simultaneous recording of FP and single neuron with microelectrodes have shown that FR are caused by neuronal firing (Ibarz et al., 2010). Considering that pyramidal cells can fire at a maximum frequency of 300 Hz, an intriguing question arises: how FR can reach frequencies up to 600 Hz? The most accepted hypothesis suggests an out-of-phase firing between different groups of neurons (Foffani et al., 2007b; Ibarz et al., 2010). Ephaptic conduction, neuronal loss,

circuit reorganization, and gap junctions can be implicated in out-of-phase conduction (Jefferys, 1995; Staba et al., 2007; Traub et al., 2001).

In 2006, the MNI group led by Gotman demonstrated the possibility of recording HFO with sEEG macroelectrodes (Jirsch et al., 2006; Urrestarazu et al., 2006). However, the extent to which HFO recorded with macro and microelectrodes hold the same significance remains to be determined. A study using hybrid micro-macro sEEG electrodes showed that all the FR captured by the macrocontacts were visible on the microelectrodes. However, 18% of FR visible in microelectrode were not on the closest macroelectrode (Curot et al., 2023). Even using ECoG macroelectrodes, several groups have successfully recorded HFO (Crepon Brain 2010; Van Klink et al., 2014; Yang et al., 2014). ECoG benefits from the ability to reposition electrodes during surgery, allowing for the assessment and removal of HFOs, making it more effective than sEEG recordings, which remain fixed and are performed preoperatively.

The presence of HFO has been consistently associated with the EZ, both fast ripples (Bragin et al., 1999, 2002; Staba et al., 2002) and ripples (Jacobs et al., 2010; Urrestarazu et al., 2006). In particular, FR appears to have a stronger link to the EZ. Several retrospective studies have shown that the removal of cortical areas generating FR improve epileptic outcomes (Fedele et al., 2016; Jacobs et al., 2018; van't Klooster et al., 2015; Van Klink et al., 2014; Zweiphenning et al., 2016). HFO shows a dynamic behavior over time. In a study of 12 patients, authors found an increase in the duration and rate of HFO when ASM was reduced, suggesting an association between HFO and epilepsy activity (Zijlmans et al., 2009). Additionally, some authors reveal that HFO rate and frequency predominance can change during the preictal period, in the 30 minutes previous to a seizure (Pearce et al., 2013). Understanding the temporal evolution of HFO during the interictal, the preictal, and the ictal period would provide keys to use it for seizure forecasting, identifying "seizure high-risk periods".

The only prospective trial is "the HFO trial" from the Netherlands (Zweiphenning et al., 2022). It consisted of a non-inferiority analysis comparing HFO-guided surgery with spike-guided surgery. The primary endpoint was seizure freedom at one year. They included a total of 78 patients. In the HFO-guided group, 67% of patients were seizure-free at one year, while 90% in the spike-guided group achieved seizure freedom at one year. The authors concluded that HFO-guided surgery was not non-inferior to spike-guided surgery (Zweiphenning et al., 2022). However, this study had some notable limitations. Firstly, the two groups were not homogeneous. The mean age was 15 in the spike group and 21 in the HFO group. Longer epilepsy duration is associated with a worse prognosis. Regarding ASM, 38% of patients in the spike group received less than 2 ASM, while 21% in the HFO group did. A history of previous epilepsy surgery was present in 13% of patients in the HFO group, while it was the case only for 3% of patients in the spike group. Good prognosis factors, such as the presence of a vascular malformation, focal cortical dysplasia, or hippocampal sclerosis, were also heterogeneous between groups, with 87% of spike group patients presenting good prognosis factors compared to only 64% of HFO group patients. Secondly, no automated detector of HFO was used. HFO were detected visually during the surgery for a limited period. That may be prone to errors since HFO visual detection is highly time-consuming, even when semiautomatic detectors are used (Zijlmans et al., 2017). Thirdly, the study did not separately analyze ripples and fast ripples, which can have an impact, as FR are considered a better marker of the EZ than ripples (Fedele et al., 2016; Jacobs et al., 2018; van't Klooster et al., 2015; Van Klink et al., 2014; Zweiphenning et al.,

2016). Years before, a retrospective analysis comparing the value of FR to localize the EZ with interictal spikes at the patient level concluded that FR are not superior to spikes (Roehri et al., 2018).

However, there is no universal consensus on the value of FR as a biomarker of the EZ. FR can be recorded at a low rate in non-pathological areas, such as the occipital cortex, the pre and postcentral gyrus, and the transverse temporal gyrus. In contrast, ripples can be found in the occipital cortex, basal temporal region, and transverse temporal gyrus (Frauscher et al., 2018; Melani et al., 2013). It is well known that HFO can be either physiological or pathological, but how to differentiate them is still a matter of debate. Another limitation of HFO use is that no analyses are studying the underlying histology beneath HFO electrodes.

HFO can be present during the interictal period. HFO nested in a continuous oscillating background are not associated with the SOZ, while HFO emerging from a silent background are strongly linked to epileptic tissue (Minthe et al., 2020). Some authors found that HFO appeared more frequently associated with spikes (approximately 64% of HFO), but they can also emerge independently (Urrestarazu et al., 2007). Another study has shown that the HFO rate increase in the minutes preceding a seizure (Jirsch et al., 2006). Conversely, a study including seven patients found increased HFO rates and decreases during the preictal period. The rates were heterogeneous, without any clear tendency (Jacobs et al., 2009). One possible explanation for this variability is that the recording was made with EEG electrodes with limited spatial resolution. HFOs are very local signals, and macrocontacts can present difficulties in identifying HFOs. Moreover, the sEEG electrodes position is fixed once implanted, and if they are placed some µm away from the source, they cannot record HFO. In the results chapter, I will further develop this topic, by describing the temporal and spatial evolution of HFO during the preictal period in an ex vivo human peritumoral slice model.

As explained previously, the peritumoral tissue is at the origin of interictal discharges (Mittal et al., 2016; Pallud et al., 2012). So far, only two studies have focused on HFO in glioma ECoG. In the first one, 16 patients were recorded during awake glioma surgery using macroelectrodes. The authors found that epileptic patients presented more likely with oscillations between 80 and 100 Hz (75% of epileptic patients) compared to non-epileptic ones (0%). Moreover, patients with an IDH1/2 mutation showed higher rates of fast oscillations than IDH-WT (Feyissa et al., 2018). The main limitation of this study was the limited sampling rate of 500 Hz, which prevented them from recording ripples or fast ripples. Furthermore, the fast oscillations around 100 Hz have not shown any specific epileptogenicity.

The second study examined 41 epileptic patients with low-grade tumors, including 25 gangliogliomas, seven dysembryoplastic neuroepithelial tumors (DNETs), seven gliomas, and two extraventricular neurocytomas. The electrodes were classified as tumor, peritumoral (if placed in the resected area), or outside the resection. FR presented higher rates in tumor and peritumoral electrodes than those set outside the resection. Additionally, gliomas and extraventricular neurocytoma showed higher FR rates than ganglioglioma and DNETs. Notably, FR in electrodes placed outside the resection was associated with a poor postoperative seizure outcome (van Klink et al., 2021).

Challenges in detection

One of the main challenges encountered when studying HFO is their brief duration (tens of milliseconds) and low amplitude compared to interictal spikes, making it possible to miss them in the noise signal. Currently, the gold standard for their detection is visual inspection.

The most widely accepted criteria for visually defining an HFO are as follows (Zijlmans et al., 2017):

1) HFOs are oscillations with a clear onset and end that stand out from the background activity, with a minimum length of four cycles.
2) The raw signal must exhibit a sinusoidal oscillation.
3) A bubble-shaped primary peak should be observed in the frequency range of interest in the spectrogram.

Given the low SNR, using an adapted amplifier with a high sampling rate, at least three times higher than the higher frequency of interest, is essential. Also, noise levels are critical, as high noise can completely obscure HFO. Spectrum whitening can be applied to improve the visibility of HFO (Roehri et al., 2016).

Once the signal is recorded, we need to visualize it with software allowing filtering. A high pass filter of 80 Hz is typically applied to visualize ripples, while a higher frequency of 250 Hz is used for FR. However, it is important to be cautious, as any sharp event in the recording can result in artifacts after filtering, which can closely resemble HFO. These spike-induced HFOs are often called “false ripples” (Bénar et al., 2010).

Real-time detection algorithms

Visual detection of HFO is considered the gold standard technique, but a meta-analysis has shown that automatic detectors can be as effective as visual inspection (Höller et al., 2015). HFO visual detection can be very time-consuming as it involves manually inspecting the data channel by channel using a time window of 1-2 seconds. Moreover, it requires trained individuals who can distinguish HFO from artifacts. Automated algorithms for HFO detection follow several steps. First of all, HFO need to be separated from the background. To do so, algorithms often use energy-based metrics such as the root-mean-square (RMS) amplitude (Staba et al., 2002), power (Birot et al., 2013), line length (Gardner et al., 2007) and the Hilbert transform enveloped (Crépon et al., 2010). Second, a threshold selection is applied to identify candidate HFO. After that, postprocessing is necessary to exclude false positives. Machine learning techniques can help exclude artifacts. Two different approaches are possible. The first approach is supervised, where HFOs are manually marked in a subset of data to train the algorithm, and then the remaining data are used to test the algorithm. Neural networks, support vector machines, and logistic regression are supervised methods (Pearce et al., 2013). The second approach is an unsupervised technique, where the algorithm base its detections on the presence of similar characteristics, based on pattern recognition (Liu et al., 2018).

RIPPLELAB, one of the most famous and widely used software for automatic HFO detection, is an open-source Matlab toolbox offering a graphical user interface ((https://github.com/BSP-Uniandes/RIPPLELAB) (Navarrete et al., 2016). It provides four

different methods for semiautomatic detection. The first one is the Short-Time Energy algorithm, developed by Staba (Staba et al., 2002). The second is the Short Line Length detector, based on Gardner's work (Gardner et al., 2007). The third method is based on the Hilbert transform (Crépon et al., 2010). The last one is the MNI detector (Zelmann et al., 2012). The variability in the methodology (for example, differences in the electrodes and amplifiers) used by different groups makes that is very difficult to compare the automatic HFO detectors (Sindhu et al., 2020). Currently, no method allows for the direct real-time detection of HFO, which limits the impact of clinical trials comparing epilepsy surgery guided by HFO or by spikes.

3.2.2.2. Peritumoral infiltration

3.2.2.2.1. HFO

Interestingly, recording HFO on human peritumoral slices ex vivo provides valuable insights into the distribution of these oscillations in relation to tumor-associated tissues. The study conducted by Pallud showed that higher rates of HFO were observed in highly infiltrated peritumoral areas (Pallud, Le Van Quyen, et al., 2014). This funding suggests that HFO may be more prevalent or prominent in regions directly affected by tumor infiltration. On the other hand, HFO were not recorded from the tumor core or non-infiltrated tissues.

These data suggest that HFO could serve as an electrophysiological biomarker of the presence of tumor cells ex vivo. However, this hypothesis needs to be validated in vivo during awake glioma surgery. If HFO are a biomarker of peritumoral infiltration, this information could be used during the surgery to better tailor the resection. To test if HFO are biomarkers of peritumoral infiltration, we have organized a clinical trial that should start at the beginning of 2024. In this trial, to improve HFO detection, we will use PEDOT:PSS coated microelectrodes of 30 µm and 500 µm in diameter during ECoG perioperative recordings. To validate our hypothesis, the presence of HFO will be correlated with the degree of tumor infiltration beneath the HFO electrodes. If the hypothesis is finally valid, real-time HFO detection will be a valuable perioperative tool. The potential implications of this finding are profound. Using HFO as a biomarker during glioma surgery could enable better tailoring of tumor resection, improving oncological outcomes while reducing postsurgical neurological impairment.

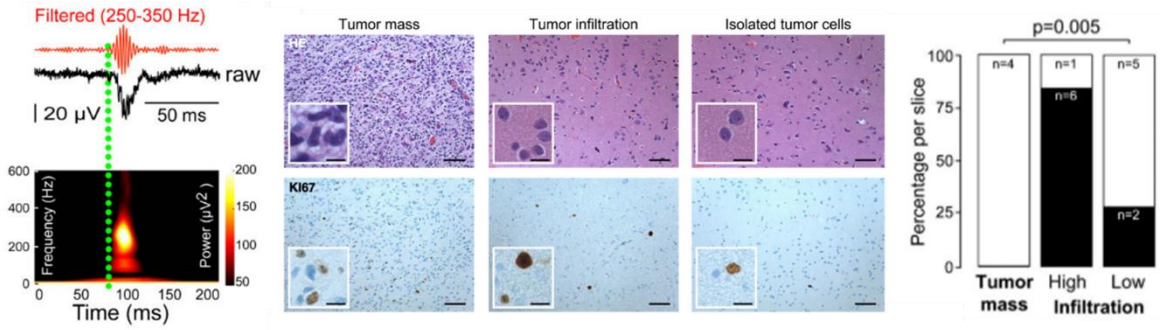

Figure 30: HFO are recorded from highly infiltrated peritumoral areas.
From Pallud et al, 2014.

Results

4.1 Objectives of the research

In the first chapter, I described the latest glioma classification and emphasized the significant role of the IDH status. Additionally, I enlightened the high frequency of epilepsy in glioma patients and its interactions with the oncological process. Epilepsy develops as the tumor grows, and its presence is linked to a more favorable oncological prognosis. I discussed the main complementary exams used for glioma diagnosis and the challenges in identifying peritumoral glioma cells. Furthermore, I described the main glioma treatments, focusing on surgery and how the supra-total approach may improve oncological and epileptological outcomes. Nonetheless, gliomas remain fatal due to our inability to detect all the peritumoral glioma cells, leading to patient relapse.

The second chapter defines the surrounding peritumoral tissue and explores how epileptogenesis, ictogenesis, and glioma growth occur in that area. I discussed the critical mechanisms involved in these processes and how the dysregulation of GABA and Glu signaling, due to the presence of tumor cells modifying the microenvironment and neuronal activity, are involved in these dynamic processes. The presence of tumor cells increases the excitability of neurons, leading to seizures, while neuronal hyperactivity promotes tumor growth. Biomarkers like 5-ALA, Glu-CEST, and D2HG-SMR are used to detect tumor cells, but more is needed to define the limits of the peritumoral compartment.

In the third chapter, I presented the main data about the electrophysiology of peritumoral tissue, both ex vivo and in vivo. In vivo ECoG recordings enable us to capture IIDs and seizures from the peritumoral cortex. Still, the use of macroelectrodes limits our spatial resolution and lacks access to single-neuron firing. The development of innovative microelectrodes with an organic PEDOT:PSS lining offers the potential to improve the SNR and enhance the detection of new signals, such as HFO, which are already promising biomarkers of epileptogenesis. Since one study has already colocalized the presence of HFO with the peritumoral glioma infiltration, we hypothesized that HFO might also be used as a biomarker of tumor cells.

Considering all previous studies, our hypothesis suggests that the presence of tumor cells impacts the electrophysiological activities recorded in the peritumoral area, altering neuronal activity and contributing to epileptogenesis, ictogenesis, and tumor growth. Throughout this thesis, I have studied the behavior of peritumoral electrophysiological activities both in vivo during awake glioma surgery and ex vivo on peritumoral human slices.

Therefore, my thesis objectives are:

1) To characterize in vivo electrophysiological features of the peritumoral cortex using canonical frequency bands and the aperiodic components of the power spectrum.
2) To investigate local the impact of tumor cells on in vivo electrophysiology.
3) To develop an algorithm based on the electrophysiological characteristics of the peritumoral cortex to assist in its delimitation.

4) To study the spatio-temporal dynamics of different electrophysiological activities (FP, MUA, and HFO) during the preictal period leading to an ILE in the human peritumoral cortex ex vivo.

5) To find a biomarker of glioma cell peritumoral infiltration.

4.2 Materials and Methods

Patients:

We retrospectively analyzed ECoG data from 29 adult glioma patients recorded during awake surgery between November 2020 and March 2023 at Sainte-Anne Hospital and Pitié-Salpêtrière Hospital (Paris, France). We collected peritumoral tissue and tumor samples from 34 patients. The samples were taken from the security margin when it was large enough, and not all the tissue was transferred to the neuropathology service. These peritumoral slices were analyzed to study the spatiotemporal dynamics of the preictal state. Several clinical features such as the presence of TRE, tumor location, WHO tumoral grade, and IDH mutation status were collected.

This retrospective study was approved by the Comité d'Evaluation et d'Ethique de l'INSERM - IRB00003888 (approval n°21-864).

Surgery:

The function-based resection was performed using an asleep-awake-asleep technique. Patients were initially anesthetized with propofol to perform a craniotomy. Once the dura mater was opened and the cortex exposed, anesthesia was stopped. The craniotomy exposed the lesion in addition to two to three cm of peritumoral cortex around the lesion to ensure a positive functional brain mapping. Surgery was not modified for the research protocol and consisted of resection after functional mapping in awake patients.

ECoG recordings:

ECoG is routinely used in glioma awake surgery in both hospitals (Pitié-Salpêtrière and Sainte-Anne, Paris). ECoG is used for intraoperative monitoring to identify spontaneous interictal discharges and after-discharges or epileptic seizures induced by direct electrical stimulations.

Once the patients were awake and able to perform the intraoperative functional testing, the neurosurgeon placed the sterile electrodes directly in contact with the cortex. The same position was kept for at least two minutes. Then, the electrode was moved to an adjacent area to map the whole exposed cortex. Typically, between four to six different positions were possible. A picture was taken for every electrode position, and information about the placement of the electrode in relation to the tumor border was carefully annotated. We tried to use a GoPro camera attached to the neurosurgeon's front, but since our goal was just to classify the positions of the electrodes in relation to the tumoral borders, the picture system was easier. A 6 X 1 strip and a 4 X 2 grid (DIXI Medical) were used, depending on the morphology and size of the craniotomy. We privilege DIXI Medical electrodes due to their higher flexibility and adaptability to the cortex compared to AdTech electrodes. The electrodes' diameter was 4 mm and the interelectrode space was 10 mm. Data were acquired using an Atlas System (Neuralynx) or an ISIS Inomed amplifier using a 20 KHz sampling rate. The first recordings were performed with the ISIS Inomed system, and once

we acquired the Atlas System we moved only to Atlas. We chose this amplifier because it already had CE approval, and it allows for a high sampling rate (20 KHz) and a high number of channels with a good quality of the recording compared to other systems such as BlackRock. To optimize the recording's quality several configurations for the reference placement were tested. For the ISIS Inomed amplifier the best results were obtained with a single reference needle placed in the scalp, next to the craniotomy. For the Atlas System, the configuration was different, one of the macroelectrodes was used as a reference, and a ground needle electrode was placed in the scalp, next to the craniotomy. To improve the quality and avoid pulsatility artifacts, a cotton pad was always placed above the electrodes. Data were acquired before the cortical functional mapping that precedes the function-based resection. The recording did not modify the surgery.

Electrodes classification:

The neurosurgeon identified the anatomic location of the tumor both by macroscopic direct visual analysis and echography. The position of the electrodes was noted and pictures of every position were taken. 3D-MRI volume rendering was obtained using 3D-Slicer reconstruction, using FLAIR and T1 Gadolinium MRI sequences (https://www.slicer.org, Brigham and Women's Hospital, Boston, USA). The intraoperative pictures with the electrode position were merged into the 3D-MRI reconstructions, matching the gyral patterns, to measure the distance between the tumoral border visible on MRI on the FLAIR sequence and the contacts. Therefore, an electrode was classified as: "tumoral" if it was contacting an MRI-positive area on FLAIR sequence and/or if it has a suspicious appearance macroscopically: "close peritumoral" if placed at less than 15 mm from the tumor border visible on MRI on FLAIR sequence; "far peritumoral" if placed between 16 and 30 mm from the tumoral margin and; "healthy" if placed at more than 31 mm. We chose those cut-off values since there is evidence of the presence of tumoral cells in the surrounding peritumoral tissue up to 20 mm, so we added another 10 mm to be sure that the healthy tissue did not contain tumoral cells.

ECoG data preprocessing:

For each recording, we plotted the raw signal from all channels using our graphical interface developed in Matlab (The Mathworks, Natick, MA, USA). For the visualization, we used a monopolar setup taking as a reference the reference electrode of the acquisition system (needle electrode for ISIS Inomed and DIXI electrode for Atlas System) and, we forward-backward filtered the signals (to avoid phase shift) between 0.1 and 50 Hz using a Chebyshev type II bandpass IIR filter. The monopolar configuration was chosen because our purpose was to correlate a signal with a distance and an underlying histology when possible. The use of a bipolar montage gave us information of two electrodes.

After visual inspection, we removed noisy channels. Segments with artifacts were excluded. The remaining data segments were subsampled (2000 Hz) and classified according to their position in the brain (tumoral, close peritumoral, far peritumoral, and healthy), and in the electrode strip. In these classified segments, we conduct a power spectrum analysis.

Power spectrum analysis:

To assess the power distribution into the different frequency components of ECoG signals, we computed the power spectral density (PSD) over the raw data using the Welch method in each signal segment (Hanning window of n = 2* Sample Rate with an overlap of 50%). Afterward, we removed from the PSD the electrical noise peaks (50 Hz and its harmonics) and computed the total power by summing the remaining points.

We calculated the absolute and relative power (Bell et al., 1990) in the six following frequency bands: delta (0.5 to 4 Hz), theta (4 to 8 Hz), alpha (8 to 12 Hz), beta (12 to 29 Hz), low gamma (30 to 45 Hz) and high gamma (55 to 100 Hz). The absolute power values were obtained by summing the PSD into each frequency band, while the relative power, was by dividing this sum by the total power. To be able to compare data from different patients, these power values were normalized using the maximum power value from each patient, to obtain values between 0 and 1.

Aperiodic components frequency analysis:

To study the 1/f-like aperiodic component of the PSD, we estimate the offset and the exponent of the PSD. To compute these values, we use the FOOOF algorithm (Donoghue et al., 2020), which parameterizes the power spectra as a combination of periodic and aperiodic components. Power spectra were parameterized across the frequency ranges 1 to 200 Hz, 20 to 30, 20 to 40, 30 to 45, 40 to 60, and 60 to 120 Hz. We chose those ranges to study the slope behavior in different frequency ranges and to avoid the 50 Hz noise.

Phase Locking Value (PLV):

As a measure of connectivity between the different compartments (tumoral, close peritumoral, far peritumoral, and healthy) we studied the phase synchrony over contacts. Specifically, these phase interactions were accessed using the Phase Locking Value (PLV). For that, first, we filtered the signals in six frequency bands (0.5 - 4 Hz, 4.5 - 8 Hz, 8.5 - 12 Hz, 12.5 - 30 Hz, 30.5 - 45 Hz, and 55 - 100 Hz) using a Chebyshev type II bandpass IIR filter. Then, for each one of these bands we calculated the Hilbert transform and obtained the phase of every signal. Afterward, we got the phase difference and computed the PLV between the contacts recorded at the same time in the operating room but covering different tissue areas (for example, contact number one located in a tumoral region vs contact number five located in a healthy region). At the end of this process, we had around 1962 phase locking values distributed in all the possible categories.

Neural Network Classifier:

We separated the training and test group with 493 recordings for training and 215 recordings for testing (70% training and 30% test) maintaining the ratio of each tissue. After dividing the database, we selected the features for the final classification model: absolute and relative power values (from delta to high gamma) and the slopes (1-200, 20-30, 20-40, 30-45, 40-60 and 60-120 Hz). Using the Python library SKLearn we trained multiple models increasing the number of features in each model, and selected the one with

the best performance. For training, we used a multi-layer perceptron classifier with a lbfgs solver over three layers with an alpha of 1e-5. Finally, we validated the classifier over the test data and obtained the confusion matrix, precision-recall curve, and F1 score. Initially, we combined the non-tumoral categories to assess if the neural network classifier was similar to other classifiers previously published by other groups.

Afterward, classified the data considering the peritumoral versus the rest of the contacts; three categories (tumoral, peritumoral, and healthy). We balanced the resulting database, to remove bias due to the increasing number of peritumoral elements, and trained a new model using the features which provided the best neural network in the previous step (1-200, 20-30, 20-40, 30-45, 40-60 and 60-120 Hz slopes, and the absolute and relative values from delta to high gamma). Finally, the model was trained to be used in classifying four categories – tumoral, close peritumoral, far peritumoral, and healthy-.

Human tissue:

During surgery, the peritumoral tissue samples were taken out and immediately immersed in an oxygenated, cold (1-4°C) aCSF solution (250 mM sucrose, 10 mM D-glucose, 3 mM KCl, 25 mM $NaHCO_3$, 1 mM for 14/46 slices and 110 mM Choline, 26 mM $NaHCO_3$, 10 mM Glucose, 11.6 mM Na-ascorbate, 7 mM $MgCl_26H_20$, 3.1 mM Na-pyruvate, 2,5 mM KCl, 1,25 mM $NaH_2PO_4H_2O$ for the remaining 32/46 slices) to slow down metabolism.

The operative piece was transported to the laboratory, where meninges were taken out to facilitate the slicing process. Using a vibratome (Leica VT1200S), 400 µm neocortical slices were cut off. Then, the slices were placed in an interface chamber for recovery for at least one hour, perfused by an oxygenated physiologic aCSF solution (124 mM NaCl, 3 mM KCl, 26 mM NaHCO3, 11.1 mM D-glucose, 1,6 mM CaCl2, 1,3 mM MgCl2) at 37°C.

MEA:

We used planar MEA with titanium nitride electrodes (30 µm diameter), arranged in two different configurations: i) a big one: 12 x 10 matrix with 1000 µm interelectrode spacing in the "x" plan and 1500 µm in the "y" plan, ii) a small one: 12 x 12 matrix with 200 µm interelectrode spacing in both directions. MEA size was chosen depending on the size of the brain slices. The recordings were made using a sampling rate of 10.000 Hz. They were filtered between 0.1 and 10.000 Hz (Logiciel MC Rack, MultiChannel Systems).

To keep alive slices for several hours, the MEA chamber was perfused with a high flow (6 ml/min) of oxygenated aCSF at 37°C. Two different types of aCSF were used: during the first ten minutes, physiologic aCSF was to record spontaneous activities (IIDs), and after ten minutes, ictogenic aCSF (6-8 mM K^+, 0 Mg^+ aCSF) to induce ILE and PIDs.

Immunostaining:

To study the histology underlying the in vivo ECoG recordings, nine brain samples from the peritumoral security margin beneath one of the DIXI electrodes were obtained for 9 patients (one biopsy per patient). Slices were cut using a vibratome (Leica VT1200S) in 400 µm. Then, they were fixed in formalin-zinc (Diapath) for 24-72 hours. They were

embedded on agar to be resliced in 40 µm sections. Only IDH mutated gliomas were analyzed, since we were using an antibody against the IDH-mutation to detect the presence of tumor cells. After 10 minutes of H_2O_2 application to block internal peroxidase, the slices were heated at 100 °C in Tri-Sodium citrate buffer 10 mM for antigen retrieval over 30 minutes. Slices were permeabilized with PGT 0,1% for 1 hour, then they were incubated overnight with a mouse primary antibody against IDHR321H mutation (1:200, Quartett). Immunochemistry was performed with a DAB reagent (Abcam).

MEA data analysis:

MC-Rack software (Multi Channel Systems) was used to visualize FP data. For measuring the temporal evolution of FP, the electrode displaying the higher amplitudes was selected and exported to Clampfit (suite pClamp, Molecular Devices). We defined the preictal transitional period as going from adding ictogenic solution until the seizure onset. Seizure onset was determined visually.

The transitional preictal period was divided into three subperiods: build-up, steady state, and trigger period. To delimit the build-up period, we selected the recordings from the appearance of the first PID > 15 µV to the end of the increase in amplitude. The trigger period was visually identified, as PID showed a change in frequency in the seconds preceding the ILE. The steady-state period was defined as the period between the build-up and the beginning of the trigger period.

FPs were analyzed after applying a low pass filter of 30 Hz (Butterworth – 8 poles) and, if needed, a high pass filter of 1 Hz (Bessel – 8 poles). Amplitude, rising slope, and frequency were measured using an " up-only" algorithm with a user-defined threshold.

As slices were highly heterogeneous in terms of FP's amplitude and duration of the preictal period, and as we were interested in the dynamics more than in the absolute values, to be able to compare the data, normalization was performed. Amplitude, rising slope, and frequency were normalized to the maximum value of the slice. Means and standard deviation were calculated for every parameter in the three periods. To evaluate the temporal evolution by subperiods, data were organized in 10% BINS for the build-up period and 33% BINS for the trigger period.

HFA temporal analysis:

HFA analyses were performed using data from 25 slices (18 big matrix, seven small matrix). The most representative electrode from each slice was selected for this analysis. The build-up, steady-state, and trigger periods were clearly distinguished for each electrode. Still, since the beginning and end of each of these period between slices, they were normalized in time (between 0 and 1) to compare the data from all recordings. To characterize the HFA behavior, two measures were extracted from these data: HFA duration and HFA amplitude.

A semi-automatic algorithm was used to compute the HFA duration. First, our script forward and backward filtered the raw signals around each PID (600 ms window) using a Chebyshev type II bandpass IIR filter (100 to 600 Hz). Then, the envelope of this signal

was calculated using the Hilbert transform. The envelope was filtered again (low pass 40 Hz) to smooth its high-frequency components and used in the HFA begin and end detection. To detect the beginning and end of each HFA, we used an amplitude threshold on this signal; specifically, for each segment, we searched for a first local maximum, and from there, our algorithm moved to the left or right (detecting the beginning or end, respectively) until the filtered envelope value was lower than the mean plus four standard deviations. Finally, if necessary, each detection was visually inspected and manually adjusted using our graphical interface. The HFA duration was calculated as the sample difference between the start and end points over the sample rate.

To evaluate the HFA amplitude, we filtered the raw signals again, but this time around the previously detected starting and ending points (±100 ms). A Chebyshev type II bandpass IIR filter was used between 100 and 550 Hz. The envelope of the filtered signal was calculated, and its maximum value was defined as the HFA amplitude.

HFO temporal analysis:

HFO temporal analysis was performed using the 19 electrodes with a larger number of HFOs over 19 slices (1 electrode per slice, seven big matrix, 12 small matrix). To perform this analysis, first, the HFOs were detected. Their features (number in time, frequency, PID ratio, and duration) were extracted, and finally, a more detailed analysis of the phase relationship between HFOs and LFP was performed. For all these analyses, the separation between the build-up, steady-state and trigger periods was not considered (due to the limited number of events).

A semi-automatic algorithm was used to detect HFOs. Our algorithm filters the raw data between 180 and 400 Hz using an infinite impulse response filter with a forward-backward filtering strategy that introduces no phase shift. It calculates the filtered signal envelope using the Hilbert transform and extracts the candidates for HFOs using a threshold equal to the envelope mean plus five standard deviations (Crépon et al., 2010; Richard J. Staba et al., 2004). Any envelope segment that met this threshold criterion and had a minimum duration of 10 ms was considered a candidate HFO. The time-frequency spectrum of all HFO candidates was obtained between 50 and 500 Hz with a Gabor wavelet, implemented with a modulated Gaussian window (Valderrama et al., 2012) of 1.5 cycles, and then used in the visual inspection stage. Two examiners (BD, DH) independently evaluated all previously obtained candidates for HFOs, using their time frequency, raw signal, filtered signal, and envelope to reject artifactual and false-positive events. On average, the two researchers agreed on 70% of the events; for the remaining 30%, they reevaluated the events and reached an agreement.

Once HFOs were detected, they were classified as ripples or fast ripples according to their predominant frequency in the spectrogram (ripples: 80 Hz< f <250 Hz and fast ripples: 250 Hz< f <550 Hz) and their duration and temporal event density were extracted. For slice 101013S1, an additional analysis was performed, including the five electrodes with the highest number of HFOs. The signal from each of these electrodes was divided into bins, and in each bin, all HFOs from these five electrodes were grouped. The FP was averaged within each group, and each event was fitted to this average. Likewise, the envelope of the filtered HFO (+-50 Hz of its dominant frequency) was calculated and plotted in a color matrix, considering the same time reference found with the FP average. Finally, a grouped

representation is obtained, with the PID onset at the top of the figure and the seizure onset at the bottom.

Spatial analysis :

For spatial analysis, the characterization of PIDs (in amplitude and time), HFA (in amplitude), and HFOs (in number of events) was extended to all electrodes of a single slice. Timestamps marked as build-up, steady state, and trigger from the same representative electrode were kept, and two color maps were generated for each of these periods and for each of the following five features: PID amplitude, PID firing order, PID firing time, HFA amplitude, and number of electrodes with HFOs.

First, we averaged the filtered signals (FP < 50 Hz) from all electrodes. Then, the local maxima of this average were detected, and a window of 4000 samples (400 ms) centered on each of these peaks was constructed to define co-occurrence in all 120 electrodes. Co-occurring events with less than 10 PIDs were excluded from the analysis, and the five features mentioned above were calculated for the rest of the events. Each feature was stored in a two-dimensional matrix that was normalized between 0 and 1. Finally, a color map was generated by interpolating the color values according to the normalized values of the matrix.

Statistics:

In both cases statistics were made using Prism (GraphPad). Exact p values are given unless $p < 0.001$. The level of significance was set at $p < 0.05$. Descriptive statistics are given as mean and standard deviations (SD).

In vivo analysis:

The data did not follow a gaussian distribution. The different spectral features were compared between all four different positions (tumoral, close peritumoral, far peritumoral, and healthy) using a Kruskall-Wallis test. A post hoc Dunn's test was applied afterward to compare the positions between them considering the multiple comparisons. Astrocytoma and oligodendroglioma patients were compared using the Mann-Whitney test. A Spearman correlation test was used to compare the distance in mm and the tumoral infiltration with all the features.

Ex vivo analysis:

The data did not follow a normal distribution. Comparisons between two continuous variables were made using the Mann-Whitney test. Comparisons between repeated measurements of continuous variables were made using the Wilcoxon test with a post hoc Dunn's test to correct for multiple comparisons.

4.3 ECoG Signatures of the Peritumoral Tissue

The first part of my thesis involves examining the electrophysiological features of the peritumoral cortex as compared to the tumor and the healthy areas. Glioma surgery aims to eliminate the largest amount of peritumoral cells without causing postoperative neurological impairment. Since gliomas can be located within or around functional areas, surgeries are conducted in awake condition to assess functionality through direct electrical stimulation. During the testing, ECoG recordings are used to monitor the presence of after-discharges or seizures induced by the stimulus.

The objectives of this work were as follows:

1) To investigate the canonical frequency bands and aperiodic components of the power spectra behavior in the tumor, close peritumoral, far peritumoral, and healthy areas.

2) To determine whether infiltration of tumor cells alters physiological brain rhythms.

3) To examine if the underlying histological classification (astrocytoma and oligodendroglioma) influences these characteristics.

4) To develop an automatic classifier of the compartments based on the electrophysiological characteristics.

Our methodology involved in vivo ECoG recordings during awake glioma surgery. We employed DIXI electrodes, each with a diameter of 4 mm and an interelectrode spacing of 10 mm. I was responsible for the recordings, in close collaboration with the neurosurgeons, and providing real-time feedback regarding the presence of IIDs, after discharges or emerging seizures. I selected noise-free segments recorded before the onset of electrical stimulation for analysis. Using MRI data, I generated 3D volume renderings of the brains and lesions, and together with the perioperative pictures, I measured the distance from the electrode center to the tumor borders. In nine cases, samples were obtained from areas beneath electrodes. In these cases, I conducted immunohistochemistry to identify tumor cells, employing a primary antibody against IDH mutated forms and a DAB reagent coupled with a secondary antibody. Then, I quantified the mean number of tumor cells in the samples. The power spectrum features were analyzed using a homemade script based on the FOOOF method developed by my colleague David Henao-Herreno. Statistical analysis was made using GraphPad. Additionally, my colleague Juan Nieto designed a neural network-based automatic classifier. In the end, I created all the figures and drafted the paper and cover letter.

Our findings revealed that tumor contacts exhibited decreased activity across all frequency bands except for an increased delta activity. That suggests that gliomas induce alterations in EEG physiological rhythms. The peritumoral cortex demonstrated heightened relative beta activity and slopes in the 20-30 and 20-40 Hz ranges, likely attributed to modifications in neuronal activity or synaptic input balances. No disparities were observed between close and far peritumoral compartments. However, tumor cell infiltration in the peritumoral region was associated with reduced physiological brain rhythms. This indicates that infiltration and its electrophysiological counterpart do not follow a linear radial distribution but rather an asymmetric propagation along axon bundles and vessels. The offset and 1-

200 Hz slope of astrocytomas and oligodendrogliomas differed. Finally, our neural network-based automatic classifier performed better classifying electrodes based on power spectrum characteristics than a random classifier.

This intraoperative pilot study underscores the electrophysiological attributes of the peritumoral cortex in comparison to the tumor and healthy cortex, thereby contributing to our understanding of diffuse gliomas. The presence of infiltrative tumor cells in the peritumoral region was correlated to specific ECoG features. Our automatic detection tool facilitates the classification of cortex regions as tumor, peritumoral, and healthy based on their electrophysiological traits.

The utilization of ECoG during glioma awake surgeries holds promise as a valuable tool for investigating interactions between neurons and tumor cells. This study lays the foundation for real-time electrophysiological mapping, enhancing the precision of resection procedures. Consequently, this approach improves oncological and epileptological outcomes, increasing patient survival rates and enhancing quality of life.

4.3.1 Article 1, submitted: Differentiation of Tumoral vs Peritumoral Compartments in Brain Gliomas by Intraoperative ECoG Frequency Signatures.

Title **Differentiation of Tumoral vs Peritumoral Compartments in Brain Gliomas by Intraoperative ECoG Frequency Signatures.**

*Author(s), and Corresponding Author(s)**

*David Henao-Herre*ño [§], *Belén Diaz-Fernandez* [§] *, Juan Nieto, Alesya Evstratova, Alexandre Roux, Edouard Dezamis, Marc Zanello, Bertrand Mathon, Carine Karachi, Alexandre Carpentier, Johan Pallud, Laurent Capelle, *Gilles Huberfeld* [‡], *Michel Le Van Quyen* [‡].

§ both authors contributed equally

‡ both authors contributed equally

B. D-F., D. H-H., J. N., A. E., G. H.

Center for Interdisciplinary Research in Biology,

Collège de France, CNRS UMR 7241, INSERM U1050, Université PSL Paris, France

E-mail : belen.diazfernandez@aphp.fr

Collège de France, 11 place Marcelin Berthelot, 75005 Paris, France.

B. D-F., M.LVQ.

Laboratoire d'Imagerie Biomedicale

75005 Paris, France

B. D-F.

Panaxium SAS

13100 Aix-en-Provence, France

B. D-F.

Department of Neurology

Pitié-Salpêtrière Hospital,

75013 Paris, France

A.R, E.D., M.Z., J. P.

Department of Neurosurgery,

GHU Paris Psychiatry and Neurosciences, Sainte-Anne Hospital,

75014 Paris, France
A.R, E.D., M.Z., J. P.
Institute of Psychiatry and Neuroscience of Paris
University Paris Cité, INSERM U1266,
75014 Paris, France

M.Z., J. P.
Université Paris Cité
75005 Pris, France

B.M, C.K, A.C, L.C.
Department of Neurosurgery,
Pitié-Salpêtrière Hospital,
75013 Paris, France

G.H.
Department of Neurology,
Hopital Fondation Adolphe de Rothschild,
75019 Paris, France

Keywords: tumors, gliomas, electrocorticography, power spectrum, biomarker

Abstract

Brain diffuse gliomas are highly epileptic and infiltrative tumors. Glioma surgery consists in the resection of the tumor core and the maximum of the peritumoral infiltrated zone, infiltrated by tumor cells, guided by the intraoperative assessment of brain functionality and connectivity. Its electrophysiological characteristics are poorly characterized. We study the characteristics of Electrocorticography (ECoG), in the context of glioma surgery in awake condition, using EEG activity sampled on the tumor itself versus on its borders and on healthy areas, in an attempt to characterize the peritumoral cortex. We explore the canonical frequency bands and aperiodic components of ECoG power spectra. First, we find that tumor contacts present a decrease in activity for all the frequency bands except for delta activity, which was increased. Second, the peritumoral cortex was characterized by increased relative beta activity and slopes between 20-30 and 20-40 Hz. Cortical tumor cell infiltration was correlated with a reduction in the production of physiological brain rhythms. Finally, an automatic classifier based on neural networks allows the classification of the electrodes based on their power spectrum characteristics. This intraoperative study shows that the peritumoral cortex displays specific electrophysiological features to be considered for diffuse glioma knowledge and surgery.

1. Introduction

Brain gliomas are the most frequent primary brain tumor and are highly epileptogenic. Between 35-89 % of patients present epileptic seizures at diagnosis.(Huberfeld & Vecht, 2016; Pallud et al., 2014, 2022) Seizure frequency increases as the tumor progresses, and patients may become resistant to antiseizure medication, which greatly impacts their health-related quality of life.[(Correia et al., 2021; S. Liang et al., 2016; Pallud et al., 2014; Rudà et al., 2012)] Multiple mechanisms are implicated in tumor related epilepsy, including Glutamate and GABA signaling impairment [(Huberfeld & Vecht, 2016; Johan Pallud et al., 2013, 2014)], which also affect glioma growth processes. Epilepsy is key in glioma management since, in addition to the effect of seizure control on the health-related quality of life [(Hu et al., 2022; Klein et al., 2003; Taphoorn et al., 2010)] epilepsy and glioma survival are linked.[(Berendsen et al., 2016; Lote et al., 1998; Pallud et al., 2014)]. On the other hand, neuronal activities contribute to glioma growth,[(Huang-Hobbs et al., 2023; Venkataramani et al., 2019, 2022; Venkatesh et al., 2015, 2019)], interactions between tumor and surrounding cortex providing a feedback effect on tumor growth.[(Krishna et al., 2023)]

Gliomas are diffuse tumors, formed by a macroscopic core, identifiable on conventional MRI, surrounded by sparser tumor cells infiltration, extending beyond MRI-defined limits,[(J. Pallud et al., 2010; Zetterling et al., 2016)] known as peritumoral tissue. Oncological and epileptological processes converge at this interface between healthy and pathological tissues. Tumor cells spread in the peritumoral tissue, and epilepsy discharges arise at distance, sometimes at even more than 1.5-3 cm from the tumoral core.[(Mittal et al., 2016; Johan Pallud et al., 2014; Tran et al., 1997)] Peritumoral cortices also produce high-frequency oscillations,[(Feyissa et al., 2018; Nicole E.C. van Klink et al., 2021)] suggesting a hyperexcitability state. Such epileptic activities have been suggested to colocalize with peritumoral infiltration in human postoperative tissues.[(Johan Pallud et al., 2014)]

Peritumoral tissues are critical for surgery, the first-line glioma treatment. Maximal removal of infiltrated tumor cells requires intraoperative functional assessment of peritumoral areas, which warrants prolonged survival and safer surgery.[(De Witt Hamer et al., 2012)] Such supramaximal resection encompassing isolated glioma cells is performed under awake condition to identify brain connectivity within peritumoral cortex and white matter bundles and to achieve a function-based resection.[(H. Duffau, 2007; J Pallud & Dezamis, 2017)] Brain functions are tested intraoperatively using direct electrical stimulations. Electrocorticography (ECoG) can detect spontaneous inter-ictal epileptic activities and after discharges and epileptic seizures induced by direct electrical stimulations.[(Demuru et al., 2020; Park et al., 2014; Trebuchon et al., 2012; Zanello et al., 2020)] The value of the integration of the epileptic activity detected by intraoperative ECoG in the resection is still a matter of debate.[(Boetto et al., 2016; Englot et al., 2011; P. Sen Yao et al., 2018)]

However, the characterization of tumoral vs. peritumoral areas using electrophysiology gathers limited attention, as tumor detection is performed by imaging. Older reports suggest that “The data provided by the stereo-EEG … did not permit, alone, a histological diagnosis, excepted when electrodes explored a solid tumor”,[(Munari et al., 1985)] while electrodes impedances allow the location of gliomas and surrounding edema. In recent years, analysis of the canonical frequency bands of the power spectrum has shown

differences between the tumor and the healthy tissue.[(Boussen et al., 2016)] Indeed, the aperiodic components of the power spectrum, such as the offset and slope, have been studied in several pathologies, such as schizophrenia or Parkinson's disease, but it is less known about gliomas and their surrounding tissue.[(Belova et al., 2021; Donoghue et al., 2020; Ghinda et al., 2021; Molina et al., 2020)] In particular, the slope of the power spectrum is thought to be a marker of the excitation-inhibition balance,[(Gao et al., 2017; H. Jiang et al., 2022; Molina et al., 2020)] known to be key both in epileptic and glioma growth processes.[(Huberfeld & Vecht, 2016)]

This study aims to identify *in vivo* electrophysiological biomarkers recorded intraoperatively using ECoG to better characterize the peritumoral cortices and to delimitate the extension of the peritumoral area during awake surgery by studying the

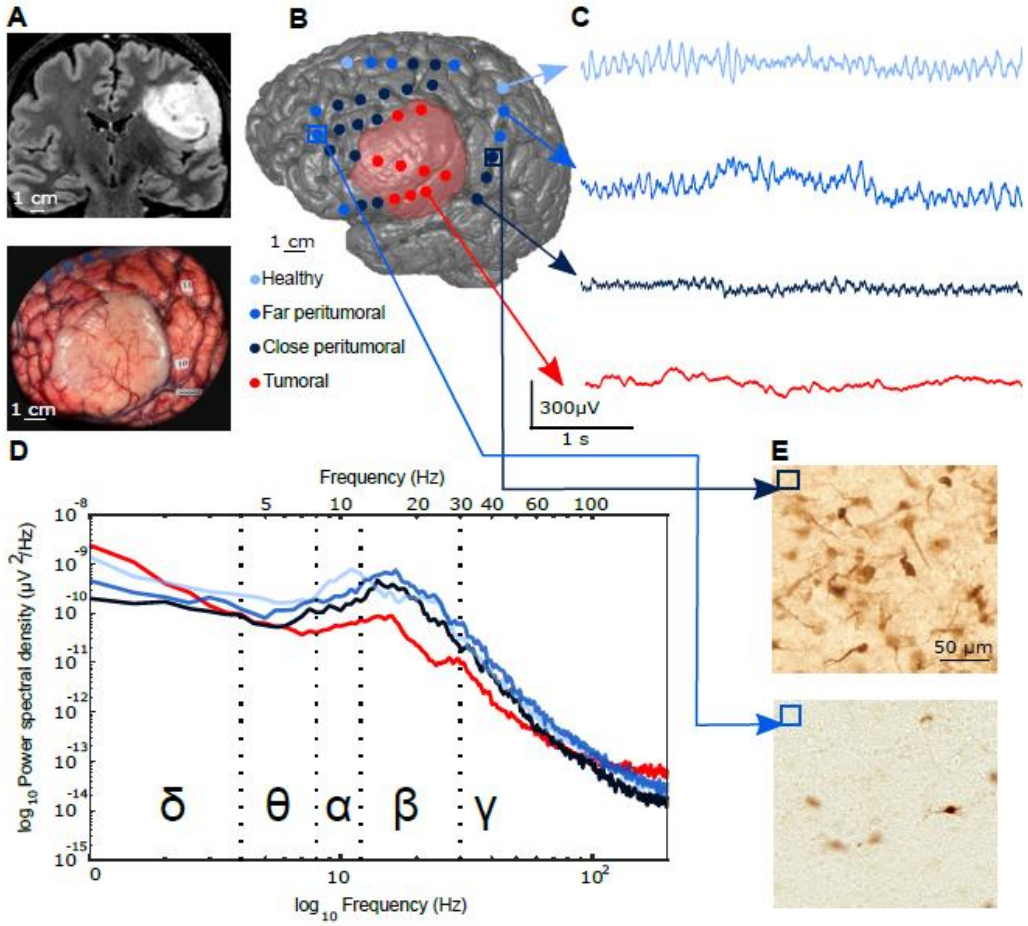

canonical frequency bands of the power spectrum as well as the aperiodic components recorded in the different areas (**Figure 1**).

Figure 1: Intraoperative ECoG recording during glioma surgery. A: MRI sagital view of a left tumor and perioperative picture. B: 3D volume rendering with the position of the contacts superimposed- tumoral (red), close peritumoral (dark blue), far peritumoral (mild blue), and healthy (pale blue). C: ECoG traces of the four compartments. D: Welch periodogram of 4 contacts, one from every location. E: Immunohistochemistry (IDH1R132H labeling) showing a high peritumoral infiltration (> 15 tumoral cells / 250 µm^2) at the top, and low infiltration (< 15 tumoral cells / 250 µm$^{2)}$ at the bottom.

2. Results and Discussion.

We obtained electrophysiological data from 718 contacts from 29 glioma subjects recorded with ECoG during awake surgery. Most cases were astrocytoma, IDH-mutant (19/29 patients; 65.51%), followed by oligodendroglioma, IDH-mutant and 1p19q codeleted (6/29 patients; 20.68 %), glioblastoma, IDH-wildtype (2/29 patients; 6.89%), and two non-typable gliomas (**Table 1**). WHO grade 3 was the most represented grade (13/29 patients; 44.82%), followed by WHO grade 2 (11/29 patients; 37.93%) and WHO grade 4 (5/29 patients; 17.24%). Most patients (27/29 patients; 93.1%) presented with epileptic seizures at diagnosis, and none of them were drug-resistant before surgery. The most frequent tumor location was frontal (19/29, 65.5%), followed by temporal (5/29, 17.2%) and insular (5/29, 17.2%). Unilobar location (21/29, 72.4%) was more frequent than multilobar implication (8/29, 27.6%). Cortical involvement (18/29, 62.1%) was more frequent than pure subcortical location (11/29, 37.9%). From the 718 electrodes, 126 were placed over the tumoral area, 456 were placed in the peritumoral area (243 close - <1.5 cm and 213 far- 1.5-3 cm), and 136 were placed over healthy tissue. Of all the 29 patients, 7 (24,1%) presented spontaneous interictal discharges (IIDs). IIDs were never recorded at the tumor level. The mean distance from the tumoral border to the IIDs was 17 mm (min 2.89 mm, max 32.65 mm).

Patient	Lobe	Side	Contacts	Location	Pathology	IDH	IIDs	Grade	Epilepsy
1	Frontal	Right	25: 2 T, 6 CP, 7 FP, 9 H	C	A	R132H	No	3	Yes
2	Frontal	Right	32: 12 T, 8 CP, 7 FP, 5 H	C	O	R132H	No	2	No
3	Frontal	Right	49: 11 T, 17 CP, 15 FP, 4 H	C	NT	R132H	No	3	Yes
4	Fronto-parietal	Left	18: 4 T, 11 CP, 3 FP	C	O	R132H	No	2	Yes
5	Frontal	Left	28: 11 T, 5 CP, 12 FP	C	A	R132H	No	3	Yes
6	Frontal	Left	20: 8 T, 10 CP, 2 FP	C	A	R132H	Yes	4	Yes
7	Parieto-occipital	Left	20: 3 T, 10 CP, 7 FP	C	GB	WT	No	4	Yes
8	Temporo-parietal	Right	14: 6 CP, 6 FP, 2 H	SC	GB	WT	No	4	Yes
9	Occipital	Left	12: 2 T, 3 CP, 4 FP, 3 H	C-SC	A	R132H	No	2	Yes
10	Frontal	Right	24: 1 T, 9 CP, 8 F, 6 H	C	A	R132H	No	4	Yes
11	Frontal	Left	15: 10 T, 5 CP	C	O	R132H	No	3	Yes
12	Insula	Left	24: 9 CP, 7 FP, 8 H	SC	A	R132H	Yes	2	Yes
13	Frontal	Left	32: 2 T, 9 CP, 14 FP, 7 H	SC	A	R132H	No	4	Yes
14	Frontal	Left	20: 10 CP, 5 FP, 5 H	SC	A	R132H	No	2	Yes
15	Insula	Right	20: 5 CP, 8 FP, 7 H	SC	A	R132H	No	2	Yes
16	Temporo-parietal	Left	16: 8 T, 5 CP, 3 FP	C	A	R132H	No	2	Yes
17	Frontal	Left	8: 4 T, 3 CP, 1 FP	C	A	R132H	No	2	Yes
18	Frontal	Right	16: 2 T, 10 CP, 4 FP	C	NT	R132H	No	3	Yes
19	Fronto-temporal	Left	20: 12 CP, 7 FP, 1 H	SC	A	R132H	No	3	Yes
20	Frontal	Left	48: 10 T, 10 CP, 15 FP, 13 H	C	O	R132H	No	2	Yes
21	Fronto-temporal	Right	40: 8 CP, 11 FP, 21 H	SC	A	R132H	No	3	Yes
22	Fronto-parietal	Left	40: 12 T, 13 CP, 15 FP	C	O	R132H	Yes	3	Yes
23	Insula	Right	18: 4 CP, 4 FP, 10 H	SC	A	R132H	No	3	Yes
24	Insula	Left	20: 6 CP, 9 FP, 5 H	SC	O	R132H	Yes	2	No
25	Frontal	Right	15: 4 T, 9 CP, 2 FP	C	A	R132H	Yes	3	Yes
26	Insula	Left	48: 15 CP, 11 FP, 22 H	SC	A	R132H	No	2	Yes
27	Fronto-parieto-occipital	Left	31: 7 T, 9 CP, 15 FP, 1 H	C	A	R132H	Yes	2	Yes
28	Temporal	Right	16: 6 T, 7 CP, 3 FP	C	O	R132H	No	2	Yes
29	Frontal	Left	24: 2 T, 10 CP, 8 FP, 4 H	C	A	R132H	Yes	3	Yes

Table 1: Clinical characteristics of the studied population. Tumoral contacts (T), close peritumoral contacts (CP), far peritumoral contacts (FP), and healthy contacts (H). Cortical (C), subcortical (SC), astrocytoma (A), oligodendroglioma (O), no typable (NT).

2.1. Assessment of glioma cortical compartments according to ECoG frequency bands.

We first looked for differences in the frequency signature between peritumoral tissue, tumoral and healthy contacts. We found differences between the compartments in all the frequency bands and aperiodic features except theta and high gamma relative values (**Table 2**). ECoG recordings from contacts located on tumoral areas were characterized by a reduction in all the frequency bands (from theta to high gamma) both in absolute and relative values, except for the delta band, in which an increased activity was observed (0.287 ± 0.16 in absolute and 0.727 ± 0.14 in relative values), compared to close peritumoral (0.296 ± 0.23 in absolute and 0.652 ± 0.17 in relative, p = 0.43 and p = 0.016), far peritumoral (0.27 ± 0.2 in absolute and 0.633 ± 0.16 in relative, p = 0.11 and 0.002) and healthy contacts (0.196 ± 0.14 in absolute and 0.642 ± 0.16 in relative, p < 0.0001 and 0.009) (**Figure 2**).

	Tumoral	SD	Close Peritumoral	SD	Far Peritumoral	SD	Healthy	SD	*p*
δ Absolute	0.28	0.16	0.29	0.23	0.27	0.2	0.19	0.14	**0.0002**
θ Absolute	0.27	0.2	0.38	0.22	0.39	0.2	0.46	0.21	**<0.0001**
α Absolute	0.19	0.13	0.34	0.21	0.37	0.21	0.38	0.21	**<0.0001**
β Absolute	0.17	0.15	0.41	0.24	0.42	0.24	0.33	0.19	**<0.0001**
Low γ Absolute	0.21	0.13	0.38	0.22	0.42	0.24	0.37	0.21	**<0.0001**
High γ Absolute	0.34	0.21	0.43	0.22	0.42	0.21	0.44	0.21	**0.006**
δ Relative	0.73	0.14	0.65	0.17	0.63	0.18	0.64	0.16	**0.002**
θ Relative	0.32	0.19	0.38	0.22	0.36	0.22	0.39	0.24	0.16
α Relative	0.24	0.15	0.40	0.24	0.41	0.25	0.36	0.22	**<0.0001**
β Relative	0.22	0.19	0.45	0.28	0.45	0.26	0.37	0.25	**<0.0001**
Low γ Relative	0.20	0.14	0.35	0.23	0.35	0.23	0.33	0.23	**<0.0001**
High γ Relative	0.29	0.19	0.36	0.23	0.35	0.21	0.39	0.26	0.15
Slope 1-200 Hz	0.81	0.09	0.85	0.07	0.85	0.07	0.85	0.08	**0.001**
Offset	0.89	0.07	0.86	0.11	0.87	0.07	0.91	0.05	**0.03**
Slope 20-30 Hz	0.62	0.14	0.69	0.14	0.68	0.15	0.62	0.15	**<0.0001**
Slope 20-40 Hz	0.62	0.18	0.74	0.85	0.77	0.11	0.71	0.12	**<0.0001**
Slope 40-60 Hz	0.61	0.17	0.71	0.16	0.73	0.16	0.68	0.17	**<0.0001**
Slope 30-45 Hz	0.53	0.21	0.69	0.17	0.71	0.14	0.65	0.16	**<0.0001**
Slope 60-120 Hz	0.56	0.16	0.65	0.16	0.69	0.17	0.72	0.13	**<0.0001**

Table 2: Mean values of the power spectrum features in the tumoral, close, far peritumoral, and healthy compartments.

The close peritumoral contacts were characterized by an increase in the delta absolute values (0.296 ± 0.23) compared to healthy contacts (0.196 ± 0.14, p= 0.007). However, no significant difference was observed between the close and far groups (p= 0.51). Interestingly, an increase in beta relative values was also observed at the close peritumoral level (0.45 ± 0.28) and far peritumoral contacts (0.45 ± 0.26) compared to both tumoral (0.22 ± 0.19, p= <0.0001 and p < 0.0001) and healthy contacts (0.37 ± 0.25, p= 0.24 and p= 0.05). The values were not different between close and far peritumoral contacts (p= 0.62) (**Figure 2**).

Electrodes in direct contact with the macroscopic tumor presented a slow background activity (**Figure 1**). Previous studies performed in glioma patients using scalp EEG and sEEG already described such a pattern at the tumoral level.[(Munari et al., 1985; Newmark et al., 1983)] Tumor electrodes were also characterized by increased delta power compared to peritumoral and healthy ones, as already reported.[(Boussen et al., 2016; Munari et al., 1985; Nagata et al., 1985; Newmark et al., 1983)] The decrease in all the other frequency bands has also been reported at the tumoral level in a study of 16 glioma ECoGs,[(Boussen et al., 2016)] which stresses the significant effects of tumor development on brain tissues. Nevertheless, previous studies only classified contacts as tumoral or non-tumoral, without considering the dynamics at the peritumoral or healthy level. In our study, the peritumoral electric behavior consisted in an increase in beta relative activity at the peritumoral level. Even if the underlying mechanisms of beta rhythm generation are still under debate, we hypothesized that the increase of beta power at the peritumoral level reflects a dysregulation of neuronal activity, possibly linked to an impairment in GABA [(Johan Pallud et al., 2014)] and glutamate signaling [(Buckingham et al., 2011; Ye et al., 1999; Yuen et al., 2012)] or imbalance.

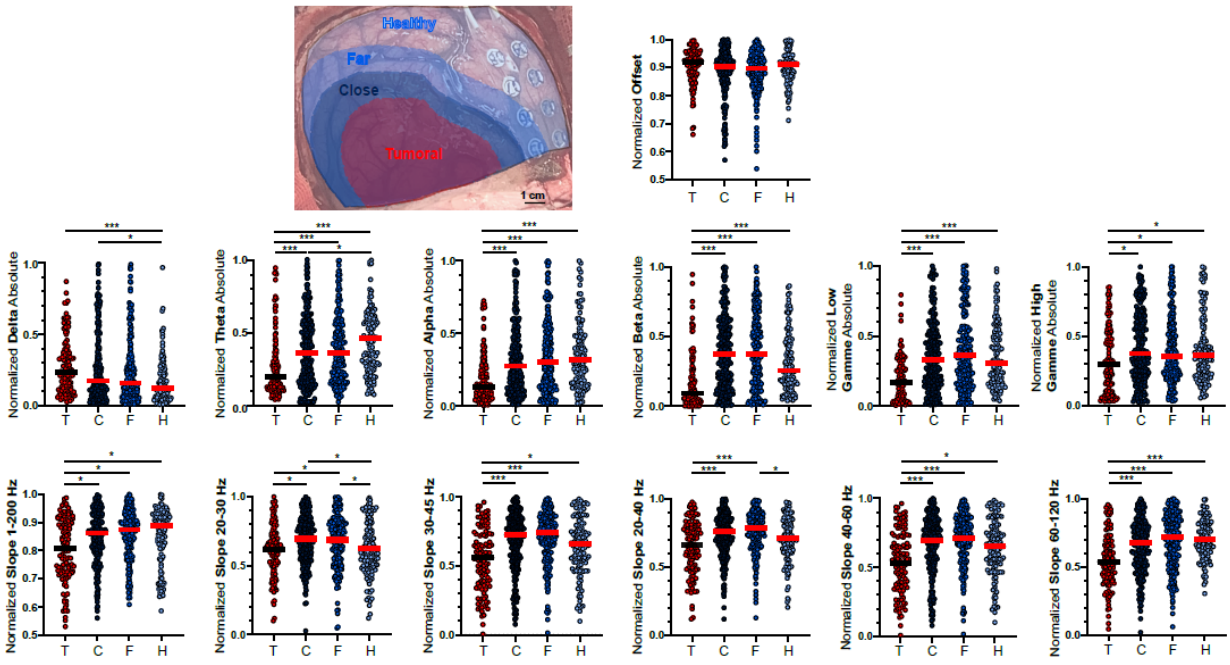

Figure 2: Frequency bands and aperiodic components analysis of tumoral and peritumoral cortices. A: Intraoperative picture showing the limits of the four compartments: tumoral (red), close peritumoral (dark blue), far peritumoral (mild blue), healthy (pale blue). B: Plot showing the normalized spectrum features: delta, theta, alpha, beta, low gamma, high gamma, offset, slope 1-200, 20-30, 20-40, 30-45, 40-60, and 60-120 Hz. * p<0.05, *** p< 0.001.

2.2. Assessment of glioma cortical compartments according to ECoG aperiodic components.

We next examined how the aperiodic components of the power spectrum changed according to the location. We analyzed the offset and different sets of slopes (from 1 to 200

Hz, 20 to 40, 30 to 40, 30 to 45, 40 to 60, and 60 to 120 Hz) to determine which bandwidths were more useful to differentiate tumoral, peritumoral and healthy compartments. Regarding the tumoral contacts, they presented a decrease of the 1-200 Hz slope (0.809 ± 0.09) compared to close peritumoral (0.85 ± 0.07, p= 0.017), far peritumoral (0.858 ± 0.07, p= 0.002) and healthy contacts (0.854 ± 0.08, p=0.006) (**Figure 2**). The slope between 20-30 Hz showed specific patterns at peritumoral locations. For close peritumoral positions, we recorded an increase (0.769 ± 0.14) compared to tumoral (0.62 ± 0.14, p = 0.001) and healthy contacts (0.62 ± 0.15 p= 0.017). Far peritumoral contacts also presented a slope increase (0.68 ± 0.15) compared to tumoral (p= 0.004) and to healthy contacts (p= 0.005). No differences were observed between close and far peritumoral contacts (p=0.72). At the far peritumoral level, the slope between 20 and 40 Hz (0.769 ± 0.11) differed from healthy ones (0.708 ± 0.12; p = 0.0003) (**Figure 2**).

2.3. Intra- and Inter-compartment functional connectivity features.

We then assessed the intra- and inter- compartment connectivity using the phase locking value (PLV). PLV was higher between tumoral contacts (0.59 ± 0.27), followed by close peritumoral (0.46 ± 0.23), far peritumoral (0.43 ± 0.22) and healthy ones (0.36 ±0.17) in the delta range, but also theta range (0.5 ± 0.25 for tumoral, 0.37 ± 0.18 close peritumoral, 0.37 ±0.19 far peritumoral and 0.32 ± 0.17 inside the healthy compartment), alpha (0.55 ± 0.25 intratumoral, 0.37 ±0.19 for close peritumoral, 0.38 ±0.2 for far peritumoral and 0.34 ± 0.2 for healthy), beta (0.54 ± 0.25 intratumoral, 0.34 ± 0.2 for close peritumoral, 0.34 ± 0.19 for far peritumoral and 0.36 ± 0.18 in healthy), low gamma (0.53 ± 0.23 intratumoral, 0.27 ± 0.18 for close peritumoral, 0.27 ± 0.19 for far peritumoral and 0.28 ± 0.17 for healthy) and high gamma (0.56 ± 0.2 intratumoral, 0.35 ± 0.18 for close peritumoral, 0.3 ± 0.18 for far peritumoral and 0.3 ± 0.19 for healthy). The PLV values comparing connectivity between different compartments are summarized in a matrix in **Figure 3.**

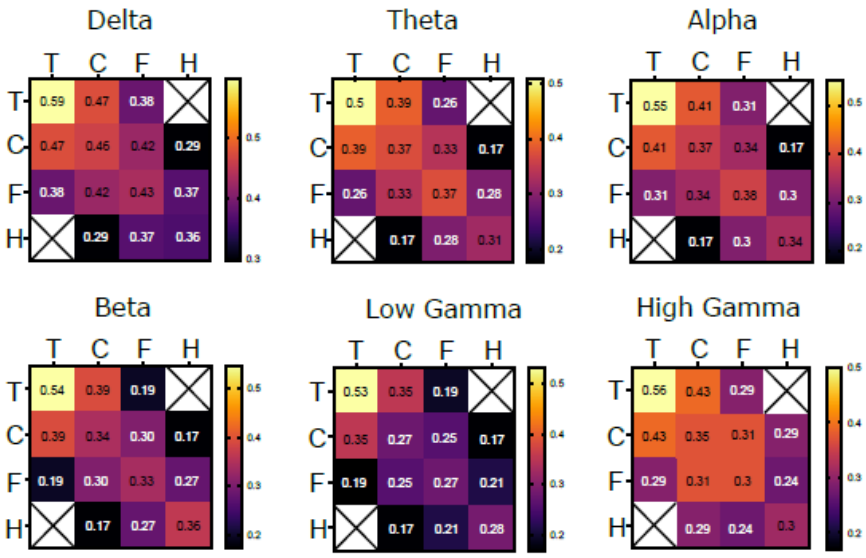

Figure 3: Phase Locking Value (PLV) of tumoral, close, far peritumoral, and healthy compartments for each frequency band. PLV matrix represented in a heat map, with the mean values inside, for the different frequency ranges (from delta to high gamma).

Previous studies have also shown increased connectivity values inside gliomas.[(Boussen et al., 2016)] We hypothesized that gliomas disrupt the normal cortical architecture, favoring long-range conduction of electrical signals.

2.4. ECoG activity differences between astrocytomas and oligodendrogliomas.

We analyzed whether astrocytomas and oligodendrogliomas presented differential frequency bands and aperiodic components characteristics. Astrocytoma presented with higher values of offset compared to oligodendrogliomas at the close peritumoral (0.915 ± 0.06 vs. 0.889 ± 0.04, p = 0.035), far peritumoral (0.9 ± 0.05 vs. 0.88 ± 0.04, p=0.03) and healthy level (0.93 ± 0.03 vs. 0.89 ± 0.04) (**Figure 4**). Two hypotheses may explain the differences found at the healthy level between astrocytoma and oligodendroglioma. First, oligodendrogliomas are thought to be more infiltrative than astrocytomas, which displace the functional fiber bundles towards the periphery. [(Landers et al., 2023)] So, in the case of astrocytomas, the functional areas can be moved towards the healthy level. Second, depending on the placement of the electrodes, healthy contacts can be in contact with functional areas, that present higher neuronal activity, impacting the offset levels.

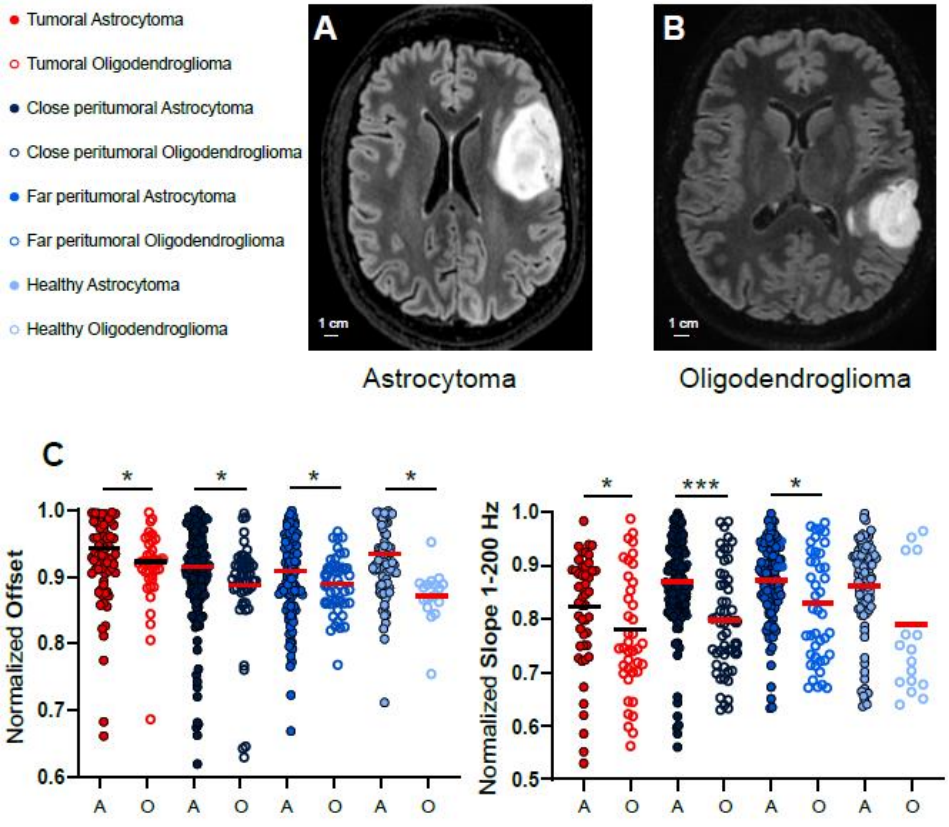

Figure 4: ECoG differential frequency features between oligodendrogliomas and astrocytomas. A: MRI axial view of an astrocytoma. B: MRI axial view of an oligodendroglioma. C: Plot comparing the offset and 1-200 Hz slope between astrocytomas (filled dot) and oligodendrogliomas (empty dot). * p<0.05, *** p< 0.001.

Slope values were also higher in astrocytoma patients at the tumoral (0.82 ± 0.09 vs. 0.78 ± 0.1, p= 0.04), close peritumoral (0.87 ± 0.07 vs. 0.79 ± 0.08, p<0.0001) and far peritumoral levels (0.87 ± 0.06 vs. 0.83 ± 0.09, p=0.02). No differences were found for the rest of the features (**Table 3**).

	Astrocytoma				Oligodendroglioma			
	Tumoral	Close Peritumoral	Far Peritumoral	Healthy	Tumoral	Close Peritumoral	Far Peritumoral	Healthy
δ Absolute	0.28	0.28	0.26	0.18	0.31	0.22	0.16	0.24
θ Absolute	0.26	0.37	0.39	0.47	0.29	0.39	0.38	0.34
α Absolute	0.19	0.35	0.36	0.35	0.24	0.35	0.34	0.53
β Absolute	0.13	0.39	0.39	0.34	0.16	0.47	0.38	0.23
Low γ Absolute	0.18	0.38	0.42	0.37	0.23	0.44	0.37	0.29
High γ Absolute	0.34	0.42	0.43	0.45	0.397	0.52	0.36	0.34
δ Relative	0.77	0.66	0.66	0.68	0.72	0.68	0.72	0.72
θ Relative	0.36	0.35	0.35	0.37	0.25	0.39	0.42	0.35
α Relative	0.27	0.41	0.39	0.35	0.18	0.35	0.44	0.34
β Relative	0.20	0.45	0.42	0.33	0.08	0.36	0.39	0.21
Low γ Relative	0.23	0.34	0.35	0.29	0.13	0.35	0.33	0.35
High γ Relative	0.33	0.34	0.35	0.38	0.26	0.39	0.32	0.30
Slope 1-200 Hz	0.82	0.87	0.87	0.86	0.78	0.79	0.83	0.79
Offset	0.92	0.92	0.91	0.93	0.92	0.89	0.89	0.87
Slope 20-30 Hz	0.64	0.70	0.69	0.61	0.6	0.76	0.72	0.61
Slope 20-40 Hz	0.64	0.74	0.76	0.69	0.62	0.73	0.77	0.77
Slope 40-60 Hz	0.6	0.71	0.76	0.67	0.63	0.69	0.71	0.76
Slope 30-45 Hz	0.52	0.69	0.71	0.66	0.56	0.75	0.8	0.66
Slope 60-120 Hz	0.55	0.68	0.7	0.69	0.60	0.59	0.67	0.77

Table 3: Table showing the mean values of the power spectrum features in the tumoral, close peritumoral, far peritumoral, and healthy compartments in astrocytoma and oligodendroglioma patients.

2.5. Distance influence on the power spectrum.

We then studied if there was a correlation between the distance of the electrode from the tumor border and the changes in the power spectrum features. A two-tailed Spearman correlation test did not show a strong correlation between the distance and the different features. The strongest association was found with offset (R= 0.28, IC 95% 0.19-0.36, p< 0.0001). Those results suggest that the peritumoral area does not follow a radial distribution but rather an eccentric one, sculpted by glioma cell infiltration. We, therefore, performed a correlation analysis between the ECoG signal and tumor cell infiltration quantified in the tissue directly sampled during surgery.

2.6. Peritumoral infiltration by tumor cells impact the power spectrum.

To go further in our analysis, we studied how the intensity of peritumoral infiltration modified the power spectrum. To do so, we measured the density of tumoral cells in 9

peritumoral fragments coming from 9 different patients obtained from the security margin during the surgery in eight cases, and from the macroscopic tumor in one case, for which their exact placement was noted in contact with a recorded channel. We performed immunohistochemistry to quantify the number of infiltrative tumoral cells (tumoral cells/250 µm^2). In the case of IDH mutation, tumor cells were identified by R132H IDH1 labeling and the number of tumor cells per area correlated with the spectrum's different features previously calculated.

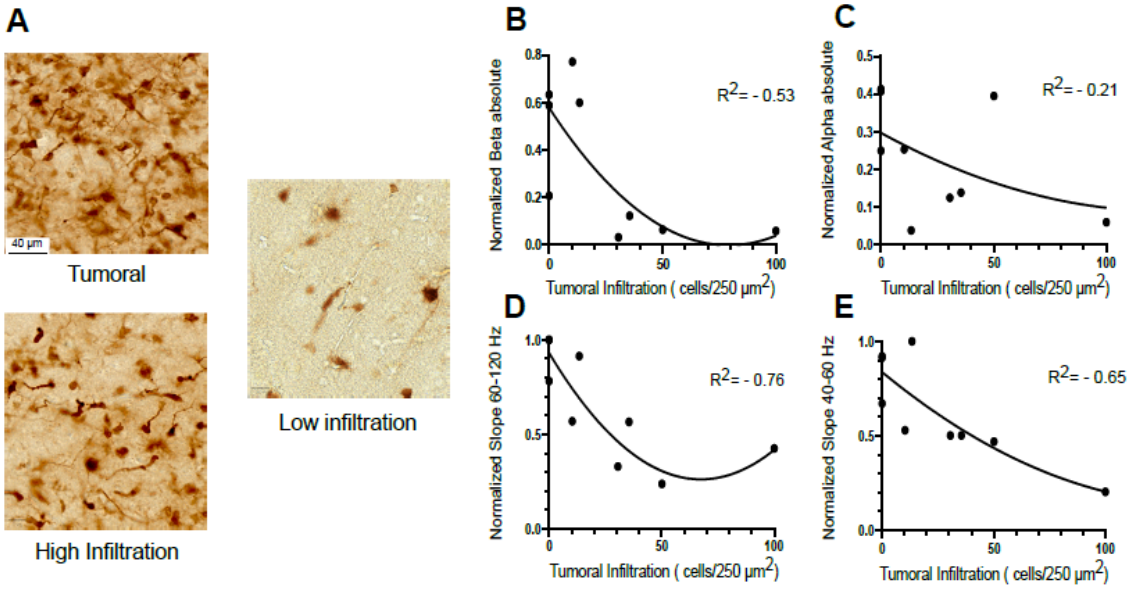

Figure 5: Correlation between glioma cells infiltration and ECoG frequency features. A: Immunohistochemistry (IDH1R132H labeling) shows tumor cells (dark brown). The tumor compartment is characterized by the presence of more than 50 tumoral cells/ 250 µm^2 and neuronal architecture lost, high infiltrated peritumoral tissue contains between 15 to 50 tumoral cells/ 250 µm^2 and low infiltrated peritumoral tissue less 15 cells/ 250 µm^2. B: Correlation between beta frequencies and tumoral infiltration. C: Correlation between alpha frequencies and tumoral infiltration. D: Correlation between 60-120 Hz slope and tumoral infiltration. E: Correlation between 40-60 Hz slope and tumoral infiltration.

We found that the higher the peritumoral infiltration was, the lower the beta absolute values were (R= -0.53, p=0.05) (**Figure 5**). We also found a tendency towards lower values on low gamma activity in highly infiltrated specimens (R= -0.66, p= 0.06). Considering the aperiodic components, the most strongly correlated values were the slope from 60 to 120 Hz (R= -0.76, p= 0.009), followed by the slope from 40 to 60 Hz (R= -0.65, p=0.02). The other features did not show any correlation (**Table 4**).

Biopsy	1	2	3	4	5	6	7	8	9	R^2
Infiltration (tum cells/ μm^2)	0	0	0	10.3	13.4	30.6	35.5	50.1	100	
δ absolute	0.06	0.17	1	0.04	0.25	0.71	1	0.21	0.24	-0.09
δ relative	0.49	0.93	0.64	0.64	0.48	0.88	0.95	0.62	0.82	-0.12
θ absolute	0.13	0.45	0.52	0.12	0.13	0.08	0.17	0.47	0.16	-0.04
θ relative	0.78	0.97	0.02	0.18	0.11	0.04	0.2	0.24	0.17	-0.27
α absolute	0.25	0.41	0.41	0.25	0.04	0.12	0.14	0.39	0.06	-0.21
α relative	0.77	0.62	0.03	0.42	0.27	0.06	0.16	0.2	0.07	-0.37
β absolute	0.63	0.21	0.59	0.77	0.59	0.03	0.12	0.06	0.06	-0.53
β relative	0.72	0.3	0.03	1	0.49	0.01	0.14	0.03	0.06	-0.25
Low γ absolute	0.94	0.33	0.37	0.43	0.41	0.02	0.19	0.03	0.27	-0.57
Low γ relative	0.99	0.52	0.03	0.43	0.3	0.01	0.19	0.01	0.21	-0.38
High γ Absolute	0.99	0.45	0.25	0.57	0.39	0.07	0.48	0.03	0.8	-0.43
High γ relative	0.99	0.82	0.02	0.55	0.29	0.02	0.27	0.01	0.57	-0.41
Slope 1-200 Hz	0.81	0.92	0.91	0.65	0.84	0.78	0.89	0.74	0.64	-0.35
Offset	0.9	0.96	0.86	0.95	0.98	0.96	0.93	1	0.95	-0.36
Slope 20-30 Hz	0.82	0.42	0.79	0.77	1	0.95	0.84	0.97	0.34	-0.68
Slope 20-40 Hz	0.53	0.57	0.85	0.87	0.98	0.84	0.77	0.77	0.37	-0.6
Slope 30-45 Hz	0.51	0.6	0.65	0.73	0.7	0.48	0.51	0.61	0.19	-0.68
Slope 40-60 Hz	0.92	0.67	0.91	0.53	1	0.5	0.5	0.47	0.2	-0.72
Slope 60-120 Hz	0.99	0.78	0.99	0.56	0.91	0.33	0.56	0.24	0.43	-0.76

Table 4: Table showing the mean values of the power spectrum features for the nine peritumoral biopsies.

Even if our study is limited to tumoral cell quantification in 9 contacts, our results showed that contacts sampling highly infiltrated areas present with lower beta and high gamma values, probably because tissues with high tumoral infiltration lost their capacity to generate physiological brain rhythms. We observed the same phenomenon at the tumoral level, characterized by a decrease in frequencies ranging from alpha to high gamma. Lower infiltrated areas presented higher values of beta activity, as is the case at the peritumoral level.

2.7. Neural network classifier of peritumoral vs. tumoral and healthy cortical recordings.

After identifying specific differences in the periodic and aperiodic components based on the compartments, we developed a method to automatically classify the contacts based on the power spectrum features, using a neural network (SKLearn library in Python) with three layers and solving it with “lbfgs”. We included the following features: all the absolute and relative frequency bands (from delta to high gamma) and the slopes (1 to 200 Hz, 20-40, 20-30, 30-45, 40-60, and 60 to 120 Hz).

First, we tried to replicate previous results by comparing only tumoral behavior with no tumoral contacts. We found a F1 score of 0.7 for tumoral and 0.7 for no tumoral, similar to

values described previously in other studies.[(Boussen et al., 2016)] The sensitivity and specificity of the classifier were 0.79 and 0.79, respectively. When comparing to a random classifier, we obtain a sensitivity of 0.26 and a specificity of 0.25 (**Figure 6**).

Since our main interest is the delimitation of the peritumoral area, we classified the contacts in peritumoral versus the rest to test whether we could distinguish specifically the peritumoral area. Using the same features, we obtained a 0.5 F1 score for peritumoral contacts and 0.6 for non-peritumoral ones, with a sensitivity of 0.64 and a 0.64 specificity. Random classification obtained a 0.26 and 0.25 sensibility and specificity in this case.

To increase our spatial precision, we classified the contacts into three groups: tumoral, peritumoral (considering both close and far contacts), and healthy. We used the same features and obtained a 0.6 F1 score for tumoral contacts, 0.4 for peritumoral, and 0.5 for healthy. The sensitivity and specificity were 0.62 and 0.63, respectively, showing an improvement over the random classifier with 0.33 and 0.33 sensitivity and specificity.

Finally, we divided the contacts into four categories (tumoral, peritumoral close, peritumoral far, and healthy). In this case, we obtain an F1 Score of 0.5 for the tumor, 0.3 for close peritumoral, 0.4 for far peritumoral, and 0.4 for healthy contacts. The sensibility was 0.46 and the specificity 0.46, compared to 0.26 and 0.26 from the random classifier. In all cases, the neural network classifier was superior to a random classifier, even if the number of categories increased, the performance was reduced.

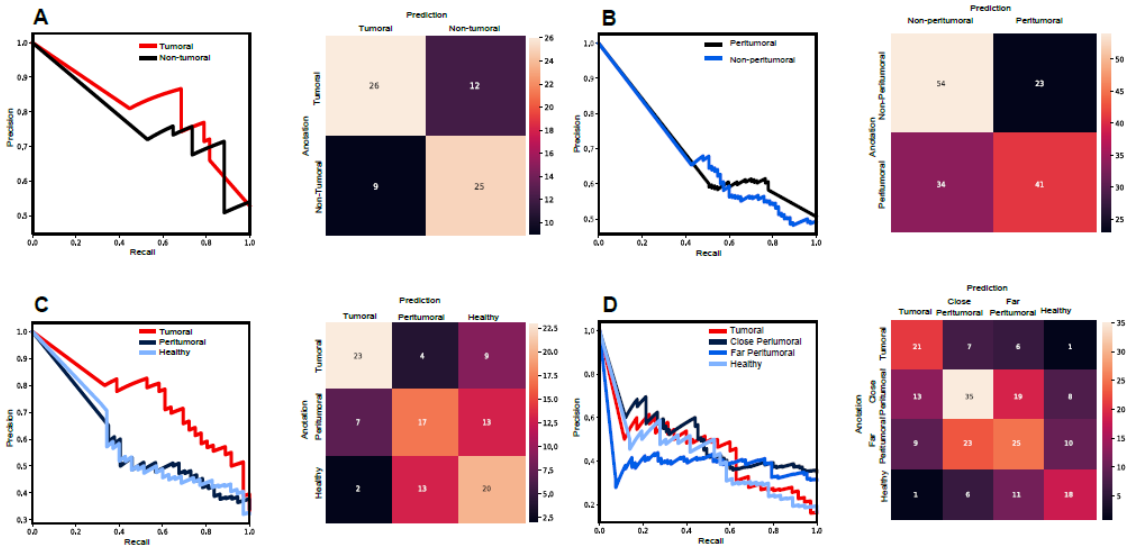

Figure 6: A neuronal network classifier of the electrode location according to recorded activity. A: Neural Network classifier for the tumoral versus non-tumoral categories and the corresponding confusion matrix. B: Neural Network classifier for two categories, peritumoral versus non-peritumoral and the corresponding confusion matrix C: Neural Network classifier for three categories, tumoral versus peritumoral versus healthy and the corresponding confusion matrix. D: Confusion matrix of neural network classifier for four categories, tumoral versus close peritumoral versus far peritumoral versus healthy, and the corresponding confusion matrix.

These results suggest that electrophysiological markers may be considered for the classification of tumoral vs. peritumoral vs. healthy cortices. Larger datasets for training

and implementation of a deep-learning model may improve the classifier performances in the future.

3. Limitations

Our preliminary study enrolled a limited number of patients. Analysis was restricted to recordings without major artifacts, which is still an issue in the surgery theatre. Most patients had astrocytomas and due to the reduced practice of awake surgery and ECoG recording in glioblastomas, histological categories were disequilibrated. Larger studies will be needed to confirm our findings. Our main limitation is the lack of information about the density of peritumoral infiltration for every EcoG channel. We only obtained biopsy samples from 9 cases immediately located beneath a recording contact. Infiltration is rather organized in patches than in radius, and the extent of infiltration is unknown. We tried to overcome this limitation by directly correlating ECoG features with quantified infiltration, which resulted in coherent results showing that the higher the infiltration was, the lower physiological rhythms were recorded. Regarding the neural network classifier, a limitation in the capacity of classification could be the imbalance of the data as peritumoral contacts were more frequent (243 close peritumoral and 213 far peritumoral compared to tumoral (126) or healthy (136), which can imbalance the data, creating a bias during the training and leading to a decrease in performance in the test. Another limitation was the reduced spatial resolution since we used routine 4 mm diameter electrodes spaced by 10 mm. Using smaller electrodes, such as new microECoGs [(Khodagholy et al., 2015; J. C. Yang et al., 2021)] would help us to overcome that limitation and be more precise.

4. Perspectives

The current study suggests, for the first time, that distinct spectral features could provide potential novel electrophysiological markers of the presence or absence of infiltration of tumor cells into the peritumoral tissue. In particular, electrodes overlying the peritumoral tissue revealed a higher slope over higher frequency ranges (20-30 Hz and 20-40 Hz) of the power spectrum compared to healthy cortices. The distinct features confirmed previous findings suggesting an alteration of GABAergic signaling in the peritumoral neocortex infiltrated by glioma cells.[(Johan Pallud et al., 2014)] Deciphering the underlying mechanism of this alteration is beyond the scope of this work. Still, it has been suggested that steeper slopes reflect an impairment in the E-I balance [(Gao et al., 2017)] already reported in gliomas from animal models and ex vivo human tissues.[(Huberfeld & Vecht, 2016)] Such modifications of the aperiodic EEG components have been identified in different conditions such as schizophrenia, temporal lobe epilepsy, and Parkinson's disease [(Belova et al., 2021; H. Jiang et al., 2022; Molina et al., 2020)] but our study is the first one performed on gliomas comparing the tumoral areas with the peritumoral and healthy ones. A recent study performed on temporal lobe epilepsy patients implanted intracranially reported that the seizure onset zone is characterized by steeper slope values [(H. Jiang et al., 2022)] which is in line with the seizure onset zone in gliomas.[(Mittal et al., 2016)] In addition to the frequency band analysis, our data suggest that peritumoral cortices present an imbalance in the excitatory-inhibitory ratio, compatible with its epileptic features, but

also with the complex interactions between glioma tissues and its neuronal microenvironment.[(Krishna et al., 2023)]

The following steps will be to analyze larger sets of patients with a more significant number of biopsies. Then, the use of smaller electrodes using conductive polymers such as PEDOT:PSS, known as microECoG [(Khodagholy et al., 2015; J. C. Yang et al., 2021)] will improve not only the spatial resolution but also will allow recording precisely and with accuracy other kinds of electrophysiological activities, such as multiunit and high-frequency oscillations (> 200 Hz).[(Johan Pallud et al., 2014)] The ability to record such rhythms should be tested during anesthetized surgeries in which brain activity is modified by anesthesia. Finally, after validation of the electrophysiological biomarkers, the electrode classifier algorithm could be used in real-time, in the operative theater, to inform the neurosurgeons about the extension of the peritumoral area. Such advances would allow for better tailoring of the resection, improving the chances of longer survival with a higher quality of life and a lesser probability of having a postsurgical functional impairment.

5. Conclusion

Our pilot study on awake ECoG recording of patients undergoing surgery for glioma in awake condition shows that tumoral and peritumoral are characterized by specific periodic and aperiodic components of the power spectrum, suggesting that they may be used as potential biomarkers of the peritumoral areas. Further, peritumoral infiltration by tumor cells was correlated to specific ECoG features. This key but difficult to delineate zone surrounding gliomas must be removed to improve both epilepsy and oncological outcomes.

We showed that the tumoral compartment was characterized by an increase in delta activity and a decrease in all the other frequency bands, highlighting the disrupting effects of the tumor on EEG physiological rhythms. In contrast, the peritumoral tissue increases relative beta activity and the 20 to 30 and 20 to 40 Hz slopes, indicating modifications of neuronal activities or synaptic input balances. Astrocytomas present different features as compared to oligodendrogliomas. We did not identify differences between close and far peritumoral contacts but rather a correlation between the reduction of physiological rhythms and tumor cell infiltration quantified by immunohistochemistry. This suggests that infiltration and its electrophysiological correlate do not follow a linear, radial distribution, at least guided by nervous bundles and vessels. An automatic classifier based on neural networks allowed us to classify the electrodes based on their power spectrum characteristics. The degree of peritumoral infiltration can impact the generation of physiological brain rhythms, especially beta, and low gamma activities, which may contribute to cognitive issues experimented on by patients.

Our study indicates that ECoG during glioma surgery in awake condition might improve our knowledge of the effects of tumor cell infiltration in nervous tissue and the surgical procedure by better delineating the cortical areas to be removed. It paves the way to real-time electrophysiological mapping to guide better the resection, which would impact the patients' oncological and epileptological outcomes, with larger survivals and improved quality of life.

6. Methods

Patients:
We retrospectively analyzed ECoG data from 29 adult glioma patients recorded during awake surgery between November 2020 and March 2023 at Saint-Anne Hospital and Pitié-Salpêtrière Hospital (Paris, France). The presence of TRE, tumor location, WHO tumoral grade and IDH mutation status were assessed.
This retrospective study was approved by the Comité d'Evaluation et d'Ethique de l'INSERM - IRB00003888 (approval n°21-864)

Surgery:
The function-based resection was performed using an asleep-awake-asleep technique using a previously described methodology in Center 1 (J. Pallud, Rigaux-Viode, et al., 2017; Zanello et al., 2020) and as follows in Center 2. Patients were initially anesthetized with propofol to perform a craniotomy. Once the dura mater was opened and the cortex exposed, anesthesia was stopped. The craniotomy exposed the lesion in addition to two to three cm of peritumoral cortex around the lesion to ensure a positive functional brain mapping (J Pallud & Dezamis, 2017).

ECoG recordings: ECoG is routinely used in glioma awake surgery in both hospitals (Pitié-Salpêtrière and Sainte-Anne, Paris). ECoG is used for intraoperative monitoring to identify spontaneous interictal discharges and after-discharges or epileptic seizures induced by direct electrical stimulations. Once the patients were awake and able to perform the intraoperative functional testing, the neurosurgeon placed the sterile electrodes directly in contact with the cortex. The same position was kept for at least two minutes. Then, the electrode was moved to an adjacent area to map the exposed cortex. A 6 X 1 strip and a 4 X 2 grid (DIXI Medical) were used, depending on the morphology and size of the craniotomy. The electrodes' diameter was 4 mm, and the interelectrode space was 10 mm. A needle reference and ground electrodes were placed in the scalp next to the craniotomy. Data were acquired using an Atlas System (Neuralynx) or an ISIS Inomed amplifier using a 20 KHz sampling rate. Only the presurgical mapping before electrical stimulation was analyzed.
Data were acquired before the cortical functional mapping that precedes the function-based resection. The recording did not modify the surgery.

Electrodes classification:
The neurosurgeon identified the anatomic location of the tumor both by macroscopic direct visual analysis and echography. The position of the electrodes was noted, and pictures of every position were taken. 3D-MRI volume rendering was obtained using 3D-Slicer reconstruction, using FLAIR and T1 Gadolinium MRI sequences (https://www.slicer.org, Brigham and Women's Hospital, Boston, USA). The intraoperative pictures with the electrode position were merged into the 3D-MRI reconstructions, matching the gyral patterns, to measure the distance between the tumoral border visible on MRI on the FLAIR sequence and the contacts. Therefore, an electrode was classified as: "tumoral" if it was contacting a MRI positive area on FLAIR sequence and/or if it has a suspicious appearance macroscopically: "close peritumoral" if placed at less than 15 mm from the tumor border visible on MRI on FLAIR sequence; "far peritumoral" if placed between 16 and 30 mm from the tumoral margin and; "healthy" if set at more than 31 mm.

Immunostaining:
Nine brain biopsies from the peritumoral security margin of 9 patients (one biopsy per patient) were obtained during the surgery of IDH-mutated gliomas. Slices were cut using a vibratome (Leica VT1200S) in 400 µm. Then, they were fixed in formalin-zinc (Diapath) for 24-72 hours. They were embedded on agar to be resliced in 40 µm sections.
After 10 minutes of H_2O_2 application to block internal peroxidase, the slices were heated at 100 °C in Tri-Sodium citrate buffer ten mM for antigen retrieval over 30 minutes. Slices were permeabilized with PGT 0,1% for 1 hour, then they were incubated overnight with a mouse primary antibody against IDHR321H mutation (1:200, Quartett). Immunochemistry was performed with a DAB reagent (Abcam).

Data preprocessing:
We plotted the raw signal from all channels for each recording using our graphical interface developed in Matlab (The Mathworks, Natick, MA, USA). For the visualization, we used a monopolar setup taking as a reference the needle electrode of the acquisition system, and we forward-backward filtered the signals (to avoid phase shift) between 0.1 and 50 Hz using a Chebyshev type II bandpass IIR filter.
After visual inspection, we removed noisy channels and excluded the signal segments with artifacts. The remaining data segments were subsampled (2000 Hz) and classified according to their position in the brain (tumoral, close peritumoral, far peritumoral, and healthy) and in the electrode strip. In these classified segments, we conduct a power spectrum analysis.

Power spectrum analysis:
To assess the power distribution into the different frequency components of ECoG signals, we computed the power spectral density (PSD) over the raw data using the Welch method in each signal segment (hanning window of n = 2* Sample Rate with an overlap of 50%). Afterward, we removed the electrical noise peaks (50 Hz and its harmonics) from the PSD and computed the total power by summing the remaining points.
We calculated the absolute and relative power (Bell et al., 1990) in the six following frequency bands: delta (0.5 to 4 Hz), theta (4 to 8 Hz), alpha (8 to 12 Hz), beta (12 to 29 Hz), low gamma (30 to 45 Hz) and high gamma (55 to 100 Hz). The absolute power values were obtained by summing the PSD into each frequency band, while the relative power by dividing this sum by the total power. To compare data from different patients, these power values were normalized using the maximum power value from each patient.

Aperiodic components frequency analysis:
To study the 1/f-like aperiodic component of the PSD, we estimate the offset and exponent. To compute these values, we use the FOOOF algorithm (Donoghue et al., 2020), which parameterizes the power spectra as a combination of periodic and aperiodic components. Power spectra were parameterized across the frequency ranges 1 to 200 Hz, 20 to 30, 20 to 40, 30 to 45, 40 to 60, and 60 to 120 Hz.

Phase Locking Value (PLV):
We studied the phase synchrony over contacts to measure connectivity between the different compartments (tumoral, close peritumoral, far peritumoral, and healthy). Specifically, these phase interactions were accessed using the Phase Locking Value (PLV). For that, first, we filtered the signals in six frequency bands (0.5 - 4 Hz, 4.5 - 8 Hz, 8.5 - 12 Hz, 12.5 - 30 Hz, 30.5 - 45 Hz, and 55 - 100 Hz) using a Chebyshev type II bandpass IIR

filter. Then, for each of these bands, we calculated the Hilbert transform and obtained the phase of every signal. Afterward, we got the phase difference and computed the PLV between the contacts recorded simultaneously in the operating room but covering different tissue areas (for example, contact number one in a tumoral region vs. contact number five in a healthy region). At the end of this process, we had around 1962 phase locking values distributed in all the possible categories (combinations with repetitions).

Statistics:
Data were expressed as mean and SD for continuous variables and percentages for categorical variables. We used GraphPad software to analyze the results. The different spectral features were compared between all four different positions (tumoral, close peritumoral, far peritumoral, and healthy) using a Kruskall-Wallis test. A *post hoc* Dunn's test was applied afterward to compare the positions between them considering the multiple comparisons. We considered significant values of p inferior to 0.05. Astrocytoma and oligodendroglioma patients were compared using a U Mann-Whitney test. A Spearman correlation test was used to compare the distance in mm and the tumoral infiltration with all the features.

Neural Network Classifier:
We separated the training and test group with 493 recordings for training and 215 recordings for testing (70% training and 30% test), maintaining the ratio of each tissue. After dividing the database, we selected the features for the final classification model: absolute and relative power values (from delta to high gamma) and the slopes (1-200, 20-30, 20-40, 30-45, 40-60 and 60-120 Hz). Using the library SKLearn from Python we trained multiple models, increasing the number of features in each model, and selected the best performance. For training, we used a multi-layer perceptron classifier with an lbfgs solver over three layers with an alpha of 1e-5. Finally, we validated the classifier over the test data and obtained the confusion matrix, precision-recall curve, and F1 score. Initially, we combined the non-tumoral categories to asses if the neural network classifier was similar to other classifiers previously published by other groups.
Afterward, classified the data considering the peritumoral versus the rest of contacts; three categories (tumoral, peritumoral, and healthy). We balanced the resulting database, to remove bias due to the increasing number of peritumoral elements, and trained a new model using the features which provided the best neural network in the previous step (1-200, 20-30, 20-40, 30-45, 40-60 and 60-120 Hz slopes, and the absolute and relative values from delta to high gamma).
Finally, the model was trained to be used in classifying four categories – tumoral, close peritumoral, far peritumoral, and healthy-.

Supporting Information

Supporting Information is available from the Wiley Online Library or from the author.

Acknowledgments

This work was supported in part by the European Research Council to GH (Consolidator grant #865592) and by the Fondation pour la Recherche Medicale to BDF (FDM201906008544 grant). The authors thank participating patients.

David Henao-Herreño *and* Belén Diaz-Fernandez *contributed equally to this work, as well as* ***Gilles Huberfeld and Michel Le Van Quyen*** *as the senior last author.*

Conflict of interest All the authors declare that they have no competing interests.

References

1. Pallud J, Audureau E, Blonski M, Sanai N, Bauchet L, Fontaine D, Mandonnet E, Dezamis E, Psimaras D, Guyotat J, Peruzzi P, Page P, Gal B, Párraga E, Baron M H, Vlaicu M, Guillevin R, De'aux B, Duffau H, Taillandier L, Capelle L, Huberfeld, G. Epileptic seizures in diffuse low-grade gliomas in adults. *Brain*. 2014;137(2):449-462. doi:10.1093/brain/awt345

2. Huberfeld G, Vecht CJ. Seizures and gliomas - Towards a single therapeutic approach. *Nat Rev Neurol*. 2016;12(4):204-216. doi:10.1038/nrneurol.2016.26

3. Pallud J, Huberfeld G, Dezamis E, Peeters S, Moiraghi A, Gavaret M, Guinard E, Dhermain F, Varlet P, Oppenheim C, Chrétien F, Roux A, Zanello M. et al. Effect of Levetiracetam Use Duration on Overall Survival of Isocitrate Dehydrogenase Wild-Type Glioblastoma in Adults: An Observational Study. *Neurology*. 2022;98(2):E125-E140. doi:10.1212/WNL.0000000000013005

4. Correia CE, Umemura Y, Flynn JR, Reiner AS, Avila EK. Pharmacoresistant seizures and IDH mutation in low-grade gliomas. *Neuro-oncology Adv*. 2021;3(1). doi:10.1093/NOAJNL/VDAB146

5. Liang S, Zhang J, Zhang S, Fu X. Epilepsy in adults with supratentorial glioblastoma: Incidence and influence factors and prophylaxis in 184 patients. *PLoS One*. 2016;11(7). doi:10.1371/journal.pone.0158206

6. Rudà R, Bello L, Duffau H, Soffietti R. Seizures in low-grade gliomas: natural history, pathogenesis, and outcome after treatments. *Neuro Oncol*. 2012;14 Suppl 4:iv55-64. doi:10.1093/neuonc/nos199

7. Pallud J, Capelle L, Huberfeld G, Pellegrino C. Tumoral epileptogenicity: How does it happen?. *Epilepsia*. 2013;54(SUPPL. 9):30-34. doi:10.1111/epi.12440

8. Pallud J, Le Van Quyen M, Bielle F, Varlet P, Labussiere M, Cresto N, Dieme M J, Baulac M, Duyckaerts C, Kourdougli N, Chazal G, Devaux B, Rivera C, Miles R, Capelle L, Huberfeld, G. Cortical GABAergic excitation contributes to epileptic activities around human glioma. *Sci Transl Med*. 2014;6(244):244ra89. doi:10.1126/scitranslmed.3008065

9. Klein M, Engelberts NHJ, Van der Ploeg HM, Kasteleijn-Nolst Trenité D G A, Aaronson N K, Taphoorn M J B, Baaijen H, Vandertop, W P, Muller M, Postma T J, Heimans J J. Epilepsy in low-grade gliomas: The impact on cognitive function and quality of life. *Ann Neurol*. 2003;54(4):514-520. doi:10.1002/ana.10712

10. Taphoorn MJB, Sizoo EM, Bottomley A. Review on Quality of Life Issues in Patients with Primary Brain Tumors. *Oncologist*. 2010;15(6):618-626.

doi:10.1634/theoncologist.2009-0291

11. Hu Y, Deng F, Zhang L, Hu K, Liu S, Zhong S, Yang J, Zeng X, Peng, X. Depression and Quality of Life in Patients with Gliomas: A Narrative Review. *J Clin Med*. 2022;11(16). doi:10.3390/JCM11164811

12. Lote K, Stenwig AE, Skullerud K, Hirschberg H. Prevalence and prognostic significance of epilepsy in patients with gliomas. *Eur J Cancer*. 1998;34(1):98-102. doi:10.1016/S0959-8049(97)00374-2

13. Berendsen S, Varkila M, Kroonen J, Seute T, Snijders T J, Kauw F, Spliet W G M, Willems M, Poulet C, Broekman M L, Bours V, Robe, P A. Prognostic relevance of epilepsy at presentation in glioblastoma patients. *Neuro Oncol*. 2016;18(5):700-706. doi:10.1093/neuonc/nov238

14. Huang-Hobbs E, Cheng Y-T, Ko Y, Luna-Figueroa E, Lozzi B, Taylor K R, McDonald M, He P, Chen H-C, Yang Y, Maleki E, Lee Z-Fu, Murali S, Williamson M R,Choi D, Curry R, Bayley J, Woo J, Jalali A, Monje M, Noebels J L, Harmanci A S, Rao G, Deneen B. Remote neuronal activity drives glioma progression through SEMA4F. *Nature*. Published online June 28, 2023. doi:10.1038/S41586-023-06267-2

15. Venkatesh HS, Morishita W, Geraghty AC, Silverbush D, Gillespie S M, Arzt M, Tam L T, Espenel C, Ponnuswami A, Ni L, Woo P J, Taylor K R, Agarwal A, Regev A, Brang D, Vogel H, Hervey-Jumper S, Bergles D E, Suvà M L, Malenka R C, Monje M. Electrical and synaptic integration of glioma into neural circuits. *Nature*. 2019;573(7775):539-545. doi:10.1038/s41586-019-1563-y

16. Venkatesh HS, Johung TB, Caretti V, Silverbush D, Gillespie S M, Arzt M, Tam L T, Espenel C, Ponnuswami A, Ni L, Woo P J, Taylor K R, Agarwal A, Regev A, Brang D, Vogel H, Hervey-Jumper S, Bergles D E, Suvà M L, Malenka R C, Monje M. Neuronal activity promotes glioma growth through neuroligin-3 secretion. *Cell*. 2015;161(4):803-816. doi:10.1016/j.cell.2015.04.012

17. Venkataramani V, Yang Y, Schubert MC, Reyhan E, Tetzlaff S K, Wißmann N, Botz M, Soyka S J, Beretta C A, Pramatarov R L, Fankhauser L, Garofano L, Freudenberg A, Wagner J, Tanev D I, Ratliff M, Xie R, Kessler T, Hoffmann D C, Hai L, Dörflinger Y, Hoppe S, Yabo Y A, Golebiewska A, Niclou S P, Sahm F, Lasorella A, Slowik M, Döring L, Iavarone A, Wick W, Kuner T, Winkler F. Glioblastoma hijacks neuronal mechanisms for brain invasion. *Cell*. 2022;185(16):2899-2917.e31. doi:10.1016/J.CELL.2022.06.054

18. Venkataramani V, Tanev DI, Strahle C, Studier-Fischer A, Fankhauser L, Kessler T, Körber C, Kardorff M, Ratliff M, Xie R, Horstmann H, Messer M, Paik S P, Knabbe J, Sahm F, Kurz F T, Acikgöz A A, Herrmannsdörfer F, Agarwal A, Bergles

D E, Chalmers A, Miletic H, Turcan S, Mawrin C, Hänggi D, Liu H K, Wick W, Winkler F, Kuner T. Glutamatergic synaptic input to glioma cells drives brain tumour progression. *Nature*. 2019;573(7775):532-538. doi:10.1038/s41586-019-1564-x

19. Krishna S, Choudhury A, Keough MB, Seo K, Ni L, Kakaizada S, Lee A, Aabedi A, Popova G, Lipkin B, Cao C, Nava Gonzales C, Sudharshan R, Egladyous A, Almeida N, Zhang Y, Molinaro A M, Venkatesh H S, Daniel A G S, Shamardani K, Hyer J, Chang E F, Findlay A, Phillips J J, Nagarajan S, Raleigh D R, Brang D, Monje M, Hervey-Jumper S L. Glioblastoma remodelling of human neural circuits decreases survival. *Nature*. 2023;617(7961). doi:10.1038/S41586-023-06036-1

20. Pallud J, Varlet P, Devaux B, Geha, S. Badoual M, Deroulers C, Page P, Dezamis E, Daumas-Duport C, Roux F X. Diffuse low-grade oligodendrogliomas extend beyond MRI-defined abnormalities. *Neurology*. 2010;74(21):1724-1731. doi:10.1212/WNL.0b013e3181e04264

21. Zetterling M, Roodakker KR, Berntsson SG, Edqvist P H, Latini F, Landtblom A M, Pontén F, Alafuzoff I, Larsson E M, Smits A. Extension of diffuse low-grade gliomas beyond radiological borders as shown by the coregistration of histopathological and magnetic resonance imaging data. *J Neurosurg*. 2016;125(5):1155-1166. doi:10.3171/2015.10.JNS15583

22. Mittal S, Barkmeier D, Hua J, Pai D S, Fuerst D, Basha M, Loeb J A, Shah A K. Intracranial EEG Analysis in Tumor-Related Epilepsy: Evidence of Distant Epileptic Abnormalities. Vol 127. I*nternational Federation of Clinical Neurophysiology;* 2016. doi:10.1016/j.clinph.2015.06.028

23. Tran TA, Spencer SS, Javidan M, Pacia S, Marks D, Spencer DD. Significance of spikes recorded on intraoperative electrocorticography in patients with brain tumor and epilepsy. *Epilepsia*. 1997;38(10):1132-1139. doi:10.1111/j.1528-1157.1997.tb01203.x

24. Feyissa AM, Worrell GA, Tatum WO, Mahato D, Brinkmann B H, Rosenfeld S S, Refaey K, Bechtle P S, Quinones-Hinojosa, A. High-frequency oscillations in awake patients undergoing brain tumor-related epilepsy surgery. *Neurology*. 2018;90(13):e1119-e1125. doi:10.1212/WNL.0000000000005216

25. van Klink NEC, Zweiphenning WJEM, Ferrier CH, Gosselaar P H, Miller K J, Aronica E, Braun K P J, Zijlmans M. Can we use intraoperative high-frequency oscillations to guide tumor-related epilepsy surgery? *Epilepsia*. 2021;62(4):997-1004. doi:10.1111/epi.16845

26. De Witt Hamer PC, Robles SG, Zwinderman AH, Duffau H, Berger MS. Impact of intraoperative stimulation brain mapping on glioma surgery outcome: A meta-

analysis. *J Clin Oncol*. 2012;30(20):2559-2565. doi:10.1200/JCO.2011.38.4818

27. Duffau H. Contribution of cortical and subcortical electrostimulation in brain glioma surgery: Methodological and functional considerations. *Neurophysiol Clin*. 2007;37(6):373-382. doi:10.1016/j.neucli.2007.09.003

28. Pallud J, Dezamis E. Functional and oncological outcomes following awake surgical resection using intraoperative cortico-subcortical functional mapping for supratentorial gliomas located in eloquent areas. *Neurochirurgie*. 2017;63(3):208-218. doi:10.1016/j.neuchi.2016.08.003

29. Demuru M, Kalitzin S, Zweiphenning W, van Blooijs D, van't Klooster M, Van Eijsden P, Leijten F, Zijlmans M, Braun K, Ferrier C, Gebbink T, Gosselaar P, Huiskamp G, van Klink N, Ophorst J, van Rijen P, van der Salm S, Winter, A V. The value of intra-operative electrographic biomarkers for tailoring during epilepsy surgery: from group-level to patient-level analysis. *Sci Rep*. 2020;10(1). doi:10.1038/s41598-020-71359-2

30. Park YS, Hochberg LR, Eskandar EN, Cash SS, Truccolo W. Early detection of human focal seizures based on cortical multiunit activity. *Annu Int Conf IEEE Eng Med Biol Soc IEEE Eng Med Biol Soc Annu Int Conf*. 2014;2014:5796-5799. doi:10.1109/EMBC.2014.6944945

31. Trebuchon A, Guye M, Tcherniack V, Tramoni E, Bruder N, Metellus P. Intérêt du monitoring électrophysiologique au cours d'une chirurgie éveillée en neurochirurgie. *Ann Fr Anesth Reanim*. 2012;31(6):87-90. doi:10.1016/j.annfar.2012.04.010

32. Zanello M, Roux A, Zah-Bi G, Trancart B, Parraga E, Edjlali M, Tauziede-Espariat A,Sauvageon X, Sharshar T, Oppenheim C, Varlet P, Dezamis E, Pallud J. Predictors of early postoperative epileptic seizures after awake surgery in supratentorial diffuse gliomas. *J Neurosurg*. 2020;134(3):683-692. doi:10.3171/2020.1.JNS192774

33. Yao P Sen, Zheng SF, Wang F, Kang DZ, Lin YX. Surgery guided with intraoperative electrocorticography in patients with low-grade glioma and refractory seizures. *J Neurosurg*. 2018;128(3):840-845. doi:10.3171/2016.11.JNS161296

34. Boetto J, Bertram L, Moulinié G, Herbet G, Moritz-Gasser S, Duffau H. Electrocorticography Is Not Necessary During Awake Brain Surgery for Gliomas. *World Neurosurg*. 2016;91:656-657. doi:10.1016/j.wneu.2016.03.030

35. Englot DJ, Berger MS, Barbaro NM, Chang EF. Predictors of seizure freedom after resection of supratentorial low-grade gliomas: A review. *J Neurosurg*. 2011;115(2):240-244. doi:10.3171/2011.3.JNS1153

36. Munari C, Musoiino A, Daumas-Duport C, Missir O, Brunei P, Giallonardo A T, Chodkiewicz J P, Bancaud J. Correlation between stereo-EEG, CT-scan and stereotactic biopsy data in epileptic patients with low-grade gliomas. *Appl Neurophysiol*. 1985;48(1-6):448-453. doi:10.1159/000101176

37. Boussen S, Velly L, Benar C, Metellus P, Bruder N, Trébuchon A. In Vivo Tumour Mapping Using Electrocorticography Alterations During Awake Brain Surgery: A Pilot Study. *Brain Topogr*. 2016;29(5):766-782. doi:10.1007/s10548-016-0502-6

38. Belova EM, Semenova U, Gamaleya AA, Tomskiy AA, Sedov A. Voluntary movements cause beta oscillations increase and broadband slope decrease in the subthalamic nucleus of parkinsonian patients. *Eur J Neurosci*. 2021;53(7):2205-2213. doi:10.1111/EJN.14715

39. Donoghue T, Haller M, Peterson EJ, Varma P, Sebastian P, Gao R, Noto T, Lara A H, Wallis J D, Knight, R T, Shestyuk A, Voytek B. Parameterizing neural power spectra into periodic and aperiodic components. *Nat Neurosci 2020 2312*. 2020;23(12):1655-1665. doi:10.1038/s41593-020-00744-x

40. Ghinda DC, Lambert B, Lu J, Jiang N, Tsai E, Sachs A, Wu J S, Northoff G. Scale-Free Analysis of Intraoperative ECoG During Awake Craniotomy for Glioma. *Front Oncol*. 2021;10(February):1-12. doi:10.3389/fonc.2020.625474

41. Molina JL, Voytek B, Thomas ML, Joshi Y B, Bhakta S G, Talledo J A, Swerdlow N R, Light G A. Memantine Effects on Electroencephalographic Measures of Putative Excitatory/Inhibitory Balance in Schizophrenia. *Biol Psychiatry Cogn Neurosci Neuroimaging*. 2020;5(6):562-568. doi:10.1016/j.bpsc.2020.02.004

42. Gao R, Peterson EJ, Voytek B. Inferring synaptic excitation/inhibition balance from field potentials. *Neuroimage*. 2017;158(March):70-78. doi:10.1016/j.neuroimage.2017.06.078

43. Jiang H, Kokkinos V, Ye S, Urban A, Bagić A, Richardson M, He B. Interictal SEEG Resting-State Connectivity Localizes the Seizure Onset Zone and Predicts Seizure Outcome. *Adv Sci*. 2022;9(18):1-11. doi:10.1002/advs.202200887

44. Newmark ME, Theodore WH, Sato S, Paz R, Patronas N, Brooks R, Jabbari B, Chiro G. EEG, transmission computed tomography, and positron emission tomography with fluorodeoxyglucose 18F. Their use in adults with gliomas. *Arch Neurol*. 1983;40(10):607-610. doi:10.1001/ARCHNEUR.1983.04050090043005

45. Nagata K, Gross CE, Kindt GW, Geier JM, Adey GR. Topographic electroencephalographic study with power ratio index mapping in patients with malignant brain tumors. *Neurosurgery*. 1985;17(4):613-619.

doi:10.1227/00006123-198510000-00014

46. Buckingham SC, Campbell SL, Haas BR, Montana V, Robel S, Ogunrinu T, Sontheimer H. Glutamate release by primary brain tumors induces epileptic activity. *Nat Med*. 2011;17(10):1269-1274. doi:10.1038/nm.2453

47. Ye ZC, Rothstein JD, Sontheimer H. Compromised glutamate transport in human glioma cells: Reduction- mislocalization of sodium-dependent glutamate transporters and enhanced activity of cystine-glutamate exchange. *J Neurosci*. 1999;19(24):10767-10777. doi:10.1523/jneurosci.19-24-10767.1999

48. Yuen TI, Morokoff AP, Bjorksten A, D'Abaco G, Paradiso L, Finch S, Wong D, Reid C A, Powell K L, Drummond K J, Rosenthal M A, Kaye A H, O'Brien T J. Glutamate is associated with a higher risk of seizures in patients with gliomas. *Neurology*. 2012;79(9):883-889. doi:10.1212/WNL.0b013e318266fa89

49. Landers MJF, Brouwers HB, Kortman GJ, Boukrab I, De Baene W, Rutten GJM. Oligodendrogliomas tend to infiltrate the frontal aslant tract, whereas astrocytomas tend to displace it. *Neuroradiology*. Published online 2023. doi:10.1007/S00234-023-03153-6

50. Khodagholy D, Gelinas JN, Thesen T, Doyle W, Devinsky O, Malliaras G G, Buzsáki G. NeuroGrid: Recording action potentials from the surface of the brain. *Nat Neurosci*. 2015;18(2):310-315. doi:10.1038/nn.3905

51. Yang JC, Paulk AC, Salami P, Lee S H, Ganji M, Soper D J, Cleary D, Simon M, Maus D, Lee J W, Nahed B V, Jones P S, Cahill D P, Cosgrove G R, Chu C J, Williams Z, Halgren E, Dayeh S, Cash S S. Microscale dynamics of electrophysiological markers of epilepsy. *Clin Neurophysiol*. 2021;132(11):2916-2931. doi:10.1016/J.CLINPH.2021.06.024

52. Pallud J, Rigaux-Viode O, Corns R, Muto J, Lopez Lopez C, Mellerio C, Sauvageon X, Dezamis E. Direct electrical bipolar electrostimulation for functional cortical and subcortical cerebral mapping in awake craniotomy. Practical considerations. *Neurochirurgie*. 2017;63(3):164-174. doi:10.1016/J.NEUCHI.2016.08.009

Table of Contents.

In this work, we differentiate glioma tumoral areas compared to the surrounding tissue, based on their power spectrum characteristics. The tumor presents an increase in delta activities, whereas the peritumoral area was characterized by an increase in beta activity and slopes between 20 to 30 and 20 to 40 Hz. An automatic algorithm classifier allowed the classification of the electrodes based on their power spectrum characteristics.

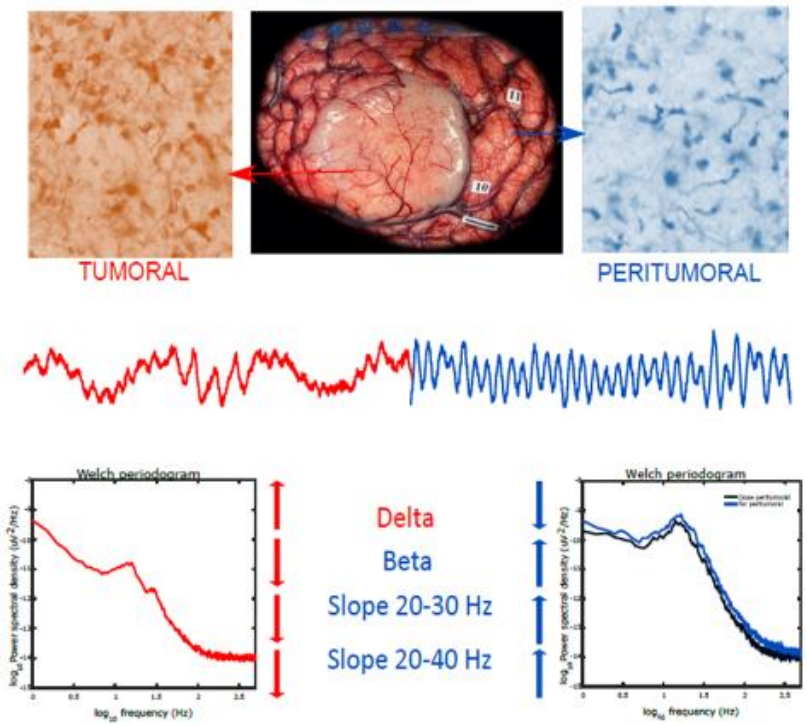

4.4 Spatio-temporal dynamics of seizure initiation

The second work of my thesis explored the spatiotemporal dynamics of field potential, high frequency activities (HFA), and HFO during the transition to an ILE. This phase, known as the preictal period, lasting tens of minutes before the onset of a seizure, holds significant importance in deciphering the mechanisms underlying seizure generation. Furthermore, given the unforeseen nature of seizures, early detection of these patterns could facilitate the development of new algorithms for identifying periods of heightened seizure risk.

The objectives of this work are the following:

1)To characterize the spatiotemporal evolution of PIDs during the preictal period.
2)To investigate the dynamics of HFA and their interplay with PIDs.
3)To explore the dynamics of HFO and their correlation with PIDs.
4)To discern whether the seconds immediately preceding the onset of the ILE present different behavior compared to the rest of the preictal period.

We performed this work by using ex vivo extracellular multielectrode array (MEA) recording of peritumoral human slices. Since gliomas are highly epileptogenic tumors and as epilepsy arises from the peritumoral tissue, these slices provide an excellent model to study ictogenesis. I performed the recordings with Multichannel arrays. Two different configurations were used depending on the size of the peritumoral slices. The big one contained 120 microelectrodes (30 µm in diameter) with an interelectrode space of 1000 µm in the "x" plane and 1500 µm in the "y" plane. The small configuration employed a different microelectrodes arrangement, with an interelectrode spacing of 200 µm. The slices were maintained alive for several hours to do the recordings. The first ten minutes of recording were made in basal aCSF conditions to assess spontaneous IID presence. Then, to induce ILE, the excitability of the medium was increased with 6 to 8 K^+- 0 Mg^{2+} CSF. The analysis of the FP was done using Clampfit. The analysis of HFA and HFO were performed with homemade MATLAB algorithms developed by my colleague David Henao.

Our findings unveil that PIDs undergo temporal and spatial dynamic changes during the preictal period, indicating increased neuronal synchronization and network recruitment. Notably, the behaviors of HFA and HFO mirror those of PIDs, underscoring the presence of this dynamic recruitment pattern and complex neuronal interactions in seizure generation.

While certain analyses pertinent to this paper remain ongoing, notably those related to the evolution of HFA and HFO, as well as the spatial dynamics, our current state allows us to conclude that ex vivo human slices serve as a model where we can artificially induce ILE to study ictogenesis. The observed PIDs, HFA, and HFO dynamics could be used to develop an *in vivo* seizure anticipation biomarker.

4.4.1 Article 2, under preparation: Spatiotemporal dynamics of seizure initiation in the ex vivo human periglioma neocortex.

Spatiotemporal dynamics of seizure initiation in the ex vivo human periglioma neocortex.

Belén Diaz-Fernandez[1,2,3,4,5,†], David Henao-Herreno[1,5,†], Elena Dossi[1], Alesya Evstratova[1], Johan Pallud[6,7,8], Laurent Capelle[9], Nathalie Rouach[1], Michel Le Van Quyen [2,‡], and Gilles Huberfeld[1,5,10,‡]

† These authors contributed equally to this work.

‡ These authors contributed equally to this work as senior authors.

Author affiliations:

1 Center for Interdisciplinary Research in Biology, Collège de France, CNRS UMR 7241, INSERM U1050, Université PSL 75005 Paris, France

2 Laboratoire d'Imagerie Biomedicale 75005 Paris, France

3 Panaxium SAS 13100 Aix-en-Provence, France

4 Department of Neurology, Pitié-Salpêtrière Hospital, 75013 Paris, France

5 Université Paris Cité, Institute of Psychiatry and Neuroscience of Paris (IPNP), INSERM U1266, Neuronal Signaling in Epilepst and Glioma, 75014 Paris, France.

6 Department of Neurosurgery, GHU Paris Psychiatry and Neurosciences, Sainte-Anne Hospital, 75014 Paris, France

7 Institute of Psychiatry and Neuroscience of Paris, University Paris Cité, INSERM U1266, IMABRAIN, 75014 Paris, France

8 Université Paris Cité, 75005 Paris, France

9 Department of Neurosurgery, Pitié-Salpêtrière Hospital, 75013 Paris, France

10 Department of Neurology, Hopital Fondation Adolphe de Rothschild, 75019 Paris, France

Correspondence to: David Henao-Herreno
Full address Université Paris Cité, Institute of Psychiatry and Neuroscience of Paris (IPNP), INSERM U1266, Neuronal Signaling in Epilepsy and Glioma, 102 rue de la Santé, 75014 Paris, France.
E-mail: david.henao@college-de-france.fr

Keywords: ictogenesis; epilepsy; Glioma, neocortex, spatio-temporal dynamics, MEA

Abstract

Seizure initiation is a dynamic process still poorly understood. We aimed to assess ex vivo the spatiotemporal dynamics of neuronal activities during the preictal period by extracellular electrophysiological recordings in human postoperative cortical tissues resected from patients with epileptic gliomas. This transition period was characterized by the emergence of preictal discharges (PIDs) which evolved in their temporal and spatial dynamics, suggesting increased neuronal synchronization and network recruitment. High-frequency oscillations (HFOs) followed the same dynamics as PIDs, reinforcing the dynamic recruitment pattern and the complex neuronal interactions at play in seizure generation. The main feature was a progressive shift and expansion of both neuronal population activities, a reinforcement of HFOs accompanied by a progressive prolongation and delay according to population activities, peaking at seizure onset. This study suggests that, in the epileptic human cortex, seizures do not arise unexpectedly but that neuronal assemblies are progressively recruited and sculpted together with HFOs.

Introduction:

Epilepsy is characterized by seizures' sudden and unpredictable occurrence (Fisher et al., 2014), which contrasts with the permanent background reorganization and abnormal short lasting neuronal activities, suggesting that such paroxysms were paradoxical (Huberfeld et al., 2013). Better understanding how the transition to seizures occurs is still fundamental since up to 30% of patients suffering from epilepsy continue to present seizures despite a well-conducted pharmacological treatment (Kwan et al., 2010).

Although poorly characterized, especially at the clinical level, the preictal period during which ictogenesis processes operate, has been identified by brain recordings (Stacey et al., 2011). Previous data showed changes in cerebral hemodynamics 20 minutes before an electroencephalogram (EEG) seizure (Baumgartner et al., 1998). An increase in the BOLD fMRI signal has also been described before the beginning of a seizure (Federico et al., 2005). Moreover, changes in the heart rate (Kerem & Geva, 2005) or even clinical prodromes, such as self-prediction of the seizure or noise sensitivity, have been reported during this transitional preictal period (Cousyn et al., 2021).

Our scarce knowledge about the preictal period arises mostly from *ex vivo* animal studies and recordings in patients with epilepsy implanted with deep electrodes (sEEG) or penetrating microarrays (Perucca et al., 2014; Weiss et al., 2016). Patient recordings can provide temporal evolution information during the preictal period, but the spatial resolution is limited. At a cellular level, microelectrodes recordings in humans did not provide relevant neuronal preictal behavior (Lambrecq et al., 2017).

The use of postsurgical human tissue offers a valuable platform for studying preictal changes, as postsurgical tissues can be kept alive for several hours ex vivo, and they can be recorded with high spatial resolution using MultiElectrode Array (MEA) (Dossi et al., 2014). In recent years, the development and improvement of MEA have provided an excellent approach to studying the spatiotemporal patterns of spontaneous and evoked activity, as they allowed the recording of electrophysiological activity from several sites of the tissue simultaneously.

In vitro, human tissues can produce spontaneous interictal discharges (IIDs) (Fig 1.A). IIDs are considered a marker of tissue's epileptogenicity, as they are not recorded in non-epileptic tissues (Blauwblomme et al., 2019; Dossi et al., 2018; Huberfeld et al., 2011; Pallud et al., 2014). Ictal-like events (ILEs) can be induced by increasing the excitability of the tissue. Different methods can be used, for instance, the increase of K^+ concentration, the decrease of Mg^{2+} concentration, or the alkalization of the extracellular medium (Huberfeld et al., 2011).

Towards the transition to an ILE, a new kind of field potential (FP) discharges progressively appears: the preictal discharges (PIDs) (Fig 1.A). PIDs emerge gradually during the preictal transitional period, in line with both the increase of excitability and excitatory glutamatergic synaptic plasticity. PIDs are high-amplitude FP mostly generated by synchronized pyramidal cells discharges driven by glutamatergic signaling (Huberfeld et al., 2011). During this transition, less attention has been paid to high frequency activities (HFAs), including high frequency oscillations (HFOs) behavior. HFA had been recorded in ex vivo human cortical dysplasia associated with IIDs, while PIDs have been associated with HFA and occasionally HFO (Blauwblomme et al., 2019). Moreover, HFO have been

considered in the last years as a very promising epilepsy biomarker (Jacobs et al., 2010; Park & Hong, 2019; Wu et al., 2021; Zijlmans et al., 2012). But their dynamics in the seizure transition period is still to be deepened.

Brain gliomas provide an excellent model to study ictogenesis because they are highly epileptic tumors. The incidence of epilepsy varies from 60-90% in low-grade gliomas (Pallud et al. 2014) and 25-60% in high-grade gliomas (Lote et al. 1998; Pallud et al. 2023). Indeed, epileptic seizures are the most frequent symptom at diagnosis. Epileptic activities are initiated in peritumoral tissues, probably in areas infiltrated by tumor cells (Mittal et al., 2016; Pallud et al., 2014) (Fig 1.B-C).

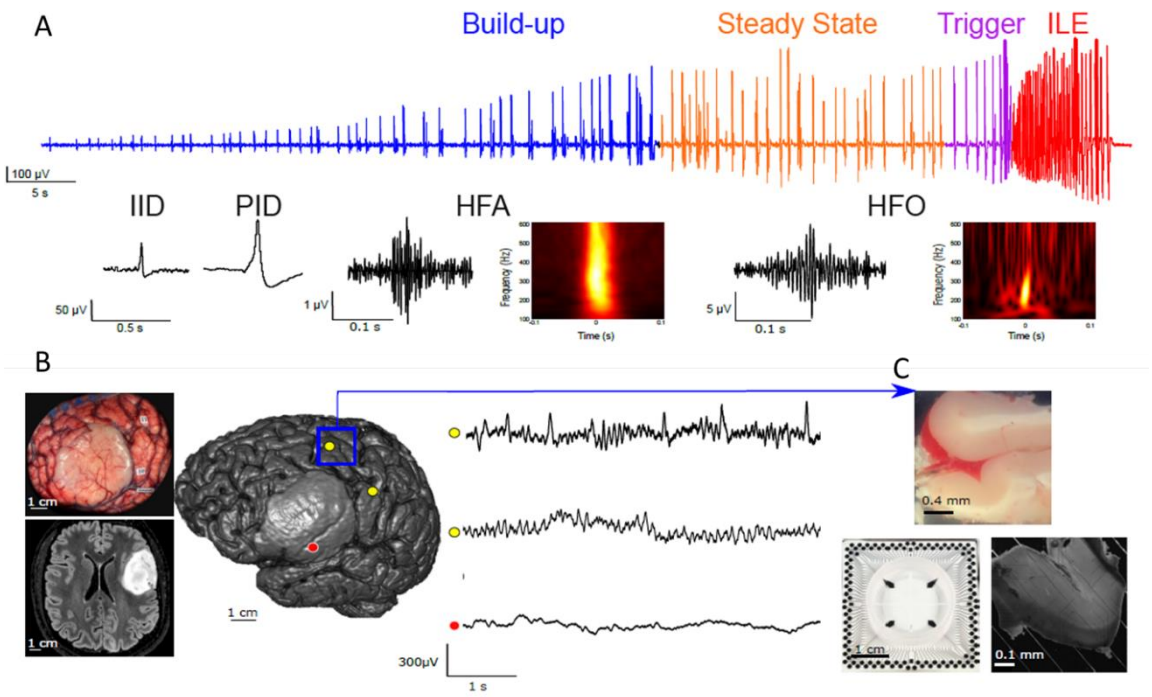

Figure 1: Methodological pipeline. A: Extracellular recording of a peritumoral slice during the preictal period induced by 6 K^+ 0 Mg^{2+}- aCSF. We can observe three subperiods: the build-up (blue) with a progressive increase in PIDs amplitude, the steady state (orange) characterized by a plateau, and the trigger period (purple) with an increase in frequency. Examples of the electrophysiological activities we can observed during the preictal period: IIDs, PIDs, HFA and HFO. B: Perioperative picture and MRI axial view of an astrocytoma. MRI 3D reconstruction of the patient with the astrocytoma visible in pale grey. Position of two peritumoral electrodes (yellow) and a tumoral electrode (red). Electrocorticography recording showing IIDs at the peritumoral level. C: Brain sample obtained from the peritumoral tissue (square blue in the 3D MRI reconstruction), MEA matrix and a peritumoral slice placed on the matrix.

Ex vivo MEA recordings of human peritumoral tissues allow analysis of both spontaneous interictal activities, a hallmark of epileptic tissues, and of the progressive route to the seizure by increasing the perfusion milieu excitability (Fig 1.C). We aim to describe the spatiotemporal dynamics of PID emergence and their relation with HFA and HFO on the way to the ILE, both during the transition period and at seizure onset.

Results:

Tissue characterization

We have recorded using a MEA 30 slices from 22 glioma patients, where ILE were induced using 6-8 K^+/0 Mg^{2+} artificial Cerebro Spinal Fluid (aCSF) perfusion. Twenty patients suffered from tumor-related epilepsy (90.9 %), from which 26 slices were recorded (86.6 %). The most frequently recorded tumor was astrocytoma (15/30 slices- 50 %), followed by oligodendroglioma (11/30 slices- 36.6 %), and glioblastoma (GB) (4/30 slices- 13.3%). The most common WHO grade was grade 2 in 16/30 slices (53.3 %), followed by grade 3 in 9/30 slices (30 %) and grade 4 in 4/30 slices (13.3%). A total of 26/30 slices (86.6 %) were obtained from tumors harboring an IDH mutation, which is known to enhance epileptogenesis. Two different ILE patterns were recorded: the most frequent (17/30 slices, 56.6 %) was characterized by a low voltage fast activity discharges (LVFA) onset followed by a progressive increase in amplitude, and the second one was formed by hypersynchronous discharges (HS), consisting in directly rhythmic, high-amplitude activity without fast discharges (13/30 slices, 43.3 %) (Figure 2.A). ILE presented a mean duration of 43.31 ± 24.29 seconds (min 15.28 s, max 127.8 s) in the case of LVFA and 31.1 ± 13.37 seconds (range 17.83 - 67.58 seconds) in the HS pattern.

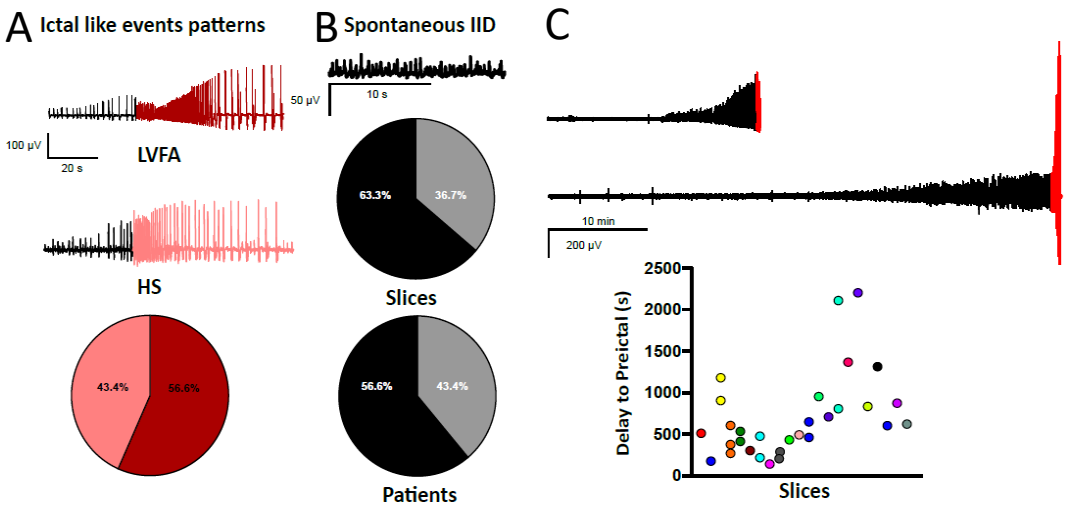

Figure 2: Descriptive features of the slices. A: Two types of ictal patterns were observed. Example of low voltage fast activity pattern (LVFA) and hypersynchronous pattern (HS). Proportion of slices exhibiting LVFA vs. HS pattern. B: Example of spontaneous IIDs at the top. Proportion of slices and patients displaying spontaneous IIDs. C: Two extracellular recordings of two different slices showing the variation in duration until the appearance of the first PID and in the duration of the preictal period. Plot showing the delay until the appearance of the first PID in all the slices. The different 22 colors represent the 22 patients, for some patients several slices were recorded.

The transition to the ictal state is characterized by the progressive emergence of PIDs.

Basal behavior of periglioma cortical tissues was first assessed in normal aCSF condition. During this period, spontaneous IIDs were recorded from 17/30 slices (56.6 %) from 14/22 patients (63.6% %), 13 of them suffering from epilepsy (76.5%) (Fig 2.B). Spontaneous

IIDs were characterized by a mean amplitude of 13.61 ± 6.35 µV (range 2.66 - 33.52 µV), a rising slope of 0.65 ± 0.43 ms/µV (range 0.18- 1.71 ms/µV) and a frequency of 0.99 ± 0.36 Hz (range 0.39 - 1.85 Hz). aCSF was then modified by increasing K^+ up to 6mM and by omitting Mg^{2+} in order to increase tissue excitability (Huberfeld et al., 2011), thereby initiating the transitional period. The progressive emergence of PIDs characterized such transitional preictal period. PIDs appeared at 680.08 ± 354.62 seconds (range 140-2203.66 seconds) after adding the ictogenic solution (Fig 1.C). Astrocytoma slices presented the shortest delay with 437.56 ± 152.14 seconds, followed by oligodendroglioma slices with 877.15 ± 387.3 seconds. GB slices presented the most prolonged delay with 987 ± 608.32 seconds (p = 0.03, Kruskall Wallis test). IDH mutated slices presented shorter delays than IDH wild types (630.97 ± 320.04 vs. 987 ± 608.33 seconds, p = 0.37, U-Mann-Whitney test). The preictal period lasted 613.5 ± 399.14 seconds in average (range 16.09 - 1738.8 seconds).

This transitional period can be subdivided into three different subperiods: the build-up period, during which a progressive increase in PIDs amplitude was observed, the steady-state period, with PIDs amplitude stability, and the trigger period in the seconds preceding the beginning of the ILE, during which PIDs' amplitude and frequency evolved just before the seizure onset (Fig 1.A).

PIDs emerged as FPs of progressively increasing amplitude during the build-up period. The build-up period had a mean duration of 426.32 ± 289.94 seconds (range 27.47-1402.08 seconds). After the build-up period, a plateau phase was reached, the steady-state period. The steady-state had a mean duration of 219.25 ± 178.5 seconds (range 7.2-1080.98 seconds). Once established, the amplitude of PIDs (98.83 ± 38.52 µV) was significantly higher than the amplitude of spontaneous IIDs (Mann-Whitney test, $p < 0.001$). The rising slope (1.55 ± 0.64 ms/µV) was higher than IIDs (Mann-Whitney test, $p = 0.001$). The frequency of PIDs (0.58 ± 0.24 Hz) was slower than IIDs (Mann-Whitney test, $p= 0.004$) (Fig 3.C).

PIDs temporal evolution

We first look to the temporal evolution of PIDs. In contrast to IIDs, which did not show any progressive dynamic in amplitude, rising slope, or frequency (Figure 3.A), PIDs evolved during the transition period. The evolution was more evident during the build-up period, in which amplitude, rising slope, and frequency increased progressively (Figure 3.B) (Friedman test, $p < 0.0001$, < 0.0001, and <0.0001, respectively).

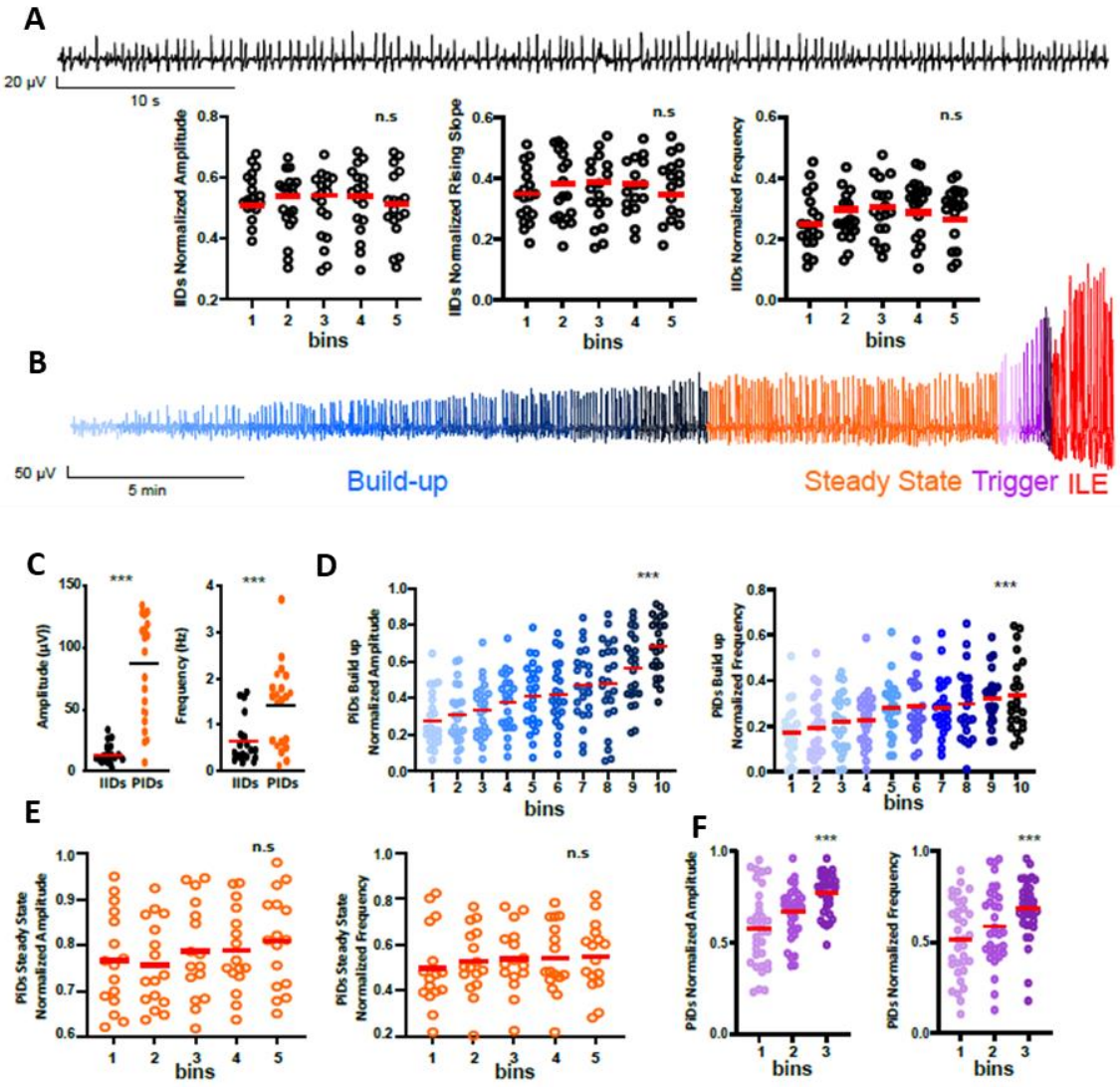

Figure 3: Field potential temporal evolution. A: IIDs example and plots showing IIDs temporal evolution using 20% bins. IIDs present stability in amplitude (p= 0.07), rising slope (p = 0.09) and frequency (p = 0.1, Friedman test). B: Extracellular recording (one electrode) showing the subperiods of the preictal state: build-up (blue), steady state (orange) and trigger (purple). C: Comparison between IIDs and steady state PIDs. PIDs present higher amplitude ($p < 0.0001$) and frequency ($p = 0.001$, U-Mann Whitney test) than IIDs. D: Temporal evolution of build up PIDs. Histograms showing a progressive increase in amplitude ($p < 0.001$) and frequency ($p < 0.001$, Friedman test) using 10% bins. E: Temporal evolution of steady state PIDs. Histograms showing stability in amplitude ($p = 0.07$) and frequency ($p = 0.12$, Friedman test) using 20% bins. F: Temporal evolution of trigger period PIDs. Plots showing an increase in amplitude ($p < 0.001$) and frequency ($p= 0.001$, Friedman test) using 33% bins.

At the beginning of the build-up period (during the first 10% bin), the mean amplitude value was 31.85 ± 12.35 µV (range 8.44 - 82.1 µV), the rising slope was 0.53 ± 0.28 ms/µV (range 0.07 - 1.11 ms/µV)) and the frequency was 0.36 ± 0.2 Hz (range 0.07 - 1.25 Hz), while at the end of the period (in the last 10% bin), the values raised to an amplitude of 111.1 ± 51.89 µV (range 29.09 - 266.92 µV), a rising slope of 2.05 ± 0.99 ms/µV (range 0.22 - 4.99 ms/µV) and a frequency of 0.69 ± 0.32 Hz (range 0.14 - 1.52 Hz).

We then assed the specific temporal evolution of PIDs in the final seconds before the beginning of the ILE, during the trigger period. PIDs also showed an increased in amplitude (140.34 ± 77.49 µV, range 22.33 - 408.16 µV), rising slope (2.82 ± 1.76 ms/µV, range 0.45 - 11.02 ms/µV) and frequency (0.96 ± 0.42 Hz, range 0.26 - 2.82 Hz) compared to the steady state period amplitude (90.49 ± 43.07 µV, range 7.01 - 232.68 µV), rising slope (1.49 ± 0.68 ms/µV, range 0.11 - 3.71 ms/µV) and frequency (0.79 ± 0.53 Hz, range 0.24 - 6.05 Hz) (Wilcoxon test, $p < 0.001$, $p = 0.001$ and $p = 0.001$ respectively). The trigger period lasted 34.17 ± 19.11 seconds (range 7.83 - 107.82 seconds), presenting an average of 20.44 ± 9.72 PIDs (range 5-50 PIDs). Once again, astrocytomas presented the shortest trigger duration with 29.12 ± 15.78 seconds (range 10.37 - 107.82 seconds) compared to oligodendrogliomas (41.76 ± 22.53 seconds) and GB (32.22 ± 16.51 seconds) (p = 0.4, Kruskall Wallis test). Focusing on the last PID before the ILE onset, 14/25 presented a higher amplitude than the mean of the trigger period, 5/25 showed no change in amplitude, and 6/30 showed a decrease.

Since we observed an increase in PIDs frequency, we analyzed the evolution of the propagation speed over time. An increase in PIDs propagation speed was seen between the steady state (0.11 ± 0.004 m/s, range 0.08 - 0.15 m/s), (n = 50 events from 3 slices), and the trigger period (0.28 ± 0.01 m/s, range 0.16 - 0.34 m/s) (n = 50 events from 3 slices) (Wilcoxon test, p= 0.002).

Preictal HFA temporal Dynamics

To understand better the mechanisms implicated in the increased in the PID features we then studied the evolution of HFA. HFA were composed by HFO and multiunit activity. We decided to study HFA because it gives us information about neuronal firing and also since in several slices it was impossible to differentiate HFO from MUA bursts. We observed a clear evolution of PIDs-associated HFA activity. Specifically, our results reveal a progressive increase in HFA amplitude and duration. During the build-up period, we observed a mean HFA burst duration of 759.6 ± 352.41 ms and a mean amplitude of 15.2 ± 9.23 µV (n= 2048 events). Through the steady-state period, the mean duration (893.15 ± 403.4 ms) and amplitude increased (19.2 µV ± 11.99 µV) (n= 1779 events). In the trigger period, the mean duration was 999.7 ± 533.27 ms, and the mean amplitude was 24.8 ± 16.47 µV (n= 505 events) (Fig 4). These values show an increase in mean HFA amplitude of 20.83% and 22.58% between periods and a similar increase in mean HFA duration of 14.95% and 10.65%.

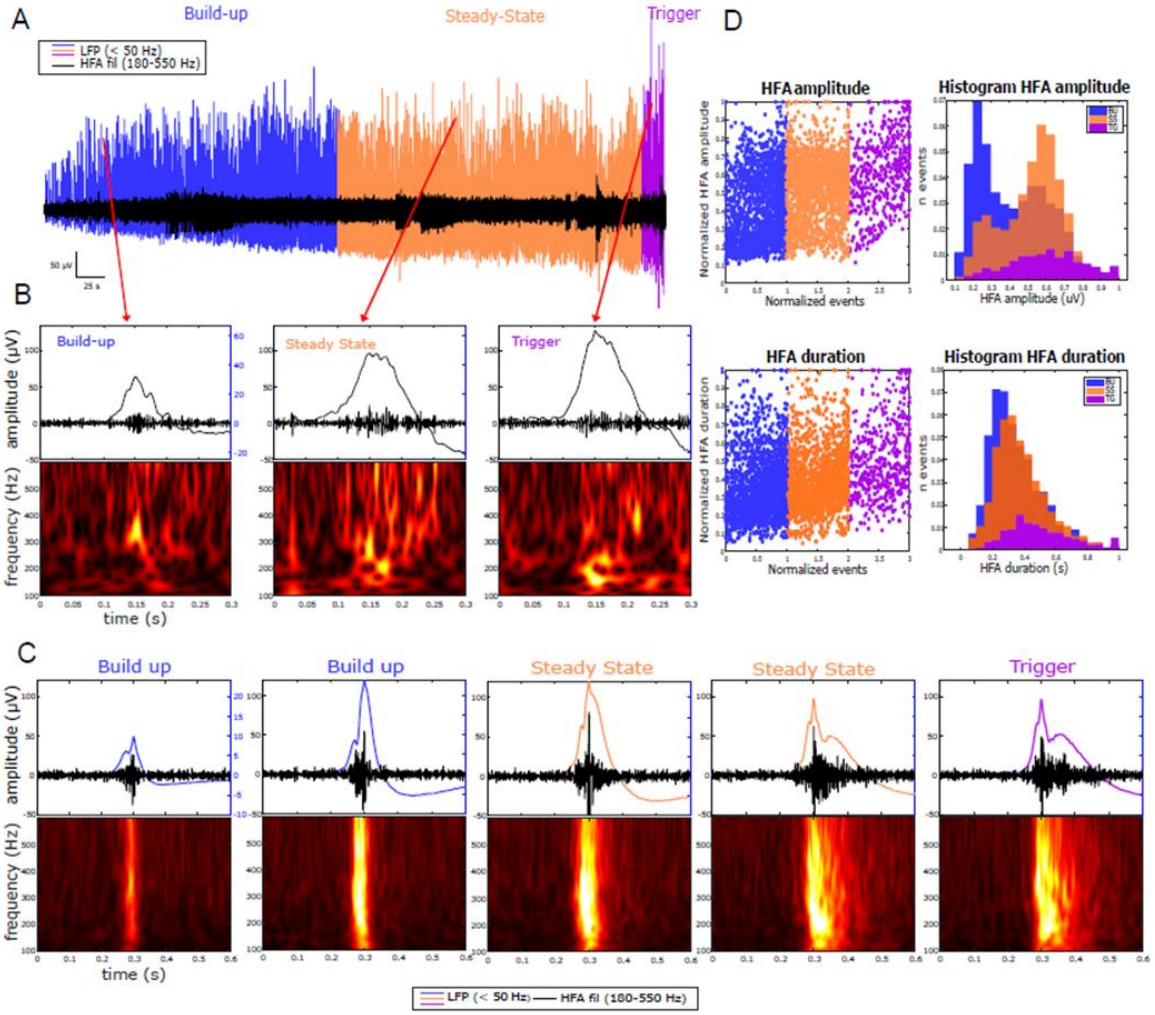

Figure 4: HFA temporal evolution. A: Extracellular recording (one electrode) of the preictal period after increasing the milieu excitability with $6K^{+}0Mg^{2+}$-aCSF. Preictal discharges (blue for the build up period, orange for the steady state, and purple for the trigger period) and HFA (superimposed in black) are shown. B: Individual examples by subperiod (build-up, steady state, and trigger period). At the top the filtered signal from 180- 550 Hz and the field potential, at the bottom, the spectrogram. C: Average HFA of one slice at five time points showing a progressive increase in amplitude and duration. Each of these averages was performed on 20 events (PID). At the top, the field potential (blue for build up, orange for steady state, and purple for trigger period), the filtered signal from 180-550 Hz, and enveloped (red) are represented. At the bottom, the spectrogram is shown. D: HFA normalized amplitude and duration evolution during the build-up (blue), steady state (orange), and trigger period (purple) (n= 25 slices, events= 4333). Histograms presenting the amplitude and frequency distribution of HFA during the build-up period (blue), steady state (orange) and trigger period (purple) show higher amplitudes and longer durations during the trigger period.

Preictal HFO temporal Dynamics

After identifying the temporal evolution of HFA, we then focused on HFO temporal dynamics, since they are known as an epileptogenesis biomarker. A total of 19/30 slices presented HFO (63.3%). 6/15 (90%) of oligodendrogliomas presented HFO, 6/15 (46%) of astrocytomas, and 2/4 (50%) of GB. In line with our HFA results, our data showed an evolution in the behavior of HFOs over time. To study the temporal dynamics of HFO, only one electrode by slice was analyzed and a total of 663 HFO were detected. Specifically, the number of HFOs tended to increase as seizure onset approached. At the beginning of the

build-up period, only 3 HFO were observed, while at the end of the trigger period, we observed 48 HFO. Almost 95% of the HFOs were nested within a PID (n = 630 / 663 events), and only 5% of them were seen outside PIDs (n = 33 / 663 events) (Fig 3.C). The number of PIDs with HFOs was nine times higher than the number of HFOs without PIDs at the end of the trigger period.

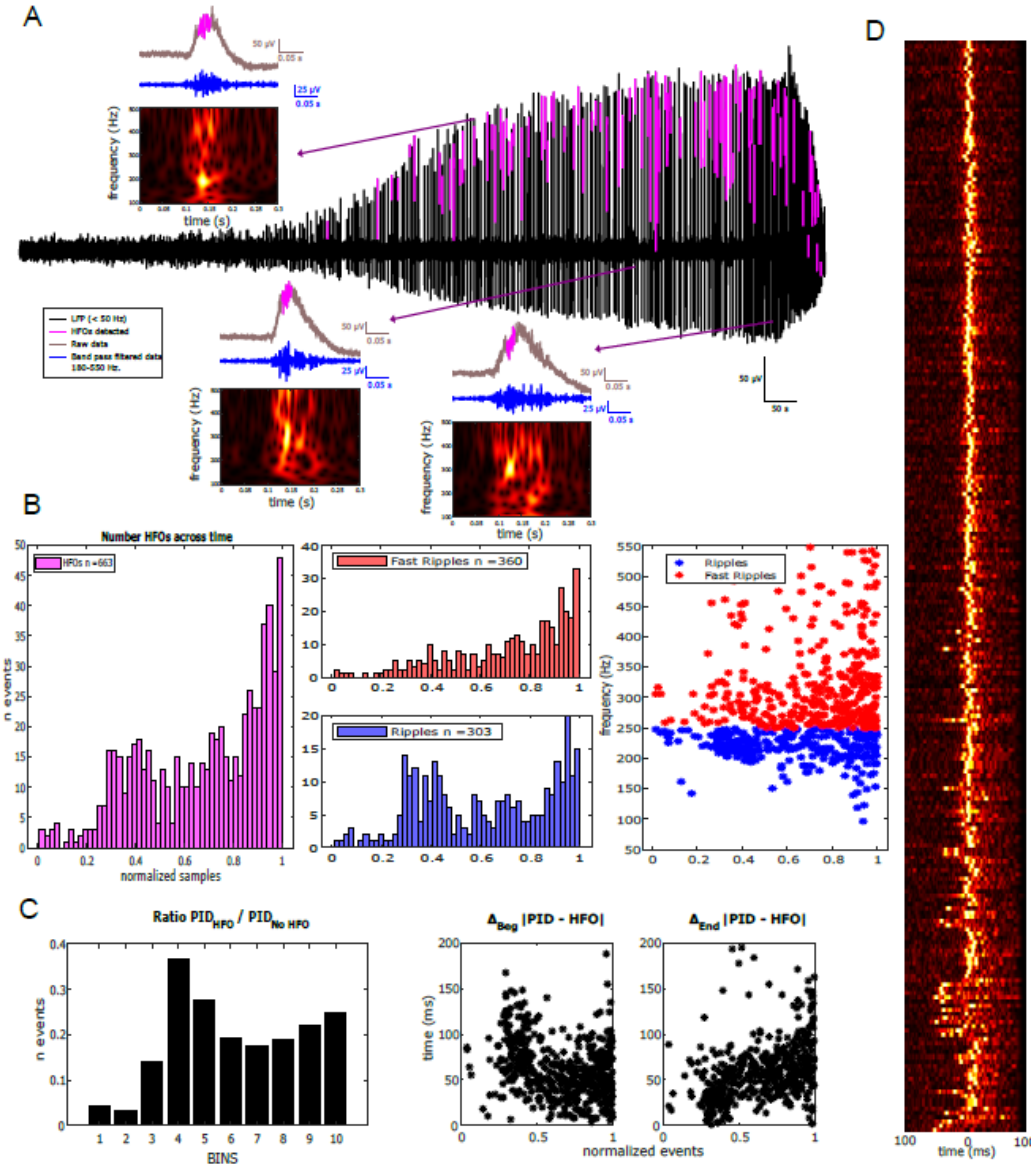

Figure 5: HFO temporal evolution. A: Extracellular recording (one electrode) of the preictal period with HFO marked in pink, and one example by subperiod showing the raw signal, filtered between 180-55 Hz, and the spectrogram. B: Histogram showing the increasing number of HFO with time and their classification in ripples and fast ripples (19 slices, 663 events). C: Ratio between PIDs associated to an HFO vs PIDs without HFO. Temporal evolution of the delay between PID and HFO onset. Temporal evolution of the delay between PID and HFO end. D: Temporal evolution of the HFO envelope in relation to the PIDs (5 slices). Color matrix showing the envelope of HFO using as a zero the time of the PID maximum. The beginning of the build up period is situated at the top of the matrix, and the end correspond to the seizure onset.

To evaluate the phase relationship between the PIDs and the HFOs, we measured the delay between PID and HFO onsets and between the end of the PID and HFO. Although the PID duration and the HFO duration increased with time, there was no phase shift of the HFO concerning the PID (Fig 5. D). The delay between PID and HFO onsets appeared to be constant (mean 61.38 ± 31.01 ms), while the end of the PID relative to the end of the HFO tended to increase (mean 65.69 ± 69.30 ms (Fig 5.C). In other words, the onset of the HFO seemed to be phase-locked with the beginning of the PID, and the duration of the HFOs increased in parallel with the duration of the PIDs. The phase relationship between PIDs and HFO not only tended to remain constant over time but occurred mainly in the rising slope of the PIDs (84.6% of the events).

Dividing HFOs into ripples (80-250 Hz) and fast ripples (250-550 Hz) according to their frequency, we observed that 45.71% of HFOs were ripples and 54.29% were fast ripples. In addition to the balance between these percentages, both oscillations maintained a constant increasing distribution in which the number of ripples and fast ripples increased toward the onset of the seizure, keeping the ratio of ripples/fast ripples (Figure 5.B).

Spatial dynamics of PIDs

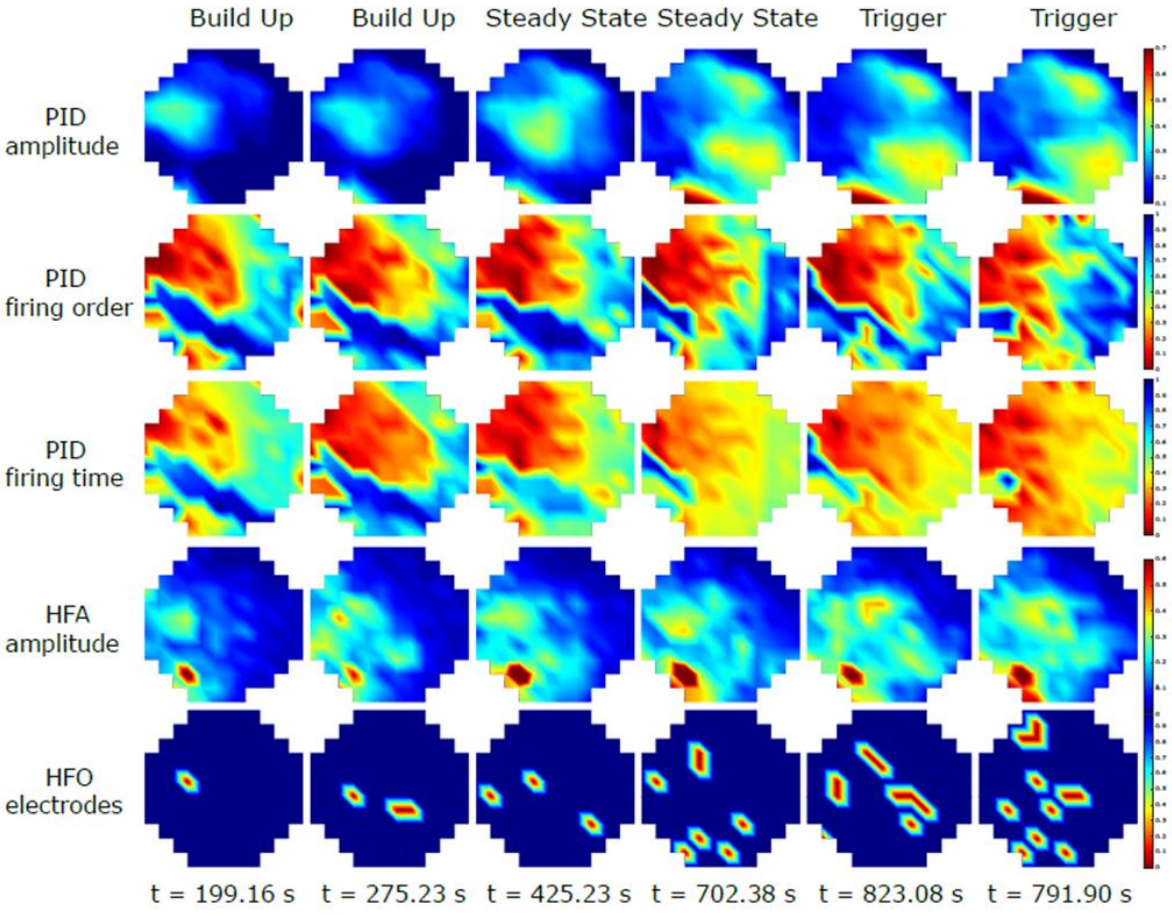

Figure 6: Spatial evolution of PID, HFA and HFO. Heat-map of the matrix showing the spatial evolution of PID amplitude, firing order, firing time, HFA amplitude and number of electrodes with HFO at six time-points in one slice. Larger areas display PID, HFA and HFO as we approach the seizure onset.

The regions where PIDs amplitude was higher coincided precisely with the electrodes where the PID discharges occurred first. PIDs tended to extend with time over larger areas. The firing order of PIDs remained relatively constant over time, in contrast to the firing time, which changed and tended to span more regions with the seizure onset approach.

Even if most of the slices displayed HFA, a region with higher amplitude values existed. This region progressively enlarged over time. Regarding HFO, they were limited to microdomains of tens of μm^2. The number of electrodes displaying HFO increased over time but always consisted of small islets (Figure 6).

Discussion:

This study shows that PIDs evolved through the way to a seizure, showing a progressive increase in amplitude, rising slope, and frequency. This increase is evident during the build up and the trigger period, while the steady state shows a stability of PIDs features. Moreover, PID present an increase in their speed propagation as we approach the seizure onset. Regarding HFA and HFO, we observed larger amplitudes and durations as we approach to the seizure onset. HFA areas are located very close to PID initiation areas and they present a gradual enlargement in space. Areas generating HFO spread progressively during the preictal period, but were limited to microdomains.

Interestingly, PIDs needed a minimum of 140 seconds to appear since the enhancement of the excitability, suggesting that some plastic mechanisms are required for PID generation (Huberfeld et al., 2011). Neuronal firing increases rapidly after extracellular K^+ rises (Contreras et al., 2021; Huberfeld et al., 2011). Still, time is needed for PID generation, and the underlying mechanisms probably stabilize once they reach the steady state. Astrocytomas and oligodendrogliomas presented shorter delays until the appearance of the first PID than GB. Astrocytomas and oligodendrogliomas are known for presenting higher rates of seizures than GB. Maybe that difference can be due to the more robust epileptic networks present in astrocytomas and oligodendrogliomas.

The temporal evolution of PIDs is evident during the build-up period until reaching a plateau. Subsequently, during the trigger period, further growth ensues. Although this increase is at its maximum during the trigger period, the final PID before the onset of ILE is not necessarily the largest. This finding suggests that ILE generation depends not only on the number of neurons involved but also on their synchronicity, as the last PID before ILE onset might have smaller amplitudes than preceding PIDs.

In vivo recordings of epileptic patients using sEEG also present similar PID patterns (Chen et al., 2018; Lagarde et al., 2019; Weiss et al., 2016). Additionally, in vivo PIDs exhibit a progressive increase in amplitude and frequency (Chen et al., 2018). The presence of a preictal spiking pattern before seizure onset correlated with 57.9% of patients achieving seizure freedom post-surgery (Lagarde et al., 2019). Comparable propagation speed ranges (0.3 to 0.8 m/s) have been recorded in epileptic patients (Matarrese et al., 2023). IIDs and PIDs propagation primarily depends on synaptic connections (Chizhov et al., 2019, 2022). The augmented speed of PID propagation from the steady state to the trigger period might be attributed to more efficient propagation along the fastest synaptic pathways. During the

build-up and the steady state, the network evolves and explores potential synaptic pathways; later on, during the trigger period, when the network becomes more streamlined, only the quickest synaptic pathways persist.

A progressive increase in HFA duration and amplitude was observed. This phenomenon suggests either an increase in the spiking rate of the neurons belonging to the network or a recruitment of more neurons into the network. The growth was maximum before the ILE onset. Interestingly, although the FP amplitude growth slowed once the build-up period ended, the HFA continued to evolve during the steady and trigger periods. So, even if we could not detect evident changes in FP, neuronal recruitment is still ongoing during the preictal period.

The quantity of HFOs also increases as ILE onset approaches. However, it is interesting to note that not all the slices exhibit HFO. Although some ILE appear without concurrent HFO, spatial analysis demonstrates that HFO can be recorded from single microelectrodes within the small matrix. This suggests that the local nature of HFO necessitates an interelectrode space of less than 200 µm to capture all the HFO. With our actual interelectrode space, some HFO can be undetectable on a slice of 400 µm thickness. This finding also suggests that sEEG electrodes, even containing microcontacts, might not capture all HFO, potentially contributing to the variable success of epilepsy surgery.

MEA recordings have the advantage of providing large spatial information. We observed spatial recruitment over time for PIDs, HFA, and HFO, suggesting that more neuronal populations joined the network as the preictal period progressed. Interestingly, HFA areas were very close to the regions where PID appears first. Maybe the HFA areas are at the origin of PID generation, but their main projection is some µm away due to volume conductance (Herreras, 2016; Kajikawa & Schroeder, 2015; Wolters & Munck, 2007). HFO follows the same behavior, with enlarging areas and the appearance of new HFO regions during the process, suggesting the presence of patchy cluster areas involved in HFO generation that are recordable only if we are situated next to them. That can explain why epilepsy surgery is not always satisfactory since we cannot detect some HFO with macro SEEG contacts, enhancing the importance of enlarging the spatial resolution when trying to catch HFO.

HFA and HFO spatiotemporal evolution followed the same behavior as PID, with a progressive enlargement of amplitude and more extensive areas involvement. We hypothesized that sharing mechanisms involved in PID, HFA, and HFO generation at the neocortical level could explain this coupled behavior. Since PIDs are driven by glutamatergic mechanisms (Huberfeld et al., 2011), maybe glutamate is one of the main mechanisms involved in HFA and HFO generation. Moreover in the peritumoral tissue case where a disbalance between excitation and inhibition is present (Krishna et al., 2023) due to GABAergic and glutamatergic signaling alterations (Lange et al., 2021; Pallud et al., 2014).

In conclusion, PIDs can be induced ex vivo in human brain slices by increased excitability. That can replicate the *in vivo* transition between the interictal period and the beginning of a seizure. Through the way to an ILE, a temporal evolution is evident in PIDs, HFA, and HFO, reflecting neuronal recruitment and synchronicity. Furthermore, a spatial enlargement of the areas producing PIDs, HFA, and HFO are observed. These findings suggest that, ictogenesis needs time and a complex dynamic of recruitment and

synchronization is necessary before a seizure arise. These dynamics, both on the temporal and spatial scale, hold the potential for developing an in vivo seizure anticipation algorithm. A deeper understanding of seizure and preictal patterns could have significant implications regarding seizure anticipation. However, a high spatial resolution is needed to capture these complex dynamics, especially of HFO.

Acknowledgments

The authors thank participating patients.

Funding

This work was supported in part by the European Research Council to GH (Consolidator grant #865592) and by the Fondation pour la Recherche Medicale to BDF (FDM201906008544 grant).

Competing interests

The authors report no competing interests.

References:

Baumgartner, C., Serles, W., Leutmezer, F., Pataraia, E., Aull, S., Czech, T., & Pietrzyk, U. (1998). *Preictal SPECT in Temporal Lobe Epilepsy : Regional Cerebral Blood Flow Is Increased Prior to Electroencephalography- Seizure Onset as process*. *39*(6).

Blauwblomme, T., Dossi, E., Pellegrino, C., Goubert, E., Iglesias, B. G., Sainte-Rose, C., Rouach, N., Nabbout, R., & Huberfeld, G. (2019). Gamma-aminobutyric acidergic transmission underlies interictal epileptogenicity in pediatric focal cortical dysplasia. *Annals of Neurology*, *85*(2), 204–217. https://doi.org/10.1002/ana.25403

Chen, I. E., Swinburne, N., Tsankova, N. M., Hefti, M. M., Aggarwal, A., Doshi, A. H., Hormigo, A., Delman, B. N., & Nael, K. (2018). Sequential Apparent Diffusion Coefficient for Assessment of Tumor Progression in Patients with Low-Grade Glioma. *AJNR. American Journal of Neuroradiology*, *39*(6), 1039–1046. https://doi.org/10.3174/AJNR.A5639

Chizhov, A. V., Amakhin, D. V., Smirnova, E. Y., & Zaitsev, A. V. (2022). Ictal wavefront propagation in slices and simulations with conductance-based refractory density model. *PLoS Computational Biology*, *18*(1). https://doi.org/10.1371/JOURNAL.PCBI.1009782

Chizhov, A. V., Amakhin, D. V., & Zaitsev, A. V. (2019). Spatial propagation of interictal discharges along the cortex. *Biochemical and Biophysical Research Communications*, *508*(4), 1245–1251. https://doi.org/10.1016/J.BBRC.2018.12.070

Contreras, S. A., Schleimer, J. H., Gulledge, A. T., & Schreiber, S. (2021). Activity-mediated accumulation of potassium induces a switch in firing pattern and neuronal excitability type. *PLoS Computational Biology*, *17*(5). https://doi.org/10.1371/JOURNAL.PCBI.1008510

Cousyn, L., Navarro, V., & Chavez, M. (2021). Preictal state detection using prodromal symptoms: A machine learning approach. *Epilepsia*, *September 2020*, 42–47. https://doi.org/10.1111/epi.16804

Crépon, B., Navarro, V., Hasboun, D., Clemenceau, S., Martinerie, J., Baulac, M., Adam, C., & Le Van Quyen, M. (2010). Mapping interictal oscillations greater than 200 Hz recorded with intracranial macroelectrodes in human epilepsy. *Brain*, *133*(1), 33–45. https://doi.org/10.1093/brain/awp277

Dossi, E., Blauwblomme, T., Moulard, J., Chever, O., Vasile, F., Guinard, E., Le Bert, M., Couillin, I., Pallud, J., Capelle, L., Huberfeld, G., & Rouach, N. (2018). Pannexin-1 channels contribute to seizure generation in human epileptic brain tissue and in a mouse model of epilepsy. *Science Translational Medicine*, *10*(443). https://doi.org/10.1126/scitranslmed.aar3796

Dossi, E., Blauwblomme, T., Nabbout, R., Huberfeld, G., & Rouach, N. (2014). Multi-electrode array recordings of human epileptic postoperative cortical tissue. *Journal of Visualized Experiments*, *92*, 1–9. https://doi.org/10.3791/51870

Federico, P., Abbott, D. F., Briellmann, R. S., Harvey, A. S., & Jackson, G. D. (2005). *Functional MRI of the pre-ictal state*. 1811–1817. https://doi.org/10.1093/brain/awh533

Fisher, R. S., Acevedo, C., Arzimanoglou, A., Bogacz, A., Cross, J. H., Elger, C. E., Engel, J., Forsgren, L., French, J. A., Glynn, M., Hesdorffer, D. C., Lee, B. I., Mathern, G. W., Moshé, S. L., Perucca, E., Scheffer, I. E., Tomson, T., Watanabe, M., & Wiebe, S. (2014). ILAE Official Report: A practical clinical definition of epilepsy. *Epilepsia*, *55*(4), 475–482. https://doi.org/10.1111/epi.12550

Herreras, O. (2016). Local field potentials: Myths and misunderstandings. *Frontiers in Neural Circuits*, *10*(DEC), 1–16. https://doi.org/10.3389/fncir.2016.00101

Huberfeld, G., Le Duigou, C., Le Van Quyen, M., Navarro, V., Baulac, M., & Miles, R. (2013). The paradox of the paroxysm: can seizure precipitants help explain human ictogenesis? *The Neuroscientist : A Review Journal Bringing Neurobiology, Neurology and Psychiatry*, *19*(5), 523–540. https://doi.org/10.1177/1073858413497430

Huberfeld, G., Menendez De La Prida, L., Pallud, J., Cohen, I., Le Van Quyen, M., Adam, C., Clemenceau, S., Baulac, M., & Miles, R. (2011). Glutamatergic pre-ictal discharges emerge at the transition to seizure in human epilepsy. *Nature Neuroscience*, *14*(5), 627–635. https://doi.org/10.1038/nn.2790

Jacobs, J., Zijlmans, M., Zelmann, R., Olivier, A., Hall, J., Gotman, J., & Dubeau, F. (2010). Value of electrical stimulation and high frequency oscillations (80-500 Hz) in identifying epileptogenic areas during intracranial EEG recordings. *Epilepsia*, *51*(4), 573–582. https://doi.org/10.1111/j.1528-1167.2009.02389.x

Kajikawa, Y., & Schroeder, C. E. (2015). Generation of field potentials and modulation of their dynamics through volume integration of cortical activity. *Journal of Neurophysiology*, *113*(1), 339–351. https://doi.org/10.1152/JN.00914.2013

Kerem, D. H., & Geva, A. B. (2005). Forecasting epilepsy from the heart rate signal. *Medical & Biological Engineering & Computing*, *43*(2), 230–239. https://doi.org/10.1007/BF02345960

Krishna, S., Choudhury, A., Keough, M. B., Seo, K., Ni, L., Kakaizada, S., Lee, A., Aabedi, A., Popova, G., Lipkin, B., Cao, C., Nava Gonzales, C., Sudharshan, R., Egladyous, A., Almeida, N., Zhang, Y., Molinaro, A. M., Venkatesh, H. S., Daniel, A. G. S., … Hervey-Jumper, S. L. (2023). Glioblastoma remodelling of human neural circuits decreases survival. *Nature*, *617*(7961). https://doi.org/10.1038/S41586-023-06036-1

Kwan, P., Arzimanoglou, A., Berg, A. T., Brodie, M. J., Hauser, W. A., Mathern, G., Moshé, S. L., Perucca, E., Wiebe, S., & French, J. (2010). Definition of drug resistant epilepsy: consensus proposal by the ad hoc Task Force of the ILAE Commission on Therapeutic Strategies. *Epilepsia*, *51*(6), 1069–1077. https://doi.org/10.1111/J.1528-1167.2009.02397.X

Lagarde, S., Buzori, S., Trebuchon, A., Carron, R., Scavarda, D., Milh, M., McGonigal, A., & Bartolomei, F. (2019). The repertoire of seizure onset patterns in human focal epilepsies: Determinants and prognostic values. *Epilepsia*, *60*(1), 85–95. https://doi.org/10.1111/EPI.14604

Lambrecq, V., Lehongre, K., Adam, C., Frazzini, V., Mathon, B., Clemenceau, S., Hasboun, D., Charpier, S., Baulac, M., Navarro, V., & Le Van Quyen, M. (2017). Single-unit activities during the transition to seizures in deep mesial structures. *Annals of Neurology*, *82*(6), 1022–1028. https://doi.org/10.1002/ana.25111

Lange, F., Hörnschemeyer, J., & Kirschstein, T. (2021). Glutamatergic Mechanisms in Glioblastoma and Tumor-Associated Epilepsy. *Cells*, *10*(5). https://doi.org/10.3390/CELLS10051226

Lote, K., Stenwig, A. E., Skullerud, K., & Hirschberg, H. (1998). Prevalence and prognostic significance of epilepsy in patients with gliomas. *European Journal of Cancer*. https://doi.org/10.1016/S0959-8049(97)00374-2

Matarrese, M. A. G., Loppini, A., Fabbri, L., Tamilia, E., Perry, M. S., Madsen, J. R., Bolton, J., Stone, S. S. D., Pearl, P. L., Filippi, S., & Papadelis, C. (2023). Spike propagation mapping reveals effective connectivity and predicts surgical outcome in epilepsy. *Brain : A Journal of Neurology*. https://doi.org/10.1093/BRAIN/AWAD118

Mittal, S., Barkmeier, D., Hua, J., Pai, D. S., Fuerst, D., Basha, M., Loeb, J. A., & Shah, A. K. (2016). Intracranial EEG analysis in tumor-related epilepsy: Evidence of distant epileptic abnormalities. In *Clinical Neurophysiology* (Vol. 127, Issue 1). International Federation of Clinical Neurophysiology. https://doi.org/10.1016/j.clinph.2015.06.028

Pallud, J., Le Van Quyen, M., Bielle, F., Pellegrino, C., Varlet, P., Labussiere, M., Cresto, N., Dieme, M. J., Baulac, M., Duyckaerts, C., Kourdougli, N., Chazal, G., Devaux, B., Rivera, C., Miles, R., Capelle, L., & Huberfeld, G. (2014). Cortical GABAergic excitation contributes to epileptic activities around human glioma. *Science Translational Medicine*, *6*(244), 244ra89. https://doi.org/10.1126/scitranslmed.3008065

Park, C. J., & Hong, S. B. (2019). High Frequency Oscillations in Epilepsy: Detection Methods and Considerations in Clinical Application. *Journal of Epilepsy Research*, *9*(1), 1–13. https://doi.org/10.14581/jer.19001

Perucca, P., Dubeau, F., & Gotman, J. (2014). Intracranial electroencephalographic seizure-onset patterns: Effect of underlying pathology. *Brain*, *137*(1), 183–196. https://doi.org/10.1093/brain/awt299

Staba, R. J., Wilson, C. L., Bragin, A., Jhung, D., Fried, I., & Engel, J. (2004). High-frequency oscillations recorded in human medial temporal lobe during sleep. *Annals of Neurology*, *56*(1), 108–115. https://doi.org/10.1002/ana.20164

Stacey, W., Le, M., Quyen, V., Mormann, F., Schulze-bonhage, A., & Pitié-salpêtrière, H. De. (2011). What is the present-day EEG evidence for a preictal state ? *Epilepsy Research*, *97*(3), 243–251. https://doi.org/10.1016/j.eplepsyres.2011.07.012

Valderrama, M., Crépon, B., Botella-Soler, V., Martinerie, J., Hasboun, D., Alvarado-Rojas, C., Baulac, M., Adam, C., Navarro, V., & Le Van Quyen, M. (2012). Human gamma oscillations during slow wave sleep. *PloS One*, *7*(4). https://doi.org/10.1371/JOURNAL.PONE.0033477

Weiss, S. A., Alvarado-Rojas, C., Bragin, A., Behnke, E., Fields, T., Fried, I., Engel, J., & Staba, R. (2016). Ictal onset patterns of local field potentials, high frequency oscillations, and unit activity in human mesial temporal lobe epilepsy. *Epilepsia*, *57*(1), 111–121. https://doi.org/10.1111/EPI.13251

Wolters, C., & Munck, J. C. de. (2007). Volume conduction. *Scholarpedia*, *2*(3), 1738. https://doi.org/10.4249/SCHOLARPEDIA.1738

Wu, D., Zhang, W., Lu, H., Liu, X., & Sun, W. (2021). Transitional Pattern as a Potential Marker of Epileptogenic Zone in Focal Epilepsy - Clinical Observations from Intracerebral Recordings.

Epilepsy Research, *174*(April), 106676. https://doi.org/10.1016/j.eplepsyres.2021.106676
Zijlmans, M., Jiruska, P., Zelmann, R., Leijten, F. S. S., Jefferys, J. G. R., & Gotman, J. (2012). High-frequency oscillations as a new biomarker in epilepsy. *Annals of Neurology*, *71*(2), 169–178. https://doi.org/10.1002/ana.22548

Materials and Methods:

Glioma surgery:

Brain tissue specimens were obtained from Pitié-Salpêtrière and Saint-Anne hospitals in Paris. All the patients gave their written consent before the surgery. Surgery was not modified for the research protocol and consisted of resection after functional mapping in awake patients. All the brain tissue specimens came from the peritumoral tissue obtained from the security margin of glioma surgery. Brain samples were collected from 22 glioma patients.
This retrospective study was approved by the Comité d'Evaluation et d'Ethique de l'INSERM - IRB00003888 (approval n°21-864).

Human tissue:

During surgery, the tissue was taken out and immediately immersed in an oxygenated, cold (1-4°C) ACSF solution (250 mM sucrose, 10 mM D-glucose, 3 mM KCl, 25 mM $NaHCO_3$, 1 mM for 10/37 slices and 110 mM Choline, 26 mM $NaHCO_3$, 10 mM Glucose, 11.6 mM Na-ascorbate, 7 mM $MgCl_26H_20$, 3.1 mM Na-pyruvate, 2,5 mM KCl, 1,25 mM $NaH_2PO_4H_2O$ for the remaining 27/37 slices) to slow down metabolism.
The operatory piece was transported to the laboratory, where meninges were removed to facilitate the slicing process. Using a vibratome (Leica VT1200S), 400 µm neocortical slices were cut off. Then, the slices were placed in an interface chamber for recovery for at least one hour, perfused by an oxygenated physiologic aCSF solution (124 mM NaCl, 3 mM KCl, 26 mM NaHCO3, 11.1 mM D-glucose, 1,6 mM CaCl2, 1,3 mM MgCl2) at 37°C.

MEA:

We used planar MEA with titanium nitride electrodes (30 µm diameter), arranged in two different configurations: i) a big one: 12 x 10 matrix with 1000 µm interelectrode spacing in the vertical plane, and 1500 µm in the horizontal plan, ii) a small one: 12 x 12 matrix with 200 µm interelectrode spacing in both directions. MEA size was chosen depending on the size of the brain slices. The recordings were made using a sampling rate of 10.000 Hz. They were filtered between 0.1 and 10.000 Hz (Logiciel MC Rack, MultiChannel Systems). To keep alive slices for several hours, the MEA chamber was perfused with a high flow (6 ml/min) of oxygenated aCSF at 37°C. Two different types of aCSF were used: during the first ten minutes, physiologic aCSF was used to record spontaneous activities (IIDs), and after ten minutes, ictogenic aCSF (6-8 mM K^+, 0 Mg^+ aCSF) to induce ILE and PIDs.

FP analysis:

MC-Rack software (Multi Channel Systems) was used to visualize FP data. For measuring the temporal evolution of FP, the electrode displaying the earliest PID was selected and exported to Clampfit (suite pClamp, Molecular Devices). We defined the preictal

transitional period as going from adding ictogenic solution until the seizure onset. Seizure onset was determined visually.
The transitional preictal period was divided into three subperiods: build-up, steady state, and trigger period. To delimit the build-up period, we selected the recordings from the appearance of the first PID > 15 µV to the end of the increase in amplitude. The trigger period was visually identified, as PID showed a change in frequency in the seconds preceding the ILE. The steady-state period was defined as the period between the build-up and the beginning of the trigger period.
FPs were analyzed after applying a low pass filter of 30 Hz (Butterworth – 8 poles) and, if needed, a high pass filter of 1 Hz (Bessel – 8 poles). Amplitude, rising slope, and frequency were measured using an " up-only" algorithm with a user-defined threshold.
As slices were highly heterogeneous in terms of FP's amplitude and duration of the preictal period, and as we were interested in the dynamics more than in the absolute values, to be able to compare the data, normalization was performed. Amplitude, rising slope, and frequency were normalized to the maximum value of the slice. Means and standard deviation were calculated for every parameter in the three periods. To evaluate the temporal evolution by subperiods, data were organized in 10% BINS for the build-up period and 33% BINS for the trigger period.

HFA temporal analysis

HFA analyses were performed using data from 25 slices (18 big matrix, seven small matrix). The most representative electrode from each slice was selected for this analysis. The build-up, steady-state, and trigger periods were clearly distinguished for each electrode. Still, since the beginning and end of each of these period between slices, they were normalized in time (between 0 and 1) to compare the data from all recordings. To characterize the HFA behavior, two measures were extracted from these data: HFA duration and HFA amplitude.

A semi-automatic algorithm was used to compute the HFA duration. First, our script forward and backward filtered the raw signals around each PID (600 ms window) using a Chebyshev type II bandpass IIR filter (100 to 600 Hz). Then, the envelope of this signal was calculated using the Hilbert transform. The envelope was filtered again (low pass 40 Hz) to smooth its high-frequency components and used in the HFA begin and end detection. To detect the beginning and end of each HFA, we used an amplitude threshold on this signal; specifically, for each segment, we searched for a first local maximum, and from there, our algorithm moved to the left or right (detecting the beginning or end, respectively) until the filtered envelope value was lower than the mean plus four standard deviations. Finally, if necessary, each detection was visually inspected and manually adjusted using our graphical interface. The HFA duration was calculated as the sample difference between the start and end points over the sample rate.

To evaluate the HFA amplitude, we filtered the raw signals again, but this time around the previously detected starting and ending points (±100 ms). A Chebyshev type II bandpass IIR filter was used between 100 and 550 Hz. The envelope of the filtered signal was calculated, and its maximum value was defined as the HFA amplitude.

HFOs temporal analysis

HFO temporal analysis was performed using the 19 electrodes with a larger number of HFOs over 19 slices (1 electrode per slice, seven big matrix, 12 small matrix). To perform this analysis, first, the HFOs were detected. Their features (number in time, frequency, PID ratio, and duration) were extracted, and finally, a more detailed analysis of the phase relationship between HFOs and LFP was performed. For all these analyses, the separation between the build-up, steady-state and trigger periods was not considered (due to the limited number of events).

A semi-automatic algorithm was used to detect HFOs. Our algorithm filters the raw data between 180 and 400 Hz using an infinite impulse response filter with a forward-backward filtering strategy that introduces no phase shift. It calculates the filtered signal envelope using the Hilbert transform and extracts the candidates for HFOs using a threshold equal to the envelope mean plus five standard deviations (Crépon et al., 2010; Staba et al., 2004). Any envelope segment that met this threshold criterion and had a minimum duration of 10 ms was considered a candidate HFO. The time-frequency spectrum of all HFO candidates was obtained between 50 and 500 Hz with a Gabor wavelet, implemented with a modulated Gaussian window (Valderrama et al., 2012) of 1.5 cycles, and then used in the visual inspection stage. Two examiners (BD, DH) independently evaluated all previously obtained candidates for HFOs, using their time frequency, raw signal, filtered signal, and envelope to reject artifactual and false-positive events. On average, the two researchers agreed on 70% of the events; for the remaining 30%, they reevaluated the events and reached an agreement.

Once HFOs were detected, they were classified as ripples or fast ripples according to their predominant frequency in the spectrogram (ripples: 80 Hz< f <250 Hz and fast ripples: 250 Hz< f <550 Hz) and their duration and temporal event density were extracted. For slice 101013S1, an additional analysis was performed, including the five electrodes with the highest number of HFOs. The signal from each of these electrodes was divided into bins, and in each bin, all HFOs from these five electrodes were grouped. The FP was averaged within each group, and each event was fitted to this average. Likewise, the envelope of the filtered HFO (+-50 Hz of its dominant frequency) was calculated and plotted in a color matrix, considering the same time reference found with the FP average. Finally, a grouped representation is obtained, with the PID onset at the top of the figure and the seizure onset at the bottom.

Spatial analysis

For spatial analysis, the characterization of PIDs (in amplitude and time), HFA (in amplitude), and HFOs (in number of events) was extended to all electrodes of a single slice. Timestamps marked as build-up, steady state, and trigger from the same representative electrode were kept, and two color maps were generated for each of these periods and for each of the following five features: PID amplitude, PID firing order, PID firing time, HFA amplitude, and number of electrodes with HFOs.

First, we averaged the filtered signals (FP < 50 Hz) from all electrodes. Then, the local maxima of this average were detected, and a window of 4000 samples (400 ms) centered on each of these peaks was constructed to define co-occurrence in all 120 electrodes. Co-occurring events with less than 10 PIDs were excluded from the analysis, and the five features mentioned above were calculated for the rest of the events. Each feature was stored in a two-dimensional matrix that was normalized between 0 and 1. Finally, a color map

was generated by interpolating the color values according to the normalized values of the matrix.

Statistics:

Statistics were made using Prism (GraphPad). Exact p values are given unless $p < 0.001$. The level of significance was set at $p < 0.05$. Descriptive statistics are given as mean and standard deviations (SD). Comparisons between two continuous variables were made using the Mann-Whitney test. Comparisons between repeated measurements of continuous variables were made using the Wilcoxon test.

4.5 MicroECoG: a precision tool for glioma surgery

Finding an electrophysiological biomarker of glioma cell peritumoral infiltration could improve the surgical approach, enhancing patients' survival and improving their quality of life with better epilepsy control. The changes in the frequency and aperiodic components of the power spectrum give us a general approach to the extent of the peritumoral tissue. Still, the spatial resolution needs to be improved to be precise. Using microelectrodes would allow us to increase the spatial resolution significantly. We have established a collaboration with French startup Panaxium, which designs microelectrodes coated with PEDOT:PSS. They will provide us with microelectrodes to be used on an ECoG setup. The innovative character of the electrodes is due to their organic PEDOT:PSS lining, which will allow us to decrease the impedances and improve the SNR. Since the device is not yet approved for human patients, we have designed a clinical trial to test their safety before CE marking.

The primary outcome will be the safety of the device. To evaluate the outcome, we will measure the incidence of adverse effects due to using the device from the surgery to four days after. The adverse effect we can face are a lesion provoked by the electrode, bleeding, aseptic meningitis, neurological impairment, and prolonged hospitalization.

We will measure the quality of the recordings as secondary outcomes compared to conventional macroelectrodes. We will measure the SNR, the impedance along the surgery, the rate of HFO, the spike rate, and the after-discharge rate. We will also measure the neurosurgeon’s perception of the microelectrodes' ease of use.

We will measure the capacity of recording MUA and the correlation between the microECoG signals and the peritumoral infiltration as exploratory outcomes.

We have planned to record 50 glioma patients during awake surgery. The first ten patients will be recorded with both macro and microelectrodes. Both devices will be placed next to each other, but never in the same region, to differentiate which one was responsible for an adverse event if that happens. Then, once the safety of the device is established. The following 40 patients will be recorded only with the microelectrodes.

Interestingly, the reglementary test to validate the device's biocompatibility did not consider any test performed on brain tissue, which is surprising as the device will be tested on the brain. For this purpose, I have completed a biocompatibility test on human slices. To study brain biocompatibility, I have placed peritumoral slices in contact with the device. Half of the slice was in contact with the electrodes and parylene matrix, and the other half was in contact with a Petri dish to use it as a control. I have used two different criteria, one electrophysiological and the other structural. The electrophysiological evaluation was done after 2 hours of contact with the device. I have recorded the slices extracellularly, using MEA, and compared the different electrophysiological activities found in the “device half” with the “control half”. I have found no differences in the ILE generation nor IIDs or PIDs presence. The structural approach consisted of quantification of neuronal density, using a NeuN marker, after 6 hours of contact with the device. No significant differences were found.

We are finalizing the “investigator brochure” and the project will be sent for ethical evaluation in the last trimester of 2023. The clinical trial will start in the first trimester of 2024. I’ve been implicated in the clinical trial since the beginning in 2020. I’ve been involved in the design of the trial and microelectrodes, writing the protocol and information letters, and performing the biocompatibility test on human tissue.

After my thesis defense, once the clinical trial starts, I will be in charge of the recording and coordination of the clinical trial.

In the following pages, you will find the clinical trial MicroECoGG and the report of the biocompatibility test. Since they are needed for French agency evaluation, both are written in French.

4.4.1: Clinical Trial: MicroECoGG

PLAN D'INVESTIGATION CLINIQUE
RECHERCHE IMPLIQUANT LA PERSONNE HUMAINE

Titre complet en français
MicroElectroCorticoGraphie peropératoire des gliomes

Titre complet en anglais
Glioma intraoperative MicroElectroCorticoGraphy

Titre abrégé/ACRONYME
MicroECoGG

☐ **Monocentrique**
☒ **Multicentrique**

☒ **Nationale**
☐ **Européenne/Internationale**

1. JUSTIFICATION DE LA RECHERCHE - HYPOTHESES DE TRAVAIL

L'ElectroEncéphaloGraphie (EEG) est un outil largement utilisé d'étude de la dynamique des activités cérébrales, développé chez l'homme à la fin des années 1920 (Berger 1929). Ses indications ont évolué alors que les techniques d'imagerie cérébrale se sont développées mais il reste extrêmement utile dans les champs de l'épileptologie, des comas, de la mort cérébrale, des encéphalopathies post-anoxiques, métaboliques, toxiques, des encéphalites infectieuses et dysimmunitaires (G Huberfeld and Kubis, N 2015).

1.1. Enregistrements EEG intracrâniens.

A côté de l'EEG de scalp, des enregistrement intracrâniens ont été développés pour optimiser la localisation des activités épileptiques, dans une optique de chirurgie de l'épilepsie (Talairach et al. 1962). Le recueil *in situ* du signal EEG permet en effet une amplification supérieure, de capter des fréquences plus élevées et offre une meilleure résolution spatiale. Le signal recueilli par les électrodes toujours utilisées à ce jour, correspondant à des macroélectrodes, est cependant le même, qu'il soit enregistré en intracrânien ou sur le scalp. Il s'agit de potentiels post-synaptiques synchrones, essentiellement excitateurs, corticaux. L'EEG par macroélectrodes n'a pas accès au fonctionnement de neurones individuels, ni même au signal porté par des ensembles neuronaux. Il s'agit uniquement d'information synchrone reçue par une population neuronale assez importante. Il en résulte qu'une masse critique minimale de tissu cérébral doit s'activer pour produire un signal EEG. Cette masse critique a été évaluée à 6 cm^2 (Tao et al. 2007) en EEG de scalp. La résolution spatiale est meilleure en EEG intracrânien, inférieure au cm^3 (Ray, Tao, and Hawes-Ebersole 2007). Des travaux récents indiquent cependant que le signal en électrocorticographie (ECoG) se propage très peu, uniquement dans un rayon de 3 mm (Dubey and Ray 2019). Les enregistrements intracrâniens permettent donc, au prix d'une invasivité, une nette amélioration de la résolution spatiale des enregistrements EEG, celle-ci restant, du fait du diamètre des électrodes (0,2 à 1 cm usuellement) et du signal enregistré (potentiels synaptiques synchrones d'une population neuronale), très nettement supérieure à l'échelle neuronale.

Deux grandes catégories d'électrodes sont actuellement utilisées. Les électrodes de StéréoElectroEncéphalopGraphie (SEEG) consistent en un stylet comprenant dans sa longueur un chapelet de contacts cylindriques. Elles sont directement implantées dans le parenchyme cérébral, permettant un échantillonnage des activités cérébrales dans presque toutes les régions cérébrales, notamment en profondeur. L'utilisation de plusieurs électrodes (jusqu'à une quinzaine) comprenant chacune plusieurs contacts (d'environ 1 mm de diamètre, jusqu'à une dizaine par électrode) vise à élargir la masse cérébrale étudiée et à reconstruire dans l'espace la dynamique des activités épileptiques. Des électrodes en forme de disque sont également utilisées pour recueillir l'activité cérébrale à la surface corticale dans le cas de l'ECoG. Des bandes (strips) ou des grilles (grids) de 4 à 64 électrodes, d'un diamètre de 0,2 à 1 cm, généralement appliquées directement sur la surface corticale permettent le recueil des activités corticales sous-jacentes. Alors que la SEEG, avec une invasivité importante, permet une étude en volume, l'ECoG, moins invasive car ne pénétrant pas le parenchyme cérébral (mais nécessitant une exposition corticale large), limite l'étude à la surface corticale. De ce fait, son rôle dans les explorations intracrâniennes des épilepsies tend à se réduire, notamment aux USA, au profit de la SEEG (Chauvel, Gonzalez-Martinez, and Bulacio 2019; Isnard et al. 2018).

Il existe cependant une circonstance très favorable à l'utilisation de l'ECoG. Lors des chirurgies cérébrales, l'exposition corticale rend possible l'enregistrement EEG cortical sans invasivité supplémentaire. L'ECoG peropératoire présente un intérêt dans la chirurgie de l'épilepsie, récemment réactivé par la découverte de meilleurs biomarqueurs électrophysiologiques.

1.2. ElectroCorticoGraphie peropératoire en épileptologie

L'ECoG peropératoire se pratique depuis la fin des années 1930, introduite par Penfield et Jasper à Montréal (Almeida, Martinez, and Feindel 2005). Elle se heurte à plusieurs difficultés techniques qui ont longtemps limité son utilisation. Nécessairement courte du fait du temps chirurgical, l'ECoG peropératoire ne capte généralement pas de crise mais uniquement des activités intericales, dont la valeur localisatrice de la zone épileptogène est imparfaite. L'anesthésie modifie par ailleurs les activités épileptiques. Il a ainsi été rapporté que le sufentanil, le fentanyl, l'alfentanil, le propofol, et le methohexital favorisent l'émergence d'activités épileptiques alors que l'halothane, les barbituriques et les benzodiazépines ont plutôt un effet suppresseur (Roessler et al. 2019).

Globalement, la « chasse aux pointes intericales » dans le but de localiser la zone épileptogène (ZE) s'est avérée plutôt décevante dans les épilepsies mésio-temporales (Tran et al. 1995; Schwartz et al. 1997; San-Juan et al. 2011), parfois utile cependant (Tripathi et al. 2010). L'ECoG peropératoire s'est surtout révélée utile en cas de lésions spécifiques s'exprimant sous le forme d'une activité intericale intense ou d'une signature électrophysiologique et de localisation similaire avec la ZE : dysplasie corticale focale, tuber de sclérose tubéreuse de Bourneville, angiome caverneux (Palmini et al. 1995; Tripathi et al. 2010; Salanova et al. 1992; Wennberg et al. 1999; D. D. Wang et al. 2013).

L'identification ces deux dernières décennies d'un nouveau biomarqueur d'épileptogénicité, les Fast Ripples (FR), où oscillations à haute fréquence (> 250 Hz) (Bragin et al. 1999) a permis de reconsidérer l'intérêt de la cartographie de la ZE par ECoG peropératoire. En effet, tant chez l'adulte que chez l'enfant, avec ou sans lésion, le fait d'emporter les régions corticales produisant des FR, qui restent très focales, est associé à un succès épileptologique en post-opératoire (Zweiphenning et al. 2016; Fedele et al. 2017; van 't Klooster, Leijten, et al. 2015; Hussain et al. 2017)**. Il est ainsi proposé d'adapter le geste chirurgical à la cartographie des FR identifiées par ECoG peropératoire et de ne pas laisser de région produisant les FR quand leur résection est possible sans déficit neurocognitif permanent** (van 't Klooster et al. 2017)**. Cette approche n'est cependant pas encore opérationnelle en pratique car i) l'enregistrement des FR est complexe, nécessitant notamment des électrodes et un système d'enregistrement performants ; 2) la détection des FR est difficile et ne se fait encore que sur des analyse *post hoc* des données d'ECoG peropératoire** (Zijlmans et al. 2017)**. Notre groupe est cependant expert dans le développement d'algorithme de détection puis de cartographie de FR et nous bénéficions d'un financement européen ERC (European Research Council) visant au développement d'un logiciel de détection en temps réel, au bloc opératoire, des FR. L'autre voix d'amélioration de la détection consiste en une amélioration des électrodes d'enregistrement, tant dans leur rapport signal / bruit que dans leur résolution spatiale. L'objectif de ce projet est la preuve de concept de l'utilisation d'électrodes innovantes permettant ces progrès et ouvrant le concept de microECoG.**

1.3. ElectroCorticoGraphie peropératoire en neuro-oncologie

Les tumeurs cérébrales désignent l'ensemble des processus lésionnels, bénins ou malins, provoqués par l'expansion d'un processus pathologique issu de divisions cellulaires anarchiques au sein du parenchyme cérébral. Elles peuvent être bénignes ou malignes – selon leur vitesse de croissance et leur invasivité, sont issues de types cellulaires divers et peuvent être originaires du système nerveux central (tumeurs primitives) ou extra-cérébrale (métastases). Parmi ces tumeurs cérébrales, les gliomes diffus représentent 25% de l'ensemble des tumeurs cérébrales et 81% des tumeurs primitives malignes avec une incidence de 4 à 6 pour 100 000 (Darlix et al. 2017; Ostrom et al. 2014). Ils se développent aux dépens des cellules gliales et peuvent être d'origine astrocytaire, oligodendrocytaire, ou indifférenciée entre ces deux types cellulaires.

1.3.1. L'épilepsie associée aux gliomes cérébraux

Les tumeurs cérébrales et l'épilepsie sont intimement liées. Les lésions tumorales sont fréquemment épileptogènes, la prévalence des crises dépendant du type histologique de la tumeur et des modalités de sa croissance, de sa localisation, de caractéristiques intrinsèques comme le profil 'moléculaire', et de spécificités de l'encéphale au sein duquel elles se développent. Les crises épileptiques sont volontiers inaugurales, faisant découvrir la tumeur et lorsqu'elles se répètent, la maladie épileptique alors installée peut elle-même être une source de handicap. La récurrence des crises est alors spécialement dépendante de l'évolution tumorale et donc des traitements oncologiques. La prise en charge de l'épilepsie associée aux tumeurs cérébrales ne se limite donc pas au diagnostic. La prise en charge médicamenteuse présente certaines spécificités : les médicaments antiépileptiques (MAE) peuvent interagir avec les traitements oncologiques mais aussi probablement directement influencer la croissance tumorale, leur profil de tolérance est plus défavorable dans ces indications, la dynamique d'évolution tumorale et donc de l'épilepsie implique une réévaluation fréquente du traitement antiépileptique. Enfin, la prévalence des épilepsies pharmacorésistantes augmente avec l'évolution tumorale et l'existence d'une épilepsie semble affecter elle-même le pronostic oncologique.

Liens épidémiologiques entre tumeurs cérébrales et épilepsie.

La fréquence des tumeurs cérébrales dans la population de patients épileptiques est estimée à 4% (van Breemen, Wilms, and Vecht 2007) et le risque de survenue d'un gliome est accru chez les patients préalablement hospitalisés pour une crise d'épilepsie (Schwartzbaum et al. 2005). Dix à 15% des crises inaugurales chez l'adulte (notamment après 66 ans (Hamilton and Kernick 2007) et 0,2 à 6% chez l'enfant sont en lien avec une tumeur cérébrale (Brogna, Gil Robles, and Duffau 2008). Chez les enfants, l'épilepsie est moins fréquemment le mode de découverte d'une tumeur cérébrale (dans 10% des cas), à l'exception des enfants de moins de 3 ans où l'épilepsie est le mode de révélation des tumeurs supratentorielles dans 70% des cas (Gaggero et al. 2009).

L'épilepsie est un trouble fréquent chez les patients porteurs d'une tumeur cérébrale : on estime qu'au moins 30% des patients porteurs d'une tumeur cérébrale présenteront une crise d'épilepsie (van Breemen, Wilms, and Vecht 2007). Elle est le symptôme révélateur dans 30 à 50% des tumeurs cérébrales primitives (van Breemen, Wilms, and Vecht 2007; Brogna, Gil Robles, and Duffau 2008; De Witt Hamer et al. 2012) et 5 à 45% des patients présenteront une crise d'épilepsie au cours de l'évolution de leur tumeur (van Breemen, Wilms, and Vecht 2007; Hildebrand et al. 2005; 2005; Hwang et al. 2001; J. W. Lee et al. 2010; C. J. Vecht and Wilms 2010). Alors que l'épilepsie est un symptôme inaugural plus fréquent dans les gliomes infiltrants de bas grade de malignité que dans ceux de haut grade, la fréquence cumulée de l'épilepsie au cours de l'histoire naturelle de la maladie est similaire dans les gliomes infiltrants de haut grade et de bas grade de malignité (van Breemen, Wilms, and Vecht 2007).

Caractéristiques tumorales et crises épileptiques.

Le risque de crise épileptique est tout d'abord dépendant de l'histopathologie tumorale (van Breemen, Wilms, and Vecht 2007). Globalement, les tumeurs à croissance lente sont nettement plus épileptogènes que celles à croissance rapide. L'incidence est de 80-90 % pour les gangliogliomes, 75% pour les tumeurs gliales de bas grade (60% pour les astrocytomes et près de 100% pour les oligodendrogliomes, 90% tous sous-types histopathologiques confondus (J Pallud, Audureau, et al. 2014)) et de 30 à 60 % pour les méningiomes. Les tumeurs dysembryoplasiques neuroépithéliales (DNET) sont associées à des crises dans plus de 95% des cas. Ces chiffres sont nettement plus faibles pour les tumeurs dites malignes : 50% pour les gliomes anaplasiques (grade III OMS), 25-60% pour les glioblastomes (grade IV OMS), 20-35% pour les métastases cérébrales et 10% pour les lymphomes primitifs du système nerveux central.

Parmi les facteurs liés aux interactions entre l'infiltration tumorale et le tissu cérébral, l'existence d'un envahissement cortical d'origine tumorale est associé au risque épileptique (Berntsson et al. 2009; Brogna, Gil Robles, and Duffau 2008; Englot, Berger, Chang, et al. 2012; Hildebrand et al. 2005; J. W. Lee et al. 2010; Johan Pallud, Llitjos, et al. 2012; Johan Pallud, Taillandier, et al. 2012; Ruda et al. 2012; You et al. 2012) aussi bien dans les gliomes infiltrants de bas grade (Chang, Smith, et al. 2008; Ruda et al. 2012) que dans ceux de haut grade de malignité (Chaichana et al. 2009). A l'inverse, les tumeurs profondes ont un risque moindre d'épilepsie (Smits et al. 2012).

L'incidence de l'épilepsie dépend de la localisation tumorale (van Breemen, Wilms, and Vecht 2007; Sirven et al. 2004). Les tumeurs sont d'autant plus épileptogènes qu'elles sont corticales, volumineuses, sus-tentorielles (J. W. Lee et al. 2010). Dans une série récente de 1509 gliomes de grade II (J Pallud, Audureau, et al. 2014), le risque de crises au diagnostic était principalement lié à la localisation anatomique, proche d'aires fonctionnelles, la localisation insulaire étant associée

à un risque accru de crises non contrôlées par le traitement. De nombreuses variables comme le volume tumoral, l'invasion corticale, la vitesse de croissance, le sous-type histopathologiques, le taux de prolifération et les marqueurs moléculaires n'étaient pas significativement associés à un risque épileptique accru. Le volume tumoral est lié au risque épileptique et son effet est dépendant du grade histopathologique : pour les gliomes infiltrants de bas grade, le risque épileptique augmente avec l'augmentation du volume tumoral du fait d'un envahissement cérébral plus important alors que pour les gliomes malins, le risque épileptique diminue avec l'augmentation du volume, du fait de l'installation rapide d'un effet de masse qui engendrera d'autres symptômes (J. W. Lee et al. 2010; Ruda et al. 2012). Ceci illustre bien le fait que l'épilepsie tumorale semble liée à la vitesse de croissance tumorale et les gliomes lentement évolutifs sont les plus épileptogènes, même si dans la sous-population des gliomes de bas grades, la vitesse de croissance ne semble pas influencer le risque et la fréquence des crises (J Pallud, Audureau, et al. 2014). Il ne semble pas exister de relation entre le degré d'effet de masse, le degré d'œdème et le risque épileptique (C. J. Vecht and Wilms 2010). Parmi les facteurs liés à la tumeur, il existe un lien fort entre le grade histopathologique de malignité et le risque épileptique (C. J. Vecht and Wilms 2010) : 60 à 100% dans les gliomes de grade II, 50 à 70% dans les gliomes de grade III et 25 à 50% dans les gliomes de grade IV. A titre d'exemple, une étude de cohorte a démontré une relation inverse entre le grade histopathologique des gliomes et la fréquence de l'épilepsie avec une incidence de 100%, 60%, 50% et 25% dans les oligodendrogliomes de grade II, les astrocytomes de grade II, les gliomes de grade III et les glioblastomes, respectivement (Lynam et al. 2007). Au-delà du grade histopathologique, il existe un lien entre le sous-type histopathologique et le risque épileptique : les oligodendrogliomes semblent plus épileptogènes que les astrocytomes (Chang, Potts, et al. 2008) et, au sein des glioblastomes, l'épilepsie est plus fréquente dans les glioblastomes secondaires que dans les glioblastomes *de novo*, sans lien connu avec le statut Isocitrate Déshydrogénase (IDH) (Englot, Berger, Chang, et al. 2012).
Les marqueurs moléculaires ont aussi été étudiés. Une étude récente portant sur plus de 500 gliomes infiltrants de bas grade de malignité a montré une absence de lien entre le risque épileptique et l'expression de nombreux facteurs moléculaires (p53, PTEN (phosphatase and tensin homolog), Ki67, proliferating cell nuclear antigen, matrix métalloprotéinase 9, EGFR, VEGF, P170, MGMT, glutathione s-transférase) (You et al. 2012). Cependant, un lien semble exister entre le coefficient de prolifération et le risque de non-contrôle des crises après traitement dans les gliomes infiltrants de bas grade, le risque épileptique étant accru dans les tumeurs ayant un coefficient de prolifération élevé (Ki67 supérieur à 10%). Le statut IDH reste le critère moléculaire d'augmentation du risque d'épileptogénicité (Chen et al. 2017).

Caractéristiques cliniques et diagnostic des crises épileptiques associées aux tumeurs cérébrales
La définition de la ligue internationale contre l'épilepsie (ILAE) définit la maladie épileptique à partir d'une seule crise épileptique en cas de présence d'un facteur prédisposant à de futures crises, comme la présence d'une tumeur cérébrale (Fisher et al. 2014). La survenue d'une crise d'épilepsie focale ou secondairement généralisée chez l'adulte est souvent le symptôme révélateur d'un gliome infiltrant, dans plus de 80% des gliomes de bas grade, dans près de 40% des gliomes anaplasiques et dans près de 20% des glioblastomes (G Huberfeld and Pallud 2015; G Huberfeld and Vecht 2016; J Pallud, Audureau, et al. 2014; C. Vecht et al. 2017). L'épilepsie peut être l'unique manifestation clinique ou, à l'inverse, être associée à un tableau d'hypertension intracrânienne et/ou à une symptomatologie neurologique focalisée. La survenue de crises d'épilepsie peut précéder de plusieurs années, dans le cadre des gliomes infiltrants de bas grade, l'apparition d'autres symptômes.
Les explorations EEG n'occupent dans cette indication plus une place prépondérante au moment du diagnostic. Les manifestations intercritiques liées à un gliome infiltrant ne se manifestent que peu en EEG de surface (G Huberfeld and Pallud 2015). L'EEG identifie 'historiquement' des anomalies évocatrices d'un processus lésionnel dans plus de 70% des cas, des anomalies pathologiques non spécifiques d'un processus lésionnel dans plus de 10 % des cas, des anomalies non significatives dans près de 13% des cas et un EEG normal dans moins de 5% des cas. Les gliomes étant découverts aujourd'hui à un stade plus précoce, leur volume ou leur influence étant volontiers moindre, la proportion d'EEG normaux serait plus élevée de nos jours. De plus, les activités mises en évidences sont imparfaitement localisatrices du gliome et non spécifiques du type tumoral, les anomalies électriques pouvant varier en fréquence et en intensité en fonction de la topographie lésionnelle, de la profondeur, de la taille, de la malignité et de l'hyperpression locale

associée. Les anomalies EEG se modifient dans le temps, en parallèle de la progression tumorale : des anomalies électriques initiales sont recueillies dans 50% des cas et dans 90% au moment du traitement chirurgical.

Effets de la chirurgie des gliomes sur l'épilepsie tumorale.

L'exérèse chirurgicale permet d'améliorer le contrôle épileptique en postopératoire, quels que soient le sous-type et le grade histopathologiques et quel que soit la localisation tumorale, avec 69 à 100% des patients libres de crises en postopératoire (Johan Pallud, Capelle, and Huberfeld 2013; J Pallud, Audureau, et al. 2014; Still et al. 2018; C. Vecht et al. 2017). L'effet antiépileptique de la résection chirurgicale dépend de plusieurs paramètres qui ont été largement étudiés pour les gliomes infiltrants de bas grade : l'étendue de la résection chirurgicale, le contrôle préopératoire des crises épileptiques et une durée d'évolution des crises inférieures à un an sont des facteurs indépendants prédictifs du bon contrôle postopératoire des crises (Englot et al. 2011). L'effet antiépileptique de la chirurgie est directement lié à l'étendue de l'exérèse chirurgicale et le caractère complet de l'exérèse est un facteur prédictif du contrôle épileptique postopératoire (Chang, Potts, et al. 2008). A titre d'exemple, 65 à 77% des patients sont libres de crise après une chirurgie de résection lésionnelle et 82 à 92% des patients le sont après une chirurgie de résection étendue au-delà des limites lésionnelles. Dans le cadre des tumeurs gliales de bas grade de localisation temporale, 79% de patients sont libres de crises après une résection complète contre 43% après une résection incomplète (Englot, Han, et al. 2012; Ruda et al. 2012). Un meilleur contrôle des crises d'épilepsie est donc obtenu si le traitement chirurgical est précoce. Il n'a pas été mis en évidence d'effet de l'âge, des caractéristiques tumorales à l'imagerie, du sous-type histologique, de l'administration de chimiothérapie ou de radiothérapie sur le contrôle épileptique post-opératoire (G Huberfeld and Pallud 2015). Il peut également être utile de réopérer les patients porteurs d'un gliome infiltrant de bas grade pour améliorer leur contrôle épileptique (Martino et al. 2009).

1.3.2. Apports de l'ElectroCorticoGraphie peropératoire dans la chirurgie des gliomes.

La chirurgie est le traitement principal des gliomes, notamment de bas grade. Mais elle ne se limite pas à l'exérèse de la tumeur comme identifiée macroscopiquement par imagerie ou en peropératoire. La chirurgie des gliomes doit prendre en compte deux particularités dans le double but d'améliorer la survie et la qualité de la survie des patients :

i- Des cellules tumorales essaiment dans le tissu cérébral à distance des limites macroscopiques

ii- Les régions péritumorales produisent les activités épileptiques

La zone péritumorale est une région clé où les processus de croissance tumorale et d'épileptogénicité sont tous deux en jeu.

Les gliomes tant de bas que de haut grade ne sont pas des tumeurs limitées. Les cellules tumorales infiltrent les tissus environnants, notamment corticaux et migrent le long de faisceaux de fibre blanche et en suivant les vaisseaux sanguins. Des cellules tumorales en migration ont été retrouvées à plusieurs centimètres des limites en imagerie par résonance magnétique (IRM) dans une étude de biopsies stéréotaxiques systématiques (J Pallud et al. 2010). L'attitude chirurgicale actuelle vise donc à réaliser une exérèse la plus large possible emportant le plus possible de contingent tumoral macroscopique mais aussi péritumoral, infiltrée de manière invisible macroscopiquement, donnant lieu au concept de chirurgie supra-totale. Une telle stratégie chirurgicale implique de tester la fonctionnalité des zones entourant les gliomes, en utilisant des stimulations cérébrales électriques directes aux niveaux cortical et sous-cortical, effectuées chez des patients éveillés (Duffau 2016; J. Pallud and Dezamis 2017). En effet, la croissance tumorale induit une plasticité remaniant les fonctions portées par les régions corticales. L'anatomie fonctionnelle n'est donc plus respectée et doit être évaluée pour chaque patient. Les limites chirurgicales de la chirurgie supra-totale ne sont dès lors plus des limites anatomiques mais des limites fonctionnelles. Elles imposent ainsi de réaliser une cartographie fonctionnelle péritumorale. Cette cartographie fonctionnelle est une autre caractéristique des chirurgies de gliome. Afin d'être menée, le patient, après ouverture cutanée, osseuse et de la dure-mère sous anesthésie générale est éveillé, une anesthésie locale permettant de contrôler la douleur osseuse et méningée. Des stimulations électriques directes, corticales et sous-corticales, dont l'effet est inhibiteur (sauf en regard du cortex moteur primaires ou elles sont activatrices) sont alors menées et leur interférence

avec les diverses fonctions cognitives, motrices et sensorielles permettent de dresser une cartographie fonctionnelle péritumorale et de fixer les limites de résection (Duffau 2016; J. Pallud and Dezamis 2017). **Dans le cadre de cette cartographie fonctionnelle menée chez les patients éveillés, l'enregistrement ECoG permet de détecter des décharges épileptiques induites par les stimulations électriques directes**. Cette pratique permet d'une part d'enregistrer des crises épileptiques précocement, permettant ainsi un traitement antiépileptique focal (infusion corticale de sérum physiologique glacé) immédiat empêchant la crise de se généraliser et évitant d'administrer un médicament antiépileptique. Une telle généralisation fait courir un danger du fait de l'agitation motrice et du risque de hernie cérébrale. L'enregistrement ECoG permet aussi d'enregistrer et de localiser une post-décharge faisant suite à la stimulation électrique. Celle-ci induit des perturbations prolongées du fonctionnement cortical qui perturbe l'interprétation de l'effet des stimulations électrique. Elles doivent donc être prise en compte dans la cartographie fonctionnelle. Enfin, l'existence de post-décharges peut conduire à moduler l'intensité de stimulation électrique**. Ainsi, dans une perspective purement clinique neurochirurgicale, la réalisation d'un enregistrement ECoG lors de la cartographie fonctionnelle réalisée par stimulation électrique directe chez les patients opérés d'un gliome en condition éveillée améliore la qualité et la sécurité de la procédure.** Elle est devenue routinière dans nos deux centres.

L'utilisation des enregistrements ECoG permet également la localisation des ZE péritumorales et leur prise en compte dans la résection. Il a été démontré que les activités épileptiques sont produites par des zones péritumorales corticales. En 1882, Hughkings-Jackson avait déjà formulé que "l'épileptogénicité de la tumeur est liée à l'implication de la matière grise corticale" (Hughlings-Jackson 1882). Les enregistrements ECoG peropératoires ont montré plus tard que les activités intericales proviennent de zones corticales éloignées (Hirsch et al. 1966; Tran et al. 1997). Les enregistrements ECoG réalisés avant l'intervention chirurgicale ont permis de cartographier les zones d'initiation des crises dans les aires corticales situées à plus de 1,5 cm de la bordure tumorale chez la plupart des patients (Mittal et al. 2016). Notre groupe a également montré que les tissus corticaux obtenus par chirurgie de gliomes de bas et haut grade conservent des propriétés épileptogènes, produisant des décharges intericales spontanées *ex vivo* (Pallud *et al.*, 2014). Nos travaux *ex vivo* ont permis d'évaluer les réseaux neuronaux générant des activités épileptiques (cf supra). Dans les tissus post-chirurgicaux, les zones corticales produisant des décharges épileptiques se caractérisent aussi par leur capacité à générer des oscillations à haute fréquence (HFO) à la fois dans la bande physiologique des ripples (80-250 Hz) que la bande des FR (250-500 Hz) (Pallud *et al.*, 2014), ces dernières étant réputées être un bon biomarqueur de la ZE. Enfin, il a été démontré que les zones corticales produisant des activités épileptiques et des HFO étaient infiltrées par des cellules de gliome migrant depuis le noyau de la tumeur mais non visibles au niveau macroscopique et situées en dehors des limites IRM du gliome (Figure 1). Cette découverte est d'un grand intérêt puisqu'elle pourrait permettre de détecter *in vivo* l'infiltration tumorale si les électrodes utilisées possédaient une meilleure résolution spatiale. Les données électrophysiologiques indiquent également que le cortex péritumoral est le générateur d'activités épileptiques, l'effet antiépileptique de la chirurgie dépendant du volume réséqué (Still et al. 2018). Les enregistrements ECoG permettent de mieux caractériser le cortex péritumoral, à l'interface d'une tumeur en croissance et du cerveau hôte, zone cruciale à la fois pour la genèse des activités épileptiques et les processus de croissance du gliome.

La localisation des activités épileptiques est d'abord nécessaire pour guérir l'épilepsie par la chirurgie. La chirurgie des gliomes est une unique occasion d'étudier les activités électriques corticales, puisque, dans la plupart des centres, elle est pratiquée en condition éveillée pour cartographier les zones fonctionnelles entourant la tumeur. Les activités corticales peuvent donc être enregistrées sans modification par l'anesthésie, qui affecte généralement les rythmes normaux, les anomalies épileptiques et les HFO. Les enregistrements ECoG effectués pendant l'opération, qui permettent une étude corticale directe sans invasivité supplémentaire, contribuent à mieux délimiter les zones épileptiques et devraient améliorer le contrôle de l'épilepsie. Différents types d'activités épileptiques intercritiques ont été décrites comme biomarqueurs de l'épilepsie, utilisés à la fois pour diagnostiquer l'épilepsie et pour localiser les zones susceptibles de générer des crises. Des pointes intermittentes peuvent être enregistrées dans de vastes zones et il a été

démontré que la « chasse aux pointes » n'améliore pas le pronostic chirurgical de l'épilepsie (Asano et al. 2009; Fernández Coello et al. 2013; San-Juan et al. 2011; Wray et al. 2012).

Dans le contexte de la chirurgie des gliomes, il a toutefois été récemment démontré que l'ECoG réalisé pendant la chirurgie des tumeurs permettait une augmentation significative de l'absence de crises postopératoires, de 38,89 % (patients sans ECoG) à 74,07 % YAO 2017. D'autres études ont par ailleurs montré que la localisation peropératoire des pointes par ECoG n'améliorait pas le pronostic épileptologique tumoral post-opératoire (C. Lee, Jeong, and Chung 2019).

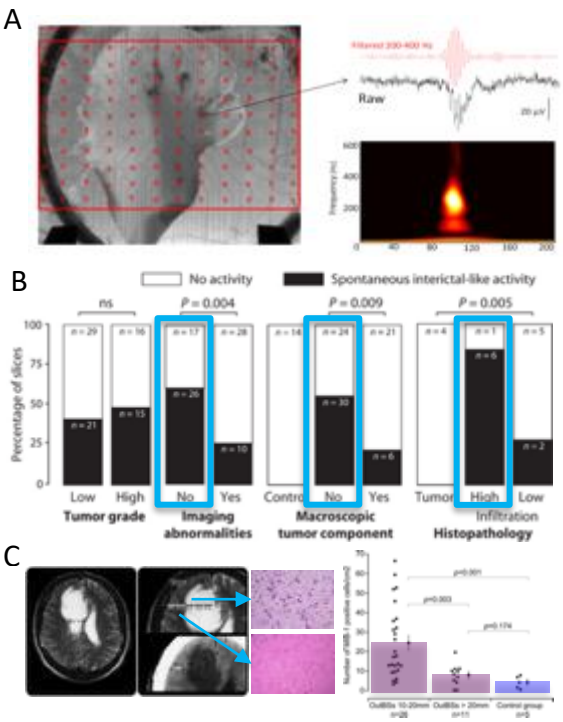

Figure 1: Peritumoral Colocalization of epileptic activities and tumor infiltration ex vivo. A) HFOs identified during epileptiform discharges from a human cortical slice containing both the solid tumor component and adjacent infiltrated neocortex. Multi-electrode arrays (MEAs). **B)** Interictal activity is associated with infiltration by glioma cells outside imaging abnormalities and macroscopic tumor component from PALLUD. **C)** Tumor cells are detected by biopsies outside imaging abnormalities from Pallud 2010.

Un autre biomarqueur électrique a été évalué plus récemment : les HFO. Les HFO (>80 Hz) sont enregistrés physiologiquement dans le cerveau des humains et des rongeurs, mais, parmi eux, les FR (>250 Hz) semblent cartographier la ZE, indépendamment de l'histologie ou de la zone corticale sous-jacente (Crépon et al. 2010; Julia Jacobs et al. 2009; Zijlmans et al. 2012). La valeur des FR a été récemment remise en question depuis qu'il a été signalé qu'elles étaient enregistrées (dans une mesure limitée et interprétées avec prudence chez les patients étudiés par voie intracrânienne pour une épilepsie) par des zones présumées non épileptiques (Frauscher et al. 2018), alors qu'un groupe a constaté que leur valeur dans la localisation de la ZE était similaire à celle des pointes intericales (Roehri et al. 2018). Cependant, la plupart des études s'accordent sur la spécificité épileptique spatiale des FR et sur la corrélation entre leur élimination et la probabilité de ne plus avoir de crises après la chirurgie (Guragain et al. 2018; Julia Jacobs et al. 2018; Liu et al. 2018). Les enregistrements ECoG permettent d'identifier les HFOs (Yang, Hakimian, and Schwartz 2014), permettant d'améliorer le résultat épileptologique lorsque les zones corticales produisant les HFO sont réséquées (Julia Jacobs et al. 2018; van Klink et al. 2014; van 't Klooster, van Klink, et al. 2015; Wu et al. 2010). L'ECoG est même probablement plus efficace pour détecter les FR en comparaison aux enregistrements SEEG, probablement parce que la procédure d'enregistrement peropératoire permet une cartographie continue pendant l'opération et la vérification qu'aucune FR ne subsiste après l'ablation. Cependant, la détection des HFO est difficile et chronophage (Zijlmans et al. 2017) et n'est actuellement effectuée que *post hoc*, c'est-à-dire après l'opération en cas d'ECoG peropératoire. Des HFO ont récemment été enregistrés en ECoG peropératoire chez des patients éveillés présentant des gliomes (Feyissa et al. 2018), mais les auteurs ne signalent que des activités dans la bande de faible fréquence (en raison d'un échantillonnage limité à 500 Hz), sans spécificité épileptique. Nos données préliminaires montrent que des HFO jusqu'à 600 Hz peuvent être enregistrés lors de la chirurgie des gliomes en condition éveillée, ainsi que des pointes intercritiques (Figure 2).

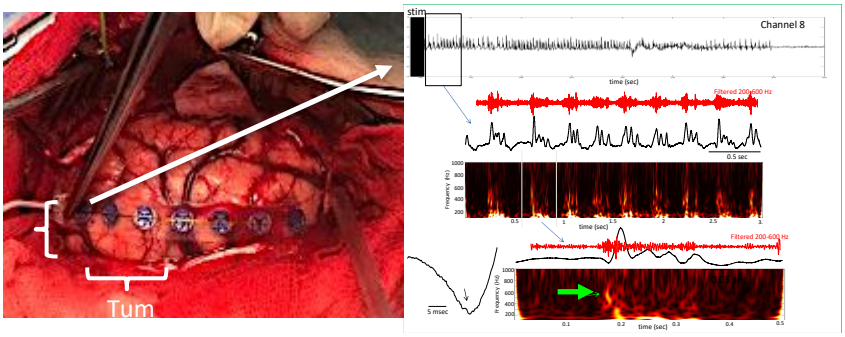

Figure 2: Intraoperative ElectroCorticoGraphical recording during a LGG surgery in awake condition with a macroelectrodes grid (0.1-10000 Hz). Right: high frequency oscillation induced by electrical stimulation reaching 600 Hz (fast ripple band).

1.3.3. Électrodes d'ElectroCorticoGraphie actuelles.

Les macroélectrodes utilisées actuellement possédant le marquage CE Classe III pour utilisation humaine sont des bandes (strips) ou des grilles (grids) de 4 à 64 électrodes, d'un diamètre de 0,2 à 1 cm, espacées de 0,4 à 1 cm. L'électrode est fabriquée en métal ou en Platinum / Iridium. L'épaisseur habituel varie entre 0.5-1 mm (Figure 3).

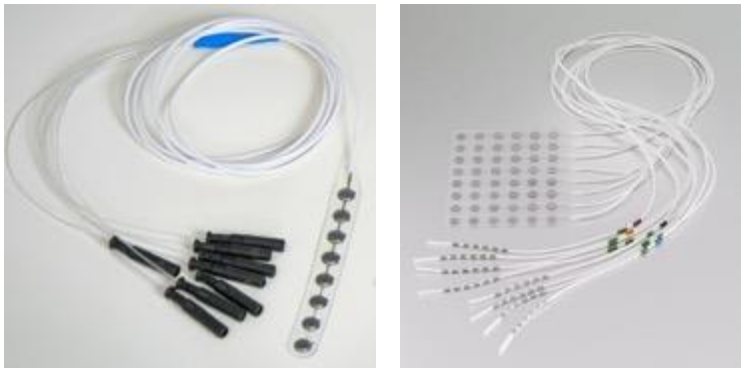

Figure 3 : bande de huit macrolectrodes et grille de 48 macroélectrodes. DIXI Medical and AdTech

Ces macroélectrodes souffrent de limitations d'usage. Du fait de leur épaisseur et de leur rigidité, leur capacité à s'adapter à la surface corticale est limitée. Ce contact imparfait réduit la surface d'enregistrement et augmente l'impédance des électrodes, réduisant leur capacité à enregistrer des signaux de faible amplitude (comme les FR). Les macroélectrodes étant rigides, elles ne suivent pas bien les mouvements corticaux, notamment la pulsatilité lors des chirurgies en condition éveillée, conduisant à un frottement potentiellement lésionnel pour le cortex. Leur encombrement gène régulièrement le neurochirurgien qui doit les déplacer. Des électrodes fabriquées avec des matériaux plus flexibles permettant une adhésion au cortex, amélioreront ainsi la qualité et la simplicité d'utilisation. Une meilleure flexibilité pourrait également permettre d'enregistrer des zones moins accessibles, comme l'intérieur des sillons cérébraux.

Par ailleurs, les macroélectrodes utilisées actuellement pour la réalisation des ECoG ont un diamètre compris entre 3 et 10 mm, et un espace inter-électrode de 10 mm. Elles ont donc une résolution spatiale limitée, ne leur permettant pas d'enregistrer un phénomène très focal. Cependant, les FR sont généralement très focales et seules les oscillations synchronisant un large volume semblent actuellement enregistrables par ces macroélectrodes. Leur taille répond par ailleurs mal à l'anatomie fonctionnelle corticale, le cortex cérébral s'organisant en colonnes fonctionnelles de 400 µm (Rockland 2010). Ainsi, la dynamique de l'organisation corticale ne peut être enregistré qu'avec des microélectrodes d'un diamètre inférieur à 40 µm (Lambrecq et al. 2017; Zijlmans et al. 2017; Le Van Quyen et al. 2016).

1.3.4. Apports potentiels de la microElectroCorticoGraphie.

Enregistrements intracérébraux par microélectrodes.

Depuis quelques années, des enregistrements par microélectrodes sont pratiqués dans un but de recherche lors d'explorations intracérébrales dans le contexte des évaluations préchirurgicales des épilepsies. En complément aux macroélectrodes d'exploration traditionnelle, des microélectrodes sont insérées dans le cerveau, ou des grilles de microélectrodes corticales pénétrantes (Utah Arrays) et permettent d'enregistrer l'activité cérébrale avec un niveau de résolution très fin. Plus précisément, deux niveaux de résolution y sont mesurable : (1) au niveau des potentiels d'actions émis par des cellules isolées (ou par un petit groupe, activité neuronale unitaire/multi-unitaire) ; (2)

au niveau des potentiels de champ locaux (Local Field Potential: LFP) qui correspondent au signal électrique résultant de la synchronisation d'une population de cellules de l'ordre du millimètre. Alors que les potentiels d'actions reflètent le traitement local des cellules, les potentiels de champ locaux reflètent principalement l'activité synaptique localisée au niveau des dendrites, ce qui correspond plus généralement aux signaux que les cellules reçoivent.

Chez l'homme, dans le contexte de la recherche en épilepsie, l'utilisation des microélectrodes a permis d'enregistrer simultanément des activités neuronales unitaires, des activités neuronales multi unitaires et des potentiels de champ locaux très localisés spatialement (Schevon et al. 2008; Schevon et al. 2010; Merricks et al. 2015; Truccolo et al. 2011; 2014; Wagner et al. 2015). Ces enregistrements ont révélé chez l'homme des dynamiques beaucoup plus complexes que celles connues dans les modèles animaux, correspondant essentiellement à une simple hypersynchronisation neuronale pendant les crises épileptiques. Une première étude a ainsi rapporté que seul un faible pourcentage de neurones augmentait son taux de décharge pendant les crises, et ce sans présenter de synchronisation (Truccolo et al. 2011). Une autre étude a, d'une part, reproduit ces résultats et, d'autre part, a réussi à enregistrer des décharges synchrones et en phase avec les oscillations critiques (Schevon et al. 2012). Ces décharges ont été observées uniquement dans de petits microdomaines d'une échelle inférieure au millimètre. En revanche, autour de ces microdomaines épileptiques, aucune hypersynchronisation n'a pu être mesurée. L'interprétation qui en a été donnée, également basée sur des observations également réalisées chez l'homme (Schevon et al. 2012), est que la ZE est entourée par une zone de "pénombre" où il existe une forte activité inhibitrice qui bloque la propagation de la crise. Dans cette zone, il est possible d'enregistrer à la fois, un potentiel de champs caractéristique des crises qui résulte de l'activité postsynaptique des neurones, et un faible taux de décharge de neurones dû à une activité inhibitrice qui empêche les trains de potentiels d'action. Cette interprétation est cohérente avec d'autres études avec microélectrodes suggérant que l'activité de petits groupes de neurones varie plusieurs minutes avant l'apparition d'une crise (Stead et al. 2010; Lambrecq et al. 2017). L'ensemble des observations suggèrent ainsi que de petits sous-ensembles de neurones sont suffisants pour initier un départ de crise et que les synchronisations sous-jacentes s'opèrent à une échelle inférieure au millimètre.

L'utilisation des microélectrodes a également permis d'étudier chez les patients épileptiques les activités pathologiques en dehors des crises, tout particulièrement lors de pointes intercritiques (Keller et al. 2010). Les pointes sont des évènements épileptiques qui se manifestent entre les crises, de façon plus ou moins prononcée selon les patients. Ces grilles de microélectrodes ont ainsi permis de mettre en évidence la grande diversité d'activités neuronales autour de ces évènements (à la fois des augmentations et des diminutions du taux de décharges à différents moments de la pointe intercritique). Une telle variété d'activités neuronale conforte l'hypothèse que les évènements épileptiques proviennent d'un réseau ayant des interactions complexes et met en avant l'importance de l'activité inhibitrice dans des évènements paroxystiques en apparence excitateurs (Alvarado-Rojas et al. 2013). Également, les enregistrements par microélectrodes ont récemment identifié chez l'homme des oscillations dans les hautes fréquences (HFO) >200 Hz en dehors des crises (Schevon et al. 2009). Ces oscillations, apparaissant en période intercritique, sont définies comme étant des évènements spontanés très brefs, composés de seulement quelques cycles distincts de l'activité de fond (Zijlmans et al. 2017). Tout particulièrement, les HFO comprises entre 200 et 600 Hz, appelées FR sont considérées pathologiques et sont supposées refléter l'hypersynchronisation des potentiels d'actions (Bragin et al. 2002). Ces oscillations sont retrouvées chez l'Homme et chez l'animal dans les structures cérébrales associées à l'épilepsie (J. Jacobs et al. 2012). Elles permettent l'identification des régions cérébrales capable de générer des crises spontanées et sont supposés refléter le substrat de l'épileptogenèse et de l'épileptogénicité (Le Van Quyen, Khalilov, and Ben-Ari 2006).

Néanmoins, l'implantation de grille de microélectrode Utah Array est une procédure délicate qui peut endommager les neurones alentours ainsi qu'impacter la vascularisation (Fernández et al. 2014). Les microélectrodes sont généralement composées de métaux et la différence de rigidité avec le cerveau crée des microlésions entrainant de la mort neuronale et la formation d'encapsulations gliales. Dans le cas de matrices, les microhémorragies ont été estimée comme fréquentes du fait de la densité des microélectrodes. Les microlésions sont très probablement la résultante de la rencontre d'un grand nombre de vaisseaux sanguins lors de l'insertion dans le

cortex. Des microhémorragies n'ont pas forcément de conséquence clinique mais elles peuvent s'étendre au-delà de l'extrémité des électrodes (Fernández et al. 2014).

Apports de la microElectroCorticoGraphie (µECoG).

L'utilisation de la µECoG vise à réduire l'invasivité et les risques encourus par le patient lors d'enregistrements corticaux, tout en apportant un niveau et une qualité d'enregistrements optimaux. Ceci implique donc l'utilisation de matériaux qui présentent une bonne fiabilité électrique tout en évitant d'endommager les tissus et n'induisant que de faibles réactions immunitaires post-implantation. Dans les dernières années, une solution à ce problème a été proposé et consiste à diminuer le plus possible le diamètre des microélectrodes pour augmenter la biocompatibilité, mais cela entraine aussi une augmentation de l'impédance. Dans ce cas, il est possible d'ajouter sur l'extrémité de l'électrode des polymères organiques conducteurs, tels que le poly(3,4-ethylenedioxythiophene (PEDOT), permettant d'améliorer les enregistrements au cours du temps en diminuant l'impédance (Ludwig et al. 2011; V. Castagnola et al. 2015; E. Castagnola et al. 2015). Dans ce cadre, plusieurs études ont montré la validité et l'innocuité *de matrices d'électrodes à base du PEDOT. Des techniques de micro fabrication ont aussi permis d'intégrer, sur un substrat de parylène (un polymère) de 4 µm d'épaisseur, une matrice d'électrodes de 10 × 10 µm². Ces matrices d'électrodes (aussi appelées par un autre « NeuroGrid ») s'adaptent parfaitement à la surface du cerveau et leur utilisation a été déjà validé* en électrophysiologie peropératoire au États-Unis (Khodagholy et al. 2015). *Chez l'animal, placées sur le cortex du rat, ces électrodes furent capables d'enregistrer des potentiels de champs locaux ainsi que l'activité unitaire de neurones. Cette dernière est révélatrice de plusieurs spécificités cellulaires, suggérant que l'enregistrement correspond à l'activité de cellules pyramidales et d'interneurones des niveaux inférieurs du cortex. Ces résultats impliquent donc que les électrodes peuvent enregistrer l'activité de neurones distants d'au moins 200 µm de la surface du cortex. La possibilité d'enregistrer de l'activité unitaire et des potentiels de champs locaux à la surface corticale est unique et devrait permettre l'obtention de données indispensables à une meilleure compréhension des mécanismes neuronaux* s'opérant à une échelle inférieure au millimètre.

C'est tout particulièrement dans le domaine de la neuro-oncologie où la µECoG est susceptible d'apporter in vivo le plus d'informations concernant les processus pathophysiologiques. Dans ce contexte, à partir de l'ECoG traditionnelle, la présence d'un silence électrique au centre de la lésion et la possible présence d'anomalies électriques dans leur périphérie a déjà été identifié dans les gliomes infiltrants (Munari et al. 1985; Hirsch et al. 1966). En particulier, dans le néocortex péritumoral, ces anomalies sont souvent constituées d'activités épileptiformes à type de pointes et activités d'ondes lentes rythmique sur la projection tumorale alors même que les circonvolutions cérébrales semblaient macroscopiquement intactes (Englot, Berger, Barbaro, et al. 2012; Tran et al. 1997), les crises elles-mêmes étant volontiers initiées à distance de la tumeur (Mittal et al. 2016). Également, comme on l'a vu plus haut, des HFO ont récemment été enregistrés en ECoG peropératoire dans le cortex péri-tumoral chez des patients présentant des gliomes (Feyissa et al. 2018). Néanmoins, les macro-électrodes n'identifient pas toujours toute la complexité de ces activités épileptiques et la meilleure résolution spatiale et temporelle offerte par l'utilisation de µECoG constitue une approche plus adaptée pour localiser précisément les oscillations pathologiques de petits groupes de neurones.

Au-delà du bénéfice en résolution spatiale, les µECoG doivent également permettre, par leur revêtement innovant en *PEDOT, d'améliorer considérablement le rapport signal / bruit. Les µ*ECoG PEDOT de type « Neurogrid » similaires à celles visant à être utilisées dans cette étude, ont déjà été testées chez l'homme (Khodagholy et al. 2015; 2016) au cours de chirurgies en condition éveillée. Les Neurogrids sont issues de la même technologie que celles produites par Panaxium, issue du même groupe de recherche (Figure 4). Sept patients ont été enregistrés par cette équipe. Ils souffraient d'épilepsie lésionnelle, dont au moins deux cas d'épilepsie tumorale, et les enregistrements étaient menés sous anesthésie générale. Le système d'enregistrement à haute fréquence d'échantillonnage n'avait pas de marquage CE. Les électrodes étaient stérilisées par une méthode gazeuse (97-100% ethylene oxide à 50 – 60 °C pendant 4 heures suivie de 12 heures de détoxification). Le signal enregistré était de qualité permettant d'enregistrer des ondes lentes

liées à l'anesthésie, des oscillations plus rapides et de l'activité multi unitaire. Un enregistrement a pu être mené chez un patient éveillé : en comparaison aux macro électrodes standards, les µECoG Neurogrids ont permis une nette augmentation de la richesse des activités enregistrées.

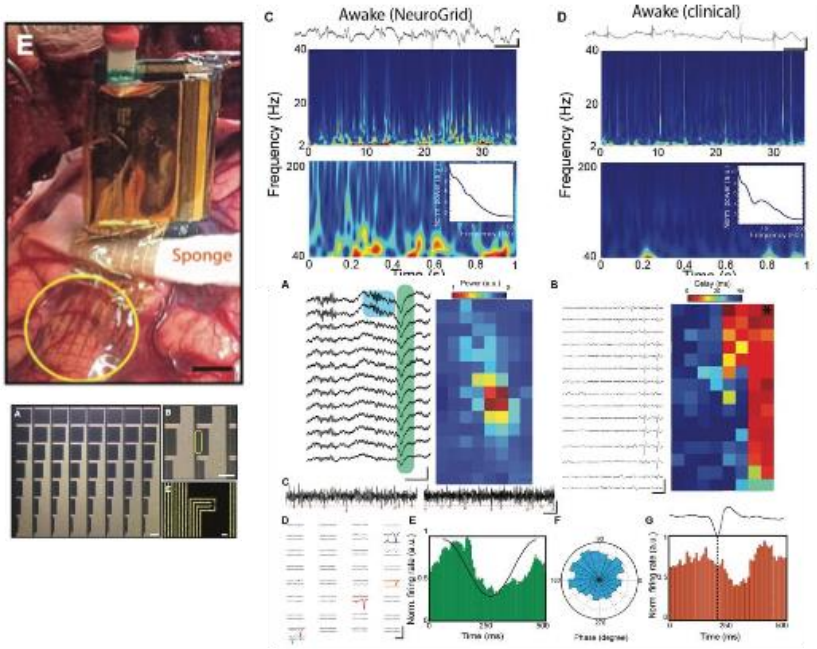

Figure 4 : Utilisation des □ECoG Neurogrids chez l'homme au cours d'une chirurgie corticale. Gauche : vision opératoire et structure de l'électrode. Droite : comparaison du signal obtenu (carte temps fréquence) entre une macro électrode (clinical) et d'une microECoG Neurogrids. Bas : activité multiunitaire enregistrée.

L'utilisation chronique chez l'animal a démontré qu'à trois mois, les signaux enregistrés étaient toujours de bonne qualité et qu'il n'y avait pas de lésion corticale en regard de l'électrode (Tybrandt et al. 2018).

Ainsi, la µECoG offre un moyen unique d'accéder à l'activité neuronale dans le cerveau humain. Elle devrait s'avérer utile pour avancer dans la compréhension des processus pathophysiologiques de façon générale mais peut également apporter des informations sur des processus fondamentaux. En autres, les enregistrements µECoG ont déjà contribués à diverses innovations technologiques telles que la découverte de mécanismes fondamentaux dans les processus cognitifs QUIROGA 2005 CHAN 2014; les oscillations physiologiques pendant le sommeil LE VAN QUYEN 2016 ; la restauration du contrôle cortical des membres supérieurs et le contrôle de prothèses robotisées HOCHERG 2006 COLLINGER 2013.

Les électrodes de µECoG développées ces dernières années permettent d'étudier les activités corticales à une échelle encore inédite. Cela est possible, en particulier grâce au grand nombre de voies qu'elles offrent et grâce à leur haute résolution spatiale. De plus, l'arrangement des microélectrodes est configurable, notamment en un arrangement en tétrode, permettant la mesure d'activité corticale localisée telle que les LFP haute fréquence.

Choix technologiques ayant présidé à au développement des microélectrodes Panaxium
Les technologies choisies pour le développement des microélectrodes Panaxium permettent d'optimiser à la fois la facilité d'utilisation, la résolution spatiale et la qualité du signal enregistré (Figure 5).

Les µECoG apportent également une souplesse et une ultra-flexibilité nécessaire pour un bon suivi de la conformité corticale.

Offer		Properties				
Company	Product	High channel count (>64)	High resolution (electrode ⌀ <0,5mm)	Ultra-conformability	Low impedance	Micro electrodes recording capacities
PMT CORPORATION		✓	✗	✗	✗	✗
DIXI medical		✗	✗	✗	✗	✗
AD-TECH		✓	✗	✗	✗	✗
NeuroOne		✓	✗	✓	✗	✗
neuroWISE		✓	✗	✓	✓	✗
CorTec Thinking ahead		✓	✓	✓	✓	✗
PANAXIUM		✓	✓	✓	✓	✓

Figure 5 : Comparatif électrodes Panaxium avec les ECoG existantes et résumé de leur apport en µECoG

Leur revêtement en PEDOT:PSS permet une conduction ionique (figure 6), optimisant la qualité du signal, élément clé pour l'enregistrement d'activités à haute fréquence et faible amplitude comme les HFO. La présence de PEDOT:PSS sur ces µECoG et leur flexibilité garantissent la réduction de l'impédance des électrodes *in situ*.

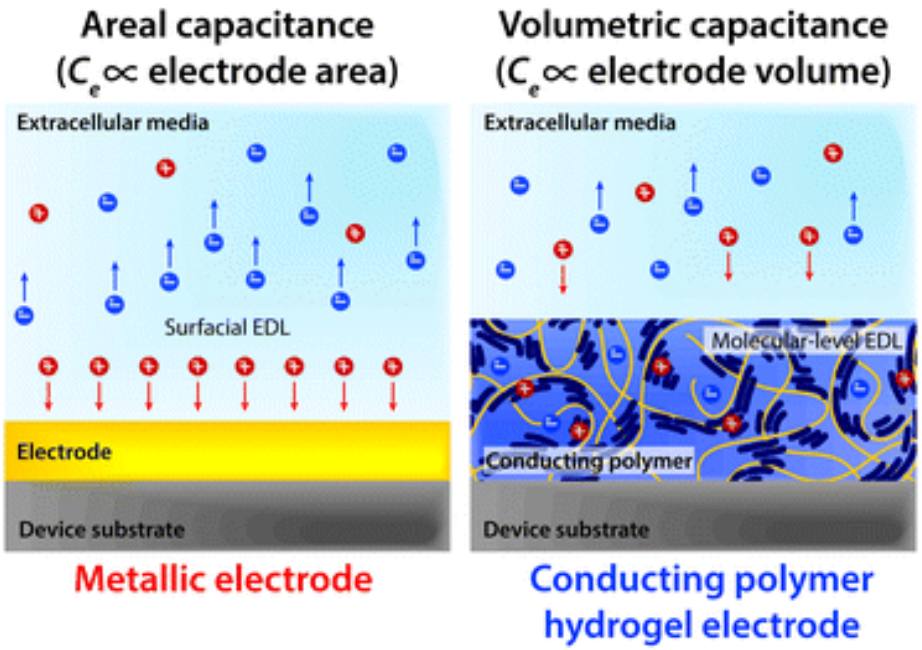

Figure 6 : Différence entre un conducteur métallique (à gauche) et un matériau conducteur organique (PEDOT:PSS à droite).

De plus, l'utilisation de câbles flexibles en polymères à cristaux liquides (LCP) permet de maintenir une bonne maniabilité pour le neurochirurgien à petite distance de la zone de contact (Figure 7). En effet, ce matériau est un polymère thermoplastique possédant une forte résistance thermique et mécanique, une stabilité et une inertie chimique ainsi qu'une isolation répondant à l'utilisation dans un environnement à forte contrainte, dont l'implantation. Grâces à ses caractéristiques thermoplastiques, il peut être thermoformé en différentes formes, même dans le cas d'un flexible à multicouches complexe encapsulant des fines pistes électriques, comme pour notre application. D'autre part, ce matériau a l'avantage d'avoir été considéré comme non cytotoxique selon la norme ISO 10993-5, et donc de réduire les risques liés à la biocompatibilité.

Figure 7 : exemple de LCP utilisé pour les électrodes Panaxium

Des électrodes utilisant du PEDOT:PSS comme matériau d'interface avec le cortex cérébral et un substrat de Parylène C ont été utilisés sur des rongeurs, et sur l'homme (Khodagholy et al. 2015; Lecomte et al. 2017) (Figure 8). Cependant, la fabrication de ces microélectrodes n'est pas identique à celle des µECoG de Panaxium, même si elles présentent les mêmes matériaux sur le dispositif fini. Ces essais ont montré l'avantage de l'ultra-conformabilité de ces électrodes sur le cortex en augmentant la stabilité et l'efficacité du contact électrique et mécanique avec le cortex. L'enregistrement de LFP et de potentiels d'action de neurones superficiels a ainsi été possible sur des rats et sur des patients humains (Khodagholy et al. 2015) et aussi sur des souris (Lecomte et al. 2017). Ainsi des tensions de l'ordre de 50µV, observables sur des temps très courts, ont pu être mesurées, avec une haute résolution spatiale.

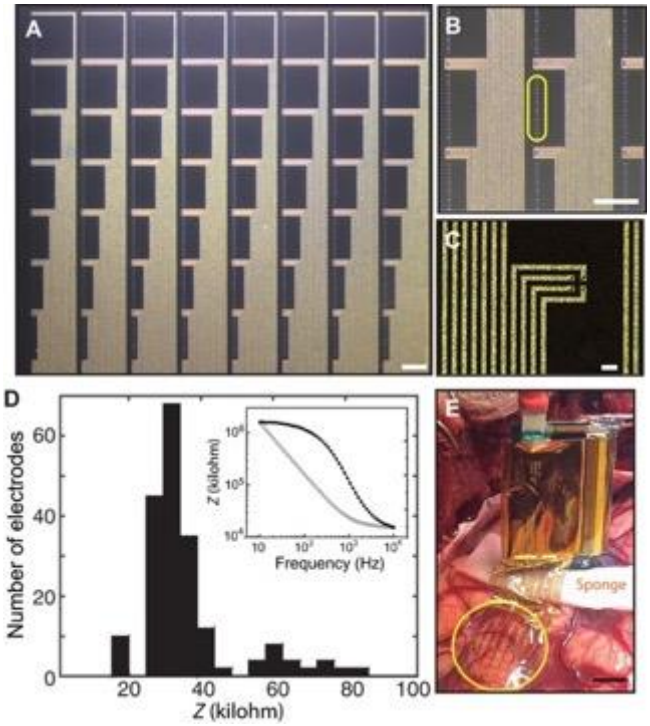

Figure 8. Neurogrids : une démonstration clinique de la sécurité et des performances des microélectrodes organiques
(A) Neurogrid : µECoG de 240 voies. échelle 1 mm (B)&(C) microscopie des électrodes arrangées en tétrodes (2X2 tétrodes de 10-µm^2) (D) Mesure des impédances (E) Photographie réalisée lors de l'usage clinique intra-opératoire du NeuroGrid

Les matrices de microélectrodes Panaxium sont très fines (4µm-12µm), ce qui permet un bon contact électrique et mécanique avec la surface cérébrale. De plus, les propriétés mécaniques de ces électrodes leur permettent de rester fixes pendant les enregistrements et minimisent les artefacts et *in fine* permettent d'améliorer la qualité du signal. L'utilisation d'un revêtement organique en PEDOT:PSS permet de réduire les valeurs d'impédance par rapport aux électrodes métalliques traditionnelles (Mantione et al. 2017). L'impédance typique d'une électrode métallique avec un diamètre de 400µm à 1 KHz est de 20kΩ (Ferlauto et al. 2018), tandis que l'impédance des microélectrodes Panaxium est de 1kΩ à 1 kHz pour un diamètre de microélectrode 300µm. Le tableau 1 résume les valeurs d'impédances obtenues dans les conditions expérimentales précédemment présentées en fonction du diamètre des µECoG de Panaxium pour une épaisseur de PEDOT:PSS de 100nm. Ainsi, à diamètre équivalent, les µEcoG Panaxium présentent des impédances inférieures aux électrodes métalliques.

Diamètre µEcoG	**3 mm**	**1 mm**	**300 µm**	**100µm**	**30µm**
Impédance à 1kHz	150 Ω	300 Ω	1 kΩ	4 kΩ	80 kΩ

Tableau 1 Correspondance entre diamètre électrode Panaxium et impédance (pour épaisseur de PEDOT:PSS de 100nm)

La diminution de l'impédance et l'augmentation du SNR sont deux facteurs améliorant la qualité du signal enregistré. D'après les résultats obtenus in vitro, nous pouvons donc améliorer le premier facteur avec les électrodes Panaxium et le deuxième sera évalué lors de l'étude sur la base de signaux spécifiques. L'objectif est de pouvoir étudier une large gamme d'activité, du potentiel de champ (LFP), aux oscillations de basse et haute fréquences (incluant les FR), jusqu'aux potentiels d'action (activité multi unitaire MUA).

Retombés cliniques :

Les résections des tumeurs cérébrales ont besoin d'un effort multidisciplinaire des neurochirurgiens, neuroradiologues, neuropsychologues, orthophoniste et neurophysiologistes, qui ensemble contribuent à la détermination de la localisation, de l'étendue et de l'implication fonctionnelle de la lésion sur l'individu.

Par conséquent, la neurochirurgie est réalisée en considérant les limites fonctionnelles et anatomiques pour atteindre une résection maximale et une préservation fonctionnelle maximale. L'identification des aires cérébrales fonctionnelles s'effectue par détermination des effets de stimulations cérébrales directes sur les fonctions cognitives, motrices, sensitives testées. L'électrophysiologie contribue à mieux localiser les activités épileptiques et à mieux identifier les effets indésirables des stimulations électriques. Nous souhaitons optimiser ces éléments en identifiant des biomarqueurs électrophysiologiques optimaux, c'est à dire sensibles et de bonne résolution spatiale, d'épileptogénicité, d'infiltration tumorale et de fonctionnalité des cortex enregistrés. L'objectif est d'améliorer la qualité de l'intervention chirurgicale, la rendant plus complète, plus sure et prenant mieux en compte les régions épileptiques, permettant *in fine* d'améliorer le pronostic fonctionnel et la survie des patients. Ces objectifs nécessitent l'utilisation d'électrodes recueillant le signal cérébral avec une meilleure résolution spatiale (précision) et temporelle (activités rapides), ainsi qu'un meilleur ratio signal / bruit (activité de faible amplitude).

La même problématique se pose pour la chirurgie de l'épilepsie. Les enregistrements corticaux peropératoires permettront d'établir une cartographie fonctionnelle des FR, nouveau biomarqueur d'épileptogénicité.

Les grilles de microélectrodes Panaxium ont été désignées pour apporter le même bénéfice que les grilles déjà commercialisés mais avec une meilleure conformabilité à la surface cérébrale, ce qui augmenterait significativement la qualité des signaux enregistrés. Particulièrement, le contact électrode/cortex amélioré aura potentiellement un impact majeur sur le SNR. Les propriétés mécaniques des électrodes pourraient aussi permettre d'accéder à des signaux inaccessibles avec des électrodes commerciales en favorisant le contact direct au niveau des sillons du cortex. Par ailleurs, la faible épaisseur des microélectrodes Panaxium permet de limiter leur invasivité et pourrait ainsi diminuer la fréquence des effets indésirables peropératoires.

1.3.5. Description des µECoG Panaxium

Le dispositif développé par Panaxium se compose des deux éléments principaux suivants (Figure 9) :

- Une partie ultra-flexible (substrat transparent) sur laquelle une matrice d'électrodes a été définie et sera en contact avec le cerveau du patient ;
- Une partie flexible (blanche) permettant la manipulation et la connexion électrique des électrodes au système d'enregistrement.

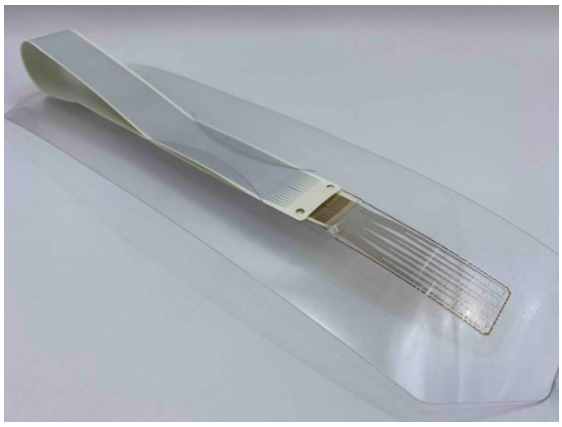

Figure 9 : Exemple de dispositif ECOG développé par Panaxium

Afin de garantir les performances et la sécurité au moment de l'utilisation pendant l'expérience clinique, les blocs suivants ont également été développés :

- Un support permettant de maintenir l'électrode durant le transport.
- Un emballage stérilisable et maintenant l'état stérile du dispositif.
- Un emballage de transport / stockage.

Dans le cadre de cette collaboration, un design spécifique de matrice d'électrodes a été prévu : il consiste en une matrice de 128 électrodes organisés en 28 électrodes de 500 µm et 96 microelectrodes de 30 µm de diamètre organisés en tétrodes (bloc de 4 électrodes) **Figure 10**.

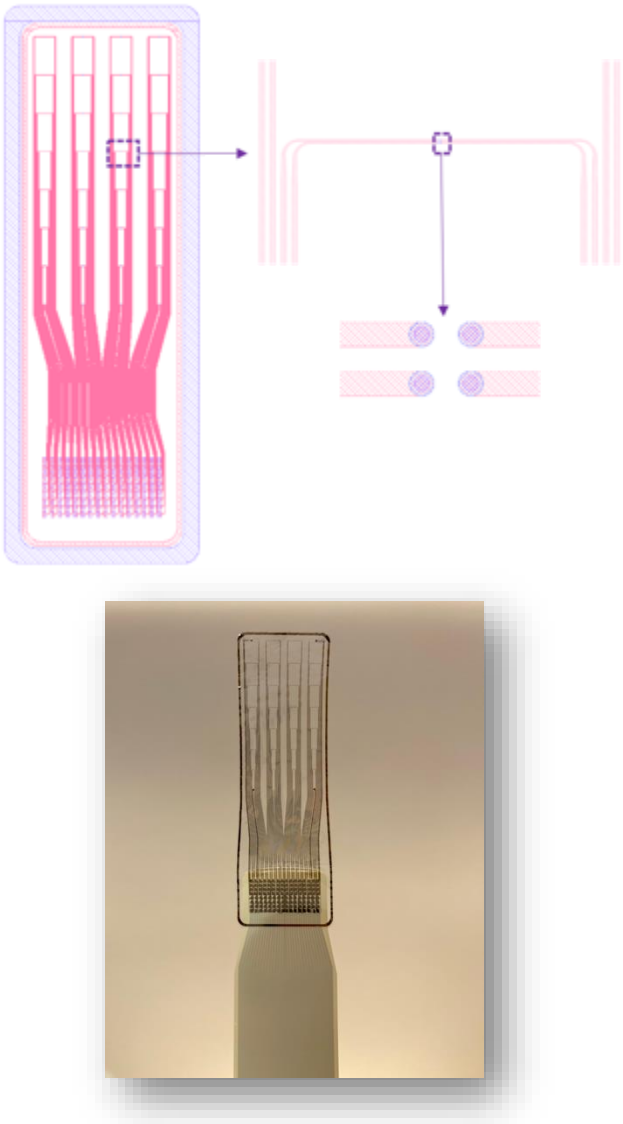

Figure 10 : Exemple de design ECoG Panaxium 128 voies, arrangement en 28 elecctrodes de 500 µm et 24 tétrodes. Zoom sur une tétrode (regroupement de 4 microélectrodes). Taille de la surface de contact : 4x2 cm.

Présentation du système global

Le système utilisé dans cette étude permet l'enregistrement de l'activité électrophysiologique cérébrale des patients pendant la chirurgie, par exemple pendant la résection tumorale ou la chirurgie de l'épilepsie. Ce système se compose de deux blocs majeurs (Figure 11) :
- Un dispositif non marqué CE développé par Panaxium qui consiste en une matrice d'électrodes flexibles, qui sera placée sur la surface du cortex du patient. Ce dispositif décrit ci-dessous concentre les attentions de ce dossier de conception du fait des risques associés à un dispositif utilisé sur le cerveau d'un patient.
- Un système d'acquisition de signaux électrophysiologiques marqué CE produit et distribué par l'entreprise NEURALYNX. Ce système électro-médical va permettre l'enregistrement de l'activité électrique corticale du patient pendant l'opération.

L'interface de connexion entre les deux blocs nécessite un développement spécifique convenu entre Neuralynx et Panaxium, et les tests de sécurité et de performances nécessaires seront réalisés durant la phase de développement afin de valider l'usage combiné des deux blocs.

Figure 11 : Schéma du système complet permettant l'usage clinique des électrodes ainsi que le post traitement des informations µECoG.

Des performances qualifiées

Les électrodes Panaxium ont été qualifiées afin d'assurer leur performance, leur sécurité et leur qualité.

Performances électriques

Les ECoG ont été testées dans des conditions représentatives de leur utilisation afin de qualifier leurs performances électriques via une analyse d'impédance sur les fréquences recherchées. Les tests sont réalisés dans une solution PBS (solution tampon phosphate salin représentant la concentration en sels du corps humain) (Figure 12).

Figure 12 : Banc de test électriques pour les microélectrodes Panaxium, à gauche : test sur support de fabrication, à droite : test après décollement de la matrice

Les tests sont réalisés sur le support de fabrication puis après leur séparation afin d'assurer la continuité des performances après l'étape de séparation du dispositif avec son support de fabrication (Figure 13).

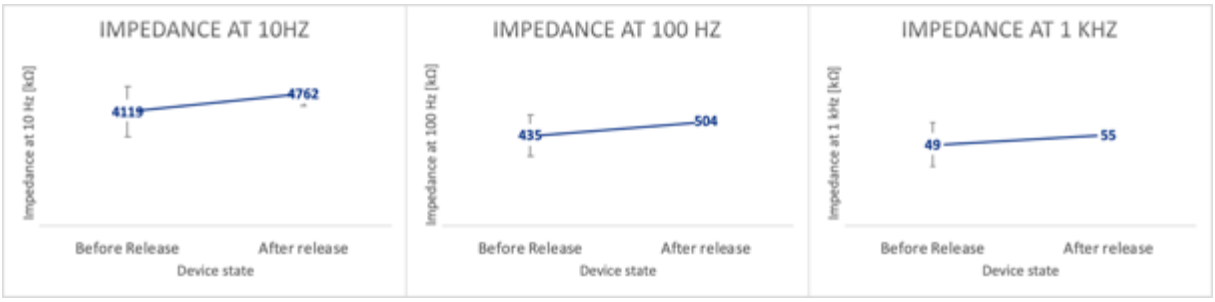

Figure 13 : Valeurs d'impédances pour des µECoG Panaxium de 30 µm de diamètre

Les impédances qualifiées montrent un bon degré de reproductibilité ainsi que le maintien des performances lorsque la matrice ultra-flexible est libérée de son support de fabrication.

Résistance mécanique

Les matrices d'électrodes ont aussi été testées après avoir subi des manipulations afin d'assurer le maintien de leur intégrité ainsi que des performances (Figure 14). Ces manipulations reproduisent les contraintes mécaniques lors du geste chirurgical (torsion, écrasement, déplacement, humidification, immersion).

Figure 14 : Exemple de contraintes mécaniques imposées aux matrices d'électrodes durant les tests, gauche : dispositif avant contrainte, milieu : dispositif mis en contraintes légères, droite : dispositif après fortes contraintes

Les caractérisations menées par microscopie ainsi que par analyse d'impédance montrent une bonne résistance ainsi que le maintien des performances électriques des électrodes Panaxium (Figure 15).

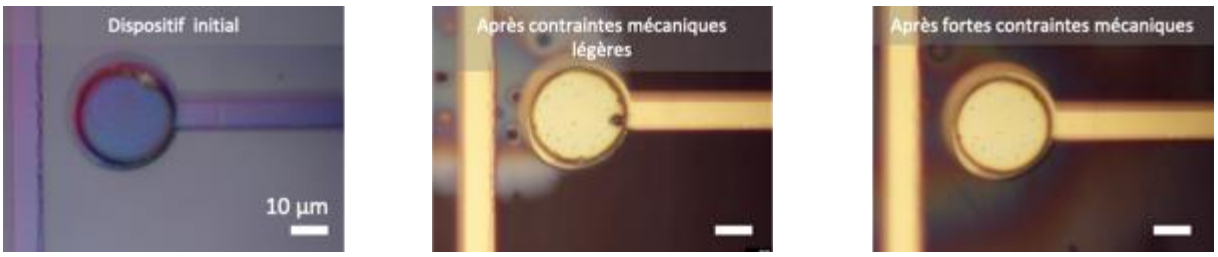

Figure 15 : Microscopie d'une électrode + piste conductrice avant et après contraintes mécaniques, nous n'observons pas de défauts malgré les contraintes imposées au dispositif

De plus les matrices montrent aussi le maintien de leurs performances électriques lorsque leur impédance est qualifiée (Figure 16).

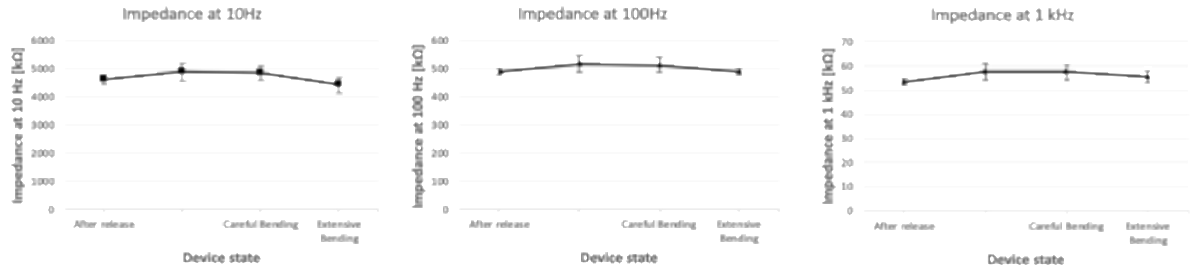

Figure 16 : Évolution de l'impédance après contraintes mécaniques, nous n'observons pas de défaut significatif impactant les performances électriques du dispositif

Tests précliniques

Des premiers tests des électrodes Panaxium ont été menés sur modèle porcin afin d'évaluer la sécurité du dispositif et ses performances en conditions représentatives (Figure 17 et 18).

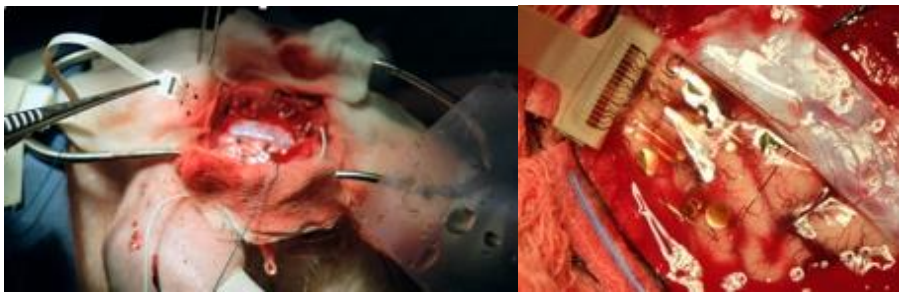

Figure 17 : Images des essais précliniques réalisés avec les électrodes Panaxium : à gauche manipulation du dispositif, à droite : dispositif positionné sur le cortex

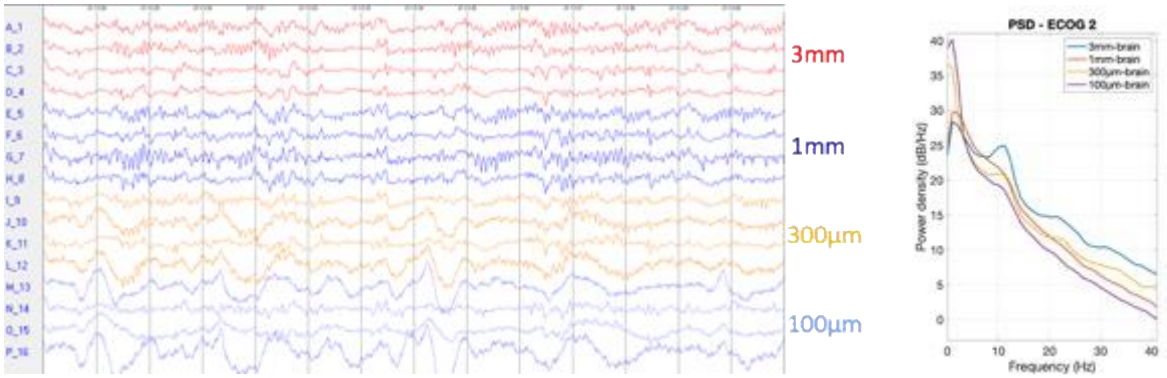

Figure 18 : Gauche : Résultat de mesures lors de l'expérience, Droite : analyse de densité spectrale de puissance avec différentes tailles d'électrodes

Les activités mesurées, pendant toute la durée de l'expérience, sont en adéquation avec l'activité cérébrale attendue sur le modèle utilisé dans les conditions anesthétiques de la chirurgie éveillée confirmant les performances des dispositifs.

D'autre part, les essais de manipulation et les observations durant et après les mesures n'ont montrés aucun risque concernant l'usage des microélectrodes. Durant toute la durée de l'expérience, aucune réaction biologique n'a été observée pendant et après l'utilisation de ces

électrodes, confirmant la biocompatibilité du dispositif en usage peropératoire en contact direct avec les tissus cérébraux (application directe sur la surface corticale), sur un modèle porcin.

De plus, des électrodes avec des matériaux identiques que celles de Panaxium mais avec des conceptions et fabrications différentes ont été effectuées sur des rats (16) et des souris (17). Ces expériences de durées variables, allant de l'utilisation intra-opératoire jusqu'à de l'implantation sur 29 semaines, n'ont montré aucune réaction biologique pouvant être causée par les dispositifs.

Packaging

Figure 19 : Exemple de Packaging permettant la protection mécanique ainsi que le maintien de la stérilité des dispositifs

Le dispositif sera packagé de façon à assurer sa protection durant les phases de transport et de stockage et sera disposé dans un double emballage compatible avec les contraintes de la stérilisation par oxyde d'éthylène.

Stérilisation

Des premiers essais de stérilisation à l'oxyde d'éthylène (EtO) du dispositif ont montré en plus de l'efficacité de la méthode de stérilisation sur des échantillons :

- Que la stérilisation n'a pas d'impact sur la fonctionnalité des µECoG
- Que les µECoG ne gardaient pas de résidus d'EtO, les résultats de dosages étaient conformes à la norme ISO 10993-7 (EtO résiduel< 0,1mg/dispositif/24h, et chlorhydrate d'éthylène <0,4mg/dispositif/24h)

Tests normatifs prévus avant l'utilisation

Pour cet essai clinique, et afin d'assurer la sécurité des patients, une évaluation de la biocompatibilité du dispositif est prévue selon la norme ISO 10993-1, en répondant aux points spécifiques de la classe du dispositif et de son utilisation (normes ISO 10993-18, ISO 10993-5, ISO 10993-10), avant le dépôt du dossier technique auprès de l'ANSM.

Une libération de stérilisation de lot selon l'annexe E de la norme ISO 11135, spécifique aux essais cliniques, est prévue sur le dispositif fini et packagé afin de garantir sa stérilité et la sécurité concernant le risque de présence de résidus d'EtO.

De plus, afin de garantir l'état stérile des dispositifs fournis pendant toute la durée de l'essai clinique, un contrôle du maintien de l'état stérile à intervalle réguliers en vieillissement en temps réel, en supplément d'un vieillissement en temps accéléré, est prévu. Dans l'éventualité de la perte de cet état stérile au cours du temps, d'autres lots de dispositifs seront stérilisés afin de pouvoir les utiliser pour la suite des essais cliniques.

Confirmation clinique prévue de la sécurité, de la performance et de l'utilisation des microélectrodes :

Les microélectrodes Panaxium n'ont pas encore été testées sur des patients. Il n'existe pas de dispositifs exactement équivalents aux microélectrodes Panaxium sur le marché. Il n'y a donc pas de données que nous pouvons considérer pour évaluer la sécurité et la performance clinique. Des électrodes comparables ont été construites de manière non industrielle et testées chez un nombre limité de patients, dans des conditions identiques à celles de cet étude, sans évènement indésirable rapporté (Khodagholy et al. 2015; 2016).

Basés sur les résultats des tests précliniques, quelques points restent encore ouverts, nécessitant une évaluation clinique. Ces points sont les suivants :
- La sécurité des microélectrodes Panaxium pendant une neurochirurgie réalisée sur des humains permettra de confirmer les résultats précliniques obtenus sur le cochon lors d'un monitorage intra-opératoire sur la surface cérébrale dans un contexte de neurochirurgie de résection tumorale ou du traitement de l'épilepsie, en condition clinique ;
- La qualité de signal pendant une neurochirurgie sur l'homme, dans un bloc opératoire avec des potentielles sources d'artéfacts et d'interférence liés à l'utilisation d'instruments chirurgicaux à proximité des microélectrodes ;
- La praticité d'utilisation des microélectrodes durant les différentes phases d'une neurochirurgie du point de vue des utilisateurs.

2. OBJECTIFS

2.1. Objectif principal

L'objectif principal de l'étude MicroECoGG est d'établir la sécurité d'utilisation des microélectrodes Panaxium lors d'enregistrements ECoG peropératoires. Cet objectif sera évalué par détermination de l'incidence des effets indésirables graves (EIG) survenus pendant la chirurgie (J0) et les quatre jours suivants (J4).

2.2. Objectifs secondaires

1. Déterminer la qualité des enregistrements avec les microélectrodes Panaxium, en comparaison aux enregistrements avec des macroélectrodes traditionnelles.
Plusieurs critères électrophysiologiques seront utilisés :
- Rapport signal / bruit ;
- Impédance des électrodes pendant la chirurgie ;
- Détection des ripples (100-250 Hz) et des fast ripples FR (250-600 Hz) ;
- Capacité à enregistrer des activités épileptiques spontanées (pointes et équivalent) ou consécutives à des stimulations électriques directes (post-décharges).
- Enregistrement des activités physiologiques évoquées gamma (*70-120 Hz*) pendant les investigations *neuropsychologiques* peropératoires (test de dénomination, comptage et test de la motricité avec déplacements de parties du corps spécifiques).

2. Établir la praticité d'utilisation et l'absence de défectuosité des microélectrodes Panaxium selon la perception des neurochirurgiens.

2.3. Objectifs exploratoires

- Capacité à enregistrer des activités multi unitaires.
- Corrélation entre activités enregistrées par µECoG et infiltration tumorale – concentration locale en oncométabolites.

3. CRITERES D'EVALUATION

3.1. Critère d'évaluation principal

Le critère d'évaluation principal est l'incidence des effets indésirables graves (EIG) liés à l'utilisation des microélectrodes Panaxium pendant la chirurgie (J0) et les quatre jours suivants (J4). Les EI sont décrits dans la section 8.

3.2. Critères d'évaluation secondaire

1. Déterminer la qualité des enregistrements avec les microélectrodes Panaxium, en comparaison aux enregistrements avec des macroélectrodes traditionnelles.

Les microélectrodes Panaxium seront comparées aux macroélectrodes DIXI de référence : électrodes corticales IOM de diamètre 4 mm, épaisseur 0,8 mm, distance inter-électrode 10 mm, largeur de la bande 10 mm, contacts en acier inoxydable.
Plusieurs critères électrophysiologiques seront utilisés :

- Rapport signal / bruit (RSB) : le RSB sera déterminé pour les segments enregistrés recueillant soit une activité oscillatoire physiologique (dépendant de la région échantillonnée), soit une figure épileptique. Le RSB sera calculé comme le rapport entre le Root Mean Square 1- de l'activité basale durant un intervalle temporel défini par l'onde ou la pointe enregistrée et 2- d'une onde (oscillation) ou d'une pointe (activité épileptique). Le RSB sera déterminé sur 20 évènements recueillis par microélectrode et par macroélectrode simultanément, au cours d'enregistrements de 2 minutes.
- Impédance des électrodes pendant la chirurgie. L'impédance est l'impédance électrique du circuit constitué par la grille d'électrodes, le cerveau du patient et l'électrode de référence. L'impédance décrit la capacité du DM pour conduire les signaux entre le cerveau du patient et le système d'enregistrement. L'impédance sera mesurée au début de l'enregistrement puis toutes les 10 minutes durant la totalité de l'enregistrement.
- Détection des ripples (100-250 Hz) et des FR (250-600 Hz). Les oscillations rapides seront détectées par le logiciel RippleLab, développé par M Le Van Quyen (Navarrete et al. 2016), sur les enregistrements par macro et microélectrodes. Elles seront quantifiées : nombre de cycles enregistrables, durée des évènements, amplitude, fréquence moyenne et maximale.
- Capacité à enregistrer des activités épileptiques spontanées (pointes et équivalent) ou post-stimulation électrique directe (post-décharges). L'amplitude, la durée et le seuil de détection de ces évènements seront analysés en comparant les données macro vs microélectrodes.
- Capacité à enregistrer les activités physiologiques dans le haut *gamma (70-120 Hz*) évoquées par les tâches cognitives au cours des tests *neuropsychologiques prédéfinis lors du bilan préopératoire* (test de dénomination, comptage et test de la motricité avec déplacements de parties du corps spécifiques). Les déviations par rapport à la ligne de base (%ERD) des activités évoquées seront estimés pendant les phases d'activités et seront comparés entre les données macro vs microélectrodes.

2. Établir la praticité d'utilisation et l'absence de défectuosité des microélectrodes Panaxium selon la perception des neurochirurgiens.

La praticité d'utilisation et l'absence de défectuosité des microélectrodes au bloc opératoire sera évaluée par les neurochirurgiens avec des questionnaires. Les questions concerneront la praticité d'utilisation, la sécurité d'utilisation pendant le dépôt des électrodes et durant leur repositionnement. Le neurochirurgien remplira le questionnaire à la fin de la chirurgie. Le nombre et le type de manipulations sera consigné. Les défectuosités possibles de l'électrode seront : un déchirement, une perte de substance, un échauffement, une perte du signal, une déconnexion du système d'enregistrement ou toute autre défectuosité constatée du DM.

3.3. Objectifs exploratoires

- Capacité à enregistrer des activités multi-unitaires
  De par leur taille, leur contact direct avec le cortex et leur impédance, les microélectrodes peuvent enregistrer les potentiels d'action neuronaux en extracellulaire. Le système d'enregistrement utilisé (Neuralynx Atlas, marqué CE pour l'usage humain, fréquence d'échantillonnage de 40 000 Hz) peut recueillir ces évènements très brefs, durant environ 1 milliseconde. Ces activités ne sont pas enregistrables par des macroélectrodes. La capacité des microélectrodes Panaxium à recueillir des potentiels d'action issus d'un (Single Unit Activity) ou de plusieurs (Multi Unit Activity) neurones sera analysée. Un résultat positif est attendu compte tenu des travaux déjà publiés d'une équipe américaine utilisant une technologie comparable (Khodagholy et al. 2015; 2016).
- Corrélation entre activités enregistrées par µECoG et infiltration tumorale – concentration locales en oncométabolites. Nos travaux préalables ont montré qu'au sein des tissus épileptiques humains péritumoraux enregistrés *ex vivo*, il existait une co-localisation entre infiltration tumorale du cortex et production d'activités épileptiques (pointes et oscillations rapides) (J Pallud, Le Van Quyen, et al. 2014). Les tissus péritumoraux présentent une autre caractéristique : divers oncométabolites sont produits par les cellules de gliomes et s'accumulent en extracellulaire, notamment en péritumoral, ou ils affectent les processus de croissance et d'infiltration tumorale mais également l'épileptogénicité locale. Le glutamate, neurotransmetteur excitateur est ainsi produit par les gliomes (Gilles Huberfeld and Vecht 2016), alors que les gliomes de bas grades mutés pour l'enzyme IDH (80 % d'entre eux) libèrent du D2-Hydroxy-Glutamate (D2HG). Les tissus péritumoraux réséqués seront explorés histologiquement (infiltration tumorale) et biochimiquement (concentration de glutamate et de D2HG). Un marquage immunohistochimique sera effectué dans des échantillons de tissus corticaux et tumoraux recoupés afin d'établir le type et le grade de la tumeur selon la classification de l'OMS de 2016 (Louis et al. 2016) et de cartographier l'infiltration des cellules tumorales : Hématoxyline-éosine, Ki67, NeuN, OLIG2, MIB-1, GFAP, IDH(R123H). L'infiltration des cellules tumorales sera mesurée en comptant le nombre de cellules tumorales par champ de haute puissance x 400, 0,2 mm^2. Une portion de 1/2 cm^3 sera congelée pour mesurer les concentrations tissulaires de glutamate et de D2HG par chromatographie en phase gazeuse couplée à la spectroscopie de masse (Gleize et al. 2015).

4. CONCEPTION DE LA RECHERCHE

4.1. Type de recherche

Il s'agit d'une recherche prospective de recherche impliquant la personne humaine interventionnelle, multicentrique, nationale, open-label, visant à étudier la sécurité d'utilisation chez l'homme d'une nouvelle électrode d'enregistrement ECoG, de type microélectrode, dispositif médical de classe III non marqué CE. La sécurité d'utilisation (effets secondaires) et les performances d'enregistrement seront comparées à celles de macroélectrodes d'usage clinique lors de la chirurgie en condition éveillée de patient souffrant d'un gliome cérébral pour lequel un enregistrement ECoG est requis dans le cadre de la cartographie fonctionnelle peropératoire pour guider la résection.

4.2. Méthodologie de la recherche

Il s'agit d'une recherche non randomisée, en ouvert, au cours de laquelle des patients souffrant d'une tumeur cérébrale, opérés en condition éveillée de manière à établir une cartographie fonctionnelle cérébrale pour la résection tumorale, bénéficiant au cours de la chirurgie d'un monitorage électrophysiologique cortical par ECoG seront enregistrés par une µECoG d'un nouveau type, en supplément de l'enregistrement normal par macroECoG usuelles.

Un nouveau DM (les µECoG Panaxium) sera testé au cours de cette recherche. L'enregistrement peropératoire sera mené simultanément pour les 10 premiers patients avec les deux électrodes, déplacées sur l'ensemble du cortex pour établir la cartographie ECoG. Dans le cas des 10 premiers patients, les électrodes seront placées en proximité, mais pas au même endroit, de façon à pouvoir déterminer dans le cas de survenue d'EI, quel type d'électrode est le responsable. Le même

système d'enregistrement EEG autorisé chez l'homme (Neuralynx Atlas) sera utilisé pour les deux électrodes de manière à comparer la qualité des signaux. Après une analyse intérimaire portant sur la sécurité, tolérance, la praticité d'utilisation, le RSB et l'impédance, les 40 patients supplémentaires bénéficieront d'un enregistrement cortical uniquement par les µECoG Panaxium de façon à augmenter les informations sur la sécurité et la qualité des signaux.

Plan expérimental :

Les patients inclus seront des adultes souffrant d'un gliome cérébral pour lequel une résection chirurgicale est indiquée, avec cartographie cérébrale fonctionnelle en condition éveillée, visant à optimiser le geste chirurgical, pour laquelle un enregistrement ECoG est programmé de manière à réaliser une cartographie des activités épileptiques corticales et à monitorer les effets des stimulations électriques corticales.

Un total de 50 patients au maximum sera inclu par les services de Neurochirurgie de 3 centres.
Les patients seront enregistrés en ECoG par électrodes macroscopiques d'usage clinique et / ou par le DM testé (µECoG Panaxium). Les 10 premiers patients seront enregistrés par les deux dispositifs simultanément et, après une analyse intermédiaire et avis du DSMB, si la sécurité d'utilisation est au moins égale et les éventuelles défectuosités du DM, par µECoG Panaxium exclusivement pour les 40 suivants. Les données préliminaires (chez l'homme pour des électrodes de même technologie (Khodagholy et al. 2015; 2016) et l'animal) indiquent que les µECoG Panaxium, de par leur configuration permettent de recueillir un signal électrique d'origine cérébrale avec une meilleure résolution spatio-temporelle. Leur faible épaisseur doit également garantir une meilleure sécurité d'utilisation.

Les patients seront recrutés par le neurochirurgien investigateur à J-1 de la chirurgie. Les enregistrements seront menés à J0 au cours de la chirurgie planifiée de résection tumorale par un des neurologues investigateurs. Les potentiels effets secondaires seront identifiés jusqu'à J4 après la chirurgie, jour de sortie habituel d'hospitalisation.

Les visites seront organisées de la façon suivante :

- Screening par le neurochirurgien investigateur pendant le mois précédant la chirurgie. Lors de cette consultation préopératoire, le patient sera informé du déroulement de la recherche si les critères d'inclusion sont remplis. Les documents d'information seront remis au patient.
- Première visite (V1) la veille de la chirurgie : information, recueil du consentement, inclusion (J-1).
- Deuxième visite (V2) le jour de la chirurgie (J0).
- Troisième visite (V3) à H24 de la chirurgie (J1).
- Quatrième visite (V4) à la sortie du patient de l'hôpital à J4.
- Une visite supplémentaire (VS) s'il est observé un effet indésirable grave associé à l'utilisation du nouveau DM, le jour de la sortie d'hôpital si celle-ci est décalée au delà de J4 pour cause d'EI, ou à J7 si le patient est toujours hospitalisé

La V1 aura lieu dans le service de Neurochirurgie, la veille de la chirurgie. Elle sera menée par le neurochirurgien investigateur devant réaliser l'intervention chirurgicale. Le patient sera informé de la recherche. La validation des critères d'inclusion et de non-inclusion sera vérifiée. Il sera ensuite proposé au patient de l'inclure et le consentement sera signé.

La V2 aura lieu le jour de la chirurgie, au bloc opératoire. Elle consiste en la réalisation de l'ECoG en condition éveillée en utilisant le DM, les µECoG Panaxium.

Le patient est opéré dans les conditions habituelles. Après réalisation d'une anesthésie générale, la ventilation étant réalisée par masque laryngé, et le crane étant fixé par une têtière, sont réalisées la craniotomie et l'ouverture de la dure-mère. Une anesthésie locale par lidocaïne est alors réalisée sur les pointes de la têtière, la peau, le muscle temporal et la dure-mère. L'anesthésie est alors levée et patient s'éveille ; il ventile spontanément et peut interagir avec le neurochirurgien.

Une cartographie fonctionnelle est alors réalisée par enregistrement ECoG. Notre équipe utilise de manière routinière des macroélectrodes possédant le marquage CE Classe III pour utilisation humaine (DIXI, électrodes corticales IOM). Il s'agit de bandes (strips) ou des grilles (grids) de respectivement 6 et 2x4 électrodes, d'un diamètre de 0,4 cm, espacées de 1 cm. L'électrode est fabriquée en acier inoxydable. L'épaisseur est de 0,8 mm. L'électrode est posée sur le cortex exposé durant la chirurgie. Une électrode aiguille de référence est insérée en bordure de champ entre la peau et l'os. Une électrode masse est variablement utilisée, collée sur la peau du patient. Les électrodes sont connectées au système d'enregistrement. Nous utilisons un système EEG évolué, dédié aux enregistrements humains, marqué CE : Système Atlas de Neuralynx. Sa caractéristique est de posséder un nombre élevé de canaux (120), possédant chacun une bande de fréquence d'enregistrement très large (DC à 40 kHz / canal), avec un RSB optimal. Le système d'enregistrement est installé sur chariot mobile dans le bloc opératoire à moins de 3 m de la tête du patient, en dehors de l'espace stérile. Les électrodes (stériles) sont connectées au système dans l'espace non stérile. Du fait de la variabilité du champ opératoire et de la nécessité de réaliser des stimulations corticales directes répétées pour la cartographie fonctionnelle au moyen d'un stylet de stimulation (espace entre les deux électrodes de stimulation bipolaire de 5 mm), les strips ou grids d'électrode ne couvrent pas tout le cortex exposé et sont déplacés à façon par le neurochirurgien pour échantillonner l'ensemble du cortex exposé. L'électrode est ainsi repositionnée toutes les 90 secondes, la durée d'enregistrement étant de 5-9 minutes.
De manière à préciser la localisation de l'électrode d'enregistrement (puis du site de stimulation corticale directe), une caméra, couplée au système EEG et synchronisée au signal EEG filmera en permanence le cortex exposé. Le visage du patient, non visible car situé de l'autre côté du champ opératoire, ne sera pas filmé.

Pendant les investigations *neuropsychologiques*, les enregistrements seront réalisés pendant que le patient effectue des tests moteurs, sensitifs, langagiers prédéfinis lors du bilan préopératoire. En peropératoire, il est en routine demandé au patient d'effectuer des tâches fonctionnelles (bouger, dénommer, compter, associer des items en fonction de leurs significations, reconnaître l'émotion exprimée par un visage, etc.) supervisée par un neuropsychologue et/ou orthophoniste en temps réel. Pendant ces tâches cognitives, le signal EEG sera synchronisé avec les réponses du patient à partir du son enregistré.

Pour une première série de 10 patients, les deux électrodes (macro grid / strip DIXI et µECoG Panaxium) seront placées côte à côte de manière à pouvoir enregistrer des activités comparables et déterminer la sécurité et la praticité d'utilisation. A cette fin, les signaux des électrodes adjacentes seront comparés (cf partie analyse).
Après cette cartographie initiale, les électrodes seront généralement laissées en périphérie du champ opératoire (si l'encombrement le permet) et continueront d'enregistrer le signal EEG pendant la phase de cartographie fonctionnelle par stimulation électrique directe corticale puis sous corticale durant habituellement 1 à 2 heures. En cas de survenue d'une post-décharge épileptique ou d'une crise organisée en lien avec les stimulations électriques, détectée par monitoring visuel continu, le neurochirurgien sera avisé en temps réel, dans le double but de mettre en place une procédure antiépileptique locale (par instillation sur le cortex de sérum physiologique glacé) et d'informer le neurochirurgien que les effets de la stimulation produisant une décharge épileptique doivent être considérés avec précaution pour la cartographie.

La résection de la tumeur sera étendue jusque dans les régions péritumorales établies comme non fonctionnelles par la cartographie. Les régions péritumorales non nécessaires à l'examen neuropathologique seront conservées pour la recherche : quantification biochimique des oncométabolites, étude histologique, étude électrophysiologique *ex vivo* et mise en culture du cortex. Leur pattern électrophysiologique aura été enregistré et la réalisation du film opératoire permettra de les localiser.
Après la résection, une nouvelle cartographie EEG est réalisée sur le cortex résiduel de manière à rechercher des activités épileptiques résiduelles.
L'impédance des électrodes sera mesurée toutes les 10 minutes, tout au long de l'enregistrement.

Au terme de la chirurgie, à J0, le neurochirurgien remplit le questionnaire d'effets indésirables et celui concernant la praticité d'usage et les défectuosités du DM.

Les données électrophysiologiques sont anonymisées (3 premières lettres de l'hôpital : PSL pour Pitié-Salpêtrière, STA pour Sainte-Anne, FOR pour Hopital Fondation Adolphe de Rothschild / numéro croissant d'inclusion).

La V3 aura lieu à H24 pendant l'hospitalisation du patient et la V4 à la sortie du patient de l'hôpital à J4, ou au jour de sortie si l'hospitalisation se prolonge. Les deux visites seront réalisées dans le service de Neurochirurgie. Pendant les visites un interrogatoire et examen clinique auront lieu, dans le cadre du soin.

Si un EIG est apparu par rapport à l'utilisation du DM, et qu'il n'est pas résolu à la sortie de l'hôpital à J4, une VS aura lieu, le jour de la sortie d'hôpital si celle-ci est décalée au delà de J4 pour cause d'EI, ou à J7 si le patient est toujours hospitalisé. Si un EIG sans rapport au DM reste présent à J4 à la sortie, le suivi sera réalisé selon les pratiques de l'hôpital.

4.3. **Calendrier prévisionnel de la recherche**

Durée des inclusions : 25 mois (environ deux patients par mois).

Durée de participation du participant : 5 jours : inclusion à J-1 de la chirurgie jusqu'à J+4. Le temps de participation active sera d'environ 6 heures (une heure d'interrogatoire / examen clinique et cinq heures de chirurgie).

Durée totale de la recherche : La durée projetée de la recherche sera de 30 mois soit 25 mois pour le recueil des données et de 5 mois pour leur analyse (traitement de signal, data management et analyse statistique).

Durée de la période d'exclusion : jusqu'à un jour après la dernière visite du patient.
Pendant toute la durée de la recherche, le patient ne pourra pas participer à d'autres recherches thérapeutiques pouvant modifier la lésion ou son environnement (qu'elle soit médicamenteuse, ou par dispositif médical) entre la V1 et la V4 ou la VS/suivi selon les pratiques de l'hôpital en cas d'EIG.

5. SELECTION DES PERSONNES

5.1. **Populations étudiées**

Adultes souffrant d'un gliome diffus cérébral pour lequel une résection chirurgicale est indiquée, avec cartographie cérébrale fonctionnelle en condition éveillée, visant à optimiser le geste chirurgical, pour laquelle un enregistrement ECoG est programmé de manière à réaliser une cartographie des activités épileptiques corticales et à monitorer les effets des stimulations électriques corticales.

5.2. **Critères d'inclusion**

- Être atteint d'un gliome diffus cérébral pour lequel une résection chirurgicale est indiquée.
- Chirurgie planifiée en condition éveillée avec cartographie fonctionnelle peropératoire.
- Intervention prévue avec monitorage électrophysiologique ECoG.
- Age supérieure ou égal à 18 ans.
- Affiliation à un régime de sécurité sociale, à la Couverture Médicale Universelle (CMU) ou à tout régime équivalent.
- Ayant donné leur consentement écrit.

5.3. **Critères de non-inclusion**

- Infection aigue avec point d'appel clinique ou biologique identifié dans le cadre du soin ou sans traitement (viral, bactérienne ou fongique).
- Patient à risque accru d'infections (par exemple sous traitement immunosuppresseur)
- Traitement actuel avec antibiotiques.
- Femmes enceinte ou à risque de grossesse ou en période d'allaitement (un test de grossesse sera demandé).
- Autres pathologies (exemple : trouble du comportement...) qui pourraient interférer sur l'évaluation neurologique ou compromettre la sécurité du sujet selon appréciation de l'investigateur.
- Participation à une recherche thérapeutique pouvant modifier la lésion ou son environnement pendant la durée de la recherche (qu'elle soit médicamenteuse ou par dispositif médical) ou soumise à une période d'exclusion pour une autre recherche.
- Personne majeure faisant l'objet d'une protection légale (curatelle, tutelle ou sauvegarde de justice).

5.4. **Modalités de recrutement**

Les patients seront recrutés par les neurochirurgiens investigateurs, dans la file active de patients pris en charge pour une tumeur cérébrale à opérer en condition éveillée.

Les patients incluables seront informés du protocole au cours de la consultation pré chirurgicale par le neurochirurgien. Ils seront de nouveau informés, après période de réflexion d'au moins 24hr entre la consultation préopératoire ambulatoire et l'hospitalisation pour la chirurgie, signeront le consentement et seront inclus la veille de la chirurgie lors de l'hospitalisation par le neurochirurgien.

6. REALISATION PRATIQUE DU PROTOCOLE

6.1. **Sélection**

Lors des consultations et hospitalisations dans un des services de Neurochirurgie des trois centres participants, le neurochirurgien investigateur informera les patients atteints d'un gliome cérébral de l'objectif, de la nature, des contraintes et des risques prévisibles de la recherche. Il vérifiera la présence des critères d'inclusion et l'absence de contre-indication.

6.2. **Inclusion, information, et accord de participation (consentement)**

L'inclusion et la signature du consentement seront faites lors d'une entrevue dédiée la veille de la chirurgie, au sein du service de Neurochirurgie dans lequel le patient est hospitalisé. Le neurochirurgien investigateur vérifiera la présence des critères d'inclusion et l'absence de contre-indication.

Le consentement éclairé sera présenté et expliqué au patient par un des investigateurs. La recherche aura au préalable été présentée lors de la consultation ambulatoire préopératoire, au moins 24 hr avant J-1. Après deux heures de réflexion minimum, le patient signera le consentement s'il souhaite participer à la recherche.

Aucun examen complémentaire ne sera réalisé au moment de l'inclusion. La V1 aura lieu pour le recueil des informations cliniques, obtenues dans le cadre du soin.

L'acceptation de participation à la recherche et la date seront notées dans le dossier médical du patient, de même, que la date éventuelle de retrait de sa participation, le cas échéant.

6.3. **Suivi**

6.3.1 : Visite 1 (J-1)

Réalisée à J-1 de la chirurgie, la visite durera **30 minutes.**

Pendant l'hospitalisation dans un service de Neurochirurgie du patient pour chirurgie tumorale.

- Inclusion : Information, vérification des critères d'inclusion et de non-inclusion, signature du consentement.

- Pseudonymisation : 3 premières lettres de l'hôpital : PSL pour Pitié-Salpêtrière, STA pour Sainte-Anne, FOR pour Hopital Fondation Adolphe de Rothschild / numéro croissant d'inclusion (gestion par le logiciel d'eCRF)

- Examen médical préalable à la recherche, réalisé dans le cadre du soin : tension artérielle, température, fréquence cardiaque, examen neurologique routinier.

- Prélèvement sanguin pour bilan préopératoire (réalisé dans le cadre du soin courant) : Le bilan biologique de routine préopératoire est réalisé la veille de la chirurgie. Il consiste en : NFS, biochimie, plaquettes, paramètres de coagulation, CRP. Tous les paramètres seront analysés dans le laboratoire de l'hôpital correspondant.

- Données issues de l'hospitalisation initiale (dans le cadre du soin courant) : Seront notées à partir du dossier médical du patient : date des premiers symptômes, du diagnostic, symptômes en rapport avec la tumeur, présence de crises épileptiques, médication habituelle.

- L'information sur la médication sera recueillie pendant la participation totale à la recherche. Le nom générique, l'indication, la date d'introduction et d'arrêt (si connues) et la voie d'administration seront renseignés.
Ces données de l'hospitalisation initiale seront recueillies dans le dossier du patient dans le cadre de la prise en charge habituelle des patients dans leur service d'hospitalisation. L'autorisation d'utiliser ces données cliniques de soins courants extraites « rétrospectivement » des dossiers patients après leur inclusion est explicitement demandée dans le consentement éclairé.

- IRM cérébrale préopératoire réalisée dans le cadre du soin courant, en l'absence de contre-indication. Les données DICOM, pseudonymisées, seront transférées sur un disque dur chiffré hors réseau.

6.3.2 : Visite 2 - Chirurgie (J0) :

Il s'agit de la chirurgie de résection tumorale réalisée en condition éveillée comme décrit en 4.2.

Le co-enregistrement par µECoG Panaxium (10 premiers patients) et l'enregistrement exclusif par µECoG Panaxium (si validé par analyse intérimaire) seront menés comme en pratique normale. L'inclusion dans la recherche ne modifiera pas le geste chirurgical ni la manière dont est menée l'enregistrement ECoG.
La chirurgie dure en moyenne 3 à 6h et la durée d'utilisation de l'électrode sera de 5 à 9 min d'enregistrement avant la phase de cartographie cérébrale. L'électrode sera laissée en périphérie de la région opérée pendant 1 à 2 h lors de la phase de stimulation électrique.

Les données comprenant : les enregistrements électrophysiologiques, le film opératoire ciblant la surface cérébrale (et non le visage), l'enregistrement sonore du patient pendant la passation des taches, les données d'impédance au cours de l'enregistrement seront pseudonymisées et transférées sur un disque dur chiffré hors réseau.

Les tissus péritumoraux non nécessaires au diagnostic neuropathologique seront étiquetés (pseudonymisation) et congelés (biochimie), fixés (histologie) ou transportés au laboratoire (Collége de France) dans du liquide cérébro-spinal artificiel glacé oxygéné (cf paragraphe 9).

Un recueil des effets indésirables et des défectuosités éventuelles du DM sera effectué après la chirurgie sur l'eCRF.

Le chirurgien remplira le questionnaire de praticité d'utilisation et de défectuosité du DM à l'issue de l'intervention chirurgicale.

6.3.3 : Visites 3, 4 et supplémentaire si besoin :

La visite se déroulera dans le service d'hospitalisation de Neurochirurgie (V3 et V4, éventuelle VS) de l'hôpital correspondant.
Durée : 30 minutes.
Elle comportera une évaluation d'évolution clinique depuis la dernière visite et un recueil des EI.
Seront notés à partir du dossier médical du patient : Examen physique similaire à celui réalisé pendant la V1, présence de crises épileptiques, événements indésirables.

La visite V3 aura lieu 24 heures après la chirurgie dans le service de Neurochirurgie.
La visite V4 aura lieu à la sortie du patient d'hospitalisation à J4.

	Visite 1	*Visite 2*	*Visite 3*	*Visite 4*
Information / Consentement	*X*			
Histoire médical (sur dossier)	*X*			
Examen clinique / neurologique	*X*		*X*	*X*
Prélèvement sanguin	*X*			
ECoG		*X*		
Mesure des impédances		*X*		
Recueil d'effets indésirables		*X*	*X*	*X*
Questionnaire de praticité d'utilisation et de défectuosité du DM		*X*		

Les éléments notés en rouge sont spécifiques à la recherche

6.4. **Visite de sortie prématurée de la recherche**

En cas de sortie prématurée, les raisons seront spécifiées dans le cahier d'observations. Les effets indésirables seront recueillis.

6.5. **Arrêt de participation de la personne à la recherche**

Les sujets participant à la recherche peuvent décider à tout moment d'interrompre leur participation, sans préjudice à leur prise en charge. La sortie de recherche ne modifiera pas le suivi du patient. Dans le cas où le participant souhaite se retirer du protocole, l'investigateur devra alors demander au participant de préciser s'il retire ou garde son consentement et, le cas échéant, s'il autorise que les données saisies avant le retrait de son consentement, ainsi que les échantillons biologiques et leurs données soient exploitées dans le cadre de la recherche, ainsi qu'une éventuelle réutilisation des données.

Il n'y a pas de modalités particulières de suivi en lien avec le protocole à mettre en place à la sortie du sujet qu'elle relève de sa décision ou de celle de l'investigateur.

Il n'y a pas de modalités particulières de suivi à la fin de participation du sujet à la recherche. A la fin de participation de la recherche, le patient consultera son neurochirurgien référent dans le cadre de son suivi habituel.

Critères de sortie d'étude :

- Impossibilité de réalisation de la chirurgie en condition éveillée (difficultés intubation/extubation du patient, agitation…) ;
- Impossibilité de réalisation de l'enregistrement ECoG.

Si le DM a été utilisé ou en contact avec le patient, un suivi des EIG doit être réalisé.

Description des modalités à mettre en place en cas de résultats significatifs concernant la santé de la personne :

En cas de découverte fortuite d'une anomalie cérébrale autre que celle connue chez les patients (tumeur cérébrale connue à l'inclusion), le sujet serait informé par le(s) investigateur(s) ou le médecin de son choix et devrait se mettre en rapport avec son neurochirurgien ou le médecin de son choix, aidé par l'investigateur, afin de déterminer la conduite à tenir.
Dans le cas de cette recherche, l'épilepsie du patient, très fréquente en cas de gliome, est déjà connue avant la chirurgie et n'est pas révélée par la recherche.

Sortie prématurée de la recherche avec retrait de consentement :

Si le sujet participant décide de quitter la recherche les datas obtenus lors des enregistrements, les échantillons biologiques et les données issues de la recherche ne seront plus utilisés pour des analyses et seront effacés. Néanmoins, si elles sont pertinentes pour l'analyse de l'objectif primaire (sécurité d'utilisation), elles seront analysées. Les échantillons biologiques humains seront détruits.

7. PRODUITS ADMINISTRES (médicament, dispositif médical, MTI…)

7.1. Dénomination et description du dispositif médical faisant l'objet de la recherche

Dénomination du dispositif médical
Le dispositif médical faisant l'objet de la recherche est une électrode corticale conçue et fabriquée par l'entreprise Panaxium pour l'enregistrement per opératoire d'activité électrophysiologique à la surface du cortex. Le dispositif se présente sous la forme d'une matrice de 128 sites d'enregistrements arrangés en 24 tétrodes (groupe de 4 électrodes rapprochées de 30µm de diamètre), 28 électrodes de 500µm de diamètre et 4 électrodes de référence.

Afin de faciliter la traçabilité des dispositifs utilisés lors de cette recherche, la dénomination suivante a été choisie :

- L'identité du fabricant : PANAXIUM
- Nom du projet : MicroECoGG
- Modèle et version associée : [Nombre de voies] [Lettre] (ex : 128 C)
- Numéro de série fabricant (permettant la traçabilité sur l'ensemble du circuit de fabrication et logistique) : #[Nombre] (ex : #014)

Un dispositif de la recherche aura donc une appellation telle que : PANAXIUM MicroECoGG 128C #001

Description du dispositif médical
Le dispositif Panaxium ne possède pas le marquage CE, cette recherche étant destinée à la validation de sa sécurité pré-marquage. Comme précisé dans la partie 1.3.5 de présentation des dispositifs conçus par Panaxium, les tests normatifs requis et de suivi des performances et des conditions de stockage et de stérilisation seront réalisés pour garantir la sécurité des patients et le maintien des performances des dispositifs fournis lors de cette recherche.

Les éléments de sécurité et de performance validés durant la recherche serviront les projets futurs de Panaxium (montage d'un dossier de marquage du dispositif, continuation du projet de recherche clinique).

Comme indiqué dans la partie 1.3.5, le dispositif est constitué de deux éléments principaux, une partie ultra-flexible, contenant les µECoG et étant directement en contact avec le cortex cérébral d'une part, et d'une partie flexible (blanche), en contact indirect avec possibilité de contact direct avec l'os d'autre part. Cet ensemble sera contenu dans un double emballage permettant la stérilisation par oxyde d'éthylène.
Pour la partie ultra-flexible, les matériaux sont : le parylène C utilisé comme substrat, l'or et le titane pour la conduction électrique, et le PEDOT:PSS pour la conduction ionique et pour limiter les ruptures d'impédance. Le parylène C et le PEDOT:PSS sont en contact direct avec l'organe cible. Le parylène C est biocompatible et est utilisé dans beaucoup d'applications médicales, y compris des dispositifs implantables. Le PEDOT :PSS est aussi utilisé dans quelques applications neurologiques (Khodagholy et al. 2015; Lecomte et al. 2017). L'or et le titane sont en contact indirect, et de ce fait le seul risque est la migration de ces métaux à travers le PEDOT:PSS et/ou le parylène C. Ce risque est très faible et n'a pas été observé dans les utilisations précédemment citées.
La partie flexible est constituée de LCP (Liquid crystal polymer), de cuivre, de nickel pour empêcher la diffusion du cuivre et d'or qui recouvre le nickel. L'ensemble est encapsulé dans le LCP, biocompatible et déjà utilisé comme matériau pour des implants rétiniens sur le lapin et pour des µECoG sur le rat, à l'exception de la zone de connexion avec la partie ultraflexible, appelée interconnexion. Cette partie présente de la colle conductrice (type ACP). L'ensemble de cette zone est encapsulé dans du silicone compatible avec une implantation de moins de 30 jours dans le corps humain, afin d'empêcher toute diffusion d'ACP ou de métaux. L'ensemble de ces matériaux ne présente pas de contre-indication à la stérilisation par oxyde d'éthylène.

7.2. **Mode de fonctionnement et d'utilisation du dispositif**

Les dispositifs fabriqués par Panaxium ne sont pas marqués CE et leur usage sera, dans le cadre de ce projet de recherche, limité aux conditions d'utilisation précisées dans ce document.
Les dispositifs seront utilisés lors de chirurgies de résection tumorale corticale, avec comme objectifs principaux de valider la sécurité et la praticité de leur utilisation ainsi que la qualité des enregistrements d'activité électrophysiologique corticale effectués lors de la chirurgie.

Les neurochirurgiens participant à la recherche seront formés au préalable à la manipulation des dispositifs (ainsi qu'à la méthode de vérification des performances du dispositif préalable à l'utilisation), ainsi que les personnels du bloc opératoire qui pourraient avoir à manipuler les dispositifs ou les emballages temporairement pendant la chirurgie.
Seul le neurochirurgien, qui a l'expérience de ce type de dispositifs et de chirurgie, utilisera le dispositif Panaxium en contact direct avec le patient.

Le dispositif sera utilisé de manière analogue à une électrode corticale commercialisée (macroélectrodes DIXI de référence : électrodes corticales IOM de diamètre 4 mm, épaisseur 0,8 mm, distance inter électrode 10 mm, largeur de la bande 10 mm, contacts en acier inoxydable, utilisées par les services de neurochirurgie, un des objectifs de l'étude étant de valider la praticité de l'utilisation des dispositifs Panaxium en comparaison avec des électrodes disponibles sur le marché). L'usage spécifique à ce projet de recherche est détaillé dans la partie 4.2 et les paramètres évalués lors de la recherche sont définis en partie 8.2.

Les conditions liées au circuit logistique de ces dispositifs sont décrites dans le paragraphe suivant 7.3. (stockage, stérilisation, expédition…). Le dispositif sera fourni stérile, pour un usage unique, limité au cadre peropératoire tel que défini dans ce protocole de recherche.

7.3. **Circuit logistique**

– ***Fourniture du dispositif médical***

Il est convenu entre le fabricant de dispositifs Panaxium et les centres investigateurs la livraison récurrente de lots de dispositifs tous les six mois comprenant un nombre de dispositifs proportionnel au besoin envisagé par les chirurgiens durant cette période.
Cette durée permettra à Panaxium d'assurer un maximum de sécurité lors de la fabrication des dispositifs ainsi que sur les étapes de packaging et de stérilisation. Cette durée permet également d'assurer une contingence temporelle en cas de délais imprévus lors du cycle de production des dispositifs et ainsi de limiter les retards dans les expériences prévues.
Il a également été convenu avec l'investigateur coordonnateur de cette recherche que des rectifications de conception pourront être envisagées entre les différentes itérations, et que leur mise en œuvre sera évaluée en fonction de leur complexité et de leur impact sur la sécurité et les performances des dispositifs fournis. La brochure investigatrice sera alors mise à jour.
En pratique :

- Les électrodes seront livrées par lots de 20 (Maximum : « 3 lots » par an au total - soit « 60 électrodes » par centre par an).
- Un réapprovisionnement est prévu tous les 6 mois (ou plus tôt si nécessaire lorsque le stock est <6 DM - maximum 3 livraisons par an). Un message est envoyé par le pharmacien responsable à Panaxium lorsque le stock est inférieur à 6 DM pour réapprovisionnement.
- En cas de non utilisation d'une électrode, toujours empaquetée de manière stérile, elle sera retournée à la pharmacie et ré-attribuable.
- Un total de 50 (nombre de sujets de la recherche) + 10 (remplacement éventuel) + 6 (marge de 10%), soit 66 sera produit.

– ***Conditionnement des dispositifs, stockage et retours***

Il est convenu que l'entreprise Panaxium fournisse les dispositifs de recherche dans un double emballage de type blister rigide et stériles (EtO) aux centres d'investigation.
Panaxium prend la responsabilité de fournir le dispositif conditionné et stérilisé aux centres d'investigation (cf 1.3.5 pour le conditionnement, la méthode de stérilisation et les tests associés).
Les emballages sont de dimensions équivalentes aux électrodes commerciales (environ 20x40x5cm).
Les dispositifs ne nécessitent pas de conditions de stockage particulières (à l'abris des UV et à température ambiante). Il est recommandé que le stockage s'effectue dans des conditions de température (T 20°C, +-10°C) et d'humidité (40% à 70%) adaptées, à l'abri de la lumière solaire directe et de contaminations de toute nature.

Les dispositifs ont une durée de stockage prévue <6 mois.
Le renvoi des dispositifs chez le fabricant est prévu pour les dispositifs non utilisés en fin de recherche ou lorsque la date de validité/péremption du fabricant est dépassée. Le transport est organisé par Panaxium.

– ***Étiquetage des dispositifs***

Il est convenu que Panaxium soit en charge de l'étiquetage des dispositifs fournis aux centres d'investigation.
L'étiquette inclura :

- La dénomination du dispositif telle que décrite en 7.1
- L'identité et les coordonnées du fabricant Panaxium
- La date limite d'utilisation (définie 6 mois après la stérilisation)
- La référence au projet MicroECoGG (l'usage du dispositif (non marqué) sera défini et limité au protocole de recherche en cours)

- Les pictogrammes de sécurité correspondant au dispositif fabriqué :
  - Dispositif stérile (et méthode de stérilisation)
  - Dispositif à usage unique
  - Pictogramme « Attention »
  - Notice d'utilisation
  - Dispositif sans latex
  - Pictogramme « ne pas utiliser si l'emballage est détérioré »
  - Pictogramme de conditions de stockage (environnement sec et à l'abri de la lumière)
  - Dispositif non pyrogène
  - L'étiquette comprendra un espace libre pour annotation du numero d'inclusion du patient et la date de l'utilisation
  - Les emballages et étiquettes seront conservées
- Mention « exclusivement pour investigations cliniques » conformément à l'arrêté du 15 mars 2010 fixant les conditions de mise en œuvre des exigences essentielles applicables aux dispositifs médicaux, pris en application de l'article R. 5211-24 du code de la santé publique.

– ***Dispensation des dispositifs***

La dispensation du DM est assurée par le pharmacien responsable :

- Hopital Sainte-Anne : Pharmacien – GHU PARIS PSYCHIATRIE & NEUROSCIENCES, 1 rue Cabanis – 75014 Paris, Téléphone: 0145658432, Télécopie : 0145658936
- Hopital Pitié-Salpêtrière : Pharmacien Dispositifs Médicaux Stériles, AP-HP.Sorbonne Université, Tél secrétariat : 01 42 16 02 83, Tél direct : 01 42 16 02 27
- Le neurochirurgien investigateur ou le médecin investigateur assurant les enregistrements établissent une ordonnance la veille de la chirurgie. Cette ordonnance est transmise à la pharmacie qui assure la libération des dispositifs. Le numéro de lot est indiqué sur l'ordonnance qui est ensuite scannée et inclues dans l'eCRF (une copie de l'ordonnance pseudonymisée sera scannée et jointe dans l'e-CRF). Le numéro de lot est également signalé dans le dossier médical et sur l'eCRF.

2 dispositifs sont prescrits pour chaque opération afin de palier une éventuelle défectuosité.
Les dispositifs non utilisés seront retournés à la pharmacie après l'opération par l'équipe investigatrice.
Les dispositifs sont indiqués pour un usage unique, ils sont ensuite directement mis aux déchets biologiques par l'équipe chirurgicale.
L'équipe investigatrice se chargera du transport entre la pharmacie et le bloc opératoire.

– **Traçabilité**

Les dispositifs feront l'objet d'un étiquetage spécifique permettant l'identification de chaque DM incluant un numéro unique, le nom de l'essai clinique et de l'investigateur principal, la date limite d'usage et mettant en avant le NON-marquage CE.
Les éventuels EIG durant la chirurgie devront pouvoir être rattachés au numéro de l'électrode.

7.4. **Modalités d'attribution**

7.4.1. **Randomisation**

Il ne sera pas réalisé de randomisation

7.4.2. **Contrôle et suivi de l'observance**

Non applicable

7.4.3. **Modalités de modification du schéma thérapeutique**

L'enregistrement ECoG sera mené avec le DM comme en routine.
Seules les mesures d'impédance toutes les 10 minutes seront ajoutées.

7.4.4. **Traitements et/ou procédures autorisés et interdits pendant la recherche y compris les traitements de secours**

Non applicable

7.4.5. **Maintien de l'insu et Procédures de levée de l'insu**

Non applicable

8. PARAMETRES ETUDIES OU CRITERES D'EFFICACITE

8.1. **Définition des paramètres étudiés ou critères d'évaluation (principaux et secondaires) de l'efficacité et technique(s) de mesure**

8.1.1. **Critère d'évaluation principal (CEP) : effets secondaires graves liés à l'utilisation des microélectrodes Panaxium**

CEP1- Le critère d'évaluation principale est l'incidence des EIG dus à l'utilisation des microélectrodes Panaxium durant la chirurgie et les quatre jours suivants. Les EIG considérés sont : lésion corticale par l'électrode, infection, saignement, méningite aseptique, déficit neurologique dû à l'utilisation de l'électrode, prolongation de l'hospitalisation, hospitalisation secondaire, décès.

8.1.2. **Critères d'évaluation secondaires (CES) : qualité des enregistrements et praticité d'utilisation des microélectrodes Panaxium.**

Détermination de la qualité des enregistrements avec les microélectrodes Panaxium (en comparaison aux enregistrements avec des macroélectrodes traditionnelles pour les 10 premiers cas). Plusieurs critères électrophysiologiques seront utilisés :

CES1- Rapport signal / bruit (RSB) :
Le RSB traduit la capacité à enregistrer un événement en fonction de son amplitude différentielle par rapport à l'activité de fond. Il définit la performance de l'électrode.
Le RSB sera déterminé sur 20 évènements constitués par des activités épileptiques (pointes) et des oscillations physiologiques recueillis par microélectrode et par macroélectrode simultanément. La valeur moyenne du RSB pour les activités physiologiques et les pointes épileptiques sera comparée entre les électrodes. Dans la seconde partie de la recherche, le RSB sera déterminé à l'identique pour la seule microélectrode Panaxium.

CES2- Impédance des électrodes pendant la chirurgie. L'impédance est l'impédance électrique du circuit constitué par la grille d'électrodes, le cerveau du patient et l'électrode de référence. L'impédance décrit la capacité du DM pour conduire les signaux entre le cerveau du patient et le système d'enregistrement.
Les macroélectrodes DIXI et microélectrodes Panaxium ne seront pas comparées pour ce critère car leur impédance est par nature différente.

CES3- Détection des ripples (100-250 Hz) et des FR (250-600 Hz).
Les oscillations rapides seront détectées par le logiciel RippleLab, développé par M Le Van Quyen (Navarrete et al. 2016), sur les enregistrements par macro et microélectrodes. Elles seront quantifiées et comparées entre macroélectrode DIXI et microélectrodes Panaxium pour les 10 premiers cas : nombre de cycles enregistrables, durée des évènements, amplitude, fréquence moyenne et maximale.

CES4- Capacité à enregistrer des activités épileptiques spontanées (pointes et équivalent) ou post stimulation électrique directe (post-décharges).
L'amplitude, la durée et le seuil de détection de ces évènements seront analysés en comparant les données macro vs microélectrodes.

CES5- Capacité à enregistrer des activités physiologiques évoquées dans le *gamma (70-120 Hz*) pendant les tâches cognitives des investigations *neuropsychologiques* peropératoires. L'amplitude et les temps d'occurrence seront estimés pendant les phases d'activités et seront comparés entre les données macro vs microélectrodes.

CES6- Praticité d'utilisation et défectuosité éventuelle des microélectrodes Panaxium selon la perception des neurochirurgiens.
La praticité d'utilisation des microélectrodes au bloc opératoire évalué par les neurochirurgiens avec des questionnaires. Les questions concerneront la praticité d'utilisation, la sécurité d'utilisation pendant le dépôt des électrodes et durant l'enlèvement pour repositionnement. Le neurochirurgien remplira le questionnaire à la fin de la chirurgie.

8.1.3. Critères d'évaluation exploratoires (CEEX)

CEEX1- Capacité à enregistrer des activités multi unitaires
De par leur taille, leur contact direct avec le cortex et leur impédance, les microélectrodes peuvent enregistrer les potentiels d'action neuronaux en extracellulaire (nommés activité multi unitaire). Le système d'enregistrement utilisé (Neuralynx Atlas, marqué CE pour l'usage humain, fréquence d'échantillonnage de 40 000 Hz) peut recueillir ces évènements très brefs, durant environ 1 milliseconde. Ces activités ne sont pas enregistrables par macroélectrodes.
La capacité des microélectrodes Panaxium à recueillir des potentiels d'action issus d'un (Single Unit Activity) ou de plusieurs (Multi Unit Activity) sera analysée. Un résultat positif est attendu compte tenu des travaux déjà publiés d'une équipe américaine utilisant une technologie comparable (Khodagholy et al. 2015; 2016).

CEEX2- Corrélation entre activités enregistrées par µECoG et infiltration tumorale – concentration locale en oncométabolites. Nos travaux préalables ont montré qu'au sein des tissus épileptiques humains péritumoraux enregistrés *ex vivo*, il existait une co-localisation entre infiltration tumorale du cortex et production d'activités épileptiques (pointes et oscillations rapides) (J Pallud, Le Van Quyen, et al. 2014). Les tissus péritumoraux présentent une autre caractéristique : divers oncométabolites sont produits par les cellules de gliomes et s'accumulent en extracellulaire, notamment en péritumoral, ou ils affectent les processus de croissance et d'infiltration tumorale mais également l'épileptogénicité locale. Le glutamate, neurotransmetteur excitateur est ainsi produit par les gliomes (Gilles Huberfeld and Vecht 2016), alors que les gliomes de bas grades mutés pour l'enzyme IDH (80 % d'entre eux) libèrent du D2-Hydroxy-Glutamate (D2HG). Les tissus péritumoraux réséqués seront explorés histologiquement (infiltration tumorale) et biochimiquement (concentration de glutamate et de D2HG). Un marquage immunohistochimique sera effectué dans des échantillons de tissus corticaux et tumoraux recoupés afin d'établir le type et le grade de la tumeur selon la classification de l'OMS de 2016 (Louis et al. 2016) et de cartographier l'infiltration des cellules tumorales.

8.2. Méthodes et calendriers prévus pour mesurer, recueillir, analyser les paramètres étudiés (critères d'efficacité ou autres)

Calendrier
CEP : établi durant la chirurgie (V2) et les 2 visites (V3 et V4) post-opératoires
CES1-6 : établis au décours de la chirurgie (V2)
CEEX1-2 : établis au décours de la chirurgie (V2)

8.2.1. Critère d'évaluation principal (CEP) : effets secondaires graves liés à l'utilisation des microélectrodes Panaxium

CEP1- Le critère d'évaluation principale est l'incidence des EIG dus à l'utilisation des microélectrodes Panaxium durant la chirurgie et les quatre jours suivants. Les EIG considérés sont : lésion corticale par l'électrode, infection, saignement, méningite aseptique déficit neurologique dû à l'utilisation de l'électrode, décès.
Technique de mesure :
Durant les enregistrements de 10 premiers patients, les électrodes seront placées côte à côte, et pas exactement au même endroit, de façon à pouvoir différentier quel dispositif médical a été le responsable dans le cas de survenu d'un EI. Le film de l'acte opératoire nous permet de savoir à tout moment où a été placé chaque électrode.
Les EIG apparaissant entre la chirurgie et J4, date de sortie de l'hôpital, seront notés sur le dossier du patient et sur le CRF. La relation entre l'évènement indésirable et les microélectrodes Panaxium sera déterminée par l'investigateur selon son expérience clinique en considérant l'état neurologique du patient à H24 et à J4, à la sortie de l'hôpital. Pour les évènements indésirables graves, une seconde évaluation de la relation de causalité sera réalisée par le service de vigilance du promoteur. Les EIG non résolus à J4 à la sortie du patient de l'hôpital bénéficieront d'un suivi jusqu'à ce que l'EIG soit résolu.

8.2.2. Critères d'évaluation secondaires (CES) : qualité des enregistrements et praticité d'utilisation des microélectrodes Panaxium.

Détermination de la qualité des enregistrements avec les microélectrodes Panaxium (en comparaison aux enregistrements avec des macroélectrodes traditionnels pour les 10 premiers cas). Les microélectrodes Panaxium seront comparées aux macroélectrodes DIXI de référence : électrodes corticales IOM de diamètre 4 mm, épaisseur 0,8 mm, distance inter électrode 10 mm, largeur de la bande 10 mm, contacts en acier inoxydable.

CES1- Rapport signal / bruit (RSB) :
Le RSB sera déterminé pour les segments enregistrés manifestant soit une activité oscillatoire physiologique spontanée (theta 4-8 Hz, alpha 8-12 Hz, béta 15-30 Hz, gamma 40-120 Hz, dépendant de la région échantillonnée), soit une figure épileptique. Le RSB sera alors calculé comme le rapport entre la densité spectrale de puissance 1- de l'activité basale avant l'onde ou la pointe enregistrée et 2- l'onde (oscillation) ou la pointe (activité épileptique) enregistrée sur une fenêtre temporelle de même durée (Suarez-Perez et al. 2018):

$$RSB(f) = \frac{PSD_{Signal}\,(f)}{PSD_{Baseline}\,(f)}$$

Dans la première partie de l'étude, le signal d'intérêt sera identifié au niveau de la macroélectrode par un seuil d'amplitude (>50 µV). Le RSB sera ensuite déterminé sur 20 évènements, pour les microélectrodes et les macroélectrodes, au cours d'enregistrements simultanés de 1,5 minutes. Trois domaines fréquentiels seront utilisés pour les moyennages des RSB : les fréquences basses (3-30 Hz), les fréquences moyennes (30-200 Hz) et les fréquences hautes (200-1500 Hz). La valeur moyenne du RSB pour les activités physiologiques et les pointes épileptiques sera comparée entre les microélectrodes et les macroélectrodes. Dans la seconde partie de l'étude, le RSB sera déterminé de manière identique pour la seule microélectrode Panaxium.

CES2- Impédance des électrodes pendant la chirurgie.
L'impédance est l'impédance électrique du circuit constitué par la grille d'électrodes, le cerveau du patient et l'électrode de référence. L'impédance décrit la capacité du DM pour conduire les signaux entre le cerveau du patient et le système d'enregistrement. Elle sera mesurée sur une bande de fréquence entre 10 Hz et 10 kHz en utilisant le système d'analyse « Minirator » (Neuralynx, Bozeman, Montana, USA). Cette mesure sera effectuée au début de l'enregistrement puis toutes

les 10 minutes durant la totalité de l'enregistrement pour les 10 premiers patients puis au début et la fin de l'enregistrement pour la seconde série de patients.
Les macroélectrodes DIXI et microélectrodes Panaxium ne seront pas comparées pour ce critère car leur impédance est par nature différente.

CES3- Détection des ripples (100-250 Hz) et des FR (250-600 Hz).
Les oscillations rapides correspondent à de brèves activités à haute fréquence d'identification difficile du fait notamment de leur faible amplitude et de leur masquage par les activités plus lentes. Les ripples sont physiologiques mais les oscillations FR sont réputées spécifiques et localisatrices des zones épileptiques. Elles sont presque exclusivement enregistrées par EEG cortical ou intracrânien et la capacité à les enregistrer reflète la qualité du système d'enregistrement (électrode et système de recueil du signal) (Zijlmans et al. 2017).
Les oscillations rapides seront détectées par le logiciel RippleLab, développé par M Le Van Quyen (Navarrete et al. 2016), sur les enregistrements par macro et microélectrodes. Quatre critères seront utilisés pour l'identification des FR : 1- Une oscillation visible à la fois dans les données brutes et dans le signal filtré (filtre passe bande de 200 à 600 Hz), 2- l'amplitude doit être d'amplitude significative par rapport à l'activité de fond (>3 déviations standards), 3- avoir au moins quatre cycles stables d'oscillations et 4- une analyse en temps/fréquence doit présenter des maxima locaux entre 250 et 500 Hz. A partir de ces critères, les paramètres électrophysiologiques suivantes seront quantifiés pour les événements identifiés : nombre de cycles enregistrables, durée des évènements, amplitude, fréquence moyenne et maximale, extension spatiale, relations temporelles avec les pointes intercritiques. Ces paramètres seront quantifiés et comparés entre macroélectrode DIXI et microélectrodes Panaxium pour les 10 premiers cas.
Seront quantifiés : nombre de cycles enregistrables, durée des évènements, amplitude, fréquence moyenne et maximale.

CES4- Capacité à enregistrer des activités épileptiques spontanées (pointes et équivalent) ou post stimulation électrique directe (post-décharges).
Les pointes seront détectées visuellement lors de l'enregistrement et par relecture des enregistrements.
Elles seront définies selon les critères de l'International Federation of Clinical Neurophysiology (Kural et al. 2020) par l'existence de 4/6 critères au moins (nous éliminerons cependant le critère 6 qui correspond à un enregistrement EEG de scalp) :

1. Di- or tri-phasic waves with sharp or spiky morphology (i.e. pointed peak)
2. Different wave-duration than the ongoing background activity, either shorter or longer
3. Asymmetry of the waveform: a sharply rising ascending phase and a more slowly decaying descending phase, or vice versa
4. The transient is followed by an associated slow after-wave
5. The background activity surrounding epileptiform discharges is disrupted by the presence of the epileptiform discharges
6. Distribution of the negative and positive potentials on the scalp suggests a source of the signal in the brain, corresponding to a radial, oblique or tangential orientation of the source

L'amplitude, la durée et le seuil de détection de ces évènements seront analysés en comparant les données macro vs microélectrodes.

CES5 Capacité à enregistrer des activités physiologiques gamma évoquées (*70-120 Hz*) pendant les tâches cognitives des investigations *neuropsychologiques* peropératoires. Afin de pouvoir interpréter correctement les variations du spectre de l'EEG lors des périodes d'activité (A), il est nécessaire de prendre un intervalle de référence (R) quelques secondes avant le début de l'évènement. La quantification des variations de la puissance dans la bande gamma est établie par la formule suivante : $ERD\% = (A - R)/ R \times 100$. Un pourcentage négatif est significatif d'une désynchronisation alors qu'un positif est significatif d'une synchronisation LACHAUX 2012.

CES6- Praticité d'utilisation et défectuosité éventuelle des microélectrodes Panaxium selon la perception des neurochirurgiens.
La praticité d'utilisation des microélectrodes au bloc opératoire évalué par les neurochirurgiens avec des questionnaires. Les questions concerneront la praticité d'utilisation, la sécurité d'utilisation

pendant le dépôt des électrodes et durant l'enlèvement pour repositionnement. Le neurochirurgien remplira le questionnaire à la fin de la chirurgie. Les défectuosités possibles de l'électrode seront : un déchirement, une perte de substance, un échauffement, une perte du signal, une déconnexion du système d'enregistrement ou toute autre défectuosité constatée du DM.

8.2.3. Critères d'évaluation exploratoires (CEEX)

CEEX1- Capacité à enregistrer des activités multi unitaires
De par leur taille, leur contact direct avec le cortex et leur impédance, les microélectrodes peuvent enregistrer les potentiels d'action neuronaux en extracellulaire. Le système d'enregistrement utilisé (Neuralynx Atlas, marqué CE pour l'usage humain, fréquence d'échantillonnage de 40 000 Hz) peut recueillir ces évènements très brefs, durant environ 1miliseconde. Ces activités ne sont pas enregistrables par macroélectrodes.
La capacité des microélectrodes Panaxium à recueillir des potentiels d'action issus d'un neurone (Single Unit Activity) ou de plusieurs (Multi Unit Activity) sera analysée par le logiciel de tri des *potentiels d'action* (*spike sorting* en anglais) « *KlustaKwik »* (Harris et al. 2000). A partir de la superposition des formes détectées, plusieurs paramètres vont être identifiés pour juger de la qualité de l'identification des neurones individuels : 1- la forme des potentiels d'action (durée et amplitude du pic), 2- la stationnarité et la stabilité temporelle des amplitudes, 3- les violations de la période réfractaire (en général 2.5 ms) à l'aide d'un autocorrélogramme (autocorrélation des temps de décharge des neurones), 4- la corrélation entre les temps de décharge des neurones de plusieurs groupes à l'aide d'un cross-corrélogramme (synchronisation des temps de décharge de plusieurs neurones). Un résultat positif est attendu compte tenu des travaux déjà publiés d'une équipe américaine utilisant une technologie comparable (Khodagholy et al. 2015; 2016).

CEEX2- Corrélation entre activités enregistrées par µECoG et infiltration tumorale – concentration locales en oncométabolites. Nos travaux préalables ont montré qu'au sein des tissus épileptiques humains péritumoraux enregistrés *ex vivo*, il existait une co-localisation entre infiltration tumorale du cortex et production d'activités épileptiques (pointes et oscillations rapides) (J Pallud, Le Van Quyen, et al. 2014). Les tissus péritumoraux présentent une autre caractéristique : divers oncométabolites sont produits par les cellules de gliomes et s'accumulent en extracellulaire, notamment en péritumoral, ou ils affectent les processus de croissance et d'infiltration tumorale mais également l'épileptogénicité locale. Le glutamate, neurotransmetteur excitateur est ainsi produit par les gliomes (Gilles Huberfeld and Vecht 2016), alors que les gliomes de bas grades mutés pour l'enzyme IDH (80 % d'entre eux) libèrent du D2-Hydroxy-Glutamate (D2HG).
Certaines zones cartographiées en ECoG seront réséquées dans le cadre du soin et pourront dès lors être étudiées *ex vivo* au laboratoire. Nous établirons des corrélations entre activités électrophysiologiques et caractéristiques histochimiques des tissus.
Étude histologique des tissus. Un marquage immunohistochimique sera effectué dans des échantillons de tissus corticaux et tumoraux recoupés afin d'établir le type et le grade de la tumeur selon la classification de l'OMS de 2016 (Louis et al. 2016) et de cartographier l'infiltration des cellules tumorales : Hématoxyline-éosine, Ki67, NeuN, OLIG2, MIB-1, GFAP, IDH(R123H). L'infiltration des cellules tumorales sera mesurée en comptant le nombre de cellules tumorales par champ de haute puissance x 400, 0,2 mm2. Les mutations IDH 1 et 2 (en plus de la mutation IDH1R132H) seront identifiées par séquençage de gènes. La localisation de l'infiltration tumorale sera corrélée aux activités enregistrées in vivo.
Dosage tissulaire du glutamate et du D2HG. Une portion de 1/2 cm^3 sera congelée pour mesurer les concentrations tissulaires de glutamate et de D2HG par chromatographie en phase gazeuse couplée à la spectroscopie de masse (Gleize et al. 2015).

9. ECHANTILLONS BIOLOGIQUES

Dans le cadre d'objectifs d'étude exploratoires, des échantillons biologiques seront prélevés en V2 : dans le cadre du schéma de résection normal du chirurgien, qui consiste à réséquer le tissu tumoral mais également le maximum de tissus péritumoraux, infiltrés par des cellules tumorales au-delà des limites macroscopiques et IRM de la lésion, après cartographie fonctionnelle des régions péritumorales, des tissus péritumoraux, non nécessaires au diagnostic neuropathologique, réséqués dans le cadre du soin, seront étudiés afin de corréler les activités électrophysiologiques avec les données histologiques (infiltration tumorale) et biochimiques (oncométabolites).

9.1. **Conditions de prélèvement**

Les tissus cérébraux, corticaux et / ou lésionnels sont prélevés par le neurochirurgien, strictement dans le cadre de la résection thérapeutique, et consisteront en des prélèvements non indispensables pour l'analyse neuropathologique. Le volume de tissu est variable, selon l'étendue de la resection et laissé à l'appréciation du neurochirurgien. Le fragment de tissu est déposé dès l'exérèse dans une bouteille remplie d'une solution d'aCSF-sucrose refroidie à 4°C ou bien dans un récipient sec pour congélation immédiate.
Une webcam filme, de manière routinière, la chirurgie, se limitant au champ opératoire (sans filmer le visage) pour localiser les électrodes en cas d'enregistrement ECoG : elle permettra de localiser le tissu prélevé. En l'absence de film, la localisation du prélèvement pourra être précisée par une photo du champ opératoire (ne permettant pas de visualiser le visage du patient).

9.2. **Modalités de codage et d'étiquetage**

Les prélèvements sont désignés par un numéro de identique à celui de codage du patient : 3 lettres de l'hôpital (PSL : Pitié-Salpêtrière, STA : Sainte-Anne, FOR : Hôpital Fondation Adolphe de Rothschild) suivi d'un numéro (ordre d'inclusion pour chaque hôpital). Les prélèvements seront numérotés par ordre croissant et leur localisation sera connue du fait du film opératoire.

9.3. **Traitement des échantillons**

Les échantillons seront fixés en paraformaldéhyde (PFA) pour étude histologique ou congelés (azote liquide) pour étude biochimique.

9.4. **Transport**

Une fois le prélèvement recueilli à l'intérieur de la bouteille, il est placé dans un container dédié aux échantillons biologiques, dans la glace. Le chercheur du laboratoire l'achemine alors directement au laboratoire (Collège de France).

9.5. **Stockage et/ou destruction**

Une fois finalisées les différentes études (histologie, biochimie et enregistrements électrophysiologiques), les tissus seront conservés sur la forme d'échantillons biologiques. Si jamais un prélèvement n'est pas utilisé dans sa totalité, il sera directement conservé.

Ils seront placés dans un congélateur à -80°C, au Collège de France, dédié, sous la responsabilité de l'investigateur principal pour la durée de de l'étude.

9.6. **Description du système qualité de la collection**

Locaux :

Adresse : 11 place Marcelin Berthelot - 75005 Paris

Surface dédiée aux activités : 40 m^2.
Procédure de nettoyage et décontamination des locaux et des équipements : les surfaces de la pièce sont nettoyées tous les deux mois avec du Surfanios par le responsable de la pièce. Les

incubateurs et les bains-marie sont nettoyés tous les mois avec Anioxy-spray. Les PSM sont nettoyés après chaque utilisation avec anioxy-spray.
Des procédures spécifiques de nettoyages ont été mises en place en cas de renversement accidentel sur les différentes surfaces.

Systèmes et circuits d'élimination des déchets : les déchets solides sont stockés dans des conteneurs pour déchets biologiques et autoclavés à la sortie de la pièce avant de suivre la filière d'évacuation des DASRI.
Les déchets liquides sont aussi autoclavés avec le programme dédié à la sortie de la pièce et éliminés dans la filière dédiée aux déchets biologiques liquides.

Équipements techniques utilisés pour les activités faisant l'objet de la déclaration :

Description des équipements et matériels dédiés aux activités :
- de préparation :
PSM : flufrance type ESIBI1012NFUVGPF
Centrifugeuse : BECKMAN GS-15R
Microscope: Floid Cell imaging station Lifetechnologie et NIKKON TMS 5
Vibratome LEICA VT1200S
Chambre de stockage en interface BS2 5

- de conservation : congélateur -80°C

- d'utilisation :
PSM: flufrance type ESIBI1012NFUVGPF
Incubateur: series800DH Co2 incubator Thermofisher
Microscope à fluorescence et biphotonique

Dispositif de sécurité pour la conservation :
La pièce de stockage (ventilée) et le congélateur peuvent être fermés à clef. L'accès au laboratoire est sécurisé (carte d'accès électronique).

Personnel.

Personnes affectées aux activités :
Gilles Huberfeld, MCUPH
Nathalie Rouach, DR1 INSERM
Giampaolo Milior, postdoc
Elena Dossi, postdoc
Belén Diaz-Fernandez, PhD
Richard Barillet, PhD

Formations suivies par le personnel dans les domaines touchant aux activités concernées (transport de matières dangereuses, assurance qualité, préparation des échantillons, gestion de bases de données, autoclave, travail en P2, etc) : formation interne au risque biologique, à la préparation des échantillons humains (gants, absence de projection ...) aux enregistrements, à la conservation et à l'élimination des déchets. Une procédure de manipulation des tissus humain postopératoires est affichée et distribuée à tout expérimentateur.

Personne responsable de la protection du personnel sur le site :
Xavier Blondeau, Responsable du Pôle Hygiène Sécurité
Téléphone : 01 44 27 11 18
Adresse électronique : xavier.blondeau@college-de-france.fr

Procédure de protection des personnels amenés à manipuler les échantillons
Risque biologique.
Une sérologie hépatite C du patient est réalisée par l'équipe neurochirurgicale. En cas de positivité, il n'y a pas de prélèvement pour la recherche.

Port de blouse et de gants. Lunettes si risque de projection. Utilisation de matériel à usage unique. Lavage des mains.
Pièces et matériel dédié à l'étude du tissu humain.
Statut infectieux des pièces opératoire : information des chirurgiens si connu.

Gestion des activités

Description des moyens utilisés pour la gestion des échantillons ou des collections et des données associées : Cahier de laboratoire. Stockage informatique sur ordinateur et serveurs protégés.

Système de Codage et règles de confidentialité Anonymisation des tissus : 3 lettres de l'hôpital d'origine + numero croissant de tissu. Conservation protégée du nom.

Modalités d'étiquetage et d'identification des ressources : Identification des fichiers (imagerie, électrophysiologie, biochimie) et des tissus conservés selon la procédure d'anonymisation

Modalités de gestion des documents justificatifs du recueil de consentement ou de l'absence d'opposition des donneurs : Information directe et consentement obtenu auprès des patients par le chirurgien (conservés dans le dossier médical)

Situation au regard de la législation sur le traitement de données à caractère personnel : Déclaration CNIL 2217233, délégué à la protection des données : dpo@inserm.fr

10. VIGILANCE DE LA RECHERCHE

10.1. Définitions

En application de la norme ISO 14155

10.1.1. Evénements Indésirables (EI)

Toute manifestation nocive, toute maladie ou blessure non intentionnelle ou tout signe clinique malencontreux, y compris un résultat de laboratoire anormal, chez des participants, des utilisateurs ou d'autres personnes, dans le cadre d'une investigation clinique, lié ou non au dispositif médical faisant l'objet d'une investigation clinique.
NOTE : Cette définition comprend les événements liés au dispositif médical sous investigation ou au comparateur et les événements liés aux procédures impliquées.

Un événement indésirable inclut :

- toute augmentation de fréquence ou d'intensité d'un événement ou d'une condition préexistante
- toute condition (même si elle était présente avant le début de l'essai) détectée après l'administration du médicament expérimental
-

Un événement indésirable n'inclut pas :

- une procédure médicale ou chirurgicale (seule la condition ayant conduit à une telle procédure est un événement indésirable)
- une pathologie préexistante ou détectée avant la première prise du traitement de l'essai et qui ne s'aggrave pas
- un événement lié à la pathologie étudiée

10.1.2. Effet indésirable du dispositif (EID)

Toute réaction nocive et non désirée lié à l'utilisation du dispositif en cours d'investigation ou tout incident qui aurait pu entraîner cette réaction si une action appropriée n'avait pas été effectuée, chez une personne qui se prête à la recherche ou chez l'utilisateur du DM, ou tout effet lié à une

défectuosité ou une altération du DM et néfaste pour la santé d'une personne qui se prête à la recherche.
NOTE 1 Cette définition inclut tout événement indésirable résultant d'insuffisances ou d'inadéquations dans les instructions d'utilisation, le déploiement, l'implantation, l'installation et le fonctionnement, ou tout dysfonctionnement du dispositif médical sous investigation.
NOTE 2 Cette définition inclut tout événement résultant d'une erreur d'utilisation ou d'un usage impropre intentionnel du dispositif médical sous investigation.

10.1.3. Evénement Indésirable Grave (EIG)

Tout événement ou effet indésirable répond à la définition de "grave" s'il :

- entraîne la mort ;
- une dégradation grave de l'état de santé du participant, laquelle est à l'origine :
  - i) d'une maladie ou blessure mettant en danger la vie du participant ;
  - ii) d'une déficience permanente d'une structure ou fonction anatomique ;
  - iii) d'une hospitalisation ou de la prolongation de l'hospitalisation du participant;
  - iv) d'une intervention médicale ou chirurgicale visant à prévenir toute maladie ou blessure mettant en danger la vie du participant ou toute déficience permanente d'une structure ou fonction anatomique ;
  - v) d'une maladie chronique ;
- une souffrance fœtale, la mort du fœtus, des déficiences physiques ou mentales congénitales ou une malformation congénitale.met en danger la vie du participant (correspond à un événement au cours duquel le participant est à risque de décès au moment de l'événement; cela ne correspond pas à un événement qui hypothétiquement aurait pu causer le décès s'il avait été plus sévère);
- est un "événement d'intérêt spécial". Pour cette recherche, les évènements d'intérêt spécial sont définis comme suit : lésion corticale par l'électrode, infection, saignement, méningite aseptique déficit neurologique dû à l'utilisation de l'électrode.

NOTE Une hospitalisation prévue en raison d'une affection préexistante ou une procédure requise par le plan d'investigation clinique, sans détérioration grave de la santé, n'est pas considérée comme un événement indésirable grave.

10.1.4. Effet Indésirable Grave Inattendu du dispositif (EIGID inattendu)

Tout effet indésirable dont la nature, la sévérité, la fréquence ou l'évolution ne concorde pas avec les informations de référence relatives au DM utilisé au cours de la recherche dans la version en cours de la brochure investigateur. Les procédures associées à l'utilisation d'un dispositif doivent être abordées dans l'évaluation des risques, ce qui permet de déterminer si les EIG liés à la procédure sont ou non des effets indésirables graves inattendus du dispositif. Les EIG liés aux procédures imposées par le plan d'investigation clinique mais pas avec l'utilisation du dispositif ne doivent pas être considérés comme des effets indésirables graves du dispositif.

10.1.5. Défectuosité du dispositif

Tout défaut d'un dispositif médical expérimental liée à son identité, sa qualité, sa durabilité, sa fiabilité, sa sécurité ou ses performances. Cela peut inclure des dysfonctionnements, des erreurs d'utilisation ou des informations inadéquates dans les informations fournies par le fabricant.

10.2. Responsabilités de l'investigateur

10.2.1 Notification des évènements indésirables graves et non graves

Que faut-il déclarer ?
L'investigateur doit reporter au promoteur, sans délai (immédiatement), et pas plus tard que dans les 3 jours calendaires à compter du moment où il en a eu connaissance :

- tout événement indésirable non grave, qu'il soit lié ou non au DM objet de la recherche sur le formulaire de "Déclaration initiale d'événement indésirable grave" (situé dans la section EIG du cahier d'observation).

- reporter tout EIG et événement d'intérêt spécial, qu'il soit lié ou non au DM objet de la recherche sur le formulaire "Déclaration initiale d'un EIG"

- Reporter toute défectuosité de l'appareil qui aurait pu conduire à un SAE si :
    - o aucune mesure appropriée n'avait été prise
    - o aucune intervention n'avait pas été faite
    - o les circonstances avaient été moins favorables

- adresser au promoteur, par email, tout document pertinent (compte-rendu d'hospitalisation, analyses biologiques, etc) après avoir supprimé toute mention du nom du participant et indiqué le numéro d'identification du participant dans la recherche

- suivre tout EIG jusqu'à la résolution de l'événement indésirable, une stabilisation à un niveau jugé acceptable par l'investigateur, ou le retour à l'état antérieur (même si le participant est sorti de l'essai, lorsque l'EIG est possiblement lié au DM expérimental)

- reporter toute nouvelle information pertinente sur un EI, un EIG, un événement d'intérêt spécial ou une défectuosité

EXCEPTIONS : EIG ne nécessitant pas de notification immédiate au promoteur :

- Pathologie préexistante ou détectée avant la réalisation des actes pratiqués pour les besoins de la recherche et qui ne s'aggrave pas.
- Événements biologiques de grade 4 détectés entre la signature du consentement par le participant à la recherche et réalisation des actes pratiqués pour les besoins de la recherche
- Les crises épileptiques déclenchées par la stimulation électrique de la cartographie fonctionnelle et enregistrées par les électrodes.

Tout événement indésirable grave doit être déclaré, s'il survient pour un participant à la recherche, pendant toute la durée de la recherche, c'est-à-dire à partir de la date de signature du consentement et jusqu'à la fin de suivi du participant.
Les événements indésirables graves subis par un participant après la fin de suivi (ex: effets graves pouvant apparaître à grande distance de l'exposition au DM, tels des cancers ou des anomalies congénitales) doivent être notifiés au promoteur si l'investigateur a connaissance de ces derniers. L'investigateur n'est pas tenu de suivre activement les participants pour détecter des événements indésirables une fois l'essai terminé, sauf indication contraire dans le protocole.

Procédure de notification des EIG
Notification des EIG via l'eCRF : Lorsque le formulaire de déclaration d'un EIG est complété, daté et signé par l'investigateur sur l'eCRF, un email est immédiatement envoyé au service de pharmacovigilance Inserm-ANRS ainsi qu'au chef de projet. Notification papier : En cas d'eCRF indisponible ou pour tout document pertinent lié à l'EIG, l'investigateur adresse les documents au service de pharmacovigilance Inserm-ANRS, par fax: 01 53 94 60 02 ou par email: pharmacovigilance.prc@inserm.fr Tout EIG déclaré selon le circuit papier doit être réenregistré dans la section appropriée du CRF.

10.2.2. Evaluation des EI graves et non graves

L'événement indésirable

L'investigateur doit documenter au mieux l'événement indésirable et en donner, si possible, le diagnostic médical.
La date de survenue de l'événement indésirable doit être antérieure (ou identique) à la date de survenue de la gravité.
En cas de procédure médicale ou chirurgicale (*ex: chirurgie, endoscopie, extraction dentaire, transfusion*…), l'investigateur doit noter l'événement ayant conduit à une telle procédure.

L'intensité

L'intensité de tous les EI (graves et non graves) doit être évaluée par l'investigateur selon l'échelle de gradation ci-dessous et reportée par l'investigateur dans le cahier d'observation.

Grade 1	**Légère**	gêne légère ou transitoire, sans limitation de l'activité quotidienne habituelle ; ne nécessite pas d'intervention médicale ou un traitement correcteur.
Grade 2	**Modéré**	limitation partielle de l'activité quotidienne habituelle ; une intervention médicale ou un traitement correcteur ne sont pas obligatoirement nécessaires.
Grade 3	**Sévère**	limitation de l'activité quotidienne habituelle ; nécessite une intervention médicale et un traitement correcteur, hospitalisation possible.
Grade 4	**Menace vitale**	activité très limitée ; nécessitant une intervention médicale et un traitement correcteur, presque toujours en milieu hospitalier.

La gravité

L'investigateur évalue chaque événement indésirable au regard de sa gravité (cf. chapitre définition d'un EIG).
Le décès de cause connue d'un participant à la recherche doit être notifié comme l'évolution d'un événement indésirable et non comme un événement indésirable. Si la cause de décès n'est pas connue, le décès doit être notifié comme "décès de cause inconnue".

Le lien de causalité

L'investigateur doit évaluer le lien de causalité entre l'événement indésirable et le DM, l'intervention mise en place pour la recherche (correspond ici à la chirurgie) et les éventuels traitements associés pris par le participant à la recherche, en utilisant les définitions ci-dessous.

Le lien de causalité est classé en 4 niveaux : non lié, lien possible, lien probable, lien certain (conformément aux définitions de la recommandation MDCG-2020-10/1).

Lien de causalité	Description
Non lié	Il n'y a aucune preuve de lien de causalité entre la survenue de l'événement et l'utilisation du dispositif expérimental ou les procédures liées à l'application du dispositif expérimental.
Possible	Le lien de causalité avec l'utilisation du dispositif expérimental ou du comparateur, ou avec les procédures d'investigation, est faible mais ne peut être totalement exclue. Des causes alternatives sont possibles (par exemple, une maladie/un état clinique sous-jacent ou concomitant ou/et un effet d'un autre dispositif, médicament ou traitement). Les cas où le lien de causalité ne peut pas être évalué ou les cas où aucune information n'a été obtenue doivent également être classés en lien possible.
Probable	Le lien de causalité avec l'utilisation du dispositif expérimental ou du comparateur, ou avec les procédures d'investigation, semble pertinent (il existe des preuves

	suggérant un lien de causalité), et/ou l'événement ne peut être raisonnablement expliqué par une autre cause (l'influence d'autres facteurs est peu probable).
Certain	- L'événement est un effet secondaire connu de dispositifs similaires. - L'événement survient dans un délai compatible avec l'utilisation/l'application ou les procédures du dispositif expérimental. - L'événement implique un site corporel ou un organe sur lequel le dispositif ou les procédures d'investigation sont appliqués ou ont un effet. - L'événement indésirable suit un schéma de réponse connu avec le dispositif médical (si le schéma de réponse est déjà connu). - L'arrêt de l'utilisation du dispositif médical (ou la réduction du niveau d'activation/d'exposition) et la reprise de son utilisation (ou l'augmentation du niveau d'activation/d'exposition), impact sur l'événement indésirable grave (lorsque cliniquement faisable). - L'événement ne peut pas être expliqué par d'autres causes (maladie/état clinique sous-jacent ou concomitant, effet d'un autre dispositif, médicament ou traitement). - L'événement est dû à une erreur d'utilisation. - l'événement dépend d'un faux résultat donné par le dispositif expérimental utilisé pour le diagnostic, si applicable ; Afin d'établir le lien, tous les critères énumérés ci-dessus peuvent ne pas être remplis en même temps, selon le type de dispositif/de procédures et l'événement indésirable grave.

Le caractère attendu ou inattendu

L'évaluation du caractère attendu/inattendu est généralement effectuée par le promoteur.
Le caractère attendu/inattendu d'un effet indésirable grave est évalué à la lumière des informations de référence décrites dans la brochure pour l'investigateur.

L'évolution de l'événement indésirable

L'évolution de l'événement au moment de la notification doit être indiquée sur le formulaire de déclaration initiale d'EIG.
Toute modification de l'évolution de l'événement (résolution, retour à l'état antérieur, aggravation …) doit être reportée sur un formulaire de déclaration complémentaire d'EIG.

10.2.4. Risques potentiels du DM et de la recherche, et conduite à tenir en cas de survenue d'événement indésirable

Les investigateurs doivent retrouver toutes les informations disponibles pour déterminer la causalité, la gravité et les conséquences de l'EI et pour différentier s'il s'agit d'un EIG qui nécessite de prévenir immédiatement le promoteur. Tous les EI seront documentés sur les documents sources et ensuite sur l'e-CRF, incluant une description de l'évènement (symptômes, signes et diagnostic), de la date de début, de la résolution, gravité, étiologie et mesures prises pour le résoudre.

Dans le cadre de cette étude, les risques identifiés sont les suivants :

- Méningite aseptique (risque de la chirurgie ou du DM)
- Altération cognitive (risque de la chirurgie)
- Fuite de liquide céphalorachidien (risque de la chirurgie)
- Hémorragie intracrânien (risque de la chirurgie ou du DM)
- Infection (risque de la chirurgie ou du DM)
- Nausées et vomissements (risque de la chirurgie)
- Déficit neurologique (risque de la chirurgie ou du DM)
- Pneumencéphalie (risque de la chirurgie)

- Accident vasculaire cérébral (risque de la chirurgie)
- Contusion cérébrale corticale (risque de la chirurgie ou du DM)

Effets indésirables graves anticipés :

Les EIG anticipés par rapport à l'utilisation des microélectrodes Panaxium sont les suivants :

- Méningite aseptique
- Hémorragie intracrânienne
- Infection
- Déficit neurologique
- Contusion corticale
- Prolongation de l'hospitalisation pour cause d'EIG lié au DM
- Ré hospitalisation pour cause d'EIG lié au DM
-

Tous les EIG en rapport avec l'utilisation des microélectrodes Panaxium ont été pris en compte pendant la phase de développement et ils le seront pendant la phase d'investigation clinique de la façon suivante :

- Hémorragie intracrânienne : plusieurs mesures de contrôle ont été implémentées pour éviter les risques hémorragiques, comme par exemple l'utilisation d'un matériel mou (Parylène) en contact avec la surface cérébrale, nettement moins traumatisant, notamment du fait de l'absence de frottement, que les macroélectrodes cliniques actuelles. En outre, les tests de vérification du design et les tests précliniques sur des animaux ont montré que les microélectrodes Panaxium résistent aux stress élastiques et de torsion qui peuvent avoir lieu pendant l'utilisation. Quoi qu'il en soit les bords de l'électrodes ne sont absolument pas vulnérants.

- Infection : le risque est limité par la procédure de nettoyage et stérilisation gazeuse des électrodes puis d'étanchéisation stérile. Les électrodes sont bien sûr à usage unique. Elles seront connectées au système EEG, no stérile, à distance du champ opératoire.

- Méningite aseptique : le risque a été pris en compte en utilisant des matières biocompatibles (Parylène). De plus, les tests de vérification et les tests précliniques sur des modèles animaux ont montré que les microélectrodes Panaxium sont résistantes au détachement de fragments qui pourraient causer une méningite aseptique.

- Déficit neurologique : le risque d'un déficit neurologique serait lié aux microélectrodes de façon indirecte, puis qu'il serait la conséquence d'une lésion cérébrale qui donnerait lieu à une hémorragie.

Cas particulier des crises épileptiques : le cortex péritumoral exposé au cours de la chirurgie des gliomes produit des activités épileptiques chez la majorité des patients et la procédure clinique de stimulation électrique corticale peut elle-même générer des crises. Il est reconnu que les macroélectrodes cliniques ne sont pas épileptogènes et servent bien évidement à détecter les crises. Les microélectrodes Panaxium n'ont pas montré d'effet épileptogène chez l'animal et au cours de leur utilisation humaine (Khodagholy et al. 2015; 2016). Dans ce contexte, nous n'utiliserons pas les crises épileptiques peropératoire comme EIG possiblement liés à l'usage du DM. Le taux de crise peropératoire est évalué à 0,6% (609 patients) (Takami, Khoshnood, and Bernstein 2020), 1,9% (1693 patients) (Oushy et al. 2018) 3,3% (611 patients) (Hervey-Jumper et al. 2015), 3,5% (202 patients) (Zanello et al. 2020), 7,3 % (41 patients) (Y.-C. Wang et al. 2019) des patients pour des séries récentes. Poolées, ces données représentent un taux de crises peropératoires de 2,1%. Cependant, l'incidence est très variable et une méta analyse récente, incluant des données anciennes indique un taux de crise peropératoire durant la chirurgie en condition éveillée de gliomes de 8% (Yuan et al. 2019).

Les défectuosités possibles de l'électrode seront : un déchirement, une perte de substance, un échauffement, une perte du signal, une déconnexion du système d'enregistrement ou toute autre défectuosité constatée du DM.

Précaution d'emploi :

De manière général, les précautions à prendre pour limiter les risques d'EIG ou de défectuosité sont :

- Ne pas réutiliser le DM afin d'éviter tout risque d'infection, de maladie de Creutzfeld-Jacob et de contact non fonctionnel du DM avec le cortex cérébral.
- Eviter tout contact entre le solvant acétone et l'électrode
- Eviter tout excès de sang ou de liquide emprisonné sous les grilles d'électrodes afin de ne pas compromettre la qualité de l'enregistrement.
- Déconnecter le dispositif de surveillance en cas de défibrillation cardiaque

Si à la sortie du patient de l'étude (soit à J4 à la sortie de l'hôpital), un EIG en rapport avec l'utilisation des microélectrodes Panaxium est encore en cours, le patient sera suivi jusqu'à la résolution de cet EIG en rapport avec les microélectrodes Panaxium (visite supplémentaire, VS). Si durant la visite finale un EI sans rapport avec les microélectrodes Panaxium est en cours, celui sera suivi selon les soins standard et le patient sortira de l'étude.

Prise en charge en cas de survenue d'un événement indésirable :

Une prise en charge médicale adéquate de l'EIG doit être mise en place. En cas d'hématome intracérébral, il peut être décidé par le médecin la simple surveillance clinique et radiologique, ou en cas de signe de gravité une intervention neurochirurgicale évacuatrice. En cas d'infection cérébrale avérée, un geste chirurgical pourra être décidé, en plus d'une antibiothérapie. En cas de déficit neurologique, une rééducation spécifique sera entreprise.

Après sa notification initiale, l'EIG doit obligatoirement faire l'objet d'un suivi jusqu'à sa résolution c'est à dire une stabilisation à un niveau jugé acceptable par l'investigateur ou le retour à l'état antérieur, même si le patient est sorti de l'essai.
Tous les EIG seront reportés dans le cahier d'observation. L'investigateur jugera de la causalité par rapport aux procédures de la recherche et à la pathologie.

Tout EIG sera étudié par le DSMB qui devra valider la poursuite de l'étude.

10.3. Responsabilités du promoteur

10.3.1. Enregistrement et évaluation des EIG

Le promoteur évalue le lien de causalité et le caractère attendu ou inattendu entre tous les événements indésirables graves et le DM faisant l'objet de la recherche, la procédure de mise en œuvre du DM, la recherche ou les traitements associés pris par le patient.
En l'absence d'informations sur la causalité de la part de l'investigateur, le promoteur devrait consulter celui-ci et l'encourager à émettre un avis à cet égard.

10.3.2. Déclaration des données de sécurité aux autorités nationales compétentes et au comité d'éthique

Le promoteur notifie à l'ANSM et le cas échéant, à toutes les autorités nationales compétentes des Etats membres de l'Union européenne où l'essai est mené :

a) tout événement indésirable grave entretenant, avec le DM faisant l'objet de l'investigation, le DM comparateur ou la procédure d'investigation, un lien de causalité avéré ou raisonnablement envisageable ;
b) toute défectuosité d'un DM qui aurait pu déboucher sur un événement indésirable grave en l'absence de mesures appropriées ou d'une intervention, ou si les circonstances avaient été moins favorables ;
c) tout nouvel élément concernant un événement visé aux points a) et b).

Le promoteur déclare aux autorités nationales compétentes, où l'essai est mené, en utilisant le tableau de déclaration spécifique aux recherches portant sur un dispositif médical :

- Pour les événements ayant entraîné la mort ou un risque de mort imminente, une blessure ou maladie grave et qui requièrent une action corrective rapide pour les participants/patients, utilisateurs ou d'autres personnes, ou toute nouvelle information ces cas : sans délai (immédiatement), et pas plus tard que 2 jours calendaires à compter du jour où le promoteur a eu connaissance de l'évènement à déclarer ou d'une nouvelle information concernant un événement déjà déclaré.
  Cela inclut les événements qui sont de nature importante et inattendue, de sorte qu'ils deviennent alarmants en tant que danger potentiel pour la santé publique. Cela inclut également la survenue de plusieurs décès à de courts intervalles. Ces problèmes peuvent être identifiés par les autorités compétentes ou le fabricant du DM.

- Pour les autres évènements ou toute nouvelle information/actualisation les concernant : sans délai (immédiatement), et pas plus tard que 7 jours calendaires à compter du jour où le promoteur a eu connaissance de l'évènement à déclarer ou d'une nouvelle information concernant un événement déjà déclaré

11. RECUEIL ET TRAITEMENT DES DONNEES

11.1. *Description des données recueillies*

Seules des données strictement nécessaires et pertinentes pour répondre aux objectifs de la recherche seront collectées de manière confidentielle pour seule finalité la réalisation de la recherche :

Les données notamment recueillies dans le eCRF :

Visite 1 :
- Les critères d'inclusion / non-inclusion
- Consentement éclairé signé
- Données démographiques : âge, sexe
- Données médicales rétrospectives liés au soin (date des premiers symptômes et du diagnostic, existence d'une épilepsie et fréquence des crises, traitement médical)
- Examen clinique : TA, FC, température, examen neurologique
- Résultat des tests de laboratoire : NFS, biochimie, plaquettes, paramètres de coagulation, CRP
- IRM cérébrale préopératoire.

Visite 2 :
- Questionnaire Neurochirurgiens (évaluation de la praticité d'utilisation)
- Enregistrements ECoG par microélectrodes Panaxium (et macroélectrodes cliniques DIXI pour les 10 premiers patients. Les enregistrements sont acquis au format propriétaire Neuralynx (système d'enregistrement) puis exportés () pour être analysés par des routines Matlab de l'équipe. Des données de RSB, impédance, capacité à enregistrer des activités épileptiques, des oscillations à haute fréquence et des activités multi unitaires seront traitées. Le film opératoire synchronisé aux données électrophysiologiques permettra de localiser les enregistrements. Le patient sera enregistré durant la cartographie fonctionnelle de manière à corréler les activités électrophysiologiques et les taches cognitives.
- Tissus peritumoraux : données histologiques (infiltration tumorale) et biochimique (oncométabolites)
- Survenue des EI ou d'une défectuosité du dispositif

Visite 3, 4 et supplémentaire si besoin :

- Examen clinique : TA, FC, température, examen neurologique
- Survenue des EI

12. ANALYSE STATISTIQUE DES DONNEES

12.1. *Responsable de l'analyse statistique*

Le responsable de l'analyse statistique et de l'analyse des signaux électrophysiologiques est le Dr Michel Le Van Quyen, ingénieur et PhD, Laboratoire d'Imagerie Biomédicale, Sorbonne Université – INSERM, Campus des Cordeliers, 15, rue de l'École de médecine, 75006 Paris.

12.2. *Calcul d'effectif*

Le nombre de sujets nécessaire est de 50 participants pour que la recherche ait une probabilité de 80% d'observer plus d'un patient avec un effet indésirable grave, considérant que l'incidence des effets indésirables graves dans la pratique clinique courante est évaluée à 10.3% (Burneo et al., 2006, Chan et al., 2017, Falowski et al., 2015, Hedegard et al., 2014, Deley et al., 2015, Fountas et al., 2007, Hersh et al., 2013, Lee et al., 2000, Liubinas et al., 2009).

La révision de la littérature sur la sécurité d'utilisation des électrodes sous durales pour le monitorage neurophysiologique peropératoire identifie comme potentiels EIG la survenue de : méningite aseptique, hémorragie intracrânienne, crises épileptiques, déficit neurologique et infection. Le calcul d'incidence d'EIG a été calculé considérant que l'hémorragie intracrânienne est l'effet indésirable grave le plus fréquemment associé à la procédure chirurgicale ou à l'utilisation du DM. Selon la littérature ce type d'effets indésirables graves est rapporté pour 5,8%. Centrés sur la valeur 5.8%, un intervalle symétrique de +/- 4 % couvrirai plus de la moitié des taux d'incidences. La limite supérieure de l'intervalle, 9.8 %, a été considérée comme une référence appropriée des EIG observés dans la pratique courante.

Avec un effectif de 50 patients, la probabilité d'observer plus d'un EIG, si la vraie incidence est de 9.8%, serait de 90%. De façon équivalente, avec 50 observations il serait possible de statuer que le DM est au moins aussi sécurisé dans son utilisation avec une probabilité de plus de 90%.

Les sujets sortis d'étude seront remplacés, afin d'obtenir le nombre requis d'observations complètes par groupe de sujet. Nous pourrons remplacer jusqu'à 20% de sorties prématurées et/ou de perdus de vue (10 patients). Le nombre total de patients participant à la recherche : 50 avec la possibilité de remplacer au maximum 10 sujets.

Les 10 premiers patients seront enregistrés à la fois par macroélectrodes cliniques DIXI et par microélectrode Panaxium. Le taux d'EIG grave sera évalué sur l'ensemble des 50 patients (critère principal) mais il sera comparé pour ces 10 premiers patients entre les 2 électrodes. Les 2 électrodes seront par ailleurs comparées pour 10 patients : ratio signal bruit, capacité à enregistrer des activités épileptiques et des oscillations à haute fréquence, stabilité des impédances (critères secondaires).

Description du plan d'analyse statistique :

Le taux d'EIG sera comparé entre macroélectrodes DIXI et microélectrodes Panaxium.

Les données électrophysiologiques seront évaluées par comparaison de moyenne (Chi2).

Les analyses descriptives seront présentées sur la forme de moyenne, écart type, médiane, range interquartile, minimum et maximum pour les datas continues. Pour les data catégoriques, les analyses descriptives seront indiquées en numéro de sujets et pourcentage.

Une erreur alpha de 5% sera considéré pour tous les analyses, sauf mention du contraire.

Critères statistiques d'arrêt de la recherche :
Si le taux d'EIG double par rapport au taux maximal (9,8%), à l'analyse intérimaire des 10 premiers patients la recherche sera arrêtée.

Méthode de prise en compte des données manquantes, inutilisées ou non valides :
Dans le cas de données manquantes les sujets pourront être exclus des analyses pour lesquels les data ne sont pas disponibles.

Variables cliniques :
Nous n'effectuerons pas de procédures d'imputabilité pour ces données manquantes

Variables « ECoG » :
Nous n'effectuerons pas de procédures d'imputabilité pour ces données manquantes (si une des actes décrits n'était pas réalisée pour raison technique).
Toutes les données manquantes seront détaillées dans le rapport final.

Gestion des modifications apportées au plan d'analyse de la stratégie initiale :

Toute modification dans la stratégie d'analyse fera l'objet d'un amendement au CPP.

Si une modification du plan d'analyse initial devait être apportée, nous l'expliquerions dans le rapport final et dans la publication des résultats de l'étude.

Délai prévisionnel de réalisation de l'analyse à partir de la fin de la recherche :

Un délai prévisionnel de 6 mois à partir de la fin de la recherche sera considéré pour la réalisation de l'analyse des donnés.

12.2.1. **Analyse des critères principaux**

Une limite supérieure de confiance à 80% de l'incidence de patient avec au moins un EIG sera réalisé et comparé avec la valeur 9.8% qui indique la limite supérieure observé dans la pratique courante. Si la limite supérieure de l'intervalle de confiance est au moins 9.8% nous pourrons conclure que la sécurité des microélectrodes Panaxium est non-inférieur à la pratique courante.

12.2.2. **Analyse des critères secondaires**

- Ratio signal / bruit : comparaison de moyenne entre le groupe macroélectrode clinique et le groupe microélectrode Panaxium (Chi2)
- Dynamique des impédances : évolution temporale dans le groupe macroélectrode clinique et dans le groupe microélectrode Panaxium (ANOVA)
- Capacité à enregistrer des pointes : analyse descriptive + comparaison de moyenne pour les co-enregistrements macroélectrode clinique / microélectrode Panaxium : amplitude, durée, nombre d'évènements enregistré par unité de temps.
- Capacité à enregistrer des oscillations à haute fréquence : analyse descriptive + comparaison de moyenne pour les co-enregistrements macroélectrode clinique / microélectrode Panaxium : amplitude, durée, nombre de cycles, nombre d'évènements enregistré par unité de temps.
- Capacité à enregistrer des activités physiologiques *gamma* évoquées pendant les tâches cognitives des investigations *neuropsychologiques* peropératoires.
- Praticité et défectuosité des électrodes : analyse descriptive.

12.2.3. **Autres analyses**

- Objectifs exploratoires : analyse descriptive

12.2.4. **Analyse (s) intermédiaire (s) : calendrier**

Une analyse intérimaire sera réalisée après les 10 premiers patients co-enregistrés par macroélectrode clinique / microélectrode Panaxium. Elle portera sur le taux d'EIG et la comparaison des signaux (ratio signal / bruit, dynamique des impédances, capacité à enregistrer des pointes, capacité à enregistre des oscillations à haute fréquence).
Si le taux d'EIG double par rapport au taux maximal (9,8%), l'étude sera arrêtée (objectif d'efficacité / tolérance).
Si les données issues de l'utilisation des microélectrodes Panaxium sont au moins équivalentes à celles obtenues par les macroélectrodes cliniques, l'étude ne sera poursuivie pour les 40 patients suivants qu'avec les électrodes Panaxium (pour éviter une futilité).

13. References bibliographiques

Almeida, Antonio N., Victor Martinez, and William Feindel. 2005. "The First Case of Invasive EEG Monitoring for the Surgical Treatment of Epilepsy: Historical Significance and Context." *Epilepsia* 46 (7): 1082–85. https://doi.org/10.1111/j.1528-1167.2005.66404.x.

Alvarado-Rojas, Catalina, Katia Lehongre, Juliana Bagdasaryan, Anatol Bragin, Richard Staba, Jerome Engel, Vincent Navarro, and Michel Le Van Quyen. 2013. "Single-Unit Activities during Epileptic Discharges in the Human Hippocampal Formation." *Frontiers in Computational Neuroscience* 7: 140. https://doi.org/10.3389/fncom.2013.00140.

Asano, Eishi, Csaba Juhász, Aashit Shah, Sandeep Sood, and Harry T. Chugani. 2009. "Role of Subdural Electrocorticography in Prediction of Long-Term Seizure Outcome in Epilepsy Surgery." *Brain: A Journal of Neurology* 132 (Pt 4): 1038–47. https://doi.org/10.1093/brain/awp025.

Berger, Hans. 1929. "Über Das Elektroenkephalogramm Des Menschen." *Archiv Für Psychiatrie Und Nervenkrankheiten*, 1929, sec. 87.

Berntsson, Shala Ghaderi, Beatrice Malmer, Melissa L. Bondy, Mingqi Qu, and Anja Smits. 2009. "Tumor-Associated Epilepsy and Glioma: Are There Common Genetic Pathways?" *Acta Oncologica (Stockholm, Sweden)* 48 (7): 955–63. https://doi.org/10.1080/02841860903104145.

Bragin, A., J. Engel, C. L. Wilson, I. Fried, and G. W. Mathern. 1999. "Hippocampal and Entorhinal Cortex High-Frequency Oscillations (100--500 Hz) in Human Epileptic Brain and in Kainic Acid--Treated Rats with Chronic Seizures." *Epilepsia* 40 (2): 127–37.

Bragin, A, C. L. Wilson, R. J. Staba, M Reddick, I Fried, and J. Jr Engel. 2002. "Interictal high-frequency oscillations (80-500 Hz) in the human epileptic brain: entorhinal cortex." *Annals of Neurology* 52 (4): 407–415.

Breemen, Melanie S M van, Erik B Wilms, and Charles J Vecht. 2007. "Epilepsy in Patients with Brain Tumours: Epidemiology, Mechanisms, and Management." *The Lancet Neurology* 6 (5): 421–430. https://doi.org/10.1016/S1474-4422(07)70103-5.

Brogna, Christian, Santiago Gil Robles, and Hugues Duffau. 2008. "Brain Tumors and Epilepsy." *Expert Review of Neurotherapeutics* 8 (6): 941–955. https://doi.org/10.1586/14737175.8.6.941.

Burneo JG, Steven DA, McLachlan RS, Parrent AG. Morbidity associated with the use of intracranial electrodes for epilepsy surgery. The Canadian journal of neurological sciences Le journal canadien des sciences neurologiques. 2006;33:223-7.

Castagnola, Elisa, Luca Maiolo, Emma Maggiolini, Antonio Minotti, Marco Marrani, Francesco Maita, Alessandro Pecora, et al. 2015. "PEDOT-CNT-Coated Low-Impedance, Ultra-Flexible, and Brain-Conformable Micro-ECoG Arrays." *IEEE Transactions on Neural Systems and Rehabilitation Engineering: A Publication of the IEEE Engineering in Medicine and Biology Society* 23 (3): 342–50. https://doi.org/10.1109/TNSRE.2014.2342880.

Castagnola, V., E. Descamps, A. Lecestre, L. Dahan, J. Remaud, L. G. Nowak, and C. Bergaud. 2015. "Parylene-Based Flexible Neural Probes with PEDOT Coated Surface for Brain Stimulation and Recording." *Biosensors & Bioelectronics* 67 (May): 450–57. https://doi.org/10.1016/j.bios.2014.09.004.

Chaichana, Kaisorn L, Scott L Parker, Alessandro Olivi, and Alfredo Quiñones-Hinojosa. 2009. "Long-Term Seizure Outcomes in Adult Patients Undergoing Primary Resection of Malignant Brain Astrocytomas. Clinical Article." *Journal of Neurosurgery* 111 (2): 282–292. https://doi.org/10.3171/2009.2.JNS081132.

Chan AY, Kharrat S, Lundeen K, Mnatsakanyan L, Sazgar M, Sen-Gupta I, et al. Length of stay for patients undergoing invasive electrode monitoring with stereoelectroencephalography and subdural grids correlates positively with increased institutional profitability. Epilepsia. 2017;58:1023-6

Chang, Edward F, Matthew B Potts, G Evren Keles, Kathleen R Lamborn, Susan M Chang, Nicholas M Barbaro, and Mitchel S Berger. 2008. "Seizure Characteristics and Control Following Resection in 332 Patients with Low-Grade Gliomas." *Journal of Neurosurgery* 108 (2): 227–235. https://doi.org/10.3171/JNS/2008/108/2/0227.

Chang, Edward F., Justin S. Smith, Susan M. Chang, Kathleen R. Lamborn, Michael D. Prados, Nicholas Butowski, Nicholas M. Barbaro, Andrew T. Parsa, Mitchel S. Berger, and Michael M. McDermott. 2008. "Preoperative Prognostic Classification System for Hemispheric Low-Grade Gliomas in Adults." *Journal of Neurosurgery* 109 (5): 817–24. https://doi.org/10.3171/JNS/2008/109/11/0817.

Chauvel, Patrick, Jorge Gonzalez-Martinez, and Juan Bulacio. 2019. "Presurgical Intracranial Investigations in Epilepsy Surgery." *Handbook of Clinical Neurology* 161: 45–71. https://doi.org/10.1016/B978-0-444-64142-7.00040-0.

Chen, Hao, Jonathon Judkins, Cheddhi Thomas, Meijing Wu, Laith Khoury, Carolina G. Benjamin, Donato Pacione, et al. 2017. "Mutant IDH1 and Seizures in Patients with Glioma." *Neurology* 88 (19): 1805–13. https://doi.org/10.1212/WNL.0000000000003911.

Crépon, Benoît, Vincent Navarro, Dominique Hasboun, Stéphane Clemenceau, Jacques Martinerie, Michel Baulac, Claude Adam, and Michel Le Van Quyen. 2010. "Mapping Interictal Oscillations Greater than 200 Hz Recorded with Intracranial Macroelectrodes in

Human Epilepsy." *Brain: A Journal of Neurology* 133 (Pt 1): 33–45. https://doi.org/10.1093/brain/awp277.
Darlix, Amélie, Sonia Zouaoui, Valérie Rigau, Faiza Bessaoud, Dominique Figarella-Branger, Hélène Mathieu-Daudé, Brigitte Trétarre, et al. 2017. "Epidemiology for Primary Brain Tumors: A Nationwide Population-Based Study." *Journal of Neuro-Oncology* 131 (3): 525–46. https://doi.org/10.1007/s11060-016-2318-3.
Delev D, Send K, Malter M, Ormond DR, Parpaley Y, von Lehe M, et al. Role of Subdural Interhemispheric Electrodes in Presurgical Evaluation of Epilepsy Patients. World neurosurgery. 2015;84:1719-25.e1.
De Witt Hamer, Philip C., Santiago Gil Robles, Aeilko H. Zwinderman, Hugues Duffau, and Mitchel S. Berger. 2012. "Impact of Intraoperative Stimulation Brain Mapping on Glioma Surgery Outcome: A Meta-Analysis." *Journal of Clinical Oncology: Official Journal of the American Society of Clinical Oncology* 30 (20): 2559–65. https://doi.org/10.1200/JCO.2011.38.4818.
Drenckhahn C, Windler C, Major S, Kang EJ, Scheel M, Vajkoczy P, et al. Complications in Aneurysmal Subarachnoid Hemorrhage Patients With and Without Subdural Electrode Strip for Electrocorticography. Journal of clinical neurophysiology : official publication of the American Electroencephalographic Society. 2016;33:250-9.
Dubey, Agrita, and Supratim Ray. 2019. "Cortical Electrocorticogram (ECoG) Is a Local Signal." *The Journal of Neuroscience: The Official Journal of the Society for Neuroscience* 39 (22): 4299–4311. https://doi.org/10.1523/JNEUROSCI.2917-18.2019.
Duffau, Hugues. 2016. "Long-Term Outcomes after Supratotal Resection of Diffuse Low-Grade Gliomas: A Consecutive Series with 11-Year Follow-Up." *Acta Neurochirurgica* 158 (1): 51–58. https://doi.org/10.1007/s00701-015-2621-3.
Englot, Dario J, Mitchel S Berger, Nicholas M Barbaro, and Edward F Chang. 2011. "Predictors of Seizure Freedom after Resection of Supratentorial Low-Grade Gliomas. A Review." *Journal of Neurosurgery* 115 (2): 240–244. https://doi.org/10.3171/2011.3.JNS1153.
———. 2012. "Factors Associated with Seizure Freedom in the Surgical Resection of Glioneuronal Tumors." *Epilepsia* 53 (1): 51–57. https://doi.org/10.1111/j.1528-1167.2011.03269.x.
Englot, Dario J., Mitchel S. Berger, Edward F. Chang, and Paul A. Garcia. 2012. "Characteristics and Treatment of Seizures in Patients with High-Grade Glioma: A Review." *Neurosurgery Clinics of North America* 23 (2): 227–35, vii–viii. https://doi.org/10.1016/j.nec.2012.01.009.
Englot, Dario J, Seunggu J Han, Mitchel S Berger, Nicholas M Barbaro, and Edward F Chang. 2012. "Extent of Surgical Resection Predicts Seizure Freedom in Low-Grade Temporal Lobe Brain Tumors." *Neurosurgery* 70 (4): 921–8– discussion 928. https://doi.org/10.1227/NEU.0b013e31823c3a30.
Falowski SM, DiLorenzo DJ, Shannon LR, Wallace DJ, Devries J, Kellogg RG, et al. Optimizations and Nuances in Neurosurgical Technique for the Minimization of Complications in Subdural Electrode Placement for Epilepsy Surgery. World neurosurgery. 2015;84:989-97.
Fedele, Tommaso, Georgia Ramantani, Sergey Burnos, Peter Hilfiker, Gabriel Curio, Thomas Grunwald, Niklaus Krayenbühl, and Johannes Sarnthein. 2017. "Prediction of Seizure Outcome Improved by Fast Ripples Detected in Low-Noise Intraoperative Corticogram." *Clinical Neurophysiology: Official Journal of the International Federation of Clinical Neurophysiology* 128 (7): 1220–26. https://doi.org/10.1016/j.clinph.2017.03.038.
Ferlauto, Laura, Antonio Nunzio D'Angelo, Paola Vagni, Marta Jole Ildelfonsa Airaghi Leccardi, Flavio Maurizio Mor, Estelle Annick Cuttaz, Marc Olivier Heuschkel, Luc Stoppini, and Diego Ghezzi. 2018. "Development and Characterization of PEDOT:PSS/Alginate Soft Microelectrodes for Application in Neuroprosthetics." *Frontiers in Neuroscience* 12: 648. https://doi.org/10.3389/fnins.2018.00648.
Fernández Coello, Alejandro, Sylvie Moritz-Gasser, Juan Martino, Matteo Martinoni, Ryosuke Matsuda, and Hugues Duffau. 2013. "Selection of Intraoperative Tasks for Awake Mapping Based on Relationships between Tumor Location and Functional Networks." *Journal of Neurosurgery* 119 (6): 1380–94. https://doi.org/10.3171/2013.6.JNS122470.
Fernández, Eduardo, Bradley Greger, Paul A. House, Ignacio Aranda, Carlos Botella, Julio Albisua, Cristina Soto-Sánchez, Arantxa Alfaro, and Richard A. Normann. 2014. "Acute Human Brain Responses to Intracortical Microelectrode Arrays: Challenges and Future Prospects." *Frontiers in Neuroengineering* 7: 24. https://doi.org/10.3389/fneng.2014.00024.
Feyissa, Anteneh M., Gregory A. Worrell, William O. Tatum, Deependra Mahato, Benjamin H. Brinkmann, Steven S. Rosenfeld, Karim ReFaey, Perry S. Bechtle, and Alfredo Quinones-Hinojosa. 2018. "High-Frequency Oscillations in Awake Patients Undergoing Brain Tumor-Related Epilepsy Surgery." *Neurology* 90 (13): e119–1125. https://doi.org/10.1212/WNL.0000000000005216.
Fisher, Robert S, Carlos Acevedo, Alexis Arzimanoglou, Alicia Bogacz, J Helen Cross, Christian E Elger, Jerome Engel, et al. 2014. "ILAE Official Report: A Practical Clinical Definition of Epilepsy." *Epilepsia* 55 (4): 475–482. https://doi.org/10.1111/epi.12550.
Fountas KN, King DW, Jenkins PD, Smith JR. Nonhabitual seizures in patients with implanted subdural electrodes. Stereotactic and functional neurosurgery. 2004;82:165-8.
Fountas KN, Smith JR. Subdural electrode-associated complications: a 20-year experience. Stereotactic and functional neurosurgery. 2007;85:264-72
Frauscher, Birgit, Nicolás von Ellenrieder, Rina Zelmann, Christine Rogers, Dang Khoa Nguyen, Philippe Kahane, François Dubeau, and Jean Gotman. 2018. "High-Frequency Oscillations in the Normal Human Brain." *Annals of Neurology* 84 (3): 374–85. https://doi.org/10.1002/ana.25304.
G Huberfeld, and Kubis, N. 2015. "Electroencephalography in Intensive Care Unit." *Reanimation*, 2015, 24 edition, sec. 5.
Gaggero, Roberto, Alessandro Consales, Francesca Fazzini, Maria Margherita Mancardi, Maria Giuseppina Baglietto, Paolo Nozza, Andrea Rossi, et al. 2009. "Epilepsy Associated with Supratentorial Brain Tumors under 3 Years of Life." *Epilepsy Research* 87 (2–3): 184–89. https://doi.org/10.1016/j.eplepsyres.2009.08.012.
Gleize, Vincent, Agusti Alentorn, Léa Connen de Kérillis, Marianne Labussière, Aravidan A Nadaradjane, Emeline Mundwiller, Chris Ottolenghi, et al. 2015. "CIC Inactivating Mutations Identify Aggressive Subset of 1p19q Codeleted Gliomas." *Annals of Neurology* 78 (3): 355–74. https://doi.org/10.1002/ana.24443.
Guragain, Hari, Jan Cimbalnik, Matt Stead, David M. Groppe, Brent M. Berry, Vaclav Kremen, Daniel Kenney-Jung, Jeffrey Britton, Gregory A. Worrell, and Benjamin H. Brinkmann. 2018. "Spatial Variation in High-Frequency Oscillation Rates and Amplitudes in Intracranial EEG." *Neurology* 90 (8): e639–46. https://doi.org/10.1212/WNL.0000000000004998.
Hamer HM, Morris HH, Mascha EJ, Karafa MT, Bingaman WE, Bej MD, et al. Complications of invasive video-EEG monitoring with subdural grid electrodes. Neurology. 2002;58:97-103.
Hamilton, William, and David Kernick. 2007. "Clinical Features of Primary Brain Tumours: A Case-Control Study Using Electronic Primary Care Records." *The British Journal of General Practice: The Journal of the Royal College of General Practitioners* 57 (542): 695–99.
Harris, K. D., D. A. Henze, J. Csicsvari, H. Hirase, and G. Buzsáki. 2000. "Accuracy of Tetrode Spike Separation as Determined by

Simultaneous Intracellular and Extracellular Measurements." *Journal of Neurophysiology* 84 (1): 401–14. https://doi.org/10.1152/jn.2000.84.1.401.
Hedegard E, Bjellvi J, Edelvik A, Rydenhag B, Flink R, Malmgren K. Complications to invasive epilepsy surgery workup with subdural and depth electrodes: a prospective population-based observational study. Journal of neurology, neurosurgery, and psychiatry. 2014;85:716-20.
Hersh EH, Virk MS, Shao H, Tsiouris AJ, Bonci GA, Schwartz TH. Bone flap explantation, steroid use, and rates of infection in patients with epilepsy undergoing craniotomy for implantation of subdural electrodes. Journal of neurosurgery. 2013;119:48-53.
Hervey-Jumper, Shawn L., Jing Li, Darryl Lau, Annette M. Molinaro, David W. Perry, Lingzhong Meng, and Mitchel S. Berger. 2015. "Awake Craniotomy to Maximize Glioma Resection: Methods and Technical Nuances over a 27-Year Period." *Journal of Neurosurgery* 123 (2): 325–39. https://doi.org/10.3171/2014.10.JNS141520.
Hildebrand, Jerzy, Cristel Lecaille, Joëlle Perennes, and Jean-Yves Delattre. 2005. "Epileptic Seizures during Follow-up of Patients Treated for Primary Brain Tumors." *Neurology* 65 (2): 212–15. https://doi.org/10.1212/01.wnl.0000168903.09277.8f.
Hirsch, J F, J Buisson-Ferey, M Sachs, J C Hirsch, and J Scherrer. 1966. "[Electrocorticogram and unitary activites with expanding lesions in man]." *Electroencephalography and clinical neurophysiology* 21 (5): 417–428.
Huberfeld, G, and J Pallud. 2015. "Brain Tumor-Related Epilepsy." *Pratique Neurologique – FMC* 6: 19–33.
Huberfeld, G, and C J Vecht. 2016. "Seizures and Gliomas – towards a Single Therapeutic Approach." *Nature Reviews Neurology* 12 (4): 204–16.
Huberfeld, Gilles, and Charles J. Vecht. 2016. "Seizures and Gliomas - towards a Single Therapeutic Approach." *Nature Reviews. Neurology* 12 (4): 204–16. https://doi.org/10.1038/nrneurol.2016.26.
Hughlings-Jackson, J. 1882. "LOCALISED CONVULSIONS FROM TUMOUR OF THE BRAIN." *Brain : A Journal of Neurology* 5 (3): 364–374. https://doi.org/10.1093/brain/5.3.364.
Hussain, Shaun A., Gary W. Mathern, Phoebe Hung, Julius Weng, Raman Sankar, and Joyce Y. Wu. 2017. "Intraoperative Fast Ripples Independently Predict Postsurgical Epilepsy Outcome: Comparison with Other Electrocorticographic Phenomena." *Epilepsy Research* 135: 79–86. https://doi.org/10.1016/j.eplepsyres.2017.06.010.
Hwang, S. L., A. S. Lieu, T. H. Kuo, C. L. Lin, C. Z. Chang, T. Y. Huang, and S. L. Howng. 2001. "Preoperative and Postoperative Seizures in Patients with Astrocytic Tumours: Analysis of Incidence and Influencing Factors." *Journal of Clinical Neuroscience: Official Journal of the Neurosurgical Society of Australasia* 8 (5): 426–29. https://doi.org/10.1054/jocn.2000.0825.
Isnard, Jean, Delphine Taussig, Fabrice Bartolomei, Pierre Bourdillon, Hélène Catenoix, Francine Chassoux, Mathilde Chipaux, et al. 2018. "French Guidelines on Stereoelectroencephalography (SEEG)." *Neurophysiologie Clinique = Clinical Neurophysiology* 48 (1): 5–13. https://doi.org/10.1016/j.neucli.2017.11.005.
Jacobs, J., R. Staba, E. Asano, H. Otsubo, J. Y. Wu, M. Zijlmans, I. Mohamed, et al. 2012. "High-Frequency Oscillations (HFOs) in Clinical Epilepsy." *Progress in Neurobiology* 98 (3): 302–15. https://doi.org/10.1016/j.pneurobio.2012.03.001.
Jacobs, Julia, Pierre Levan, Claude-Edouard Châtillon, André Olivier, François Dubeau, and Jean Gotman. 2009. "High Frequency Oscillations in Intracranial EEGs Mark Epileptogenicity Rather than Lesion Type." *Brain: A Journal of Neurology* 132 (Pt 4): 1022–37. https://doi.org/10.1093/brain/awn351.
Jacobs, Julia, Joyce Y. Wu, Piero Perucca, Rina Zelmann, Malenka Mader, Francois Dubeau, Gary W. Mathern, Andreas Schulze-Bonhage, and Jean Gotman. 2018. "Removing High-Frequency Oscillations: A Prospective Multicenter Study on Seizure Outcome." *Neurology* 91 (11): e1040–52. https://doi.org/10.1212/WNL.0000000000006158.
Keller, C J, W Truccolo, J T Gale, E Eskandar, T Thesen, C Carlson, O Devinsky, et al. 2010. "Heterogeneous Neuronal Firing Patterns during Interictal Epileptiform Discharges in the Human Cortex." *Brain : A Journal of Neurology* 133 (6): 1668–1681. https://doi.org/10.1093/brain/awq112.
Khodagholy, Dion, Jennifer N. Gelinas, Thomas Thesen, Werner Doyle, Orrin Devinsky, George G. Malliaras, and György Buzsáki. 2015. "NeuroGrid: Recording Action Potentials from the Surface of the Brain." *Nature Neuroscience* 18 (2): 310–15. https://doi.org/10.1038/nn.3905.
Khodagholy, Dion, Jennifer N. Gelinas, Zifang Zhao, Malcolm Yeh, Michael Long, Jeremy D. Greenlee, Werner Doyle, Orrin Devinsky, and György Buzsáki. 2016. "Organic Electronics for High-Resolution Electrocorticography of the Human Brain." *Science Advances* 2 (11): e1601027. https://doi.org/10.1126/sciadv.1601027.
Klink, N. E. C. van, M. A. Van't Klooster, R. Zelmann, F. S. S. Leijten, C. H. Ferrier, K. P. J. Braun, P. C. van Rijen, M. J. a. M. van Putten, G. J. M. Huiskamp, and M. Zijlmans. 2014. "High Frequency Oscillations in Intra-Operative Electrocorticography before and after Epilepsy Surgery." *Clinical Neurophysiology: Official Journal of the International Federation of Clinical Neurophysiology* 125 (11): 2212–19. https://doi.org/10.1016/j.clinph.2014.03.004.
Klooster, Maryse A. van 't, Nicole E. C. van Klink, Frans S. S. Leijten, Rina Zelmann, Tineke A. Gebbink, Peter H. Gosselaar, Kees P. J. Braun, Geertjan J. M. Huiskamp, and Maeike Zijlmans. 2015. "Residual Fast Ripples in the Intraoperative Corticogram Predict Epilepsy Surgery Outcome." *Neurology* 85 (2): 120–28. https://doi.org/10.1212/WNL.0000000000001727.
Klooster, Maryse A. van 't, Nicole E. C. van Klink, Willemiek J. E. M. Zweiphenning, Frans S. S. Leijten, Rina Zelmann, Cyrille H. Ferrier, Peter C. van Rijen, et al. 2017. "Tailoring Epilepsy Surgery with Fast Ripples in the Intraoperative Electrocorticogram." *Annals of Neurology* 81 (5): 664–76. https://doi.org/10.1002/ana.24928.
Klooster, Maryse A. van 't, Frans S. S. Leijten, Geertjan Huiskamp, Hanneke E. Ronner, Johannes C. Baayen, Peter C. van Rijen, Martinus J. C. Eijkemans, Kees P. J. Braun, Maeike Zijlmans, and HFO study group. 2015. "High Frequency Oscillations in the Intra-Operative ECoG to Guide Epilepsy Surgery ('The HFO Trial'): Study Protocol for a Randomized Controlled Trial." *Trials* 16 (September): 422. https://doi.org/10.1186/s13063-015-0932-6.
Kural, Mustafa Aykut, Hatice Tankisi, Lene Duez, Vibeke Sejer Hansen, Aparna Udupi, Richard Wennberg, Stefan Rampp, Pål G. Larsson, Reinhard Schulz, and Sándor Beniczky. 2020. "Optimized Set of Criteria for Defining Interictal Epileptiform EEG Discharges." *Clinical Neurophysiology: Official Journal of the International Federation of Clinical Neurophysiology* 131 (9): 2250–54. https://doi.org/10.1016/j.clinph.2020.06.026.
Lachaux JP, Axmacher N, Mormann F, Halgren E, Crone NE (2012) High-frequency neural activity and human cognition: past, present and possible future of intracranial EEG research. *Progress in Neurobiology*. 98: 279-301.
Lambrecq, Virginie, Katia Lehongre, Claude Adam, Valério Frazzini, Bertrand Mathon, Stéphane Clemenceau, Dominique Hasboun, et al. 2017. "Single-Unit Activities during the Transition to Seizures in Deep Mesial Structures." *Annals of Neurology* 82 (6): 1022–28. https://doi.org/10.1002/ana.25111.
Le Van Quyen, Michel, Ilgam Khalilov, and Yehezkel Ben-Ari. 2006. "The Dark Side of High-Frequency Oscillations in the Developing Brain." *Trends in Neurosciences* 29 (7): 419–427. https://doi.org/10.1016/j.tins.2006.06.001.
Le Van Quyen, Michel, Lyle E. Muller, Bartosz Telenczuk, Eric Halgren, Sydney Cash, Nicholas G. Hatsopoulos, Nima Dehghani, and Alain Destexhe. 2016. "High-Frequency Oscillations in Human and Monkey Neocortex during the Wake-Sleep Cycle." *Proceedings*

of the National Academy of Sciences of the United States of America 113 (33): 9363–68. https://doi.org/10.1073/pnas.1523583113.
Lecomte, Aziliz, Amélie Degache, Emeline Descamps, Lionel Dahan, and Christian Bergaud. 2017. "In Vitro and in Vivo Biostability Assessment of Chronically-Implanted Parylene C Neural Sensors." *Sensors and Actuators B: Chemical* 251 (November): 1001–8. https://doi.org/10.1016/j.snb.2017.05.057.
Lee, Changik, Woorim Jeong, and Chun Kee Chung. 2019. "Clinical Relevance of Interictal Spikes in Tumor-Related Epilepsy: An Electrocorticographic Study." *Journal of Epilepsy Research* 9 (2): 126–33. https://doi.org/10.14581/jer.19015.
Lee, Jong Woo, Patrick Y. Wen, Shelley Hurwitz, Peter Black, Santosh Kesari, Jan Drappatz, Alexandra J. Golby, et al. 2010. "Morphological Characteristics of Brain Tumors Causing Seizures." *Archives of Neurology* 67 (3): 336–42. https://doi.org/10.1001/archneurol.2010.2.
Lee WS, Lee JK, Lee SA, Kang JK, Ko TS. Complications and results of subdural grid electrode implantation in epilepsy surgery. Surgical neurology. 2000;54:346-51.
Liu, Su, Candan Gurses, Zhiyi Sha, Michael M. Quach, Altay Sencer, Nerses Bebek, Daniel J. Curry, et al. 2018. "Stereotyped High-Frequency Oscillations Discriminate Seizure Onset Zones and Critical Functional Cortex in Focal Epilepsy." *Brain* 141 (3): 713–30. https://doi.org/10.1093/brain/awx374.
Liubinas SV, Cassidy D, Roten A, Kaye AH, O'Brien TJ. Tailored cortical resection following image guided subdural grid implantation for medically refractory epilepsy. Journal of clinical neuroscience: official journal of the Neurosurgical Society of Australasia. 2009;16:1398-408.
Louis, David N., Arie Perry, Guido Reifenberger, Andreas von Deimling, Dominique Figarella-Branger, Webster K. Cavenee, Hiroko Ohgaki, Otmar D. Wiestler, Paul Kleihues, and David W. Ellison. 2016. "The 2016 World Health Organization Classification of Tumors of the Central Nervous System: A Summary." *Acta Neuropathologica* 131 (6): 803–20. https://doi.org/10.1007/s00401-016-1545-1.
Ludwig, Kip A., Nicholas B. Langhals, Mike D. Joseph, Sarah M. Richardson-Burns, Jeffrey L. Hendricks, and Daryl R. Kipke. 2011. "Poly(3,4-Ethylenedioxythiophene) (PEDOT) Polymer Coatings Facilitate Smaller Neural Recording Electrodes." *Journal of Neural Engineering* 8 (1): 014001. https://doi.org/10.1088/1741-2560/8/1/014001.
Lynam, Laura M., Mark K. Lyons, Joseph F. Drazkowski, Joseph I. Sirven, Katherine H. Noe, Richard S. Zimmerman, and James A. Wilkens. 2007. "Frequency of Seizures in Patients with Newly Diagnosed Brain Tumors: A Retrospective Review." *Clinical Neurology and Neurosurgery* 109 (7): 634–38. https://doi.org/10.1016/j.clineuro.2007.05.017.
Mantione, Daniele, Isabel Del Agua, Ana Sanchez-Sanchez, and David Mecerreyes. 2017. "Poly(3,4-Ethylenedioxythiophene) (PEDOT) Derivatives: Innovative Conductive Polymers for Bioelectronics." *Polymers* 9 (8). https://doi.org/10.3390/polym9080354.
Martino, Juan, Luc Taillandier, Sylvie Moritz-Gasser, Peggy Gatignol, and Hugues Duffau. 2009. "Re-Operation Is a Safe and Effective Therapeutic Strategy in Recurrent WHO Grade II Gliomas within Eloquent Areas." *Acta Neurochirurgica* 151 (5): 427–36– discussion 436. https://doi.org/10.1007/s00701-009-0232-6.
Merricks, Edward M., Elliot H. Smith, Guy M. McKhann, Robert R. Goodman, Lisa M. Bateman, Ronald G. Emerson, Catherine A. Schevon, and Andrew J. Trevelyan. 2015. "Single Unit Action Potentials in Humans and the Effect of Seizure Activity." *Brain: A Journal of Neurology* 138 (Pt 10): 2891–2906. https://doi.org/10.1093/brain/awv208.
Mittal, S., D. Barkmeier, J. Hua, D. S. Pai, D. Fuerst, M. Basha, J. A. Loeb, and A. K. Shah. 2016. "Intracranial EEG Analysis in Tumor-Related Epilepsy: Evidence of Distant Epileptic Abnormalities." *Clinical Neurophysiology: Official Journal of the International Federation of Clinical Neurophysiology* 127 (1): 238–44. https://doi.org/10.1016/j.clinph.2015.06.028.
Morace R, Di Gennaro G, Picardi A, Quarato PP, Sparano A, Mascia A, et al. Surgery after intracranial investigation with subdural electrodes in patients with drug-resistant focal epilepsy: outcome and complications. Neurosurgical review. 2012;35:519-26; discussion 26
Munari, C., A. Musolino, C. Daumas-Duport, O. Missir, P. Brunet, A. T. Giallonardo, J. P. Chodkiewicz, and J. Bancaud. 1985. "Correlation between Stereo-EEG, CT-Scan and Stereotactic Biopsy Data in Epileptic Patients with Low-Grade Gliomas." *Applied Neurophysiology* 48 (1–6): 448–53. https://doi.org/10.1159/000101176.
Navarrete, Miguel, Catalina Alvarado-Rojas, Michel Le Van Quyen, and Mario Valderrama. 2016. "RIPPLELAB: A Comprehensive Application for the Detection, Analysis and Classification of High Frequency Oscillations in Electroencephalographic Signals." *PLOS ONE* 11 (6): e0158276. https://doi.org/10.1371/journal.pone.0158276.
Ostrom, Quinn T., Luc Bauchet, Faith G. Davis, Isabelle Deltour, James L. Fisher, Chelsea Eastman Langer, Melike Pekmezci, et al. 2014. "The Epidemiology of Glioma in Adults: A 'State of the Science' Review." *Neuro-Oncology* 16 (7): 896–913. https://doi.org/10.1093/neuonc/nou087.
Oushy, Soliman, Stefan H. Sillau, Douglas E. Ney, Denise M. Damek, A. Samy Youssef, Kevin O. Lillehei, and D. Ryan Ormond. 2018. "New-Onset Seizure during and after Brain Tumor Excision: A Risk Assessment Analysis." *Journal of Neurosurgery* 128 (6): 1713–18. https://doi.org/10.3171/2017.2.JNS162315.
Ozlen F, Asan Z, Tanriverdi T, Kafadar A, Ozkara C, Ozyurt E, et al. Surgical morbidity of invasive monitoring in epilepsy surgery: an experience from a single institution. Turkish neurosurgery. 2010;20:364-72.
Pallud, J, E Audureau, M Blonski, N Sanai, L Bauchet, D Fontaine, E Mandonnet, et al. 2014. "Epileptic Seizures in Diffuse Low-Grade Gliomas in Adults." *Brain* 137 (2): 449–462. https://doi.org/10.1093/brain/awt345.
Pallud, J., and E. Dezamis. 2017. "Functional and Oncological Outcomes Following Awake Surgical Resection Using Intraoperative Cortico-Subcortical Functional Mapping for Supratentorial Gliomas Located in Eloquent Areas." *Neuro-Chirurgie* 63 (3): 208–18. https://doi.org/10.1016/j.neuchi.2016.08.003.
Pallud, J, M Le Van Quyen, F Bielle, C Pellegrino, P Varlet, M Labussiere, N Cresto, et al. 2014. "Cortical GABAergic Excitation Contributes to Epileptic Activities around Human Glioma." *Science Translational Medicine* 6 (244): 244ra89–244ra89. https://doi.org/10.1126/scitranslmed.3008065.
Pallud, J, P Varlet, B Devaux, S Geha, M Badoual, C Deroulers, P Page, E Dezamis, C Daumas-Duport, and F-X Roux. 2010. "Diffuse Low-Grade Oligodendrogliomas Extend beyond MRI-Defined Abnormalities." *Neurology* 74 (21): 1724–1731. https://doi.org/10.1212/WNL.0b013e3181e04264.
Pallud, Johan, Laurent Capelle, and Gilles Huberfeld. 2013. "Tumoral Epileptogenicity: How Does It Happen?" *Epilepsia* 54 Suppl 9 (s9): 30–34. https://doi.org/10.1111/epi.12440.
Pallud, Johan, Jean-François Llitjos, Frédéric Dhermain, Pascale Varlet, Edouard Dezamis, Bertrand Devaux, Raphaëlle Souillard-Scémama, et al. 2012. "Dynamic Imaging Response Following Radiation Therapy Predicts Long-Term Outcomes for Diffuse Low-Grade Gliomas." *Neuro-Oncology* 14 (4): 496–505. https://doi.org/10.1093/neuonc/nos069.
Pallud, Johan, Luc Taillandier, Laurent Capelle, Denys Fontaine, Matthieu Peyre, François Ducray, Hugues Duffau, and Emmanuel

Mandonnet. 2012. “Quantitative Morphological Magnetic Resonance Imaging Follow-up of Low-Grade Glioma: A Plea for Systematic Measurement of Growth Rates.” *Neurosurgery* 71 (3): 729–39; discussion 739-740. https://doi.org/10.1227/NEU.0b013e31826213de.

Palmini, A., A. Gambardella, F. Andermann, F. Dubeau, J. C. da Costa, A. Olivier, D. Tampieri, P. Gloor, F. Quesney, and E. Andermann. 1995. “Intrinsic Epileptogenicity of Human Dysplastic Cortex as Suggested by Corticography and Surgical Results.” *Annals of Neurology* 37 (4): 476–87. https://doi.org/10.1002/ana.410370410.

Ray, A, J. X. Tao, and S. M. Hawes-Ebersole. 2007. “Localizing value of scalp EEG spikes: a simultaneous scalp and intracranial study.” *Clin Neurophysiol* 118 (1): 69–79.

Rydenhag B, Silander HC. Complications of epilepsy surgery after 654 procedures in Sweden, September 1990-1995: a multicenter study based on the Swedish National Epilepsy Surgery Register. Neurosurgery. 2001;49:51-6; discussion 6-7.

Rockland, Kathleen S. 2010. “Five Points on Columns.” *Frontiers in Neuroanatomy* 4: 22. https://doi.org/10.3389/fnana.2010.00022.

Roehri, Nicolas, Francesca Pizzo, Stanislas Lagarde, Isabelle Lambert, Anca Nica, Aileen McGonigal, Bernard Giusiano, Fabrice Bartolomei, and Christian-George Bénar. 2018. “High-Frequency Oscillations Are Not Better Biomarkers of Epileptogenic Tissues than Spikes.” *Annals of Neurology* 83 (1): 84–97. https://doi.org/10.1002/ana.25124.

Roessler, Karl, Elisabeth Heynold, Michael Buchfelder, Hermann Stefan, and Hajo M. Hamer. 2019. “Current Value of Intraoperative Electrocorticography (IopECoG).” *Epilepsy & Behavior: E&B* 91: 20–24. https://doi.org/10.1016/j.yebeh.2018.06.053.

Ruda, R, L Bello, H Duffau, and R Soffietti. 2012. “Seizures in Low-Grade Gliomas: Natural History, Pathogenesis, and Outcome after Treatments.” *Neuro-Oncology* 14 (suppl 4): iv55–iv64. https://doi.org/10.1093/neuonc/nos199.

Salanova, V., F. Andermann, A. Olivier, T. Rasmussen, and L. F. Quesney. 1992. “Occipital Lobe Epilepsy: Electroclinical Manifestations, Electrocorticography, Cortical Stimulation and Outcome in 42 Patients Treated between 1930 and 1991. Surgery of Occipital Lobe Epilepsy.” *Brain: A Journal of Neurology* 115 (Pt 6) (December): 1655–80. https://doi.org/10.1093/brain/115.6.1655.

San-juan, Daniel, Claudia Alfaro Tapia, Alfaro Tapia Claudia, Maricarmen Fernández González-Aragón, González-Aragón Fernández Maricarmen, Adriana Martínez Mayorga, Martínez Mayorga Adriana, et al. 2011. “The Prognostic Role of Electrocorticography in Tailored Temporal Lobe Surgery.” *Seizure* 20 (7): 564–69. https://doi.org/10.1016/j.seizure.2011.04.006.

Schevon, C. A., R. R. Goodman, G. McKhann, and R. G. Emerson. 2010. “Propagation of Epileptiform Activity on a Submillimeter Scale.” *Journal of Clinical Neurophysiology: Official Publication of the American Electroencephalographic Society* 27 (6): 406–11. https://doi.org/10.1097/WNP.0b013e3181fdf8a1.

Schevon, C, S Ng, J Cappell, R Goodman, G McKhann, A Waziri, A Branner, A Sosunov, C Schroeder, and R Emerson. 2008. “Microphysiology of Epileptiform Activity in Human Neocortex.” *Journal of Clinical Neurophysiology : Official Publication of the American Electroencephalographic Society*, November. https://doi.org/10.1097/WNP.0b013e31818e8010.

Schevon, Catherine A., A. J. Trevelyan, C. E. Schroeder, R. R. Goodman, G. McKhann, and R. G. Emerson. 2009. “Spatial Characterization of Interictal High Frequency Oscillations in Epileptic Neocortex.” *Brain: A Journal of Neurology* 132 (Pt 11): 3047–59. https://doi.org/10.1093/brain/awp222.

Schevon, Catherine A, Shennan A Weiss, Guy McKhann, Robert R Goodman, Rafael Yuste, Ronald G Emerson, and Andrew J Trevelyan. 2012. “Evidence of an Inhibitory Restraint of Seizure Activity in Humans.” *Nature Communications* 3 (September): 1060. https://doi.org/10.1038/ncomms2056.

Schmidt RF, Wu C, Lang MJ, Soni P, Williams KA, Jr., Boorman DW, et al. Complications of subdural and depth electrodes in 269 patients undergoing 317 procedures for invasive monitoring in epilepsy. Epilepsia. 2016;57:1697-708.

Schwartz, T. H., C. W. Bazil, T. S. Walczak, S. Chan, T. A. Pedley, and R. R. Goodman. 1997. “The Predictive Value of Intraoperative Electrocorticography in Resections for Limbic Epilepsy Associated with Mesial Temporal Sclerosis.” *Neurosurgery* 40 (2): 302–9; discussion 309-311. https://doi.org/10.1097/00006123-199702000-00014.

Schwartzbaum, Judith, Fredrik Jonsson, Anders Ahlbom, Susan Preston-Martin, Beatrice Malmer, Stefan Lönn, Karin Söderberg, and Maria Feychting. 2005. “Prior Hospitalization for Epilepsy, Diabetes, and Stroke and Subsequent Glioma and Meningioma Risk.” *Cancer Epidemiology, Biomarkers & Prevention: A Publication of the American Association for Cancer Research, Cosponsored by the American Society of Preventive Oncology* 14 (3): 643–50. https://doi.org/10.1158/1055-9965.EPI-04-0119.

Sirven, Joseph I., Dean M. Wingerchuk, Joseph F. Drazkowski, Mark K. Lyons, and Richard S. Zimmerman. 2004. “Seizure Prophylaxis in Patients with Brain Tumors: A Meta-Analysis.” *Mayo Clinic Proceedings* 79 (12): 1489–94. https://doi.org/10.4065/79.12.1489.

Smits, Anja, Zhe Jin, Tamador Elsir, Hugo Pedder, Monica Nistér, Irina Alafuzoff, Anna Dimberg, et al. 2012. “GABA-A Channel Subunit Expression in Human Glioma Correlates with Tumor Histology and Clinical Outcome.” *PLoS ONE* 7 (5): e37041. https://doi.org/10.1371/journal.pone.0037041.

Stead, Matt, Mark Bower, Benjamin H Brinkmann, Kendall Lee, W Richard Marsh, Fredric B Meyer, Brian Litt, Jamie Van Gompel, and Greg A Worrell. 2010. “Microseizures and the Spatiotemporal Scales of Human Partial Epilepsy.” *Brain* 133 (9): 2789–2797. https://doi.org/10.1093/brain/awq190.

Still, Megan E. H., Alexandre Roux, Gilles Huberfeld, Luc Bauchet, Marie-Hélène Baron, Denys Fontaine, Marie Blonski, et al. 2018. “Extent of Resection and Residual Tumor Thresholds for Postoperative Total Seizure Freedom in Epileptic Adult Patients Harboring a Supratentorial Diffuse Low-Grade Glioma.” *Neurosurgery*, November. https://doi.org/10.1093/neuros/nyy481.

Suarez-Perez, Alex, Gemma Gabriel, Beatriz Rebollo, Xavi Illa, Anton Guimerà-Brunet, Javier Hernández-Ferrer, Maria Teresa Martínez, Rosa Villa, and Maria V. Sanchez-Vives. 2018. “Quantification of Signal-to-Noise Ratio in Cerebral Cortex Recordings Using Flexible MEAs With Co-Localized Platinum Black, Carbon Nanotubes, and Gold Electrodes.” *Frontiers in Neuroscience* 12: 862. https://doi.org/10.3389/fnins.2018.00862.

Swartz BE, Rich JR, Dwan PS, DeSalles A, Kaufman MH, Walsh GO, et al. The safety and efficacy of chronically implanted subdural electrodes: a prospective study. Surgical neurology. 1996;46:87-93.

Takami, Hirokazu, Nikki Khoshnood, and Mark Bernstein. 2020. “Preoperative Factors Associated with Adverse Events during Awake Craniotomy: Analysis of 609 Consecutive Cases.” *Journal of Neurosurgery*, June, 1–9. https://doi.org/10.3171/2020.4.JNS20378.

Talairach, J., J. Bancaud, A. Bonis, G. Szikla, and P. Tournoux. 1962. “Functional Stereotaxic Exploration of Epilepsy.” *Confinia Neurologica* 22: 328–31.

Tao, James X, Maria Baldwin, Amit Ray, Susan Hawes-Ebersole, and John S Ebersole. 2007. “The Impact of Cerebral Source Area and Synchrony on Recording Scalp Electroencephalography Ictal Patterns.” *Epilepsia* 48 (11): 2167–2176. https://doi.org/10.1111/j.1528-1167.2007.01224.x.

Tran, T A, S S Spencer, M Javidan, S Pacia, D Marks, and D D Spencer. 1997. “Significance of Spikes Recorded on Intraoperative Electrocorticography in Patients with Brain Tumor and Epilepsy.” *Epilepsia* 38 (10): 1132–1139.

Tran, T. A., S. S. Spencer, D. Marks, M. Javidan, S. Pacia, and D. D. Spencer. 1995. “Significance of Spikes Recorded on Electrocorticography in Nonlesional Medial Temporal Lobe Epilepsy.” *Annals of Neurology* 38 (5): 763–70. https://doi.org/10.1002/ana.410380511.

Tripathi, M., A. Garg, S. Gaikwad, C. S. Bal, Sarkar Chitra, K. Prasad, H. H. Dash, B. S. Sharma, and P. Sarat Chandra. 2010. "Intra-Operative Electrocorticography in Lesional Epilepsy." *Epilepsy Research* 89 (1): 133–41. https://doi.org/10.1016/j.eplepsyres.2009.12.007.

Truccolo, Wilson, Omar J. Ahmed, Matthew T. Harrison, Emad N. Eskandar, G. Rees Cosgrove, Joseph R. Madsen, Andrew S. Blum, N. Stevenson Potter, Leigh R. Hochberg, and Sydney S. Cash. 2014. "Neuronal Ensemble Synchrony during Human Focal Seizures." *The Journal of Neuroscience: The Official Journal of the Society for Neuroscience* 34 (30): 9927–44. https://doi.org/10.1523/JNEUROSCI.4567-13.2014.

Truccolo, Wilson, Jacob A Donoghue, Leigh R Hochberg, Emad N Eskandar, Joseph R Madsen, William S Anderson, Emery N Brown, Eric Halgren, and Sydney S Cash. 2011. "Single-Neuron Dynamics in Human Focal Epilepsy." *Nature Neuroscience* 14 (5): 635–641. https://doi.org/10.1038/nn.2782.

Tybrandt, Klas, Dion Khodagholy, Bernd Dielacher, Flurin Stauffer, Aline F. Renz, György Buzsáki, and János Vörös. 2018. "High-Density Stretchable Electrode Grids for Chronic Neural Recording." *Advanced Materials (Deerfield Beach, Fla.)* 30 (15): e1706520. https://doi.org/10.1002/adma.201706520.

Valentin A, Hernando-Quintana N, Moles-Herbera J, Jimenez-Jimenez D, Mourente S, Malik I, et al. Depth versus subdural temporal electrodes revisited: Impact on surgical outcome after resective surgery for epilepsy. Clinical neurophysiology : official journal of the International Federation of Clinical Neurophysiology. 2017;128:418-23.

Van Gompel JJ, Worrell GA, Bell ML, Patrick TA, Cascino GD, Raffel C, et al. Intracranial electroencephalography with subdural grid electrodes: techniques, complications, and outcomes. Neurosurgery. 2008;63:498-505; discussion -6

Vecht, Charles J., and Erik B. Wilms. 2010. "Seizures in Low- and High-Grade Gliomas: Current Management and Future Outlook." *Expert Review of Anticancer Therapy* 10 (5): 663–69. https://doi.org/10.1586/era.10.48.

Vecht, Charles, Louis Royer-Perron, Caroline Houillier, and Gilles Huberfeld. 2017. "Seizures and Anticonvulsants in Brain Tumours: Frequency, Mechanisms and Anti-Epileptic Management." *Current Pharmaceutical Design*, October. https://doi.org/10.2174/1381612823666171027130003.

Wagner, Fabien B., Emad N. Eskandar, G. Rees Cosgrove, Joseph R. Madsen, Andrew S. Blum, N. Stevenson Potter, Leigh R. Hochberg, Sydney S. Cash, and Wilson Truccolo. 2015. "Microscale Spatiotemporal Dynamics during Neocortical Propagation of Human Focal Seizures." *NeuroImage* 122 (November): 114–30. https://doi.org/10.1016/j.neuroimage.2015.08.019.

Wang, Doris D., Abby E. Deans, A. James Barkovich, Tarik Tihan, Nicholas M. Barbaro, Paul A. Garcia, and Edward F. Chang. 2013. "Transmantle Sign in Focal Cortical Dysplasia: A Unique Radiological Entity with Excellent Prognosis for Seizure Control." *Journal of Neurosurgery* 118 (2): 337–44. https://doi.org/10.3171/2012.10.JNS12119.

Wang, Yu-Chi, Cheng-Chi Lee, Hirokazu Takami, Stephanie Shen, Ko-Ting Chen, Kuo-Chen Wei, Min-Hsien Wu, Gregory Worrell, and Pin-Yuan Chen. 2019. "Awake Craniotomies for Epileptic Gliomas: Intraoperative and Postoperative Seizure Control and Prognostic Factors." *Journal of Neuro-Oncology* 142 (3): 577–86. https://doi.org/10.1007/s11060-019-03131-0.

Wellmer J, von der Groeben F, Klarmann U, Weber C, Elger CE, Urbach H, et al. Risks and benefits of invasive epilepsy surgery workup with implanted subdural and depth electrodes. Epilepsia. 2012;53:1322-32.

Wennberg, R., L. F. Quesney, A. Lozano, A. Olivier, and T. Rasmussen. 1999. "Role of Electrocorticography at Surgery for Lesion-Related Frontal Lobe Epilepsy." *The Canadian Journal of Neurological Sciences. Le Journal Canadien Des Sciences Neurologiques* 26 (1): 33–39.

Wong CH, Birkett J, Byth K, Dexter M, Somerville E, Gill D, et al. Risk factors for complications during intracranial electrode recording in presurgical evaluation of drug resistant partial epilepsy. Acta neurochirurgica. 2009;151:37-50.

Wray, Carter D., Sharon S. McDaniel, Russell P. Saneto, Edward J. Novotny, and Jeffrey G. Ojemann. 2012. "Is Postresective Intraoperative Electrocorticography Predictive of Seizure Outcomes in Children?" *Journal of Neurosurgery. Pediatrics* 9 (5): 546–51. https://doi.org/10.3171/2012.1.PEDS11441.

Wu, J. Y., R. Sankar, J. T. Lerner, J. H. Matsumoto, H. V. Vinters, and G. W. Mathern. 2010. "Removing Interictal Fast Ripples on Electrocorticography Linked with Seizure Freedom in Children." *Neurology* 75 (19): 1686–94. https://doi.org/10.1212/WNL.0b013e3181fc27d0.

Wyler AR, Walker G, Somes G. The morbidity of long-term seizure monitoring using subdural strip electrodes. Journal of neurosurgery. 1991;74:734-7.

Yang, Tong, Shahin Hakimian, and Theodore H. Schwartz. 2014. "Intraoperative ElectroCorticoGraphy (ECog): Indications, Techniques, and Utility in Epilepsy Surgery." *Epileptic Disorders: International Epilepsy Journal with Videotape* 16 (3): 271–79. https://doi.org/10.1684/epd.2014.0675.

You, Gan, Zhi-Yi Sha, Wei Yan, Wei Zhang, Yong-Zhi Wang, Shao-Wu Li, Lin Sang, et al. 2012. "Seizure Characteristics and Outcomes in 508 Chinese Adult Patients Undergoing Primary Resection of Low-Grade Gliomas: A Clinicopathological Study." *Neuro-Oncology* 14 (2): 230–241. https://doi.org/10.1093/neuonc/nor205.

Yuan, Yang, Zhou Peizhi, Wang Xiang, Liu Yanhui, Liang Ruofei, Jiang Shu, and Mao Qing. 2019. "Intraoperative Seizures and Seizures Outcome in Patients Undergoing Awake Craniotomy." *Journal of Neurosurgical Sciences* 63 (3): 301–7. https://doi.org/10.23736/S0390-5616.16.03880-7.

Zanello, Marc, Alexandre Roux, Gilles Zah-Bi, Bénédicte Trancart, Eduardo Parraga, Myriam Edjlali, Arnault Tauziede-Espariat, et al. 2020. "Predictors of Early Postoperative Epileptic Seizures after Awake Surgery in Supratentorial Diffuse Gliomas." *Journal of Neurosurgery*, March, 1–10. https://doi.org/10.3171/2020.1.JNS192774.

Zijlmans, Maeike, Geertjan M. Huiskamp, Olaf L. Cremer, Cyrille H. Ferrier, Alexander C. van Huffelen, and Frans S. S. Leijten. 2012. "Epileptic High-Frequency Oscillations in Intraoperative Electrocorticography: The Effect of Propofol." *Epilepsia* 53 (10): 1799–1809. https://doi.org/10.1111/j.1528-1167.2012.03650.x.

Zijlmans, Maeike, Gregory A. Worrell, Matthias Dümpelmann, Thomas Stieglitz, Andrei Barborica, Marcel Heers, Akio Ikeda, Naotaka Usui, and Michel Le Van Quyen. 2017. "How to Record High-Frequency Oscillations in Epilepsy: A Practical Guideline." *Epilepsia* 58 (8): 1305–15. https://doi.org/10.1111/epi.13814.

Zweiphenning, W. J. E. M., M. A. van 't Klooster, E. van Diessen, N. E. C. van Klink, G. J. M. Huiskamp, T. A. Gebbink, F. S. S. Leijten, et al. 2016. "High Frequency Oscillations and High Frequency Functional Network Characteristics in the Intraoperative Electrocorticogram in Epilepsy." *NeuroImage. Clinical* 12: 928–39. https://doi.org/10.1016/j.nicl.2016.09.014.

4.4.2 Neurotoxicity Test

Objectifs
L'étude fait partie de l'évaluation de la sécurité d'utilisation du dispositif médical conçu par Panaxium. Le dispositif médical consiste en une grille de microélectrodes recouvertes de PEDOT-PSS dont le substrat est en Parylène C couplée à un connecteur flex en LCP, ce dernier n'étant pas en contact direct avec la surface corticale. Ce test a pour but d'évaluer la neurotoxicité aigue du dispositif médical en amont de l'étude clinique. Seule la partie du dispositif en contact avec le cortex a été évaluée (Parylène C et PEDOT:PSS sont les composants de cette surface).
L'évaluation de la neurotoxicité a été menée à partir des critères suivants :

1) Histologiques : préservation de l'anatomie de la structure cérébrale après 6 heures de maintien en conditions de survie cellulaire (aCSF).
2) Electrophysiologique : persistance d'une activité neuronale après 2 heures de maintien en conditions de survie cellulaire.

Méthode
Le test consiste à placer une tranche de tissu cérébral humain, issue des marges de résection de sécurité de gliomes, en contact avec l'électrode Panaxium. Les tissus cérébraux ont été maintenus en survie durant 2 à 6 heures sur l'électrode Panaxium pour moitié et sur la surface en verre Sodocalcique de la boite de Petri ou de l'électrode MEA pour l'autre moitié, afin de comparer le même tissu soumis à 2 conditions différentes :

- Contrôle : **Moitié de tranche de tissu cortical humain**
- Test : **Moitié de tranche de tissu cortical humain** sur électrode

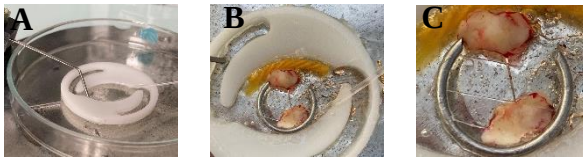

Figure 1 : A : Setup de maintien en vie des tranches en contact avec les électrodes Panaxium. B : 2 tranches à cheval entre l'électrode et la surface en verre. C : Zoom de l'image précédente.

Les **Électrodes Panaxium** ont été fournies stériles dans le même emballage que celui à destination d'usage clinique (double emballage rigide composé de Tyvek et de PETg) avec le support en PETg. La stérilisation, préalablement effectuée (conformément à aux recommandations de la norme **ISO 10993-5 :2009**), a été la même que pour l'usage clinique, soit une stérilisation par oxyde d'éthylène dont un contrôle de concentration de résidus de stérilisation aura été fait avant libération du lot destiné au test conformément à la norme **ISO 10993-7 :2008**.

Le protocole ci-dessous est inspiré du point 8.3 de la norme **ISO 10993-5** adapté pour l'évaluation de la neurotoxicité sur des tranches corticales (et non sur des cultures cellulaires monocouches).

1. Préparation du liquide céphalo-rachidien artificiel (aCSF)
    a. De coupe de tissu : 110 mM Choline, 26 mM NaHCO3, 10 mM Glucose, 11.6 mM Na-ascorbate, 7 mM MgCl26H20, 3.1 mM Na-pyruvate, 2,5 mM KCl, 1,25 mM NaH2PO4H2O

b. De maintien et d'enregistrement de tissu : 124 mM NaCl, 3 mM KCl, 26 mM NaHCO3, 11.1 mM D-glucose, 1,6 mM CaCl2, 1,3 mM MgCl2

2. Préparation de la tranche corticale : résection à la pince des méninges et vaisseaux à la surface de la tranche en milieu ACSF froids et oxygéné puis collage du bloc de tissu sur une porte-échantillon. Section au vibratome de tranches de 400 microns d'épaisseur. Les tranches sont alors maintenues dans de l'ACSF en condition d'interface pendant 1 heure pour optimiser leur viabilité.
3. Dépôt de l'élément à tester (électrode Panaxium) dans une électrode de MEA couvrant la moitié des électrodes (étude électrophysiologique) ou dans une boite de Petri (étude histologique).
4. Dépôt de la tranche corticale à cheval entre l'électrode Panaxium et la surface en verre de l'électrode MEA ou de la boite de Petri (Figure 1.B et C).
5. Perfusion d'ACSF oxygéné au carbogène (95%O2 – 5 % CO2), chauffé à 36 °C.
6. Après 2 heures de maintien, l'électrode Panaxium est retirée de sous la tranche de tissu cérébral. L'activité électrophysiologique extracellulaire est alors recueillie. L'activité de la région de la tranche maintenue sur l'électrode est comparée à celle maintenue sur le verre (contrôle interne).

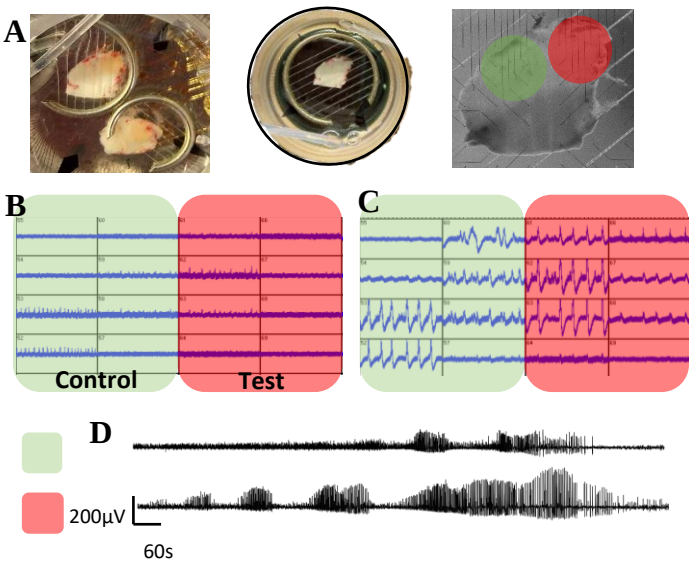

Figure 2. A : maintien des tranches en condition de survie en contact avec l'électrode et le verre. B : Activités électrophysiologiques des régions control (vert) et régions test (rouge) en conditions spontanées. C : Activités électrophysiologiques des régions control (vert) et régions test (rouge) en conditions d'hyperexcitabilité. D : Example de tracés des régions control (vert) et test (rouge).

7. L'enregistrement dure 1 heure comportant 15 minutes d'enregistrement de l'activité de base et 45 minutes d'enregistrement après augmentation de l'excitabilité cellulaire (ajout de 4 mM de KCl dans l'ACSF).
8. Évaluation histologique : après 6 heures de maintien de la tranche en survie dans l'ACSF.
9. Quantification de la survie cellulaire : Une réduction de plus de 30% de la survie cellulaire est considéré comme un effet cytotoxique. Le nombre de neurones survivants sera quantifié par marquage NeuN. La quantification sera : nombre de cellule (NeuN) par champ à 25x

Résultats

Un total de 5 tranches a été enregistré après contact de deux heures avec l'électrode Panaxium. Trois tranches présentaient des activités d'hyperexcitabilité en condition d'excitabilité cellulaire. Sur deux tranches il n'y avait pas d'activités spontanées ni d'hyperexcitabilité sur les régions test et contrôle.

Sur les trois tranches présentant des activités d'hyperexcitabilité, deux présentaient des évènement ictal-like (ILE) sur des régions test et control. Un total de cinq ILE étaient enregistrés. Pas de différence entre la durée des intervalles inter-ILE n'a été retrouvée.

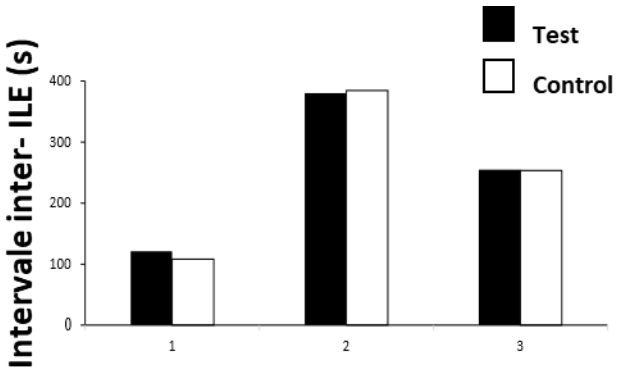

Figure 3: Durée des intervalles inter-ILE en secondes. Pas de différence entre les régions contrôle et test.

Cinq autres tranches ont été analysés histologiquement après avoir passé six heures en contact avec le dispositif médical. En moyenne, 779.2 neurones ont été présents sur les champs X25 sur des régions test, et 671.4 neurones dans le cas des régions control (Figure 1.C). Aucune réduction statistiquement significative de la viabilité cellulaire n'a été retrouvé.

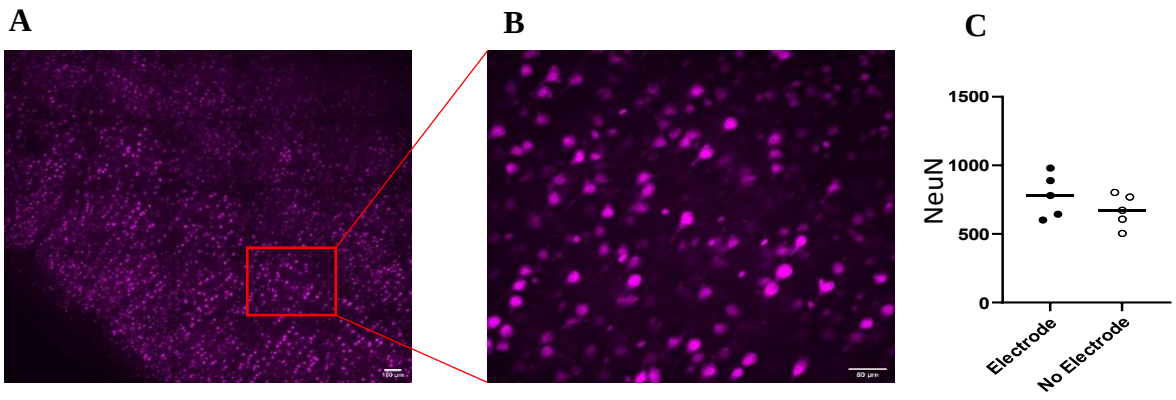

Figure 4: A Immunofluorescence de une région test. B : Zoom X25 pour contage du marquage NeuN. C : Pas de différence significative entre région test et contrôle

Conclusion :
Aucun effet neurotoxique n'a pas été observé, ni structurellement ni fonctionnellement.

Discusion

Throughout this PhD, I have focused my work on the peritumoral tissue. At the peritumoral level, tumor growth and epilepsy converge. Tumor cells spread from the tumor border to the surrounding area, and the presence of the tumor cells alters the microenvironment inducing an increase in activity in the neighboring neurons. However, the interactions between tumor cells and neurons are bidirectional since not only tumor cells enhance neuronal activity, but also neuronal activity boosts tumor growth. Communication between neurons and glioma cells depends on disrupted glutamatergic and GABA signaling; therefore, electrophysiology could also reflect this GABA/Glu impairment. A more profound knowledge of the electrophysiological behavior of the peritumoral tissue could provide information for both epileptogenesis and tumor growth processes. Moreover, from a clinical point of view, glioma management presents two big problems: first, we need a curative treatment since the surgery only allows removing some of the infiltrative tumor cells. Second, given that seizures are frequent in gliomas, patients' quality of life is impacted. Both problems converge at the peritumoral level.

Firstly, in vivo, using ECoG recordings during awake glioma surgery, I have studied: (i) the in vivo electrophysiological behavior of the peritumoral cortex compared to the tumor and healthy areas; (ii) the influence of tumor cells on brain rhythms. The final goal of this in vivo project is to better understand the interactions between tumor cells and neurons and to identify biomarkers of the presence of infiltrative tumor cells in the peritumoral cortex, to guide glioma surgery better and improve at the same time, the oncological and epileptological prognosis. A clinical trial using next-generation conductive polymer based microelectrodes has been designed and will start soon.

Secondly, ex vivo, using human peritumoral slices, I have studied the spatiotemporal dynamics of seizure initiation. Studying the electrophysiological dynamic in the minutes preceding a seizure increases our knowledge of ictogenesis. That can pave the way to designing algorithms for seizure forecasting and developing new pharmacological targets to prevent seizures, leading to a better seizure control, and improve patients' quality of life.

5.1. Contributions of research in the characterization of the peritumoral cortex

5.1.1. In vivo ECoG recordings during awake glioma surgery

While there remains controversy over the value of perioperative ECoG, as some neurosurgical teams do not perceive it as useful (Boetto et al., 2015, 2016), decades ago, before the development of neuroimage, EEG was employed for diagnosing and localizing tumors (Walter & Dovey, 1946).

In this initial study, we report that glioma peritumoral tissue scarcely displays IIDs in patients with well-controlled TRE. However, in patients with a pharmacoresistant TRE, the incidence of IIDs is higher, reaching 80% of patients (Tran et al., 1997). When present, the IIDs never originate from the tumor itself but from the peritumoral cortex at an average

distance of 17 mm from the tumor's border, ranging from 3 to 32 mm. This finding corroborates previous studies suggesting that epileptic activities arise from peritumoral tissue situated over 15 mm away from the tumor border (Mittal et al., 2016; Pallud, Le Van Quyen, et al., 2014). Furthermore, a previous study from our group had colocalized the presence of IIDs ex vivo with regions of pronounced peritumoral infiltration. This investigation also demonstrated that IIDs were never recorded from macroscopic tumor slices (Pallud, Le Van Quyen, et al., 2014).

Our ECoG recordings reveal an augmented beta activity within the peritumoral tissue and an increase in the 20 to 30 and 20 to 40 Hz slopes, with no significant differences between close and far peritumoral contacts. This increase in beta activity at the peritumoral level is a novel observation. Previous studies conducted on healthy individuals have shown that the administration of GABA agonists can elevate beta power in EEG and MEG recordings (Fingelkurts et al., 2004; Hall et al., 2010). Moreover, computational models have suggested that inhibitory postsynaptic currents (IPSCs) on inhibitory neurons are more important than those on pyramidal cells for generating beta rhythms (Jensen et al., 2005). As proposed by Gaetz and colleagues, beta power seems to correlate with levels of GABA inhibition (Gaetz et al., 2011). A study on stroke patients highlighted diminished suppression of beta oscillations during motor tasks, which corresponded to poorer motor learning abilities (Espenhahn et al., 2020), suggesting that aberrant brain functioning can manifest as higher levels of beta activities. Conversely, in Parkinson's patients, beta power increases after levodopa administration, coinciding with symptoms improvement (Cao et al., 2020). Taken together, these data suggest that beta activity may serve as an indicator of both healthy and pathological sensorimotor processing. However, the precise neural mechanisms underlying beta rhythms genesis remain poorly understood (Barone & Rossiter, 2021). While the mechanisms governing beta rhythm generation remain elusive, we hypothesize that the enhanced beta power at the peritumoral level reflects a dysregulation of neuronal activity, likely linked to GABA (Pallud, Le Van Quyen, et al., 2014) and Glu signaling impairment (Buckingham et al., 2011; Ye et al., 1999; Yuen et al., 2012), culminating in hyperexcitability within that region.

On the other hand, the tumoral compartment is characterized by an increase in delta activity accompanied by reduced activity across all the other frequency bands. This suppression of brain rhythms, except for delta activity, has also been reported at the tumor level in a study of 16 glioma ECoGs (Boussen et al., 2016). Nevertheless, their classification was binary, dividing contacts into tumoral or non-tumoral, without exploring the dynamics at the peritumoral or healthy levels. Previous EEG studies on tumor patients have consistently observed delta waves at the tumor site (Munari et al., 1985; Nagata et al., 1985; Newmark et al., 1983). While initially attributed to increased intracranial pressure, subsequent research suggested that delta activity might arise due to peritumoral edema (Hossmann et al., 1979) or structural remodeling in peritumoral areas (De Jongh et al., 2003). The increase in delta activity is thought to indicate reduced cortical inhibition stemming from GABA dysfunction (Niedermeyer et al., 1986, 1997). Regarding the suppression of brain rhythms at the tumor level, if we assume gamma activities are a proxy for neuronal spiking (Buzśaki & Wang, 2012; Fernandez-Ruiz et al., 2023), a decline in gamma activity at the tumor level is expected, given the drastic reduction in neurons within this compartment.

Turning to the aperiodic components of the power spectrum, we observed steeper slopes between 20 to 30 and 20 to 40 Hz at the peritumoral level. Deciphering the underlying mechanism for this increase is beyond the scope of this thesis, yet some authors propose

that steeper slopes signify an imbalance in the excitation-inhibition equilibrium (Gao et al., 2017). Given the heightened excitability in the peritumoral tissue, it is plausible that this excitation-inhibition balance is disrupted. A similar elevation in peritumoral excitability was observed in vivo using ECoG in TRE glioma patients, with an increase of fast activities up to 100 Hz (Feyissa et al., 2018) and HFO rates (van Klink et al., 2021). Another ECoG study on glioma patients also reported an increased slope at the peritumoral level compared to healthy tissue (Ghinda et al., 2021). Additionally, a study involving epileptic patients implanted with sEEG showed that SOZ displayed higher slope values (Jiang et al., 2022).

Our analysis of intra and intercompartment connectivity using the phase locking value (PLV) revealed that the tumor compartment presented the highest levels of connectivity. This trend was consistent with a previous study (Boussen et al., 2016). Elevated intratumoral connectivity may be attributed to the disruption of standard cortical architecture induced by the tumor mass, which promotes long-range conduction of electrical signals.

Furthermore, astrocytomas and oligodendrogliomas present different behaviors, with higher values of offset and slope from 1-200 Hz in astrocytomas at close, far peritumoral, and even healthy levels. These variations may be due to different infiltration patterns between the two entities. Recent findings indicate that oligodendrogliomas exhibit a greater tendency to infiltrate surrounding areas, whereas astrocytomas tend to displace nearby structures and bundles (Landers et al., 2023). Another study demonstrated that oligodendrogliomas infiltrate larger and more heterogeneous white matter tracks compared to astrocytomas (Latini et al., 2020). Also, in a study based on the WHO 2016 classification criteria, oligodendrogliomas tend to present more diffuse borders (83/90 patients, 92%) compared to astrocytomas (26/58 patients, 45%) (Johnson et al., 2017). These differences in infiltration imply that astrocytomas are more likely to displace functional cortex and bundles, shifting functional areas towards the periphery. An alternative explanation for the disparities found at the healthy level could be the electrode placement, as healthy contacts may come occasionally into contact with functional areas exhibiting higher neuronal activity, thereby impacting offset levels.

Given that we employed an arbitrary distance criterion for compartment classification, we then examined electrode behavior based on the distance to the tumor without applying any threshold. The distance between the macroscopic core and the contact did not correlate with the frequency bands or the aperiodic features. In TRE, IIDs and the seizure onset zone are typically eccentric to a specific area of the peritumoral tissue, and no radial distribution has ever been noted before (Mittal et al., 2016). Our data supports that peritumoral follows an eccentric rather than a radial distribution, influenced by glioma cell infiltration along axons and blood vessels.

High peritumoral infiltration in slices showed an inverse correlation with beta and low gamma activities and slopes from 40 to 60 and 60 to 120 Hz. Thus, peritumoral infiltration seems to alter brain rhythms.

Following the identification of specific differences in the periodic and aperiodic components based on compartments, we developed a method for automated contact classification based on power spectrum features using a neural network. This approach outperformed random classification, suggesting that electrophysiological markers may hold promise for classifying tumoral, peritumoral, and healthy cortices.

In summary, this study represents the first comparison of aperiodic component and frequency behavior between the tumor, peritumoral and healthy cortex. In addition to describing the electrophysiological characteristics of the peritumoral cortex, which could be useful as an ECoG biomarker to refine glioma surgery, we observed an imbalance excitatory-inhibitory state within the peritumoral cortex. This imbalance is consistent with its epileptic features and the complex interactions between glioma tissues and the surrounding neuronal microenvironment (Krishna et al., 2023).

5.1.2. Ex vivo extracellular recordings of human peritumoral slices during the transition to a seizure

This study demonstrates that PIDs exhibit larger amplitudes, steeper rising slopes, and higher frequencies compared to IIDs. These distinct characteristics are suggestive of varied underlying mechanisms governing their generation. Specifically, IIDs depend on glutamatergic and GABAergic signaling, while PIDs depend on AMPA signaling (Huberfeld et al., 2011; Johan Pallud et al., 2014). IIDs are markers of epileptogenicity since only epileptic tissues display spontaneous IIDs. Control tissues, such as the cortex from regions adjacent to deep cavernomas, do not exhibit spontaneous IIDs (Blauwblomme et al. 2019; Dossi et al. 2018; Huberfeld et al. 2011; Pallud et al. 2014). The larger amplitudes associated with PIDs suggest that larger neuronal populations are implicated in their generation. Their steeper rising slope may reflect more robust synchronous networks compared to IIDs. Moreover, whereas IIDs maintain stability over time, PIDs present progressive amplitude, rising slope, and frequency increases, implying ongoing neuronal recruitment during the preictal period.

Our findings indicate that PID generation requires time, as they do not manifest immediately following heightened excitability. Unlike neuronal firing, which rapidly increases after extracellular K^+ elevation (Contreras et al., 2021), PID generation likely necessitates some form of plasticity (Huberfeld et al., 2011). Notably, astrocytomas and oligodendrogliomas present shorter delays in the appearance of the first PID compared to GB. This discrepancy might be attributed to the more robust epileptic networks found in astrocytomas and oligodendrogliomas, which are recognized for higher seizure rates.

The temporal evolution of PIDs is evident during the build-up period until reaching a plateau. Subsequently, during the trigger period, further growth ensues. Although this increase is at its maximum during the trigger period, the final PID before the onset of ILE is not necessarily the largest. This finding suggests that ILE generation depends not only on the number of neurons involved but also on their synchronicity, as the last PID before ILE onset might have smaller amplitudes than preceding PIDs.

In vivo recordings of epileptic patients using sEEG also present similar PID patterns (I. E. Chen et al., 2018; Lagarde et al., 2019; Weiss et al., 2016). Additionally, in vivo PIDs exhibit a progressive increase in amplitude and frequency (Chen et al., 2018). The presence of a preictal spiking pattern before seizure onset correlated with 57.9% of patients achieving seizure freedom post-surgery (Lagarde et al., 2019). Comparable propagation speed ranges (0.3 to 0.8 m/s) have been recorded in epileptic patients (Matarrese et al., 2023).

IIDs and PIDs propagation primarily depends on synaptic connections (Chizhov et al., 2019, 2022). The augmented speed of PID propagation from the steady state to the trigger period might be attributed to more efficient propagation along the fastest synaptic pathways. During the build-up and the steady state, the network evolves and explores potential synaptic pathways; later on, during the trigger period, when the network becomes more streamlined, only the quickest synaptic pathways persist.

Regarding HFA, a temporal dynamic is also observed, characterized by progressive increases in duration and amplitude. This phenomenon suggests either an increase in the spiking rate of the neurons belonging to the network or a recruitment of more neurons into the network. The peak durations and amplitudes of HFA occur just before ILE onset, which had already been reported in an ex vivo hippocampal mice model, where HFA increases during the preictal period with a maximum in the seconds before the ILE (Jiruska et al., 2010). Interestingly, despite the slowing of FP amplitude growth during the steady state, HFA continues to evolve during the steady and trigger periods, indicating ongoing neuronal recruitment during the preictal phase even without evident changes in FP.

The quantity of HFOs also increases as ILE onset approaches. However, it is interesting to note that not all the slices exhibit HFO. A disrupted inhibitory network is needed for pathologic ripples and fast ripples generation (Ibarz et al., 2010; Trevelyan et al., 2007). To record fast ripples, we also need the presence of ephaptic conduction, circuit reorganization, and probably also gap junctions (Foffani et al., 2007; Ibarz et al., 2010; Jefferys, 1995; Richard J. Staba et al., 2007; Traub et al., 2011). Although some ILE appear without concurrent HFO, spatial analysis demonstrates that HFO can be recorded from single microelectrodes within the small matrix. This suggests that the local nature of HFO necessitates an interelectrode space of less than 200 µm to capture all the HFO. With our actual interelectrode space, some HFO can be undetectable on a slice of 400 µm thickness. This finding also suggests that sEEG electrodes, even containing microcontacts, might not capture all HFO, potentially contributing to the variable success of epilepsy surgery. Different techniques, such as perioperative electrocorticography, could enhance the recording of HFOs, aiding in surgical planning.

MEA recordings offer the advantage of providing extensive spatial information. Gill and colleagues described the propagation of ILE in a tumor epilepsy mice model using MEA on brain slices. They found that ILE originates at the tumor border in 50% of cases and the peritumoral tissue in 36.9% (Gill et al., 2020). However, their study focused on the spatiotemporal dynamics of ILEs, omitting the preictal phase. In our study, we observed temporal and spatial recruitment patterns for PIDs, HFA, and HFO, suggesting increasing neuronal populations joining the network as the preictal period advances. Interestingly, HFA areas were closely situated to the initial appearance of PIDs, implying a potential role in PID generation. However, their primary projection might be displaced by some µm due to volume conductance (Herreras, 2016; Kajikawa & Schroeder, 2015; Wolters & Munck, 2007). Similarly, HFO followed the same behavior, with enlarging areas and emerging HFO regions during the process, indicating the presence of patchy cluster areas involved in HFO generation that are detectable only in close proximity.

The spatiotemporal evolution of HFA and HFO mirrored that of PIDs, with gradually increasing amplitude and broader areas involved. Furthermore, most HFOs were nested within a PID, maintaining constant phase relations during the preictal period. We hypothesized that a shared mechanism underlying PID, HFA, and HFO generation at the

neocortical level could explain this coordinated behavior. Given that glutamatergic mechanisms drive PIDs (Huberfeld et al., 2011), it is conceivable that glutamate plays a significant role in enhancing HFA and HFO during the preictal period. As HFA evolves throughout the preictal period, that can suggest that neuronal recruitment is continuous during the way to the ILE. However, the fact that PIDs mainly evolve during the build-up period suggests that synchronicity remains stagnant during the steady state, only to be revived once more during the trigger period.

The analysis of this second paper are still ongoing, specially regarding HFA and HFO spatiotemporal dynamics, that need to be precisely quantified and compared to PID evolution. However, at the moment we can conclude that PIDs can be induced ex vivo in human brain slices by increased excitability. That can replicate the *in vivo* transition between the interictal period and the beginning of a seizure. Through the way to an ILE, a temporal evolution is evident in PIDs, HFA, and HFO, reflecting neuronal recruitment and synchronicity. Furthermore, a spatial enlargement of the areas producing PIDs, HFA, and HFO are observed. These dynamics, both on the temporal and spatial scale, hold the potential for developing an in vivo seizure anticipation algorithm. A deeper understanding of seizure and preictal patterns could have significant implications regarding seizure anticipation or prognosis. However, a high spatial resolution is needed to capture the complex dynamics, especially of HFO.

5.2. Methodological Limitations:

5.2.1. In vivo ECoG recordings.

We encounter two primary limitations when identifying an electrophysiological biomarker of the peritumoral cortex extension. Firstly, there is the challenge of defining peritumoral tissue. The extent of peritumoral tissue remains unknown until we confirm the presence of tumor cells through histological analysis. However, the problem is not binary since it is not only the local presence of tumor cells that impact brain activity. Additionally, the density of tumor cells can influence brain activity in a different grade, as previously described; higher peritumoral infiltration alters brain rhythms more than low infiltration. Sometimes, the electrodes were placed in functional areas where obtaining a biopsy is impossible. We tried to overcome this limitation by directly correlating ECoG features with quantified infiltration. This approach yielded coherent outcomes, demonstrating that more significant infiltration is associated with lower physiological rhythms.

Furthermore, it is essential to consider that the infiltration of tumor cells tends to be organized in patches rather than following a radial distribution since they follow axons and blood vessels for migration. Therefore, using an arbitrary radial distance criterion designates areas as peritumoral, but they can present different infiltration grades ranging from no infiltration to high infiltration. That could explain the heterogeneity of our results.

However, we must consider that gliomas secrete Glu and D2HG, which can diffuse throughout the vicinity. D2HG is detectable in patients' CSF (Kalinina et al., 2016). Nonetheless, the gradient of its diffusivity is unknown, and a comprehensive map of D2HG and Glu diffusion around the tumor is lacking. We are collecting small biopsies (0.5 cm^3)

to measure Glu and D2HG concentrations using gas chromatography coupled with mass spectroscopy to address this query.

The second limitation is the spatial resolution achievable with macroelectrodes. Nowadays, the smallest electrodes we can use in a clinical setting possess a diameter of 4 mm and are spaced by 10 mm. Smaller electrodes have yet to receive EMA or FDA approval, restricting their use to research protocols involving a limited number of patients.

Our study analyzed data from a limited pool of 29 patients, but recordings were performed on 85 patients. Most of these recordings (41) were excluded due to elevated noise levels in the monopolar montage. ECoG recordings during awake glioma surgery are susceptible to multiple artifacts, including electromagnetic interference from numerous electronic devices that cannot be switched off (perfusion, speech therapist computer, electrical bipolar stimulation, electrical scalpel, amplifier computer…). The other 15 recordings were excluded due to the diffuse nature of the tumor, making it impossible to delimitate its borders for accurate electrode distance measurement. Furthermore, the limited number of patients due to the quality of the recordings made that most patients had astrocytomas, and GB were underrepresented with only two individuals.

Our recordings presented a limited number of IIDs, which was surprising since most of the cohort presented epileptic seizures. Another surprising finding was that only a few patients presented HFO in the recordings. Even patients with spontaneous IIDs did not exhibit HFOs.

Regarding the neural network classifier, a limitation in the capacity of classification could be the imbalance of the data as peritumoral contacts were more frequent (243 close peritumoral and 213 far peritumoral) compared to tumoral (126) or healthy (136), that can imbalance the data, creating a bias during the training and leading to a decrease in performance in the test.

5.2.2. Ex vivo extracellular recordings

Using ex vivo human slices provides a valuable platform to study ictogenesis. Achieving successful and accurate recordings hinges on a meticulous slice manipulation and sectioning approach. Precision and speed are crucial to prevent tissue damage. Maintaining proper temperature control and oxygenation of the slices are pivotal factors influencing network activity recording.

Nonetheless, there exist two main limitations when employing ex vivo human slices. First, the slice loses its connections to other brain areas. Neuronal activity often undergoes modulation through inputs originating from close and distant brain regions. Second, a significant challenge arises in establishing an appropriate control tissue. Typically, we used cortex resected for accessing deep lesions like cavernomas as control tissues. However, even tissues from supposedly normal cortex can exhibit alterations stemming from the presence of the primary lesion or associated epilepsy.

Furthermore, the surgical procedure itself can damage the tissue. The ideal sample must be obtained before the beginning of glioma resection to avoid disturbing the surrounding area

with edema or bleeding. The vibratome slicing process can also damage the slice leading to neuronal death (Verwer et al., 2015). In 400 µm slices, the first 50 µm on both sides can be damaged due to the slicing. The slicing process can provoke a dysregulation of Cl^- homeostasis, ultimately inducing a GABAergic alteration (Dzhala et al., 2012).

In the context of our study, slices recorded with a small matrix configuration (200 µm of interelectrode spacing) might exhibit the SOZ located outside the recording site, thereby capturing only propagation.

5.3. New uses of microECoG

MicroECoG electrodes enhance the quality of the recordings by increasing spatial resolution and SNR. This opens a unique window to the brain, enabling the concurrent detection of field potential activities alongside single-neuron firing. Enhanced spatial resolution is precious for discerning local disparities in the power spectrum between the tumor and surrounding compartment, which is challenging with macrocontacts since electrodes might straddle compartments.

Moreover, microelectrodes can elevate the rate of HFO detections, a critical factor given the requirement for a robust SNR to identify low amplitude HFO. Additionally, evidence demonstrates that macroelectrodes fail to capture all HFO we can record with microcontacts (Curot et al., 2023). Therefore, microECoG can also help study ictogenesis in vivo through chronic recordings. Our ex vivo study has unveiled temporal dynamics in HFO, fast activities, and FP in the minutes before an ILE. However, the modulation of these activities by inputs from other brain regions during ictogenesis is unknown. This gap arises because studies focused on seizure generation have predominantly employed the Utah array or sEEG recordings confined to minute areas. Due to their specificity to epileptical processes, seizure forecasting algorithms could be developed based on the spatiotemporal dynamic of HFO and PIDs before the seizure.

Furthermore, an ex vivo investigation has successfully correlated infiltrative tumor cell presence with HFO. HFO is a promising biomarker of epileptogenicity. However, their role as perioperative electrophysiological biomarkers for tumor cells needs validation. To this end, we have designed a clinical trial employing innovative microECoGs with an organic PEDOT:PSS lining. The primary outcome of the clinical trial is the device's safety before EMA marking. As exploratory outcomes, we will study the correlation between the electrophysiological recorded activities and the degree of peritumoral infiltration assessed by histology. The most promising biomarker are HFO, but different combinations of activities will be studied: ripples alone, fast ripples alone, HFO associated with spikes, and gamma activity. After this first “proof-of-concept” clinical trial, a second trial would be needed to determine the superiority of HFO to guide glioma surgery. We would need to compare the surgery guided by HFO presence vs. surgery non-based on HFO.

If HFO shows its value as a biomarker for tumor cells in the peritumoral area, software allowing real-time detection of HFO during the surgery could be used as an “electrophysiological microscope” to unveil the presence of tumor cells. However, overcoming specific technological challenges is essential:

- High-density microelectrodes, sampled at 20 KHz, generate a massive amount of data requiring processing for relevant information extraction. While commercial solutions like Spike2 suffice for the Berger frequency range, tools for processing activities exceeding 40 Hz are lacking.
- Implementing real-time detectors is crucial, as current automatic HFO detectors need a post-processing validation stage.
- Another challenge is, once we have the information, for example, the rate of HFO in a given area, how to represent it visually intuitively for interpretation to make decisions in real-time.

MicroECoGs can also be used during epilepsy surgery, allowing better to detect HFOs, possible markers of the EZ. However, since microECoG allows for single-neuron recordings, that could also provide insight into the underlying mechanisms implicated in seizure generation in other pathologies such as focal cortical dysplasia, tuberous sclerosis, etc. Beyond epilepsy, that would help to better understand different brain functions in physiological and pathological conditions. During awake surgery, various protocols can be used to test for vision, memory, and language.

Finally, microelectrodes seem a perfect candidate for chronic setups in brain-machine interfaces like Neuralink devices. Further technological development could position them as therapeutic tools for optimizing neuronal plasticity after stroke or trauma. Their flexibility made them suitable to be implanted in chronic setups in a minimally invasive way.

5.4 Evolution of Glioma Surgery

Glioma surgery stands as the epitome of functional surgery since the boundaries of the tumor's anatomy fail to dictate the extent of resection. Instead, the evaluation of the functionality of the surrounding brain areas guides surgical decisions. While we presume the presence of tumor cells around macroscopic tumors, distinguishing between healthy and infiltrated areas in real-time during the surgery sounds like a science-fiction story. The optimal strategy, enhancing overall survival and epileptological outcomes, involves maximizing resection as guided by functional mapping. Expanding the safety margin around the tumor is associated with improved oncological and epileptological outcomes. Nevertheless, the utility of electrical direct stimulation for functional mapping is constrained in identifying associative areas. Therefore, knowing that tissue is not infiltrated could favorably lead to its preservation, potentially aiding postsurgical neuronal plasticity.

A refined surgical approach is needed to enhance outcomes, using innovative techniques to detect infiltrative tumor cells in real-time during the surgery. Imaging techniques face spatial resolution limitations due to the small dimensions of tumor cells. For example, 1H-MRS D2HG can detect D2HG presence but in voxels of 3 cm^3. Imaging techniques with higher spatial resolution, such as confocal microscopy for detecting protoporphyrin X, are time-consuming.

Our team approaches glioma cell detection from a distinctive standpoint, capitalizing on interactions between neurons and glioma cells. Beyond molecular interactions, changes in Glu and GABA signaling are also evident. Tumor cells modify the peritumoral microenvironment, triggering a hyperactivation of surrounding neurons through mechanisms previously described (Glu and GABA dysregulation, activation of mTOR pathway, alteration of ionic homeostasis …). Still, neuronal activity reciprocally influences tumor cell behavior and growth. This "bidirectional communication" between glioma cells and neurons induces changes in normal electrophysiological activities. These changes, measurable in vivo using ECoG, provide an avenue for exploitation.

The results from the ECoG pilot study reveal distinct frequency content and aperiodic components differences in the peritumoral cortex compared to the tumor and healthy cortex. These changes could be used to delimitate the extension of the peritumoral tissue using automatic detectors based on machine learning. We need to overcome the spatial resolution limitations; smaller electrodes could better detect electrophysiological changes in those different areas. Therefore, initiating a spontaneous primary cortical activity recording before functional mapping to locate and delineate the peritumoral area could be a valuable complementary tool. We propose to take advantage of those electric changes to delimit the extent of the peritumor area, to focus the measure of biomarkers of tumor cells there.

Furthermore, while electrical direct stimulation mapping excels at localizing primary functional areas –constituting about 30% of the cortex, like the primary motor or somatosensitive cortex- it is less efficient for associative areas. However, the process can be highly time-consuming since EDS evaluates one brain region at a time. Since gamma activity from 40 Hz can be recorded during multiple cognitive functions, such as visual perception, selective attention, motor tasks, speech or memory-related processes (Basirat et al., 2008; Engelhard et al., 2013; Ole Jensen et al., 2007; Jean Philippe Lachaux et al., 2000; Müsch et al., 2014), recording gamma-evoked activity during functional tasks holds promise as a functional mapping technique for identifying functional primary and associative areas. Gamma mapping, used in addition to electrical mapping, has already been used in some centers (Milsap et al., 2019; Taplin et al., 2016). Also, preliminary unpublished data from our team showed that auditory stimuli induced augmentation of gamma activities between 40 and 80 Hz in auditory cortical areas. Although further studies are required in the glioma population, envisioning a 'positive gamma functional mapping" is plausible. Placing an electrode grid on the cortex and instructing patients to perform different tasks allows simultaneous information collection from the entire grid-covered area to expedite functional mapping. Incorporating stimulation capabilities into the electrodes could confirm findings for primary functions. This approach, in my opinion, has the potential to yield a more efficient mapping process, enhancing speed and reducing patient fatigue – a common problem during awake glioma surgery.

Envisioning the future of glioma surgery, I imagine an integrated setup for functional awake surgery that offers real-time:

- Accurate positioning of electrodes merged on MRI, facilitated by a perioperative camera linked to fiducials on the grid.

- HFO and spikes mapping during a spontaneous recording before functional tasks.

- Heat maps for the various frequencies (from delta to high gamma) and aperiodic components of the power spectrum during the initial recording.

- Positive functional mapping based on gamma mapping during different tasks.

- Negative functional mapping by EDS.

- Anatomic and functional MRI with preoperative information.

- Fusion of all the heatmaps (HFO, gamma activities, power spectrum characteristics, negative mapping) with MRI and perioperative brain view.

- And the icing on the cake, since parylene is transparent, a filter adapted to the perioperative camera to detect the fluorescence of protoporphyrin IX.

Conclusion

Conclusion

My thesis aimed at assessing the electrophysiological features of the periglioma cortical tissues, both in vivo in awake patients and ex vivo in postoperative tissues.
ECoG recording of patients undergoing awake glioma surgery sheds light on distinct electroencephalographic patterns within different tumor compartments. Specifically, the tumor area exhibits an elevation in delta activity and a reduction in all the other frequency bands, thereby highlighting the disrupting effects of the tumor on EEG physiological rhythms. Conversely, the peritumoral tissue presents an increase in relative beta activity, as well as steeper slopes within the 20 to 30 and 20 to 40 Hz ranges. These observations indicate alterations in neuronal activities or synaptic input balances. Although differences between close and far peritumoral contacts are not evident, a noticeable correlation emerges between the reduction of physiological rhythms and the extent of tumor cell infiltration quantified by immunohistochemistry. This suggests that infiltration and its electrophysiological correlate do not follow a linear, radial distribution but a spreading guided by nervous bundles and vessels. This key but challenging to delineate zone surrounding gliomas must be removed to improve epilepsy and oncological outcomes. This pilot study lays the ground for real-time electrophysiological mapping, with improved spatio-temporal resolution using microECoG, a tool that can better guide the resection, ultimately impacting patient's survival rates and quality of life.

The ictogenesis study of peritumoral slices highlights the intricate dynamics followed by PIDs in time and space. PIDs show a gradual amplification in amplitude, rising slope, and frequency, indicative of increased neuronal synchronization, especially during the build-up and trigger periods. HFA and HFO increased over the preictal period, suggesting progressive neuronal recruitment and activation of small networks responsible for HFO generation, culminating in peak activity seconds before the ILE onset. PIDs, HFA, and HFO follow a progressive spatial enlargement. However, HFO recording is limited to microdomains smaller than 200 µm. Given the parallel progression of these activities, it is plausible that they arise from shared underlying mechanisms. These complex dynamics could be used to develop algorithms to detect seizure high-risk periods in patients. During these windows, adjusting the medication or avoiding dangerous activities could improve the patient's quality of life.

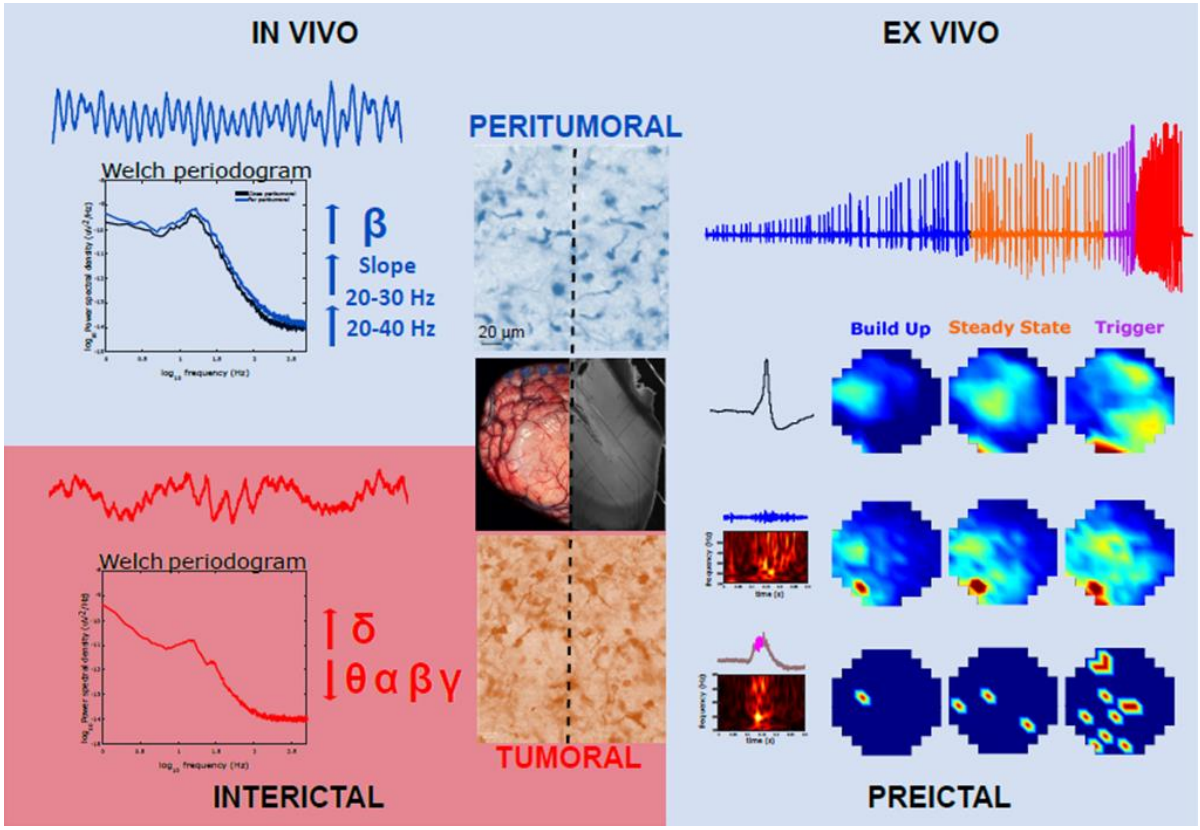

Figure 31: Peritumoral cortex: electrophysiological signals.
Left: In vivo characteristics of the power spectrum during the interictal period.
Right: Ex vivo spatiotemporal dynamics of electrophysiological signals during ictogenesis.

Bibliography

Al-Khallaf, H. (2017). Isocitrate dehydrogenases in physiology and cancer: Biochemical and molecular insight. *Cell and Bioscience*, *7*(1), 1–18.

Algharabil, J., Kintner, D. B., Wang, Q., Begum, G., Clark, P. A., Yang, S. Sen, Lin, S. H., Kahle, K. T., Kuo, J. S., & Sun, D. (2012). Inhibition of Na(+)-K(+)-2Cl(-) cotransporter isoform 1 accelerates temozolomide-mediated apoptosis in glioblastoma cancer cells. *Cellular Physiology and Biochemistry : International Journal of Experimental Cellular Physiology, Biochemistry, and Pharmacology*, *30*(1), 33–48.

Alimohamadi, M., POUR-RASHIDI, A., LARIJANI, A., RAHMANI, M., HENDI, K., SHARIAT MOHARARI, R., RAMINFARD, S., AJAM, H., & GERGANOV, V. (2023). Perioperative seizure in patients undergoing brain mapping under awake craniotomy for language-related eloquent region gliomas: a prospective study. *Journal of Neurosurgical Sciences*.

Almairac, F., Frenay, M., & Paquis, P. (2010). [Genetic diseases and glioblastomas]. *Neuro-Chirurgie*, *56*(6), 455–458.

Alms, D., Fedrowitz, M., Römermann, K., Noack, A., & Löscher, W. (2014). Marked differences in the effect of antiepileptic and cytostatic drugs on the functionality of P-glycoprotein in human and rat brain capillary endothelial cell lines. *Pharmaceutical Research*, *31*(6), 1588–1604.

Alsop, D. C., Detre, J. A., Golay, X., Günther, M., Hendrikse, J., Hernandez-Garcia, L., Lu, H., Macintosh, B. J., Parkes, L. M., Smits, M., Van Osch, M. J. P., Wang, D. J. J., Wong, E. C., & Zaharchuk, G. (2015). Recommended implementation of arterial spin-labeled perfusion MRI for clinical applications: A consensus of the ISMRM perfusion study group and the European consortium for ASL in dementia. *Magnetic Resonance in Medicine*, *73*(1), 102–116.

Amary, M. F., Bacsi, K., Maggiani, F., Damato, S., Halai, D., Berisha, F., Pollock, R., O'Donnell, P., Grigoriadis, A., Diss, T., Eskandarpour, M., Presneau, N., Hogendoorn, P. C. W., Futreal, A., Tirabosco, R., & Flanagan, A. M. (2011). IDH1 and IDH2 mutations are frequent events in central chondrosarcoma and central and periosteal chondromas but not in other mesenchymal tumours. *The Journal of Pathology*, *224*(3), 334–343.

Amorini, F., Zironi, I., Marzocchi, M., Gualandi, I., Calienni, M., Cramer, T., Fraboni, B., & Castellani, G. (2017). Electrically Controlled "Sponge Effect" of PEDOT:PSS Governs Membrane Potential and Cellular Growth. *ACS Applied Materials & Interfaces*, *9*(8), 6679–6689.

Andronesi, O. C., Kim, G. S., Gerstner, E., Batchelor, T., Tzika, A. A., Fantin, V. R., Vander Heiden, M. G., & Sorensen, A. G. (2012). Detection of 2-Hydroxyglutarate in IDH-mutated Glioma Patients by Spectral-editing and 2D Correlation Magnetic Resonance Spectroscopy. *Science Translational Medicine*, *4*(116), 116ra4.

Angulo, M. C., Kozlov, A. S., Charpak, S., & Audinat, E. (2004). Glutamate released from glial cells synchronizes neuronal activity in the hippocampus. *The Journal of Neuroscience : The Official Journal of the Society for Neuroscience*, *24*(31), 6920–6927.

Appay, R., Dehais, C., Maurage, C. A., Alentorn, A., Carpentier, C., Colin, C., Ducray, F., Escande, F., Idbaih, A., Kamoun, A., Marie, Y., Mokhtari, K., Tabouret, E., Trabelsi, N., Uro-Coste, E., Delattre, J. Y., Figarella-Branger, D., Dhermain, F., Desenclos, C., … Uro-Coste, E. (2019). CDKN2A homozygous deletion is a strong adverse prognosis factor in diffuse malignant IDH-mutant gliomas. *Neuro-Oncology*, *21*(12), 1519–1528.

Arbizu, J., Tejada, S., Marti-Climent, J. M., Diez-Valle, R., Prieto, E., Quincoces, G., Vigil, C., Idoate, M. A., Zubieta, J. L., Peñuelas, I., & Richter, J. A. (2012). Quantitative volumetric analysis of gliomas with sequential MRI and ^{11}C-methionine PET assessment: patterns of integration in therapy planning. *European Journal of Nuclear Medicine and Molecular Imaging*, *39*(5), 771–781.

Arcella, A., Biagioni, F., Antonietta Oliva, M., Bucci, D., Frati, A., Esposito, V., Cantore, G., Giangaspero, F., & Fornai, F. (2013). Rapamycin inhibits the growth of glioblastoma. *Brain Research*, *1495*, 37–51.

Arcella, A., Carpinelli, G., Battaglia, G., D'Onofrio, M., Santoro, F., Ngomba, R. T., Bruno, V., Casolini, P., Giangaspero, F., & Nicoletti, F. (2005). Pharmacological blockade of group II metabotropic glutamate receptors reduces the growth of glioma cells in vivo. *Neuro-Oncology*, *7*(3), 236–245.

Armstrong, T. S., Grant, R., Gilbert, M. R., Lee, J. W., & Norden, A. D. (2016). Epilepsy in glioma patients: mechanisms, management, and impact of anticonvulsant therapy. *Neuro-Oncology*, *18*(6), 779–789.

Aronica, E., Gorter, J. A., Jansen, G. H., Leenstra, S., Yankaya, B., & Troost, D. (2001). Expression of connexin 43 and connexin 32 gap-junction proteins in epilepsy-associated brain tumors and in the perilesional epileptic cortex. *Acta Neuropathologica*, *101*(5), 449–459.

Aronica, E., Gorter, J. A., Redeker, S., Van Vliet, E. A., Ramkema, M., Scheffer, G. L., Scheper, R. J., Van

Der Valk, P., Leenstra, S., Baayen, J. C., Spliet, W. G. M., & Troost, D. (2005). Localization of breast cancer resistance protein (BCRP) in microvessel endothelium of human control and epileptic brain. *Epilepsia*, *46*(6), 849–857.

Arya, R., Horn, P. S., & Crone, N. E. (2018). ECoG high-gamma modulation versus electrical stimulation for presurgical language mapping. *Epilepsy & Behavior : E&B*, *79*, 26–33.

Audrey, C., Lim, K. S., Ahmad Zaki, R., Fong, S. L., Chan, C. Y., Sathis Kumar, T., Narayanan, V., & Tan, C. T. (2022). Prevalence of seizures in brain tumor: A meta-analysis. *Epilepsy Research*, *187*.

Barker, F. G., & Linskey, M. E. (2004). History of the AANS/CNS joint section on tumors and preface to the 20th anniversary Journal of Neuro-Oncology Special Issue. *Journal of Neuro-Oncology*, *69*(1–3), 1–18.

Barone, J., & Rossiter, H. E. (2021). Understanding the Role of Sensorimotor Beta Oscillations. *Frontiers in Systems Neuroscience*, *15*.

Barth, K. J., Sun, J., Chiang, C. H., Qiao, S., Wang, C., Rahimpour, S., Trumpis, M., Duraivel, S., Dubey, A., Wingel, K. E., Voinas, A. E., Ferrentino, B., Doyle, W., Southwell, D. G., Haglund, M. M., Vestal, M., Harward, S. C., Solzbacher, F., Devore, S., … Viventi, J. (2023). Flexible, high-resolution cortical arrays with large coverage capture microscale high-frequency oscillations in patients with epilepsy. *Epilepsia*, *64*(7).

Bartolomei, F., Chauvel, P., & Wendling, F. (2008). Epileptogenicity of brain structures in human temporal lobe epilepsy: a quantified study from intracerebral EEG. *Brain : A Journal of Neurology*, *131*(Pt 7), 1818–1830.

Basirat, A., Sato, M., Schwartz, J. L., Kahane, P., & Lachaux, J. P. (2008). Parieto-frontal gamma band activity during the perceptual emergence of speech forms. *NeuroImage*, *42*(1), 404–413.

Bauchet, L., Rigau, V., Mathieu-Daudé, H., Figarella-Branger, D., Hugues, D., Palusseau, L., Bauchet, F., Fabbro, M., Campello, C., Capelle, L., Durand, A., Trétarre, B., Frappaz, D., Henin, D., Menei, P., Honnorat, J., & Segnarbieux, F. (2007). French brain tumor data bank: methodology and first results on 10,000 cases. *Journal of Neuro-Oncology*, *84*(2), 189–199.

Baumgartner, C., Serles, W., Leutmezer, F., Pataraia, E., Aull, S., Czech, T., & Pietrzyk, U. (1998). *Preictal SPECT in Temporal Lobe Epilepsy : Regional Cerebral Blood Flow Is Increased Prior to Electroencephalography- Seizure Onset as process*. *39*(6).

Beaumont, A., & Whittle, I. R. (2000). The pathogenesis of tumour associated epilepsy. *Acta Neurochirurgica*, *142*(1), 1–15.

Behr, C., D'Antuono, M., Hamidi, S., Herrington, R., Lévesque, M., Salami, P., Shiri, Z., Köhling, R., & Avoli, M. (2014). Limbic networks and epileptiform synchronization: The view from the experimental side. *International Review of Neurobiology*, *114*, 63–87.

Beierlein, M., Gibson, J. R., & Connors, B. W. (2000). A network of electrically coupled interneurons drives synchronized inhibition in neocortex. *Nature Neuroscience*, *3*(9), 904–910.

Belova, E. M., Semenova, U., Gamaleya, A. A., Tomskiy, A. A., & Sedov, A. (2021). Voluntary movements cause beta oscillations increase and broadband slope decrease in the subthalamic nucleus of parkinsonian patients. *The European Journal of Neuroscience*, *53*(7), 2205–2213.

Bénar, C. G., Chauvière, L., Bartolomei, F., & Wendling, F. (2010). Pitfalls of high-pass filtering for detecting epileptic oscillations: a technical note on "false" ripples. *Clinical Neurophysiology : Official Journal of the International Federation of Clinical Neurophysiology*, *121*(3), 301–310.

Bénit, C. P., & Vecht, C. J. (2016). Seizures and cancer: drug interactions of anticonvulsants with chemotherapeutic agents, tyrosine kinase inhibitors and glucocorticoids. *Neuro-Oncology Practice*, *3*(4), 245–260.

Berendsen, S., Varkila, M., Kroonen, J., Seute, T., Snijders, T. J., Kauw, F., Spliet, W. G. M., Willems, M., Poulet, C., Broekman, M. L., Bours, V., & Robe, P. A. (2016). Prognostic relevance of epilepsy at presentation in glioblastoma patients. *Neuro-Oncology*, *18*(5), 700–706.

Bergles, D. E., Roberts, J. D. B., Somogyl, P., & Jahr, C. E. (2000). Glutamatergic synapses on oligodendrocyte precursor cells in the hippocampus. *Nature*, *405*(6783), 187–191.

Besson, A., & Yong, V. W. (2001). Mitogenic signaling and the relationship to cell cycle regulation in astrocytomas. *Journal of Neuro-Oncology*, *51*(3), 245–264.

Bianchi, L., De Micheli, E., Bricolo, A., Ballini, C., Fattori, M., Venturi, C., Pedata, F., Tipton, K. F., & Della Corte, L. (2004). Extracellular levels of amino acids and choline in human high grade gliomas: an intraoperative microdialysis study. *Neurochemical Research*, *29*(1), 325–334.

Bikfalvi, A., da Costa, C. A., Avril, T., Barnier, J. V., Bauchet, L., Brisson, L., Cartron, P. F., Castel, H., Chevet, E., Chneiweiss, H., Clavreul, A., Constantin, B., Coronas, V., Daubon, T., Dontenwill, M., Ducray, F., Enz-Werle, N., Figarella-Branger, D., Fournier, I., … Virolle, T. (2023). Challenges in glioblastoma research: focus on the tumor microenvironment. *Trends in Cancer*, *9*(1), 9–27.

Birken, D. L., & Oldendorf, W. H. (1989). N-acetyl-L-aspartic acid: a literature review of a compound

prominent in 1H-NMR spectroscopic studies of brain. *Neuroscience and Biobehavioral Reviews*, *13*(1), 23–31.

Birot, G., Kachenoura, A., Albera, L., Bénar, C., & Wendling, F. (2013). Automatic detection of fast ripples. *Journal of Neuroscience Methods*, *213*(2), 236–249.

Bjørnsen, L. P., Eid, T., Holmseth, S., Danbolt, N. C., Spencer, D. D., & de Lanerolle, N. C. (2007). Changes in glial glutamate transporters in human epileptogenic hippocampus: inadequate explanation for high extracellular glutamate during seizures. *Neurobiology of Disease*, *25*(2), 319–330.

Blauwblomme, T., Dossi, E., Pellegrino, C., Goubert, E., Iglesias, B. G., Sainte-Rose, C., Rouach, N., Nabbout, R., & Huberfeld, G. (2019). Gamma-aminobutyric acidergic transmission underlies interictal epileptogenicity in pediatric focal cortical dysplasia. *Annals of Neurology*, *85*(2), 204–217.

Bobustuc, G. C., Baker, C. H., Limaye, A., Jenkins, W. D., Pearl, G., Avgeropoulos, N. G., & Konduri, S. D. (2010). Levetiracetam enhances p53-mediated MGMT inhibition and sensitizes glioblastoma cells to temozolomide. *Neuro-Oncology*, *12*(9), 917–927.

Bodalia, P. N., Grosso, A. M., Sofat, R., Macallister, R. J., Smeeth, L., Dhillon, S., Casas, J. P., Wonderling, D., & Hingorani, A. D. (2013). Comparative efficacy and tolerability of anti-epileptic drugs for refractory focal epilepsy: systematic review and network meta-analysis reveals the need for long term comparator trials. *British Journal of Clinical Pharmacology*, *76*(5), 649–667.

Boetto, J., Bertram, L., Moulinié, G., Herbet, G., Moritz-Gasser, S., & Duffau, H. (2015). Low rate of intraoperative seizures during awake craniotomy in a prospective cohort with 374 supratentorial brain lesions: Electrocorticography is not mandatory. *World Neurosurgery*, *84*(6), 1838–1844.

Boetto, J., Bertram, L., Moulinié, G., Herbet, G., Moritz-Gasser, S., & Duffau, H. (2016). Electrocorticography Is Not Necessary During Awake Brain Surgery for Gliomas. *World Neurosurgery*, *91*, 656–657.

Bondy, M. L., Scheurer, M. E., Malmer, B., Barnholtz-Sloan, J. S., Davis, F. G., Il'yasova, D., Kruchko, C., McCarthy, B. J., Rajaraman, P., Schwartzbaum, J. A., Sadetzki, S., Schlehofer, B., Tihan, T., Wiemels, J. L., Wrensch, M., & Buffler, P. A. (2008). Brain tumor epidemiology: consensus from the Brain Tumor Epidemiology Consortium. *Cancer*, *113*(7 Suppl), 1953–1968.

Bontempi, P., Rozzanigo, U., Amelio, D., Scartoni, D., Amichetti, M., & Farace, P. (2021). Quantitative Multicomponent T2 Relaxation Showed Greater Sensitivity Than Flair Imaging to Detect Subtle Alterations at the Periphery of Lower Grade Gliomas. *Frontiers in Oncology*, *11*.

Bormann, J., Hamill, O. P., & Sakmann, B. (1987). Mechanism of anion permeation through channels gated by glycine and gamma-aminobutyric acid in mouse cultured spinal neurones. *The Journal of Physiology*, *385*(1), 243–286. h

Bosma, I., Douw, L., Bartolomei, F., Heimans, J. J., Van Dijk, B. W., Postma, T. J., Stam, C. J., Reijneveld, J. C., & Klein, M. (2008). Synchronized brain activity and neurocognitive function in patients with low-grade glioma: a magnetoencephalography study. *Neuro-Oncology*, *10*(5), 734–744.

Böttcher, M., Renner, K., Berger, R., Mentz, K., Thomas, S., Cardenas-Conejo, Z. E., Dettmer, K., Oefner, P. J., Mackensen, A., Kreutz, M., & Mougiakakos, D. (2018). D-2-hydroxyglutarate interferes with HIF-1α stability skewing T-cell metabolism towards oxidative phosphorylation and impairing Th17 polarization.

Boussen, S., Velly, L., Benar, C., Metellus, P., Bruder, N., & Trébuchon, A. (2016). In Vivo Tumour Mapping Using Electrocorticography Alterations During Awake Brain Surgery: A Pilot Study. *Brain Topography*, *29*(5), 766–782.

Boxerman, J. L., Quarles, C. C., Hu, L. S., Erickson, B. J., Gerstner, E. R., Smits, M., Kaufmann, T. J., Barboriak, D. P., Huang, R. H., Wick, W., Weller, M., Galanis, E., Kalpathy-Cramer, J., Shankar, L., Jacobs, P., Chung, C., van den Bent, M. J., Chang, S., Al Yung, W. K., … Schmainda, K. M. (2020). Consensus recommendations for a dynamic susceptibility contrast MRI protocol for use in high-grade gliomas. *Neuro-Oncology*, *22*(9), 1262–1275.

Boyden, E. S., Zhang, F., Bamberg, E., Nagel, G., & Deisseroth, K. (2005). Millisecond-timescale, genetically targeted optical control of neural activity. *Nature Neuroscience*, *8*(9), 1263–1268.

Boyer, A., Ramdani, S., Duffau, H., Dali, M., Vincent, M. A., Mandonnet, E., Guiraud, D., & Bonnetblanc, F. (2021). Electrophysiological Mapping During Brain Tumor Surgery: Recording Cortical Potentials Evoked Locally, Subcortically and Remotely by Electrical Stimulation to Assess the Brain Connectivity On-line. *Brain Topography*, *34*(2), 221–233.

Bragin, A., Engel, J., Wilson, C. L., Fried, I., & Mathern, G. W. (1999). Hippocampal and entorhinal cortex high-frequency oscillations (100-500 Hz) in human epileptic brain and in kainic acid-treated rats with chronic seizures. *Epilepsia*, *40*(2), 127–137.

Bragin, A., Wilson, C. L., Staba, R. J., Reddick, M., Fried, I., & Engel, J. (2002). Interictal high-frequency oscillations (80-500Hz) in the human epileptic brain: Entorhinal cortex. *Annals of Neurology*, *52*(4), 407–415.

Brendle, C., Maier, C., Bender, B., Schittenhelm, J., Paulsen, F., Renovanz, M., Roder, C., Castaneda-Vega, S., Tabatabai, G., Ernemann, U., & la Fougère, C. (2022). Impact of 18F-FET PET/MRI on Clinical Management of Brain Tumor Patients. *Journal of Nuclear Medicine : Official Publication, Society of Nuclear Medicine*, *63*(4), 522–527.

Brocke, K. S., Staufner, C., Luksch, H., Geiger, K. D., Stepulak, A., Marzahn, J., Schackert, G., Temme, A., & Ikonomidou, C. (2010). Glutamate receptors in pediatric tumors of the central nervous system. *Cancer Biology & Therapy*, *9*(6), 455–468.

Brodie, M. J., Mintzer, S., Pack, A. M., Gidal, B. E., Vecht, C. J., & Schmidt, D. (2013). Enzyme induction with antiepileptic drugs: cause for concern? *Epilepsia*, *54*(1), 11–27.

Brodie, M. J., & Sills, G. J. (2011). Combining antiepileptic drugs—Rational polytherapy? *Seizure*, *20*(5), 369–375.

Brodie, S. A., & Brandes, J. C. (2014). Could valproic acid be an effective anticancer agent? The evidence so far. *Expert Review of Anticancer Therapy*, *14*(10), 1097–1100.

Bromley, R., Weston, J., Adab, N., Greenhalgh, J., Sanniti, A., Mckay, A. J., Tudur Smith, C., & Marson, A. G. (2014). Treatment for epilepsy in pregnancy: neurodevelopmental outcomes in the child. *The Cochrane Database of Systematic Reviews*, *2014*(10).

Brown, T. J., Bota, D. A., Van Den Bent, M. J., Brown, P. D., Maher, E., Aregawi, D., Liau, L. M., Buckner, J. C., Weller, M., Berger, M. S., & Glantz, M. (2019). Management of low-grade glioma: a systematic review and meta-analysis. *Neuro-Oncology Practice*, *6*(4), 249–258.

Buckingham, S. C., Campbell, S. L., Haas, B. R., Montana, V., Robel, S., Ogunrinu, T., & Sontheimer, H. (2011). Glutamate release by primary brain tumors induces epileptic activity. *Nature Medicine*, *17*(10), 1269–1274.

Buckingham, S. C., & Robel, S. (2013). Glutamate and tumor-associated epilepsy: Glial cell dysfunction in the peritumoral environment. *Neurochemistry International*, *63*(7), 696–701.

Bunevicius, A., Schregel, K., Sinkus, R., Golby, A., & Patz, S. (2020). REVIEW: MR elastography of brain tumors. *NeuroImage. Clinical*, *25*, 102109.

Buonocore, M. H., & Maddock, R. J. (2015). Magnetic resonance spectroscopy of the brain: a review of physical principles and technical methods. *Reviews in the Neurosciences*, *26*(6), 609–632.

Buzsáki, G., Anastassiou, C. A., & Koch, C. (2012). The origin of extracellular fields and currents-EEG, ECoG, LFP and spikes. *Nature Reviews Neuroscience*, *13*(6), 407–420.

Buzsáki, G., Horváth, Z., Urioste, R., Hetke, J., & Wise, K. (1992). High-frequency network oscillation in the hippocampus. *Science*, *256*(5059), 1025–1027.

Buzśaki, G., & Wang, X. J. (2012). Mechanisms of gamma oscillations. In *Annual Review of Neuroscience* (Vol. 35, pp. 203–225). NIH Public Access.

Calatozzolo, C., Pollo, B., Botturi, A., Dinapoli, L., Carosi, M., Salmaggi, A., & Maschio, M. (2012). Multidrug resistance proteins expression in glioma patients with epilepsy. *Journal of Neuro-Oncology*, *110*(1), 129–135.

Campbell-Washburn, A. E., Keenan, K. E., Hu, P., Mugler, J. P., Nayak, K. S., Webb, A. G., Obungoloch, J., Sheth, K. N., Hennig, J., Rosen, M. S., Salameh, N., Sodickson, D. K., Stein, J. M., Marques, J. P., & Simonetti, O. P. (2023). Low-field MRI: A report on the 2022 ISMRM workshop. *Magnetic Resonance in Medicine*.

Campbell, S. L., Buckingham, S. C., & Sontheimer, H. (2012). Human glioma cells induce hyperexcitability in cortical networks. *Epilepsia*, *53*(8), 1360–1370.

Campbell, S. L., Robel, S., Cuddapah, V. A., Robert, S., Buckingham, S. C., Kahle, K. T., & Sontheimer, H. (2015). GABAergic disinhibition and impaired KCC2 cotransporter activity underlie tumor-associated epilepsy. *Glia*, *63*(1), 23–36.

Cao, C., Li, D., Zhan, S., Zhang, C., Sun, B., & Litvak, V. (2020). L-dopa treatment increases oscillatory power in the motor cortex of Parkinson's disease patients. *NeuroImage. Clinical*, *26*.

Capelle, L., Fontaine, D., Mandonnet, E., Taillandier, L., Golmard, J. L., Bauchet, L., Pallud, J., Peruzzi, P., Baron, M. H., Kujas, M., Guyotat, J., Guillevin, R., Frenay, M., Taillibert, S., Colin, P., Rigau, V., Vandenbo, F., Pinelli, C., & Duffau, H. (2013). Spontaneous and therapeutic prognostic factors in adult hemispheric World Health Organization Grade II gliomas: a series of 1097 cases: clinical article. *Journal of Neurosurgery*, *118*(6), 1157–1168.

Capper, D., Zentgraf, H., Balss, J., Hartmann, C., & Von Deimling, A. (2009). Monoclonal antibody specific for IDH1 R132H mutation. *Acta Neuropathologica*, *118*(5), 599–601.

Carbonneau, M., Gagne, L. M., Lalonde, M. E., Germain, M. A., Motorina, A., Guiot, M. C., Secco, B., Vincent, E. E., Tumber, A., Hulea, L., Bergeman, J., Oppermann, U., Jones, R. G., Laplante, M., Topisirovic, I., Petrecca, K., Huot, M. É., & Mallette, F. A. (2016). The oncometabolite 2-hydroxyglutarate activates the mTOR signalling pathway. *Nature Communications*, *7*.

Cases-Cunillera, S., Van Loo, K. M. J., Pitsch, J., Quatraccioni, A., Sivalingam, S., Salomoni, P., Borger, V.,

Dietrich, D., Schoch, S., & Becker, A. J. (2022). Heterogeneity and excitability of BRAFV600E-induced tumors is determined by Akt/mTOR-signaling state and Trp53-loss. *Neuro-Oncology*, *24*(5), 741–754.

Castagnola, E., Maiolo, L., Maggiolini, E., Minotti, A., Marrani, M., Maita, F., Pecora, A., Angotzi, G. N., Ansaldo, A., Boffini, M., Fadiga, L., Fortunato, G., & Ricci, D. (2015). Pedot-cnt-coated low-impedance, ultra-flexible, and brain-conformable micro-ECoG arrays. *IEEE Transactions on Neural Systems and Rehabilitation Engineering*, *23*(3), 342–350.

Cela, E., McFarlan, A. R., Chung, A. J., Wang, T., Chierzi, S., Murai, K. K., & Sjöström, P. J. (2019). An Optogenetic Kindling Model of Neocortical Epilepsy. *Scientific Reports*, *9*(1).

Cepeda, C., André, V. M., Hauptman, J. S., Yamazaki, I., Huynh, M. N., Chang, J. W., Chen, J. Y., Fisher, R. S., Vinters, H. V., Levine, M. S., & Mathern, G. W. (2012). Enhanced GABAergic network and receptor function in pediatric cortical dysplasia Type IIB compared with Tuberous Sclerosis Complex. *Neurobiology of Disease*, *45*(1), 310–321.

Chaichana, K. L., Parker, S. L., Olivi, A., & Quiñones-Hinojosa, A. (2009). Long-term seizure outcomes in adult patients undergoing primary resection of malignant brain astrocytomas: Clinical article. *Journal of Neurosurgery*, *111*(2), 282–292.

Chaichana, K. L., Zadnik, P., Weingart, J. D., Olivi, A., Gallia, G. L., Blakeley, J., Lim, M., Brem, H., & Quiñones-Hinojosa, A. (2013). Multiple resections for patients with glioblastoma: prolonging survival. *Journal of Neurosurgery*, *118*(4), 812–820.

Chang, E. F., Potts, M. B., Keles, G. E., Lamborn, K. R., Chang, S. M., Barbaro, N. M., & Berger, M. S. (2008). Seizure characteristics and control following resection in 332 patients with low-grade gliomas. *Journal of Neurosurgery*, *108*(2), 227–235.

Chang, L., Munsaka, S. M., Kraft-Terry, S., & Ernst, T. (2013). Magnetic resonance spectroscopy to assess neuroinflammation and neuropathic pain. *Journal of Neuroimmune Pharmacology : The Official Journal of the Society on NeuroImmune Pharmacology*, *8*(3), 576–593.

Chang, M., Dian, J. A., Dufour, S., Wang, L., Moradi Chameh, H., Ramani, M., Zhang, L., Carlen, P. L., Womelsdorf, T., & Valiante, T. A. (2018). Brief activation of GABAergic interneurons initiates the transition to ictal events through post-inhibitory rebound excitation. *Neurobiology of Disease*, *109*(Pt A), 102–116.

Chen, C. K., Yang, S. Y., Park, S. C., Jang, O. J., Zhu, X., Xiang, Y. T., Ouyang, W. C., Javed, A., Khan, M. N. S., Grover, S., Avasthi, A., Kallivayalil, R. A., Chee, K. Y., Chemi, N., Kato, T. A., Hayakawa, K., Pariwatcharakul, P., Maramis, M., Seneviratne, L., … Lin, S. K. (2023). Clinical use of mood stabilizers beyond treatment for bipolar disorder: The REAP-MS study. *Asian Journal of Psychiatry*,

Chen, H., Judkins, J., Thomas, C., Wu, M., Khoury, L., Benjamin, C. G., Pacione, D., Golfinos, J. G., Kumthekar, P., Ghamsari, F., Chen, L., Lein, P., Chetkovich, D. M., Snuderl, M., & Horbinski, C. (2017). Mutant IDH1 and seizures in patients with glioma. *Neurology*, *88*(19), 1805–1813.

Chen, I. E., Swinburne, N., Tsankova, N. M., Hefti, M. M., Aggarwal, A., Doshi, A. H., Hormigo, A., Delman, B. N., & Nael, K. (2018). Sequential Apparent Diffusion Coefficient for Assessment of Tumor Progression in Patients with Low-Grade Glioma. *AJNR. American Journal of Neuroradiology*, *39*(6), 1039–1046.

Chiang, C. H., Won, S. M., Orsborn, A. L., Yu, K. J., Trumpis, M., Bent, B., Wang, C., Xue, Y., Min, S., Woods, V., Yu, C., Kim, B. H., Kim, S. B., Huq, R., Li, J., Seo, K. J., Vitale, F., Richardson, A., Fang, H., … Viventi, J. (2020). Development of a neural interface for high-definition, long-term recording in rodents and nonhuman primates. *Science Translational Medicine*, *12*(538), 1–13.

Ching, J., Amiridis, S., Stylli, S. S., Bjorksten, A. R., Kountouri, N., Zheng, T., Paradiso, L., Luwor, R. B., Morokoff, A. P., O'Brien, T. J., & Kaye, A. H. (2015). The peroxisome proliferator activated receptor gamma agonist pioglitazone increases functional expression of the glutamate transporter excitatory amino acid transporter 2 (EAAT2) in human glioblastoma cells. *Oncotarget*, *6*(25), 21301–21314. 9

Chizhov, A. V., Amakhin, D. V., Smirnova, E. Y., & Zaitsev, A. V. (2022). Ictal wavefront propagation in slices and simulations with conductance-based refractory density model. *PLoS Computational Biology*, *18*(1).

Chizhov, A. V., Amakhin, D. V., & Zaitsev, A. V. (2019). Spatial propagation of interictal discharges along the cortex. *Biochemical and Biophysical Research Communications*, *508*(4), 1245–1251.

Chowdhury, R., Yeoh, K. K., Tian, Y. M., Hillringhaus, L., Bagg, E. A., Rose, N. R., Leung, I. K. H., Li, X. S., Woon, E. C. Y., Yang, M., McDonough, M. A., King, O. N., Clifton, I. J., Klose, R. J., Claridge, T. D. W., Ratcliffe, P. J., Schofield, C. J., & Kawamura, A. (2011). The oncometabolite 2-hydroxyglutarate inhibits histone lysine demethylases. *EMBO Reports*, *12*(5), 463–469.

Christensen, J., Grnøborg, T. K., Srøensen, M. J., Schendel, D., Parner, E. T., Pedersen, L. H., & Vestergaard, M. (2013). Prenatal valproate exposure and risk of autism spectrum disorders and childhood autism. *JAMA*, *309*(16), 1696–1703.

Bibliography

Chung, W. Joon, & Sontheimer, H. (2009). Sulfasalazine inhibits the growth of primary brain tumors independent of nuclear factor-kappaB. *Journal of Neurochemistry*, *110*(1), 182–193.

Chung, Wook Joon, Lyons, S. A., Nelson, G. M., Hamza, H., Gladson, C. L., Yancey Gillespie, G., & Sontheimer, H. (2005). Inhibition of cystine uptake disrupts the growth of primary brain tumors. *The Journal of Neuroscience : The Official Journal of the Society for Neuroscience*, *25*(31), 7101–7110.

Clark, P. A., Gaal, J. T., Strebe, J. K., Pasch, C. A., Deming, D. A., Kuo, J. S., & Robins, H. I. (2017). The effects of tumor treating fields and temozolomide in MGMT expressing and non-expressing patient-derived glioblastoma cells. *Journal of Clinical Neuroscience : Official Journal of the Neurosurgical Society of Australasia*, *36*, 120–124.

Claus, E. B., Walsh, K. M., Wiencke, J., Molinaro, A. M., Wiemels, J. L., Schildkraut, J. M., Bondy, M. L., Berger, M., Jenkins, R., & Wrensch, M. (2015). Survival and low grade glioma: the emergence of genetic information. *Neurosurgical Focus*, *38*(1), E6.

Cobb, S. R., Buhl, E. H., Halasy, K., Paulsen, O., & Somogyi, P. (1995). Synchronization of neuronal activity in hippocampus by individual GABAergic interneurons. *Nature*, *378*(6552), 75–78.

Cochereau, J., Herbet, G., & Duffau, H. (2016). Patients with incidental WHO grade II glioma frequently suffer from neuropsychological disturbances. *Acta Neurochirurgica*, *158*(2), 305–312.

Collinger, J. L., Wodlinger, B., Downey, J. E., Wang, W., Tyler-Kabara, E. C., Weber, D. J., McMorland, A. J. C., Velliste, M., Boninger, M. L., & Schwartz, A. B. (2013). High-performance neuroprosthetic control by an individual with tetraplegia. *Lancet (London, England)*, *381*(9866), 557–564.

Colman, H., Zhang, L., Sulman, E. P., McDonald, J. M., Shooshtari, N. L., Rivera, A., Popoff, S., Nutt, C. L., Louis, D. N., Cairncross, J. G., Gilbert, M. R., Phillips, H. S., Mehta, M. P., Chakravarti, A., Pelloski, C. E., Bhat, K., Feuerstein, B. G., Jenkins, R. B., & Aldape, K. (2010). A multigene predictor of outcome in glioblastoma. *Neuro-Oncology*, *12*(1), 49–57.

Colopi, A., Fuda, S., Santi, S., Onorato, A., Cesarini, V., Salvati, M., Balistrieri, C. R., Dolci, S., & Guida, E. (2023). Impact of age and gender on glioblastoma onset, progression, and management. *Mechanisms of Ageing and Development*, *211*.

Connelly, J. M., Prah, M. A., Santos-Pinheiro, F., Mueller, W., Cochran, E., & Schmainda, K. M. (2021). Magnetic Resonance Imaging Mapping of Brain Tumor Burden: Clinical Implications for Neurosurgical Management: Case Report. *Neurosurgery Open*, *2*(4).

Conti, L., Palma, E., Roseti, C., Lauro, C., Cipriani, R., De Groot, M., Aronica, E., & Limatola, C. (2011). Anomalous levels of Cl- transporters cause a decrease of GABAergic inhibition in human peritumoral epileptic cortex. *Epilepsia*, *52*(9), 1635–1644.

Contreras, S. A., Schleimer, J. H., Gulledge, A. T., & Schreiber, S. (2021). Activity-mediated accumulation of potassium induces a switch in firing pattern and neuronal excitability type. *PLoS Computational Biology*, *17*(5).

Coppola, A., Zarabla, A., Maialetti, A., Villani, V., Koudriavtseva, T., Russo, E., Nozzolillo, A., Sueri, C., Belcastro, V., Balestrini, S., Ferlazzo, E., Giannarelli, D., Bilo, L., & Maschio, M. (2020). Perampanel Confirms to Be Effective and Well-Tolerated as an Add-On Treatment in Patients With Brain Tumor-Related Epilepsy (PERADET Study). *Frontiers in Neurology*, *11*.

Correia, C. E., Umemura, Y., Flynn, J. R., Reiner, A. S., & Avila, E. K. (2021). Pharmacoresistant seizures and IDH mutation in low-grade gliomas. *Neuro-Oncology Advances*, *3*(1).

Cossart, R., Dinocourt, C., Hirsch, J. C., Merchan-Perez, A., De Felipe, J., Ben-Ari, Y., Esclapez, M., & Bernard, C. (2001). Dendritic but not somatic GABAergic inhibition is decreased in experimental epilepsy. *Nature Neuroscience*, *4*(1), 52–62.

Coull, J. A. M., Beggs, S., Boudreau, D., Boivin, D., Tsuda, M., Inoue, K., Gravel, C., Salter, M. W., & Koninck, Y. De. (2005). *LETTERS BDNF from microglia causes the shift in neuronal anion gradient underlying neuropathic pain*. *438*(December), 1017–1021.

Cousyn, L., Navarro, V., & Chavez, M. (2021). Preictal state detection using prodromal symptoms: A machine learning approach. *Epilepsia*, *62*(2), e42–e47.

Crépon, B., Navarro, V., Hasboun, D., Clemenceau, S., Martinerie, J., Baulac, M., Adam, C., & Le Van Quyen, M. (2010). Mapping interictal oscillations greater than 200 Hz recorded with intracranial macroelectrodes in human epilepsy. *Brain*, *133*(1), 33–45.

Crino, P. B. (2016). The mTOR signalling cascade: paving new roads to cure neurological disease. *Nature Reviews. Neurology*, *12*(7), 379–392.

Croft, R. J., & Barry, R. J. (2000). Removal of ocular artifact from the EEG: a review. *Neurophysiologie Clinique = Clinical Neurophysiology*, *30*(1), 5–19.

Croteau, D., Scarpace, L., Hearshen, D., Gutierrez, J., Fisher, J. L., Rock, J. P., & Mikkelsen, T. (2001). Correlation between magnetic resonance spectroscopy imaging and image-guided biopsies: semiquantitative and qualitative histopathological analyses of patients with untreated glioma. *Neurosurgery*, *49*(4), 823–829.

Cuddapah, V. A., Habela, C. W., Watkins, S., Moore, L. S., Barclay, T. T. C., & Sontheimer, H. (2012). Kinase activation of ClC-3 accelerates cytoplasmic condensation during mitotic cell rounding. *American Journal of Physiology. Cell Physiology*, *302*(3).

Cui, M., Zorrilla-Veloz, R. I., Hu, J., Guan, B., & Ma, X. (2021). Diagnostic Accuracy of PET for Differentiating True Glioma Progression From Post Treatment-Related Changes: A Systematic Review and Meta-Analysis. *Frontiers in Neurology*, *12*.

Curot, J., Barbeau, E., Despouy, E., Denuelle, M., Sol, J. C., Lotterie, J. A., Valton, L., & Peyrache, A. (2023). Local neuronal excitation and global inhibition during epileptic fast ripples in humans. *Brain : A Journal of Neurology*, *146*(2), 561–575.

Dang, L., White, D. W., Gross, S., Bennett, B. D., Bittinger, M. A., Driggers, E. M., Fantin, V. R., Jang, H. G., Jin, S., Keenan, M. C., Marks, K. M., Prins, R. M., Ward, P. S., Yen, K. E., Liau, L. M., Rabinowitz, J. D., Cantley, L. C., Thompson, C. B., Vander Heiden, M. G., & Su, S. M. (2009). Cancer-associated IDH1 mutations produce 2-hydroxyglutarate. *Nature*, *462*(7274), 739–744.

Dasgupta, P., Balasubramanyian, V., de Groot, J. F., & Majd, N. K. (2023). Preclinical Models of Low-Grade Gliomas. *Cancers*, *15*(3).

Daumas-Duport, C., Tucker, M. L., Kolles, H., Cervera, P., Beuvon, F., Varlet, P., Udo, N., Koziak, M., & Chodkiewicz, J. P. (1997). Oligodendrogliomas. Part II: A new grading system based on morphological and imaging criteria. *Journal of Neuro-Oncology*, *34*(1), 61–78.

De Bruin, M. E., Van Der Meer, P. B., Dirven, L., Taphoorn, M. J. B., & Koekkoek, J. A. F. (2021). Efficacy of antiepileptic drugs in glioma patients with epilepsy: a systematic review. *Neuro-Oncology Practice*, *8*(5), 501–517.

De Curtis, M., & Avanzini, G. (2001). Interictal spikes in focal epileptogenesis. In *Progress in Neurobiology* (Vol. 63, Issue 5, pp. 541–567). Elsevier Ltd.

De Groot, J. F., Ta, J. L., Fuller, G., & Yung, W. K. A. (2005). The excitatory amino acid transporter-2 induces apoptosis and decreases glioma growth in vitro and in vivo. *Cancer Research*, *65*(5), 1934–1940.

De Groot, M., Douw, L., Sizoo, E. M., Bosma, I., Froklage, F. E., Heimans, J. J., Postma, T. J., Klein, M., & Reijneveld, J. C. (2013). Levetiracetam improves verbal memory in high-grade glioma patients. *Neuro-Oncology*, *15*(2), 216–223.

De Groot, M., Iyer, A., Zurolo, E., Anink, J., Heimans, J. J., Boison, D., Reijneveld, J. C., & Aronica, E. (2012). Overexpression of ADK in human astrocytic tumors and peritumoral tissue is related to tumor-associated epilepsy. *Epilepsia*, *53*(1), 58–66.

de Groot, & Sontheimer, H. (2011). Glutamate and the biology of gliomas. *GLIA*, *59*(8), 1181–1189.

De Jongh, A., Baayen, J. C., De Munck, J. C., Heethaar, R. M., Vandertop, W. P., & Stam, C. J. (2003). The influence of brain tumor treatment on pathological delta activity in MEG. *NeuroImage*, *20*(4), 2291–2301.

de Mel, A., Jell, G., Stevens, M. M., & Seifalian, A. M. (2008). Biofunctionalization of biomaterials for accelerated in situ endothelialization: a review. *Biomacromolecules*, *9*(11), 2969–2979.

De Witt Hamer, P. C., Robles, S. G., Zwinderman, A. H., Duffau, H., & Berger, M. S. (2012). Impact of intraoperative stimulation brain mapping on glioma surgery outcome: A meta-analysis. *Journal of Clinical Oncology*, *30*(20), 2559–2565.

de Zwart, P. L., van Dijken, B. R. J., Holtman, G. A., Stormezand, G. N., Dierckx, R. A. J. O., van Laar, P. J., & van der Hoorn, A. (2020). Diagnostic Accuracy of PET Tracers for the Differentiation of Tumor Progression from Treatment-Related Changes in High-Grade Glioma: A Systematic Review and Metaanalysis. *Journal of Nuclear Medicine : Official Publication, Society of Nuclear Medicine*, *61*(4), 498–504.

Del Agua, I., Marina, S., Pitsalidis, C., Mantione, D., Ferro, M., Iandolo, D., Sanchez-Sanchez, A., Malliaras, G. G., Owens, R. M., & Mecerreyes, D. (2018). Conducting Polymer Scaffolds Based on Poly(3,4-ethylenedioxythiophene) and Xanthan Gum for Live-Cell Monitoring. *ACS Omega*, *3*(7), 7424–7431.

Deuschl, C., Kirchner, J., Poeppel, T. D., Schaarschmidt, B., Kebir, S., El Hindy, N., Hense, J., Quick, H. H., Glas, M., Herrmann, K., Umutlu, L., Moenninghoff, C., Radbruch, A., Forsting, M., & Schlamann, M. (2018). 11C-MET PET/MRI for detection of recurrent glioma. *European Journal of Nuclear Medicine and Molecular Imaging*, *45*(4), 593–601.

Dhermain, F. G., Hau, P., Lanfermann, H., Jacobs, A. H., & van den Bent, M. J. (2010). Advanced MRI and PET imaging for assessment of treatment response in patients with gliomas. *The Lancet. Neurology*, *9*(9), 906–920.

Dhermain, F., Saliou, G., Parker, F., Page, P., Hoang-Xuan, K., Lacroix, C., Tournay, E., Bourhis, J., & Ducreux, D. (2010). Microvascular leakage and contrast enhancement as prognostic factors for recurrence in unfavorable low-grade gliomas. *Journal of Neuro-Oncology*, *97*(1), 81–88.

Di Carlo, D. T., Duffau, H., Cagnazzo, F., Benedetto, N., Morganti, R., & Perrini, P. (2020). IDH wild-type

WHO grade II diffuse low-grade gliomas. A heterogeneous family with different outcomes. Systematic review and meta-analysis. *Neurosurgical Review*, *43*(2), 383–395.

Dijk, G., Rutz, A. L., & Malliaras, G. G. (2020). Stability of PEDOT:PSS-Coated Gold Electrodes in Cell Culture Conditions. *Advanced Materials Technologies*, *5*(3).

Dissaux, G., Dissaux, B., Kabbaj, O. El, Gujral, D. M., Pradier, O., Salaün, P. Y., Seizeur, R., Bourhis, D., Ben Salem, D., Querellou, S., & Schick, U. (2020). Radiotherapy target volume definition in newly diagnosed high grade glioma using 18F-FET PET imaging and multiparametric perfusion MRI: A prospective study (IMAGG). *Radiotherapy and Oncology : Journal of the European Society for Therapeutic Radiology and Oncology*, *150*, 164–171.

Donoghue, T., Haller, M., Peterson, E. J., Varma, P., Sebastian, P., Gao, R., Noto, T., Lara, A. H., Wallis, J. D., Knight, R. T., Shestyuk, A., & Voytek, B. (2020). Parameterizing neural power spectra into periodic and aperiodic components. *Nature Neuroscience 2020 23:12*, *23*(12), 1655–1665.

Dossi, E., Blauwblomme, T., Moulard, J., Chever, O., Vasile, F., Guinard, E., Le Bert, M., Couillin, I., Pallud, J., Capelle, L., Huberfeld, G., & Rouach, N. (2018). Pannexin-1 channels contribute to seizure generation in human epileptic brain tissue and in a mouse model of epilepsy. *Science Translational Medicine*, *10*(443).

Dossi, E., Vasile, F., & Rouach, N. (2018). Human astrocytes in the diseased brain. In *Brain Research Bulletin* (Vol. 136, pp. 139–156). Elsevier Inc.

Douw, L., Schoonheim, M. M., Landi, D., van der Meer, M. L., Geurts, J. J. G., Reijneveld, J. C., Klein, M., & Stam, C. J. (2011). Cognition is related to resting-state small-world network topology: an magnetoencephalographic study. *Neuroscience*, *175*, 169–177.

Ducray, F., Idbaih, A., Wang, X. W., Cheneau, C., Labussiere, M., & Sanson, M. (2011). Predictive and prognostic factors for gliomas. *Expert Review of Anticancer Therapy*, *11*(5), 781–789.

Duffau, H. (2007). Contribution of cortical and subcortical electrostimulation in brain glioma surgery: Methodological and functional considerations. *Neurophysiologie Clinique*, *37*(6), 373–382.

Duffau, H., Lopes, M., Arthuis, F., Bitar, A., Sichez, J. P., Van Effenterre, R., & Capelle, L. (2005). Contribution of intraoperative electrical stimulations in surgery of low grade gliomas: A comparative study between two series without (1985-96) and with (1996-2003) functional mapping in the same institution. *Journal of Neurology, Neurosurgery and Psychiatry*, *76*(6), 845–851.

Duffau, Hugues. (2016). Long-term outcomes after supratotal resection of diffuse low-grade gliomas: a consecutive series with 11-year follow-up. *Acta Neurochirurgica*, *158*(1), 51–58.

Duffau, Hugues. (2017). A two-level model of interindividual anatomo-functional variability of the brain and its implications for neurosurgery. *Cortex*, *86*, 303–313.

Duffau, Hugues. (2022). Repeated Awake Surgical Resection(s) for Recurrent Diffuse Low-Grade Gliomas: Why, When, and How to Reoperate? *Frontiers in Oncology*, *12*.

Duffau, Hugues, & Capelle, L. (2004). Preferential brain locations of low-grade gliomas: Comparison with glioblastomas and review of hypothesis. *Cancer*, *100*(12), 2622–2626.

Duffner, F., Ritz, R., Freudenstein, D., Weller, M., Dietz, K., & Wessels, J. (2005). Specific intensity imaging for glioblastoma and neural cell cultures with 5-aminolevulinic acid-derived protoporphyrin IX. *Journal of Neuro-Oncology*, *71*(2), 107–111.

Dührsen, L., Sauvigny, T., Ricklefs, F. L., Mende, K. C., Schaper, M., Matschke, J., Goebell, E., Westphal, M., & Martens, T. (2019). Seizures as presenting symptom in patients with glioblastoma. *Epilepsia*, *60*(1), 149–154.

Dzhala, V., Valeeva, G., Glykys, J., Khazipov, R., & Staley, K. (2012). Traumatic alterations in GABA signaling disrupt hippocampal network activity in the developing brain. *The Journal of Neuroscience : The Official Journal of the Society for Neuroscience*, *32*(12), 4017–4031.

Eftekhari, S., Mehvari Habibabadi, J., Najafi Ziarani, M., Hashemi Fesharaki, S. S., Gharakhani, M., Mostafavi, H., Joghataei, M. T., Beladimoghadam, N., Rahimian, E., & Hadjighassem, M. R. (2013). Bumetanide reduces seizure frequency in patients with temporal lobe epilepsy. *Epilepsia*, *54*(1).

Elahian, B., Lado, N. E., Mankin, E., Vangala, S., Misra, A., Moxon, K., Fried, I., Sharan, A., Yeasin, M., Staba, R., Bragin, A., Avoli, M., Sperling, M. R., Engel, J., & Weiss, S. A. (2018). Low-voltage fast seizures in humans begin with increased interneuron firing. *Annals of Neurology*, *84*(4), 588–600.

Ellingson, B. M., Bendszus, M., Boxerman, J., Barboriak, D., Erickson, B. J., Smits, M., Nelson, S. J., Gerstner, E., Alexander, B., Goldmacher, G., Wick, W., Vogelbaum, M., Weller, M., Galanis, E., Kalpathy-Cramer, J., Shankar, L., Jacobs, P., Pope, W. B., Yang, D., … Kingston, A. (2015). Consensus recommendations for a standardized Brain Tumor Imaging Protocol in clinical trials. *Neuro-Oncology*, *17*(9), 1188–1198.

Ellis, H. P., & Kurian, K. M. (2014). Biological Rationale for the Use of PPARγ Agonists in Glioblastoma. *Frontiers in Oncology*, *4*.

Engelhard, B., Ozeri, N., Israel, Z., Bergman, H., & Vaadia, E. (2013). Inducing γ oscillations and precise

spike synchrony by operant conditioning via brain-machine interface. *Neuron*, *77*(2), 361–375.
Englot, D. J., Berger, M. S., Barbaro, N. M., & Chang, E. F. (2011). Predictors of seizure freedom after resection of supratentorial low-grade gliomas: A review. *Journal of Neurosurgery*, *115*(2), 240–244.
Englot, D. J., Berger, M. S., Barbaro, N. M., & Chang, E. F. (2012). Factors associated with seizure freedom in the surgical resection of glioneuronal tumors. *Epilepsia*, *53*(1), 51–57.
Englot, D. J., Han, S. J., Berger, M. S., Barbaro, N. M., & Chang, E. F. (2012). Extent of surgical resection predicts seizure freedom in low-grade temporal lobe brain tumors. *Neurosurgery*, *70*(4), 921–927.
Ernest, N. J., Weaver, A. K., Van Duyn, L. B., & Sontheimer, H. W. (2005). Relative contribution of chloride channels and transporters to regulatory volume decrease in human glioma cells. *American Journal of Physiology - Cell Physiology*, *288*(6 57-6), C1451-60.
Espenhahn, S., Rossiter, H. E., Van Wijk, B. C. M., Redman, N., Rondina, J. M., Diedrichsen, J., & Ward, N. S. (2020). Sensorimotor cortex beta oscillations reflect motor skill learning ability after stroke. *Brain Communications*, *2*(2).
Fan, X., Li, Y., Shan, X., You, G., Wu, Z., Li, Z., Qiao, H., & Jiang, T. (2018). Seizures at presentation are correlated with better survival outcomes in adult diffuse glioma: A systematic review and meta-analysis. *Seizure*, *59*, 16–23.
Farshidfar, F., Zheng, S., Gingras, M. C., Newton, Y., Shih, J., Robertson, A. G., Hinoue, T., Hoadley, K. A., Gibb, E. A., Roszik, J., Covington, K. R., Wu, C. C., Shinbrot, E., Stransky, N., Hegde, A., Yang, J. D., Reznik, E., Sadeghi, S., Pedamallu, C. S., … Stuart, J. M. (2017). Integrative Genomic Analysis of Cholangiocarcinoma Identifies Distinct IDH-Mutant Molecular Profiles. *Cell Reports*, *19*(13), 2878–2880.
Fedele, T., van 't Klooster, M., Burnos, S., Zweiphenning, W., van Klink, N., Leijten, F., Zijlmans, M., & Sarnthein, J. (2016). Automatic detection of high frequency oscillations during epilepsy surgery predicts seizure outcome. *Clinical Neurophysiology*, *127*(9), 3066–3074.
Federico, P., Abbott, D. F., Briellmann, R. S., Harvey, A. S., & Jackson, G. D. (2005). *Functional MRI of the pre-ictal state*. 1811–1817.
Fernandez-Ruiz, A., Sirota, A., Lopes-dos-Santos, V., & Dupret, D. (2023). Over and above frequency: Gamma oscillations as units of neural circuit operations. *Neuron*, *111*(7), 936–953.
Fernández, E., Greger, B., House, P. A., Aranda, I., Botella, C., Albisua, J., Soto-Sánchez, C., Alfaro, A., & Normann, R. A. (2014). Acute human brain responses to intracortical microelectrode arrays: challenges and future prospects. *Frontiers in Neuroengineering*, *7*(JUL).
Feron, K., Lim, R., Sherwood, C., Keynes, A., Brichta, A., & Dastoor, P. C. (2018). Organic Bioelectronics: Materials and Biocompatibility. *International Journal of Molecular Sciences*, *19*(8).
Ferreira, M. T., Miyake, J. A., Gomes, R. N., Feitoza, F., Stevannato, P. B., da Cunha, A. S., Serachi, F. de O., Panagopoulos, A. T., & Colquhoun, A. (2021). Cyclooxygenase Inhibition Alters Proliferative, Migratory, and Invasive Properties of Human Glioblastoma Cells In Vitro. *International Journal of Molecular Sciences*, *22*(9).
Feyissa, A. M., Worrell, G. A., Tatum, W. O., Mahato, D., Brinkmann, B. H., Rosenfeld, S. S., Refaey, K., Bechtle, P. S., & Quinones-Hinojosa, A. (2018). High-frequency oscillations in awake patients undergoing brain tumor-related epilepsy surgery. *Neurology*, *90*(13), e1119–e1125.
Fingelkurts, A. A., Fingelkurts, A. A., Kivisaari, R., Pekkonen, E., Ilmoniemi, R. J., & Kähkönen, S. (2004). Enhancement of GABA-related signalling is associated with increase of functional connectivity in human cortex. *Human Brain Mapping*, *22*(1), 27–39.
Fisher, R. S., Acevedo, C., Arzimanoglou, A., Bogacz, A., Cross, J. H., Elger, C. E., Engel, J., Forsgren, L., French, J. A., Glynn, M., Hesdorffer, D. C., Lee, B. I., Mathern, G. W., Moshé, S. L., Perucca, E., Scheffer, I. E., Tomson, T., Watanabe, M., & Wiebe, S. (2014). ILAE Official Report: A practical clinical definition of epilepsy. *Epilepsia*, *55*(4), 475–482.
Fisher, R. S., Van Emde Boas, W., Blume, W., Elger, C., Genton, P., Lee, P., & Engel, J. (2005). Epileptic seizures and epilepsy: definitions proposed by the International League Against Epilepsy (ILAE) and the International Bureau for Epilepsy (IBE). *Epilepsia*, *46*(4), 470–472.
Flanigan, P. M., Jahangiri, A., Kuang, R., Truong, A., Choi, S., Chou, A., Rick, J. W., Chang, S. M., Molinaro, A. M., McDermott, M. W., Berger, M. S., & Aghi, M. K. (2017). Improved survival with decreasedwait time to surgery in glioblastoma patients presenting with seizure. *Neurosurgery*, *81*(5), 824–833.
Foffani, G., Uzcategui, Y. G., Gal, B., & Menendez de la Prida, L. (2007). Reduced Spike-Timing Reliability Correlates with the Emergence of Fast Ripples in the Rat Epileptic Hippocampus. *Neuron*, *55*(6), 930–941.
Fox, J. E., Bikson, M., & Jefferys, J. G. R. (2007). The effect of neuronal population size on the development of epileptiform discharges in the low calcium model of epilepsy. *Neuroscience Letters*, *411*(2), 158–161.
Fraser, D. D., Duffy, S., Angelides, K. J., Perez-Velazquez, J. L., Kettenmann, H., & MacVicar, B. A. (1995).

GABAA/benzodiazepine receptors in acutely isolated hippocampal astrocytes. *The Journal of Neuroscience : The Official Journal of the Society for Neuroscience*, *15*(4), 2720–2732. 5

Frauscher, B., von Ellenrieder, N., Zelmann, R., Rogers, C., Nguyen, D. K., Kahane, P., Dubeau, F., & Gotman, J. (2018). High-Frequency Oscillations in the Normal Human Brain. *Annals of Neurology*, *84*(3), 374–385.

Freyschlag, C. F., Krieg, S. M., Kerschbaumer, J., Pinggera, D., Forster, M. T., Cordier, D., Rossi, M., Miceli, G., Roux, A., Reyes, A., Sarubbo, S., Smits, A., Sierpowska, J., Robe, P. A., Rutten, G. J., Santarius, T., Matys, T., Zanello, M., Almairac, F., … Mandonnet, E. (2018). Imaging practice in low-grade gliomas among European specialized centers and proposal for a minimum core of imaging. *Journal of Neuro-Oncology*, *139*(3), 699–711.

Fujita, Y., Nagashima, H., Tanaka, K., Hashiguchi, M., Hirose, T., Itoh, T., & Sasayama, T. (2021). The Histopathologic and Radiologic Features of T2-FLAIR Mismatch Sign in IDH-Mutant 1p/19q Non-codeleted Astrocytomas. *World Neurosurgery*, *149*, e253–e260.

Furtak, J., Rakowska, J., Szylberg, T., Harat, M., Małkowski, B., & Harat, M. (2021). Glioma Biopsy Based on Hybrid Dual Time-Point FET-PET/MRI-A Proof of Concept Study. *Frontiers in Neurology*, *12*.

Gaetz, W., Edgar, J. C., Wang, D. J., & Roberts, T. P. L. (2011). Relating MEG measured motor cortical oscillations to resting γ-aminobutyric acid (GABA) concentration. *NeuroImage*, *55*(2), 616–621.

Gagnon, M., Bergeron, M. J., Lavertu, G., Castonguay, A., Tripathy, S., Bonin, R. P., Perez-Sanchez, J., Boudreau, D., Wang, B., Dumas, L., Valade, I., Bachand, K., Jacob-Wagner, M., Tardif, C., Kianicka, I., Isenring, P., Attardo, G., Coull, J. A. M., & De Koninck, Y. (2013). Chloride extrusion enhancers as novel therapeutics for neurological diseases. *Nature Medicine*, *19*(11), 1524–1528.

Gallotto, S., & Seeck, M. (2022). EEG biomarker candidates for the identification of epilepsy. *Clinical Neurophysiology Practice*, *8*, 32–41.

Gao, R., Peterson, E. J., & Voytek, B. (2017). Inferring synaptic excitation/inhibition balance from field potentials. *NeuroImage*, *158*(March), 70–78.

Gardner, A. B., Worrell, G. A., Marsh, E., Dlugos, D., & Litt, B. (2007). Human and automated detection of high-frequency oscillations in clinical intracranial EEG recordings. *Clinical Neurophysiology : Official Journal of the International Federation of Clinical Neurophysiology*, *118*(5), 1134–1143.

Garrett, M., Sperry, J., Braas, D., Yan, W., Le, T. M., Mottahedeh, J., Ludwig, K., Eskin, A., Qin, Y., Levy, R., Breunig, J. J., Pajonk, F., Graeber, T. G., Radu, C. G., Christofk, H., Prins, R. M., Lai, A., Liau, L. M., Coppola, G., & Kornblum, H. I. (2018). Metabolic characterization of isocitrate dehydrogenase (IDH) mutant and IDH wildtype gliomaspheres uncovers cell type-specific vulnerabilities. *Cancer & Metabolism*, *6*(1).

Garzon-Muvdi, T., Schiapparelli, P., ap Rhys, C., Guerrero-Cazares, H., Smith, C., Kim, D. H., Kone, L., Farber, H., Lee, D. Y., An, S. S., Levchenko, A., & Quiñones-Hinojosa, A. (2012). Regulation of brain tumor dispersal by NKCC1 through a novel role in focal adhesion regulation. *PLoS Biology*, *10*(5).

Gastaut, J. L., Michel, B., Sabet Hassan, S., Cerda, M., Bianchi, L., & Gastaut, H. (1979). Electroencephalography in brain edema (127 cases of brain tumor investigated by cranial computerized tomography). *Electroencephalography and Clinical Neurophysiology*, *46*(3), 239–255.

Gerin, C., Pallud, J., Grammaticos, B., Mandonnet, E., Deroulers, C., Varlet, P., Capelle, L., Taillandier, L., Bauchet, L., Duffau, H., & Badoual, M. (2012). Improving the time-machine: estimating date of birth of grade II gliomas. *Cell Proliferation*, *45*(1), 76–90.

Gerin, Chloé, Pallud, J., Deroulers, C., Varlet, P., Oppenheim, C., Roux, F. X., Chrétien, F., Thomas, S. R., Grammaticos, B., & Badoual, M. (2013). Quantitative characterization of the imaging limits of diffuse low-grade oligodendrogliomas. *Neuro-Oncology*, *15*(10), 1379–1388.

Ghinda, D. C., Lambert, B., Lu, J., Jiang, N., Tsai, E., Sachs, A., Wu, J. S., & Northoff, G. (2021). Scale-Free Analysis of Intraoperative ECoG During Awake Craniotomy for Glioma. *Frontiers in Oncology*, *10*(February), 1–12.

Gholami, M., Hosseinmardi, N., Mirnajafi-Zadeh, J., Javan, M., Semnanian, S., Naghdi, N., & Fathollahi, Y. (2020). Long-term potentiation enhancing effect of epileptic insult in the CA1 area is dependent on prior-application of primed-burst stimulation. *Experimental Brain Research*, *238*(4), 897–903.

Gilbert, M. R., Liu, Y., Neltner, J., Pu, H., Morris, A., Sunkara, M., Pittman, T., Kyprianou, N., & Horbinski, C. (2014). Autophagy and oxidative stress in gliomas with IDH1 mutations. *Acta Neuropathologica*, *127*(2), 221–233.

Gill, B. J. A., Wu, X., Khan, F. A., Sosunov, A. A., Liou, J., Dovas, A., Eissa, T. L., Banu, M. A., Bateman, L. M., Mckhann, G. M., Canoll, P., & Schevon, C. (2021). *Ex vivo multi-electrode analysis reveals spatiotemporal dynamics of ictal behavior at the infiltrated margin of glioma*.

Gill, B. J. A., Wu, X., Khan, F. A., Sosunov, A. A., Liou, J. you, Dovas, A., Eissa, T. L., Banu, M. A., Bateman, L. M., McKhann, G. M., Canoll, P., & Schevon, C. (2020). Ex vivo multi-electrode analysis reveals spatiotemporal dynamics of ictal behavior at the infiltrated margin of glioma. *Neurobiology of*

Disease, *134*(October 2019), 104676.

Glantz, M. J., Cole, B. F., Forsyth, P. A., Recht, L. D., Wen, P. Y., Chamberlain, M. C., Grossman, S. A., & Cairncross, J. G. (2000). Practice parameter: anticonvulsant prophylaxis in patients with newly diagnosed brain tumors. Report of the Quality Standards Subcommittee of the American Academy of Neurology. *Neurology*, *54*(10), 1886–1893.

Glutamate Inhibitors in Glioblastoma - Full Text View - ClinicalTrials.gov. (n.d.). Retrieved July 21, 2023, from https://classic.clinicaltrials.gov/ct2/show/NCT05664464

Gogos, A. J., Young, J. S., Morshed, R. A., Hervey-Jumper, S. L., & Berger, M. S. (2020). Awake glioma surgery: technical evolution and nuances. *Journal of Neuro-Oncology*.

Goncharova, I. I., Alkawadri, R., Gaspard, N., Duckrow, R. B., Spencer, D. D., Hirsch, L. J., Spencer, S. S., & Zaveri, H. P. (2016). The relationship between seizures, interictal spikes and antiepileptic drugs. *Clinical Neurophysiology : Official Journal of the International Federation of Clinical Neurophysiology*, *127*(9), 3180–3186.

Gonzalez, D., & Elvidge, A. R. (1962). On the occurrence of epilepsy caused by astrocytoma of the cerebral hemispheres. *Journal of Neurosurgery*, *19*, 470–482.

Gotman, J., & Marciani, M. G. (1985). Electroencephalographic spiking activity, drug levels, and seizure occurrence in epileptic patients. *Annals of Neurology*, *17*(6), 597–603.

Green, R. A., Baek, S., Poole-Warren, L. A., & Martens, P. J. (2010). Conducting polymer-hydrogels for medical electrode applications. *Science and Technology of Advanced Materials*, *11*(1).

Grommes, C., Conway, D. S., Alshekhlee, A., & Barnholtz-Sloan, J. S. (2010). Inverse association of PPARγ agonists use and high grade glioma development. *Journal of Neuro-Oncology*, *100*(2), 233–239.

Gust, J., Hay, K. A., Hanafi, L. A., Li, D., Myerson, D., Gonzalez-Cuyar, L. F., Yeung, C., Liles, W. C., Wurfel, M., Lopez, J. A., Chen, J., Chung, D., Baker, S. H., Ozpolat, T., Fink, K. R., Riddell, S. R., Maloney, D. G., & Turtle, C. J. (2017). Endothelial Activation and Blood-Brain Barrier Disruption in Neurotoxicity after Adoptive Immunotherapy with CD19 CAR-T Cells. *Cancer Discovery*, *7*(12), 1404–1419.

Guyotat, J., Pallud, J., Armoiry, X., Pavlov, V., & Metellus, P. (2016). 5-Aminolevulinic Acid-Protoporphyrin IX Fluorescence-Guided Surgery of High-Grade Gliomas: A Systematic Review. *Advances and Technical Standards in Neurosurgery*, *43*, 61–90.

Haas, B. R., & Sontheimer, H. (2010). Inhibition of the sodium-potassium-chloride cotransporter isoform-1 reduces glioma invasion. *Cancer Research*, *70*(13), 5597–5606.

Habela, C. W., Ernest, N. J., Swindall, A. F., & Sontheimer, H. (2009). Chloride accumulation drives volume dynamics underlying cell proliferation and migration. *Journal of Neurophysiology*, *101*(2), 750–757.

Haglund, M. M., Berger, M. S., Kunkel, D. D., Franck, J. E., Ghatan, S., & Ojemann, G. A. (1992). Changes in gamma-aminobutyric acid and somatostatin in epileptic cortex associated with low-grade gliomas. *Journal of Neurosurgery*, *77*(2), 209–216.

Hall, S. D., Barnes, G. R., Furlong, P. L., Seri, S., & Hillebrand, A. (2010). Neuronal network pharmacodynamics of GABAergic modulation in the human cortex determined using pharmaco-magnetoencephalography. *Human Brain Mapping*, *31*(4), 581–594.

Hamdan, N., & Duffau, H. (2021). Extending the multistage surgical strategy for recurrent initially low-grade gliomas: functional and oncological outcomes in 31 consecutive patients who underwent a third resection under awake mapping. *Journal of Neurosurgery*, *136*(4), 1035–1044.

Hamilton, W., & Kernick, D. (2007). Clinical features of primary brain tumours: A case-control study using electronic primary care records. *British Journal of General Practice*, *57*(542), 695–699.

Han, Q., Liang, H., Cheng, P., Yang, H., & Zhao, P. (2020). Gross Total vs. Subtotal Resection on Survival Outcomes in Elderly Patients With High-Grade Glioma: A Systematic Review and Meta-Analysis. *Frontiers in Oncology*, *10*.

Hansen, K. B., Yi, F., Perszyk, R. E., Furukawa, H., Wollmuth, L. P., Gibb, A. J., & Traynelis, S. F. (2018). Structure, function, and allosteric modulation of NMDA receptors. *The Journal of General Physiology*, *150*(8), 1081–1105.

Happold, C., Gorlia, T., Chinot, O., Gilbert, M. R., Nabors, L. B., Wick, W., Pugh, S. L., Hegi, M., Cloughesy, T., Roth, P., Reardon, D. A., Perry, J. R., Mehta, M. P., Stupp, R., & Weller, M. (2016). Does Valproic Acid or Levetiracetam Improve Survival in Glioblastoma? A Pooled Analysis of Prospective Clinical Trials in Newly Diagnosed Glioblastoma. *Journal of Clinical Oncology : Official Journal of the American Society of Clinical Oncology*, *34*(7), 731–739.

Hasegawa, K., & Aird, R. B. (1963). AN EEG STUDY OF DEEP-SEATED CEREBRAL AND SUBTENTORIAL LESIONS IN COMPARISON WITH CORTICAL LESIONS. *Electroencephalography and Clinical Neurophysiology*, *15*(6), 934–946.

Hassibi, A., Navid, R., Dutton, R. W., & Lee, T. H. (2004). Comprehensive study of noise processes in electrode electrolyte interfaces. *Journal of Applied Physics*, *96*(2), 1074–1082.

Haubold, J., Demircioglu, A., Gratz, M., Glas, M., Wrede, K., Sure, U., Antoch, G., Keyvani, K., Nittka, M., Kannengiesser, S., Gulani, V., Griswold, M., Herrmann, K., Forsting, M., Nensa, F., & Umutlu, L. (2020). Non-invasive tumor decoding and phenotyping of cerebral gliomas utilizing multiparametric 18F-FET PET-MRI and MR Fingerprinting. *European Journal of Nuclear Medicine and Molecular Imaging*, *47*(6), 1435–1445.

Hausmann, D., Hoffmann, D. C., Venkataramani, V., Jung, E., Horschitz, S., Tetzlaff, S. K., Jabali, A., Hai, L., Kessler, T., Azoŕin, D. D., Weil, S., Kourtesakis, A., Sievers, P., Habel, A., Breckwoldt, M. O., Karreman, M. A., Ratliff, M., Messmer, J. M., Yang, Y., … Winkler, F. (2023). Autonomous rhythmic activity in glioma networks drives brain tumour growth. *Nature*, *613*(7942), 179–186.

Haydon, P. G. (2001). GLIA: listening and talking to the synapse. *Nature Reviews. Neuroscience*, *2*(3), 185–193.

He, J., Zhang, G., Yuan, Q., Wang, S., Liu, Z., Wang, M., Cai, H., Wan, J., & Zhao, B. (2023). Overexpression of Podoplanin Predicts Poor Prognosis in Patients With Glioma. *Applied Immunohistochemistry & Molecular Morphology : AIMM*, *31*(5), 295–303.

Hegi, M. E., Diserens, A.-C., Gorlia, T., Hamou, M.-F., de Tribolet, N., Weller, M., Kros, J. M., Hainfellner, J. A., Mason, W., Mariani, L., Bromberg, J. E. C., Hau, P., Mirimanoff, R. O., Cairncross, J. G., Janzer, R. C., & Stupp, R. (2005). MGMT gene silencing and benefit from temozolomide in glioblastoma. *The New England Journal of Medicine*, *352*(10), 997–1003.

Heinemann, U., Lux, H. D., & Gutnick, M. J. (1977). Extracellular free calcium and potassium during paroxsmal activity in the cerebral cortex of the cat. *Experimental Brain Research*, *27*(3–4), 237–243.

Helmstaedter, C., & Witt, J. A. (2008). The effects of levetiracetam on cognition: a non-interventional surveillance study. *Epilepsy & Behavior : E&B*, *13*(4), 642–649.

Henker, C., Hiepel, M. C., Kriesen, T., Scherer, M., Glass, Ä., Herold-Mende, C., Bendszus, M., Langner, S., Weber, M. A., Schneider, B., Unterberg, A., & Piek, J. (2019). Volumetric assessment of glioblastoma and its predictive value for survival. *Acta Neurochirurgica*, *161*(8), 1723–1732.

Herman, M. A., Nahir, B., & Jahr, C. E. (2011). Distribution of extracellular glutamate in the neuropil of hippocampus. *PloS One*, *6*(11).

Herreras, O. (2016). Local field potentials: Myths and misunderstandings. *Frontiers in Neural Circuits*, *10*(DEC), 1–16.

Hervey-Jumper, S. L., & Berger, M. S. (2019). Evidence for Improving Outcome Through Extent of Resection. *Neurosurgery Clinics of North America*, *30*(1), 85–93.

Higashimori, H., & Sontheimer, H. (2007). Role of Kir4.1 channels in growth control of glia. *Glia*, *55*(16), 1668–1679.

Hirsch, J. F., Buisson-Ferey, J., Sachs, M., Hirsch, J. C., & Scherrer, J. (1966). [Electrocorticogram and unitary activites with expanding lesions in man]. *Electroencephalography and Clinical Neurophysiology*, *21*(5), 417–428.

Hirschler, L., Sollmann, N., Schmitz-Abecassis, B., Pinto, J., Arzanforoosh, F., Barkhof, F., Booth, T., Calvo-Imirizaldu, M., Cassia, G., Chmelik, M., Clement, P., Ercan, E., Fernández-Seara, M. A., Furtner, J., Fuster-Garcia, E., Grech-Sollars, M., Guven, N. T., Hatay, G. H., Karami, G., … Hangel, G. (2023). Advanced MR Techniques for Preoperative Glioma Characterization: Part 1. *Journal of Magnetic Resonance Imaging : JMRI*, *57*(6).

Höller, Y., Kutil, R., Klaffenböck, L., Thomschewski, A., Höller, P. M., Bathke, A. C., Jacobs, J., Taylor, A. C., Nardone, R., & Trinka, E. (2015). High-frequency oscillations in epilepsy and surgical outcome. A meta-analysis. *Frontiers in Human Neuroscience*, *9*(OCTOBER), 574.

Hollmann, M., & Heinemann, S. (1994). Cloned glutamate receptors. *Annual Review of Neuroscience*, *17*, 31–108.

Hossmann, K. A., Wechsler, W., & Wilmes, F. (1979). Experimental peritumorous edema - Morphological and pathophysiological observations. *Acta Neuropathologica*, *45*(3), 195–203.

Houillier, C., Wang, X., Kaloshi, G., Mokhtari, K., Guillevin, R., Laffaire, J., Paris, S., Boisselier, B., Idbaih, A., Laigle-Donadey, F., Hoang-Xuan, K., Sanson, M., & Delattre, J. Y. (2010a). IDH1 or IDH2 mutations predict longer survival and response to temozolomide in low-grade gliomas. *Neurology*, *75*(17), 1560–1566.

Huang-Hobbs, E., Cheng, Y.-T., Ko, Y., Luna-Figueroa, E., Lozzi, B., Taylor, K. R., McDonald, M., He, P., Chen, H.-C., Yang, Y., Maleki, E., Lee, Z.-F., Murali, S., Williamson, M. R., Choi, D., Curry, R., Bayley, J., Woo, J., Jalali, A., … Deneen, B. (2023). Remote neuronal activity drives glioma progression through SEMA4F. *Nature*.

Huberfeld, G., Menendez De La Prida, L., Pallud, J., Cohen, I., Le Van Quyen, M., Adam, C., Clemenceau, S., Baulac, M., & Miles, R. (2011). Glutamatergic pre-ictal discharges emerge at the transition to seizure in human epilepsy. *Nature Neuroscience*, *14*(5), 627–635.

Huberfeld, G., & Vecht, C. J. (2016). Seizures and gliomas - Towards a single therapeutic approach. *Nature*

Reviews Neurology, *12*(4), 204–216.

Huberfeld, G., Wittner, L., Clemenceau, S., Baulac, M., Kaila, K., Miles, R., & Rivera, C. (2007). Perturbed chloride homeostasis and GABAergic signaling in human temporal lobe epilepsy. *Journal of Neuroscience*, *27*(37), 9866–9873.

Ibarz, J. M., Foffani, G., Cid, E., Inostroza, M., & De La Prida, L. M. (2010). Emergent dynamics of fast ripples in the epileptic hippocampus. *Journal of Neuroscience*, *30*(48), 16249–16261. 0

Inal, S., Rivnay, J., Suiu, A. O., Malliaras, G. G., & McCulloch, I. (2018). Conjugated Polymers in Bioelectronics. *Accounts of Chemical Research*, *51*(6), 1368–1376.

Ishihara, R., Katayama, Y., Watanabe, T., Yoshino, A., Fukushima, T., & Sakatani, K. (2007). Quantitative spectroscopic analysis of 5-aminolevulinic acid-induced protoporphyrin IX fluorescence intensity in diffusely infiltrating astrocytomas. *Neurologia Medico-Chirurgica*, *47*(2), 53–57.

Ishiuchi, S., Tsuzuki, K., Yoshida, Y., Yamada, N., Hagimura, N., Okado, H., Miwa, A., Kurihara, H., Nakazato, Y., Sasaki, T., & Ozawa, S. (2002). Blockage of Ca 2+ -permeable AMPA receptors suppresses migration and induces apoptosis in human glioblastoma cells. *Nature Medicine*, *8*(9), 971–978.

Ishiuchi, S., Yoshida, Y., Sugawara, K., Aihara, M., Ohtani, T., Watanabe, T., Saito, N., Tsuzuki, K., Okado, H., Miwa, A., Nakazato, Y., & Ozawa, S. (2007). Ca2+-permeable AMPA receptors regulate growth of human glioblastoma via Akt activation. *The Journal of Neuroscience : The Official Journal of the Society for Neuroscience*, *27*(30), 7987–8001.

Ius, T., Ng, S., Young, J. S., Tomasino, B., Polano, M., Ben-Israel, D., Kelly, J. J. P., Skrap, M., Duffau, H., & Berger, M. S. (2022). The benefit of early surgery on overall survival in incidental low-grade glioma patients: A multicenter study. *Neuro-Oncology*, *24*(4), 624–638.

Ivens, S., Kaufer, D., Flores, L. P., Bechmann, I., Zumsteg, D., Tomkins, O., Seiffert, E., Heinemann, U., & Friedman, A. (2007). TGF-beta receptor-mediated albumin uptake into astrocytes is involved in neocortical epileptogenesis. *Brain : A Journal of Neurology*, *130*(Pt 2), 535–547.

Izumoto, S., Miyauchi, M., Tasaki, T., Okuda, T., Nakagawa, N., Nakano, N., Kato, A., & Fujita, M. (2018). Seizures and Tumor Progression in Glioma Patients with Uncontrollable Epilepsy Treated with Perampanel. *Anticancer Research*, *38*(7), 4361–4366.

Jacobs, J., Wu, J. Y., Perucca, P., Zelmann, R., Mader, M., Dubeau, F., Mathern, G. W., Schulze-Bonhage, A., & Gotman, J. (2018). Removing high-frequency oscillations: A prospective multicenter study on seizure outcome. *Neurology*, *91*(11), e1040–e1052.

Jacobs, J., Zelmann, R., Jirsch, J., Chander, R., Dubeau, C. É. C. F., & Gotman, J. (2009). High frequency oscillations (80-500 Hz) in the preictal period in patients with focal seizures. *Epilepsia*, *50*(7), 1780–1792.

Jacobs, J., Zijlmans, M., Zelmann, R., Chatillon, C. É., Hall, J., Olivier, A., Dubeau, F., & Gotman, J. (2010). High-frequency electroencephalographic oscillations correlate with outcome of epilepsy surgery. *Annals of Neurology*, *67*(2), 209–220.

Jadvar, H., & Colletti, P. M. (2014). Competitive advantage of PET/MRI. *European Journal of Radiology*, *83*(1), 84–94.

JASPER, H. H., ARFEL-CAPDEVILLE, G., & RASMUSSEN, T. (1961). Evaluation of EEG and cortical electrographic studies for prognosis of seizures following surgical excision of epileptogenic lesions. *Epilepsia*, *2*, 130–137.

Jefferys, J. G. R. (1995). Nonsynaptic modulation of neuronal activity in the brain: electric currents and extracellular ions. *Physiological Reviews*, *75*(4), 689–723.

Jensen, M. S., & Yaari, Y. (1997). Role of intrinsic burst firing, potassium accumulation, and electrical coupling in the elevated potassium model of hippocampal epilepsy. *Journal of Neurophysiology*, *77*(3), 1224–1233.

Jensen, O., Goel, P., Kopell, N., Pohja, M., Hari, R., & Ermentrout, B. (2005). On the human sensorimotor-cortex beta rhythm: sources and modeling. *NeuroImage*, *26*(2), 347–355.

Jensen, Ole, Kaiser, J., & Lachaux, J. P. (2007). Human gamma-frequency oscillations associated with attention and memory. *Trends in Neurosciences*, *30*(7), 317–324.

Ji, S. Y., Kim, J. W., & Park, C.-K. (2019). Experience Profiling of Fluorescence-Guided Surgery I: Gliomas. *Brain Tumor Research and Treatment*, *7*(2), 98.

Jiang, B., Chaichana, K., Veeravagu, A., Chang, S. D., Black, K. L., & Patil, C. G. (2017). Biopsy versus resection for the management of low-grade gliomas. *The Cochrane Database of Systematic Reviews*, *4*(4).

Jiang, H., Kokkinos, V., Ye, S., Urban, A., Bagić, A., Richardson, M., & He, B. (2022). Interictal SEEG Resting-State Connectivity Localizes the Seizure Onset Zone and Predicts Seizure Outcome. *Advanced Science*, *9*(18), 1–11.

Jirsch, J. D., Urrestarazu, E., LeVan, P., Olivier, A., Dubeau, F., & Gotman, J. (2006). High-frequency

oscillations during human focal seizures. *Brain : A Journal of Neurology*, *129*(Pt 6), 1593–1608.

Jiruska, P., Csicsvari, J., Powell, A. D., Fox, J. E., Chang, W., Vreugdenhil, M., Li, X., Palus, M., Bujan, A. F., Dearden, R. W., & Jefferys, J. G. R. (2010). *High-Frequency Network Activity , Global Increase in Neuronal Activity , and Synchrony Expansion Precede Epileptic Seizures In Vitro*. *30*(16), 5690–5701.

Jiruska, P., de Curtis, M., Jefferys, J. G. R., Schevon, C. A., Schiff, S. J., & Schindler, K. (2013). Synchronization and desynchronization in epilepsy: controversies and hypotheses. *The Journal of Physiology*, *591*(4), 787–797. 0

Jo, J., Diaz, M., Horbinski, C., Mackman, N., Bagley, S., Broekman, M., Rak, J., Perry, J., Pabinger, I., Key, N. S., & Schiff, D. (2023). Epidemiology, biology, and management of venous thromboembolism in gliomas: An interdisciplinary review. *Neuro-Oncology*.

Jo, J., Nevel, K., Sutyla, R., Smolkin, M., Lopes, M. B., & Schiff, D. (2020). Predictors of early, recurrent, and intractable seizures in low-grade glioma. *Neuro-Oncology Practice*, *8*(1), 40–47.

Johnson, D. R., Diehn, F. E., Giannini, C., Jenkins, R. B., Jenkins, S. M., Parney, I. F., & Kaufmann, T. J. (2017). Genetically Defined Oligodendroglioma Is Characterized by Indistinct Tumor Borders at MRI. *AJNR. American Journal of Neuroradiology*, *38*(4), 678–684.

Joseph, J. W., Jensen, M. V., Ilkayeva, O., Palmieri, F., Alárcon, C., Rhodes, C. J., & Newgard, C. B. (2006). The mitochondrial citrate/isocitrate carrier plays a regulatory role in glucose-stimulated insulin secretion. *The Journal of Biological Chemistry*, *281*(47), 35624–35632.

Kahle, K. T., Barnett, S. M., Sassower, K. C., & Staley, K. J. (2009). Decreased seizure activity in a human neonate treated with bumetanide, an inhibitor of the Na(+)-K(+)-2Cl(-) cotransporter NKCC1. *Journal of Child Neurology*, *24*(5), 572–576.

Kaila, K. (1994). Ionic basis of GABAA receptor channel function in the nervous system. *Progress in Neurobiology*, *42*(4), 489–537.

Kajikawa, Y., & Schroeder, C. E. (2015). Generation of field potentials and modulation of their dynamics through volume integration of cortical activity. *Journal of Neurophysiology*, *113*(1), 339–351.

Kalinina, J., Ahn, J., Devi, N. S., Wang, L., Li, Y., Olson, J. J., Glantz, M., Smith, T., Kim, E. L., Giese, A., Jensen, R. L., Chen, C. C., Carter, B. S., Mao, H., He, M., & Van Meir, E. G. (2016). Selective Detection of the D-enantiomer of 2-Hydroxyglutarate in the CSF of Glioma Patients with Mutated Isocitrate Dehydrogenase. *Clinical Cancer Research : An Official Journal of the American Association for Cancer Research*, *22*(24), 6256–6265.

Kaneoka, A., Fujimoto, S. H., Tamura, K., Inaji, M., & Maehara, T. (2023). Nonconvulsive status epilepticus characteristics in glioma patients: a retrospective study. *Discover. Oncology*, *14*(1).

Karoly, P. J., Freestone, D. R., Boston, R., Grayden, D. B., Himes, D., Leyde, K., Seneviratne, U., Berkovic, S., O'Brien, T., & Cook, M. J. (2016). Interictal spikes and epileptic seizures: their relationship and underlying rhythmicity. *Brain : A Journal of Neurology*, *139*(Pt 4), 1066–1078.

Karoly, P. J., Rao, V. R., Gregg, N. M., Worrell, G. A., Bernard, C., Cook, M. J., & Baud, M. O. (2021). Cycles in epilepsy. *Nature Reviews. Neurology*, *17*(5), 267–284.

Karschnia, P., Vogelbaum, M. A., van den Bent, M., Cahill, D. P., Bello, L., Narita, Y., Berger, M. S., Weller, M., & Tonn, J. C. (2021). Evidence-based recommendations on categories for extent of resection in diffuse glioma. *European Journal of Cancer (Oxford, England : 1990)*, *149*, 23–33.

Kast, R. E. (2021). Adding high-dose celecoxib to increase effectiveness of standard glioblastoma chemoirradiation. *Annales Pharmaceutiques Francaises*, *79*(5), 481–488.

Kayser-Gatchalian, M. C., & Kayser, K. (1975). Thrombosis and intracranial tumors. *Journal of Neurology*, *209*(3), 217–224.

Kelly, P. J., Daumas-Duport, C., Kispert, D. B., Kall, B. A., Scheithauer, B. W., & Illig, J. J. (1987). Imaging-based stereotaxic serial biopsies in untreated intracranial glial neoplasms. *Journal of Neurosurgery*, *66*(6), 865–874.

Kerem, D. H., & Geva, A. B. (2005). Forecasting epilepsy from the heart rate signal. *Medical & Biological Engineering & Computing*, *43*(2), 230–239.

Kerkhof, M., Dielemans, J. C. M., van Breemen, M. S., Zwinkels, H., Walchenbach, R., Taphoorn, M. J., & Vecht, C. J. (2013). Effect of valproic acid on seizure control and on survival in patients with glioblastoma multiforme. *Neuro-Oncology*, *15*(7), 961–967.

Kerkhof, M., & Vecht, C. J. (2013). Seizure characteristics and prognostic factors of gliomas. *Epilepsia*, *54*(SUPPL. 9), 12–17.

Khodagholy, D., Gelinas, J. N., Thesen, T., Doyle, W., Devinsky, O., Malliaras, G. G., & Buzsáki, G. (2015). NeuroGrid: Recording action potentials from the surface of the brain. *Nature Neuroscience*, *18*(2), 310–315.

Khodagholy, D., Gelinas, J. N., Zhao, Z., Yeh, M., Long, M., Greenlee, J. D., Doyle, W., Devinsky, O., & Buzsáki, G. (2016). Organic electronics for high-resolution electrocorticography of the human brain. *Science Advances*, *2*(11), e1601027.

Khodagholy, D., Rivnay, J., Sessolo, M., Gurfinkel, M., Leleux, P., Jimison, L. H., Stavrinidou, E., Herve, T., Sanaur, S., Owens, R. M., & Malliaras, G. G. (2013). High transconductance organic electrochemical transistors. *Nature Communications*, *4*, 2133.

Kim, D., Chun, J. H., Kim, S. H., Moon, J. H., Kang, S. G., Chang, J. H., & Yun, M. (2019). Re-evaluation of the diagnostic performance of 11C-methionine PET/CT according to the 2016 WHO classification of cerebral gliomas. *European Journal of Nuclear Medicine and Molecular Imaging*, *46*(8), 1678–1684.

Kim, Y. H., Kim, T., Joo, J. D., Han, J. H., Kim, Y. J., Kim, I. A., Yun, C. H., & Kim, C. Y. (2015). Survival benefit of levetiracetam in patients treated with concomitant chemoradiotherapy and adjuvant chemotherapy with temozolomide for glioblastoma multiforme. *Cancer*, *121*(17), 2926–2932.

Kipp, B. R., Voss, J. S., Kerr, S. E., Barr Fritcher, E. G., Graham, R. P., Zhang, L., Edward Highsmith, W., Zhang, J., Roberts, L. R., Gores, G. J., & Halling, K. C. (2012). Isocitrate dehydrogenase 1 and 2 mutations in cholangiocarcinoma. *Human Pathology*, *43*(10), 1552–1558.

Kirson, E. D., Dbalý, V., Tovaryš, F., Vymazal, J., Soustiel, J. F., Itzhaki, A., Mordechovich, D., Steinberg-Shapira, S., Gurvich, Z., Schneiderman, R., Wasserman, Y., Salzberg, M., Ryffel, B., Goldsher, D., Dekel, E., & Palti, Y. (2007). Alternating electric fields arrest cell proliferation in animal tumor models and human brain tumors. *Proceedings of the National Academy of Sciences of the United States of America*, *104*(24), 10152–10157.

Kirson, E. D., Gurvich, Z., Schneiderman, R., Dekel, E., Itzhaki, A., Wasserman, Y., Schatzberger, R., & Palti, Y. (2004). Disruption of cancer cell replication by alternating electric fields. *Cancer Research*, *64*(9), 3288–3295.

Kirson, E. D., Schneiderman, R. S., Dbal, V., Tovary, F., Vymazal, J., Itzhaki, A., Mordechovich, D., Gurvich, Z., Shmueli, E., Goldsher, D., Wasserman, Y., & Palti, Y. (2009). Chemotherapeutic treatment efficacy and sensitivity are increased by adjuvant alternating electric fields (TTFields). *BMC Medical Physics*, *9*(1).

Klein, M., Engelberts, N. H. J., Van der Ploeg, H. M., Kasteleijn-Nolst Trenité, D. G. A., Aaronson, N. K., Taphoorn, M. J. B., Baaijen, H., Vandertop, W. P., Muller, M., Postma, T. J., & Heimans, J. J. (2003). Epilepsy in low-grade gliomas: The impact on cognitive function and quality of life. *Annals of Neurology*, *54*(4), 514–520.

Knobbe, C. B., Merlo, A., & Reifenberger, G. (2002). Pten signalling in gliomas. *Neuro-Oncology*, *4*(3), 196–210.

Koekkoek, J. A. F., Dirven, L., Heimans, J. J., Postma, T. J., Vos, M. J., Reijneveld, J. C., & Taphoorn, M. J. B. (2016). Seizure reduction is a prognostic marker in low-grade glioma patients treated with temozolomide. *Journal of Neuro-Oncology*, *126*(2), 347–354.

Koekkoek, J. A. F., Kerkhof, M., Dirven, L., Heimans, J. J., Reijneveld, J. C., & Taphoorn, M. J. B. (2015). Seizure outcome after radiotherapy and chemotherapy in low-grade glioma patients: a systematic review. *Neuro-Oncology*, *17*(7), 924–934. 2

Kölker, S., Pawlak, V., Ahlemeyer, B., Okun, J. G., Hörster, F., Mayatepek, E., Krieglstein, J., Hoffmann, G. F., & Köhr, G. (2002). NMDA receptor activation and respiratory chain complex V inhibition contribute to neurodegeneration in d-2-hydroxyglutaric aciduria. *The European Journal of Neuroscience*, *16*(1), 21–28.

Konteatis, Z., Artin, E., Nicolay, B., Straley, K., Padyana, A. K., Jin, L., Chen, Y., Narayaraswamy, R., Tong, S., Wang, F., Zhou, D., Cui, D., Cai, Z., Luo, Z., Fang, C., Tang, H., Lv, X., Nagaraja, R., Yang, H., … Biller, S. A. (2020). Vorasidenib (AG-881): A First-in-Class, Brain-Penetrant Dual Inhibitor of Mutant IDH1 and 2 for Treatment of Glioma. *ACS Medicinal Chemistry Letters*, *11*(2), 101–107.

Korshunov, A., Casalini, B., Chavez, L., Hielscher, T., Sill, M., Ryzhova, M., Sharma, T., Schrimpf, D., Stichel, D., Capper, D., Reuss, D. E., Sturm, D., Absalyamova, O., Golanov, A., Lambo, S., Bewerunge-Hudler, M., Lichter, P., Herold-Mende, C., Wick, W., … Sahm, F. (2019). Integrated molecular characterization of IDH-mutant glioblastomas. *Neuropathology and Applied Neurobiology*, *45*(2), 108–118.

Krishna, S., Choudhury, A., Keough, M. B., Seo, K., Ni, L., Kakaizada, S., Lee, A., Aabedi, A., Popova, G., Lipkin, B., Cao, C., Nava Gonzales, C., Sudharshan, R., Egladyous, A., Almeida, N., Zhang, Y., Molinaro, A. M., Venkatesh, H. S., Daniel, A. G. S., … Hervey-Jumper, S. L. (2023). Glioblastoma remodelling of human neural circuits decreases survival. *Nature*, *617*(7961).

Kuffler, S. W. (1967). Neuroglial cells: physiological properties and a potassium mediated effect of neuronal activity on the glial membrane potential. *Proceedings of the Royal Society of London. Series B, Biological Sciences*, *168*(1010), 1–21.

Kurimoto, M., Hayashi, N., Kamiyama, H., Nagai, S., Shibata, T., Asahi, T., Matsumura, N., Hirashima, Y., & Endo, S. (2004). Impact of neuronavigation and image-guided extensive resection for adult patients with supratentorial malignant astrocytomas: a single-institution retrospective study. *Minimally Invasive Neurosurgery : MIN*, *47*(5), 278–283.

Kwan, P., Arzimanoglou, A., Berg, A. T., Brodie, M. J., Hauser, W. A., Mathern, G., Moshé, S. L., Perucca, E., Wiebe, S., & French, J. (2010). Definition of drug resistant epilepsy: consensus proposal by the ad hoc Task Force of the ILAE Commission on Therapeutic Strategies. *Epilepsia*, *51*(6), 1069–1077.

Laack, N. N., Pafundi, D., Anderson, S. K., Kaufmann, T., Lowe, V., Hunt, C., Vogen, D., Yan, E., Sarkaria, J., Brown, P., Kizilbash, S., Uhm, J., Ruff, M., Zakhary, M., Zhang, Y., Seaberg, M., Wan Chan Tseung, H. S., Kabat, B., Kemp, B., & Brinkmann, D. (2021). Initial Results of a Phase 2 Trial of 18F-DOPA PET-Guided Dose-Escalated Radiation Therapy for Glioblastoma. *International Journal of Radiation Oncology, Biology, Physics*, *110*(5), 1383–1395.

Lachaux, J. Ph, Rudrauf, D., & Kahane, P. (2003). Intracranial EEG and human brain mapping. *Journal of Physiology Paris*, *97*(4–6), 613–628.

Lachaux, Jean Philippe, Rodriguez, E., Martinerie, J., Adam, C., Hasboun, D., & Varela, F. J. (2000). A quantitative study of gamma-band activity in human intracranial recordings triggered by visual stimuli. *The European Journal of Neuroscience*, *12*(7), 2608–2622.

Lagarde, S., Buzori, S., Trebuchon, A., Carron, R., Scavarda, D., Milh, M., McGonigal, A., & Bartolomei, F. (2019). The repertoire of seizure onset patterns in human focal epilepsies: Determinants and prognostic values. *Epilepsia*, *60*(1), 85–95.

Lairy-Bounes, G. C., & Dreyfus-Brisac, C. (1950). [EEG. of cerebral intra- and sub-ventricular tumors]. *Revue Neurologique*, *83*(6), 613–618.

Lambrecq, V., Lehongre, K., Adam, C., Frazzini, V., Mathon, B., Clemenceau, S., Hasboun, D., Charpier, S., Baulac, M., Navarro, V., & Le Van Quyen, M. (2017). Single-unit activities during the transition to seizures in deep mesial structures. *Annals of Neurology*, *82*(6), 1022–1028.

Landers, M. J. F., Brouwers, H. B., Kortman, G. J., Boukrab, I., De Baene, W., & Rutten, G. J. M. (2023). Oligodendrogliomas tend to infiltrate the frontal aslant tract, whereas astrocytomas tend to displace it. *Neuroradiology*.

Lange, F., Hartung, J., Liebelt, C., Boisserée, J., Resch, T., Porath, K., Hörnschemeyer, J., Reichart, G., Sellmann, T., Neubert, V., Kriesen, S., Hildebrandt, G., Schültke, E., Köhling, R., & Kirschstein, T. (2020). Perampanel Add-on to Standard Radiochemotherapy in vivo Promotes Neuroprotection in a Rodent F98 Glioma Model. *Frontiers in Neuroscience*, *14*.

Lange, F., Hörnschemeyer, J., & Kirschstein, T. (2021). Glutamatergic Mechanisms in Glioblastoma and Tumor-Associated Epilepsy. *Cells*, *10*(5).

Lange, F., Weßlau, K., Porath, K., Hörnschemeyer, J., Bergner, C., Krause, B. J., Mullins, C. S., Linnebacher, M., Köhling, R., & Kirschstein, T. (2019). AMPA receptor antagonist perampanel affects glioblastoma cell growth and glutamate release in vitro. *PloS One*, *14*(2).

Larjavaara, S., Mäntylä, R., Salminen, T., Haapasalo, H., Raitanen, J., Jääskeläinen, J., & Auvinen, A. (2007). Incidence of gliomas by anatomic location. *Neuro-Oncology*, *9*(3), 319–325.

Latini, A., Da Silva, C. G., Ferreira, G. C., Schuck, P. F., Scussiato, K., Sarkis, J. J., Dutra Filho, C. S., Wyse, A. T. S., Wannmacher, C. M. D., & Wajner, M. (2005). Mitochondrial energy metabolism is markedly impaired by D-2-hydroxyglutaric acid in rat tissues. *Molecular Genetics and Metabolism*, *86*(1–2), 188–199.

Latini, F., Fahlström, M., Hesselager, G., Zetterling, M., & Ryttlefors, M. (2020). Differences in the preferential location and invasiveness of diffuse low-grade gliomas and their impact on outcome. *Cancer Medicine*, *9*(15), 5446–5458.

Law, I., Albert, N. L., Arbizu, J., Boellaard, R., Drzezga, A., Galldiks, N., la Fougère, C., Langen, K. J., Lopci, E., Lowe, V., McConathy, J., Quick, H. H., Sattler, B., Schuster, D. M., Tonn, J. C., & Weller, M. (2019). Joint EANM/EANO/RANO practice guidelines/SNMMI procedure standards for imaging of gliomas using PET with radiolabelled amino acids and [18F]FDG: version 1.0. *European Journal of Nuclear Medicine and Molecular Imaging*, *46*(3), 540–557.

Lebrun, C., Fontaine, D., Ramaioli, A., Vandenbos, F., Chanalet, S., Lonjon, M., Michiels, J. F., Bourg, V., Paquis, P., Chatel, M., & Frenay, M. (2004). Long-term outcome of oligodendrogliomas. *Neurology*, *62*(10), 1783–1787.

Leclercq, K., Liefferinge, J. Van, Albertini, G., Neveux, M., Dardenne, S., Mairet-Coello, G., Vandenplas, C., Deprez, T., Chong, S. A., Foerch, P., Bentea, E., Sato, H., Maher, P., Massie, A., Smolders, I., & Kaminski, R. M. (2019). Anticonvulsant and antiepileptogenic effects of system inactivation in chronic epilepsy models. *Epilepsia*, *60*(7), 1412–1423.

Lee, H. H. C., Deeb, T. Z., Walker, J. A., Davies, P. A., & Moss, S. J. (2011). NMDA receptor activity downregulates KCC2 resulting in depolarizing GABAA receptor-mediated currents. *Nature Neuroscience*, *14*(6), 736–743.

Lee, J. W., Norden, A. D., Ligon, K. L., Golby, A. J., Beroukhim, R., Quackenbush, J., Wells, W., Oelschlager, K., Maetzold, D., & Wen, P. Y. (2014). Tumor associated seizures in glioblastomas are influenced by survival gene expression in a region-specific manner: A gene expression imaging study.

Epilepsy Research, *108*(5), 843–852.

Lee, J. W., Wen, P. Y., Hurwitz, S., Black, P., Kesari, S., Drappatz, J., Golby, A. J., Wells, W. M., Warfield, S. K., Kikinis, R., & Bromfield, E. B. (2010). Morphological characteristics of brain tumors causing seizures. *Archives of Neurology*, *67*(3), 336–342.

Lehnertz, K., & Litt, B. (2005). The First International Collaborative Workshop on Seizure Prediction: summary and data description. *Clinical Neurophysiology : Official Journal of the International Federation of Clinical Neurophysiology*, *116*(3), 493–505.

Leighton, F., Poole, B., Lazarow, P. B., & De Duve, C. (1969). THE SYNTHESIS AND TURNOVER OF RAT LIVER PEROXISOMES : I. Fractionation of Peroxisome Proteins. *The Journal of Cell Biology*, *41*(2), 521.

Lemaitre, A. L., Herbet, G., Duffau, H., & Lafargue, G. (2021). Personality and behavioral changes after brain tumor resection: a lesion mapping study. *Acta Neurochirurgica*, *163*(5), 1257–1267.

Lemaitre, A. L., Herbet, G., Ng, S., Moritz-Gasser, S., & Duffau, H. (2022). Cognitive preservation following awake mapping-based neurosurgery for low-grade gliomas: A longitudinal, within-patient design study. *Neuro-Oncology*, *24*(5), 781–793.

Lenz, G., & Avruch, J. (2005). Glutamatergic regulation of the p70S6 kinase in primary mouse neurons. *The Journal of Biological Chemistry*, *280*(46), 38121–38124.

Leroy, H. A., Delmaire, C., Le Rhun, E., Drumez, E., Lejeune, J. P., & Reyns, N. (2019). High-field intraoperative MRI and glioma surgery: results after the first 100 consecutive patients. *Acta Neurochirurgica*, *161*(7), 1467–1474.

Liang, C., Li, M., Gong, J., Zhang, B., Lin, C., He, H., Zhang, K., & Guo, Y. (2019). A new application of ultrasound-magnetic resonance multimodal fusion virtual navigation in glioma surgery. *Annals of Translational Medicine*, *7*(23), 736–736.

Liang, S., Zhang, J., Zhang, S., & Fu, X. (2016). Epilepsy in adults with supratentorial glioblastoma: Incidence and influence factors and prophylaxis in 184 patients. *PLoS ONE*, *11*(7).

Lillis, K., MA, K., J, M., KJ, S., & JA, W. (2012). Pyramidal cells accumulate chloride at seizure onset. *Neurobiology of Disease*, *47*(3), 358–366.

Linninger, A., Hartung, G. A., Liu, B. P., Mirkov, S., Tangen, K., Lukas, R. V., Unruh, D., David James, C., Sarkaria, J. N., & Horbinski, C. (2018). Modeling the diffusion of D-2-hydroxyglutarate from IDH1 mutant gliomas in the central nervous system. *Neuro-Oncology*, *20*(9), 1197–1206.

Lipton, J. O., & Sahin, M. (2014). The neurology of mTOR. *Neuron*, *84*(2), 275–291.

Litt, B., & Lehnertz, K. (2002). Seizure prediction and the preseizure period. *Current Opinion in Neurology*, *15*(2), 173–177.

Liu, R., Wang, J., Liang, S., Zhang, G., & Yang, X. (2019). Role of NKCC1 and KCC2 in Epilepsy: From Expression to Function. *Frontiers in Neurology*, *10*, 1407.

Liu, S., Gurses, C., Sha, Z., Quach, M. M., Sencer, A., Bebek, N., Curry, D. J., Prabhu, S., Tummala, S., Henry, T. R., & Ince, N. F. (2018). Stereotyped high-frequency oscillations discriminate seizure onset zones and critical functional cortex in focal epilepsy. *Brain : A Journal of Neurology*, *141*(3), 713–730.

Liubinas, S. V., D'Abaco, G. M., Moffat, B. M., Gonzales, M., Feleppa, F., Nowell, C. J., Gorelik, A., Drummond, K. J., O'Brien, T. J., Kaye, A. H., & Morokoff, A. P. (2014). IDH1 mutation is associated with seizures and protoplasmic subtype in patients with low-grade gliomas. *Epilepsia*, *55*(9), 1438–1443.

Llaguno, S. R. A., & Parada, L. F. (2016). Cell of origin of glioma: biological and clinical implications. *British Journal of Cancer*, *115*(12), 1445–1450.

Lohmann, P., Stavrinou, P., Lipke, K., Bauer, E. K., Ceccon, G., Werner, J. M., Neumaier, B., Fink, G. R., Shah, N. J., Langen, K. J., & Galldiks, N. (2019). FET PET reveals considerable spatial differences in tumour burden compared to conventional MRI in newly diagnosed glioblastoma. *European Journal of Nuclear Medicine and Molecular Imaging*, *46*(3), 591–602.

Long, Y., Tao, H., Karachi, A., Grippin, A. J., Jin, L., Chang, Y., Zhang, W., Dyson, K. A., Hou, A. Y., Na, M., Deleyrolle, L. P., Sayour, E. J., Rahman, M., Mitchell, D. A., Lin, Z., & Huang, J. (2020). Dysregulation of Glutamate Transport Enhances Treg Function That Promotes VEGF Blockade Resistance in Glioblastoma. *Cancer Research*, *80*(3), 499–509.

Lopes, D. V., de Fraga Dias, A., Silva, L. F. L., Scholl, J. N., Sévigny, J., Battastini, A. M. O., & Figueiró, F. (2021). Influence of NSAIDs and methotrexate on CD73 expression and glioma cell growth. *Purinergic Signalling*, *17*(2), 273–284.

Losi, G., Marcon, I., Mariotti, L., Sessolo, M., Chiavegato, A., & Carmignoto, G. (2016). A brain slice experimental model to study the generation and the propagation of focally-induced epileptiform activity. *Journal of Neuroscience Methods*, *260*, 125–131.

Louis, D. N., Perry, A., Wesseling, P., Brat, D. J., Cree, I. A., Figarella-Branger, D., Hawkins, C., Ng, H. K., Pfister, S. M., Reifenberger, G., Soffietti, R., Von Deimling, A., & Ellison, D. W. (2021). The 2021

WHO classification of tumors of the central nervous system: A summary. *Neuro-Oncology*, *23*(8), 1231–1251.

Lu, C., Venneti, S., Akalin, A., Fang, F., Ward, P. S., DeMatteo, R. G., Intlekofer, A. M., Chen, C., Ye, J., Hameed, M., Nafa, K., Agaram, N. P., Cross, J. R., Khanin, R., Mason, C. E., Healey, J. H., Lowe, S. W., Schwartz, G. K., Melnick, A., & Thompson, C. B. (2013). Induction of sarcomas by mutant IDH2. *Genes & Development*, *27*(18), 1986–1998.

Lu, Y., Kwintkiewicz, J., Liu, Y., Tech, K., Frady, L. N., Su, Y. T., Bautista, W., Moon, S. I., MacDonald, J., Ewend, M. G., Gilbert, M. R., Yang, C., & Wu, J. (2017). Chemosensitivity of IDH1-Mutated Gliomas Due to an Impairment in PARP1-Mediated DNA Repair. *Cancer Research*, *77*(7), 1709–1718.

Ludwig, K. A., Langhals, N. B., Joseph, M. D., Richardson-Burns, S. M., Hendricks, J. L., & Kipke, D. R. (2011). Poly(3,4-ethylenedioxythiophene) (PEDOT) polymer coatings facilitate smaller neural recording electrodes. *Journal of Neural Engineering*, *8*(1).

Luyken, C., Blümcke, I., Fimmers, R., Urbach, H., Elger, C. E., Wiestler, O. D., & Schramm, J. (2003). The spectrum of long-term epilepsy-associated tumors: Long-term seizure and tumor outcome and neurosurgical aspects. *Epilepsia*, *44*(6), 822–830.

Lyons, S. A., Chung, W. J., Weaver, A. K., Ogunrinu, T., & Sontheimer, H. (2007). Autocrine glutamate signaling promotes glioma cell invasion. *Cancer Research*, *67*(19), 9463–9471.

Maas, S., Patt, S., Schrey, M., & Rich, A. (2001). Underediting of glutamate receptor GluR-B mRNA in malignant gliomas. *Proceedings of the National Academy of Sciences of the United States of America*, *98*(25), 14687–14692.

Malliaras, G., & Abidian, M. R. (2015). Organic Bioelectronic Materials and Devices. *Advanced Materials (Deerfield Beach, Fla.)*, *27*(46), 7492.

Malmer, B., Henriksson, R., & Grönberg, H. (2003). Familial brain tumours-genetics or environment? A nationwide cohort study of cancer risk in spouses and first-degree relatives of brain tumour patients. *International Journal of Cancer*, *106*(2), 260–263.

Mandonnet, E., De Witt Hamer, P., Pallud, J., Bauchet, L., Whittle, I., & Duffau, H. (2014). Silent diffuse low-grade glioma: toward screening and preventive treatment? *Cancer*, *120*(12), 1758–1762.

Mandonnet, E., Taillandier, L., & Duffau, H. (2017). [Proposal of screening for diffuse low-grade gliomas in the population from 20 to 40years]. *Presse Medicale (Paris, France : 1983)*, *46*(10), 911–920.

Mandonnet, E., Winkler, P. A., & Duffau, H. (2010). Direct electrical stimulation as an input gate into brain functional networks: Principles, advantages and limitations. *Acta Neurochirurgica*, *152*(2), 185–193.

Mantione, D., del Agua, I., Sanchez-Sanchez, A., & Mecerreyes, D. (2017). Poly(3,4-ethylenedioxythiophene) (PEDOT) Derivatives: Innovative Conductive Polymers for Bioelectronics. *Polymers*, *9*(8).

Mantione, D., del Agua, I., Schaafsma, W., Diez-Garcia, J., Castro, B., Sardon, H., & Mecerreyes, D. (2016). Poly(3,4-ethylenedioxythiophene):GlycosAminoGlycan Aqueous Dispersions: Toward Electrically Conductive Bioactive Materials for Neural Interfaces. *Macromolecular Bioscience*, *16*(8), 1227–1238.

Mao, J., Deng, D., Yang, Z., Wang, W., Cao, M., Huang, Y., & Shen, J. (2020). Pretreatment structural and arterial spin labeling MRI is predictive for p53 mutation in high-grade gliomas. *The British Journal of Radiology*, *93*(1115).

Marco, P., Sola, R. G., Cajal, S. R. Y., & DeFelipe, J. (1997). Loss of inhibitory synapses on the soma and axon initial segment of pyramidal cells in human epileptic peritumoural neocortex: Implications for epilepsy. *Brain Research Bulletin*, *44*(1), 47–66.

Marcus, H. J., Carpenter, K. L. H., Price, S. J., & Hutchinson, P. J. (2010). In vivo assessment of high-grade glioma biochemistry using microdialysis: A study of energy-related molecules, growth factors and cytokines. *Journal of Neuro-Oncology*, *97*(1), 11–23.

Marczynski, T. J. (1998). GABAergic deafferentation hypothesis of brain aging and Alzheimer's disease revisited. *Brain Research Bulletin*, *45*(4), 341–379.

Mardis, E. R., Ding, L., Dooling, D. J., Larson, D. E., McLellan, M. D., Chen, K., Koboldt, D. C., Fulton, R. S., Delehaunty, K. D., McGrath, S. D., Fulton, L. A., Locke, D. P., Magrini, V. J., Abbott, R. M., Vickery, T. L., Reed, J. S., Robinson, J. S., Wylie, T., Smith, S. M., … Ley, T. J. (2009). Recurring mutations found by sequencing an acute myeloid leukemia genome. *The New England Journal of Medicine*, *361*(11), 1058–1066.

Marson, A. G., Appleton, R., Baker, G. A., Chadwick, D. W., Doughty, J., Eaton, B., Gamble, C., Jacoby, A., Shackley, P., Smith, D. F., Tudur-Smith, C., Vanoli, A., & Williamson, P. R. (2007). A randomised controlled trial examining the longer-term outcomes of standard versus new antiepileptic drugs. The SANAD trial. *Health Technology Assessment (Winchester, England)*, *11*(37), 1–108.

Maschio, M., Dinapoli, L., Sperati, F., Pace, A., Fabi, A., Vidiri, A., & Muti, P. (2011). Levetiracetam monotherapy in patients with brain tumor-related epilepsy: seizure control, safety, and quality of life. *Journal of Neuro-Oncology*, *104*(1), 205–214.

Maschio, M., Maialetti, A., Mocellini, C., Domina, E., Pauletto, G., Costa, C., Mascia, A., Romoli, M., & Giannarelli, D. (2020). Effect of Brivaracetam on Efficacy and Tolerability in Patients With Brain Tumor-Related Epilepsy: A Retrospective Multicenter Study. *Frontiers in Neurology*, *11*.

Maschio, M., Pauletto, G., Zarabla, A., Maialetti, A., Lus, T., Villani, V., Fabi, A., Koudriavtseva, T., & Giannarelli, D. (2019). Perampanel in patients with brain tumor-related epilepsy in real-life clinical practice: a retrospective analysis. *The International Journal of Neuroscience*, *129*(6), 593–597.

Matarrese, M. A. G., Loppini, A., Fabbri, L., Tamilia, E., Perry, M. S., Madsen, J. R., Bolton, J., Stone, S. S. D., Pearl, P. L., Filippi, S., & Papadelis, C. (2023). Spike propagation mapping reveals effective connectivity and predicts surgical outcome in epilepsy. *Brain : A Journal of Neurology*.

Matta, J. A., Ashby, M. C., Sanz-Clemente, A., Roche, K. W., & Isaac, J. T. R. (2011). mGluR5 and NMDA receptors drive the experience- and activity-dependent NMDA receptor NR2B to NR2A subunit switch. *Neuron*, *70*(2), 339–351.

Mayer, M. L. (2005). Crystal structures of the GluR5 and GluR6 ligand binding cores: molecular mechanisms underlying kainate receptor selectivity. *Neuron*, *45*(4), 539–552.

Mbizvo, G. K., Dixon, P., Hutton, J. L., & Marson, A. G. (2012). Levetiracetam add-on for drug-resistant focal epilepsy: an updated Cochrane Review. *The Cochrane Database of Systematic Reviews*, *2012*(9).

Mccarthy, L., Verma, G., Hangel, G., Neal, A., Moffat, B. A., Stockmann, J. P., Andronesi, O. C., Balchandani, P., & Hadjipanayis, C. G. (2022). Application of 7T MRS to High-Grade Gliomas. *AJNR. American Journal of Neuroradiology*, *43*(10), 1378–1395.

McCoy, E., & Sontheimer, H. (2007). Expression and function of water channels (aquaporins) in migrating malignant astrocytes. *GLIA*, *55*(10), 1034–1043.

McCullough, B. J., Ader, V., Aguedan, B., Feng, X., Susanto, D., Benkers, T. L., Henson, J. W., Mayberg, M., Cobbs, C. S., Gwinn, R. P., Monteith, S. J., Newell, D. W., Delashaw, J., Fouke, S. J., Rostad, S., & Keogh, B. P. (2018). Preoperative relative cerebral blood volume analysis in gliomas predicts survival and mitigates risk of biopsy sampling error. *Journal of Neuro-Oncology*, *136*(1), 181–188.

Melani, F., Zelmann, R., Mari, F., & Gotman, J. (2013). Continuous High Frequency Activity: a peculiar SEEG pattern related to specific brain regions. *Clinical Neurophysiology : Official Journal of the International Federation of Clinical Neurophysiology*, *124*(8), 1507–1516.

Mellinghoff, I. K., van den Bent, M. J., Blumenthal, D. T., Touat, M., Peters, K. B., Clarke, J., Mendez, J., Yust-Katz, S., Welsh, L., Mason, W. P., Ducray, F., Umemura, Y., Nabors, B., Holdhoff, M., Hottinger, A. F., Arakawa, Y., Sepulveda, J. M., Wick, W., Soffietti, R., … Cloughesy, T. F. (2023a). Vorasidenib in IDH1- or IDH2-Mutant Low-Grade Glioma. *The New England Journal of Medicine*.

Mellinghoff, I. K., van den Bent, M. J., Blumenthal, D. T., Touat, M., Peters, K. B., Clarke, J., Mendez, J., Yust-Katz, S., Welsh, L., Mason, W. P., Ducray, F., Umemura, Y., Nabors, B., Holdhoff, M., Hottinger, A. F., Arakawa, Y., Sepulveda, J. M., Wick, W., Soffietti, R., … Cloughesy, T. F. (2023b). Vorasidenib in IDH1- or IDH2-Mutant Low-Grade Glioma. *The New England Journal of Medicine*, *389*(7).

Mesny, E., Barritault, M., Izquierdo, C., Poncet, D., d'Hombres, A., Guyotat, J., Jouanneau, E., Ameli, R., Honnorat, J., Meyronet, D., & Ducray, F. (2022). Gyriform infiltration as imaging biomarker for molecular glioblastomas. *Journal of Neuro-Oncology*, *157*(3), 511–521.

Milior, G., Morin-Brureau, M., Pallud, J., Miles, R., & Huberfeld, G. (2023). Animal models and human tissue compared to better understand and treat the epilepsies. *Epilepsia*, *64*(5), 1175–1189.

Milsap, G., Collard, M., Coogan, C., Rabbani, Q., Wang, Y., & Crone, N. E. (2019). Keyword Spotting Using Human Electrocorticographic Recordings. *Frontiers in Neuroscience*, *13*(FEB).

Minthe, A., Janzarik, W. G., Lachner-Piza, D., Reinacher, P., Schulze-Bonhage, A., Dümpelmann, M., & Jacobs, J. (2020). Stable high frequency background EEG activity distinguishes epileptic from healthy brain regions. *Brain Communications*, *2*(2).

Mirsattari, S. M., Chong, J. J. R., Hammond, R. R., Megyesi, J. F., Macdonald, D. R., Lee, D. H., & Cairncross, J. G. (2011). Do epileptic seizures predict outcome in patients with oligodendroglioma? *Epilepsy Research*, *94*(1–2), 39–44.

Mittal, S., Barkmeier, D., Hua, J., Pai, D. S., Fuerst, D., Basha, M., Loeb, J. A., & Shah, A. K. (2016). Intracranial EEG analysis in tumor-related epilepsy: Evidence of distant epileptic abnormalities. In *Clinical Neurophysiology* (Vol. 127, Issue 1). International Federation of Clinical Neurophysiology.

Mohammadi, A. M., Sullivan, T. B., Barnett, G. H., Recinos, V., Angelov, L., Kamian, K., & Vogelbaum, M. A. (2014). Use of high-field intraoperative magnetic resonance imaging to enhance the extent of resection of enhancing and nonenhancing gliomas. *Neurosurgery*, *74*(4), 339–348.

Moiraghi, A., & Pallud, J. (2020). *Intraoperative ultrasound techniques for cerebral gliomas resection : usefulness and pitfalls*. *8*(8), 8–10.

Molina, J. L., Voytek, B., Thomas, M. L., Joshi, Y. B., Bhakta, S. G., Talledo, J. A., Swerdlow, N. R., & Light, G. A. (2020). Memantine Effects on Electroencephalographic Measures of Putative Excitatory/Inhibitory Balance in Schizophrenia. *Biological Psychiatry: Cognitive Neuroscience and*

Neuroimaging, *5*(6), 562–568.

Molinaro, A. M., Hervey-Jumper, S., Morshed, R. A., Young, J., Han, S. J., Chunduru, P., Zhang, Y., Phillips, J. J., Shai, A., Lafontaine, M., Crane, J., Chandra, A., Flanigan, P., Jahangiri, A., Cioffi, G., Ostrom, Q., Anderson, J. E., Badve, C., Barnholtz-Sloan, J., … Berger, M. S. (2020). Association of Maximal Extent of Resection of Contrast-Enhanced and Non-Contrast-Enhanced Tumor With Survival Within Molecular Subgroups of Patients With Newly Diagnosed Glioblastoma. *JAMA Oncology*, *6*(4), 495–503.

Moody, W. (1984). Effects of intracellular H+ on the electrical properties of excitable cells. *Annual Review of Neuroscience*, *7*(1), 257–278.

Mormann, F., Andrzejak, R. G., Elger, C. E., & Lehnertz, K. (2007). *Seizure prediction : the long and winding road*. 314–333.

Mortazavi, A., Fayed, I., Bachani, M., Dowdy, T., Jahanipour, J., Khan, A., Owotade, J., Walbridge, S., Inati, S. K., Steiner, J., Wu, J., Gilbert, M., Yang, C. Z., Larion, M., Maric, D., Ksendzovsky, A., & Zaghloul, K. A. (2022). *IDH-mutated gliomas promote epileptogenesis through d-2-hydroxyglutarate-dependent mTOR hyperactivation*. *January*, 1–13.

Mostofa, A. G. M., Punganuru, S. R., Madala, H. R., Al-Obaide, M., & Srivenugopal, K. S. (2017). The Process and Regulatory Components of Inflammation in Brain Oncogenesis. *Biomolecules*, *7*(2).

Mountcastle. (1957). Modality and topographic properties of single neurons of cat's somatic sensory cortex. *Journal of Neurophysiology*, *20*, 408–434.

Mukamel, R., Gelbard, H., Arieli, A., Hasson, U., Fried, I., & Malach, R. (2005). Coupling between neuronal firing, field potentials, and FMRI in human auditory cortex. *Science (New York, N.Y.)*, *309*(5736), 951–954.

Müller, L., Tokay, T., Porath, K., Köhling, R., & Kirschstein, T. (2013). Enhanced NMDA receptor-dependent LTP in the epileptic CA1 area via upregulation of NR2B. *Neurobiology of Disease*, *54*, 183–193.

Munari, C., Musoiino, A., Daumas-Duport, C., Missir, O., Brunei, P., Giallonardo, A. T., Chodkiewicz, J. P., & Bancaud, J. (1985). Correlation between stereo-EEG, CT-scan and stereotactic biopsy data in epileptic patients with low-grade gliomas. *Applied Neurophysiology*, *48*(1–6), 448–453.

Munkvold, B. K. R., Jakola, A. S., Reinertsen, I., Sagberg, L. M., Unsgård, G., & Solheim, O. (2018). The Diagnostic Properties of Intraoperative Ultrasound in Glioma Surgery and Factors Associated with Gross Total Tumor Resection. *World Neurosurgery*, *115*, e129–e136.

Muñoz, A., Méndez, P., Defelipe, J., & Alvarez-Leefmans, F. J. (2007). Cation-chloride cotransporters and GABA-ergic innervation in the human epileptic hippocampus. *Epilepsia*, *48*(4), 663–673.

Müsch, K., Hamamé, C. M., Perrone-Bertolotti, M., Minotti, L., Kahane, P., Engel, A. K., Lachaux, J. P., & Schneider, T. R. (2014). Selective attention modulates high-frequency activity in the face-processing network. *Cortex; a Journal Devoted to the Study of the Nervous System and Behavior*, *60*, 34–51.

Nagata, K., Gross, C. E., Kindt, G. W., Geier, J. M., & Adey, G. R. (1985). Topographic electroencephalographic study with power ratio index mapping in patients with malignant brain tumors. *Neurosurgery*, *17*(4), 613–619.

Najafi, K., Ji, J., & Wise, K. D. (1990). Scaling limitations of silicon multichannel recording probes. *IEEE Transactions on Bio-Medical Engineering*, *37*(1), 1–11.

Nakada, M., Kita, D., Watanabe, T., Hayashi, Y., Teng, L., Pyko, I. V., & Hamada, J. I. (2011). Aberrant signaling pathways in glioma. *Cancers*, *3*(3), 3242–3278.

Nataf, F., Koziak, M., Ricci, A. C., Varlet, P., Devaux, B., Beuvon, F., Roujeau, T., Page, P., Cioloca, C., Turak, B., Schlienger, M., Touboul, E., Haie-Meder, C., Vannetzel, J. M., Dhermain, F., Honnorat, J., Jouvet, A., De Saint-Pierre, G., Daumas-Duport, C., … Roux, F. X. (2005). [Results of the Sainte-Anne - Lyons series of 318 oligodendroglioma in adults]. *Neuro-Chirurgie*, *51*(3-4 Pt 2), 329–351.

Navarrete, M., Alvarado-Rojas, C., Le Van Quyen, M., & Valderrama, M. (2016). RIPPLELAB: A Comprehensive Application for the Detection, Analysis and Classification of High Frequency Oscillations in Electroencephalographic Signals. *PLOS ONE*, *11*(6), e0158276.

Neal, A., Moffat, B. A., Stein, J. M., Nanga, R. P. R., Desmond, P., Shinohara, R. T., Hariharan, H., Glarin, R., Drummond, K., Morokoff, A., Kwan, P., Reddy, R., O'Brien, T. J., & Davis, K. A. (2019). Glutamate weighted imaging contrast in gliomas with 7 Tesla magnetic resonance imaging. *NeuroImage. Clinical*, *22*.

Newmark, M. E., Theodore, W. H., Sato, S., Paz, R., Patronas, N., Brooks, R., Jabbari, B., & Chiro, G. (1983). EEG, transmission computed tomography, and positron emission tomography with fluorodeoxyglucose 18F. Their use in adults with gliomas. *Archives of Neurology*, *40*(10), 607–610.

Newton, H. B., Goldlust, S. A., & Pearl, D. (2006). Retrospective analysis of the efficacy and tolerability of levetiracetam in brain tumor patients. *Journal of Neuro-Oncology*, *78*(1), 99–102.

Niedermeyer, E., Naidu, S. B., & Plate, C. (1997). Unusual EEG Theta Rhythms over Central Region in Rett

Syndrome: Considerations of the Underlying Dysfunction. *Clinical EEG and Neuroscience*, *28*(1), 36–43.

Niedermeyer, E., Rett, A., Renner, H., Murphy, M., Naidu, S., Opitz, J. M., & Reynolds, J. F. (1986). Rett syndrome and the electroencephalogram. *American Journal of Medical Genetics*, *25*(S1), 195–199.

Nimsky, C., Ganslandt, O., Hastreiter, P., Wang, R., Benner, T., Sorensen, A. G., & Fahlbusch, R. (2005). Intraoperative diffusion-tensor MR imaging: shifting of white matter tracts during neurosurgical procedures--initial experience. *Radiology*, *234*(1), 218–225.

Niyazi, M., Brada, M., Chalmers, A. J., Combs, S. E., Erridge, S. C., Fiorentino, A., Grosu, A. L., Lagerwaard, F. J., Minniti, G., Mirimanoff, R. O., Ricardi, U., Short, S. C., Weber, D. C., & Belka, C. (2016). ESTRO-ACROP guideline "target delineation of glioblastomas." *Radiotherapy and Oncology : Journal of the European Society for Therapeutic Radiology and Oncology*, *118*(1), 35–42.

Noch, E., & Khalili, K. (2009). Molecular mechanisms of necrosis in glioblastoma: The role of glutamate excitotoxicity. In *Cancer Biology and Therapy* (Vol. 8, Issue 19, pp. 1791–1797). Landes Bioscience.

Numan, T., Breedt, L. C., Maciel, B. de A. P. C., Kulik, S. D., Derks, J., Schoonheim, M. M., Klein, M., de Witt Hamer, P. C., Miller, J. J., Gerstner, E. R., Stufflebeam, S. M., Hillebrand, A., Stam, C. J., Geurts, J. J. G., Reijneveld, J. C., & Douw, L. (2022). Regional healthy brain activity, glioma occurrence and symptomatology. *Brain : A Journal of Neurology*, *145*(10), 3654–3665.

Nunez, P. L., Srinivasan, R., Westdorp, A. F., Wijesinghe, R. S., Tucker, D. M., Silberstein, R. B., & Cadusch, P. J. (1997). EEG coherency I: Statistics, reference electrode, volume conduction, Laplacians, cortical imaging, and interpretation at multiple scales. *Electroencephalography and Clinical Neurophysiology*, *103*(5), 499–515.

Okadome, T., Yamaguchi, T., Mukaino, T., Sakata, A., Ogata, K., Shigeto, H., Isobe, N., & Uehara, T. (2022). The effect of interictal epileptic discharges and following spindles on motor sequence learning in epilepsy patients. *Frontiers in Neurology*, *13*.

Olsen, M. L., & Sontheimer, H. (2008). Functional implications for Kir4.1 channels in glial biology: from K+ buffering to cell differentiation. *Journal of Neurochemistry*, *107*(3), 589–601.

Osswald, M., Jung, E., Sahm, F., Solecki, G., Venkataramani, V., Blaes, J., Weil, S., Horstmann, H., Wiestler, B., Syed, M., Huang, L., Ratliff, M., Karimian Jazi, K., Kurz, F. T., Schmenger, T., Lemke, D., Gömmel, M., Pauli, M., Liao, Y., … Winkler, F. (2015). Brain tumour cells interconnect to a functional and resistant network. *Nature*, *528*(7580), 93–98.

Ostrom, Q. T., Price, M., Neff, C., Cioffi, G., Waite, K. A., Kruchko, C., & Barnholtz-Sloan, J. S. (2022). CBTRUS Statistical Report: Primary Brain and Other Central Nervous System Tumors Diagnosed in the United States in 2015-2019. *Neuro-Oncology*, *24*(5), v1–v95.

Ostrom, Q. T., Rubin, J. B., Lathia, J. D., Berens, M. E., & Barnholtz-Sloan, J. S. (2018). Females have the survival advantage in glioblastoma. *Neuro-Oncology*, *20*(4), 576–577.

Otsuki, T. (2004). Neuroimaging and presurgical evaluation of symptomatic epilepsies. *Psychiatry and Clinical Neurosciences*, *58*(3).

Overwater, I. E., Rietman, A. B., van Eeghen, A. M., & de Wit, M. C. Y. (2019). Everolimus for the treatment of refractory seizures associated with tuberous sclerosis complex (TSC): current perspectives. *Therapeutics and Clinical Risk Management*, *15*, 951–955.

Öz, G., Alger, J. R., Barker, P. B., Bartha, R., Bizzi, A., Boesch, C., Bolan, P. J., Brindle, K. M., Cudalbu, C., Dinçer, A., Dydak, U., Emir, U. E., Frahm, J., Gilberto González, R., Gruber, S., Gruetter, R., Gupta, R. K., Heerschap, A., Henning, A., … Kauppinen, R. A. (2014). Clinical proton MR spectroscopy in central nervous system disorders. *Radiology*, *270*(3), 658–679.

Pace, A., Vidiri, A., Galiè, E., Carosi, M., Telera, S., Cianciulli, A. M., Canalini, P., Giannarelli, D., Jandolo, B., & Carapella, C. M. (2003). Temozolomide chemotherapy for progressive low-grade glioma: clinical benefits and radiological response. *Annals of Oncology : Official Journal of the European Society for Medical Oncology*, *14*(12), 1722–1726.

Pallud, Audureau, E., Blonski, M., Sanai, N., Bauchet, L., Fontaine, D., Mandonnet, E., Dezamis, E., Psimaras, D., Guyotat, J., Peruzzi, P., Page, P., Gal, B., Párraga, E., Baron, M. H., Vlaicu, M., Guillevin, R., De'aux, B., Duffau, H., … Huberfeld, G. (2014). Epileptic seizures in diffuse low-grade gliomas in adults. *Brain*, *137*(2), 449–462.

Pallud, Huberfeld, G., Dezamis, E., Peeters, S., Moiraghi, A., Gavaret, M., Guinard, E., Dhermain, F., Varlet, P., Oppenheim, C., Chrétien, F., Roux, A., & Zanello, M. (2022). Effect of Levetiracetam Use Duration on Overall Survival of Isocitrate Dehydrogenase Wild-Type Glioblastoma in Adults: An Observational Study. *Neurology*, *98*(2), E125–E140.

Pallud, J., & Dezamis, E. (2017). Functional and oncological outcomes following awake surgical resection using intraoperative cortico-subcortical functional mapping for supratentorial gliomas located in eloquent areas. *Neurochirurgie*, *63*(3), 208–218.

Pallud, J., Mandonnet, E., Corns, R., Dezamis, E., Parraga, E., Zanello, M., & Spena, G. (2017). Technical

principles of direct bipolar electrostimulation for cortical and subcortical mapping in awake craniotomy. *Neurochirurgie*, *63*(3), 158–163.

Pallud, J., Varlet, P., Devaux, B., Geha, S., Badoual, M., Deroulers, C., Page, P., Dezamis, E., Daumas-Duport, C., & Roux, F. X. (2010). Diffuse low-grade oligodendrogliomas extend beyond MRI-defined abnormalities. *Neurology*, *74*(21), 1724–1731.

Pallud, Johan, Capelle, L., Taillandier, L., Fontaine, D., Mandonnet, E., Guillevin, R., Bauchet, L., Peruzzi, P., Laigle-Donadey, F., Kujas, M., Guyotat, J., Baron, M. H., Mokhtari, K., & Duffau, H. (2009). Prognostic significance of imaging contrast enhancement for WHO grade II gliomas. *Neuro-Oncology*, *11*(2), 176–182.

Pallud, Johan, Huberfeld, G., Dezamis, E., Peeters, S., Moiraghi, A., Gavaret, M., Guinard, E., Dhermain, F., Varlet, P., Oppenheim, C., Chrétien, F., Roux, A., & Zanello, M. (2021). Effect of Levetiracetam use duration on overall survival of isocitrate dehydrogenase wildtype glioblastoma in adults: an observational study. *Neurology*, *98*(2), 10.1212/WNL.0000000000013005.

Pallud, Johan, Le Van Quyen, M., Bielle, F., Pellegrino, C., Varlet, P., Labussiere, M., Cresto, N., Dieme, M. J., Baulac, M., Duyckaerts, C., Kourdougli, N., Chazal, G., Devaux, B., Rivera, C., Miles, R., Capelle, L., & Huberfeld, G. (2014). Cortical GABAergic excitation contributes to epileptic activities around human glioma. *Science Translational Medicine*, *6*(244), 244ra89.

Pallud, Johan, Llitjos, J. F., Dhermain, F., Varlet, P., Dezamis, E., Devaux, B., Souillard-Scémama, R., Sanai, N., Koziak, M., Page, P., Schlienger, M., Daumas-Duport, C., Meder, J. F., Oppenheim, C., & Roux, F. X. (2012). Dynamic imaging response following radiation therapy predicts long-term outcomes for diffuse low-grade gliomas. *Neuro-Oncology*, *14*(4), 496–505.

Pallud, Johan, Mandonnet, E., Duffau, H., Kujas, M., Guillevin, R., Galanaud, D., Taillandier, L., & Capelle, L. (2006). Prognostic value of initial magnetic resonance imaging growth rates for World Health Organization grade II gliomas. *Annals of*

Pallud, Johan, & McKhann, G. M. (2019). Diffuse Low-Grade Glioma-Related Epilepsy. *Neurosurgery Clinics of North America*, *30*(1), 43–54.

Pallud, Johan, Roux, A., & Mellerio, C. (2019). Glioma Resection Unmasks Eloquent Brain Areas. *World Neurosurgery*, *132*, 251–252.

Pallud, Johan, Zanello, M., Kuchcinski, G., Roux, A., Muto, J., Mellerio, C., Dezamis, E., & Oppenheim, C. (2018). Individual Variability of the Human Cerebral Cortex Identified Using Intraoperative Mapping. *World Neurosurgery*, *109*, e313–e317.

Palma, E., Amici, M., Sobrero, F., Spinelli, G., Di Angelantonio, S., Ragozzino, D., Mascia, A., Scoppetta, C., Esposito, V., Miledi, R., & Eusebi, F. (2006). Anomalous levels of Cl- transporters in the hippocampal subiculum from temporal lobe epilepsy patients make GABA excitatory. *Proceedings of the National Academy of Sciences of the United States of America*, *103*(22), 8465–8468.

Palmini, A., Gambardella, A., Andermann, F., Dubeau, F., da Costa, J. C., Olivier, A., Tampieri, D., Gloor, P., Quesney, F., Andermann, E., Paglioli, E., Paglioli-Neto, E., Andermann, L. C., Leblanc, R., & Kim, H. -I. (1995). Intrinsic epileptogenicity of human dysplastic cortex as suggested by corticography and surgical results. *Annals of Neurology*, *37*(4), 476–487.

Pamir, M. N., Özduman, K., Dinçer, A., Yildiz, E., Peker, S., & Özek, M. M. (2010). First intraoperative, shared-resource, ultrahigh-field 3-Tesla magnetic resonance imaging system and its application in low-grade glioma resection. *Journal of Neurosurgery*, *112*(1), 57–69.

Pappa, A. M., Parlak, O., Scheiblin, G., Mailley, P., Salleo, A., & Owens, R. M. (2018). Organic Electronics for Point-of-Care Metabolite Monitoring. *Trends in Biotechnology*, *36*(1), 45–59.

Párraga, E., & Pallud, J. (2012). [Velocity of diametric expansion for high-grade gliomas]. *Radiologia*, *54*(5), 468.

Parrish, R., NK, C., C, M.-G. S., & AJ, T. (2019). Feedforward inhibition ahead of ictal wavefronts is provided by both parvalbumin- and somatostatin-expressing interneurons. *The Journal of Physiology*, *597*(8), 2297–2314.

Pascual, O., Casper, K. B., Kubera, C., Zhang, J., Revilla-Sanchez, R., Sul, J. Y., Takano, H., Moss, S. J., McCarthy, K., & Haydon, P. G. (2005). Astrocytic purinergic signaling coordinates synaptic networks. *Science (New York, N.Y.)*, *310*(5745), 113–116.

Pasternack, M., Bountra, C., Voipio, J., & Kaila, K. (1992). Influence of extracellular and intracellular pH on GABA-gated chloride conductance in crayfish muscle fibres. *Neuroscience*, *47*(4), 921–929.

Patel, K. S., Labar, D. R., Gordon, C. M., Hassnain, K. H., & Schwartz, T. H. (2013). Efficacy of vagus nerve stimulation as a treatment for medically intractable epilepsy in brain tumor patients. A case-controlled study using the VNS therapy Patient Outcome Registry. *Seizure*, *22*(8), 627–633.

Payne, J. A. (1997). Functional characterization of the neuronal-specific K-Cl cotransporter: implications for [K+]o regulation. *The American Journal of Physiology*, *273*(5).

Pearce, A., Wulsin, D., Blanco, J. A., Krieger, A., Litt, B., & Stacey, W. C. (2013). Temporal changes of

neocortical high-frequency oscillations in epilepsy. *Journal of Neurophysiology*, *110*(5), 1167–1179.
Peña-Ceballos, J., Moloney, P. B., Munteanu, T., Doyle, M., Colleran, N., Liggan, B., Breen, A., Murphy, S., El-Naggar, H., Widdess-Walsh, P., & Delanty, N. (2023). Adjunctive cenobamate in highly active and ultra-refractory focal epilepsy: A "real-world" retrospective study. *Epilepsia*, *64*(5).
Pepin, K. M., McGee, K. P., Arani, A., Lake, D. S., Glaser, K. J., Manduca, A., Parney, I. F., Ehman, R. L., & Huston, J. (2018). MR Elastography Analysis of Glioma Stiffness and IDH1-Mutation Status. *AJNR. American Journal of Neuroradiology*, *39*(1), 31–36.
Perry, J. R. (2012). Thromboembolic disease in patients with high-grade glioma. *Neuro-Oncology*, *14 Suppl 4*(Suppl 4).
Piao, Y., Lu, L., & De Groot, J. (2009). AMPA receptors promote perivascular glioma invasion via beta1 integrin-dependent adhesion to the extracellular matrix. *Neuro-Oncology*, *11*(3), 260–273.
Poetsch, L., Bronnimann, C., Loiseau, H., Frénel, J. S., Siegfried, A., Seizeur, R., Gauchotte, G., Cappellen, D., Carpentier, C., Figarella-Branger, D., Eimer, S., Meyronet, D., Ducray, F., Desenclos, C., Sevestre, H., Menei, P., Rousseau, A., Cruel, T., Lopez, S., … Dhermain, F. (2021). Characteristics of IDH-mutant gliomas with non-canonical IDH mutation. *Journal of Neuro-Oncology*, *151*(2), 279–286.
Pope, W. B., Prins, R. M., Thomas, M. A., Nagarajan, R., Yen, K. E., Bittinger, M. A., Salamon, N., Chou, A. P., Yong, W. H., Soto, H., Wilson, N., Driggers, E., Jang, H. G., Su, S. M., Schenkein, D. P., Lai, A., Cloughesy, T. F., Kornblum, H. I., Wu, H., … Liau, L. M. (2012). Non-invasive detection of 2-hydroxyglutarate and other metabolites in IDH1 mutant glioma patients using magnetic resonance spectroscopy. *Journal of Neuro-Oncology*, *107*(1), 197–205.
Povlich, L. K., Cho, J. C., Leach, M. K., Corey, J. M., Kim, J., & Martin, D. C. (2013). Synthesis, copolymerization and peptide-modification of carboxylic acid-functionalized 3,4-ethylenedioxythiophene (EDOTacid) for neural electrode interfaces. *Biochimica et Biophysica Acta*, *1830*(9), 4288–4293.
Press, R. H., Shafer, S. L., Jiang, R., Buchwald, Z. S., Abugideiri, M., Tian, S., Morgan, T. M., Behera, M., Sengupta, S., Voloschin, A. D., Olson, J. J., Hasan, S., Blumenthal, D. T., Curran, W. J., Eaton, B. R., Shu, H. K. G., & Zhong, J. (2020). Optimal timing of chemoradiotherapy after surgical resection of glioblastoma: Stratification by validated prognostic classification. *Cancer*, *126*(14), 3255–3264.
Pressler, R. M., Boylan, G. B., Marlow, N., Blennow, M., Chiron, C., Cross, J. H., de Vries, L. S., Hallberg, B., Hellström-Westas, L., Jullien, V., Livingstone, V., Mangum, B., Murphy, B., Murray, D., Pons, G., Rennie, J., Swarte, R., Toet, M. C., Vanhatalo, S., & Zohar, S. (2015). Bumetanide for the treatment of seizures in newborn babies with hypoxic ischaemic encephalopathy (NEMO): an open-label, dose finding, and feasibility phase 1/2 trial. *The Lancet. Neurology*, *14*(5), 469–477.
Price, S. J., Fryer, T. D., Cleij, M. C., Dean, A. F., Joseph, J., Salvador, R., Wang, D. D., Hutchinson, P. J., Clark, J. C., Burnet, N. G., Pickard, J. D., Aigbirhio, F. I., & Gillard, J. H. (2009). Imaging regional variation of cellular proliferation in gliomas using 3'-deoxy-3'-[18F]fluorothymidine positron-emission tomography: an image-guided biopsy study. *Clinical Radiology*, *64*(1), 52–63.
Price, S. J., Green, H. A. L., Dean, A. F., Joseph, J., Hutchinson, P. J., & Gillard, J. H. (2011). Correlation of MR relative cerebral blood volume measurements with cellular density and proliferation in high-grade gliomas: an image-guided biopsy study. *AJNR. American Journal of Neuroradiology*, *32*(3), 501–506.
Price, Stephen J. (2010). Advances in imaging low-grade gliomas. *Advances and Technical Standards in Neurosurgery*, *35*, 1–34.
Price, Stephen J., Jena, R., Burnet, N. G., Hutchinson, P. J., Dean, A. F., Peña, A., Pickard, J. D., Carpenter, T. A., & Gillard, J. H. (2006). Improved delineation of glioma margins and regions of infiltration with the use of diffusion tensor imaging: An image-guided biopsy study. *American Journal of Neuroradiology*, *27*(9), 1969–1974.
Quick, J., Gessler, F., Dützmann, S., Hattingen, E., Harter, P. N., Weise, L. M., Franz, K., Seifert, V., & Senft, C. (2014). Benefit of tumor resection for recurrent glioblastoma. *Journal of Neuro-Oncology*, *117*(2), 365–372.
Quiroga, R. Q., Reddy, L., Kreiman, G., Koch, C., & Fried, I. (2005). Invariant visual representation by single neurons in the human brain. *Nature*, *435*(7045), 1102–1107.
Rades, D., Witteler, J., Trillenberg, P., Olbrich, D., Schild, S. E., Tvilsted, S., & Kjaer, T. W. (2022). Increasing Seizure Activity During Radiation Treatment for High-grade Gliomas - Final Results of a Prospective Interventional Study. *In Vivo (Athens, Greece)*, *36*(5), 2308–2313.
Ramuz, M., Hama, A., Huerta, M., Rivnay, J., Leleux, P., & Owens, R. M. (2014). Combined optical and electronic sensing of epithelial cells using planar organic transistors. *Advanced Materials (Deerfield Beach, Fla.)*, *26*(41), 7083–7090.
Rasmussen, T. (1983). Characteristics of a pure culture of frontal lobe epilepsy. *Epilepsia*, *24*(4), 482–493.
Ray, S., Crone, N. E., Niebur, E., Franaszczuk, P. J., & Hsiao, S. S. (2008). Neural correlates of high-gamma oscillations (60-200 Hz) in macaque local field potentials and their potential implications in

electrocorticography. *The Journal of Neuroscience : The Official Journal of the Society for Neuroscience*, *28*(45), 11526–11536.

Reddy, K. B., Nabha, S. M., & Atanaskova, N. (2003). Role of MAP kinase in tumor progression and invasion. *Cancer Metastasis Reviews*, *22*(4), 395–403.

Remakanthakurup Sindhu, K., Staba, R., & Lopour, B. A. (2020). Trends in the use of automated algorithms for the detection of high-frequency oscillations associated with human epilepsy. *Epilepsia*.

Rheims, S., Represa, A., Ben-Ari, Y., & Zilberter, Y. (2008). Layer-specific generation and propagation of seizures in slices of developing neocortex: Role of excitatory GABAergic synapses. *Journal of Neurophysiology*, *100*(2), 620–628.

Ricard, D., Idbaih, A., Ducray, F., Lahutte, M., Hoang-Xuan, K., & Delattre, J. Y. (2012). Primary brain tumours in adults. *Lancet (London, England)*, *379*(9830), 1984–1996.

Richardson, M. P., & Jefferys, J. G. R. (2011). Introduction —– Epilepsy Research UK Workshop 2010 on ‘“ Preictal Phenomena .”’ *Epilepsy Research*, *97*(3), 229–230.

Riedl, J., Preusser, M., Nazari, P. M. S., Posch, F., Panzer, S., Marosi, C., Birner, P., Thaler, J., Brostjan, C., Lötsch, D., Berger, W., Hainfellner, J. A., Pabinger, I., & Ay, C. (2017). Podoplanin expression in primary brain tumors induces platelet aggregation and increases risk of venous thromboembolism. *Blood*, *129*(13), 1831–1839.

Riviere-Cazaux, C., Lacey, J. M., Carlstrom, L. P., Laxen, W. J., Munoz-Casabella, A., Hoplin, M. D., Ikram, S., Zubair, A. Bin, Andersen, K. M., Warrington, A. E., Decker, P. A., Kaufmann, T. J., Campian, J. L., Eckel-Passow, J. E., Kizilbash, S. H., Tortorelli, S., & Burns, T. C. (2023). Cerebrospinal fluid 2-hydroxyglutarate as a monitoring biomarker for IDH-mutant gliomas. *Neuro-Oncology Advances*, *5*(1).

Rivnay, J., Ramuz, M., Leleux, P., Hama, A., Huerta, M., & Owens, R. M. (2015). Organic electrochemical transistors for cell-based impedance sensing. *Applied Physics Letters*, *106*(4).

Rizzo, A., Donzelli, S., Girgenti, V., Sacconi, A., Vasco, C., Salmaggi, A., Blandino, G., Maschio, M., & Ciusani, E. (2017). In vitro antineoplastic effects of brivaracetam and lacosamide on human glioma cells. *Journal of Experimental & Clinical Cancer Research : CR*, *36*(1).

Roa, W., Brasher, P. M. A., Bauman, G., Anthes, M., Bruera, E., Chan, A., Fisher, B., Fulton, D., Gulavita, S., Hao, C., Husain, S., Murtha, A., Petruk, K., Stewart, D., Tai, P., Urtasun, R., Cairncross, J. G., & Forsyth, P. (2004). Abbreviated course of radiation therapy in older patients with glioblastoma multiforme: a prospective randomized clinical trial. *Journal of Clinical Oncology : Official Journal of the American Society of Clinical Oncology*, *22*(9), 1583–1588.

Roehri, N., Lina, J. M., Mosher, J. C., Bartolomei, F., & Benar, C. G. (2016). Time-Frequency Strategies for Increasing High-Frequency Oscillation Detectability in Intracerebral EEG. *IEEE Transactions on Bio-Medical Engineering*, *63*(12), 2595–2606.

Roehri, N., Pizzo, F., Lagarde, S., Lambert, I., Nica, A., McGonigal, A., Giusiano, B., Bartolomei, F., & Bénar, C. G. (2018). High-frequency oscillations are not better biomarkers of epileptogenic tissues than spikes. *Annals of Neurology*, *83*(1), 84–97.

Roelz, R., Strohmaier, D., Jabbarli, R., Kraeutle, R., Egger, K., Coenen, V. A., Weyerbrock, A., & Reinacher, P. C. (2016). Residual Tumor Volume as Best Outcome Predictor in Low Grade Glioma - A Nine-Years Near-Randomized Survey of Surgery vs. Biopsy. *Scientific Reports*, *6*.

Romstöck, J., Fahlbusch, R., Ganslandt, O., Nimsky, C., & Strauss, C. (2002). Localisation of the sensorimotor cortex during surgery for brain tumours: feasibility and waveform patterns of somatosensory evoked potentials. *Journal of Neurology, Neurosurgery, and Psychiatry*, *72*(2), 221–229.

Roodakker, K. R., Alhuseinalkhudhur, A., Al-Jaff, M., Georganaki, M., Zetterling, M., Berntsson, S. G., Danfors, T., Strand, R., Edqvist, P. H., Dimberg, A., Larsson, E. M., & Smits, A. (2019). Region-by-region analysis of PET, MRI, and histology in en bloc-resected oligodendrogliomas reveals intra-tumoral heterogeneity. *European Journal of Nuclear Medicine and Molecular Imaging*, *46*(3), 569–579.

Rosati, A., Marconi, S., Pollo, B., Tomassini, A., Lovato, L., Maderna, E., Maier, K., Schwartz, A., Rizzuto, N., Padovani, A., & Bonetti, B. (2009). Epilepsy in glioblastoma multiforme: Correlation with glutamine synthetase levels. *Journal of Neuro-Oncology*, *93*(3), 319–324.

Rosenow, F., & Lüders, H. (2001). Presurgical evaluation of epilepsy. *Brain : A Journal of Neurology*, *124*(Pt 9), 1683–1700.

Rosenow, F., Schade-Brittinger, C., Burchardi, N., Bauer, S., Klein, K. M., Weber, Y., Lerche, H., Evers, S., Kovac, S., Hallmeyer-Elgner, S., Winkler, G., Springub, J., Niedhammer, M., Roth, E., Eisensehr, I., Berrouschot, J., Arnold, S., Schröder, M., Beige, A., … Hamer, H. M. (2012). The LaLiMo Trial: lamotrigine compared with levetiracetam in the initial 26 weeks of monotherapy for focal and generalised epilepsy--an open-label, prospective, randomised controlled multicenter study. *Journal of Neurology, Neurosurgery, and Psychiatry*, *83*(11), 1093–1098.

Rossi, J., Cavallieri, F., Bassi, M. C., Biagini, G., Rizzi, R., Russo, M., Bondavalli, M., Iaccarino, C., Pavesi, G., Cozzi, S., Giaccherini, L., Najafi, M., Pisanello, A., & Valzania, F. (2023). Efficacy and Tolerability of Perampanel in Brain Tumor-Related Epilepsy: A Systematic Review. *Biomedicines*, *11*(3), 651.

Rossi, M., Ambrogi, F., Gay, L., Gallucci, M., Nibali, M. C., Leonetti, A., Puglisi, G., Sciortino, T., Howells, H., Riva, M., Pessina, F., Navarria, P., Franzese, C., Simonelli, M., Rudà, R., & Bello, L. (2019). Is supratotal resection achievable in low-grade gliomas? Feasibility, putative factors, safety, and functional outcome. *Journal of Neurosurgery*, *132*(6), 1692–1705.

Rossi, M., Gay, L., Ambrogi, F., Conti Nibali, M., Sciortino, T., Puglisi, G., Leonetti, A., Mocellini, C., Caroli, M., Cordera, S., Simonelli, M., Pessina, F., Navarria, P., Pace, A., Soffietti, R., Rudà, R., Riva, M., & Bello, L. (2021). Association of supratotal resection with progression-free survival, malignant transformation, and overall survival in lower-grade gliomas. *Neuro-Oncology*, *23*(5), 812–826.

Rouach, N., Koulakoff, A., Abudara, V., Willecke, K., & Giaume, C. (2008). Astroglial metabolic networks sustain hippocampal synaptic transmission. *Science (New York, N.Y.)*, *322*(5907), 1551–1555.

Roux, A., Aboubakr, O., Elia, A., Moiraghi, A., Benevello, C., Fathallah, H., Parraga, E., Oppenheim, C., Chretien, F., Dezamis, E., Zanello, M., & Pallud, J. (2023). Carmustine wafer implantation for supratentorial glioblastomas, IDH-wildtype in "extreme" neurosurgical conditions. *Neurosurgical Review*, *46*(1), 140.

Rudà, R., Bello, L., Duffau, H., & Soffietti, R. (2012). Seizures in low-grade gliomas: natural history, pathogenesis, and outcome after treatments. *Neuro-Oncology*, *14 Suppl 4*, iv55-64.

Rudà, R., Houillier, C., Maschio, M., Reijneveld, J. C., Hellot, S., De Backer, M., Chan, J., Joeres, L., Leunikava, I., Glas, M., & Grant, R. (2020). Effectiveness and tolerability of lacosamide as add-on therapy in patients with brain tumor-related epilepsy: Results from a prospective, noninterventional study in European clinical practice (VIBES). *Epilepsia*, *61*(4), 647–656.

Rudà, R., Magliola, U., Bertero, L., Trevisan, E., Bosa, C., Mantovani, C., Ricardi, U., Castiglione, A., Monagheddu, C., & Soffietti, R. (2013). Seizure control following radiotherapy in patients with diffuse gliomas: a retrospective study. *Neuro-Oncology*, *15*(12), 1739–1749.

Ruff, R. L., & Posner, J. B. (1983). Incidence and treatment of peripheral venous thrombosis in patients with glioma. *Annals of Neurology*, *13*(3), 334–336.

Ryu, J. Y., Min, K. L., & Chang, M. J. (2019). Effect of anti-epileptic drugs on the survival of patients with glioblastoma multiforme: A retrospective, single-center study. *PLoS ONE*, *14*(12).

Rzeski, W., Turski, L., & Ikonomidou, C. (2001). Glutamate antagonists limit tumor growth. *Proceedings of the National Academy of Sciences of the United States of America*, *98*(11), 6372–6377.

Saha, L., Bhandari, S., Bhatia, A., Banerjee, D., & Chakrabarti, A. (2014). Anti-kindling Effect of Bezafibrate, a Peroxisome Proliferator-activated Receptors Alpha Agonist, in Pentylenetetrazole Induced Kindling Seizure Model. *Journal of Epilepsy Research*, *4*(2), 45–54.

Salari, N., Ghasemi, H., Fatahian, R., Mansouri, K., Dokaneheifard, S., Shiri, M. hossain, Hemmati, M., & Mohammadi, M. (2023). The global prevalence of primary central nervous system tumors: a systematic review and meta-analysis. *European Journal of Medical Research*, *28*(1).

Salmaggi, A., Corno, C., Maschio, M., Donzelli, S., D'urso, A., Perego, P., & Ciusani, E. (2021). Synergistic Effect of Perampanel and Temozolomide in Human Glioma Cell Lines. *Journal of Personalized Medicine*, *11*(5).

Sami, A., & Karsy, M. (2013). Targeting the PI3K/AKT/mTOR signaling pathway in glioblastoma: novel therapeutic agents and advances in understanding. *Tumour Biology : The Journal of the International Society for Oncodevelopmental Biology and Medicine*, *34*(4), 1991–2002.

Sanai, N., Polley, M. Y., McDermott, M. W., Parsa, A. T., & Berger, M. S. (2011). An extent of resection threshold for newly diagnosed glioblastomas. *Journal of Neurosurgery*, *115*(1), 3–8.

Sanai, N., Snyder, L. A., Honea, N. J., Coons, S. W., Eschbacher, J. M., Smith, K. A., & Spetzler, R. F. (2011). Intraoperative confocal microscopy in the visualization of 5-aminolevulinic acid fluorescence in low-grade gliomas: Clinical article. *Journal of Neurosurgery*, *115*(4), 740–748.

Sang, H., Cho, Y. K., Han, K., & Koh, E. H. (2023). Impact of abdominal obesity on the risk of glioma development in patients with diabetes: A nationwide population-based cohort study in Korea. *PloS One*, *18*(3), e0283023.

Sanson, M., Marie, Y., Paris, S., Idbaih, A., Laffaire, J., Ducray, F., Hallani, S. El, Boisselier, B., Mokhtari, K., Hoang-Xuan, K., & Delattre, J. Y. (2009). Isocitrate dehydrogenase 1 codon 132 mutation is an important prognostic biomarker in gliomas. *Journal of Clinical Oncology*, *27*(25), 4150–4154.

Saria, M. G., Corle, C., Hu, J., Rudnick, J. D., Phuphanich, S., Mrugala, M. M., Crew, L. K., Bota, D. A., Fu, B. D., Kim, R. Y., Brown, T., Feely, H., Brechlin, J., Brown, B. D., Drappatz, J., Wen, P. Y., Chen, C. C., Carter, B., Lee, J. W., & Kesari, S. (2013). Retrospective analysis of the tolerability and activity of lacosamide in patients with brain tumors: clinical article. *Journal of Neurosurgery*, *118*(6), 1183–1187.

Sauvageot, S., Boetto, J., & Duffau, H. (2023). Surgical, functional, and oncological considerations regarding

awake resection for giant diffuse lower-grade glioma of more than 100 cm3. *Journal of Neurosurgery*, 1–10.

Savaskan, N. E., Heckel, A., Hahnen, E., Engelhorn, T., Doerfler, A., Ganslandt, O., Nimsky, C., Buchfelder, M., & Eyüpoglu, I. Y. (2008). Small interfering RNA-mediated xCT silencing in gliomas inhibits neurodegeneration and alleviates brain edema. *Nature Medicine*, *14*(6), 629–632.

Schevon, C. A., Weiss, S. A., McKhann, G., Goodman, R. R., Yuste, R., Emerson, R. G., & Trevelyan, A. J. (2012). Evidence of an inhibitory restraint of seizure activity in humans. *Nature Communications*, *3*.

Schubert-Bast, S., Rosenow, F., Klein, K. M., Reif, P. S., Kieslich, M., & Strzelczyk, A. (2019). The role of mTOR inhibitors in preventing epileptogenesis in patients with TSC: Current evidence and future perspectives. *Epilepsy & Behavior : E&B*, *91*, 94–98.

Schunemann, D. P., Grivicich, I., Regner, A., Leal, L. F., De Araújo, D. R., Jotz, G. P., Fedrigo, C. A., Simon, D., & Da Rocha, A. B. (2010). Glutamate promotes cell growth by EGFR signaling on U-87MG human glioblastoma cell line. *Pathology Oncology Research : POR*, *16*(2), 285–293.

Schüz, J., Pirie, K., Reeves, G. K., Floud, S., & Beral, V. (2022). Cellular Telephone Use and the Risk of Brain Tumors: Update of the UK Million Women Study. *JNCI: Journal of the National Cancer Institute*, *114*(5), 704–711.

Schwartz, T. H., Bazil, C. W., Walczak, T. S., Chan, S., Pedley, T. A., & Goodman, R. R. (1997). The predictive value of intraoperative electrocorticography in resections for limbic epilepsy associated with mesial temporal sclerosis. *Neurosurgery*, *40*(2), 302–311.

Senner, V., Köhling, R., Püttmann-Cyrus, S., Straub, H., Paulus, W., & Speckmann, E. J. (2004). A new neurophysiological/neuropathological ex vivo model localizes the origin of glioma-associated epileptogenesis in the invasion area. *Acta Neuropathologica*, *107*(1), 1–7.

Sessolo, M., Marcon, I., Bovetti, S., Losi, G., Cammarota, M., Ratto, G. M., Fellin, T., & Carmignoto, G. (2015). Parvalbumin-Positive Inhibitory Interneurons Oppose Propagation But Favor Generation of Focal Epileptiform Activity. *The Journal of Neuroscience : The Official Journal of the Society for Neuroscience*, *35*(26), 9544–9557.

Shamji, M. F., Fric-Shamji, E. C., & Benoit, B. G. (2009). Brain tumors and epilepsy: pathophysiology of peritumoral changes. *Neurosurgical Review*, *32*(3), 274–284.

Shen, X., Chen, L., Pan, J., Hu, Y., Li, S., & Zhao, J. (2016). Improved Work Function of Poly(3,4-ethylenedioxythiophene): Poly(styrenesulfonic acid) and its Effect on Hybrid Silicon/Organic Heterojunction Solar Cells. *Nanoscale Research Letters*, *11*(1).

Sherman, J. H., Moldovan, K., Yeoh, H. K., Starke, R. M., Pouratian, N., Shaffrey, M. E., & Schiff, D. (2011). Impact of temozolomide chemotherapy on seizure frequency in patients with low-grade gliomas. *Journal of Neurosurgery*, *114*(6), 1617–1621.

Shete, S., Hosking, F. J., Robertson, L. B., Dobbins, S. E., Sanson, M., Malmer, B., Simon, M., Marie, Y., Boisselier, B., Delattre, J. Y., Hoang-Xuan, K., Hallani, S. El, Idbaih, A., Zelenika, D., Andersson, U., Henriksson, R., Bergenheim, A. T., Feychting, M., Lönn, S., … Houlston, R. S. (2009). Genome-wide association study identifies five susceptibility loci for glioma. *Nature Genetics*, *41*(8), 899–904.

Shi, L., Gao, L. li, Cai, S. zhong, Xiong, Q. wei, & Ma, Z. rui. (2021). A novel selective mitochondrial-targeted curcumin analog with remarkable cytotoxicity in glioma cells. *European Journal of Medicinal Chemistry*, *221*.

Shibasaki, H., Ikeda, A., & Nagamine, T. (2007). Use of magnetoencephalography in the presurgical evaluation of epilepsy patients. *Clinical Neurophysiology : Official Journal of the International Federation of Clinical Neurophysiology*, *118*(7), 1438–1448.

Shofty, B., Haim, O., Costa, M., Kashanian, A., Shtrozberg, S., Ram, Z., & Grossman, R. (2020). Impact of repeated operations for progressive low-grade gliomas. *European Journal of Surgical Oncology : The Journal of the European Society of Surgical Oncology and the British Association of Surgical Oncology*, *46*(12), 2331–2337.

Sibille, J., Pannasch, U., & Rouach, N. (2014). Astroglial potassium clearance contributes to short-term plasticity of synaptically evoked currents at the tripartite synapse. *The Journal of Physiology*, *592*(1), 87–102.

Silva, M., Vivancos, C., & Duffau, H. (2022). The Concept of «Peritumoral Zone» in Diffuse Low-Grade Gliomas: Oncological and Functional Implications for a Connectome-Guided Therapeutic Attitude. *Brain Sciences*, *12*(4).

Simon, D. T., Kurup, S., Larsson, K. C., Hori, R., Tybrandt, K., Goiny, M., Jager, E. W. H., Berggren, M., Canlon, B., & Richter-Dahlfors, A. (2009). Organic electronics for precise delivery of neurotransmitters to modulate mammalian sensory function. *Nature Materials*, *8*(9), 742–746.

Sizoo, E. M., Braam, L., Postma, T. J., Pasman, H. R. W., Heimans, J. J., Klein, M., Reijneveld, J. C., & Taphoorn, M. J. B. (2010). Symptoms and problems in the end-of-life phase of high-grade glioma patients. *Neuro-Oncology*, *12*(11), 1162–1166.

Skinner, F. K., Zhang, L., Perez Velazquez, J. L., & Carlen, P. L. (1999). Bursting in inhibitory interneuronal networks: A role for gap-junctional coupling. *Journal of Neurophysiology*, *81*(3), 1274–1283.

Solomons, M. R., Jaunmuktane, Z., Weil, R. S., El-Hassan, T., Brandner, S., & Rees, J. H. (2020). Seizure outcomes and survival in adult low-grade glioma over 11 years: living longer and better. *Neuro-Oncology Practice*, *7*(2), 196–201.

Solomou, G., Finch, A., Asghar, A., & Bardella, C. (2023). Mutant IDH in Gliomas: Role in Cancer and Treatment Options. *Cancers*, *15*(11), 2883.

Song, I., & Huganir, R. L. (2002). Regulation of AMPA receptors during synaptic plasticity. *Trends in Neurosciences*, *25*(11), 578–588.

Song, S., Wang, L., Yang, H., Shan, Y., Cheng, Y., Xu, L., Dong, C., Zhao, G., & Lu, J. (2021). Static 18F-FET PET and DSC-PWI based on hybrid PET/MR for the prediction of gliomas defined by IDH and 1p/19q status. *European Radiology*, *31*(6), 4087–4096.

Sontheimer, H. (2003). Malignant gliomas: perverting glutamate and ion homeostasis for selective advantage. *Trends in Neurosciences*, *26*(10), 543–549.

Spencer, S. S. (2002). Neural networks in human epilepsy: evidence of and implications for treatment. *Epilepsia*, *43*(3), 219–227.

Spitzer, N. C. (2010). How GABA generates depolarization. In *Journal of Physiology* (Vol. 588, Issue 5, pp. 757–758). Wiley-Blackwell.

Staba, R. J., Wilson, C. L., Bragin, A., & Fried, I. (2002). Quantitative analysis of high-frequency oscillations (80-500 Hz) recorded in human epileptic hippocampus and entorhinal cortex. *Journal of Neurophysiology*, *88*(4), 1743–1752.

Staba, Richard J., Frighetto, L., Behnke, E. J., Mathern, G. W., Fields, T., Bragin, A., Ogren, J., Fried, I., Wilson, C. L., & Engel, J. (2007). Increased fast ripple to ripple ratios correlate with reduced hippocampal volumes and neuron loss in temporal lobe epilepsy patients. *Epilepsia*, *48*(11), 2130–2138.

Staba, Richard J., Wilson, C. L., Bragin, A., Jhung, D., Fried, I., & Engel, J. (2004). High-frequency oscillations recorded in human medial temporal lobe during sleep. *Annals of Neurology*, *56*(1), 108–115.

Stam, C. J., van Straaten, E. C. W., Van Dellen, E., Tewarie, P., Gong, G., Hillebrand, A., Meier, J., & Van Mieghem, P. (2016). The relation between structural and functional connectivity patterns in complex brain networks. *International Journal of Psychophysiology : Official Journal of the International Organization of Psychophysiology*, *103*, 149–160.

Stavrinidou, E., Gabrielsson, R., Gomez, E., Crispin, X., Nilsson, O., Simon, D. T., & Berggren, M. (2015). Electronic plants. *Science Advances*, *1*(10).

Stead, M., Bower, M., Brinkmann, B. H., Lee, K., Marsh, W. R., Meyer, F. B., Litt, B., Van Gompel, J., & Worrell, G. A. (2010). Microseizures and the spatiotemporal scales of human partial epilepsy. *Brain : A Journal of Neurology*, *133*(9), 2789–2797.

Stepulak, A., Luksch, H., Gebhardt, C., Uckermann, O., Marzahn, J., Sifringer, M., Rzeski, W., Staufner, C., Brocke, K. S., Turski, L., & Ikonomidou, C. (2009). Expression of glutamate receptor subunits in human cancers. *Histochemistry and Cell Biology*, *132*(4), 435–445.

Still, M. E. H., Roux, A., Huberfeld, G., Bauchet, L., Baron, M. H., Fontaine, D., Blonski, M., Mandonnet, E., Guillevin, R., Guyotat, J., Taillandier, L., Capelle, L., Duffau, H., & Pallud, J. (2019a). Extent of Resection and Residual Tumor Thresholds for Postoperative Total Seizure Freedom in Epileptic Adult Patients Harboring a Supratentorial Diffuse Low-Grade Glioma. *Neurosurgery*, *85*(2), E332–E339.

Stirling, R. E., Cook, M. J., Grayden, D. B., & Karoly, P. J. (2021). Seizure forecasting and cyclic control of seizures. *Epilepsia*, *62 Suppl 1*(S1), S2–S14.

Stummer, W., Pichlmeier, U., Meinel, T., Wiestler, O. D., Zanella, F., & Reulen, H. J. (2006). Fluorescence-guided surgery with 5-aminolevulinic acid for resection of malignant glioma: a randomised controlled multicentre phase III trial. *The Lancet. Oncology*, *7*(5), 392–401.

Stupp, R., & Roila, F. (2009). Malignant glioma: ESMO clinical recommendations for diagnosis, treatment and follow-up. *Annals of Oncology : Official Journal of the European Society for Medical Oncology*, *20 Suppl 4*(SUPPL. 4).

Stupp, Roger, Mason, W. P., van den Bent, M. J., Weller, M., Fisher, B., Taphoorn, M. J. B., Belanger, K., Brandes, A. A., Marosi, C., Bogdahn, U., Curschmann, J., Janzer, R. C., Ludwin, S. K., Gorlia, T., Allgeier, A., Lacombe, D., Cairncross, J. G., Eisenhauer, E., & Mirimanoff, R. O. (2005). Radiotherapy plus concomitant and adjuvant temozolomide for glioblastoma. *The New England Journal of Medicine*, *352*(10), 987–996.

Su, C., Xu, S., Lin, D., He, H., Chen, Z., Damen, F. C., Ke, C., Lv, X., & Cai, K. (2022). Multi-parametric Z-spectral MRI may have a good performance for glioma stratification in clinical patients. *European Radiology*, *32*(1), 101–111.

Sulkowski, P. L., Corso, C. D., Robinson, N. D., Scanlon, S. E., Purshouse, K. R., Bai, H., Liu, Y., Sundaram, R. K., Hegan, D. C., Fons, N. R., Breuer, G. A., Song, Y., Mishra-Gorur, K., De Feyter, H. M., De Graaf, R. A., Surovtseva, Y. V., Kachman, M., Halene, S., Günel, M., … Bindra, R. S. (2017). 2-Hydroxyglutarate produced by neomorphic IDH mutations suppresses homologous recombination and induces PARP inhibitor sensitivity. *Science Translational Medicine*, *9*(375).

Sun, J., Barth, K., Qiao, S., Chiang, C. H., Wang, C., Rahimpour, S., Trumpis, M., Duraivel, S., Dubey, A., Wingel, K. E., Rachinskiy, I., Voinas, A. E., Ferrentino, B., Southwell, D. G., Haglund, M. M., Friedman, A. H., Lad, S. P., Doyle, W. K., Solzbacher, F., … Viventi, J. (2022). Intraoperative microseizure detection using a high-density micro-electrocorticography electrode array. *Brain Communications*, *4*(3).

Sun, T., Warrington, N. M., Luo, J., Brooks, M. D., Dahiya, S., Snyder, S. C., Sengupta, R., & Rubin, J. B. (2014). Sexually dimorphic RB inactivation underlies mesenchymal glioblastoma prevalence in males. *The Journal of Clinical Investigation*, *124*(9), 4123–4133.

Tabaee Damavandi, P., Pasini, F., Fanella, G., Cereda, G. S., Mainini, G., DiFrancesco, J. C., Trinka, E., & Lattanzi, S. (2023). Perampanel in Brain Tumor-Related Epilepsy: A Systematic Review. *Brain Sciences*, *13*(2).

Takano, T., Lin, J. H. C., Arcuino, G., Gao, Q., Yang, J., & Nedergaard, M. (2001). Glutamate release promotes growth of malignant gliomas. *Nature Medicine*, *7*(9), 1010–1015.

Talairach, J., & Bancaud, J. (1966). Lesion, "irritative" zone and epileptogenic focus. *Confinia Neurologica*, *27*(1), 91–94. https://doi.org/10.1159/000103937

Talos, D. M., Sun, H., Kosaras, B., Joseph, A., Folkerth, R. D., Poduri, A., Madsen, J. R., Black, P. M., & Jensen, F. E. (2012). Altered inhibition in tuberous sclerosis and type IIb cortical dysplasia. *Annals of Neurology*, *71*(4), 539–551.

Tamimi, A. F., & Juweid, M. (2017). Epidemiology and Outcome of Glioblastoma. *Glioblastoma*, 143–153.

Tang, C. M., Dichter, M., & Morad, M. (1990). Modulation of the N-methyl-D-aspartate channel by extracellular H+. *Proceedings of the National Academy of Sciences of the United States of America*, *87*(16), 6445–6449.

Tantillo, E., Vannini, E., Cerri, C., Spalletti, C., Colistra, A., Mazzanti, C. M., Costa, M., & Caleo, M. (2020). Differential roles of pyramidal and fast-spiking, GABAergic neurons in the control of glioma cell proliferation. *Neurobiology of Disease*, *141*, 104942.

Taphoorn, M. J. B., Sizoo, E. M., & Bottomley, A. (2010). Review on Quality of Life Issues in Patients with Primary Brain Tumors. *The Oncologist*, *15*(6), 618–626.

Taplin, A. L. M., de Pesters, A., Brunner, P., Hermes, D., Dalfino, J. C., Adamo, M. A., Ritaccio, A. L., & Schalk, G. (2016). Intraoperative mapping of expressive language cortex using passive real-time electrocorticography. *Epilepsy & Behavior Case Reports*, *5*, 46–51.

Tatekawa, H., Yao, J., Oughourlian, T. C., Hagiwara, A., Wang, C., Raymond, C., Lai, A., Cloughesy, T. F., Nghiemphu, P. L., Liau, L. M., Salamon, N., & Ellingson, B. M. (2020). Maximum Uptake and Hypermetabolic Volume of 18F-FDOPA PET Estimate Molecular Status and Overall Survival in Low-Grade Gliomas: A PET and MRI Study. *Clinical Nuclear Medicine*, *45*(12), E505–E511.

Tatsuoka, J., Sano, E., Hanashima, Y., Yagi, C., Yamamuro, S., Sumi, K., Hara, H., Takada, K., Kanemaru, K., Komine-Aizawa, S., Katayama, Y., & Yoshino, A. (2022). Anti-tumor effects of perampanel in malignant glioma cells. *Oncology Letters*, *24*(6).

Timp, J. F., Braekkan, S. K., Versteeg, H. H., & Cannegieter, S. C. (2013). Epidemiology of cancer-associated venous thrombosis. *Blood*, *122*(10), 1712–1723.

Tinchon, A., Oberndorfer, S., Marosi, C., Gleiss, A., Geroldinger, A., Sax, C., Sherif, C., Moser, W., & Grisold, W. (2015). Haematological toxicity of Valproic acid compared to Levetiracetam in patients with glioblastoma multiforme undergoing concomitant radio-chemotherapy: a retrospective cohort study. *Journal of Neurology*, *262*(1), 179–186.

Tobochnik, S., Lapinskas, E., Vogelzang, J., Ligon, K. L., & Lee, J. W. (2022). Early EEG hyperexcitability is associated with decreased survival in newly diagnosed IDH-wildtype glioma. *Journal of Neuro-Oncology*, *159*(1), 211–218.

Tofts, P. S., Benton, C. E., Weil, R. S., Tozer, D. J., Altmann, D. R., Jäger, H. R., Waldman, A. D., & Rees, J. H. (2007). Quantitative analysis of whole-tumor Gd enhancement histograms predicts malignant transformation in low-grade gliomas. *Journal of Magnetic Resonance Imaging : JMRI*, *25*(1), 208–214.

Tran, T. A., Spencer, S. S., Javidan, M., Pacia, S., Marks, D., & Spencer, D. D. (1997). Significance of spikes recorded on intraoperative electrocorticography in patients with brain tumor and epilepsy. *Epilepsia*, *38*(10), 1132–1139.

Traub, R. D., Cunningham, M. O., & Whittington, M. A. (2011). Chemical synaptic and gap junctional interactions between principal neurons: partners in epileptogenesis. *Neural Networks : The Official Journal of the International Neural Network Society*, *24*(6), 515–525.

Traub, R. D., Whittington, M. A., Buhl, E. H., LeBeau, F. E. N., Bibbig, A., Boyd, S., Cross, H., & Baldeweg, T. (2001). A possible role for gap junctions in generation of very fast EEG oscillations preceding the onset of, and perhaps initiating, seizures. *Epilepsia*, *42*(2), 153–170.

Traynelis, S. F., Wollmuth, L. P., McBain, C. J., Menniti, F. S., Vance, K. M., Ogden, K. K., Hansen, K. B., Yuan, H., Myers, S. J., & Dingledine, R. (2010). Glutamate receptor ion channels: structure, regulation, and function. *Pharmacological Reviews*, *62*(3), 405–496.

Trebuchon, A., Guye, M., Tcherniack, V., Tramoni, E., Bruder, N., & Metellus, P. (2012). Intérêt du monitoring électrophysiologique au cours d'une chirurgie éveillée en neurochirurgie. *Annales Francaises d'Anesthesie et de Reanimation*, *31*(6), 87–90.

Trevelyan, A. J., Sussillo, D., & Yuste, R. (2007). Feedforward inhibition contributes to the control of epileptiform propagation speed. *The Journal of Neuroscience : The Official Journal of the Society for Neuroscience*, *27*(13), 3383–3387.

Tripathi, M., Garg, A., Gaikwad, S., Bal, C. S., Chitra, S., Prasad, K., Dash, H. H., Sharma, B. S., & Chandra, P. S. (2010). Intra-operative electrocorticography in lesional epilepsy. *Epilepsy Research*, *89*(1), 133–141.

Truccolo, W., Donoghue, J. A., Hochberg, L. R., Eskandar, E. N., Madsen, J. R., Anderson, W. S., Brown, E. N., Halgren, E., & Cash, S. S. (2011). Single-neuron dynamics in human focal epilepsy. *Nature Neuroscience*, *14*(5), 635–643.

Tybrandt, K., Khodagholy, D., Dielacher, B., Stauffer, F., Renz, A. F., Buzsáki, G., & Vörös, J. (2018). High-Density Stretchable Electrode Grids for Chronic Neural Recording. *Advanced Materials*, *30*(15), e1706520.

Unruh, D., Schwarze, S. R., Khoury, L., Thomas, C., Wu, M., Chen, L., Chen, R., Liu, Y., Schwartz, M. A., Amidei, C., Kumthekar, P., Benjamin, C. G., Song, K., Dawson, C., Rispoli, J. M., Fatterpekar, G., Golfinos, J. G., Kondziolka, D., Karajannis, M., … Horbinski, C. (2016). Mutant IDH1 and thrombosis in gliomas. *Acta Neuropathologica*, *132*(6), 917–930.

Uppstrom, T. J., Singh, R., Hadjigeorgiou, G. F., Magge, R., & Ramakrishna, R. (2016). Repeat surgery for recurrent low-grade gliomas should be standard of care. *Clinical Neurology and Neurosurgery*, *151*, 18–23.

Urrestarazu, E., Chander, R., Dubeau, F., & Gotman, J. (2007). Interictal high-frequency oscillations (10-500 Hz) in the intracerebral EEG of epileptic patients. *Brain*, *130*(9), 2354–2366.

Urrestarazu, E., Jirsch, J. D., LeVan, P., Hall, J., & Gotman, J. (2006). High-frequency intracerebral EEG activity (100-500 Hz) following interictal spikes. *Epilepsia*, *47*(9), 1465–1476.

Vacher, E., Rodriguez Ruiz, M., & Rees, J. H. (2023). Management of brain tumour related epilepsy (BTRE): a narrative review and therapy recommendations. *British Journal of Neurosurgery*, 1–8.

Vajda, F., O'Brien, T., Graham, J., Hitchcock, A., Perucca, P., Lander, C., & Eadie, M. (2023). Specific fetal malformations following intrauterine exposure to antiseizure medication. *Epilepsy & Behavior : E&B*, *142*.

Valderrama, M., Crépon, B., Botella-Soler, V., Martinerie, J., Hasboun, D., Alvarado-Rojas, C., Baulac, M., Adam, C., Navarro, V., & Le Van Quyen, M. (2012). Human gamma oscillations during slow wave sleep. *PloS One*, *7*(4).

van't Klooster, M. A., Van Klink, N. E. C., Leijten, F. S. S., Zelmann, R., Gebbink, T. A., Gosselaar, P. H., Braun, K. P. J., Huiskamp, G. J. M., & Zijlmans, M. (2015). Residual fast ripples in the intraoperative corticogram predict epilepsy surgery outcome. *Neurology*, *85*(2), 120–128.

Van Breemen, M. S. M., Rijsman, R. M., Taphoorn, M. J. B., Walchenbach, R., Zwinkels, H., & Vecht, C. J. (2009). Efficacy of anti-epileptic drugs in patients with gliomas and seizures. *Journal of Neurology*, *256*(9), 1519–1526.

van Breemen, M. S., Wilms, E. B., & Vecht, C. J. (2007). Epilepsy in patients with brain tumours: epidemiology, mechanisms, and management. *Lancet Neurology*, *6*(5), 421–430.

van Dellen, E., Douw, L., Hillebrand, A., Ris-Hilgersom, I. H. M., Schoonheim, M. M., Baayen, J. C., de Witt Hamer, P. C., Velis, D. N., Klein, M., Heimans, J. J., Stam, C. J., & Reijneveld, J. C. (2012). MEG network differences between low- and high-grade glioma related to epilepsy and cognition. *PloS One*, *7*(11).

Van Den Bent, M. J., Afra, D., De Witte, O., Ben Hassel, M., Schraub, S., Hoang-Xuan, K., Malmström, P. O., Collette, L., Piérart, M., Mirimanoff, R., & Karim, A. B. M. F. (2005). Long-term efficacy of early versus delayed radiotherapy for low-grade astrocytoma and oligodendroglioma in adults: the EORTC 22845 randomised trial. *Lancet (London, England)*, *366*(9490), 985–990.

Van Den Bent, Martin J., Brandes, A. A., Taphoorn, M. J. B., Kros, J. M., Kouwenhoven, M. C. M., Delattre, J. Y., Bernsen, H. J. J. A., Frenay, M., Tijssen, C. C., Grisold, W., Sipos, L., Enting, R. H., French, P. J., Dinjens, W. N. M., Vecht, C. J., Allgeier, A., Lacombe, D., Gorlia, T., & Hoang-Xuan, K. (2013). Adjuvant procarbazine, lomustine, and vincristine chemotherapy in newly diagnosed anaplastic

oligodendroglioma: long-term follow-up of EORTC brain tumor group study 26951. *Journal of Clinical Oncology : Official Journal of the American Society of Clinical Oncology*, *31*(3), 344–350.

van Klink, N. E.C., Van't Klooster, M. A., Zelmann, R., Leijten, F. S. S., Ferrier, C. H., Braun, K. P. J., Van Rijen, P. C., Van Putten, M. J. A. M., Huiskamp, G. J. M., & Zijlmans, M. (2014). High frequency oscillations in intra-operative electrocorticography before and after epilepsy surgery. *Clinical Neurophysiology*, *125*(11), 2212–2219.

van Klink, Nicole E.C., Zweiphenning, W. J. E. M., Ferrier, C. H., Gosselaar, P. H., Miller, K. J., Aronica, E., Braun, K. P. J., & Zijlmans, M. (2021). Can we use intraoperative high-frequency oscillations to guide tumor-related epilepsy surgery? *Epilepsia*, *62*(4), 997–1004.

Van Quyen, M. Le, Muller, L. E., Telenczuk, B., Halgren, E., Cash, S., Hatsopoulos, N. G., Dehghani, N., & Destexhe, A. (2016). High-frequency oscillations in human and monkey neocortex during the wake-sleep cycle. *Proceedings of the National Academy of Sciences of the United States of America*, *113*(33), 9363–9368.

Vecht, C. J., Kerkhof, M., & Duran-Pena, A. (2014). Seizure Prognosis in Brain Tumors: New Insights and Evidence-Based Management. *The Oncologist*, *19*(7), 751–759.

Venkataramani, V., Tanev, D. I., Strahle, C., Studier-Fischer, A., Fankhauser, L., Kessler, T., Körber, C., Kardorff, M., Ratliff, M., Xie, R., Horstmann, H., Messer, M., Paik, S. P., Knabbe, J., Sahm, F., Kurz, F. T., Acikgöz, A. A., Herrmannsdörfer, F., Agarwal, A., … Kuner, T. (2019). Glutamatergic synaptic input to glioma cells drives brain tumour progression. *Nature*, *573*(7775), 532–538.

Venkataramani, V., Yang, Y., Schubert, M. C., Reyhan, E., Tetzlaff, S. K., Wißmann, N., Botz, M., Soyka, S. J., Beretta, C. A., Pramatarov, R. L., Fankhauser, L., Garofano, L., Freudenberg, A., Wagner, J., Tanev, D. I., Ratliff, M., Xie, R., Kessler, T., Hoffmann, D. C., … Winkler, F. (2022). Glioblastoma hijacks neuronal mechanisms for brain invasion. *Cell*, *185*(16), 2899-2917.e31.

Venkatesh, H. S., Johung, T. B., Caretti, V., Silverbush, D., Gillespie, S. M., Arzt, M., Tam, L. T., Espenel, C., Ponnuswami, A., Ni, L., Woo, P. J., Taylor, K. R., Agarwal, A., Regev, A., Brang, D., Vogel, H., Hervey-Jumper, S., Bergles, D. E., Suvà, M. L., … Monje, M. (2015). Neuronal activity promotes glioma growth through neuroligin-3 secretion. *Cell*, *161*(4), 803–816.

Venkatesh, H. S., Morishita, W., Geraghty, A. C., Silverbush, D., Gillespie, S. M., Arzt, M., Tam, L. T., Espenel, C., Ponnuswami, A., Ni, L., Woo, P. J., Taylor, K. R., Agarwal, A., Regev, A., Brang, D., Vogel, H., Hervey-Jumper, S., Bergles, D. E., Suvà, M. L., … Monje, M. (2019). Electrical and synaptic integration of glioma into neural circuits. *Nature*, *573*(7775), 539–545.

Venkatesh, H. S., Tam, L. T., Woo, P. J., Lennon, J., Nagaraja, S., Gillespie, S. M., Ni, J., Duveau, D. Y., Morris, P. J., Zhao, J. J., Thomas, C. J., & Monje, M. (2017). Targeting neuronal activity-regulated neuroligin-3 dependency in high-grade glioma. *Nature*, *549*(7673), 533–537.

Verburg, N., Koopman, T., Yaqub, M. M., Hoekstra, O. S., Lammertsma, A. A., Barkhof, F., Pouwels, P. J. W., Reijneveld, J. C., Heimans, J. J., Rozemuller, A. J. M., Bruynzeel, A. M. E., Lagerwaard, F., Vandertop, W. P., Boellaard, R., Wesseling, P., De, P. C., Hamer, W., & De, P. (2020). Improved detection of diffuse glioma infiltration with imaging combinations: a diagnostic accuracy study. *Neuro-Oncology*, *22*(3), 412–422.

Verwer, R. W. H., Sluiter, A. A., Balesar, R. A., Baaijen, J. C., De Witt Hamer, P. C., Speijer, D., Li, Y., & Swaab, D. F. (2015). Injury Response of Resected Human Brain Tissue In Vitro. *Brain Pathology (Zurich, Switzerland)*, *25*(4), 454–468.

Viitanen, T., Ruusuvuori, E., Kaila, K., & Voipio, J. (2010). The K+-Cl cotransporter KCC2 promotes GABAergic excitation in the mature rat hippocampus. *The Journal of Physiology*, *588*(Pt 9), 1527–1540.

Villanueva, V., Santos-Carrasco, D., Cabezudo-García, P., Gómez-Ibáñez, A., Garcés, M., Serrano-Castro, P., Castro-Vilanova, M. D., Sayas, D., Lopez-Gonzalez, F. J., Rodríguez-Osorio, X., Torres-Gaona, G., Saiz-Diaz, R. A., Hampel, K. G., Martinez-Ferri, M., Aguilar-Amat, M. J., Mercedes-Alvarez, B., García-Morales, V., del Villar-Igea, A., Massot-Tarrús, A., & Rodríguez-Uranga, J. J. (2023). Real-world safety and effectiveness of cenobamate in patients with focal onset seizures: Outcomes from an Expanded Access Program. *Epilepsia Open*.

Vinogradov, E., Sherry, A. D., & Lenkinski, R. E. (2013). CEST: from basic principles to applications, challenges and opportunities. *Journal of Magnetic Resonance (San Diego, Calif. : 1997)*, *229*, 155–172.

Voloshin, T., Munster, M., Blatt, R., Shteingauz, A., Roberts, P. C., Schmelz, E. M., Giladi, M., Schneiderman, R. S., Zeevi, E., Porat, Y., Bomzon, Z., Urman, N., Itzhaki, A., Cahal, S., Kirson, E. D., Weinberg, U., & Palti, Y. (2016). Alternating electric fields (TTFields) in combination with paclitaxel are therapeutically effective against ovarian cancer cells in vitro and in vivo. *International Journal of Cancer*, *139*(12), 2850–2858.

Walter, W. G., & Dovey, V. J. (1946). DELIMITATION OF SUBCORTICAL TUMOURS BY DIRECT

ELECTROGRAPHY. *The Lancet*, *247*(6384), 5–9.
Walz, W. (2002). Chloride/anion channels in glial cell membranes. *Glia*, *40*(1), 1–10.
Wang, C., Xu, Z., Wang, S., Peng, L., Zhang, W., Li, X., Yang, L., Luan, Y., Su, T., Li, Z., & Hu, X. (2021). Clinical importance of ADC in the prediction of 125I in the treatment for gliomas. *Journal of Cancer*, *12*(7), 1945–1951.
Warnert, E. A. H., Wood, T. C., Incekara, F., Barker, G. J., Vincent, A. J. P., Schouten, J., Kros, J. M., van den Bent, M., Smits, M., & Tamames, J. A. H. (2022). Mapping tumour heterogeneity with pulsed 3D CEST MRI in non-enhancing glioma at 3 T. *Magma (New York, N.Y.)*, *35*(1), 53–62.
Watanabe, M., Tanaka, R., & Takeda, N. (1992). Magnetic resonance imaging and histopathology of cerebral gliomas. *Neuroradiology*, *34*(6), 463–469.
Watanabe, S., Takahashi, H., & Torimitsu, K. (2017). Electroconductive polymer-coated silk fiber electrodes for neural recording and stimulation in vivo. *Japanese Journal of Applied Physics*, *56*(3), 037001.
Watanabe, T., Nobusawa, S., Kleihues, P., & Ohgaki, H. (2009). IDH1 mutations are early events in the development of astrocytomas and oligodendrogliomas. *The American Journal of Pathology*, *174*(4), 1149–1153.
Watkins, S., & Sontheimer, H. (2011). Hydrodynamic cellular volume changes enable glioma cell invasion. *Journal of Neuroscience*, *31*(47), 17250–17259.
Weil, S., Osswald, M., Solecki, G., Grosch, J., Jung, E., Lemke, D., Ratliff, M., Hänggi, D., Wick, W., & Winkler, F. (2017). Tumor microtubes convey resistance to surgical lesions and chemotherapy in gliomas. *Neuro-Oncology*, *19*(10), 1316–1326.
Weiss, S. A., Alvarado-Rojas, C., Bragin, A., Behnke, E., Fields, T., Fried, I., Engel, J., & Staba, R. (2016). Ictal onset patterns of local field potentials, high frequency oscillations, and unit activity in human mesial temporal lobe epilepsy. *Epilepsia*, *57*(1), 111–121.
Weller, M., Gorlia, T., Cairncross, J. G., Van Den Bent, M. J., Mason, W., Belanger, K., Brandes, A. A., Bogdahn, U., Macdonald, D. R., Forsyth, P., Rossetti, A. O., Lacombe, D., Mirimanoff, R. O., Vecht, C. J., & Stupp, R. (2011). Prolonged survival with valproic acid use in the EORTC/NCIC temozolomide trial for glioblastoma. *Neurology*, *77*(12), 1156–1164.
Weller, Michael, & Le Rhun, E. (2020). How did lomustine become standard of care in recurrent glioblastoma? *Cancer Treatment Reviews*, *87*.
Weller, Michael, Stupp, R., & Wick, W. (2012). Epilepsy meets cancer: when, why, and what to do about it? *The Lancet. Oncology*, *13*(9).
Weller, Michael, van den Bent, M., Preusser, M., Le Rhun, E., Tonn, J. C., Minniti, G., Bendszus, M., Balana, C., Chinot, O., Dirven, L., French, P., Hegi, M. E., Jakola, A. S., Platten, M., Roth, P., Rudà, R., Short, S., Smits, M., Taphoorn, M. J. B., … Wick, W. (2021). EANO guidelines on the diagnosis and treatment of diffuse gliomas of adulthood. *Nature Reviews. Clinical Oncology*, *18*(3), 170–186.
Wenzel, M., Hamm, J. P., Peterka, D. S., & Yuste, R. (2019). Acute Focal Seizures Start As Local Synchronizations of Neuronal Ensembles. *The Journal of Neuroscience : The Official Journal of the Society for Neuroscience*, *39*(43), 8562–8575.
Werner, J. M., Weller, J., Ceccon, G., Schaub, C., Tscherpel, C., Lohmann, P., Bauer, E. K., Schäfer, N., Stoffels, G., Baues, C., Celik, E., Marnitz, S., Kabbasch, C., Gielen, G. H., Fink, G. R., Langen, K. J., Herrlinger, U., & Galldiks, N. (2021). Diagnosis of Pseudoprogression Following Lomustine-Temozolomide Chemoradiation in Newly Diagnosed Glioblastoma Patients Using FET-PET. *Clinical Cancer Research : An Official Journal of the American Association for Cancer Research*, *27*(13), 3704–3713.
Wheless, J. W. (2020). Adjunctive cenobamate for the treatment of focal onset seizures in adults with epilepsy: a critical review. *Expert Review of Neurotherapeutics*, *20*(11), 1085–1098.
Whitaker, H. A., & Ojemann, G. A. (1977). Graded localisation of naming from electrical stimulation mapping of left cerebral cortex. *Nature*, *270*(5632), 50–51.
Wiemels, J. L., Wiencke, J. K., Sison, J. D., Miike, R., McMillan, A., & Wrensch, M. (2002). History of allergies among adults with glioma and controls. *International Journal of Cancer*, *98*(4), 609–615.
Willems, P. W. A., Taphoorn, M. J. B., Burger, H., Van Der Sprenkel, J. W. B., & Tulleken, C. A. F. (2006). Effectiveness of neuronavigation in resecting solitary intracerebral contrast-enhancing tumors: a randomized controlled trial. *Journal of Neurosurgery*, *104*(3), 360–368.
Williams, P. A., White, A. M., Clark, S., Ferraro, D. J., Swiercz, W., Staley, K. J., & Dudek, F. E. (2009). Development of spontaneous recurrent seizures after kainate-induced status epilepticus. *The Journal of Neuroscience : The Official Journal of the Society for Neuroscience*, *29*(7), 2103–2112.
Wilson, T. W., Heinrichs-Graham, E., & Aizenberg, M. R. (2012). Potential role for magnetoencephalography in distinguishing low- and high-grade gliomas: a preliminary study with histopathological confirmation. *Neuro-Oncology*, *14*(5), 624–630.
Winkler, F., & Wick, W. (2018). Harmful networks in the brain and beyond. *Science (New York, N.Y.)*,

359(6380), 1100–1101.

Wirsching, H. G., Silginer, M., Ventura, E., Macnair, W., Burghardt, I., Claassen, M., Gatti, S., Wichmann, J., Riemer, C., Schneider, H., & Weller, M. (2020). Negative allosteric modulators of metabotropic glutamate receptor 3 target the stem-like phenotype of glioblastoma. *Molecular Therapy Oncolytics*, *20*, 166–174.

Witt, J. A., & Helmstaedter, C. (2013). Monitoring the cognitive effects of antiepileptic pharmacotherapy--approaching the individual patient. *Epilepsy & Behavior : E&B*, *26*(3), 450–456.

Wittner, L., Eross, L., Czirják, S., Halász, P., Freund, T. F., & Maglóczky, Z. (2005). Surviving CA1 pyramidal cells receive intact perisomatic inhibitory input in the human epileptic hippocampus. *Brain : A Journal of Neurology*, *128*(Pt 1), 138–152.

Wolters, C., & Munck, J. C. de. (2007). Volume conduction. *Scholarpedia*, *2*(3), 1738.

Wong, S. C., Kamarudin, M. N. A., & Naidu, R. (2021). Anticancer Mechanism of Curcumin on Human Glioblastoma. *Nutrients*, *13*(3), 1–19.

Wrensch, M., Jenkins, R. B., Chang, J. S., Yeh, R. F., Xiao, Y., Decker, P. A., Ballman, K. V., Berger, M., Buckner, J. C., Chang, S., Giannini, C., Halder, C., Kollmeyer, T. M., Kosel, M. L., Lachance, D. H., McCoy, L., O'Neill, B. P., Patoka, J., Pico, A. R., … Wiencke, J. K. (2009). Variants in the CDKN2B and RTEL1 regions are associated with high-grade glioma susceptibility. *Nature Genetics*, *41*(8), 905–908.

Wright, A., & Vissel, B. (2012). The essential role of AMPA receptor GluR2 subunit RNA editing in the normal and diseased brain. *Frontiers in Molecular Neuroscience*, *5*(APRIL).

Wyler, A. R., Ojemann, G. A., Lettich, E., & Ward, A. A. (1984). Subdural strip electrodes for localizing epileptogenic foci. *Journal of Neurosurgery*, *60*(6), 1195–1200.

Xi, C., Jinli, S., Jianyao, M., Yan, C., Huijuan, L., Zhongjie, S., Zhangyu, L., Liwei, Z., Yukui, L., Sifang, C., & Guowei, T. (2023). Fluorescein-guided surgery for high-grade glioma resection: a five-year-long retrospective study at our institute. *Frontiers in Oncology*, *13*.

Xu, D. S., Awad, A. W., Mehalechko, C., Wilson, J. R., Ashby, L. S., Coons, S. W., & Sanai, N. (2018). An extent of resection threshold for seizure freedom in patients with low-grade gliomas. *Journal of Neurosurgery*, *128*(4), 1084–1090.

Xu, W., Yang, H., Liu, Y., Yang, Y., Wang, P., Kim, S. H., Ito, S., Yang, C., Wang, P., Xiao, M. T., Liu, L. X., Jiang, W. Q., Liu, J., Zhang, J. Y., Wang, B., Frye, S., Zhang, Y., Xu, Y. H., Lei, Q. Y., … Xiong, Y. (2011). Oncometabolite 2-hydroxyglutarate is a competitive inhibitor of α-ketoglutarate-dependent dioxygenases. *Cancer Cell*, *19*(1), 17–30.

Yan, H., Parsons, D. W., Jin, G., McLendon, R., Rasheed, B. A., Yuan, W., Kos, I., Batinic-Haberle, I., Jones, S., Riggins, G. J., Friedman, H., Friedman, A., Reardon, D., Herndon, J., Kinzler, K. W., Velculescu, V. E., Vogelstein, B., & Bigner, D. D. (2009). IDH1 and IDH2 mutations in gliomas. *New England Journal of Medicine*, *360*(8), 765–773.

Yang, H., Ye, D., Guan, K. L., & Xiong, Y. (2012). IDH1 and IDH2 mutations in tumorigenesis: mechanistic insights and clinical perspectives. *Clinical Cancer Research : An Official Journal of the American Association for Cancer Research*, *18*(20), 5562–5571.

Yang, L. J., Liu, Y. L., Wang, S. Bin, & Jin, Z. G. (2014). IDH1 and IDH2 Mutations in Gliomas. *Zhongguo Zhen Jiu = Chinese Acupuncture & Moxibustion*, *34*(4), 334–336.

Yang, T., HakiYangmian, S., & Schwartz, T. H. (2014). Intraoperative electroCorticoGraphy (ECog): Indications, techniques, and utility in epilepsy surgery. *Epileptic Disorders*, *16*(3), 271–279.

Yang, W., Warrington, N. M., Taylor, S. J., Whitmire, P., Carrasco, E., Singleton, K. W., Wu, N., Lathia, J. D., Berens, M. E., Kim, A. H., Barnholtz-Sloan, J. S., Swanson, K. R., Luo, J., & Rubin, J. B. (2019). Sex differences in GBM revealed by analysis of patient imaging, transcriptome, and survival data. *Science Translational Medicine*, *11*(473).

Yao, C., Li, Q., Guo, J., Yan, F., & Hsing, I. M. (2015). Rigid and flexible organic electrochemical transistor arrays for monitoring action potentials from electrogenic cells. *Advanced Healthcare Materials*, *4*(4), 528–533.

Yao, P. Sen, Zheng, S. F., Wang, F., Kang, D. Z., & Lin, Y. X. (2018). Surgery guided with intraoperative electrocorticography in patients with low-grade glioma and refractory seizures. *Journal of Neurosurgery*, *128*(3), 840–845.

Ye, Z. C., Rothstein, J. D., & Sontheimer, H. (1999). Compromised glutamate transport in human glioma cells: Reduction- mislocalization of sodium-dependent glutamate transporters and enhanced activity of cystine-glutamate exchange. *Journal of Neuroscience*, *19*(24), 10767–10777.

Yekhlef, L., Breschi, G. L., Lagostena, L., Russo, G., & Taverna, S. (2015). Selective activation of parvalbumin- or somatostatin-expressing interneurons triggers epileptic seizurelike activity in mouse medial entorhinal cortex. *Journal of Neurophysiology*, *113*(5), 1616–1630.

Yohay, K., Tyler, B., Weaver, K. D., Pardo, A. C., Gincel, D., Blakeley, J., Brem, H., & Rothstein, J. D.

(2014). Efficacy of local polymer-based and systemic delivery of the anti-glutamatergic agents riluzole and memantine in rat glioma models. *Journal of Neurosurgery*, *120*(4), 854–863.

Yoo, R. E., Yun, T. J., Hwang, I., Hong, E. K., Kang, K. M., Choi, S. H., Park, C. K., Won, J. K., Kim, J. hoon, & Sohn, C. H. (2020). Arterial spin labeling perfusion-weighted imaging aids in prediction of molecular biomarkers and survival in glioblastomas. *European Radiology*, *30*(2), 1202–1211.

Yordanova, Y. N., Moritz-Gasser, S., & Duffau, H. (2011). Awake surgery for WHO Grade II gliomas within "noneloquent" areas in the left dominant hemisphere: toward a "supratotal" resection. Clinical article. *Journal of Neurosurgery*, *115*(2), 232–239.

You, G., Huang, L., Yang, P., Zhang, W., Yan, W., Wang, Y., Bao, Z., Li, S., Li, S., Li, G., & Jiang, T. (2012). Clinical and molecular genetic factors affecting postoperative seizure control of 183 Chinese adult patients with low-grade gliomas. *European Journal of Neurology*, *19*(2), 298–306.

Yuan, H. X., Xiong, Y., & Guan, K. L. (2013). Nutrient sensing, metabolism, and cell growth control. *Molecular Cell*, *49*(3), 379–387.

Yuan, Y., Xiang, W., Yanhui, L., Ruofei, L., Jiewen, L., Shu, J., & Qing, M. (2017). Activation of the mTOR signaling pathway in peritumoral tissues can cause glioma-associated seizures. *Neurological Sciences : Official Journal of the Italian Neurological Society and of the Italian Society of Clinical Neurophysiology*, *38*(1), 61–66.

Yuen, T. I., Morokoff, A. P., Bjorksten, A., D'Abaco, G., Paradiso, L., Finch, S., Wong, D., Reid, C. A., Powell, K. L., Drummond, K. J., Rosenthal, M. A., Kaye, A. H., & O'Brien, T. J. (2012). Glutamate is associated with a higher risk of seizures in patients with gliomas. *Neurology*, *79*(9), 883–889.

Zaitsev, A. V., Malkin, S. L., Postnikova, T. Y., Smolensky, I. V., Zubareva, O. E., Romanova, I. V., Zakharova, M. V., Karyakin, V. B., & Zavyalov, V. (2019). Ceftriaxone Treatment Affects EAAT2 Expression and Glutamatergic Neurotransmission and Exerts a Weak Anticonvulsant Effect in Young Rats. *International Journal of Molecular Sciences*, *20*(23).

Zelmann, R., Mari, F., Jacobs, J., Zijlmans, M., Dubeau, F., & Gotman, J. (2012). A comparison between detectors of high frequency oscillations. *Clinical Neurophysiology : Official Journal of the International Federation of Clinical Neurophysiology*, *123*(1), 106–116.

Zetterling, M., Roodakker, K. R., Berntsson, S. G., Edqvist, P. H., Latini, F., Landtblom, A. M., Pontén, F., Alafuzoff, I., Larsson, E. M., & Smits, A. (2016). Extension of diffuse low-grade gliomas beyond radiological borders as shown by the coregistration of histopathological and magnetic resonance imaging data. *Journal of Neurosurgery*, *125*(5), 1155–1166.

Zhang, C., Zuo, Z., Kwan, P., & Baum, L. (2011). In vitro transport profile of carbamazepine, oxcarbazepine, eslicarbazepine acetate, and their active metabolites by human P-glycoprotein. *Epilepsia*, *52*(10), 1894–1904.

Zhang, J., Zhu, W., Tain, R., Zhou, X. J., & Cai, K. (2018). Improved Differentiation of Low-Grade and High-Grade Gliomas and Detection of Tumor Proliferation Using APT Contrast Fitted from Z-Spectrum. *Molecular Imaging and Biology*, *20*(4), 623–631.

Zhang, L., Min, Z., Tang, M., Chen, S., Lei, X., & Zhang, X. (2017). The utility of diffusion MRI with quantitative ADC measurements for differentiating high-grade from low-grade cerebral gliomas: Evidence from a meta-analysis. *Journal of the Neurological Sciences*, *373*, 9–15.

Zhang, R. R., Schroeder, A. B., Grudzinski, J. J., Rosenthal, E. L., Warram, J. M., Pinchuk, A. N., Eliceiri, K. W., Kuo, J. S., & Weichert, J. P. (2017). Beyond the margins: real-time detection of cancer using targeted fluorophores. *Nature Reviews. Clinical Oncology*, *14*(6), 347–364.

Zhong, Z., Wang, Z., Wang, Y., You, G., & Jiang, T. (2015). IDH1/2 mutation is associated with seizure as an initial symptom in low-grade glioma: A report of 311 chinese adult glioma patients. *Epilepsy Research*, *109*(1), 100–105.

Zhu, H., & Barker, P. B. (2011). MR spectroscopy and spectroscopic imaging of the brain. *Methods in Molecular Biology (Clifton, N.J.)*, *711*, 203–226.

Ziburkus, J., Cressman, J. R., Barreto, E., & Schiff, S. J. (2006). Interneuron and pyramidal cell interplay during in vitro seizure-like events. *Journal of Neurophysiology*, *95*(6), 3948–3954.

Zijlmans, M., Jacobs, J., Zelmann, R., Dubeau, F., & Gotman, J. (2009). High-frequency oscillations mirror disease activity in patients with epilepsy. *Neurology*, *72*(11), 979–986.

Zijlmans, Maeike, Worrell, G. A., Dümpelmann, M., Stieglitz, T., Barborica, A., Heers, M., Ikeda, A., Usui, N., & Le Van Quyen, M. (2017). How to record high-frequency oscillations in epilepsy: A practical guideline. *Epilepsia*, *58*(8), 1305–1315.

Zouaoui, S., Rigau, V., Mathieu-Daudé, H., Darlix, A., Bessaoud, F., Fabbro-Peray, P., Bauchet, F., Kerr, C., Fabbro, M., Figarella-Branger, D., Taillandier, L., Duffau, H., Trétarre, B., & Bauchet, L. (2012). [French brain tumor database: general results on 40,000 cases, main current applications and future prospects]. *Neuro-Chirurgie*, *58*(1), 4–13.

Zu, Z., Louie, E. A., Lin, E. C., Jiang, X., Does, M. D., Gore, J. C., & Gochberg, D. F. (2017). Chemical

exchange rotation transfer imaging of intermediate-exchanging amines at 2 ppm. *NMR in Biomedicine*, *30*(10).

Zurolo, E., de Groot, M., Iyer, A., Anink, J., van Vliet, E. A., Heimans, J. J., Reijneveld, J. C., Gorter, J. A., & Aronica, E. (2012). Regulation of Kir4.1 expression in astrocytes and astrocytic tumors: a role for interleukin-1 β. *Journal of Neuroinflammation*, *9*.

Zweiphenning, W. J. E. M., van 't Klooster, M. A., van Diessen, E., van Klink, N. E. C., Huiskamp, G. J. M., Gebbink, T. A., Leijten, F. S. S., Gosselaar, P. H., Otte, W. M., Stam, C. J., Braun, K. P. J., & Zijlmans, G. J. M. (2016). High frequency oscillations and high frequency functional network characteristics in the intraoperative electrocorticogram in epilepsy. *NeuroImage: Clinical*, *12*, 928–939.

Zweiphenning, W., Klooster, M. A. va. t., van Klink, N. E. C., Leijten, F. S. S., Ferrier, C. H., Gebbink, T., Huiskamp, G., van Zandvoort, M. J. E., van Schooneveld, M. M. J., Bourez, M., Goemans, S., Straumann, S., van Rijen, P. C., Gosselaar, P. H., van Eijsden, P., Otte, W. M., van Diessen, E., Braun, K. P. J., Zijlmans, M., … Dankbaar, J. W. (2022). Intraoperative electrocorticography using high-frequency oscillations or spikes to tailor epilepsy surgery in the Netherlands (the HFO trial): a randomised, single-blind, adaptive non-inferiority trial. *The Lancet. Neurology*, *21*(11), 982–993.

Cortex péritumotal : signaux électrophysiologiques

Résumé :

Les gliomes cérébraux sont des tumeurs hautement épileptogènes formées d'un noyau macroscopique entouré de tissus infiltrés par des cellules tumorales, le tissu péritumoral. Les processus de croissance de la tumeur et d'épileptogenèse convergent à son niveau. Ce travail à visé à caractériser au plan électrophysiologique le tissu péritumoral. Pendant la chirurgie éveillée des gliomes, lors d'enregistrements électrocorticographiques (ECoG), la tumeur et les zones péritumorales présentent des caractéristiques distinctes dans les composantes périodiques et apériodiques du spectre fréquentiel. Ces différences ont le potentiel de servir de biomarqueurs des zones péritumorales. Bien qu'aucune différence apparente ne soit pas observable entre les zones péritumorales proches et éloignées, il existe une corrélation entre la réduction des rythmes physiologiques et l'infiltration des cellules tumorales. Ces données suggèrent que l'infiltration tumorale ne suis pas une distribution radiale mais se propage guidée par les faisceaux neuronaux et les vaisseaux sanguins. Cette zone clé mais difficile à délimiter entournant les gliomes doit être réséquée pour améliorer à la fois les pronostics épileptiques et oncologiques, ce que sa caractérisation fine doit optimiser. Le tissu péritumoral est aussi le site de genèse des crises épileptiques, dont j'ai caractérisé ex vivo, dans les tissus postopératoires, la dynamique spatiotemporelle. La transition vers la crise, complexe, comprend une augmentation progressive de l'amplitude, de la pente ascendante et de la fréquence d'activité de populations neuronales, spécifiques de la période préictale et initiatrices de la crise une fois déployées, nommées décharges préictales (PIDs). Cette évolution indique une synchronisation et un recrutement neuronaux accrus. Les oscillations à haute fréquence augmentent aussi pendant la période préictale, atteignant leur apogée quelques secondes avant le début de la crise. Les PIDs et les oscillations à haute fréquence suivent une propagation spatiale progressive, ces dernières se limitant à des microdomaines de moins de 200 μm, soulignant l'importance d'améliorer la résolution spatiale pour les capturer précisément. Étant donné l'évolution temporelle et spatiale commune des toutes ces activités, il est plausible que des mécanismes communs de plasticité synaptique excitatrice sous-tendent leur génération. Ces dynamiques complexes peuvent être utilisées pour développer des algorithmes de détection des périodes à haut risque de crises chez les patients. Ce travail de caractérisation électrophysiologique du tissu péritumoral, in vivo et ex vivo permettra de développer des outils de détection pour optimiser la chirurgie et pour mieux comprendre les interactions entre cellules tumorales et micro-environnement neuronal.

Mots clés : Gliome, peritumoral, ECoG, épilepsie, ictogenèse

Peritumotal cortex: electrophysiological signals

Abstract:

Brain gliomas are highly epileptogenic tumors formed by a macroscopic core and by the surrounding tissue infiltrated by tumor cells, called the peritumoral tissue. At this level, the tumor growth and the epileptogenesis converge. The aim of this work was to characterize electrophysiologically the peritumoral tissue. During awake glioma surgery cortical EEG recording (ECoG), the tumor and peritumoral areas exhibit distinctive features in the periodic and aperiodic components of the frequency power spectrum. These differences have the potential to serve as biomarkers of the peritumoral areas. Although no apparent differences are noticeable between close and far peritumoral areas, a correlation exists between the reduction of physiological rhythms and the infiltration of tumor cells. These data suggest that infiltration do not follow a radial distribution but spread guided by neural bundles and vessels. This key

but challenging to delineate zone surrounding gliomas must be removed to improve both epilepsy and oncological outcomes, which requires its accurate characterization. The peritumoral tissue is also the site of epileptic seizure genesis. I have characterized ex vivo, in postoperative tissues, its spatiotemporal dynamics. The complex transition to seizure involves a progressive increase in the amplitude, upward slope and frequency of neuronal populations activity, specific to the preictal period and triggering the seizure once mature, called preictal discharges (PIDs). This evolution indicates increased neuronal synchronization and recruitment. High frequency oscillations also intensify during the preictal period, suggesting gradual neuronal recruitment and activation of small networks responsible for high frequency oscillations generation, peaking seconds before the seizure onset. PIDs and high frequency oscillations follow a progressive spatial spreading. However, high frequency oscillations are confined to microdomains smaller than 200 µm, underscoring the importance of enhancing spatial resolution to capture them accurately. Given the shared temporal and spatial evolution of all these activities, it is plausible that common mechanisms based on excitatory synaptic plasticity underlie their generation. These complex dynamics can be used to develop algorithms for detecting seizure high-risk periods in patients, thereby advancing our understanding of the pathophysiological mechanisms implicated in seizure generation. This electrophysiological characterization of peritumoral tissues, both in vivo and ex vivo, will enable us to develop detection tools to optimize surgery and better understand the interactions between tumor cells and the neuronal microenvironment.

Keywords: Glioma, peritumoral, ECoG, epilepsy, ictogenesis